

INDIAN JOURNAL OF PHYSICS

VOL. 30

AND

PROCEEDINGS

OF THE

Indian Association for the Cultivation of Science, Vol. 39

(Published in Collaboration with the Indian Physical Society)

(With Twentytwo Plates)

Printed by Kalipada Mukherjee, Eka Press, 2041. B. T. Road, Calcutta
and published by the Registrar, Indian Association for the Cultivation
of Science, Jadavpur, Calcutta 32

1956

Price Rs. 20 or £ 2

BOARD OF EDITORS

R. K. ASUNDI	S. K. MITRA
K. BANERJEE	P. RAY
D. M. BOSE	K. R. RAO
S. N. BOSE	M. N. SAHA
K. R. DIXIT	S. C. SIRKAR (<i>Secretary</i>)
P. S. GILL	B. N. SRIVASTAVA

EDITORIAL COLLABORATORS

PROF. D. BASU, PH.D.
DR. A. BOSE, D.Sc.
DR. N. N. DASGUPTA, M.Sc., PH.D.
DR. S. GHOSH, D.Sc.
DR. S. R. KHASTGIR, D.Sc., F.N.I., F.R.S.E.
PROF. P. K. KICHLU, D.Sc., F.N.I.
PROF. D. S. KOTHARI, D.Sc., F.N.I.
DR. K. S. KRISHNAN, D.Sc., F.R.S.
PROF. P. C. MAHANTI, D.Sc., F.N.I.
PROF. B. D. NAG CHOWDHURY, PH.D.
PROF. S. R. PALIT, D.Sc., F.R.I.C., F.N.I.
DR. S. PARTHASARATHY, D.Sc., F.N.I.
DR. H. RAKSHIT, D.Sc., F.N.I.
DR. R. GOPALAMURTY RAO.
DR. VIKRAM A. SARABHAI, M.A., PH.D.
PROF. N. R. SEN, D.Sc., F.N.I.
PROF. N. R. TAWDE, D.Sc., F.N.I.

ASSISTANT EDITOR

MR. A. N. BANERJEE, M.Sc.

NOTICE

TO INTENDING AUTHORS

Manuscripts for publication should be sent to the Assistant Secretary, Indian Journal of Physics, Jadavpur, Calcutta 32.

The manuscripts submitted must be type-written with double space on thick foolscap paper with sufficient margin on the left and at the top. The original copy, and not the carbon copy, should be submitted. Each paper must contain an abstract at the beginning.

All references should be given in the text by quoting the surname of the author, followed by year of publication, e.g., (Ghosh, 1954). The full reference should be given in a list at the end, arranged alphabetically, as follows; Ghosh, D. K., 1954, *Ind. J. Phys.*, **28**, 485.

Line diagrams should be drawn on white Bristol board or tracing paper with black India ink, and letters and numbers inside the diagrams should be written neatly in capital type with India ink. The size of the diagrams submitted and the lettering inside should be large enough so that it is legible after reduction to one-third the original size. A simple style of lettering such as gothic, with its uniform line width and no serifs should be used, e.g.,

A·B·E·F·G·M·P·T·W·

Photographs submitted for publication should be printed on glossy paper with somewhat more contrast than that desired in the reproduction, and should, if possible, be mounted on thick white paper.

Captions to all figures should be typed in a separate sheet and attached at the end of the paper.

The mathematical expressions should be written carefully by hand. Care should be taken to distinguish between capital and small letters and superscripts and subscripts. Repetition of a complex expression should be avoided by representing it by a symbol. Greek letters and unusual symbols should be identified in the margin. Fractional exponents should be used instead of root signs.

Annual Subscription—

Inland Rs. 20

Foreign £ 2

INDIAN JOURNAL OF PHYSICS. VOL. 30, 1956

CONTENTS

No. 1. January

	PAGE
1. Analysis of Spuriousness of Geiger-Muller Tubes at High Temperatures —By Satya Pal Puri and P. S. Gill	1
2. Rectification and Crystal Structure—By K. R. Dixit	10
3. On the Anomalous Magnetic Moments of the Nucleons—By S. P. Misra and B. B. Deo	16
4. On the Nature of Extra Reflections in the Laue Photographs of some Diamonds of known Relative Fluorescence Efficiencies—By S. C. Sirkar and S. N. Sen	29
5. Polarization of the Echoes from the Ionosphere—By J. K. D. Verma and R. Roy	36
REVIEW :	
Beta and Gamma-Ray Spectroscopy —By Kai Siegbahn	47

No. 2. February

Obituary —Professor Meghnad Saha, F.R.S.	51
6. The Flow of a Viscous Liquid in a Circular Tube Under Pressure-Gradients Varying Exponentially with time—By Lakshmi Sanyal	57
7. The Temperature-Dependence of Geiger-Muller Counter Characteristics (Part I)—By Satya Pal Puri and P. S. Gill	62
8. The Temperature-Dependence of Geiger-Muller Counter Characteristics. (Part II)—By Satya Pal Puri and P. S. Gill	70
9. Determination of Absolute Cross-Section of (n, p) Reaction in S^{32} —By N. K. Saha and L. Kasturi Rangan	80
10. Dielectric Properties of 2,4-Dinitrofluorobenzene—By D. V. G. L. Narasimha Rao	91

LETTER TO THE EDITOR:

Structure of the Spectrum of Singly Ionised Bromine—Y. Bhupala Rao	95
--	----

REVIEW :

Light Calculations and Measurements—By H. A. E. Keitz	97
---	----

No. 3. March

11. A Time of Flight Neutron Velocity Selector using Scintillation Counter—By A. P. Patro.	99
12. Ultraviolet Absorption Spectra of α -Methyl Naphthalene and β -Methyl Naphthalene in the Liquid and Solid States—By S. B. Banerjee	106

	Page
13. Analysis of the near Ultraviolet Absorption Spectrum of Ortho-chloroanisole—By V. Suryanarayana and V. Ramakrishna Rao	117
14. Behaviour of Saturable Reactors in Magnetic Amplifiers—By P. N. Das	129
15. On the Fluorescence of Parachlorotoluene in the Solid State at Low Temperature—By D. C. Biswas	143
LETTER TO THE EDITOR	
The Ultraviolet Absorption Spectrum of Meta-fluorochlorobenzene—S. L. N. G. Krishnamachari	151

No. 4. April

	PAGE
16. Geomagnetic Activity and Solar M-Regions for the Current Epoch of the Sunspot Minimum— By J. N. Tandon	153
17. Studies on the Magnetic Susceptibility of the Cr^{+3} Alums in the Range 300°K to 100°K—By S. K. Dutta Roy	169
18. Ionospheric Prediction Methods and the Probable Sources of Error—By S. S. Baral	189
19. Calculation of Dipole Moments of the Tetra-Substituted Benzenes Part I— By K. V. Gopal Krishna	206

No. 5. May

20. A Nuclear Magnetic Resonance Apparatus - By A. Saha, B. Banerjee, T. Das, D. Roy, S. Ghosh Roy and T. Ghose	211
21. On the Crystal Structure of Para Dichlorobenzene at Different Temperatures- By G. S. R. Krishna Murti and S. N. Sen	242
22. Dependence of Limit of Resolution on Background Intensity, Detecting Instrument and Stage of Resolution in X-ray Spectra—By D. C. Purkayastha	250
23. On the Dependence of the Intensity of Fluorescence of Frozen <i>p</i> -Chlorotoluene on the Wavelength of the Exciting Radiation -- By D. C. Biswas	255

LETTERS TO THE EDITOR

(1) Boiling Point and other Physical Properties of the Halogens and Halides—G. R. Somayajulu	258
(2) Boiling Point and Atomic Size—G. R. Somayajulu and Santi R. Palit	262

No. 6. June

24. Compton Scattering of Light by Electron—By D. Basu and D. P. Sural	265
--	-----

	Page
25. On Wave Nature of Matter—Part II—By Brahmananda Mishra ..	273
26. Ultraviolet Absorption Spectra of Frozen Solutions of <i>o</i> -, <i>m</i> - and <i>p</i> -Chlorotoluene in Isobutyl Alcohol—By S. B. Roy ..	276
27. Origin of the Zodiacal Light and the Variations of its Brightness—By Prabhat K. Sen Gupta	285
28. Polarisation in p-p Scattering—By C. C. Banerjee	292
29. Test of the Workability of Lotmar's Potential Energy Function—By N. R. Tawde and N. N. Gejji	299
30. Spectroscopic Constants of Molecules. V. Similarities in Constants of Different Groups—By Y. P. Varshni and K. Majumdar ..	303
31. Raman Spectra of Frozen Solutions of Toluene and Benzene in Aliphatic Solvents—By G. S. Kastha	313
LETTER TO THE EDITOR	
The Ultraviolet Absorption Spectrum of Para-fluorochlorobenzene—By S. L. N. G. Krishnamachari	319

No. 7. July

	PAGE
32. Ultraviolet Absorption Spectra of Phenyl Acetonitrile, Phenyl Acetate, Phenyl Salicylate and Monomeric Styrene in the Liquid and Solid States—By S. K. Sen	321
33. Analysis of the Absorption and Fluorescence spectra of Uranyl Salts. Part I. Uranyl Acetate (Absorption) By V. Ramakrishna Rao and K. V. Narasimham	334
34. Measurement of Surface Tension by Unstable Pendant Drops—By N. R. Tawde and K. G. Parvatikar	348
35. Ultraviolet Absorption Spectra of Phenol, <i>o</i> -Bromophenol and Diphenyl Ether in Different States—By S. B. Banerjee ..	353
36. Mass Measurements in Nuclear Emulsions by Multiple Scattering and Gap Distribution—By Inder Sain Mittra	363
LETTER TO THE EDITOR.	
Structure of the Spectrum of Doubly Ionised Bromine—Y. Bhupala Rao	371

No. 8. August

37. Radiations from Two Radioactive Isotopes of Gold—By V. R. Potnis	375
38. On the Raman Spectra of 1, 1-Dichloroethane and 1, 1, 1-Trichloroethane in the Vapour State—By Monomohan Mazumder ..	384
39. Circular Arc Antennas—By S. Balaram Rao	390
40. On the Fluorescence of para-Bromotoluene, ortho-Bromo- and ortho-Chlorotoluene in the Solid State at Low Temperature—By D. C. Biswas	407

	Page
41. $L_{2,3}$ and K Emission Spectra of Magnesium, Aluminium and Lithium in Higher Orders—By A. K. Sen	415
42. Surface Tension-Temperature Relation from Free-Volume Concept - By Shashanka Shekhar Mitra	423

No. 9. September

43. The Inverse Kinetic Energy Matrix Elements for the out-of-plane Vibrations in Furan, Thiophene, Cyclopentadiene and their Substituted Compounds —By V. Santhamma	429
44. Magnetic Moments of the Nucleons-- By S. K. Kundu	450
45. Cloud Chamber Analysis of Cosmic-Ray Showers under 10 to 23 cms. of Lead-- By P. K. Sen Choudhury and S. N. Sen Gupta	453
46. On the Determination of Electron Density Distribution in the Ionospheric Regions from h.f Records—By A. K. Saha	464
47. Ultraviolet Absorption Spectra of Pyridine in the Liquid and Solid States —By S. B. Banerjee	480
48. Deformation of a Fixed-Free bar under a Compressive Impact of Short Duration- By S. K. Ghosh	485

LETTER TO THE EDITOR

The Ultraviolet Absorption Spectra of <i>o</i> -, <i>m</i> -, <i>p</i> -Fluorobromobenzene —S. L. N. G. Krishnamachari	487
---	-----

BOOK REVIEW

Paramagnetic Nuclear Resonance—By P. Grivet	489
---	-----

No. 10. October

49. Resolution of Spectral Lines of Unequal Intensity—By K. C. Chaturvedi and M. S. Sodha	491
50. Theory of Spherical Symmetry Method for Measurement of Thermal Neutron Absorption-- By A. M. Ghose and N. K. Ganguly	500
51. Raman Spectra of Pyridine and its Solutions in Ethyl Alcohol at Different Temperatures-- By G. S. Kastha	519
52. Sommerfeld's Fine Structure Formula from a Second Order Equation without Thomas Correction—By C. C. Banerji	525
53. Raman Spectra of three Monosubstituted Benzene Compounds in the Solid State at Low Temperatures—By D. C. Biswas	530

No. 11. November

54. The Crystal Structure of Anthracene at Different Temperatures— By G. S. R. Krishna Murti	537
55. On Dependence of Resolving Power on Background Intensity, Stage of Resolution and Detecting Instrument—By K. C. Chaturvedi and M. S. Sodha	543

	PAGE
56. Ultraviolet Absorption Spectra of <i>o</i> -Methoxyphenol and 2, 4, 6-Trichlorophenol in Different States—By S. K. Sen	553
57. On the Radial Pulsation of Magnetic Stars—By S. P. Talwar and J. N. Tandon	561
58. Fluorescence Spectra of Methyl Benzoate, <i>m</i> -Chlorotoluene and <i>m</i> -Bromotoluene—By D. C. Biswas	565
59. On Thermoluminescence Spectra—By B. C. Dutta and A. K. Ghosh ..	570
LETTER TO THE EDITOR	
Dipole Moments of Tri-Substituted Benzenes—D. V. G. L. Narasimha Rao	580

No. 12. December

60. Growing of Organic Phosphors for Scintillation Counters—By Rangalal Bhattacharyya, Uma Basu Roy and Santimay Chatterjee	585
61. Ultraviolet Absorption Spectra of Solutions of Bromotoluenes in Isobutyl Alcohol at Different Temperatures—By S. B. Roy ..	590
62. Effect of Background Intensity on Resolving Power of Lummer-Gehrke Plate and Transmission Echelon—By K. C. Chaturvedi and M. S. Sodha	599
63. On the Induction Drag of a Sphere Moving in a Conducting Fluid in the Presence of a Magnetic field—By K. P. Chopra	605
64. Variation of the Binding Energies of Neutrons and Protons in Heavy Nuclei—By H. K. Raut	611
65. On the Fluorescence in Diamond Excited by X-Rays—By S. N. Sen and B. M. Bishui	620
LETTER TO THE EDITOR	
Theory of Specific Heat of Liquid Hydrogen—S. C. Misra ..	626

AUTHOR INDEX

Author	Subject	Page
Banerjee, B. and A. Saha, T. Das, D. Roy, S. Ghosh Roy and T. Ghose	A nuclear magnetic resonance apparatus	211
Banerjee, C. C.	Sommerfeld's fine structure formula from a second order equation without Thomas correction	525
" "	Polarisation in p-p scattering	292
Bauerjee, S. B.	Ultraviolet absorption spectra of α - methyl naphthalene and β -methyl naphthalene in the liquid and solid states	106
" "	Ultraviolet absorption spectra of phenol, <i>o</i> -bromophenol and diphenyl ether in different states	353
" "	Ultraviolet absorption spectra in pyri- dine in the liquid and solid states	480
Baral, S.S.	Ionospheric prediction methods and probable sources of error	189
Basu, D. and D. P. Sural	Characteristics of light by laser	265
Basu Roy, Uma; R. Bhattacharyya and S. Chatterjee	Growing of organic phosphors for scintil- lation counters	585
Bhattacharyya, R., Uma Basu Roy and S. Chatterjee	" " " " " "	585
Bishui, B. M. and S. N. Sen	On the fluorescence in diamond excited by X-rays	620
Biswas, D. C.	On the fluorescence of parachloroto- luene in the solid state at low temp- erature	143
" "	On the dependence of the intensity of fluorescence of frozen <i>p</i> -chlorotoluene on the wavelength of the exciting radiation	255
" "	On the fluorescence of parabromotoluene in the solid state at low temperatures	407
" "	Raman spectra of three mono-substi- tuted benzene compounds in the solid state at low temperatures	530
" "	Fluorescence spectra of methyl ben- zoate, <i>m</i> -chlorotoluene and <i>m</i> -bromo- toluene	565
	vii	

Author	Subject	Page
Chatterjee, S., R. Bhattacharyya and Uma Basu Roy	Growing of organic phosphors for scintillation counters	585
Chaturvedi K. C. and M. S. Sodha	Resolution of spectral lines of unequal intensity	491
" " " "	On the dependence of resolving power on background intensity, stage of resolution and detecting instrument	543
" " " "	Effect of background intensity on resolving power of Lummer-Gebrcke plate and transmission echelon	599
Chopra, K. P.	On the induction drag of a sphere moving in conducting fluid in the presence of a magnetic field	605
Das, P. N.	Behaviour of saturable reactor in magnetic amplifiers	129
Das, T., and A. Saha B. Banerjee D. Ray, S. Ghosh Roy, T. Ghose	A nuclear magnetic resonance apparatus	211
Deo, B. B. and S. P. Misra	On the anomalous magnetic moments of the nucleons	16
Dixit, K. R.	Rectification and crystal structure	10
Dutta Roy, S. K.	Studies on the magnetic susceptibility of the Cr^{+3} alumina in the range 300°K to 100°K	169
Dutta B. C. and A. K. Ghosh	On thermoluminescence spectra	570
Ganguly, N. K. and A. M. Ghosh	Theory of spherical symmetry method for measurement of thermal neutron absorption	500
Gejji, N. V. and N. R. Tawde	Test of the workability of Lotmar's potential energy function	299
Ghosh, A. M. and N. K. Ganguly	Theory of spherical symmetry method for measurement of thermal neutron absorption	500
Ghosh, S. K.	Deformation of a fixed-free bar under a compressive impact of short duration	485
Ghose, T. A. Saha, B. Banerjee, T. Das, D. Roy and S. Ghosh Roy	A nuclear magnetic resonance apparatus	211
Ghosh Roy, S., A. Saha, B. Banerjee, T. Das, D. Roy and T. Ghose	A nuclear magnetic resonance apparatus	211
Ghosh, A. K. and B. C. Dutta	On thermoluminescence spectra	570

Author	Subject	Page
Gill, P. S. and S. P. Puri	Analysis of spuriousness of Geiger-Muller tubes at high-temperatures	1
" P. S. and S. P. Puri	The temperature-dependence of Geiger-Muller counter characteristics (Part I)	62
" P. S. and S. P. Puri	" " " " (Part II)	70
Gopal Krishna, K. V.	Calculation of dipole moments of the tetra-substituted benzenes (I)	206
Kasturi Rangan, L. and N. K. Saha	Determination of absolute cross-section (n, p) reaction in S ³²	80
Kastha, G. S.	Raman spectra of frozen solutions of toluene and benzene in aliphatic solvents	313
" G. S.	Raman spectra of pyridine and its solution in ethyl alcohol at different temperatures	519
Krishna Murti, G. S. R.	The crystal structure of anthracene at different temperatures	537
Krishnamachari, S. L. N. G.	The ultraviolet absorption spectrum of meta-fluorobenzene (L)	151
" "	The ultraviolet absorption spectrum of para-fluorochlorobenzene (L)	319
" "	The ultraviolet absorption spectra of o-, m-, p-fluorobromobenzene (L)	487
Krishna Murti, G. S. R. and S. N. Sen	On the crystal structure of para-dichlorobenzene at different temperatures	242
Kundu, S. K.	Magnetic moments of nucleons	450
Mazumder, M. M.	On the Raman spectra of 1, 1-dichloroethane and 1, 1, 1-trichloroethane in the vapour state	384
Majumdar, K. and Y. P. Varshni	Spectroscopic constants of molecules. V. Similarities in constants of different groups	303
Mishra, Brahmananda	On wave nature of matter. Part II	273
Misra, S. C.	Theory of specific heat of liquid hydrogen (L)	626
Misra, S. P. and B. B. Deo,	On the anomalous magnetic moments of the nucleons	16
Mitra, I. S.	Mass measurements in nuclear emulsions by multiple scattering and gas distribution	363

Author	Subject	Page
Mitra, S. S.	Surface tension-temperature relation from free-volume concept	423
Narasimham, K. V. and V. R. Rao.	Analysis of absorption and fluorescence spectra of uranyl salts. I. Uranyl acetate (absorption)	334
Palit, S. R. and G. R. Somaya-julu	Boiling point and atomic size (L)	262
Parvatikar, K. G. and N. R. Tawde	Measurement of surface tension by unstable pendant drops	348
Patro, A. P.	A time of flight neutron velocity selector using scintillation counter	99
Potnis, V. R.	Radiations from two radio-active isotopes of gold	375
Puri, S. P. and P. S. Gill	Analysis of spuriousness of Geiger-Muller tubes at high temperatures	1
Puri, S. P. and P. S. Gill	The temperature-dependence of Geiger Muller counter characteristics (Part I)	62
Puri, S. P. and P. S. Gill	" " (Part II)	70
Purkayastha, D. C.	Dependence of limit of resolution on background intensity, detecting instrument and stage of resolution in x-ray spectra	250
Rao, S. B.	Circular arc antennas	390
Rao, V. R. and K. V. Narasimham	Analysis of the absorption and fluorescence spectra of uranyl salts. I. Uranyl acetate (absorption)	334
Rao, V. R. and V. Suryanarayana	Analysis of the near ultraviolet absorption spectrum of orthochloroanisole	117
Rao, D. V. G. L. N.	Dielectric properties of 2, 4-dinitro-fluorobenzene	91
" "	Dipole moments of tri-substituted benzenes (L)	580
Rao, Y. B.	Structure of the spectrum of singly ionised bromine (L)	95
Rao, Y. B.	Structure of the spectrum of doubly ionised bromine (L)	371
Roy, D. and A. Saha, B. Banerjee, T. Das, S. Ghosh Roy, T. Ghose	A nuclear magnetic resonance apparatus	211
Roy, R. and J. K. D. Verma	Polarization of echoes from the ionosphere	36

Author	Subject	Page
Roy, S. B.	Ultraviolet absorption spectra of solutions of bromotoluene in isobutyl alcohol at different temperatures	590
Roy, S. B.	Ultraviolet absorption spectra of frozen solutions of <i>o</i> -, <i>m</i> - and <i>p</i> -chlorotoluene in isobutyl alcohol	276
Raut, H. K.	Variation of binding energies of neutrons and protons in heavy nuclei	611
Saha, A. K.	On the determination of electron density distribution in ionospheric regions from h-f records	464
Saha, A. and B. Banerjee, T. Das, D. Roy, S. Ghosh Roy, T. Ghose	A nuclear magnetic resonance apparatus	211
Saha, N. K. and L. Kasturi Rangan	Determination of absolute cross-section of (n p) reaction in S ³²	80
Sanyal, Lakshmi	The flow of a viscous liquid in a circular tube under pressure gradients varying exponentially with time	57
Santhamma, V.	The inverse kinetic energy matrix elements for the out-of-plane vibrations in furan, thiophene, cyclopentadiene and their substituted compounds	429
Sen, A. K.	L ₂₋₃ and K emission spectra of magnesium, aluminium and lithium in higher orders	415
Sen, S. N. and B. M. Bishui	On the fluorescence in diamond excited by X-rays	620
Sen, S. N. and S. C. Sirkar	On the nature of extra reflections in the Laue photographs of some diamonds of known relative fluorescence efficiencies	29
Sen, S. N. and G. S. R. Krishna Murti	On the crystal structure of para dichlorobenzene at different temperatures	242
Sen, S. K.	Ultraviolet absorption spectra of phenyl acetonitrile, phenyl acetate, phenyl salicylate and monomeric styrene in the liquid and solid states	321
Sen, S. K.	Ultraviolet absorption spectra of <i>o</i> -methoxyphenol and 2, 4, 6-trichlorophenol in different states	553

Author	Subject	Page
Sen Choudhury, P. K. and S. N. Sen Gupta	Cloud chamber analysis of cosmic ray showers under 10 to 23 cms of lead	453
Sen Gupta, P. K.	Origin of the zodiacal light and the variations of its brightness	285
Sengupta, S. N. and P. K. Sen Choudhury	Cloud chamber analysis of cosmic ray showers under 10 to 23 cms of lead	453
Sirkar, S. C. and S. N. Sen	On the nature of extra reflections in Laue photographs of some diamonds of known relative fluorescence efficiencies	29
Sodha, M. S. and K. C. Chaturvedi	Resolution of spectral lines of unequal intensity	491
" "	On dependence of resolving power on background intensity, stage of resolution and detecting instrument	543
" "	Effect of back ground intensity on resolving power of Lummer-Gehreke plate and transmission echelon	599
Somayajulu, G. R.	Boiling point and other physical properties of the halogens and halides (L)	258
Somayajulu G. R. and S. R. Palit	Boiling point and atomic size (L)	262
Sural, D. P. and D. Basu	Compton scattering of light by electron	265
Suryanarayana, V. and V. R. Rao	Analysis of the near ultraviolet absorption spectrum of ortho-chloroanisole	117
Talwar, S. P. and J. N. Tandon	On the radial pulsation of magnetic stars	561
Tandon, J. N.	Geomagnetic activity and solar M-regions for the current epoch of the sunspot minimum	153
Tandon, J. N. and S. P. Talwar	On the radial pulsation of magnetic stars	561
Tawde, N. R. and N. V. Gejji	Test of the workability of Lotmar's potential energy function	299
Tawde, N. R. and K. G. Parvatikar	Measurement of surface tension by unstable pendant drops	348
Varshni, Y. P. and K. Majumdar	Spectroscopic constants of molecules V. Similarities in the constants of different groups	303
Verma, J. K. D. and R. Roy	Polarization of the echoes from the ionosphere	36

SUBJECT INDEX

Subject	Author	Page
Antennas. Circular arc	S. Balaram Rao	390
Binding energies of neutrons and protons in heavy nuclei. Variation of the	H. K. Raut	611
Boiling point and other physical properties of the halogens and halides (L)	G. R. Somayajulu	258
Boiling point and atomic size (L)	G. R. Somayajulu and S. R. Palit	262
Cross-section of (n, p) reaction in S^{32} . Determination of absolute	N. K. Saha and L. Kasturi Rangan	80
Compton scattering of light by electron	D. Basu and D. P. Sural	265
Cosmic ray showers under 10 to 23 cms of lead. Cloud chamber analysis of	P. K. Sen Choudhury and S. N. Sengupta	453
Crystal structure of anthracene at different temperatures. The	G. S. R. Krishna Murti	537
Crystal structure of para-dichlorobenzene at different temperatures. On the	G. S. R. Krishna Murti and S. N. Sen	242
Deformation of a fixed-free bar under a compressive impact of short duration	S. K. Ghosh	485
Dielectric properties of 2, 4-dinitrofluorobenzene	D. V. G. L. Narasimha Rao	91
Dipole moments of tetra substituted benzenes. Part I. Calculation of	K. V. Gopal Krishna	206
Dipole moments of tri-substituted benzenes (L)	D. V. G. L. N. Rao	580
Electron density distribution in the ionospheric regions from h-f records. On the determination of	A. K. Saha	464
Emission spectra of magnesium, aluminium and lithium in higher orders. $L_{2,3}$ and K	A. K. Sen	415
Extra reflection in the Laue photographs of some diamonds of known relative fluorescence efficiencies. On the nature of	S. C. Sirkar and S. N. Sen	29
Flow of viscous liquid in a circular tube under pressure gradients varying exponentially with time. The	Lakshmi Sanyal	57

Subject	Author	Page
Geiger-Muller counter tubes at high temperatures. Analysis of spuriousness of	S. P. Puri and P. S. Gill	1
Geiger-Muller counter characteristics (Part I). The temperature dependence of	" "	62
" " " (Part II)	" "	70
Geomagnetic activity and solar M-regions for the current epoch of sunspots minimum	J. N. Tandon	153
Induction drag of a sphere moving in a conducting fluid in the presence of magnetic field. On the	K.P. Chopra	606
Inverse kinetic energy matrix elements for the out-of-plane vibrations in furan thiophenes, cyclopentadiene and their substituted compounds. The	V. Santhamma	429
Ionospheric prediction methods and probable sources of error	S. S. Boral	189
Lotmar's potential energy function. Test of the workability of	N. R. Tawde and N. V. Gejji	299
Limit of resolution on background intensity, detecting instrument and stage of resolution in X ray spectra. Dependence of	D. C. Purkayastha	250
Magnetic susceptibility of C_r^{+3} alums in the range 300° K. Studies on the	S. K. Datta Ray	169
Magnetic moments of nucleons	S. K. Kundu	450
Magnetic moments of the nucleons. On the anomalous	S. P. Mishra and B. B. Deo	16
Mass measurement in nuclear emulsion by multiple scattering and gap distribution	I. S. Mittra	363
Nuclear magnetic resonance apparatus. A	A. Saha, B. Banerjee, T. Das, D. Roy, S. Ghosh Roy, and T. Ghose	211
Organic phosphors for scintillation counters. Growing of	R. Bhattacharyya, U. Basu Roy and S. Chatterjee	585
Polarisation echoes from the ionosphere.	J. K. D. Verma and R. Ray	36
Polarisation in p.p. scattering.	C. C. Banerjee	292
Radial pulsation of magnetic stars. On the	S. P. Talwar and J. N. Tandon	561
Radio-active isotopes of gold. Radiation from two	V. R. Potnis	375

Subject	Author	Page
Rectification and crystal structure.	K. R. Dixit	10
Resolution of spectral lines of unequal intensity	K. C. Chaturvedi and M. S. Sodha	491
Resolving power on background intensity, stage of resolution and detecting instrument. On dependence of	K. C. Chaturvedi and M. S. Sodha	543
Resolving power of Lummer Gehrcke plate and transmission echelon. Effect of background intensity on	K. C. Chaturvedi and M. S. Sodha	599
Saturable reactors in magnetic amplifiers. Behaviour of	P. N. Das	129
Sommerfeld's fine structure formula from a second order equation without thomas correction	C. C. Banerjee	525
Specific heat of liquid hydrogen. Theory of (L)	S. C. Misra	625
 SPECTRA		
Absorption and fluorescence spectra of uranyl salts. (Part I) Uranyl acetate (absorption). Analysis of	V. Ramakrishna Rao and K. V. Narasimham	334
Absorption spectra of frozen solution of <i>o</i> -, <i>m</i> -, and <i>p</i> -chlorotoluene in isobutyl alcohol. Ultraviolet	S. B. Roy	276
Absorption spectra of phenyl acetone, phenyl acetate, phenyl salicylate and monomeric styrene in the liquid and solid states. Ultraviolet	S. K. Sen	321
Absorption spectra of phenol, <i>o</i> -bromophenol and diphenyl ether in different states. Ultraviolet	S. B. Banerjee	353
Absorption spectra of pyridene in the liquid and solid states. Ultraviolet	S. B. Banerjee	480
Absorption spectrum of meta-fluorochlorobenzene. The ultraviolet (L)	S. L. N. G. Krishnamachari	151
Absorption spectrum of para-fluorochlorobenzene. The ultraviolet (L)	S. L. N. G. Krishnamachari	319
Absorption spectra of <i>o</i> -, <i>m</i> -, <i>p</i> -fluorobromobenzene. The ultraviolet	"	487
Absorption spectra of <i>o</i> -methoxy phenol and 2, 4, 6-trichlorophenol. Ultraviolet	S. K. Sen	553

	Page
Absorption spectra of solutions of bromotoluene in isobutyl alcohol at different temperatures. Ultraviolet	S. B. Roy 590
Absorption spectra of α -methyl naphthalene and β -methyl naphthalene in the liquid and solid states. Ultraviolet	S. B. Banerjee 106
Absorption spectrum of ortho-chloro anisole. Analysis of the near ultraviolet	V. Suryanarayana and V. R. Rao 117
Fluorescence in diamonds excited by X-rays. On the	S. N. Sen and B. M. Bishui 620
Fluorescence of frozen para-chlorotoluene on the wave length of the exciting radiation. On the dependence of the intensity of	D. C. Biswas 255
Fluorescence spectra of methyl benzoate, <i>m</i> -chlorotoluene and <i>m</i> -bromotoluene	D. C. Biswas 565
Fluorescence of para-bromotoluene, ortho-chlorotoluene in the solid state at low temperature. On the	D. C. Biswas 407
Fluorescence of para-chlorotoluene in the solid state at low temperature. On the	D. C. Biswas 143
Raman Spectra of 1,1- dichloroethane and 1, 1, 1- trichloroethane in the vapour state. On the	M. M. Mazumder 384
Raman spectra of pyridine and its solution in ethyl alcohol at different temperatures.	G. S. Kastha 519
Raman Spectra of three mono-substituted benzene in the solid state at low temperatures.	D. C. Biswas 530
Raman spectra of frozen solution of toluene and benzene in aliphatic solvents.	G. S. Kastha 313
Spectrum of the singly ionised bromine. Structure of the (L)	Y. B. Rao 95
Spectrum of doubly ionised bromine. Structure of the (L)	Y. B. Rao 371
Spectroscopic constants of molecules. V. Similarities of constants of different groups	Y. P. Varshni and K. Majumdar 303

	Page
Spherical symmetry method for measurement of thermal neutron absorption.	A. M. Ghosh and N. K. Ganguli 500
Theory of	
Surface tension by unstable pendant drops. Measurement of	N. R. Tawde and K. G. Parvatikar 348
Surface tension-temperature relation from free-volume concept	S. S. Mitra 423
Thermoluminescence spectra. On the	B. C. Dutta and A. K. Ghosh 570
Time of flight neutron velocity selector using scintillation counter. A	A. P. Patro 99
Wave nature of matter. On the	B. Mishra 273
Zodiacal light and the variation of its brightness. Origin of	P. K. Sen Gupta 285
 BOOK REVIEWS	
Beta and Gamma Ray Spectroscopy	Kai Siegbahn 47
Light Calculations and Measurements	H. A. E. Keitz 97
Paramagnetic Nuclear Resonance	P. Grivet 489
 OBITUARY	
Professor Meghnad Saha, F. R. S.	51

ANALYSIS OF SPURIOUSNESS OF GEIGER-MULLER TUBES AT HIGH TEMPERATURES

SATYA PAL PURI AND P. S. GILL

DEPARTMENT OF PHYSICS, MUSLIM UNIVERSITY, ALIGARH.

(Received for publication, October 19, 1955)

ABSTRACT. The present communication is a sequel to the earlier report by the authors regarding the temperature-dependence of spurious discharges in G-M counters. A quantitative confirmation of the conclusions arrived at therein, is obtained by studying the time-distribution of pulses at higher temperatures by the method of delayed coincidence. The results of the present investigation indicate that :

- (i) The dead and transit times remain constant with temperature.
- (ii) The coefficient of secondary emission remains constant in the case of internal counters, whereas there is an exponential increase in its value in the case of Mazo type of counter.
- (iii) The high counting rate decays with the time of heating and the curve is analogous to that of the desorption of the quenching vapour.

These observations are discussed in light of possible mechanisms and it is inferred that desorption of the vapour at high temperatures is the cause of temperature effect. The mechanism of emission of the adsorbed vapour is not clear.

INTRODUCTION

Puri and Gill (1956) studied the temperature-dependence of spurious discharges in G-M. counters, and reported that there is a large increase in the counting rate at higher temperatures and decrease in overall width of the plateau characteristic. It was shown that the increase is only in frequency and not in multiplicity of pulses as the temperature is raised. The tentative explanation was given on the basis of the desorption of the quenching vapour at higher temperatures.

In view of the fact that the delay of occurrence of a spurious pulse from a genuine one is dependent on the mechanism of its production, it was considered necessary to study the time-distribution of pulses at high temperatures. The present study of time correlation between ionising events will indicate whether any time correlation exists between the pulses or that these are randomly distributed. Also to see whether the temperature has any effect on dead and transit times.

EXPERIMENTAL SET-UP

Three counters, all of the self-quenching type with different quenching vapours, were employed in the present investigation. The constructional details

of the counters are given in the accompanying paper (Part I, Puri and Gill, 1956). The counters could be enclosed in a brass cylinder and placed in a thermostatically controlled tank, which could be easily raised to any temperature and kept there by employing a thermoregulator.

The time interval analyzer, (Puri and Gill, 1956) was made use of for studying the time-distribution of pulses. A radioactive source was employed as the source of radiation.

OBSERVATIONS

The time-distribution was studied at different temperatures, keeping the overvoltage the same in all the cases with each type of counter. The counting rate decayed to the background rate with time of heating at the same temperature, so the study of time-distribution was resorted to only after the counting rate had become almost constant.

One of the curves was obtained at the temperature where no spuriousness had set in, which served as a reference for the rest of the curves for the same counter.

Figure 1 gives the delayed coincidence rate *vs* delay time at temperatures of 62°C, 100°C, and 128°C respectively for the internal petroleum ether-filled counter. The dead and transit times for this counter remain constant at all temperatures studied. Differences in the background coincidence rate is due to the fact

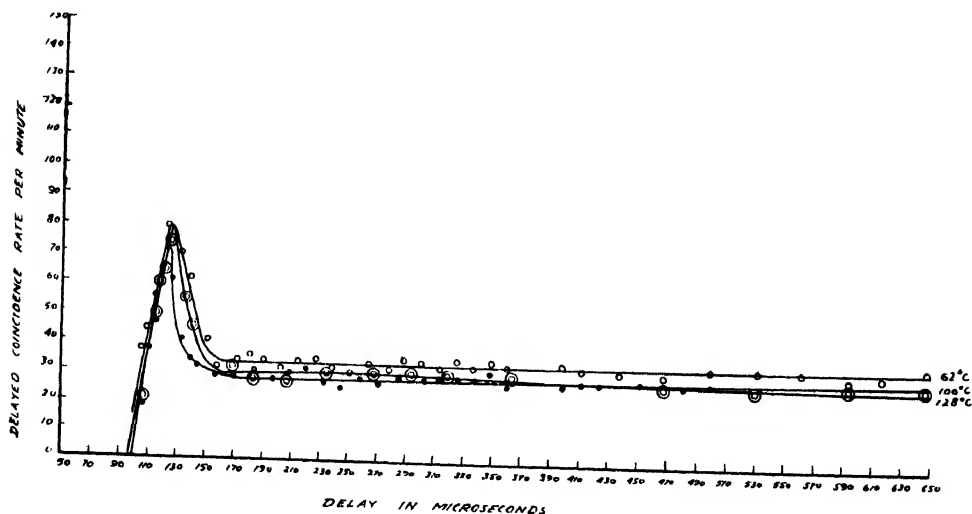


Fig. 1. Delayed coincidence rate versus delay time for internal petroleum ether-filled counter.

that any slight change in the position of the source would change the value of r_c .

The values of the coefficient of secondary emission, as calculated from figure 1 are tabulated in Table I, making use of the formula (Puri and Gill, 1956)

$$\frac{A_1}{r_c} = \frac{K}{n_1 \{1 - K - K^2 + K^3\}}$$

where K is the probability that a discharge creates an after discharge ; in this case it pertains to the cathodic emission only, so it is the coefficient of secondary emission,

A_1 is the area of the 1st peak superimposing the background.

r_c is the rate of background coincidences.

n_1 is the rate of counting from the direct channel. This is observed from the output of shaping circuit in the direct channel.

TABLE I

Counter No.	Temperature	K	Dead time in microseconds	Transit time in microseconds
1	62°C	.2632	95	126
	100°C	.2169	95	126
	128°C	.2391	95	126
2	41°C	.2909	72	120
	73.5°C	.3300	72	120
3	60°C	.1262	122	158
	94°C	.1977	122	158
	124°C	.2622	122	158

Figure 2 gives the time-distribution for the internal butane-filled counter at 41°C and 73.5°C respectively, whereas Table I gives the dead and transit times and the coefficient of secondary emission for counter No. 2, as calculated from figure 2.

Figure 3 gives the plateau characteristics for the butane-filled counter at 93.5°C at different hours of heating keeping the temperature the same. There is a progressive downward shifting of the plateau, whereas the slope substantially remains the same throughout.

Figure 4 gives the decay of counting rate *vs* time after the rise in temperature was stopped and the counter kept at that constant temperature of 93.5°C. This curve can be obtained from the curves of figure 3.

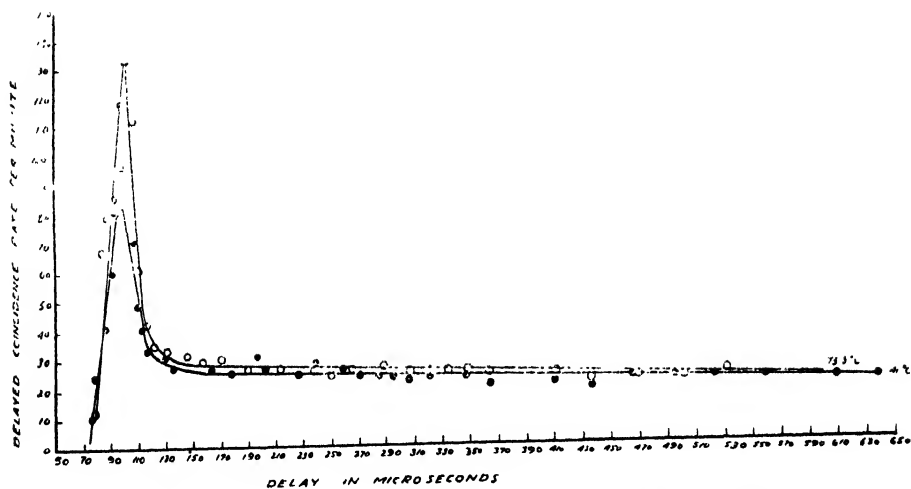


Fig. 2. Delayed coincidence rate versus delay time for internal butane-filled counter.

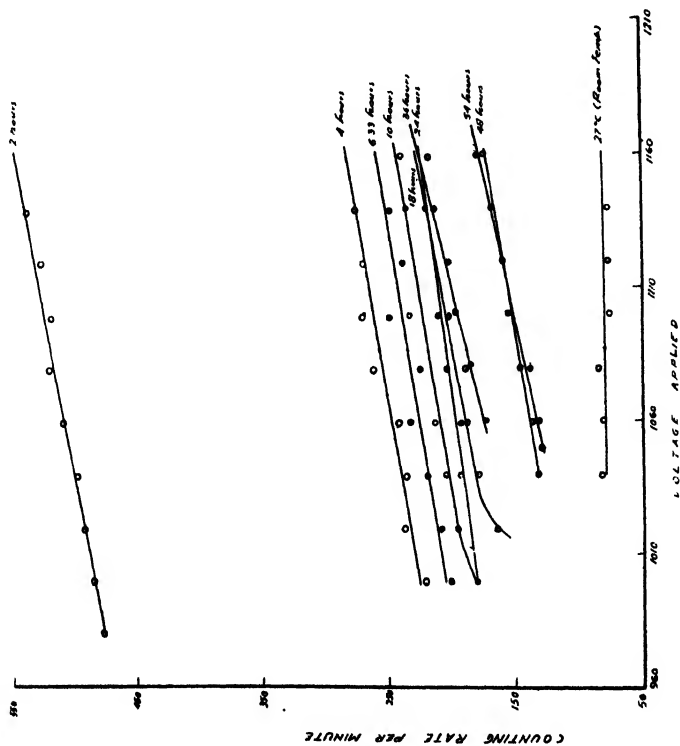


Fig. 3. Plateau characteristics at 93.5°C, but after different hours of heating for butane-filled counter.

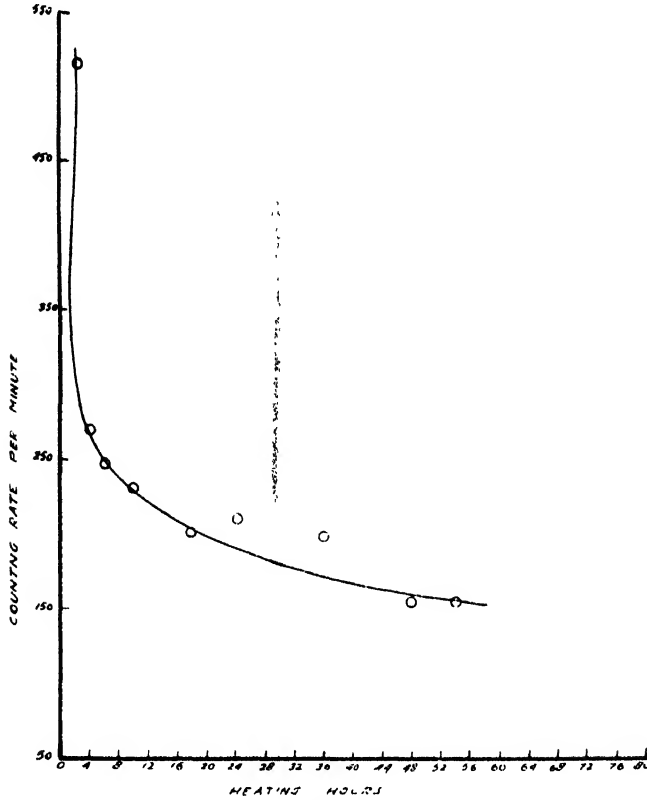


Fig. 4. Decay of counting rate versus heating hours after the rise in temperature was stopped and the counter kept at that constant temperature of $93^{\circ}\text{C} \pm 1^{\circ}\text{C}$.

Figure 5 gives the delayed coincidence rate *vs* delay time at temperatures of 60° , 94° and 124°C respectively for counter No. 3. Figure 6 gives the decay of

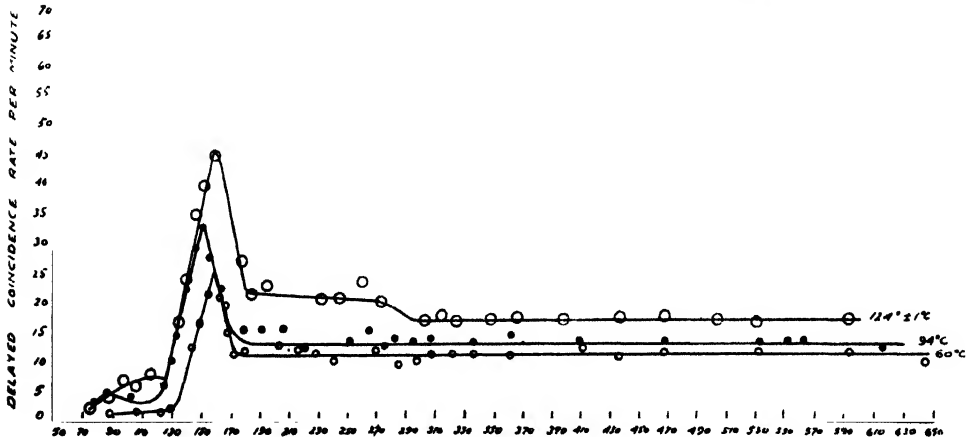


Fig. 5. Delayed coincidence rate versus delay time for external alcohol-filled counter.

counting rate *vs* time when the external counter is kept at the constant temperature of 124°C . Here again the dead time and the transit time remain constant at all temperatures. Figure 7 gives the plot of the coefficient of secondary emission against temperature.

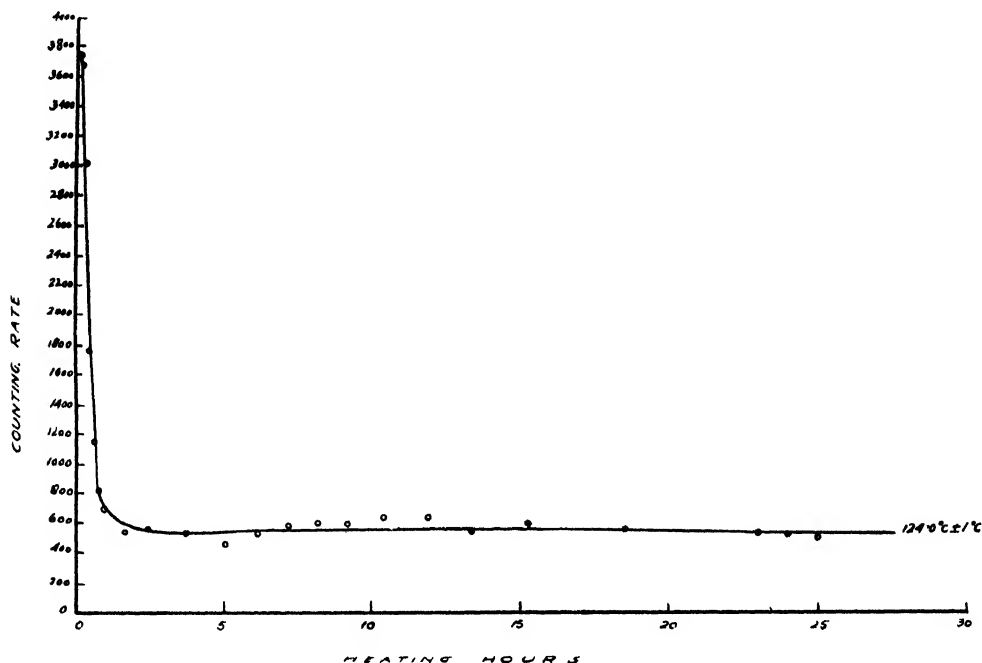


Fig. 6. Decay of counting rate versus heating time for external counter.

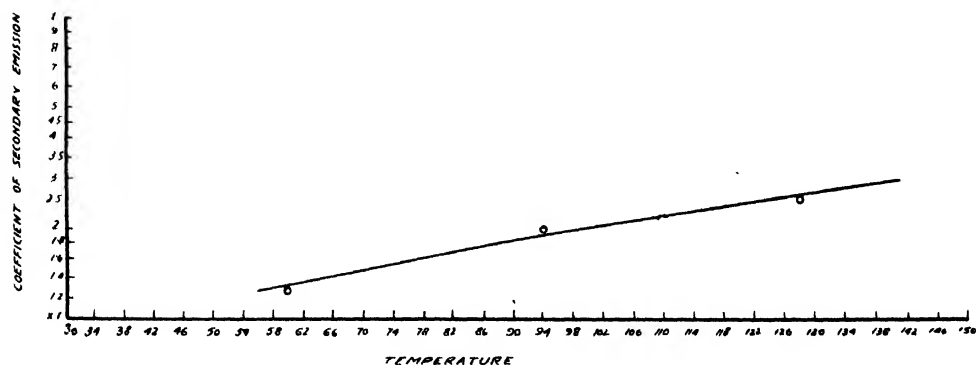


Fig. 7. Coefficient of secondary emission versus temperature of counter for external alcohol-filled counter.

The data mentioned above can be summarized as follows:

1. The dead and transit times as shown in Table I remain constant as the temperature is increased in all the three cases.
2. The values of the coefficient of secondary emission remain constant in the case of internal counters, whereas there is an exponential increase in its value with temperature for the external counter (figure 7).
3. In all the three cases, no peaks additional to that at the room temperature are observed, —figures 1, 2 & 5.
4. The curves showing the decay of counting rate vs time of heating when the counter is kept at the same high temperature, are somewhat similar to those of the desorption of the adsorbed vapour on the cylinder and glass surfaces.
5. There seems to be no permanent effect of heating on the counting rate of the counter, but for the fact that the threshold does not regain its original value.

DISCUSSION

Puri and Gill (1955) suggested possible mechanisms, which could explain the temperature-dependence of G-M. counters. In the light of these mechanisms the observations of the present paper are discussed.

Parkash (1950) offered the suggestion that secondary emission, caused by the impact of positive ions of mercury on the cathode was responsible for the high counting rate at high temperatures, while Joshi (1953) ascribed it to the formation of the long lived metastables 2^3P_0 states of mercury atoms with a longer life. If such were the case the dead and transit times would show an increase with temperature due to the fact that the mobilities of the Hg ions are less compared to that of alcohol. But the results of this investigation show that dead and transit times remain constant with temperature.

Hereford (1950) obtained shorter recovery times at higher temperatures in the case of parallel plate counter. His explanation was based on the negative temperature coefficient of higher resistivity ($\sim 10^{14}$ ohms -cm) of Si O_2 particles on the cathode, which might be released on baking the counter at 425°C . as well as the presence of minute droplets in the gas mixture. The constant values of the dead and transit times observed for all three counters show that in the case of G-M. tubes Hereford's interpretation does not play any part.

Parkash and Kapur (1950) explained the high counting rates at higher temperatures due to increased secondary emission, because the average energy and the number of positive ions is greater at higher temperature. As shown by Puri and Gill (1955), the increase in average energy is

$$\frac{(3n-6)}{2} kT \text{ where } n \text{ is the atomicity of the molecule, } \sim .385 \text{ e.v.}$$

which is negligible as compared to 200 e.v., the energy due to the intense field.

Moreover the constancy of the value of K does not lend any support to their suggestion.

The reduction of CuO to Cu and the oxidation of alcohol to acetic acid, was cited by Parkash (1950) as a possible mechanism at higher temperatures. The process of reduction of copper oxide will reduce the work function and consequently will increase the probability of a discharge creating an after discharge. The constancy of K in the case of internal counters would rule out this suggestion.

The absence of any extra peak, additional to that at the room temperature, indicates that the increase in the number of counts is not influenced by any external agency. Moreover, there is no interaction between the impinging molecules and those adsorbed on the cathode, as neither any peak is obtained at twice the transit time nor any increase in the value of K is observed. There seems to be no emission of electrons or negative ions, as a result of the energy freed during elementary exothermic reaction between the impinging molecules and those adsorbed on the cathode as put forward by Seidl and Roubinek (1952).

It is observed that in the case of external counter the coefficient of secondary emission increases exponentially. As this counter was not baked for a sufficiently long period, there may be a release of adsorbed oxygen molecules. Due to the presence of oxygen at higher temperatures, attachment of the electron formed in the initial ionizing event can cause a mean time-lag of as much as the transit time between the passage of the ionizing particle and initiation of the discharge; for the mobility of a negative ion is roughly the same as that of the positive ion. Lennard-Jones and Devonshire (1936) analysed that for a given desorption process

the rate of evaporation of particles per unit area is proportional to $A\theta e^{-\frac{\chi}{kT}}$ where χ is the energy of desorption per molecule from the lowest state and A is a constant. Thus the amount of oxygen desorbed will increase exponentially with temperature, consequently the value of K .

The feeble inclination of the time-distribution curve in case of external counter may be due to the following phenomenon. Ordinarily the impulses of the counter, which come just after dead-time, present in general an amplitude too feeble to be detected by the input amplifier. Exceptionally the amplitude of such an impulse can surpass the threshold of sensibility, which can take place when the first of the two impulses comes during a period lying between dead-time and time of recovery of the impulse which precedes it. Since such a pulse will be accompanied by a lesser space charge and thus will have lesser dead-time, consequently we get a coincidence for delay less than the dead-time. But such an effect remains feeble.

The curves of Figs. 4 and 6, showing decay of counting rate with time after the counter is raised to given higher temperature and kept there, resemble the desorption of the vapour at high temperatures. The abrupt fall in the beginning

is due to the desorption of the vapour that is held by Van der Waals forces, whereas the almost constant part is due to the desorption of the vapour held by chemisorption. The adsorbed vapour may be given out in the form of negative ions but the mechanism of emission is not clear at present. Some further work is required to understand such an emission process.

ACKNOWLEDGMENTS

One of the authors (S.P.P.) acknowledges very gratefully the help of Union Education Ministry for the grant of a Senior Research Scholarship.

REFERENCES

- Hereford, Frank, L., 1950, *Phys. Rev.*, **77**, 559.
Joshi, C. P., 1953, *Ind. J. Phys.*, **36**, **8**, 48.
Lennard Jones, J. E., and Devonshire, A. F., 1936, *Proc. Roy. Soc. A.*, **156**, 6.
Parkash, Om, 1950, *Phys. Rev.*, **80**, 303.
„ and Kapur, P. L., 1950, *Proc. Phys. Soc.*, **63A**, 453.
„ 1950, *Curr. Sci.*, **9**, 273.
Puri, S. P. and Gill, P. S., 1955, *Ind. J. Phys.*, **29**, 95.
„ „ „ *Ind. J. Phys.* (under publication), 1956
Seidl, R. and Roubinek, F., 1952, *Czech. J. Phys.*, **1**, No. 3-4, 207.

RECTIFICATION AND CRYSTAL STRUCTURE*

K. R. DIXIT

GUJARAT COLLEGE, AHMEDABAD.

(Received for publication, December 21, 1955)

ABSTRACT. The work done by Welker on alloy rectifiers, by Hoffmann and Rose and Strosche on the structure of selenium barrier layer, and by the author and his colleagues on the structure of cuprous oxide rectifiers is critically examined. This leads us to expect that a structure like diamond is necessary for an efficient rectifier.

INTRODUCTION

The first rectifiers were all crystals with a metallic point contact. The crystals used were either cubic or those which represent a close packed lattice. This fact naturally led one to expect that the rectification might have something to do with the crystal structure. The discovery of the barrier layer rectifiers, like cuprous oxide or selenium, appeared to question the validity of this view. This happened because the selenium metal has either a spiral chain or a closed ring structure with two neighbours only —i.e. a structure which is neither cubic nor close packed, —and the nature of the crystal structure of the cuprous oxide rectifier was not fully known. Here we shall examine some recent work of Welker (1952, 1953, 1954) on alloy rectifiers, work of Hoffmann and Rose (1953) and of Strosche (1955) on the structure of selenium barrier layer, the work done by us (1941, 1955) on the structure of cuprous oxide rectifiers and some theoretical work specially that of Krebs and Schottky (1954). This leads us to expect that a face-centred cubic structure, like diamond or zincblende, is a necessary condition for an efficient rectifier.

WELKER'S WORK ON ALLOY RECTIFIERS

Welker started with the idea that the most efficient rectifiers (excluding selenium) are diamond, silicon, germanium and grey tin. All these have the face-centred interpenetrating cubic lattice of diamond, in which every atom is surrounded by four neighbours which lie at the corners of a regular tetrahedron. These elements belong to the IVth group of the periodic table. Welker prepared compounds (alloys or mixtures), by melting together the elements Al, Ga or In

* Presidential address read before the annual meeting of the Indian Physical Society Agra, January, 1956.

from the IIIrd group and P, As or Sb from the Vth group. This gave nine compounds of the intermetallic type. All these, having a structure similar to the diamond or zincblende lattice, are compounds of lighter elements and show pronounced semi-conducting properties. Whereas a compound like TlBi, also composed of elements from the IIIrd and Vth groups, but the elements of which are heavier, shows a pronounced metallic character. Some properties of these compounds are better than those of the elements of the IVth group, e.g. the electron mobility of InSb is 25,000 cm²/volt sec. Welker also tried to investigate other compounds of elements from the IInd and the VIth groups and from the Ist and the VIIth groups. In the case of such compounds the binding is more ionic and they act like insulators.

GENERALISATION

If we generalise from Welker's experiments and ideas, we come to the conclusion that an ideal semi-conductor rectifier should have,

(a) a close packed structure like diamond or zincblende so as to reduce the thermal oscillations and increase the electron mobility,

(b) the intensity of the ionic bond as low as possible so as to reduce the width of the forbidden electron band,

(c) the goal mentioned in (b) attained by the introduction of a homopolar character, because this would also give a low effective value for the mass of the conductivity electron.

STRUCTURE OF SELENIUM RECTIFIERS

The usual selenium rectifiers are formed on plates which are alloys of cadmium. The rectifying layer is formed either thermally by heating under pressure or electrically by allowing about 10 times the normal current to flow in the wrong direction (Sperrichtung). X-ray diffraction pictures show that this active layer consists of cadmium selenide, and that the rectifier characteristics change with the thickness of this layer. Cadmium selenide is known to have two modifications, which are isomorphous with zincblende (cubic) or wurtzite (hexagonal). Previous workers, (Yamaguchi and Katayama, 1950, Pickar and Morris, 1951) could not say definitely whether the structure was of the zincblende or the wurtzite type. This was essentially due to the presence of small crystallites which gave rather diffuse rings. Recent examination of the cadmium selenide layer by Hoffmann and Rose (1953) by X-rays and electrons shows that the cadmium selenide is of the zincblende type and that no wurtzite lines are seen. Strosche (1955) also finds that the films prepared by vacuum evaporation and examined by X-rays show the existence of cadmium selenide of the zincblende type. The rings are rather broad and correspond to a crystal size smaller than 10⁻⁵ cm. Thus this most recent work on selenium appears to justify our generalisation.

STRUCTURE OF CUPROUS OXIDE

Layers of cuprous oxide were formed under different conditions of pressures temperatures and processing (i.e. heat treatment by slow cooling after the layer is formed). All these layers were examined by electron reflection (Dixit, 1941, 1955).

Cuprous oxide has a cubic structure in which the oxygen atoms lie on a body-centred cube, while the copper atoms lie on a face-centred cube. The two lattices interpenetrate to a distance of $1/4$. When cuprous oxide is formed at atmospheric pressure, in the beginning when the layer is very thin, we can see only the face-centred rings $\sqrt{3}$, $\sqrt{4}$, $\sqrt{8}$, $\sqrt{11}$, $\sqrt{12}$; but as the thickness increases we also begin to see the body-centred rings $\sqrt{2}$, $\sqrt{6}$, and $\sqrt{18}$. This is due to the difference in the scattering power of Cu and O. But when Cu_2O is formed at low pressures (1 to 10 mm of Hg in the range 1000°C to 600°C) for an interval of time which is a few minutes, we see prominently the rather broad rings corresponding to $\sqrt{3}$, $\sqrt{12}$, $\sqrt{27}$, and $\sqrt{48}$. (This is true for the bulk of oxide forming the barrier layer. The outermost layer at the surface, about 1000 \AA thick, shows definite (111) orientation and recrystallisation). There are two other rings also present but they are very faint and rather broad. At this stage the cuprous oxide is able to show a small rectification. The rectification is considerably increased and the low resistance becomes favourable by the subsequent heat treatment. At this stage we see only the four broad rings $\sqrt{3}$, $\sqrt{12}$, $\sqrt{27}$, $\sqrt{48}$. These rings are really arcs, about 30° wide, visible at the centre, indicating that a large number of crystallites of Cu_2O are so oriented that the (111)face is parallel to the substrate.

The cuprous oxide rectifier is known to contain excess of oxygen but the amount of oxygen present is less than that (Dubar, 1932) given by the formula $\text{Cu}_2\text{O} + 1.5/100 \text{ CuO}$. Perakis and Serres (1955) have suggested, for the semiconductor, the formula $\text{Cu}_{11} \text{ Cu}^+ \text{ O}_6$, where Cu^+ represents the vacancy of Cu^+ ion.

The general picture of the formation of the Cu_2O barrier layer is as follows: At low pressures at which the layers are prepared small crystallites of Cu_2O are formed on the surface of the block. By exposing these crystals to oxygen at low pressures, it is possible to have a few oxygen atoms diffusing in these crystallites, forming a solid solution. During the process of slow cooling most of the excess oxygen is ejected out retaining a few oxygen atoms, as required by the formulae.

Let us assume that the structure now becomes the same as that of the zinc-blende lattice and that in addition a homopolar character is introduced in the bond. Consider a cube side 4.26 \AA , the length of a Cu_2O cell, and assume that the copper atoms are situated at the corners and the centres of the six faces of this cube. Divide this cube into eight smaller cubes, with lower cubes 1, 2, 3, 4 and the upper 5,6,7,8. In the normal Cu_2O crystal the oxygen atoms would be

at the centres of cubes 1 and 7 and they would share electrons from the copper atoms associated with these cubes. Suppose now that a homopolar character is developed in this structure. Then we could expect, that the oxygen atom which was in cube 1 and which was sharing electrons from copper atoms associated only with cube 1, can now share at different successive times electrons associated with all the copper atoms in the nearest cubes 1, 2, 4 and 5. Similarly the oxygen atom which was in cube 7 can now share at different successive times electrons associated with copper atoms in its nearest neighbour cubes 3, 6, 7 and 8. The sharing of these electrons is really equivalent to the oxygen atom 1 occupying successively positions at the centres of cubes 1, 2, 4 and 5 and oxygen atom 7 occupying positions at the centres of cubes 3, 6, 7 and 8. Such a distributed attachment is characteristic of the homopolar bond and the particular distribution suggested above between the nearest neighbours corresponds to what should be expected from the zincblende lattice. The formation of this kind of structure is probably helped by the dissolved oxygen which is slowly removed during the process of cooling and yet permitting some excess oxygen to stay behind. In this process we visualise a copper atom getting used to more than its normal share of oxygen, but this being no longer permanently available is made available on a time average basis.

The result of this kind of combination will be to reinforce the rings 111, 222, 333 and 444 and almost cancel all others. Further 222 and 444 will be stronger than they normally would be. This is exactly what we observe. The breadth of the rings observed suggests that the crystal size is small but this is not unexpected in the light of work done on cadmium selenide. Thus our work on cuprous oxide rectifiers also appears to support the generalisation we have made. As a matter of fact, the generalisation has enabled us to interpret the results we had already obtained.

DISCUSSION AND CONCLUSION

Let us now turn to the theoretical aspect of the problem. In the theoretical investigation of semi-conductor rectifiers we must consider the following:

- (a) The width of the forbidden electron band.
- (b) The mobility of the electrons or holes.
- (c) The mechanism which produces asymmetry.

Let us consider these points in that order.

The width of the forbidden electron band depends on the binding energy of the atoms concerned. In general, an ionic binding is stronger than a homopolar or covalent binding and an ionic binding indicates a broader forbidden electron band. The widths of the forbidden bands are 6 to 7 volts for diamond, 1.1 volt for Si and 0.7 volt for Ge. For a good rectifier, with an appreciable current carrying capacity, it is necessary that the width of the forbidden electron band should

be small. That is why Si and Ge are widely used. But we could also choose an ionic binding and reduce the width of the forbidden band. This could happen if a part of the ionic character of the bond is replaced by a homopolar or covalent character. Such a partial replacement gives rise to a quantum mechanical resonance between the homopolar and the heteropolar components, and an exact calculation of the resonance will enable us to predict the semi-conductor rectifier properties of the compounds.

Now let us turn to the second question of the mobility of the electrons or the holes. In this connection we have to consider the effective mass of the conductivity electrons and the thermal oscillations of the material through which they have to move. The effective mass of the conductivity electrons can be obtained from the energy spectrum by a differentiating process and we find that the homopolar binding is able to give a low effective value to the mass of the conductivity electron. Thus even here the homopolar character appears to be favourable. The thermal oscillations are least in a lattice which represents most closely packed atoms. The best lattice of this type, from the point of view of a good rectifier, is the diamond or the zincblende lattice. This type of lattice in addition to being a most closely packed lattice also happens to favour homopolar binding. This peculiar crystal structure, therefore, could be expected to help in the formation of a good rectifier.

Turning to the third aspect, we observed that Mott (1946) and Schottky (1939 and 1942) explain the asymmetry as due to the presence of a barrier layer; a chemical layer or a physical layer respectively. In the barrier layer with a diamond like structure every atom has four neighbours at the corners of a tetrahedron. They are bound by exchange forces between the electrons, in the quantum state of a (sp^3) hybrid. The binding electron pair is practically localised in the space between two neighbours, so that every (sp^3) eigenfunction becomes one-sided and situated near the neighbour. In the case of ionic crystals like ZnS, zincblende, the p -electron system is comparable with the π -electron system in organic compounds. In such a case the eigenvalues of the p -electrons can have large values in two directions separated by 180° , thus producing a spin-like coupling. Such a coupling gives rise to a resonance and a sort of directed homopolar bond. This may be regarded as a probable cause of asymmetry in the physical or chemical barrier layer.

Thus our investigations lead us to expect that a very close-packed structure like diamond or zincblende, which is favourable for the formation of a superimposed homopolar bond, is very helpful in the formation of a good rectifier.

REFERENCES

- Dixit, K. R., 1941. *Proc. Ind. Acad. Sci.*, **13**, 498.
Dixit, K. R. and Agashe, V. V., 1955. *Z. Naturforschg.*, **10a.**, 152.
Dubar, L., 1952. *C.R.*, **194**, 1332.

- Hoffman, A. and Rose, F., 1953. *Z. Phys.*, **136**, 152.
- Krebs, H., 1953. *Naturwissen.*, **40**, 525.
- „ 1953. *Z. angew. Chem.*, **65**, 293.
- „ 1954. *Physica.*, **20**, 1125.
- Krebs, H. and Schottky, W., 1954. 'Halbleiterprobleme' Vieweg.
- Mott, N. F. and Gurney, R. W., 1946. 'Electronic processes in ionic crystals', Oxford.
- Perakis, N. and Serres, A., 1955. *J. Physique Rad.*, **16**, 387.
- Pickar, P. B. and Morris, L. W., 1951. *Phys. Rev.*, **83**, 488.
- Schottky, W., 1939. *Z. Phys.*, **113**, 367.
- „ 1942. *Z. Phys.*, **118**, 359.
- Strosche, H., 1955. *Z. Phys.*, **140**, 409.
- Welker, H., 1952. *Z. Naturforschg.* **7a**, 744.
- „ 1953. *Z. Naturforschg.* **8a**, 248.
- „ 1954. *Physica.*, **20**, 893.
- Yamaguchi, J. and Katayama, S., 1950. *J. Phys. Soc. Japan.*, **5**, 386.

ON THE ANOMALOUS MAGNETIC MOMENTS OF THE NUCLEONS

S. P. MISRA

MATHEMATICS DEPARTMENT, RAVENSHAW COLLEGE, CUTTACK

AND

B. B. DEO

PHYSICAL LABORATORY, RAVENSHAW COLLEGE, CUTTACK

(Received for publication, October 19, 1955).

ABSTRACT. We have here calculated the anomalous magnetic moments of the nucleons with the help of a fourth order meson equation given by Bhabha and Thirring. The electromagnetic current density of this meson field has been evaluated for our purpose. The results are in much better agreement with the experiments than what we get in conventional meson theories.

1. INTRODUCTION

Several attempts have been made to get a correct value of the anomalous magnetic moments of the nucleons making use of conventional meson theories (Case, 1949 ; Slotnick and Heitler, 1949 ; Borowitz and Kohn 1949 ; Goto, 1954) ; Except for partial qualitative success, the disagreements of the results obtained by them with the experiments are too conspicuous. Even the ratio of the anomalous neutron and proton moments is almost eight times the experimental value, although this ratio is independent of the rather uncertain coupling constants. The treatment of Sachs (1952) with the help of a definite model is more or less made to agree with experiments; but the arbitrariness of this model is an essential defect of this approach. Such failures suggest that an altogether different meson theory may help us in this direction. We have here chosen a fourth order meson equation given by Bhabha (1950) and Thirring (1950) for the consideration of the same problem. It is seen here that for our calculations no infinite renormalisation is necessary and that the values thus obtained agree with the experiments to a much greater extent.

2. FIELD EQUATIONS AND MESON CURRENT DENSITIES

The fourth order meson field equation is

$$(\square^2 - \kappa^2)^2 \phi_i = 0 \quad \dots (1)$$

The invariant lagrangian density $L(x)$ which, with the general field equation

$$\frac{\partial L}{\partial \phi_i} - \frac{\partial}{\partial x_\mu} \frac{\partial L}{\partial \frac{\partial \phi_i}{\partial x_\mu}} + \frac{\partial^2}{\partial x_\mu \partial x_\nu} \frac{\partial L}{\partial \frac{\partial^2 \phi_i}{\partial x_\mu \partial x_\nu}} = 0 \quad \dots (2)$$

gives us the field equation (1) which can be written as

$$L = - \left(-\frac{1}{2\kappa^2} \frac{\partial^2 \phi_i}{\partial x_\mu} \frac{\partial^2 \phi_i^*}{\partial x_\mu} + \frac{\partial \phi_i}{\partial x_\mu} \frac{\partial \phi_i^*}{\partial x_\mu} - \frac{1}{2} \kappa^2 \phi_i \phi_i^* \right) \quad \dots (3)$$

Here we have adopted the summation convention for repeated indices, and

$$x = (\vec{x}, ct) \text{ and } x_\mu x_\mu = x^2 - c^2 t^2.$$

For our purpose it is necessary to deduce a current density for the above field. The lagrangian here contains the second order derivatives of the field operators. But proceeding according to Wentzel (1949), the gauge invariance of the first kind enables us to write the current density s_μ as

$$= -ie \left\{ \frac{\partial L}{\partial \frac{\partial \phi_i}{\partial x_\mu}} \phi_i - \frac{\partial L}{\partial x_\nu} \frac{\partial}{\partial \frac{\partial^2 \phi_i}{\partial x_\mu \partial x_\nu}} \phi_i + \frac{\partial L}{\partial \frac{\partial^2 \phi_i}{\partial x_\mu \partial x_\nu}} \frac{\partial \phi_i}{\partial x_\nu} \right. \\ \left. - \text{the complex conjugate expression} \right\} \quad (4)$$

where e is a constant related to the charge. A direct evaluation of $\frac{\partial s_\mu}{\partial x_\mu}$ with the subsequent application of the field equations(2) gives us

$$\frac{\partial s_\mu}{\partial x_\mu} = -ie \left\{ \frac{\partial L}{\partial \phi_i} \phi_i + \frac{\partial L}{\partial \frac{\partial \phi_i}{\partial x_\mu}} \frac{\partial \phi_i}{\partial x_\mu} + \frac{\partial L}{\partial \frac{\partial^2 \phi_i}{\partial x_\mu \partial x_\nu}} \frac{\partial^2 \phi_i}{\partial x_\mu \partial x_\nu} - c.c. \right\}$$

But the above quantity is the coefficient of α under an infinitesimal gauge transformation $\phi_i \rightarrow \phi_i \exp(i\alpha)$, $\phi_i^* \rightarrow \phi_i^* \exp(-i\alpha)$ and thus must vanish. This was at the basis of the choice of the current density (4). Thus for (3) we obtain

$$s_\mu = ie \left\{ \left(\frac{\partial \phi_i^*}{\partial x_\mu} \phi_i - \frac{\partial \phi_i}{\partial x_\mu} \phi_i^* \right) - \frac{1}{2\kappa^2} \left(\frac{\partial \square^2 \phi_i^*}{\partial x_\mu} \phi_i - \frac{\partial \square^2 \phi_i}{\partial x_\mu} \phi_i^* \right) \right. \\ \left. + \frac{1}{2\kappa^2} \left(\square^2 \phi_i^* \frac{\partial \phi_i}{\partial x_\mu} - \square^2 \phi_i \frac{\partial \phi_i^*}{\partial x_\mu} \right) \right\} \quad (5)$$

However, when there is an external electromagnetic field with the four vector potential A_μ , then the lagrangian density (3) must be changed to

$$L(x) = - \left\{ -\frac{1}{2\kappa^2} \left(\frac{\partial}{\partial x_\mu} - \frac{ie}{\hbar c} A_\mu \right)^2 \phi_i \left(\frac{\partial}{\partial x_\mu} + \frac{ie}{\hbar c} A_\mu \right)^2 \phi_i^* \right. \\ \left. + \left(\frac{\partial}{\partial x_\mu} - \frac{ie}{\hbar c} A_\mu \right) \phi_i \left(\frac{\partial}{\partial x_\mu} + \frac{ie}{\hbar c} A_\mu \right) \phi_i^* - \frac{1}{2} \kappa^2 \phi_i \phi_i^* \right\} \quad \dots (6)$$

and equation (1) is to be changed similarly.

Thus by (4) the current density s_μ becomes

$$s_\mu = \frac{ie}{\hbar c} \left\{ \left(\frac{\partial \phi_i^*}{\partial x_\mu} \phi_i - \frac{\partial \phi_i}{\partial x_\mu} \phi_i^* \right) - \frac{1}{2\kappa^2} \left(\frac{\partial \square^2 \phi_i^*}{\partial x_\mu} \phi_i - \frac{\partial \square^2 \phi_i}{\partial x_\mu} \phi_i^* - \square^2 \phi_i^* \frac{\partial \phi_i}{\partial x_\mu} + \square^2 \phi_i \frac{\partial \phi_i^*}{\partial x_\mu} \right) \right\} - \frac{2e^2}{(\hbar c)^2} A_\mu \left\{ \phi_i^* \phi_i + \frac{1}{2} \left(\square^2 \phi_i^* \phi_i + \square^2 \phi_i \phi_i^* \right) \right\} - \frac{ie^3}{(\hbar c)^3} A_\mu A_\nu \frac{1}{\kappa^2} \left(\frac{\partial \phi_i^*}{\partial x_\nu} \phi_i - \frac{\partial \phi_i}{\partial x_\nu} \phi_i^* \right) + \frac{2e^4}{(\hbar c)^4} \frac{1}{\kappa^2} A_\mu A_\nu^2. \quad \dots (7)$$

Here we have made the substitution $\epsilon = e/\hbar c$ and have arranged the terms in the ascending powers of e .

The continuity equation follows from the gauge invariance of the first kind of the lagrangian density (6). The theory is also invariant for gauge transformations of the second kind (Wentzel, 1949, p. 68), this gauge invariance being necessary since $F_{\mu\nu} = \frac{\partial A_\nu}{\partial x_\mu} - \frac{\partial A_\mu}{\partial x_\nu}$ determines the electromagnetic field.

In our calculations we shall keep only the terms involving the first power of e .

3. GENERAL THEORY

We can take the Tomonaga equation as

$$i\hbar \frac{\partial \Psi(\sigma)}{\partial \sigma(x)} = H(x) \Psi(\sigma)$$

Here $H(x) = H_i + H_1^{ext} + H_2^{ext}$

$$H_i(x) = i f_\mu \bar{\psi}(x) \gamma_5 \tau_\mu \psi(x) \phi_\mu(x) \quad \dots (8)$$

$$H_1^{ext} = j_\mu A_\mu = -ie \bar{\psi} \frac{1-\tau_3}{2} \gamma_\mu \psi A_\mu \quad \dots (9)$$

$$H_2^{ext} = s_\mu A_\mu$$

$$= -(e/\hbar c) A_\mu \left(\phi_1 \frac{\partial \phi_2}{\partial x_\mu} - \phi_2 \frac{\partial \phi_1}{\partial x_\mu} \right)$$

$$+ e/\hbar c A_\mu (1/2\kappa^2) \left(\phi_1 \frac{\partial \square^2 \phi_2}{\partial x_\mu} - \phi_2 \frac{\partial \square^2 \phi_1}{\partial x_\mu} - \frac{\partial \phi_1}{\partial x_\mu} \square^2 \phi_2 + \frac{\partial \phi_2}{\partial x_\mu} \square^2 \phi_1 \right) \dots (10)$$

In the above τ_1, τ_2, τ_3 are the isotopic spin matrices, τ_4 is unit matrix in isotopic spin space, ψ is the nucleon wave function denoting the proton and neutron states for $\tau_3 = \mp 1$ respectively. $\phi_\mu, \mu = 1, 2, 3, 4$ are real fields, pseudoscalar in space-time with the corresponding complex fields describing the charge mesons given as $\phi = \frac{1}{\sqrt{2}} (\phi_1 - i\phi_2)$ and $\phi^* = \frac{1}{\sqrt{2}} (\phi_1 + i\phi_2)$ which has been applied in deducing (10). $f_\mu, \mu = 1, 2, 3, 4$ are the corresponding coupling constants for

the above fields. As mentioned earlier in deducing (10) we have neglected the higher powers of e . The anticommutation relations and the vacuum expectation values for the nucleon fields are written as

$$[\psi_\alpha(x), \psi_\beta(x')]_+ = -iS_{\alpha\beta}(x-x') \quad \dots (11)$$

$$\langle P(\bar{\psi}_\alpha(x)\psi_\beta(x')) \rangle_0 = \frac{1}{2} S_{F\beta\alpha}(x-x') \quad \dots (11a)$$

$$\text{where } S_{F\beta\alpha}(x) = -\left(\gamma_\mu \frac{\partial}{\partial x_\mu} + \kappa_0\right)_{\beta\alpha} \Delta_F(x) \quad \dots (11b)$$

$$\Delta_F(x) = -2i/(2\pi)^4 \int d^4k (k_\mu^2 + \kappa_0^2)^{-1} \exp(ik_\mu x_\mu). \quad \dots (11c)$$

The integral in (11c) is to be understood with the usual convention of adding a small negative imaginary part to the mass of the nucleon.

The commutation relations and the vacuum expectation values of the meson field can be written as (Thirring, 1950).

$$[\phi_\mu(x), \phi_\nu(x')] = i\hbar c \delta_{\mu\nu} D(x-x') \quad \dots (12)$$

$$\langle P(\phi_\mu(x)\phi_\nu(x')) \rangle_0 = \frac{1}{2}\hbar c \delta_{\mu\nu} D_F(x-x') \quad \dots (12a)$$

$$\text{where } D_F(x) = \frac{-2i}{(2\pi)^4} \kappa^2 \int d^4k (k_\mu^2 + \kappa^2)^{-2} \exp(ik_\mu x_\mu). \quad \dots (12b)$$

The convention of the (12b) integral is the similar to that of (11c). The κ^2 was introduced in the above integral to keep the dimensions of the propagation function remain unchanged; it could as well have been absorbed in the hamiltonian, as has been done by Thirring.

4. CALCULATIONS

Because of the presence of the virtual meson fields, the electromagnetic properties of the nucleons will be modified. In the second order for the meson field, this change is given by (Case, 1949)

$$H'_{eff}(x_0) = \frac{1}{2} (-i/\hbar c)^2 \int_{-\infty}^{\infty} d^4x_1 \int_{-\infty}^{\infty} d^4x_2 P(H^{ext}(x_0) H_i(x_1) H_i(x_2))$$

which are split up into the terms

$$\begin{aligned} H_1(x_0) &= \frac{-ief_\nu f_\sigma}{2\hbar^2 c^2} A_\mu(x_0) \int_{-\infty}^{\infty} d^4x_1 \int_{-\infty}^{\infty} d^4x_2 P(\phi_\nu(x_1)\phi_\sigma(x_2)) \\ &\times P(\psi(x_0) \frac{1-\tau_3}{2} \gamma_\mu \bar{\psi}(x_1) \tau_\nu \gamma_5 \psi(x_1) \bar{\psi}(x_2) \tau_\sigma \gamma_5 \psi(x_2)) \quad \dots (13) \end{aligned}$$

$$\begin{aligned}
H_2(x_0) = & -\frac{ief_1 f_2}{2\hbar^3 c^3} A_\mu(x_0) \int_{-\infty}^{\infty} d^4 x_1 \int_{-\infty}^{\infty} d^4 x_2 P(\bar{\psi}(x_1) \tau_\nu \gamma_5 \psi(x_1) \bar{\psi}(x_2) \tau_\sigma \gamma_5 \psi(x_2)) \\
& \times P\left((\phi_1(x_0) \frac{\partial \phi_2(x_0)}{\partial x_{0\mu}} - \phi_2(x_0) \frac{\partial \phi_1}{\partial x_{0\mu}}) \phi_\nu(x_1) \phi_\sigma(x_2) \right. \\
& + \frac{ef_1 f_2}{2\hbar^3 c^3} A_\mu(x_0) (1/2\kappa^2) \int_{-\infty}^{\infty} d^4 x_1 \int_{-\infty}^{\infty} d^4 x_2 P(\bar{\psi}(x_1) \tau_\nu \gamma_5 \psi(x_1) \bar{\psi}(x_2) \tau_\sigma \gamma_5 \psi(x_2)) \\
& \times P\left((\phi_1(x_0) \frac{\partial \square_{0\mu}^\circ \phi_2}{\partial x_{0\mu}} - \phi_2(x_0) \frac{\partial \square_{0\mu}^\circ \phi_1}{\partial x_{0\mu}} - \frac{\partial \phi_1}{\partial x_{0\mu}} \square_{0\mu}^\circ \phi_2 + \frac{\partial \phi_2}{\partial x_{0\mu}} \square_{0\mu}^\circ \phi_1) \phi_\nu(x_1) \phi_\sigma(x_2) \right) \dots \quad (14)
\end{aligned}$$

Equations (13) and part of (14) are identical with those of (Case, 1949) (equations (20) and (21)).

For our problem we now take the one-nucleon, zero-meson vacuum expectation values. As has been shown in the appendix, then we can write in terms of a single momentum variable

$$\begin{aligned}
H_1(x_0) = & -\frac{ieA_\mu(x_0)}{8\hbar c} \frac{i\kappa^2}{2\pi^4} \int d^4 k \bar{\psi}(x_0) T \gamma_\nu \gamma_\mu \gamma_\lambda \psi(x_0) \\
& \times k_\nu k_\lambda ((k_\mu - P_\mu)^2 + \kappa_0^2)^{-1} ((k_\mu - P'_\mu)^2 + \kappa_0^2)^{-1} (k_\mu^2 + \kappa^2)^{-2}, \quad \dots \quad (15)
\end{aligned}$$

and

$$\begin{aligned}
H_2(x_0) = & \frac{ie}{2\hbar c} f_1 f_2 A_\mu(x_0) \frac{\kappa^2}{2\pi^4} \int d^4 k \bar{\psi}(x_0) \tau_3 i \gamma_\nu \psi(x_0) \\
& \times \frac{(k_\nu - P'_\nu)(P_\mu - k_\mu)}{(k_\mu^2 + \kappa_0^2)((k_\mu - P_\mu)^2 + \kappa^2)^2((k_\mu - P'_\mu)^2 + \kappa^2)^2} \\
& + \frac{ef_1 f_2}{2\hbar c} \frac{\partial A_\mu(x_0)}{\partial x_{0\lambda}} \frac{\kappa^2}{2\pi^4} \int d^4 k \bar{\psi}(x_0) \tau_3 i \gamma_\nu \psi(x_0) \\
& \times \frac{(k_\nu - P_\nu)(P_\mu - k_\mu)(P_\lambda - k_\lambda)}{(k_\mu^2 + \kappa_0^2)((k_\mu - P_\mu)^2 + \kappa^2)^2(k_\mu - P'_\mu)^2 + \kappa^2)^2} \quad \dots \quad (16)
\end{aligned}$$

The description of the symbols appears in the appendix along with the calculations. Using the representations

$$1/(abc) = 2 \int_0^1 dx \int_0^x dy (ay - b(x-y) - c(1-x))^{-3}$$

for the product denominators in (15) and (16), we get

$$\begin{aligned}
 H_1 &= \frac{-ie}{8\hbar c} A_\mu(x_0) \frac{i^2}{2\pi^4} 6 \int d^4k \int_0^1 dx \int_0^x dy \frac{(1-x)\bar{\psi}(x_0)T\gamma_\nu\gamma_\mu\gamma_\lambda\psi(x_0)k_\lambda}{(k_\mu^2 - 2k_\mu(P'_\mu y + P_\mu(x-y)) + \kappa^2(1-x))^4} \\
 H_2 &= \frac{ief_1 f_2}{2\hbar c} A_\mu(x_0) \frac{\kappa^2}{2\pi^4} 6 \int d^4k \int_0^1 dx \int_0^x dy (1-x)\bar{\psi}(x_0)\tau_3 i\gamma_\nu \psi(x) \\
 &\quad \times \frac{(k_\nu - P'_\nu)(P_\mu - k)}{(k_\mu^2 - 2k_\mu(P_\mu(x-y) + P'_\mu(1-x)) + \kappa_\nu^2(1-2y) + \kappa^2(1-y))^4} \\
 &\quad + \frac{ef_1 f_2}{2\hbar c} \frac{\partial A_\mu(x_0)}{\partial x_{0\lambda}} \frac{\kappa^2}{2\pi^4} 24 \int d^4k \int_0^1 dx \int_0^x dy (1-x)(x-y)\bar{\psi}(x_0)\tau_3 i\gamma_\nu \psi(x) \\
 &\quad \times \frac{(k_\nu - P_\nu)(k_\mu - P_\mu)(k_\gamma - P_\lambda)}{(k_\mu^2 - 2k_\mu(P_\mu(x-y) + P'_\mu(1-x)) + \kappa_\nu^2(1-2y) + \kappa^2(1-y))^6}
 \end{aligned}$$

We find that the k -integration above is automatically convergent. Proceeding as in Feynman, (1949), we get.

$$\begin{aligned}
 H_1 &= -\frac{ieA_\mu(x_0)}{8\hbar c} \frac{\kappa^2}{2\pi^4} \int_0^1 dx \int_0^x dy (1-x)\bar{\psi}(x_0)T(K_1)^{-2} \\
 &\quad \times (-\gamma_\nu\gamma_\mu\gamma_\lambda(\Delta P_\nu y - P_\nu x)(\Delta P_\lambda y - P_\lambda x) + \gamma_\mu K_1)\psi(x_0),
 \end{aligned}$$

where

$$K_1 = y(x-y)(\Delta P_\nu)^2 - \phi(x) \quad \dots (17)$$

$$\phi(x) = \kappa_0^2 x^2 + \kappa^2(1-x) \quad \dots (18)$$

$$\text{and} \quad \Delta P_\nu = P_\nu - P'_\nu. \quad \dots (19)$$

Similarly

$$\begin{aligned}
 H_2 &= -\frac{ief_1 f_2}{8\pi^2 \hbar c} A_\mu(x_0) \kappa^2 \int_0^1 dx \int_0^x dy (1-x)\bar{\psi}(x_0)\tau_3 \gamma_\nu \psi(x_0) \\
 &\quad (K_2)^{-2} (2(x\Delta P_\nu - yP_\nu)((1-x)\Delta P_\mu - yP_\mu) - \delta_{\mu\nu} K_2) \\
 &\quad - \frac{ef_1 f_2}{8\pi^2 \hbar c} \frac{\partial A_\mu(x_0)}{\partial x_{0\nu}} \kappa^2 \int_0^1 dx \int_0^x dy (1-x)(x-y)\bar{\psi}(x_0)\tau_3 \\
 &\quad [(K_2)^{-2} (\gamma_\nu(\Delta P_\mu(1-x) + P_\mu y) + \gamma_\mu(\Delta P_\nu(1-x) - P_\nu y)) \\
 &\quad - (K_2)^{-2} \gamma_\lambda (P_\lambda y + \Delta P_\lambda(1-x))(P_\mu y + \Delta P_\mu(1-x))(P_\nu y + \Delta P_\nu(1-x))] \psi(x_0) \quad \dots (20)
 \end{aligned}$$

where $K_2 = (1-x)(x-y)(\Delta P_\nu)^2 + \phi(y)$.

In deducing (20) we have used

$$\int \frac{k_\nu k_\mu k_\lambda d^4 k}{(k_\mu^2 - 2k_\mu Q_\mu - \Delta)^6} = \frac{\pi^2}{48i} \left[\frac{4Q_\nu Q_\lambda Q_\mu}{(Q_\mu^2 + \Delta)^3} - \frac{Q_\nu \delta_{\mu\lambda} + Q_\mu \delta_{\nu\lambda} + Q_\lambda \delta_{\mu\nu}}{(Q_\mu^2 + \Delta)^2} \right]$$

and the continuity equation $\frac{\partial A_\mu(x_0)}{\partial x_{0\mu}} = 0$

Equations (17) and (20) are simplified by repeated use of (A3) and the anti-commutation rules of the γ -matrices. We also use the result

$$\bar{\psi}(x_0)(2iP_\mu)\psi(x_0) = \bar{\psi}(x_0)(\sigma_{\mu\nu}\Delta P_\nu - 2\kappa_0\gamma_\mu + i\Delta P_\mu)\psi(x_0)$$

with

$$\sigma_{\mu\nu} = (-i/2)(\gamma_\mu\gamma_\nu - \gamma_\nu\gamma_\mu)$$

We also use the result

$$\int d^4 x_0 \frac{\partial A_\mu(x_0)}{\partial x_{0\nu}} \bar{\psi}(x_0)Q\psi(x_0) = -i\Delta P_\nu \int d^4 x_0 A_\mu(x_0)\bar{\psi}(x_0)Q\psi(x_0) \quad \dots \quad (21)$$

(21) is employed to simplify the second term in (20). It gives as a particular case that terms of the type

$$A_\mu(x_0) (\text{constant}) \bar{\psi}(x_0)\Delta P_\mu f((\Delta P_\nu)^2)\psi(x)$$

are effectively zero, as has been mentioned in Case (1949).

Now we write,

$$H_1 = \frac{ieA_\mu(x_0)}{16\pi^2\hbar c} \kappa^2 \int_0^1 dx \int_0^x dy (1-x)\bar{\psi}(x_0)T[(K_1)^{-2}\kappa_0^2\sigma_{\mu\nu}\Delta P_\nu - \gamma_\mu(K_1)^{-2}(\kappa_0^2x^2 + \phi(x)) + \gamma_\mu(\phi(x))^{-2}(\kappa_0^2x^2 + \phi(x))]$$

The last term above inside the square bracket has been added for renormalisation. It is to be noted that this renormalising term is finite, as has been mentioned in the introduction. The physical significance of this renormalisation may be realised when we see that the matrix element above vanishes when ΔP is zero, and that the correction due to renormalisation is independent of the momenta P and P' . We may also add that the concept of renormalisation has nothing to do with the divergencies as such, although necessarily the arguments are *more* consistent when the renormalising terms are finite, as is the case here (Kallen, 1953). Thus H_1 simplifies to

$$H_1 = \frac{ieA_\mu(x_0)}{16\pi^2\hbar c} \kappa^2 \int_0^1 dx \int_0^x dy (1-x)\bar{\psi}(x_0)T[(K_1)^{-2}\kappa_0^2\sigma_{\mu\nu}\Delta P_\nu - (K_1\phi(x))^{-2}\gamma_\mu y(x-y)(\Delta P_\nu)^2(\kappa_0^2x^2 + \phi(x)) - (2\phi(x) + y(x-y)(\Delta P_\nu)^2)\psi(x_0)] \quad \dots \quad (22)$$

For the simplification of H_2 we remember (21) and proceed in a similar way as before. Thus we get

$$H_2 = \frac{ief_1 f_2}{8\pi^2 \hbar c} A_\mu(x_0) \kappa^2 \int_0^1 dx \int_0^x dy (1-x) \bar{\psi}(x_0) \tau_3 [(K_3)^{-2} \kappa_0 y^2 \sigma_{\mu\nu} \Delta P_\nu - (K_3 \phi(y))^{-2} \gamma_\mu (1-x)(x-y) (\Delta P_\nu)^2 (4\phi(y) \kappa_0 y^2 - (\phi(y))^2 - (1-x)(x-y) (\Delta P_\nu)^2 (\phi(y) - 2\kappa_0^2 y^2) \psi(x) \dots \quad (23)$$

+ terms that involve $(\Delta P)^2$ throughout, and thus by the subsequent section will not contribute anything to the magnetic moment.

5. MAGNETIC MOMENTS

The terms involving $\sigma_{\mu\nu} \Delta P_\nu$ above will contribute to the anomalous magnetic moments of the nucleons. For this purpose we neglect $(\Delta P_\nu)^2$ and write $A_\mu(x_0) \bar{\psi}(x_0) \Delta P_\nu \Gamma \psi(x_0)$ in the form $+ i \frac{\partial A_\mu}{\partial x_{0\nu}} \bar{\psi}(x_0) \Gamma \psi(x_0)$, the Γ above being an operator depending on the γ 's and the τ 's. This gives

$$H_1 = \frac{e\kappa^2}{16\pi^2 \hbar c} I_{1\frac{1}{2}} F_{\mu\nu}(x_0) \bar{\psi}(x_0) T \sigma_{\mu\nu} \psi(x_0).$$

$$H_2 = \frac{ef_1 f_2}{8\pi^2 \hbar c} I_{2\frac{1}{2}} F_{\mu\nu}(x_0) \bar{\psi}(x_0) \tau_3 \sigma_{\mu\nu} \psi(x_0)$$

where

$$I_1 = \int_0^1 dx \int_0^x dy (\phi(x))^{-2} ((1-x) \kappa_0 x^2),$$

$$I_2 = \int_0^1 dx \int_0^x dy (\phi(y))^{-2} ((1-x) \kappa_0 y^2).$$

This finally with $\vec{H} = (F_{23}, F_{31}, F_{12})$ giving the only nonzero kennzahlen of the field tensor $F_{\mu\nu}$ and with the usual spin matrix vector $\vec{\sigma}$ we get for a proton

$$H'_{eff} = \left(- \frac{e(f_3^2 + f_4^2) \kappa^2}{16\pi^2 \hbar c} I_1 - \frac{ef^2}{8\pi^2 \hbar c} \kappa^2 I_2 \right) (-\psi^*(x_0) \vec{\sigma} \cdot \vec{H} \psi(x_0))$$

and for the neutron

$$H'_{eff} = \left(- \frac{ef^2}{8\pi^2 \hbar c} \kappa^2 I_1 - \frac{ef^2}{8\pi^2 \hbar c} \kappa^2 I_2 \right) (-\psi^*(x_0) \vec{\sigma} \cdot \vec{H} \psi(x_0)).$$

In the above $f_1 = f_2 = f$ has been taken. Confining our attention to the symmetrical

theory ($f_1 = f_2 = f_3 = f$, $f_4 = 0$) we get the respective anomalous magnetic moments as

$$\Delta\mu_P = \frac{ef^2\kappa^2}{8\pi^2\hbar c} (I_2 - \frac{1}{2}I_1)$$

and

$$\Delta\mu_N = - \frac{ef^2\kappa^2}{8\pi^2\hbar c} (I_2 + I_1)$$

The integrals I_1 and I_2 are elementary although lengthy. Evaluating them we have

$$I_1 = \frac{1}{\kappa_0^3} \left(-3/2 + \frac{1}{2} \ln(1/\lambda) + \frac{\lambda^{1/2}}{(4-\lambda)^{3/2}} (18-13\lambda+2\lambda^2) \cos^{-1}(\lambda^{1/2}/2) \right. \\ \left. + \frac{1}{2}\lambda - \frac{3\lambda-\lambda^2}{4(4-\lambda)} - \lambda \ln(1/\lambda) \right),$$

and

$$I_2 = \frac{1}{\kappa_0^3} \left(1 - \frac{1}{2} \ln(1/\lambda) + \frac{2-12\lambda+9\lambda^2}{\lambda^{1/2}(4-\lambda)^{3/2}} \cos^{-1}(\lambda^{1/2}/2) - \frac{2-4\lambda+\lambda^2}{4(4-\lambda)} \right. \\ \left. + \frac{1}{2} \ln(1/\lambda) - 4\lambda \right).$$

where $\lambda = \left(\frac{\kappa}{\kappa_0} \right)^2$. With $\lambda^{1/2} = 0.15$, we get

$$I_1 = \frac{1}{\kappa_0^3} \quad 0.80 \text{ nearly,}$$

and

$$I_2 = \frac{1}{\kappa_0^3} \quad 1.20 \text{ nearly.}$$

Hence

$$\Delta\mu_P = (G^2/4\pi^2\hbar c) \quad 0.80$$

and

$$\Delta\mu_N = -(G^2/4\pi^2\hbar c) \quad 2.00$$

where the quantities are expressed in nuclear magnetons and we have substituted

$$\frac{f\kappa}{\kappa_0} = G.$$

Thus $|\Delta\mu_P/\Delta\mu_N| = 0.40$ nearly.

If we take $\Delta\mu_P = 1.79$, then $G^2/4\pi^2\hbar c = 7$ nearly, ... (24)

and if we take $\Delta\mu_N = -1.91$, then $G^2/4\pi^2\hbar c = 3$ nearly. ... (25)

DISCUSSIONS

The above results are in qualitative agreement with experiments as regards the signs and the relative magnitudes of the magnetic moments. The quantitative values, though not satisfactory, do not 'contradict violently the experimental results' (Goto, 1954) as in earlier theories. Our result 2.50 for the coupling-constant-independent ratio $|\Delta\mu_N/\Delta\mu_P|$ is a significant improvement over those of Case (1949), and Borowitz and Kohn (1949), which is 8 nearly, as compared to the experimental value 1.07. Even the relativistic cut-off method of Goto (1954), yields the value 3.1 nearly, which is slightly worse than ours.

Again, the calculated values of the coupling constants in (24) and (25) do not differ widely (previously they differed as much as 56 and 7), and although the values thus obtained are comparatively small, they are not small enough to make the second order calculations very reliable, and the differences still present may be attributed to this fact.

In our calculations here no infinite renormalisation was necessary, which is an encouraging feature of this theory. But it may be noted that higher order corrections to this theory will contain infinite renormalisations, since the meson self-energy remains unchanged. Thus the processes which involve this graph will have to be dealt with more or less in the usual manner of subtracting infinite quantities.

ACKNOWLEDGMENTS

The authors wish to express their sincere thanks to Dr. D. Basu for suggesting the problem and also for pointing out an error in the calculations.

APPENDIX

Evaluation of H_1 :

After taking the vacuum expectation values, we can write $H_1 = H_1^a + H_1^b$ where

$$H_1^a = \frac{ief_v^2}{8\hbar c} A_\mu(x_0) \int_{-\infty}^{\infty} d^4x_1 \int_{-\infty}^{\infty} d^4x_2 D_F(x_1-x_2) \bar{\psi}(x_2) \gamma_5 \tau_\nu \psi(x_2) \\ S p(\tau_\nu \gamma_5 S_F(x_0-x_1) \gamma_\mu \frac{1-\tau_3}{2} S_F(x_1-x_0)) \dots \quad (A1)$$

and

$$H_1^b = - \frac{ief_v^2}{8\hbar c} A_\mu(x_0) \int_{-\infty}^{\infty} d^4x_1 \int_{-\infty}^{\infty} d^4x_2 \bar{\psi}(x_1) \gamma_5 \tau_\nu S_F(x_0-x_1) \gamma_\mu \frac{1-\tau_3}{2} \\ S_F(x_2-x_0) \tau_\nu \gamma_5 \psi(x_2) D_F(x_1-x_2)$$

To evaluate H_1^a we note that the spur written down in (A1) vanishes, as has been shown by Case (1949) with the same quantities as in (A1), but with a different D_F function. Thus the arguments of Case for the vanishing of the H_1^a with the conventional D_F function continues to hold here as well.

Rearranging the isotopic spin matrices, H_1^b can be simplified to

$$H_1^b = - \frac{ie}{8\hbar c} A_\mu(x_0) \int_{-\infty}^{\infty} d^4x_1 \int_{-\infty}^{\infty} d^4x_2 \bar{\psi}(x_1) T \gamma_5 S_F(x_0 - x_1) \gamma_\mu S_F(x_2 - x_0) \gamma_5 \psi(x_2) D_F(x_1 - x_2),$$

where

$$T = \frac{1}{2}(1 - \tau_3)(f_3^2 + f_4^2) + \frac{1}{2}(1 + \tau_3)(f_1^2 + f_2^2). \quad \dots \quad (\text{A2})$$

Also we take

$$\psi(x) = u_p \exp(iP_\mu x_\mu), \quad \bar{\psi}(x) = u'_p \exp(-iP'_\mu x_\mu)$$

such that $P_\mu^2 = P'^2_\mu = -\kappa_0^2$. We now represent the invariant functions by means of the integrals (11c) and (12b) and integrate with respect to x_1 and x_2 , giving rise to δ -functions with the help of which we finally express

$$H_1^b = - \frac{ie}{8\hbar c} A_\mu(x_0) \frac{i\kappa^2}{2\pi^4} \int d^4k \bar{\psi}(x_0) T \gamma_5 \times \\ \times \frac{(i\gamma_\nu (P'_\nu - k_\nu) - \kappa_0) \gamma_\mu (i\gamma_\lambda (P_\lambda - k_\lambda) - \kappa_0) \gamma_5 \psi(x_0)}{((k_\mu - P_\mu)^2 + \kappa_0^2)((k_\mu - P'_\mu)^2 + \kappa_0^2)(k_\mu^2 + \kappa^2)^2}$$

With repeated applications of the results

$$(i\gamma_\mu P_\mu + \kappa_0) u_p = u'_p \quad (i\gamma_\mu P'_\mu + \kappa_0) = 0 \quad \dots \quad (\text{A3})$$

and $\gamma_5^2 = 1$, the above expression for H_1^b can be seen to simplify to the expression (15) already written down.

Evaluation of H_2 :

We first write $H_2 = H'_2 + H''_2$, where

$$H'_2 = - \frac{ef_\nu f_\mu}{2\hbar^3 c^3} A_\mu(x_0) \int_{-\infty}^{\infty} d^4x_1 \int_{-\infty}^{\infty} d^4x_2 P(\bar{\psi}(x_1) \tau_\nu \gamma_5 \psi(x_1) \bar{\psi}(x_2) \tau_\sigma \gamma_5 \psi(x_2)) \\ \times P \left(\left(\phi_1(x_0) \frac{\partial \phi_2}{\partial x_{0\mu}} - \phi_2(x_0) \frac{\partial \phi_1}{\partial x_{0\mu}} \right) \phi_\nu(x_1) \phi_\sigma(x_2) \right) \\ H''_2 = \frac{ef_\nu f_\mu}{2\hbar^3 c^3} A_\mu(x_0) \frac{1}{2\kappa^2} \int_{-\infty}^{\infty} d^4x_1 \int_{-\infty}^{\infty} d^4x_2 P(\bar{\psi}(x_1) \tau_\nu \gamma_5 \psi(x_1) \bar{\psi}(x_2) \tau_\sigma \gamma_5 \psi(x_2)) \\ \times P \left(\left(\phi_1(x_0) \frac{\partial \square_\sigma^2 \phi_2}{\partial x_{0\mu}} - \phi_2(x_0) \frac{\partial \square_\sigma^2 \phi_1}{\partial x_{0\mu}} - \frac{\partial \phi_1}{\partial x_{0\mu}} \square_\sigma^2 \phi_2 + \frac{\partial \phi_2}{\partial x_{0\mu}} \square_\sigma^2 \phi_1 \right) (\phi_\nu(x_1) \phi_\sigma(x_2)) \right)$$

The calculation of H'_2 is similar to that of Case (1949), and proceeding as before, the final result can be written as

$$H'_2 = + \frac{ie f_1 f_2}{2\hbar c} A_\mu(x_0) \frac{\kappa^4}{2\pi^4} \int d^4k \bar{\psi}(x_0) \tau_3 i \gamma_\nu \psi(x_0) \\ \times \frac{(k_\nu - P'_\nu)(P_\mu - k_\mu)}{(k_\mu^2 + \kappa_0^2)((k_\mu - P_\mu)^2 + \kappa^2)((k_\mu - P'_\mu)^2 + \kappa^2)}$$

To simplify H'_2 we note that

$$< P(\phi_\nu(x_1)\phi_\nu(x_2)(\phi_1(x_0) \frac{\partial \square_0^2 \phi_2}{\partial x_{0\mu}} - \phi_2(x_0) \frac{\partial \square_0^2 \phi_1}{\partial x_{0\mu}} - \frac{\partial \phi_1}{\partial x_{0\mu}} \square_0^2 \phi_2(x_0) + \frac{\partial \phi_2}{\partial x_{0\mu}} \square_0^2 \phi_1)) >_0 \\ = (\hbar^2 c^2/4)(\delta_{1\nu}\delta_{2\nu} - \delta_{1\sigma}\delta_{2\nu})(D_F(x_0-x_1) \frac{\partial \square_0^2 D_F(x_0-x_2)}{\partial x_{0\mu}} - D_F(x_0-x_2) \frac{\partial \square_0^2 D_F(x_0-x_1)}{\partial x_{0\mu}} \\ - \frac{\partial D_F(x_0-x_1)}{\partial x_{0\mu}} \square_0^2 D_F(x_0-x_2) + \frac{\partial D_F(x_0-x_2)}{\partial x_{0\mu}} \square_0^2 D_F(x_0-x_1))$$

This gives

$$H''_2 = - \frac{ef_1 f_2}{8\hbar c} A_\mu(x_0) \frac{1}{2\kappa^2} \int_{-\infty}^{\infty} d^4x_1 \int_{-\infty}^{\infty} d^4x_2 \bar{\psi}(x_1) (\tau_1 \gamma_5 S_F(x_2-x_1) \tau_2 \gamma_5 \\ - \tau_2 \gamma_5 S_F(x_2-x_1) \tau_1 \gamma_5) \psi(x_2) \\ \times \left[D_F(x_0-x_1) \frac{\partial \square_0^2 D_F(x_0-x_2)}{\partial x_{0\mu}} - D_F(x_0-x_2) \frac{\partial \square_0^2 D_F(x_0-x_1)}{\partial x_{0\mu}} \right. \\ \left. - \frac{\partial D_F(x_0-x_1)}{\partial x_{0\mu}} \square_0^2 D_F(x_0-x_2) + \frac{\partial D_F(x_0-x_2)}{\partial x_{0\mu}} \square_0^2 D_F(x_0-x_1) \right] \quad \dots \quad (\text{A4})$$

We now use $\tau_1 \tau_2 = -\tau_2 \tau_1 = i\tau_3$. Also in (A4), the x_0 integration is implicit. Carrying out partial integration with respect to x_0 and using the result $\frac{\partial A_\mu(x_0)}{\partial x_{0\mu}}$

= 0, the second and third terms inside the square bracket can be seen to be respectively equal to the first and fourth terms. For example,

$$- \int_{-\infty}^{\infty} dx_{0\mu} A_\mu(x_0) \frac{\partial D_F(x_0-x_1)}{\partial x_{0\mu}} \square_0^2 D_F(x_0-x_2) \\ = \int_{-\infty}^{\infty} dx_{0\mu} \frac{\partial}{\partial x_{0\mu}} (A_\mu(x_0) \square_0^2 D_F(x_0-x_2)) D_F(x_0-x_1) \\ = \int_{-\infty}^{\infty} dx_{0\mu} A_\mu(x_0) \frac{\partial \square_0^2 D_F(x_0-x_2)}{\partial x_{0\mu}} D_F(x_0-x_1).$$

But again applying partial integration two times in the different variables for the fourth term in (A4), we obtain this term as equal to

$$\int d^4x_0 \left[\square_0^2 \left(A_\mu(x_0) \frac{\partial D_F(x_0-x_2)}{\partial x_{0\mu}} \right) D_F(x_0-x_1) \right. \\ \left. - \int d^4x_0 \left[A_\mu(x_0) \frac{\partial \square_0^2 D_F(x_0-x_2)}{\partial x_{0\mu}} + 2 \frac{\partial A_\mu(x_0)}{\partial x_{0\nu}} \frac{\partial^2 D_F(x_0-x_2)}{\partial x_{0\nu} \partial x_{0\mu}} \right] D_F(x_0-x_1) \right]$$

where we have applied $\square_0^2 A_\mu(x_0) = 0$.

Thus we get

$$H_2'' = - \frac{ief_1 f_2}{2\hbar c} \frac{1}{\kappa^2} \int_{-\infty}^{\infty} d^4x_1 \int_{-\infty}^{\infty} d^4x_2 \bar{\psi}(x_1) \tau_3 \gamma_5 S_F(x_2-x_1) \gamma_5 \psi(x_2) \\ \times \left[A_\mu(x_0) D_F(x_0-x_1) \frac{\partial \square_0^2 D_F(x_0-x_2)}{\partial x_{0\mu}} \right. \\ \left. + \frac{\partial A_\mu(x_0)}{\partial x_{0\nu}} D_F(x_0-x_1) \frac{\partial^2 D_F(x_0-x_2)}{\partial x_{0\mu} \partial x_{0\nu}} \right].$$

We again apply the integrals (11c) and (12b) and thus finally obtain, as in case of H_1' and H_2' ,

$$H_2'' = \frac{ief_1 f_2}{2\hbar c} \frac{\kappa^2}{2\pi^4} \int d^4k \bar{\psi}(x_0) \tau_3 i \gamma_\nu \psi(x_0) \\ \times \frac{A_\mu(x_0) (k_\nu - P'_\nu) (P_\mu - k_\mu) (P_\lambda - k_\lambda)^2 - i \frac{\partial A_\mu(x_0)}{\partial x_{0\lambda}} (k_\nu - P'_\nu) (P_\mu - k_\mu) (P_\lambda - k_\lambda)}{(k_\mu^2 + \kappa_0^2) ((k_\mu - P_\mu)^2 + \kappa^2)^2 ((k_\mu - P'_\mu)^2 + \kappa^2)^2}.$$

Thus adding the values of H_2' and H_2'' and simplifying, we get the value of H_2 as mentioned in formula (16) earlier.

REFERENCES

- Bhabha H. J., 1950, *Phys. Rev.*, **77**, 665.
 Borowitz S. and Kohn, W., 1949, *Phys. Rev.*, **76**, 818.
 Case, K. M., 1949, *Phys. Rev.*, **76**, 1.
 Feynman, R. P., 1949, *Phys. Rev.*, **76**, 784 (appendix).
 Goto S., 1954, *Progress of Theor. Phys.*, **12**, 699.
 Källén G., 1953, *Physica*, **19**, 850.
 Sachs R. G., 1952, *Phys. Rev.*, **87**, 1100;
 Slotnick, M. and Heitler W., 1949, *Phys. Rev.*, **75**, 1645;
 Thirring, W., 1950, *Phil. Mag.* **41**, 653.
 Wontzel G., 1949, *Quantum Theory of Fields*, Interscience Publishers. p. 68

ON THE NATURE OF EXTRA REFLECTIONS IN THE LAUE PHOTOGRAPHS OF SOME DIAMONDS OF KNOWN RELATIVE FLUORESCENCE EFFICIENCIES

S. C. SIRKAR AND S. N. SEN

OPTICS DEPARTMENT, INDIAN ASSOCIATION FOR THE CULTIVATION OF SCIENCE, JADAVPUR, CALCUTTA

(Received for publication, November 25, 1955)

Plates 1A, 1B, 1C, & 1D.

ABSTRACT. The positions and approximate relative intensities of extra spots accompanying the $\{111\}$ reflection in the Laue photographs of eleven specimens of diamond have been determined using a Seifert X-ray tube provided with a copper target and nickel filter and running at 30 Kv, 28 mA. In order to measure the directions of extra reflections accurately in some cases the front surface of the crystals as dusted with powdered NaCl, so that the Debye-Scherrer pattern of NaCl was superimposed on the Laue photographs. The specimens studied were used by Bishui (1950, 52) in previous investigations on the relative intensities of the fluorescence band at 4156 \AA and on the ultraviolet absorption limits. The results show that all the specimens excepting D 6 possess partial mosaic structure, so that they produce extra reflections from $\{111\}$ planes of different intensities in the direction making an angle $2\theta_H$ with the incident rays when the disorientation from the Bragg angle θ_H is less than 3° .

It is observed that neither the intensities of the extra reflections nor those of the extra reflections in other directions present in the Laue photographs of some of the crystals can be correlated either with the intensity of the band at 4156 \AA or with the impurity present in the crystals. Also, these intensities cannot be correlated with the respective thicknesses of the specimens.

INTRODUCTION

It was first shown by Lonsdale and Smith (1941) that the secondary X-ray reflections consisting of groups of extra spots observed in the Laue photographs of diamonds of Type I do not appear in the Laue photographs of diamonds of Type II. Later, Lonsdale (1941) reviewed the existing theories put forward to explain the origin of these secondary extra reflections and pointed out that all the observed facts could not be explained satisfactorily by any of the existing theories. Guinier (1942) put forward a new theory in which he suggested that partial irregularities of spacing along the cube edges might give rise to these extra reflections. Lonsdale (1948) studied the divergent-beam X-ray photographs of specimens of diamond of Type I and Type II and observed that diamonds of Type I produced bad divergent-beam photographs which showed that the crystals had perfect structure. On the other hand, all Type II diamonds studied by her gave excellent divergent-beam photographs. So, she pointed out that

although Guinier's hypothesis could explain many features of the extra spots satisfactorily it was difficult to understand why such partial irregularity in spacing should occur only in diamonds having a perfect structure and should be absent in Type II diamonds having a mosaic structure. More recently, Grenville-Wells (1952) studied the divergent-beam photographs of 38 specimens of diamond of different qualities and also the relative intensities of the fluorescence and the secondary extra reflections produced by these diamonds in order to find out whether the texture of the specimens could be correlated with their counting properties, which had been determined along with the ultraviolet transparency earlier by Champion (1952), and also with the intensity of extra reflections produced by these diamonds. The results obtained by her do not confirm the conclusions drawn by Lonsdale (1942) that only diamonds having perfect structure produce intense extra reflections and those having mosaic structure do not produce such reflections. Some of the specimens produced neither good divergent-beam photographs nor secondary extra reflections while some other specimens producing good extra reflections yielded good divergent beam photographs. She also proved conclusively that the intensity of fluorescence of the diamonds could not be correlated either with texture or with the intensity of extra reflections.

There are, however, several points which are not quite clear from the results reported by Grenville-Wells (1952). First, while studying the extra reflections, she considered only the intensities without measuring accurately the directions in which these extra reflections took place. It is not known whether some of the specimens giving good divergent beam photographs also produced sharp extra reflections in the direction making an angle equal to double the Bragg angle with the incident X-rays, indicating thereby the existence of mosaicity in the crystals. Secondly, as regards the fluorescence she probably estimated the total intensity of the light emitted by the crystals without considering its spectral distribution. It was shown by Bishui (1952) that diamonds should not be classified as Type I and Type II on the criterion of mere transparency in the ultraviolet region, because specimens having absorption limit at 2300 \AA , but showing absorption bands at 2360 \AA and 2363.5 \AA give strong fluorescence band at 4156 \AA and these should be classified as Type I diamond. Bishui (1950, 52) estimated the relative fluorescence efficiencies at 4156 \AA of 14 specimens of diamond and also studied the ultraviolet absorption limits of the specimens. The present investigation was undertaken to find out whether there was any correlation between the intensity of the band at 4156 \AA and intensities of the extra reflections given by these diamonds. It was also intended to attempt at a separation of the reflection due to mosaicity from other types of secondary reflections not satisfying Bragg's law for Cu $K\alpha$ radiation and to find out whether these residual extra reflections can be correlated with either the intensity of the band at 4156 \AA or with the ultraviolet transparency.

EXPERIMENTAL

The Laue photographs were taken with a cylindrical camera having a radius of about 5.1 cm in order to measure the angles accurately. The divergence of the X-ray beam incident on the crystal was about $2^{\circ}18'$. A Seifert X-ray tube giving 28 m.A. at 30 Kv and provided with copper anticathode was used in this investigation. A nickel filter was used to cut off the Cu $K\beta$ radiation. An exposure of 2 hours was required for getting intense Laue photograph of diamond. As the crystals were all of large size the Laue spots were elongated in the direction at right angles to the plane of incidence corresponding to the width of the incident beam. The horizontal width of the vertical Laue spots is, however, determined mainly by the thickness of the crystals, because two divergent rays, reflected by two parallel planes in the crystal produce two convergent rays, the angle of convergence being equal to the angle of divergence of the incident rays. The distance of the point of convergence is $D \cos 2\theta$, where D is the distance of the slit from the crystal and θ is the glancing angle. The diamonds used in the present investigation are the same as those used by Bishui (1950,52). The thickness of crystals varies from .647 mm to 2 mm as shown in Table I. The ultraviolet absorption limits of most of these diamonds are also given in this table.

The specimen D 13 gave no fluorescence at 4156 \AA and D 4 produced an extremely weak band at this position. So, these two were classified as Type II diamonds. D 11 and D 14 exhibited absorption bands at 2360 \AA and 2363 \AA and gave strong fluorescence bands. These two diamonds were classified by Bishui as diamonds of Type I.

TABLE I

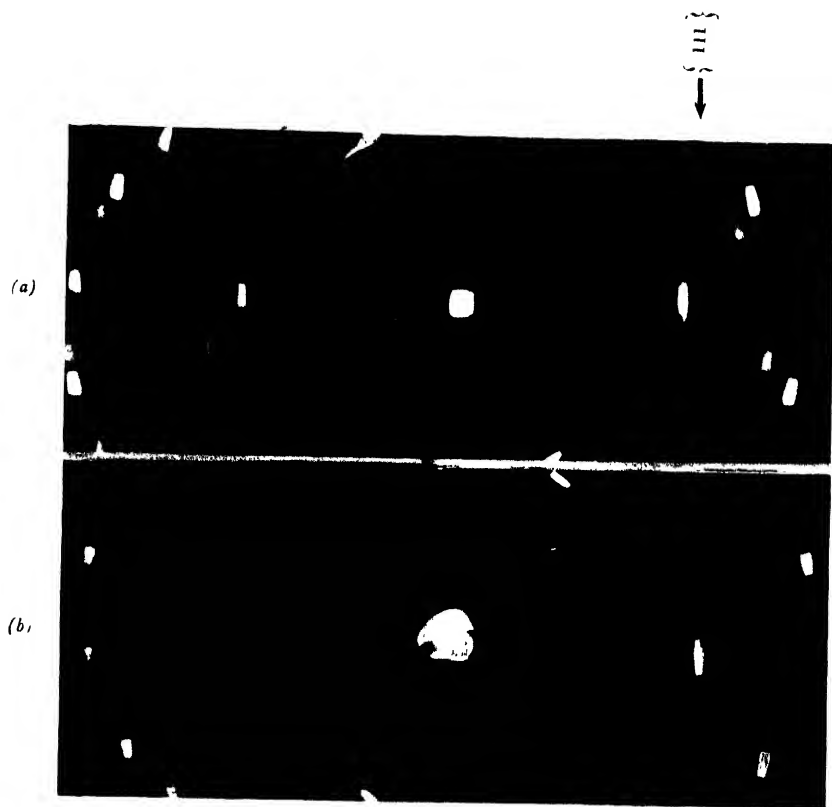
Specimen used	thickness in mm.	UV absorption limit in A.U.	
D 1	1.5	--	
D 4	1.5	2300	
D 6	2.0	--	
D 7	1.353	2560	
D 8	1.30	3000	
D 9	0.8	2550	
D 10	1.092	2810	
D 11	0.952	2270	(absorption bands at 2360 etc.)
D 12	0.647	2720	
D 13	0.838	2240	
D 14	0.812	2300	(absorption bands at 2360 etc.)

Preliminary investigations showed that some of the specimens produced extra reflections in the directions making an angle $2\theta_B$ with incident rays, where θ_B is Bragg angle for $\{111\}$ planes of diamond for Cu $K\alpha$ radiation. In order to verify this, attempts were made to measure the angles correctly by superimposing Debye-Scherrer photographs of rocksalt on the Laue photographs. This was done by dusting the front surface of the specimen with fine powders of chemically pure NaCl. It was found that when both the surfaces were dusted in this way two sharp ring systems of NaCl were produced corresponding to the two surfaces separated by the thickness of the crystal. This happens because in the case of reflection by powdered crystal, the partial focussing effect observed in the case of Laue spots is absent. So, care was taken to put a narrow line of powdered NaCl on the surface of the crystal through which the X-rays emerged. In measuring the distance of the crystal from the film, half the thickness of the crystal was added to the distance obtained from the position of the Bragg reflection from the $\{220\}$ plane of NaCl. As this spacing of NaCl and that of $\{111\}$ planes of diamond are near to each other the angle between the reflections from these two planes could be measured very accurately by this method. For each diamond several Laue photographs were taken with different disorientations from the Bragg angle. The angle between the direction of the incident beam and that of the Laue spot due to $\{111\}$ plane and the corresponding angle for the extra reflection accompanying it were measured accurately in each case. Altogether eleven specimens were studied.

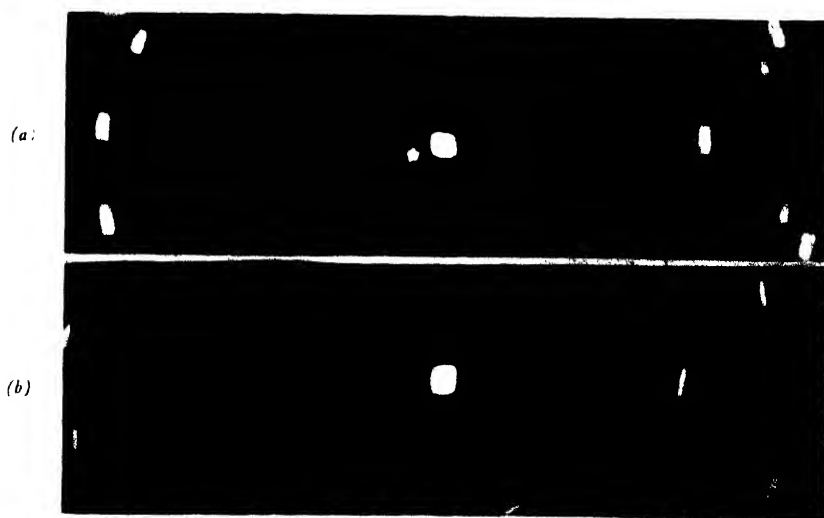
RESULTS AND DISCUSSION

Some of the Laue photographs are reproduced in Plate I to show that in some of the photographs the extra reflections are extremely sharp and their positions could be determined very accurately. The results are tabulated in Table II in which 2θ is the angle made with the incident rays by the ray corresponding to the Laue spot and $\theta + \phi$ is the angle made similarly by the extra reflection. The approximate intensities of extra reflections are indicated as strong, medium weak and very weak by the letters s, m, w and v.w respectively. The widths of the extra reflections are given as sharp, broad and diffuse. The intensities of the fluorescence band at 4156 \AA are taken from the results reported by Bishui (1950, 52). As regards D1 and D4, absolute fluorescence efficiencies were not determined by Bishui, but visual examination of the spectrograms shows that the value of the constant K is about 6.

It can be seen from Table II that all the specimens, excepting D6, give extra reflections in the direction making an angle of about $43^\circ 56'$ with the incident rays for different positions of the Laue spot. This shows that these extra reflections are produced by the Bragg reflection of Cu $K\alpha$ rays from the $\{111\}$ planes even when the glancing angle is slightly different from $21^\circ 58'$. This is possible

Fig. 1. Diamond D 1. $|110|$ vertical.

(a) $2\theta = 39^{\circ}20'$ $\theta + \varphi = 42^{\circ}51'$
 (b) $2\theta = 42^{\circ}29'$ $\theta + \varphi = 43^{\circ}57'$

Fig. 2. Diamonds D 4 and D 9. $|110|$ vertical.

(a) D 4 ; $2\theta = 45^{\circ}51'$, $\theta + \varphi = 43^{\circ}51'$
 (b) D 9 ; $2\theta = 41^{\circ}36'$, $\theta + \varphi = 43^{\circ}58'$

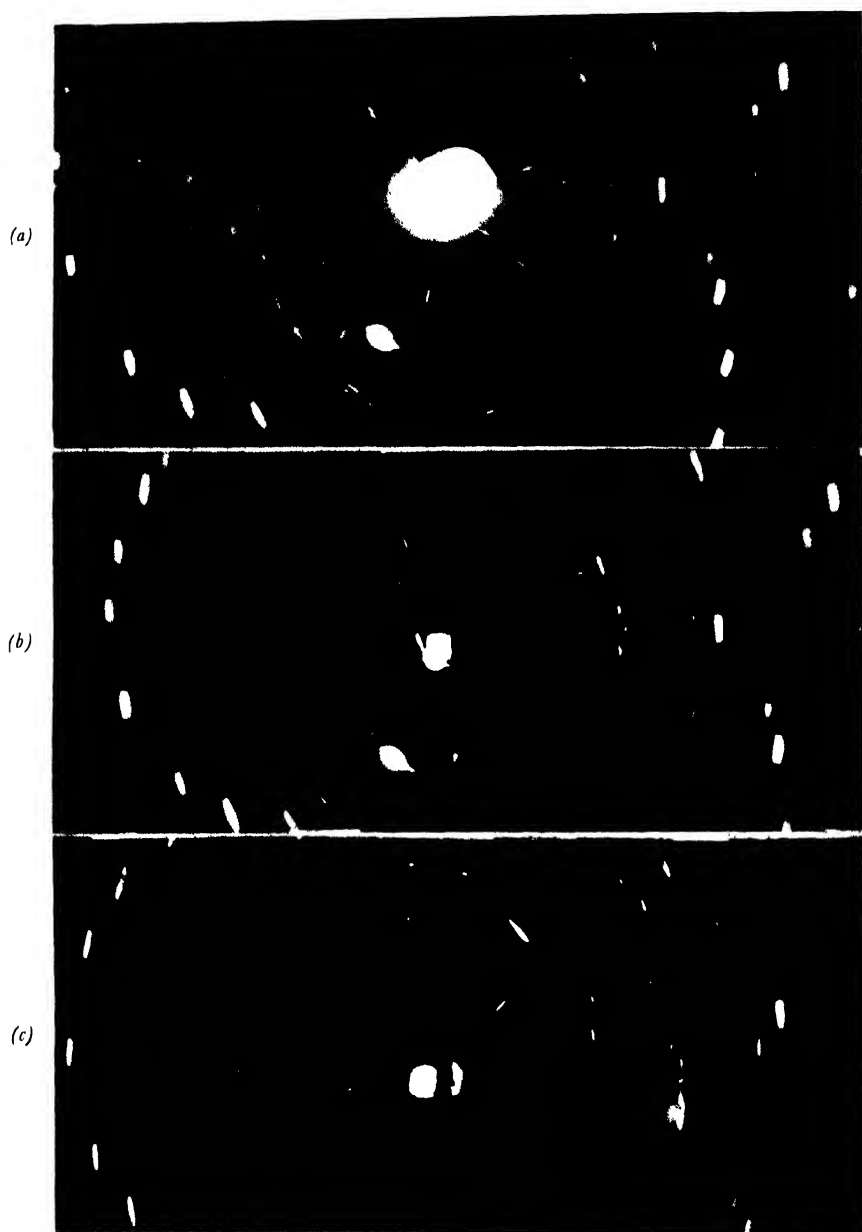


Fig. 3. Diamonds D 7 and D 11. $[110]$ vertical.

(a) D 7 ; $2\theta = 40^\circ 35'$, $\theta + \varphi = 43^\circ 45'$

(b) D 7 ; $2\theta = 49^\circ 40'$, $\theta + \varphi = 43^\circ 50'$

(c) D 11 ; $2\theta = 45^\circ 48'$, $\theta + \varphi = 43^\circ 58'$

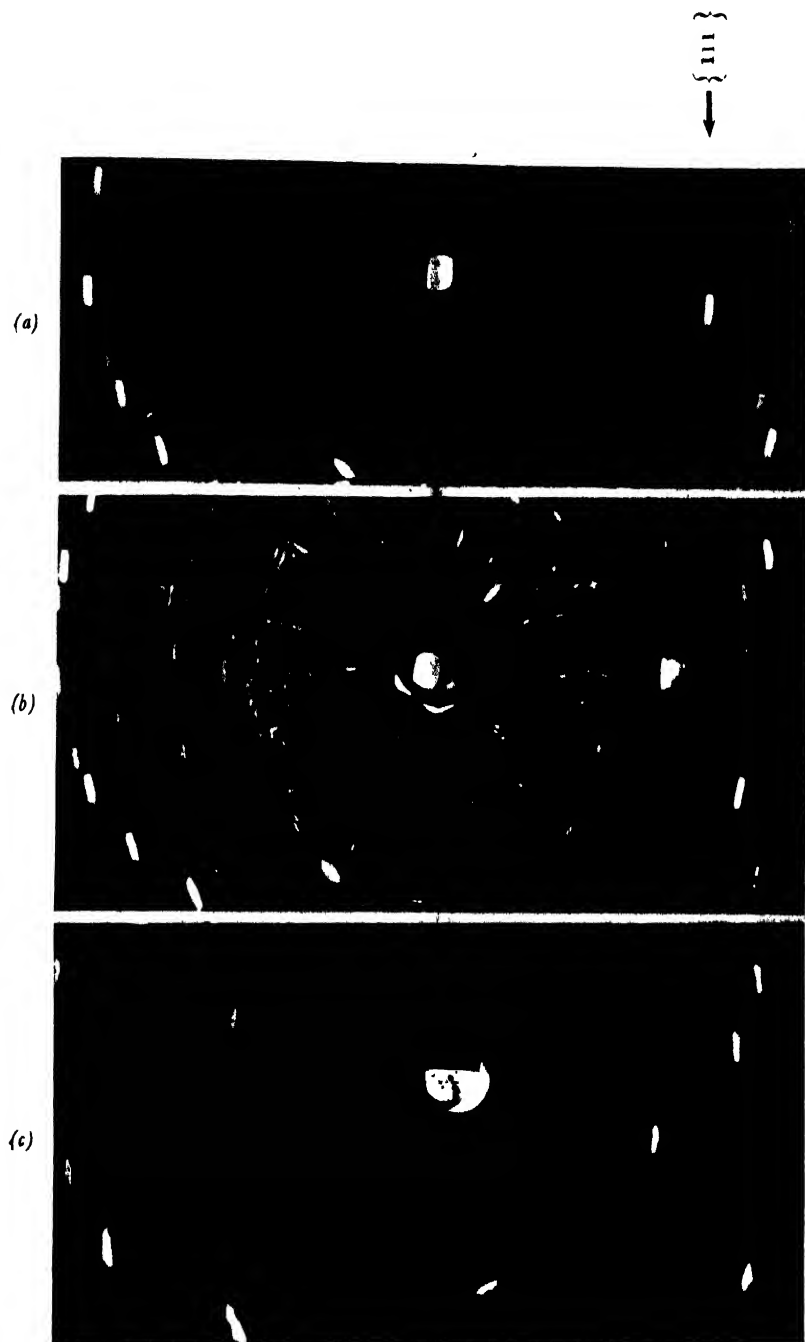


Fig. 4. Diamonds D 8 and D 10. $[\bar{1}10]$ vertical.

- | | |
|--|------------------------------------|
| (a) D 8 ; $2\theta = 47^{\circ}30'$, | $\theta + \varphi = 43^{\circ}52'$ |
| (b) D 8 ; $2\theta = 41^{\circ}33'$, | $\theta + \varphi = 43^{\circ}48'$ |
| (c) D 10 ; $2\theta = 39^{\circ}26'$, | $\theta + \varphi = 43^{\circ}56'$ |

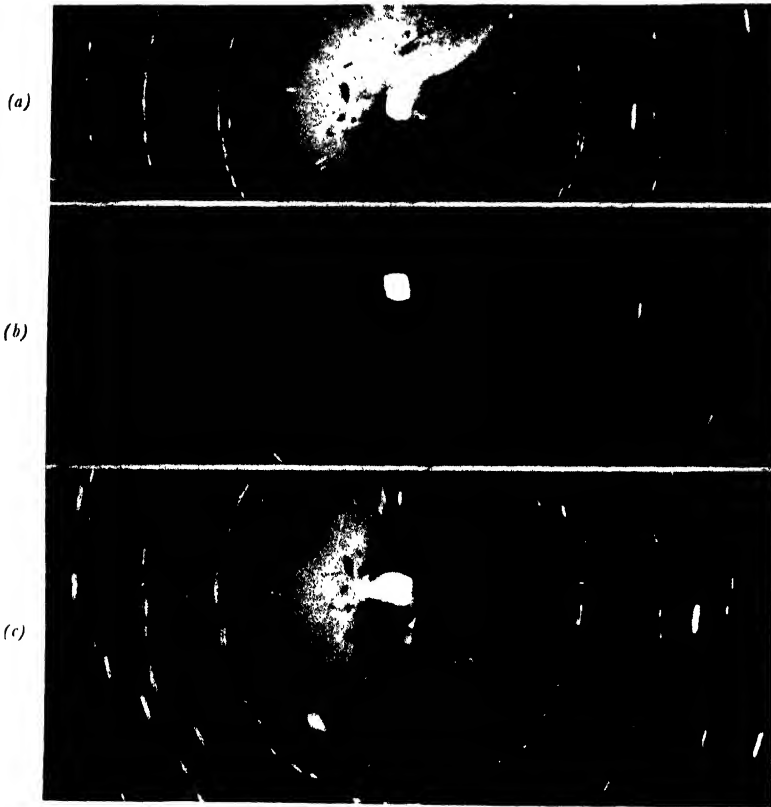


Fig. 5. Diamond D 12. $[110]$ vertical.

- (a) $2\theta = 40^\circ 48'$, $\theta + \varphi = 43^\circ 58'$
 (b) $2\theta = 41^\circ 36'$, $\theta + \varphi = 43^\circ 58'$
 (c) $2\theta = 51^\circ 42'$, $\theta + \varphi = 46^\circ 1'$

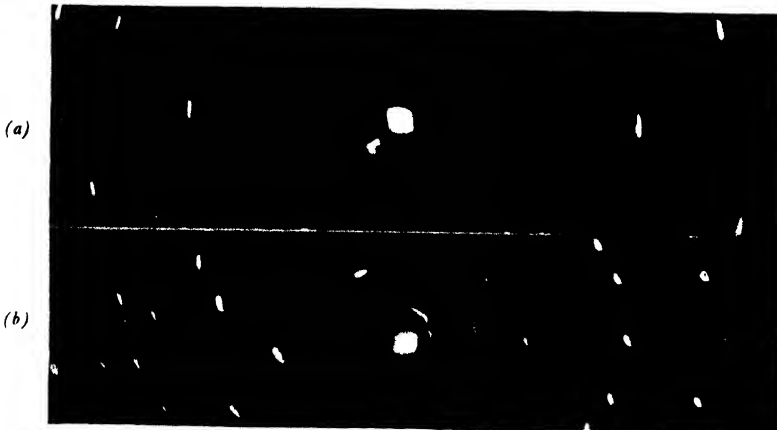


Fig. 6. Diamonds D 13 and D 14. $[110]$ vertical.

- (a) D 13 ; $2\theta = 41^\circ 38'$, $\theta + \varphi = 43^\circ 57'$
 (b) D 14 ; $2\theta = 41^\circ 2'$, $\theta + \varphi = 43^\circ 57'$ (smaller camera)

TABLE II

Specimen No.	2θ	$\theta + \varphi$	Width	Intensity	I_{4156}/I_R	Remarks
D 1	37°39'	42°29'	B and D	w	57/ $K \sim 9.5$	K is an unknown constant. Visual comparison of the spectrograms shows that $K \approx 6$.
	39°20'	42°51'	B and D	m	"	
	42°29'	43°57'	sharp	s	"	
D 4	45°51'	43°51'	B and D	w	1	
	39°48'	42°56'	"	v.w.	"	
D 6	38°9'	42°45'	B	v.w.	54/ $K \approx 9$	
D 7	39°35'	43°42'	sharp	w	5.2	
	40°35'	43°45'	"	m	"	
	49°40'	43°50'	"	m	"	
D 8	36°37'	42°34'	sharp	w	1.5	
	41°33'	43°48'	sharp	s	"	
	45°44'	43°50'	"	s	"	
	47°30'	43°52'	"	s	"	
	51°10'	43°57'	B	m	"	
D 9	41°36'	43°58'	B	m	9.26	
	37°32' (sharp)	41°58'	B	v.w.	"	
D 10	39°26'	43°56'	B	w	8.4	
	41°58'	43°59'	sharp	m	"	
	47°54'	44°58'	sharp	m	"	
	35°49'	43°38'	V.B.	v.w.	"	
D 11	42°9'	43°58'	B	s	7.1	
	41°22'	43°58'	B	w	"	
	47°12'	43°58'	B	v.w.	"	
	45°48'	43°58'	sharp	strong	"	
D 12	40°48'	43°38'	B	s	3.8	
	45°51'	44°0'	B	v.s.	"	
	51°42'	46°1'	sharp	w	"	
	35°45'	43°3'	B	w	"	
	41°36'	43°28'	sharp	s	"	
		43°56'	"	m	"	
	41°8'	43°3'	sharp	s	"	
D 13		43°58'	"	m	"	
	41°36'	43°57'	B	w	0	
	42°43'	43°59'	sharp	m	"	
	41°0'	43°17'	B	w	"	
D 14	36°51'	43°26'	B	v.w.	6	
	41°2'	43°57'	B	w	"	

only when there is mosaicity in the crystal and in a small volume of the crystal the $\{111\}$ planes make a small angle with those planes in the major portion of the crystal. Some of the specimens, however, give extra reflections in other directions and these cannot be attributed to mosaicity of the crystals.

It can clearly be seen, however, from the data given in Table II that neither the mosaicity of the crystal indicated by the presence of extra reflection in the direction making the angle $43^{\circ}56'$ with the incident rays nor the intensity of the extra reflection in other directions can be correlated with the intensity of the fluorescence band at 4156 \AA . The intensity of this band is very small in the case of D 4, and D 13 does not exhibit this band at all, but the extra reflection due to mosaicity is present in both the cases. Also the intensity of the band due to D 8 or D 12 is much smaller than that of the band due to any of the crystals D 7, D 9 and D 10, but the extra reflections due to mosaicity given by D 8 and D 12 are much stronger than those given by the latter crystals. As regards the extra reflection in other directions it is absent in the case of D 11 and D 7, but the intensity of the fluorescence band is large. Also, the extra reflections due to D 6 and D 14 are very weak, but the fluorescence band is very strong. On the other hand, D 13 does not show any fluorescence at 4156 \AA , but it shows weak extra reflections in the direction $43^{\circ}17'$. It is thus evident that the fluorescence band and the extra reflections are produced by two entirely different causes.

It was pointed out by Bishui (1952) that the fluorescence band at 4156 \AA is produced by a particular type of impurity which produces two ultraviolet absorption bands at 2360 \AA and 2363.5 \AA respectively. The results obtained in the present investigation show that the amount of these impurities does not depend on either the partial mosaicity of the crystal or on the irregularities which produce extra reflections in directions other than that making an angle $2\theta_B$ with the incident rays. It was also pointed out by him that other impurities which are not responsible for the production of the fluorescence band at 4156 \AA are present in most of the specimens of diamond and produce a shift in the ultraviolet absorption limit towards longer wavelengths. As D 13 produces weak extra reflections due to partial mosaicity as well as those due to other irregularities and is a specimen of diamond containing absolutely no impurity, it is evident that the defects in the structure mentioned above does not depend much on the presence of impurity, but it appears from Tables I and II that any kind of impurity tends to enhance the formation of mosaic blocks in the crystal. It might be pointed out that the extra reflection in directions other than that making an angle $2\theta_B$ with incident rays observed in the present investigation cannot be attributed to thermal scattering, because these are very weak in the case of some of the crystal such as D 8 and D 11 and are present with large intensities in other cases e.g., D 1, D 10 and D 12. Also, these intensities cannot be correlated with the thickness of the crystals. These extra reflections may be due to permanent irregularities in the

spacing along cube edges, as pointed out by Guinier (1952). It is quite clear from the data given in Table II for D 12 that both partial mosaic structure and the irregularities in spacing can be present simultaneously in a single specimen. This particular specimen is a thin triangular plate of thickness 0.647 mm and it is observed that with gradual increase in the disorientation from the Bragg angle the two sharp reflections corresponding to the mosaic structure and the other type of irregularity are gradually separated from each other, and when 2θ is diminished to $35^{\circ}45'$ the intensities of both these reflections diminish abruptly. So, the fraction of the volume in which the $\{111\}$ planes make an angle of about $4^{\circ}5'$ with these planes in the rest of the volume is very small. It is found that in most of the specimens, this angle lies within 3° . The partial mosaic structure indicated above is different from the mosaic structure indicated by divergent-beam photography. In the latter case the orientation of the planes varies gradually and continuously within narrow limits throughout the whole volume of the crystal, so that all the rays in the incident X-ray beam making a small angle upto about 1° or 2° with each other are reflected by the planes satisfying Bragg condition. In the present case the crystals showing weak reflections due to mosaic structure possess such mosaic blocks only in small parts of the whole volume.

Finally, it may be pointed out that these conclusions are generally in agreement with those drawn by Grenville Wells (1952) who studied only the integrated intensities of the total fluorescent light and the intensities of the extra reflections without giving their actual directions. Probably some of the extra reflections observed by her in the case of the diamonds giving good divergent-beam X-ray photographs were actually in the direction making an angle $2\theta_B$ with the incident rays. As regards the intensities of fluorescence given by her in Column (3), these are indicated as zero in the case of many of the diamonds showing ultraviolet absorption limit longer than 2400 \AA . It is doubtful whether the intensities of the fluorescence band 4156 \AA is zero in all these cases, because previous workers have observed the fluorescence band in the case of all crystals having such absorption limits in the ultraviolet region.

REFERENCES

- Bishui, B. M., 1950, *Ind. J. Phys.*, **24**, 441.
Bishui, B. M., 1952, *Ind. J. Phys.*, **26**, 347.
Champion, F. C., 1952, *Proc. Phys. Soc. London B.*, **65**, 465.
Grenville-Wells, H. J. 1952, *Proc. Phys. Soc. London B.*, **65**, 313.
Guinier, A., 1942, *C. R. Acad. Sci.*, **215**, 114.
Lonsdale, K., 1942, *Proc. Phys. Soc. London A.*, **54**, 314.
Lonsdale, K., 1948, *Phil. Trans. Roy. Soc. A.*, **240**, 219.
Lonsdale, K. and Smith, H., 1941, *Nature*, **148**, 112, 257.

POLARIZATION OF THE ECHOES FROM THE IONOSPHERE*

J. K. D. VERMA AND R. ROY

INSTITUTE OF NUCLEAR PHYSICS, CALCUTTA

(Received for publication, December 15, 1955)

Plates IIA & IIB

ABSTRACT. Some experimental studies on the polarization characteristics of the echoes from the ionospheric layers have been presented. The details of an improved type of radio polarimeter which can work in conjunction with a high resolution radio sonde equipment have been described. The high resolving limit of the equipment made it possible to record the true polarization patterns of the echoes due to normal reflection and those due to irregularities in the ionized regions. A method has been indicated for the identification of the thin layer type of E_s echoes from other types on the basis of their polarization characteristics.

1. INTRODUCTION

The experimental study of the polarization of echoes from the ionosphere, had started as early as in 1932 (Appleton and Watson-Watt, 1932) for a correct identification of the magneto-ionically split waves. For the delineation of the true polarization patterns of the echoes, it is essential to separate them from each other on the time scale; otherwise due to superposition of the waves, the polarization patterns of the echoes become extremely unstable in character (Martyn, Piddington and Munro, 1937, Eckersley and Farmer, 1945). In case the echoes appear on the type A display, as resolved from one another, the character of their polarization is studied, now-a-days, by the method of echo-selection, originally evolved by Eckersley and Farmer. In case the separation between the pair of echoes falls below the resolving limit of the equipment, attempts are made to suppress one component echo by monitoring the nature of polarization of the transmitted beam. Morgan (1952, 1953) at Hanover, New Hampshire, utilized an equipment in which the transmitted beam was elliptically polarized; he found that any of the interfering pairs of echoes could be eliminated completely if the transmitted beam had an elliptical polarization with a sense opposite to that of the particular echo. The suppression of one of the interfering waves makes it possible to record the steady polarization pattern of the other echo.

Mention may be made here of some experiments on the polarization of the reflected waves from the E-layer at low frequencies (Benner and Nearhoof, 1950, Kilpatrick, 1952). Kilpatrick recorded the polarization patterns of the echoes at 160 Kc/sec; he found that whenever the echo became elongated, the leading and lagging portions of the echo envelope showed patterns with opposite sense

* Communicated by Prof. M. N. Saha, F.R.S.

of rotation. The presence of an echo with a right handed sense of rotation rendered the polarization pattern unsteady, i.e. the pattern changed from left handed elliptical, linear to right handed elliptical shapes cyclically. Watts (1952) utilized a pulse transmitter emitting waves of circular polarization at 160 Kc/sec, and found that specially during the disturbed nights, the polarization pattern of the echo showed similar instability, possibly due to the superposition of several reflections from the E-layer occurring simultaneously.

From the above review of the extant works, it is apparent that the success of the polarization measurements depends to a marked extent on the resolving power of the equipment. For obtaining the true polarization patterns of the echoes, it is desirable to utilize an equipment with higher resolving power. An improved type of radio polarimeter, which can operate in conjunction with a high resolution radio sonde equipment, and the typical polarization patterns of the echoes from the ionospheric layers will be described in this paper.

2. SOUNDING EQUIPMENT

The ionospheric sounding equipment (Banerjee and Roy, 1952) which is in operation at the Institute of Nuclear Physics, Calcutta, has a resolving limit of 2 Km. only. A 50 K.W. pulse transmitter radiates R/F pulses of 6-30 μ secs duration with the help of a terminated vertical delta antenna. The echo-signals are picked up by a pair of horizontal dipole antennas situated on the top of the antenna mast (140 feet above the ground level) and after pre-amplification they are fed to a superhetrodyne receiver of 90 Kc/sec bandwidth. These echoes are displayed on a raster time base (Banerjee and Roy, 1950) of twelve lines; each line of which corresponds to 50 Km. of equivalent height.

The use of a short duration pulse helps in separating the magneto-ionic component echoes from each other, even when the operating frequency of transmission is sufficiently away from the penetration frequency of any of the ionized layers. Also it is possible to separate these normal echoes effectively from the back-scattered echoes (Roy and Verma, 1953), from electron clouds or from the echoes due to other types of irregularities in the ionized region.

3. THE RADIO POLARIMETER

The radio polarimeter utilized, follows in principle, a design similar to that evolved by Eckersley and Farmer. The method of operation of the polarimeter has been outlined in the block diagram in figure 1. The signal received at vertical incidence is picked up by a pair of crossed loop antennae, the planes of the loops being oriented in the N-S and E-W directions respectively. Each arm of the loop is of length one metre which is small compared to the operating wavelengths. The loop antennae assembly is housed in a hut on the topmost part of the institute building at a height of 70 ft. from the ground level, fairly away from the proximity of other conductors. Each individual loop, whose centre is grounded, is

tuned by means of a variable double-ganged condenser operated with remote control selsyns. The signal from each loop is fed directly to a wide-band pre-amplifier (figure 2). The amplified signal from the pre-amplifier for each loop is fed through

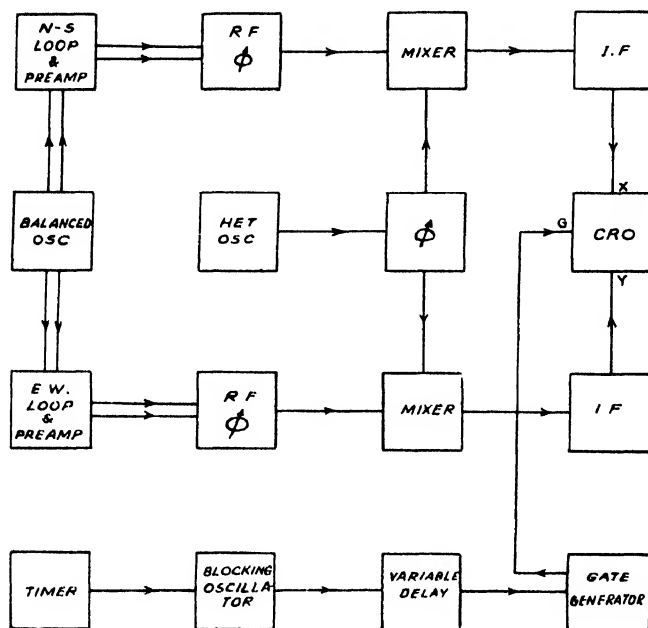


Fig. 1. Block diagram of the radio polarimeter.

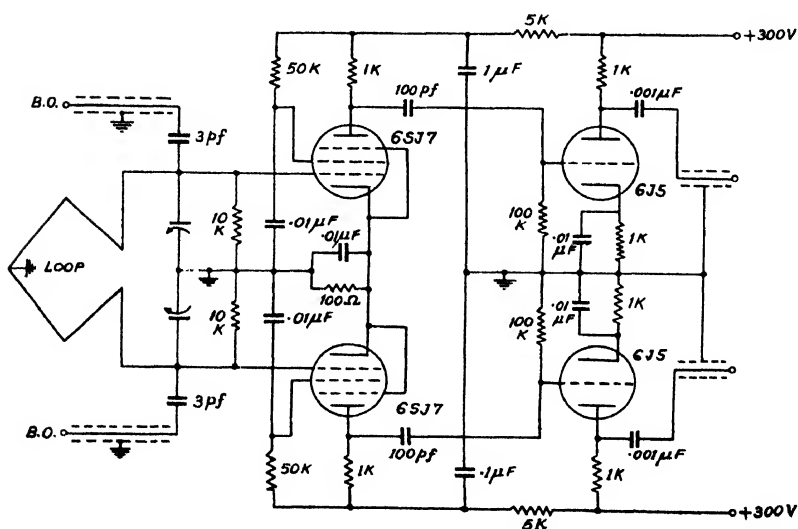


Fig. 2. Pre-amplifier.

equal lengths of shielded co-axial cables to the input of a receiver (figure 3). The centre of the input coupling coil is grounded, and the first stage of the receiver is a push-pull RF amplifier. These circuit arrangements ensure perfect balancing of the signal leads from the loops with respect to ground.

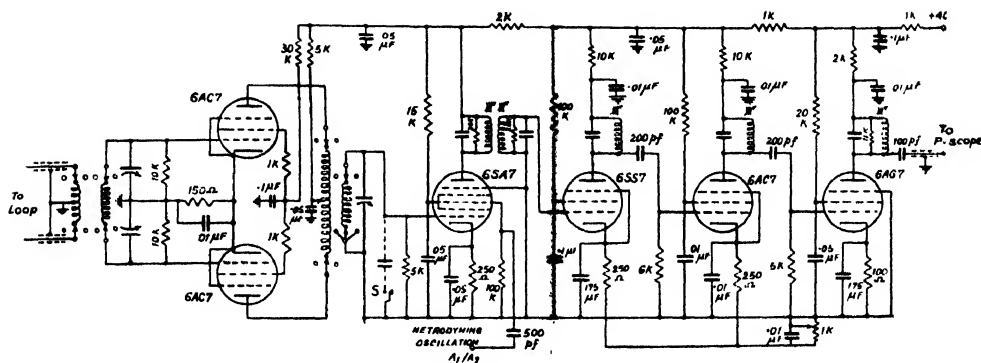


Fig. 3. Receiver.

The two receivers, one for the N-S and another for the E-W channels, are identical in operation and design: each has a maximum gain of 120 db. and a minimum overall bandwidth 50 Kc/sec., the intermediate frequency being 1.2 Mc/sec. The signal circuits are designed for a frequency range 2.8 Mc/sec. to 6.3 Mc/sec. and the number of turns in each loop is selected according to the operating frequency. A common oscillator (figure 4) feeds the heterodyning signal through an adjustable phase-shift network. The output from the final I/F stages of the receiver is applied through small lengths of shielded co-axial cables to the quadrature plates of the oscilloscope (*P-Scope* figure 5). The oscilloscope circuit

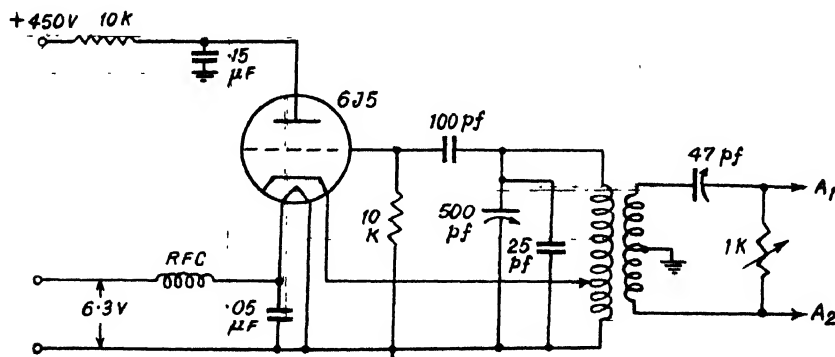


Fig. 4. Common heterodyning oscillator.

is so arranged that the beam of the tube remains blanked for the whole repetition period (20 milliseconds) except for a short duration of 8 microseconds. The

control) and a 100 kilo ohm (fine control) potentiometers and a set of capacitors connected to the grid of the second half of the tube 6SN7(V_2). The square wave is then differentiated, and the differentiated output is applied to a biased amplifier V_3 , which gives a positive spike synchronous with the trailing edge of the delay multivibrator output. This spike again triggers the gate generator V_4 —a cathode coupled multivibrator, delivering an output of 150 volts and of duration 8 microseconds only. This positive gate pulse is then led through a cathode follower V_5 and applied to the grid of the cathode ray tube 89D (figure 5). The time constant of the grid circuit of the CRT is kept large compared to the gate pulse duration, as otherwise the intensification of the beam occurs for a shorter interval. A small part of the gate pulse obtained from a capacity divider network at the cathode of V_5 is also applied to the Y -deflection plate of the cathode ray tube 09J for type A presentation. Thus, by monitoring the controls of the delay multivibrator, the gate pulse can be so adjusted that it occupies the central part of any echo (figure 7) appearing on the second or higher lines of the raster time base.

For calibrating the two receiving channels for identical phase and equal amplification, a balanced oscillator (figure 8) feeds through twin pair of shielded coaxial cables a small input signal of the order of 50 microvolts at the operating

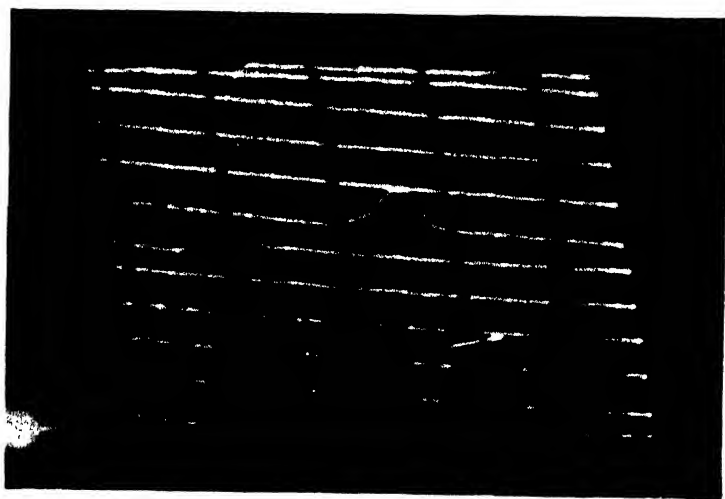


Fig. 7. The gate pulse is on the central part of α -echo on the sixth line of the raster time base. The ground pulse is on the first (lowest) line. The α -echo is on the seventh line.

mid-frequency of the transmitter pulse, through a very small capacity 3 pf to the loops. With proper adjustment of the tuning controls in the two receiving

channels, and the phase-shift network in the heterodyning oscillator, a straight line (figure 9) inclined 45° to N-S direction is delineated on the oscillograph screen;

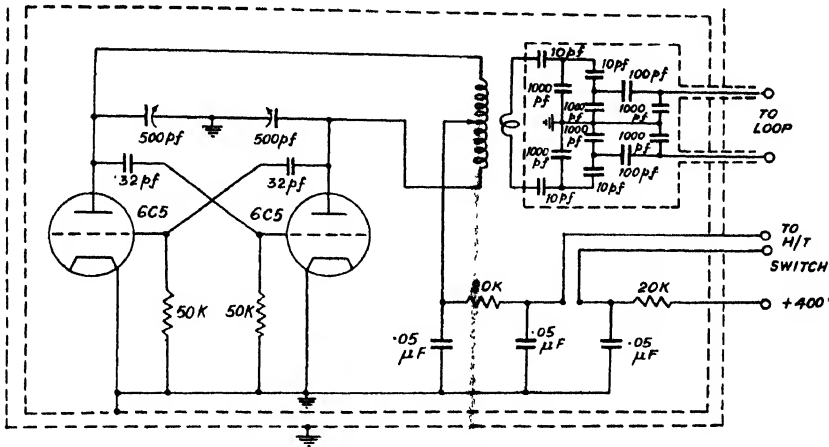


Fig. 8. Balanced oscillator

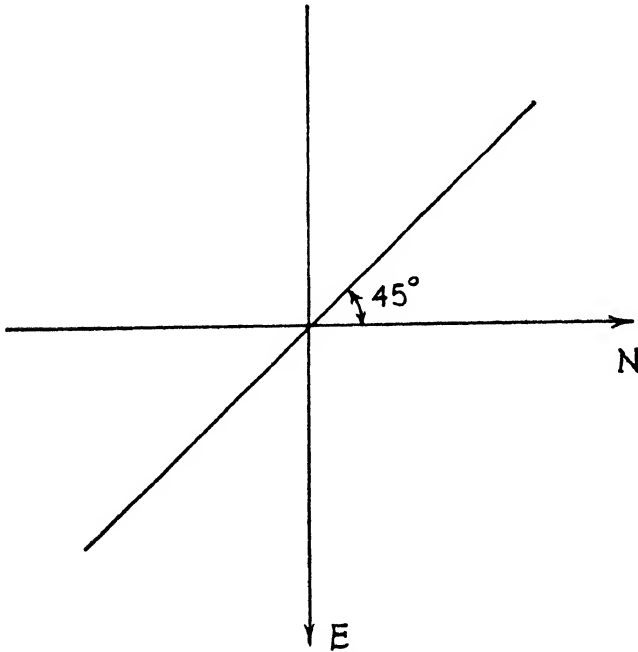


Fig. 9. Orientation of the calibration line.

this indicated the standard reference adjustment for perfect alignment of the two receiving channels. Next, the balanced oscillator H/T is switched off instead of disconnecting the calibrating RF signal-leads from the pre-amplifier inputs, since the latter step has been found to affect the phase adjustment. The above proce-

ture for the calibration of the polarimeter is carried out at each operating frequency.

4. SENSE OF ROTATION

It is well known that for observations at vertical incidence, the phase relation between the electric vector components in the N-S and E-W directions in any echo, will be the same as that obtained in the observed polarization patterns. Any decrease in the phase difference between the two electric vector components will tend to rotate the pattern depending on the sense of rotation of the resultant electric vector in the wavefront. When the resultant electric vector rotates in an anticlockwise direction, it may be seen that a decrease in phase difference will make the polarized pattern rotate in the clockwise direction and vice versa. Reduction of resistance in the phase-shift network of the heterodyning oscillator gives the aforesaid reduction in phase. The reduction in phase relation can be obtained by adjusting the phase-shift network or switching in a small capacity in the single-tuned circuit at the signal grid of the mixer of one receiver. Thus the sense of rotation in the polarization patterns can be inferred by operating the phase change switch (S in figure 3).

5. RESULTS AND DISCUSSION

Polarization patterns of both o - and x -waves from E- and F-layers had been recorded during both day and night for a period of fifteen months—January 1954 to March 1955. Figures 10 (a), (b), (c) and (d), [Plate IIA] show some typical patterns of the normal echoes, the tilt angle (ψ) and the ratio of axes which are given in the (x) of following:

F-layer:

Figure 10 (a)— o -echo, $\psi = 91^\circ$, $x = 0.28$

Figure 10 (b)— x -echo, $\psi = 180^\circ$, $x = 0.47$

E-layer:

Figure 10 (c)— o -echo, $\psi = 101^\circ$, $x = 0$

Figure 10 (d)— x -echo, $\psi = 182^\circ$, $x = 0.43$

The detailed description of the ranges in which the characteristics of these patterns vary, have been reported elsewhere (Roy and Verma, 1955).

The senses of rotation of the o - and x -ellipses were observed to be opposite in general, the o -wave having the counter-clockwise sense of rotation. But occasionally when the x -wave patterns appeared in the N-W quadrant, but the o -wave pattern remained in the N-E quadrant [Figure 11 (a) and (b)], the x -wave was found to have the same sense of rotation as that of the o -wave. On some occasions, though rare, both o - and x -ellipses, were found to lie in the N-W quadrant [figure 12 (a) and (b)]; the sense of rotation of both the waves were always similar (anti-clockwise) under such anomalous conditions. These tend to

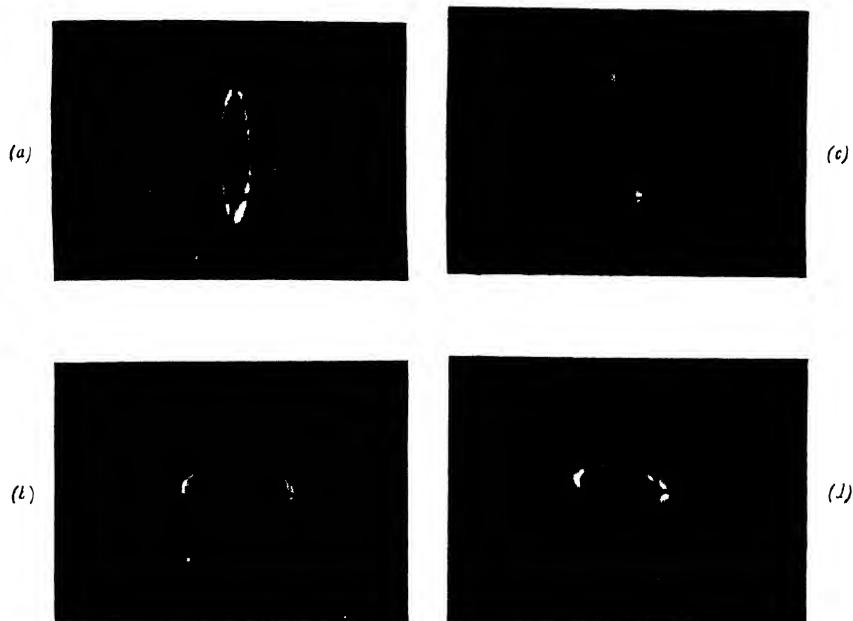


Fig. 10. (a) Pattern of α -echo from F -layer

$\psi = 91^\circ$, $x = 0.28$
(b) Pattern of α -echo from F -layer
 $\psi = 180^\circ$, $x = 0.47$

(c) Pattern of α -echo from E -layer

$\psi = 101^\circ$, $x = 0$
(d) Pattern of α -echo from E -layer
 $\psi = 162^\circ$, $x = 0.43$

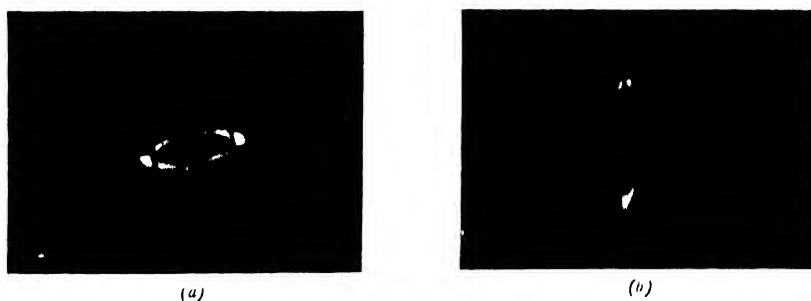


Fig. 11

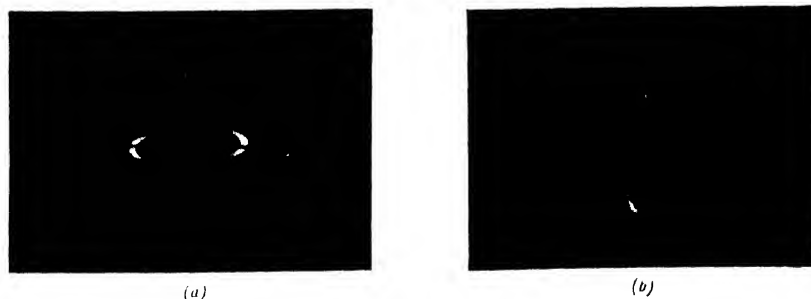


Fig. 12

Fig. 11. (a) The α -ellipse in $N-E$ quadrant

$\psi = 92^\circ$, $x = 0.24$

(b) The α -ellipse in $N-W$ quadrant
 $\psi = 6^\circ$, $x = 0.31$

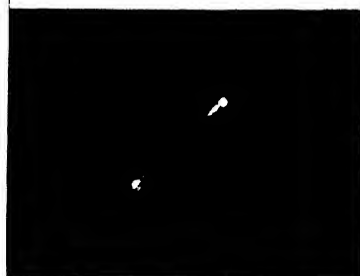
Fig. 12. (a) The α -ellipse in $N-W$ quadrant
 $\psi = 85^\circ$, $x = 0.25$

(b) The α -ellipse in $N-W$ quadrant
 $\psi = 2^\circ$, $x = 0.33$

(a)



(b)



(c)



(d)



(e)



Unsteady patterns of an echo from a thin layer type of E_3 recorded at half-a-minute intervals.

(a) $\psi = 34^\circ$,	$x = 0.33$
(b) $\psi = 41^\circ$,	$x = 0$
(c) $\psi = 79^\circ$,	$x = 0.09$
(d) $\psi = 101^\circ$,	$x = 0.39$
(e) $\psi = 114^\circ$,	$x = 0.18$

show that the method of identification of a substratification within a layer from the observed similar sense of rotation in the polarization patterns of twin echoes from the same layer is doubtful.

In a broad type of echo, which owes its origin to different retardation of the component frequencies of the short duration RF exploring pulse, the leading and lagging portions of the echo-envelope never showed any polarization pattern. However large the base-width of the echo may be, its pattern could be obtained only when the selecting gate pulse is monitored to the centre of the echo-envelope. Mixed type of polarization detected by Kilpatrick in an elongated echo appears to be due to the presence of both *o*- and *x*-echoes with a separation smaller than the resolving limit of the equipment.

It has already been described that the high resolution offered by the sounding equipment made it possible to separate the scattered echoes from the normally reflected echoes. The scattered echoes fluctuate in intensity and persist for a few minutes only, whereas the reflected echoes are fairly steady. These fluctuating echoes from both E- and F-layers had also been selected and studied for the determination of their polarization characteristics. Detailed investigations throughout the period of observation showed that the back-scattered echoes from the electron clouds are completely unpolarized in character; they do not exhibit any polarization pattern at all. There is, however, another type of E_s , the thin-layer type of irregularity, which differs in the polarized character from those of the normally reflected echoes. The pattern obtained from this type of sporadic E_s shows an extremely unsteady character i.e., the pattern continuously changes from circular, elliptic to linear forms and does not orient itself in any quadrant steadily even for a minute. Plates IIB, (a)—(e) are a set of five records (at 0800 hrs. IST on 6.12.54 at 3.1 Mc/sec) of varying polarization patterns of an echo from a thin layer, taken at half-a-minute intervals; the varying values of the tilt-angle and the ratio of axes of the records illustrate the unsteadiness of the patterns. A similar unsteady pattern is obtained whenever the normal *o*- and *x*-echoes interfere i.e. when the separation between the component echoes falls below 4 Km. The similarity of these two cases of unsteady polarized character tends to suggest that the thin layer type of E_s reflects both the magneto-ionic components.

Thus the studies on the polarization of the echoes with an equipment of high resolving power offers an easy method for the identification of the thin layer type of E_s from the electron cloud type of irregularities or the normal echoes, since the characters of polarization of these echoes are different from one another.

The polarization of the normally reflected echoes were observed to remain steady throughout the day and the night except during the sunset hours. At the time of sunset, even though each individual echo remains resolved from other echoes, the polarization of each echo assumes an unsteady character, i.e., the pattern varies from linear, elliptical to circular forms at random. Such varying

patterns are found for both o - and x -echoes from both E-and F-layers, and the unsteadiness of the patterns persists for about one to two hours around sunset.

It may be mentioned here that it is possible to determine the magnitude of the collision frequency of the electrons in the ionized layer from the tilt angle and the ratio of axes of any of the normal echo-patterns (Roy and Verma, 1955). This is possible from an analysis of the data of the patterns—carried out on the basis of the wave theory of propagation (Saha, Banerjee and Guha, 1951) of the c.m. waves for vertical propagation in the ionosphere.

ACKNOWLEDGMENTS

The authors wish to record their heartfelt gratitude to Prof. M. N. Saha, D.Sc., F.R.S., for his keen interest and continued guidance. Grateful thanks are also due to Sri B. M. Banerjee for his kind suggestions and helpful discussions.

REFERENCES

- Appleton, E. V. and Watson Watt, R. A., 1932, *Wireless World*, July 8, 17.
Banerjee, B. M. and Roy, R., 1950, *Ind. J. Phys.*, **24**, 411.
Banerjee, B. M. and Roy, R., 1952, *Ind. J. Phys.*, **26**, 473.
Benner, A. H., and Nearhoof, H. J., 1950, *Rev. Sci. Instrum.*, **21**, 830.
Eckersley, T. L. and Farmer, F. T., 1945, *Proc. Roy. Soc. A.*, **184**, 196.
Kilpatrick, E. L., 1952, *J. Geophys. Res.*, **57**, 221.
Martyn, D. F., Piddington, J. H. and Munro, J. H., 1937, *Proc. Roy. Soc. A.*, **158**, 536.
Morgan, M. G., 1952, Proceedings of the General Assembly of the URSI at Sydney on Aug. 11-21, p. 97; Ionospheric Research Technical Report No. 4 of Dartmouth College, Hanover, New Hampshire, Jan. 1, 1952.
Morgan, M. G., 1953, "Polarization observations at Dartmouth College with twin-channel transmitting and receiving equipment of MF ionospherically reflected pulse signals at vertical incidence"—presented at Joint URSI -IRE meetings, National Bureau of Standards, Washington, on 27-30 April.
Roy, R. and Verma, J. K. D., 1953, *J. Geophys. Res.*, **58**, 473.
Roy, R. and Verma, J. K. D., 1955, *J. Geophys. Res.*, December issue.
Saha, M. N., Banerjee, B. K. and Guha, U. C., 1951, *Proc. Nat. Sci. India.*, **17**, 205.
Watts, J. M., 1952, *J. Geophys. Res.*, **57**, 221.

REVIEW

BETA- AND GAMMA-RAY SPECTROSCOPY. Edited by Kai Siegbahn. Pp i-xxiii + 959. North Holland Publishing Company, Amsterdam. 1955. Price £7. 12. 0.

This book is a comprehensive treatise on the theory and experimental methods of the study of β - and γ -ray spectra. Besides the introduction written by the Editor himself, there are altogether 26 chapters and 8 appendices written by different specialists working in these lines. The very fact that the Editor has secured the cooperation of an international team of 42 such specialists in writing the different chapters clearly indicates his attempt to incorporate in the treatise authoritative treatments of the different problems in the theoretical and experimental domains of this subject, and even a brief survey of the different chapters will convince the reader that the Editor has been thoroughly successful in this attempt.

The introduction contains a brief but masterly survey of some of the main experimental methods and of the conclusions drawn from the experimental results.

The first chapter contributed by W. Paul and H. Steinwedel and the second chapter written by C. M. Davisson deal respectively with the interaction of β -electrons and γ -rays with matter. The existing theories have been discussed and the experimental results have been compared with those deduced theoretically in these two chapters. The theories and design of different types of β -ray spectrometers have been discussed by K. Siegbahn in Chapter III. This chapter extending over 47 pages includes beautiful diagrams and reproductions of some spectra recorded on photographic plates and also by automatic recording system. The fourth chapter dealing with crystal diffraction spectroscopy of nuclear γ -rays has been written by J. W. M. Dumond whose own contributions in this line are well known. The scintillation method has been discussed by P. R. Bell in the fifth chapter using 33 diagrams to illustrate the observed results. The sixth chapter has been contributed by four writers. S. C. Curran has dealt with proportional counter spectrometry, H. Bulbright has discussed the use of a high pressure proportional counter in β -ray spectroscopy and G. Bishop and R. Wilson have discussed some special methods in γ -ray spectroscopy, such as measurement of photoneutron and photoproton energies. In Chapter VII A. C. G. Mitchell has discussed the methods of counting coincidences between beta-rays and gamma-rays or between two γ -rays, and application of the method in the measurement of internal conversion electrons, determination of efficiency of γ -ray counters, etc. In the next chapter he has dealt with the investigations of disintegration schemes and H. Slätis has discussed various methods of preparing sources for beta-ray spectroscopy and the thin films on which these sources are spread. M. E. Rose has given in brief the theory of allowed β -decay in Chapter IX and the theory of internal conversion in Chapter XIV. The theory of forbidden β -decay has been

given by E. Konopinsky in Chapter X. C. S. Wu has described experiments on shapes of β -spectra due to allowed and forbidden transitions in Chapter XI and in the next chapter O. Kofoed-Hansen has described some experiments on recoil of neutrino and has discussed the significance of the results.

The theory of multipole radiation has been investigated in detail by S. A. Moszkowski in Chapter XIII. The shell model of the nuclei has been discussed in detail by J. H. D. Jensen in Chapter XV. In the next chapter M. Goeppert-Mayer has dealt with classification of β -transitions including a table giving spin of the daughter nuclei, half life, branching ratio etc. In the same chapter M. Goldhaber and A. W. Sunyar have discussed the classification of nuclear isomers. Unified nuclear model has been discussed by A. Bohr and B. R. Mottelson in Chapter XVII. Measurement of short life times of excited states by delayed coincidence methods has been discussed by R. E. Bell and measurement of such life times by studying the resonant scattering of γ -rays has been dealt with in detail by K. G. Malmfors in Chapter XVIII. The next chapter dealing with angular distribution of nuclear radiation has been contributed by six specialists who have themselves made valuable contributions in this line of research. H. Frauenfelder has covered 68 pages dealing with angular correlation, incorporating in the treatment the theory of γ - γ direction correlation in free nuclei and a general theory of angular correlation. Similarly, α - γ and β - γ directional correlations as well as methods for the determination of several nuclear constants have also been discussed by him. R. J. Blin-Stoyle, M. A. Grace and H. Halban have surveyed the experimental methods used in investigations with oriented nuclei, and the experimental results have been discussed in detail. Finally, S. R. Groot and H. A. Tolhoek have given the theory of angular effects of radiations from oriented nuclei in the same chapter.

In Chapter XX, I. Bergstrom has described in detail the results of investigations on Auger electrons emitted by radioactive atoms and has discussed the significance of the experimental results, R. Wilson has dealt with internal pair formation at different ranges of energy and C. S. Wu has discussed internal *bremsstrahlung*. The next chapter deals with the application of scintillation technique to the study of particular problems. Discussions on the application to the study of the Compton effect by P. E. Cavanagh, on the usefulness of the technique in a search for double β -decay by H. Fulbright and on its use in the study of annihilation of positrons by S. de Benedetti, R. E. Bell and M. Deutsch have been incorporated in this chapter.

Some typical results of investigations on the artificial disintegration of nuclei have been discussed in Chapter XXII by R. E. Bell, D. E. Alburger, A. C. G. Mitchell and P. Preiswerk and in the next chapter N. Feather has dealt with β - and γ -disintegration of some heavy radio elements with Z greater than 80. The next two chapters are devoted to γ -radiation. D. E. Alburger has discussed the γ -radiation observed in charged particle reactions and B. B. Kinsey has discussed the emission of γ -rays after neutron capture. Measurement of disintegration rate has been discussed in Chapter XXVI by J. L. Putman.

In Appendix I, M. Davisson has given absorption coefficients of various elements for photon of energies ranging from .01 Mev. to 100 Mev. The other appendices compiled by different workers give Fermi functions, forbidden β -decay functions, internal conversion coefficients, values of some parameters used in directional correlation, critical X-ray absorption energies, details of β -ray spectra of some elements and values of $B\rho$ for different values of Kev.

It can be easily seen from the summary of the contents given above that the treatise under review will be useful as a valuable book of reference not only to research workers, but also to post-graduate students interested in nuclear physics. Of course, the price is beyond the reach of students of average means, but considering the fact that the number of figures exceeds 400 and the number of pages 1000, the price is found to be only moderate.

S. C. S.



Professor Meghnad Saha, F.R.S.

Born—October 6, 1893

Died—February 16, 1956

OBITUARY

Professor Meghnad Saha

The sudden death of Professor Meghnad Saha at about 10 a.m. on the 16th February this year under tragic circumstances has snatched away from our midst one of the most distinguished scientists of the world. Only two years ago his 60th birthday was celebrated by his students, friends and admirers in India and the messages, which were received on that occasion and were published by the Sixtieth Birthday Committee in his biography, show that he had won the affection not only of his friends in India but also of many distinguished scientists of foreign countries. His unexpected death, taking place so soon after the celebration of the 60th birthday will, therefore, be mourned deeply by his friends all over the world.

EARLY CAREER

Professor Meghnad Saha was born on the 6th October, 1893 as the fifth child to his parents Sri Jagannath Saha and Srimati Bhubaneswari Debi who belonged to a middle class family in the village Seoratali situated at a distance of 30 miles to the north of Dacca in East Bengal. He got his early education first upto 1905 in a Middle English School in a village about seven miles away from his native village and then in the Dacca Collegiate School and he passed the Entrance Examination in 1909, standing first among those who appeared from East Bengal. He passed the Intermediate Examination in Science in 1911 from Dacca College and shifted to Presidency College, Calcutta for higher studies. He passed the B.Sc. Examination with First Class Honours in Mathematics in 1913 and secured a First Class M.Sc. degree in Applied Mathematics in 1915.

EARLY RESEARCH WORK

Saha was selected as a Lecturer in Mathematics of the Calcutta University when Sir Asutosh Mookerjee, who was then the Vice-Chancellor of

the University, started Post Graduate teaching in science at the University. He was transferred to the Department of Physics in 1917. Besides organising the laboratory and courses for the M.Sc. degree, he started research work on theoretical and experimental physics, and even in 1917 he could publish a paper entitled 'On Maxwell's Stresses' in the *Philosophical Magazine* and another paper entitled 'On the limit of Interference in the Febry-Perot interferometer' in *Physical Review*. Next year, he published three papers dealing respectively with experimental verification of pressure of light, a new theorem in elasticity, the dynamics of the electron, and another paper jointly with Professor S. N. Bose giving a new equation of state which was an improvement upon Dietrici's. He was admitted to the D.Sc. degree of the Calcutta University in 1918 for his thesis which included besides the papers mentioned above also results of other investigations on—(a) Fundamental law of electrical action, (b) Radiation pressure and quantum theory and (c) Selective radiation pressure and its applications. Of these the last paper was published locally in 1919, but the other two papers and also a third paper on the mechanical and electrodynamical properties of the electron were published in foreign journals in 1919.

He was married to Srimati Radharani Saha (née Roy) in June, 1918.

THE THEORY OF THERMAL IONIZATION

Professor Saha left for a study tour in Europe in 1919, but before sailing for London he communicated the paper entitled "On ionization in solar chromosphere" for publication in *Philosophical Magazine*. Saha's famous equation of thermal ionization was given in this paper and it came out in the journal in 1920 after he had reached England. The importance of this discovery can be judged from the statements made by some of the famous astrophysicists in their messages sent on the occasion of his 60th birthday anniversary in 1953. Dr. Harlow Shapley of Harvard College Observatory says :

"The Harvard College Observatory owes much to Professor Meghnad Saha. His pioneer work of thirty years ago on temperature ionization in sun and stars inspired the activities of the British scientists which in turn inspired the work here at Harvard of Mrs. Cecilia Payne Gaposchkin, Donald H. Menzel and Frank Hogg; and their work established modern astrophysics at Harvard."

Dr. H. Spencer Jones, Astronomer Royal, Royal Greenwich Observatory, Sussex writes :

"I well remember how on the publication of his early and important paper on ionization in stellar atmosphere the late Professor Alfred Fowler

drew my attention to it and emphasized its fundamental importance. And so it proved, for this paper was the stimulus to the work of Milne, R. H. Fowler and others in subsequent years. In fact, almost all work on stellar atmosphere has been based on it either directly or indirectly. The paper provided a new method of attack and opened the way to the solution of many problems that had been puzzling."

Many other renowned scientists, including Professor Niels Bohr and Professor E. Fermi expressed similar views in their messages.

WORK DONE IN ENGLAND AND OTHER COUNTRIES OF EUROPE

Professor Saha worked at the Imperial College of Science & Technology, London, for about a year under Prof. A. Fowler and wrote a paper entitled "On a Physical theory of stellar spectra" which was published in 1921. He then shifted to Prof. Nernst's laboratory in Berlin and started an experiment on the verification of his theory of thermal ionization, but as he was requested by Sir Asutosh Mookerjee to come back to India to accept the post of Khaira Professor of Physics at the Calcutta University, he could not finish the experiment and came back to Calcutta and was appointed Khaira Professor of Physics in November, 1921.

CAREER AT ALLAHABAD

As the financial condition of the Post Graduate Department in Science of the Calcutta University was far from being satisfactory when Professor Saha joined as the Khaira Professor of Physics he could not get any laboratory facilities. Being unable to carry on any experimental work, he resigned the post a year later and joined the Allahabad University as the Head of the Department of Physics. It is at Allahabad that he first gathered around him a band of enthusiastic research workers who shined in their later career. He created there three schools of research, one in spectroscopy, another in ionospheric problems and the third in astrophysics, besides carrying on some experiments on thermal ionization of elements. During his stay of about 15 years (from 1923 upto 1938) at Allahabad, Professor Saha himself published 33 papers either independently or in collaboration with his students, besides a very large number of papers published independently by his students under his guidance in the subjects mentioned above. Professor D. S. Kothari is one of his distinguished students. In recognition of his earlier work Professor Saha was elected a Fellow of the Royal Society of London in 1927 at the age of 34. He left Allahabad to join the post of Palit Professor of Physics of the Calcutta University in 1938.

RECENT CAREER AT CALCUTTA

During the latter part of his stay at Allahabad, Professor Saha began to take interest in the discoveries made in nuclear physics and cosmic rays, and after returning to Calcutta as the Palit Professor of Physics he started reorganising the laboratory for investigations in these lines. In 1939 he published in collaboration with others a paper entitled "On the structure of atomic nuclei" giving a nuclear chart in which all known isotopes are plotted in a $(A - I)$ diagram, A being the atomic weight and I the difference between the number of neutrons and protons. Some of his students started investigations on cosmic rays, and after securing a grant of Rs. 60,000 from the Tata Sons Ltd., he started the work of installation of a 35-inch cyclotron at the University College of Science with the help of Dr. B. D. Nag Choudhury who had been sent to California for training in research in nuclear physics. This Cyclotron Laboratory gradually developed into the Institute of Nuclear Physics which started functioning as an All-India Institute in July 1951. There is also a section of biophysics in this Institute and Dr. N. Das Gupta has been using a Siemens vertical type electron microscope for the study of biophysical problems. First as the Palit Professor of Physics and then as the Honorary Director of the Institute Professor Saha organised research and teaching in nuclear physics in this institute and the workers have made valuable contributions in this line of research. Professor Saha himself also continued theoretical investigations on propagation of radio waves in upper atmosphere, ionosphere and in solar atmosphere.

EXPANSION OF THE ACTIVITIES OF INDIAN ASSOCIATION FOR THE
CULTIVATION OF SCIENCE

Being handicapped by want of proper facilities for research throughout his earlier career, Professor Saha felt the necessity of creating facilities for younger generation. It is well known that although the discovery of the Raman effect was made by Professor C. V. Raman while working in the laboratories of the Indian Association for the Cultivation of Science, the resources of the Association were meagre and it was through the personal efforts of Professor Raman that a donation was received by him for the creation of a professorship at the Association, called Mahendra Lal Sircar Professorship, after the name of the Founder. The recurring annual grants received from the Government was Rs. 10,000/- before the award of the Nobel Prize to Professor Raman and it was raised to Rs. 20,000/- after he was awarded the Nobel Prize. When the first M. L. S. Professor, Dr. K. S.

Krishnan, F.R.S. left the Association just after the bombardment of the city by Japanese planes Professor Saha took initiative in bringing the equipments back from the place of safety to which they had been transferred and in appointing a new M. L. S. Professor (Prof. K. Banerjee). He next felt that the Association was a suitable place for carrying on fundamental investigations in molecular physics and drew up a scheme for the expansion of its activities. In this scheme he proposed to create two new professorships in physics and three professorships in chemistry, and also to erect a new building for providing suitable accommodation for all these laboratories. This scheme was accepted in principle by the Government of India in 1947 and the work under the new scheme started by the end of 1947. It is now generally known that Dr. J. C. Ghosh, one of his most intimate friends helped him in getting the scheme accepted by the Government of India. All the professorships could not be filled up initially owing to want of accommodation till new laboratory buildings were erected at Jadavpur and the Association shifted to its new premises in 1951. Professor Saha was elected President of the Association in 1950. From 1948 to 1951 the Association did not appoint any wholetime Director, but Professor P. Ray, Palit Professor of Chemistry of the Calcutta University, served as the Honorary Director. At the initiative of Late Dr. S. S. Bhatnagar, who was then Secretary to the Government of India, Ministry of Natural Resources and Scientific Research, the post of wholetime Director was created by the Council of the Association and as a member of the Selection Committee Dr. Bhatnagar advised the Council to offer the post to Professor Saha. The Council gladly agreed to this proposal and Professor Saha had been serving as the Director of this Association till he breathed his last under tragic circumstances while going to attend an important meeting at Delhi.

PROFESSOR SAHA AS AUTHOR OF TEXT BOOKS

Besides the numerous papers in which original contributions have been made Professor Saha also published four books. These are (1) *The Principle of Relativity* (1919), (2) *Treatise on Heat* (jointly with Dr. B. N. Srivastava, first published in 1931), (3) *Treatise on Modern Physics* (jointly with Dr. N. K. Saha, first published in 1934) and (4) *Junior Text Book of Heat* (jointly with Dr. B. N. Srivastava, first published in 1932). Except the first one, the other books have run into several editions.

CONNECTION WITH LEARNED SOCIETIES

Besides being a Fellow of the Royal Society of London, Professor Saha was connected with numerous other learned societies. He was one of

the Honorary Members of the American Astronomical Society. He was elected President of the section of physics of the Indian Science Congress in 1925 and the General President of the Indian Science Congress in 1934. He was the Founder President of the U.P. Academy of Sciences which was established at his initiative in 1931 and was renamed National Academy of Sciences, India, in 1934. It was through his efforts that the National Institute of Sciences of India was founded in 1935 with Professor Saha as one of its Vice-Presidents, and during the year 1937-39 he served as the President of the Institute. In 1934 he came occasionally to Calcutta from Allahabad, and with the help of his friends founded Indian Science News Association which started publishing *Science & Culture*, a popular journal meant for dissemination of scientific knowledge among educated people of India. It was some of his famous articles published in *Science & Culture* which were responsible for the creation of the Damodar Valley Corporation and Council of Scientific and Industrial Research. He was also responsible for the formation of the Indian Physical Society in 1934 of which he was the President during the years 1936-1937. He was a member of the Council of Scientific and Industrial Research and a Fellow of the Asiatic Society of Bengal. He served as the President of the Society during the years 1945-1946. He was also elected a member of the Parliament of India in 1951.

Professor Saha was connected with Indian Journal of Physics as its Editorial Collaborator from 1936 upto 1938 and as a member of the Board of Editors since January 1939 till his death. It was in the latter capacity that he converted this journal from a bimonthly to a monthly journal and it is through his efforts that the regularity in the publication of the journal has been assured by the transfer of the printing of the journal to a new press.

Professor Saha is survived by his wife, three sons and four daughters and a host of near relatives and friends to mourn his death. His eldest son, Dr. A. K. Saha is now Professor of Theoretical Nuclear Physics at the Institute of Nuclear Physics, Calcutta. His sudden demise came as a bolt from the blue and much of his work is left unfinished. It is too early to make a proper estimate of his contribution to science and to his countrymen. Only the future generation will be able to do it.

It has been mentioned that the end came under tragic circumstances. He could not pay attention to himself even at the last moment of his life, as he was deeply engrossed in the work for his countrymen. Throughout his life he was anxious for the welfare of mankind. May his soul, caressed by Knowledge Infinite, rest in eternal peace!

S. C. Sirkar.

THE FLOW OF A VISCOUS LIQUID IN A CIRCULAR TUBE UNDER PRESSURE-GRADIENTS VARYING EXPONENTIALLY WITH TIME.

LAKSHMI SANYAL

APPLIED MATHEMATICS DEPARTMENT, CALCUTTA UNIVERSITY

(Received for publication, February 17, 1955)

ABSTRACT. In the present paper the flow of a viscous liquid in a circular tube under pressure-gradients proportional to $\exp(\nu\alpha^2t)$ and $\exp(-\nu\alpha^2t)$ is studied. It is found that when αR is very small (R radius of the tube) the motions in the two cases are similar, in the sense that the velocity distribution in a cross-section of the tube is parabolic in both the cases. But when αR is very large the two motions are completely different. In the first case the flow has the boundary layer character while this characteristic is completely absent in the second case and the velocity depends on the wall distance.

INTRODUCTION

The flow of a viscous liquid in a circular tube under a periodic pressure-gradient has been investigated experimentally by Richardson and Tyler (1929) and theoretically by Sexl (1930). Assuming the pressure gradient to be proportional to $\cos nt$, Sexl has shown that when the dimensionless number $R(n/\nu)^{1/2}$, (ν = kinematic coefficient of viscosity of the liquid and R the radius of the tube) is very small, the distribution of velocity in a cross-section of the tube is parabolic and when $R(n/\nu)^{1/2}$ is very large, the velocity at some distance away from the wall of the tube is independent of the wall distance, that is, the solution has the boundary layer character. These facts have been experimentally confirmed by Richardson and Tyler. In the present paper, the flow of a viscous liquid in a tube of circular section is considered in two cases:

- (1) when the pressure-gradient rises exponentially with time, and
- (2) when the pressure-gradient falls exponentially with time.

Assuming that, in the first case, the pressure-gradient is proportional to $\exp(\nu\alpha^2t)$, it is found that when αR (R , radius of the tube) is very small, the distribution of velocity in a cross-section of the tube is parabolic, but when αR is very large, the velocity at some distance away from the wall of the tube is independent of the wall distance, so that the solution has the boundary layer character. Assuming that, in the second case, the pressure gradient is proportional to $\exp(-\nu\alpha^2t)$, it has been found that for small values of αR , the distribution of the velocity in a cross-section of the tube is parabolic, while for large values of αR the velocity in

a cross-section of the tube depends on the distance from the wall, showing that the boundary layer character is completely absent in the motion. Thus, for small values of αR , the two flows in the tube under pressure gradients increasing and decreasing exponentially with time are similar, while, for large values of αR , the two flows are completely different, one having the boundary layer character and the other depending on the wall distance.

We measure x along the axis of the tube and r along the radius of a cross-section. The motion is symmetrical about the axis of the tube and we assume that it is one dimensional, in the direction of the x -axis. The velocity component u in the direction of the axis of the tube is assumed to be independent of x , while the two other components of velocity are assumed to vanish. With these assumptions, Stokes-Navier equations of motion in cylindrical coordinates r, θ, x , reduce to

$$\begin{aligned}\frac{\partial u}{\partial t} &= -\frac{1}{\rho} \frac{\partial p}{\partial x} + \nu \left(\frac{\partial^2 u}{\partial r^2} + \frac{1}{r} \frac{\partial u}{\partial r} \right) \\ 0 &= -\frac{1}{\rho} \frac{\partial p}{\partial r} \\ 0 &= -\frac{1}{\rho} \frac{\partial p}{r \partial \theta}\end{aligned}$$

The last two equations show that the pressure is independent of r, θ . Since u is independent of x it appears from the first equation that $\frac{\partial p}{\partial x}$ is a function of t alone.

1. Pressure-gradient rising exponentially with time.

We take the pressure gradient to be given by

$$-\frac{1}{\rho} \frac{\partial p}{\partial x} = k e^{\nu \alpha^2 t}.$$

The equation of motion then becomes

$$\frac{\partial u}{\partial t} = k e^{\nu \alpha^2 t} + \nu \left(\frac{\partial^2 u}{\partial r^2} + \frac{1}{r} \frac{\partial u}{\partial r} \right). \quad \dots (1)$$

Assuming

$$u = f(r) e^{\nu \alpha^2 t}, \quad \dots (2)$$

to be a solution of the equation (1), we see that f satisfies the equation

$$f'' + \frac{1}{r} f' - \alpha^2 f = -\frac{k}{\nu}. \quad \dots (3)$$

A solution of this equation which does not become infinite on the axis is

$$f = \frac{k}{v\alpha^2} + AJ_0(i\alpha r), \quad \dots (4)$$

where $J_0(i\alpha r)$ is the Bessel's function of order zero of the imaginary argument $i\alpha r$.

Hence

$$u = \left(\frac{k}{v\alpha^2} + AJ_0(i\alpha r) \right) e^{\nu\alpha^2 t}, \quad \dots (5)$$

where the constant A is determined from the condition that the velocity is zero on the wall of the tube. If R be the radius of the tube, $u = 0$ when $r = R$. This gives

$$A = - \frac{k}{v\alpha^2} \frac{1}{J_0(i\alpha R)}. \quad \dots (6)$$

Therefore

$$u = \frac{k}{v\alpha^2} \left(1 - \frac{J_0(i\alpha r)}{J_0(i\alpha R)} \right) e^{\nu\alpha^2 t} \quad \dots (7)$$

Since

$$J_0(z) = 1 - \frac{z^2}{2^2 \cdot 1} + \frac{z^4}{2^4 \cdot 1^2 \cdot 2^2} - \dots \quad \dots (8)$$

we have for small values of αR and therefore of αr

$$\begin{aligned} u &= \frac{k}{v\alpha^2} \left[1 - \frac{1 + \frac{\alpha^2 r^2}{4}}{1 + \frac{\alpha^2 R^2}{4}} \right] e^{\nu\alpha^2 t} \\ &= \frac{k}{4\nu} (R^2 - r^2) e^{\nu\alpha^2 t}. \quad \dots (9) \end{aligned}$$

This equation shows that, at a given point the velocity increases exponentially with time, and that the distribution of velocity in a cross-section of the tube is parabolic.

From the formula of the asymptotic expansion of $J_n(z)$ [Whittaker and Watson, 1927] we have for large values of αR and αr ,

$$\begin{aligned} J_0(i\alpha R) &= (2/\pi\alpha iR)^{\frac{1}{2}} \cos \left(i\alpha R - \frac{\pi}{4} \right) \\ &= \frac{1}{2}(2/\pi\alpha R)^{\frac{1}{2}} e^{\alpha r} \quad \dots (10) \end{aligned}$$

and

$$J_0(i\alpha r) = \frac{1}{2}(2/\pi\alpha r)^{\frac{1}{2}} e^{\alpha r} \quad \dots (11)$$

so that

$$u = \frac{k}{v\alpha^2} \left[1 - \sqrt{\frac{R}{r}} e^{-\alpha(R-r)} \right] e^{v\alpha^2 t} \quad \dots (12)$$

This equation shows that, at a given point, the velocity rises exponentially with time. It further shows that for an appreciable value of $(R-r)$, $e^{-\alpha(R-r)}$ is very small so that the velocity is independent of the wall distance. Only for very small values of $(R-r)$ the velocity depends on the wall distance. Hence the solution has the boundary layer character.

2. Pressure-gradient falling exponentially with time.

We take the pressure gradient to be given by

$$-\frac{1}{\rho} \frac{\partial p}{\partial x} = k e^{-v\alpha^2 t} \quad \dots (13)$$

The equation of motion becomes

$$\frac{\partial u}{\partial t} = k e^{-v\alpha^2 t} + v \left(\frac{\partial^2 u}{\partial r^2} + \frac{1}{r} \frac{\partial u}{\partial r} \right) \quad \dots (14)$$

Assuming

$$u = f(r) e^{-v\alpha^2 t} \quad \dots (15)$$

to be a solution of equation (14), we see that f satisfies the equation

$$f'' + \frac{1}{r} f' + \alpha^2 f = -\frac{k}{v} \quad \dots (16)$$

A solution of this equation which does not become infinite on the axis is

$$f = -\frac{k}{v\alpha^2} + B J_0(\alpha r), \quad \dots (17)$$

where $J_0(\alpha r)$ is the Bessel's function of order zero of the argument αr
Hence

$$u = \left[-\frac{k}{v\alpha^2} + B J_0(\alpha r) \right] e^{-v\alpha^2 t} \quad \dots (18)$$

The constant B is determined from the condition that the velocity is zero on the wall of the tube, i.e., $u = 0$ when $r = R$.

This gives

$$B = \frac{k}{v\alpha^2} \frac{1}{J_0(\alpha R)} \quad \dots (19)$$

Therefore

$$u = -\frac{k}{v\alpha^2} \left(1 - \frac{J_0(\alpha r)}{J_0(\alpha R)} \right) e^{-\nu\alpha^2 t}. \quad \dots (20)$$

For small values of αR and therefore of αr ,

$$\begin{aligned} u &= -\frac{k}{v\alpha^2} \left[1 - \frac{1 - \frac{\alpha^2 r^2}{4}}{1 - \frac{\alpha^2 R^2}{4}} \right] e^{-\nu\alpha^2 t} \\ &= \frac{k}{4\nu} (R^2 - r^2) e^{-\nu\alpha^2 t} \quad \dots (21) \end{aligned}$$

which shows that the distribution of velocity in a cross-section of the tube is parabolic.

For large values of αR and αr

$$J_0(\alpha r) = \left(\frac{2}{\pi\alpha r} \right)^{\frac{1}{2}} \cos \left(\alpha r - \frac{\pi}{4} \right) \quad \dots (22)$$

$$J_0(\alpha R) = \left(\frac{2}{\pi\alpha R} \right)^{\frac{1}{2}} \cos \left(\alpha R - \frac{\pi}{4} \right) \quad \dots (23)$$

Therefore, we have

$$u = -\frac{k}{v\alpha^2} \left[1 - \sqrt{\frac{R}{r}} \frac{\cos \left(\alpha r - \frac{\pi}{4} \right)}{\cos \left(\alpha R - \frac{\pi}{4} \right)} \right] e^{-\nu\alpha^2 t} \quad \dots (24)$$

This shows that the distribution of velocity depends on the wall distance. Hence the solution has not the boundary layer character.

ACKNOWLEDGMENT

In conclusion the author wishes to express her thanks to Dr. S. Ghosh for helpful suggestions.

REFERENCES

- Richardson, E. G. and Tyler, E., 1929, *Proc. Phys. Soc. London*, **42**, 1.
 Sez1, Th., 1930, *Z. Phys.*, **61**, 349.
 Whittaker, E. T. and Watson, G. N. *A Course of Modern Analysis* (4th Ed.), Cambridge, 368,

THE TEMPERATURE-DEPENDENCE OF G-M. COUNTER CHARACTERISTICS. (PART I).

SATYA PAL PURI AND P. S. GILL

DEPARTMENT OF PHYSICS, MUSLIM UNIVERSITY, ALIGARH.

(Received for publication. October 19, 1955)

ABSTRACT. A study of the characteristics of a self-quenching argon-petroleum ether internal and an argon-alcohol filled external counters was carried out in the range of 16°C to -20°C . The internal counter is found to be independent of temperature in the above mentioned range of temperature. The changes of the characteristics of the argon-alcohol filled external cathode counter are ascribed to the condensation of the alcohol content. This counter is temperature-independent upto -7°C . The threshold voltage falls by about 100 volts at -11.5°C . and decreases by further lowering the temperature. The operation remains the same down to a few degrees lower than the saturation temperature. Beyond -11.5°C , the electrical resistance of the glass envelope becomes too high to allow this type of counter to operate satisfactorily.

INTRODUCTION

This investigation arose out of some difficulties experienced in the use of externally coated cathode G-M. tubes at the Gulmarg Research Observatory, where these tubes were occasionally subjected to fairly low temperatures. The role of the polyatomic constituent in the self-quenching counters was explained by Korff and Present (1944) as follows: (a) The positive ions of argon transfer their ionization energy to polyatomic molecules, (b) the polyatomic molecules degrade the recombination photons and (c) suppress the secondary emission through the well-known process of predissociation.

By lowering the temperature a change in the characteristics of a self-quenching counter is expected to occur only at the temperature at which the partial pressure of quenching vapour decreases. On further lowering the temperature the partial pressure will gradually fall and render the counter progressively useless.

In recent years studies of the temperature-dependence of G-M. tubes have been reported by Korff *et al* (1942), Parkash (1946), Parkash and Kapur (1950), Loosemore and Taylor (1950), Fujioka *et al* (1950), Stanisiz (1952) and Mader (1954). Parkash and Kapur (1950) reported the shortening of the plateau and high increase in the slope with no shift in the threshold at 16°C , whereas at 9°C the plateau disappeared totally. They interpreted their results on the basis of partial condensation of the vapour. Their explanation is improbable as it is known that the vapour is unsaturated at this temperature and consequently

no condensation can take place. Mader (1954) reported that the plateau contracted to about 30 volts at 20°C in the case of a G-M. tube filled with 85 mm of argon and 15 mm of ethanol vapour. Korff *et al* (1942) reported the complete disappearance of plateau at -22°C.

APPARATUS AND EXPERIMENTAL ARRANGEMENT

The G-M. counters employed in this study were of the self-quenching type. One had the internal Cu cathode (No. 1) and the other was of the Maze type (No.2) The internal diameter of the Cu cathode counter was 1.5 cm and it was 13 cm. long. A 3 mil tungsten wire along the axis served as anode. It was filled with spectroscopically pure argon 9 cm. and petroleum ether vapour 1.1 cm. (B.P. 40-60°C). Before filling, the central wire was flashed under vacuum and the assembly was roasted at 250°C for two hours to drive off water vapour and occluded gases. The second counter had an external aquadag coated cathode. It was filled with spectroscopically pure argon 9 cm. and of absolute alcohol vapour, 1 cm. The glass wall was 2.12 mm thick. It was baked at 140°C for one hour.

The counters were enclosed in a brass cylinder which was placed in a thermostatically controlled cooling cabinet. The temperature was varied in small steps from 16°C to -21.5°C. The lowering of temperature from 16°C to 5°C was done by employing water as the bath liquid, from 5° to -6.9°C using brine and for the rest of the temperatures eutectic-mixtures were availed of. This mode of cooling ensured constancy of temperature within $\pm 1^\circ\text{C}$ for a period of several hours..

Cosmic radiation served as the source for tracing the plateau characteristics at different temperatures. The counter pulses were amplified and recorded in the usual way.

At the end of the investigation, the characteristics were redetermined after the counters had returned to the room temperature in order to see whether there was any permanent effect of cooling or not.

OBSERVATIONS AND RESULTS

The measurements were carried out in the range from 16° C to -21.5°C, over small intervals of temperature. Sufficient time was allowed at every setting of temperature before the characteristics were taken.

Figures 1 and 2 give the plateau characteristics of counters No. 1 and No. 2 respectively. The plateau tracing was abandoned on the appearance of a distorted or double pulse. The curves of figure 3 show the pulse size *vs* temperature at different overvoltages in the two cases. The curves of figure 4 show the threshold voltages *vs* temperature. These data show the following :

(i) The characteristic curves of counter No. 1 remain normal over the temperature range of 16.1°C to -21.5°C, whereas for counter No. 2 the range is from

16.1°C to -7°C. For temperature below -7°C, the plateau of counter No. 2 shifts towards lower operating voltages and there is a gradual contraction of the plateau which does not disappear completely even at -21.5°C.

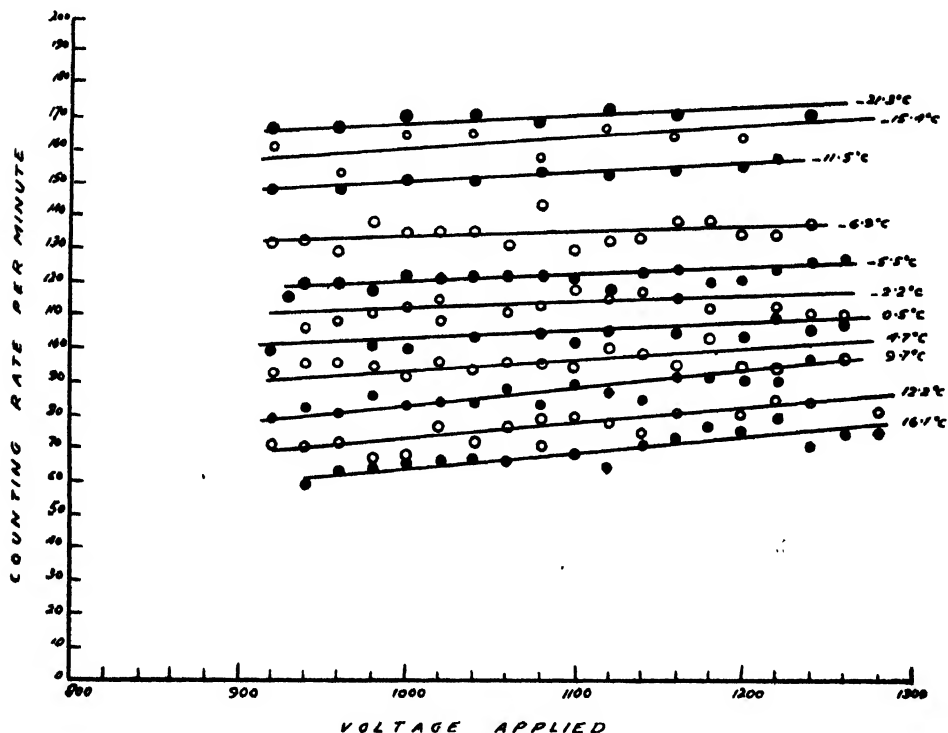


Fig. 1. Plateau characteristics of internal petroleum-ether filled counter at different temperatures. In each of the curves the scale giving the ordinate has been shifted upwards by one scale division so as to bring out all the changes prominently.

- (ii) Within the ranges given above the slopes remain substantially the same.
- (iii) At -11.5°C, the threshold voltage of counter No. 2 decreases by about 100 volts. At this temperature alcohol begins to condense from the super-saturated vehicular gas argon.
- (iv) These counters do not show any increase in counting rate throughout the temperature range similar to that reported by Parkash and Kapur (1950) and Stanisiz (1951).

(v) In the case of counter No. 2 even at a temperature below the temperature of condensation, the operation seems to be satisfactory. There set in certain anomalies such as, an abnormal increase in pulse size when the voltage across is increased instantaneously, which falls to a finite lower value after some time.

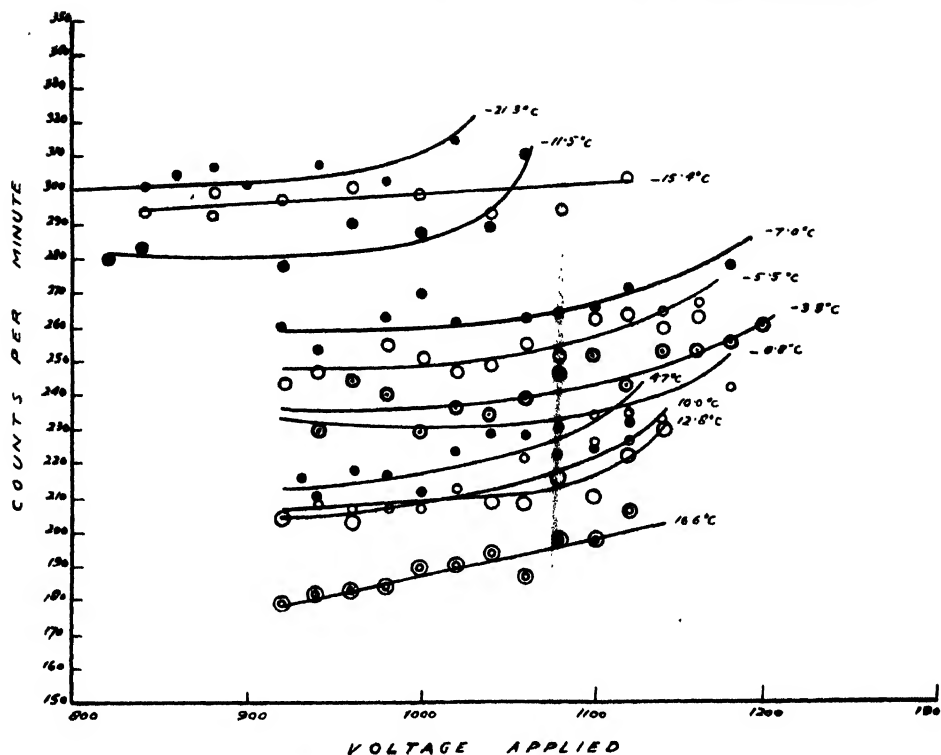


Fig. 2. Plateau characteristics of externally coated alcohol filled counter at different temperatures. In each of the curves the scale giving the ordinate has been shifted upwards by one scale division, so as to bring out all the changes prominently.

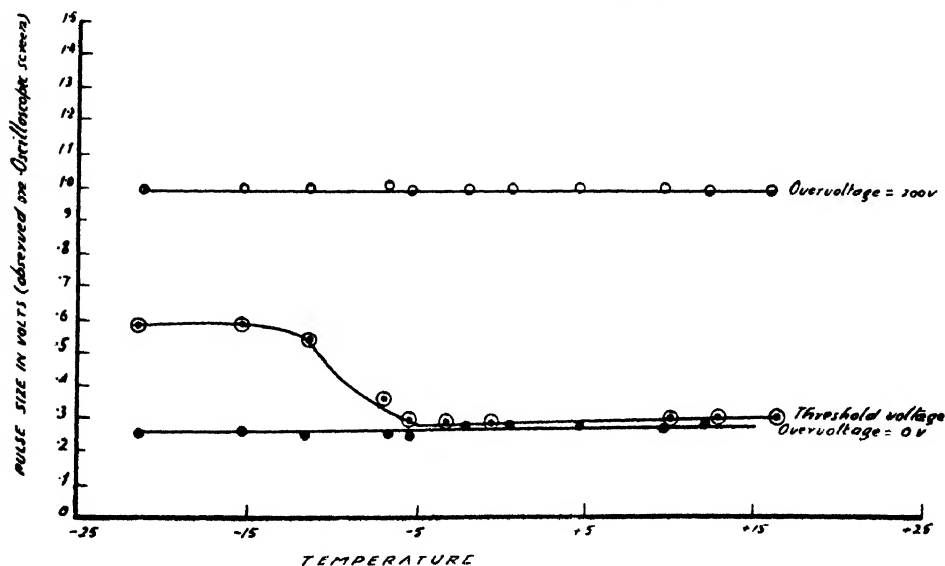


Fig. 3. Pulse size versus temperature for internal (petroleum-ether filled) and external (alcohol-filled) counters. o, ● = Internal counter, ⊕ = External counter.

The counter becomes insensitive for a considerable period when the working voltage is reduced. The threshold voltage increases with greater counting rate and the pulse size decreases.

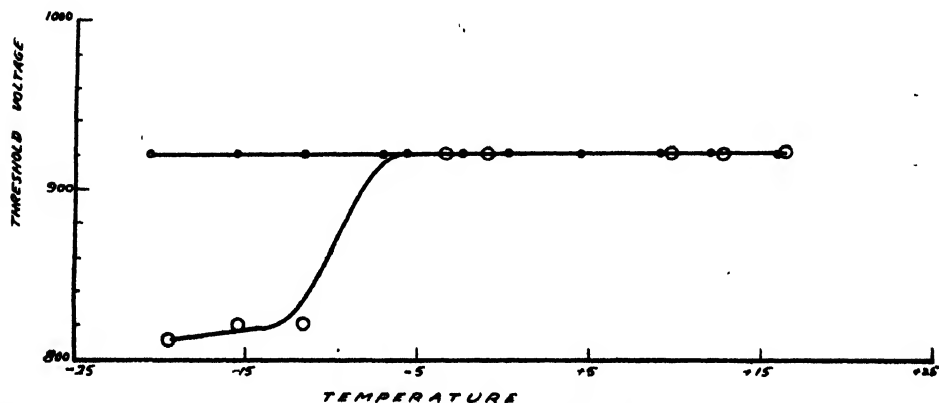


Fig. 4. Threshold voltage versus temperature for internal and external counters.
 o = Internal counter : O = External counter.

(vi) The counters regained their original characteristics at room temperature.

DISCUSSION

Lowering of threshold voltage

The lowering of threshold voltage in the case of counter No. 2 at -11.5°C , may be due to the decrease in pressure caused by condensation of some alcohol vapour. When the decrease of the alcohol vapour pressure has taken place by condensation, the free path of the electron bringing about the avalanche increases and the threshold voltage decreases. This view is supported by the fact that the threshold has been shown to shift towards lower voltages as the amount of poly-atomic constituent is lowered (Trost, 1937 and Weisz, 1948). There is a qualitative agreement between these results.

In the case of counter No. 1, lowering of threshold does not occur as the constituents of petroleum ether mainly hexane and heptane remain unsaturated throughout the range investigated.

The threshold voltage is shifted beyond -7°C for counter No. 2, whereas Stanisiz (1951) reports the shift at -2.5°C , the temperature of saturation for an internal cathode counter having the same filling as counter No. 2. From the theory of droplet formation, condensation can occur only when the vehicular gas is supersaturated with the vapour at that temperature. A certain degree of supersaturation, defined as the ratio of the density of the vapour in the gaseous mixture in the supersaturated state to the corresponding density in the saturated state

at the same temperature, must be attained for condensation to take place, (Das Gupta and Ghosh, 1946).

The following mechanisms are considered for the explanation of these observations:

- (i) Insufficient quenching material.
- (ii) Leakage across the semiconducting paths in the liquid condensed near the electrodes.
- (iii) Increased adsorption of the vapour on the cathode cylinder.
- (iv) The role of the glass wall in the case of external counter.

The curves of figures 1 and 2 showing plateaus for counters No. 1 and 2 seem to improve slightly as the temperature is lowered but is still above the condensation temperature. This is caused by the increased adsorption of the polyatomic vapour which improves upon the surface layer already formed. The importance of formation of suitable surface layer which prevents spontaneous discharges and electron escape from the cathode was pointed out by Trost (1937).

The decrease of the number of alcohol vapour molecules accounts for the shortening of the counter plateau and the increase in its slope. When the amount of alcohol has fallen lower than the optimum value, some positive ions of argon will reach the cathode, which will give rise to multiple and spurious pulses at lower overvoltage, as is confirmed by the oscilloscopic observation. Even at a temperature where the alcohol pressure reduces to inappreciable value, the counter will still function as a non-selfquenching counter. So we expect no complete disappearance of plateau as reported by Parkash and Kapur (1950) at 9°C, and by Mader (1954) at 20°C.

Parkash and Kapur (1950) ascribed these results to condensation of alcohol at 9°C. The partial pressure of alcohol employed by them cannot cause saturation at temperatures higher than 2.5°C, and supersaturation would occur at still lower temperatures. They also did not observe any lowering of the threshold, which should have been the case if condensation had set in.

Another explanation advanced by Parkash and Kapur (1950) and Stanis (1951) was that the liquid might condense near the electrodes in such a way as to cause semiconducting paths across the insulating material between the wire and the cylinder. Leakage across such paths can manifest itself as spurious counts. There is very little likelihood of alcohol condensing between the electrodes, where it can give rise to spurious counts. The resistivity of ethyl alcohol (at 15°C) is 0.3×10^6 ohms per cm cube, (Handbook of Chemistry and Physics, 1949), and this comes in parallel with the quenching resistance. It would result in the reduction of pulse size. But no such reduction was noted, as shown in figure 3.

The glass envelope of counter No. 2 acts like a leaky capacitor, which acquires a positive charge during its operation, which sets up an opposing e.m.f. This

counter e.m.f. increases with mean pulse rate and the overvoltage. If V_a is the applied voltage, the effective voltage V_e is given by

$$V_e = V_a - n \times R \times q(V_e)$$

where n = mean pulse rate

$q(V_e)$ = the charge per pulse at voltage V_e

and R = the resistance of glass.

R , the resistance of glass envelope ($\sim 9.0 \times 10^{13}$ ohms per cm^3) is strongly temperature-dependent. The decrease in temperature increases the counter e.m.f. and consequently decreases the effective voltage. At sufficiently low temperatures when R has become quite high, the above equation explains the intensity-dependence of counter characteristics. Considering the equivalent circuit of the external counter, the distributed capacity becomes

$$\frac{kL}{2k} \log \frac{b'}{a} + 2 \log \frac{b}{b'}$$

where k —the dielectric constant of the glass wall

b' —the inner radius of the glass envelope

b —the outer radius of the glass envelope

a —the radius of the central wire

and L —the effective length of the counter.

The increase in the distributed capacity of the counter caused by the glass wall increases the recovery time of the counter. This capacitor has a high leakage resistance ($\sim 10^{14}$ ohms per cm^3), represented as a shunt across it.

At lower temperatures, the resistance of the glass envelope becomes very high with the consequence that the effective e.m.f. is lower than that at a higher temperature for a particular operating voltage. Now if the working voltage is lowered, the excess positive charge accumulated on the glass envelope will require sometime, depending upon the leakage resistance at the time, before it sets to the charge density corresponding to the decreased voltage. With the leakage of the positive charge, the effective voltage builds up and the pulse size increases till it attains the maximum value. Similarly when the operating voltage is increased, the counter e.m.f. builds up to a higher value, depending upon the rate of accumulation of positive charge, and effective voltage decreases till a balance is reached between the rate of accumulation and rate of leakage of positive ions. The pulse size gradually becomes minimum. This explanation is further endorsed by a similar observation in case of an externally coated pyrex G-M. counter, (Yasin *et al*, 1951), at, room temperature.

ACKNOWLEDGMENTS

One of the authors (S.P.P.) is grateful to the Union Government for financial assistance in the form of a research scholarship. We acknowledge the help of the glass blower Mr. Ajit Singh.

REFERENCES

- Das Gupta, N. N., and Ghosh, S. K., 1946, *Rev. Mod. Phys.*, **18**, 225.
Fujioka Goro *et al*, 1950, *J. Phys. Soc. Japan*, **8**, 103.
Hodgman, Charles, D, (1949). *Handbook of Chemistry & Physics*, Chemical Rubber Publishing Co., Cleveland, Ohio.
Korff, S. A. and Present, R. D., 1944, *Phys. Rev.*, **65**, 274.
Korff, S. A. *et al*, 1942, *Rev. Sci. Instrum.*, **13**, 127.
Loosemore, W. R., Raylor, Denis, 1950, *Proc. Phys. Soc.*, **63B**, 728.
Mader, H. J., 1954, *Z. f. Phys.*, **137**, No. 2, 216.
Parkash, O, 1946, *Phys. Rev.*, **76**, 568.
„ „ and Kapur, P. L., 1950, *Proc. Phys. Soc.*, **63A**, 453.
Stanisz, O., 1952, *Acta. Phys. Polon.*, **11**, No. 2, 140.
Trost, A., 1937, *Z. f. Phys.*, **105**, 399.
Weisz, P. B., 1948, *Phys. Rev.*, **74**, 1807.
Yasin, M., Ahmad, R. and Gill P. S., 1951, *Ind. J. Phys.*, **25**, 182.

THE TEMPERATURE-DEPENDENCE OF G-M. COUNTER CHARACTERISTICS. (PART II).

SATYA PAL PURI AND P. S. GILL

DEPARTMENT OF PHYSICS, MUSLIM UNIVERSITY, ALIGARH

(Received for publication, October 19, 1955)

ABSTRACT. The measurements were made on self-quenching argon-petroleum ether, argon-butane, and argon-alcohol filled Geiger-Muller counters in the range of 32° to 150°C, 34° to 100°C. and 27° to 138°C. respectively. The results of the present investigation indicate the following :

- (i) There is a progressive rise of the threshold as the temperature is increased.
- (ii) The above mentioned three counters seem to be substantially temperature-independent, up to 80°C, 55°C. and 105°C. respectively.
- (iii) There is an exponential increase in slope with temperature and decrease in overall width of the plateau characteristics at higher temperatures.
- (iv) A large increase in counting rate is experienced at higher temperatures. However, there is increase only in frequency and not in multiplicity.
- (v) There is a sudden deterioration of these counters at 100°C., 85°C. and 105°C. respectively.

It is inferred that it is the desorption of the quenching vapour at higher temperatures, which causes the rise of the threshold. The increase in counting rate with temperature may be due to the formation of negative ions of the absorbed gas at the cathode.

INTRODUCTION

The theory of discharge mechanism in Geiger-Muller counters was developed by Rose and Korff (1941), Ramsay (1940), and Montgomery and Montgomery (1941), and it predicts that the internally quenched type must show some change in its characteristics with temperature. It has also been reported by Korff (1948) that self-quenching counters, usually employing argon or some other gas mixed with some organic vapour show a temperature-dependence of their counting rate which can sometimes be troublesome.

In recent years studies of the temperatures-dependence of G-M tubes have been reported by Korff *et al* (1942); Parkash (1946); Parkash (1950) Parkash and Kapur (1950); Tanyel (1950); Loosemore and Taylor (1950); Hereford (1950) Fujioka *et al* (1950); Kimura (1951); Seidl and Roubinek (1952); Stanisiz (1952) Joshi (1953) Mader (1954). Putman (1948) found that there was a bodily shifting of the plateau towards higher operating potentials as the temperature was increased.

The self-quenching counters using argon and alcohol, argon and petroleum ether are the most widely used in cosmic-ray and other experiments. This investigation was undertaken to study the temperature-dependence of counter characteristics at different temperatures which may give a clue to the discharge mechanism as well.

APPARATUS AND EXPERIMENTAL ARRANGEMENT

Three counters all of the self-quenching type, with different quenching vapours were employed in the present investigation.

Counter No. 1 was the same as described in Part I, counter No. 2 was 20 cm in length and 1 cm in diameter. The filling consisted of 86% argon and 14% butane at a total pressure of 12 cm of Hg. Counter No. 3 was the same as No. 2 of Part I.

The counters could be enclosed in a brass cylinder with three outlet holes, the extreme ones for the leads and central one for the mercury thermometer.

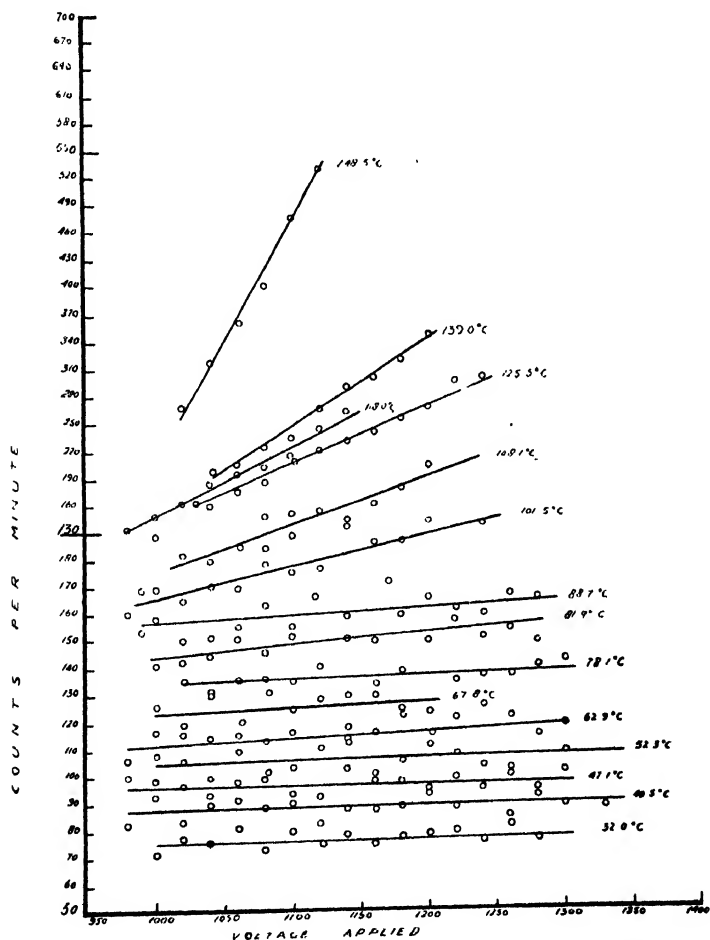


Fig. 1. Plateau characteristics at different temperatures (petroleum-ether filled) of counter No. 1.

In each of the curves the scale division giving the ordinate has been shifted upwards by one scale division, so as to bring out all the changes prominently.

The assembly was placed in thermostatically controlled tank, whose temperature sensitivity was 0.1°C in most of the settings. Upto 90°C toluene (B.P. 110°C) was the thermoregulator liquid, which was replaced by glycerine (B.P. 291°C). The liquid used as bath was a non-fuming; non-inflammable Houghton's Tempering Oil No; 80 (B.P. 700°C).

Recording was made with a scaling unit, with input sensitivity of 3V , and resolving time of 10 microseconds. Small resolving time was specially suited for the present investigation as it was desirable to resolve the "Nachentladung" from the previous discharges, Trost (1937).

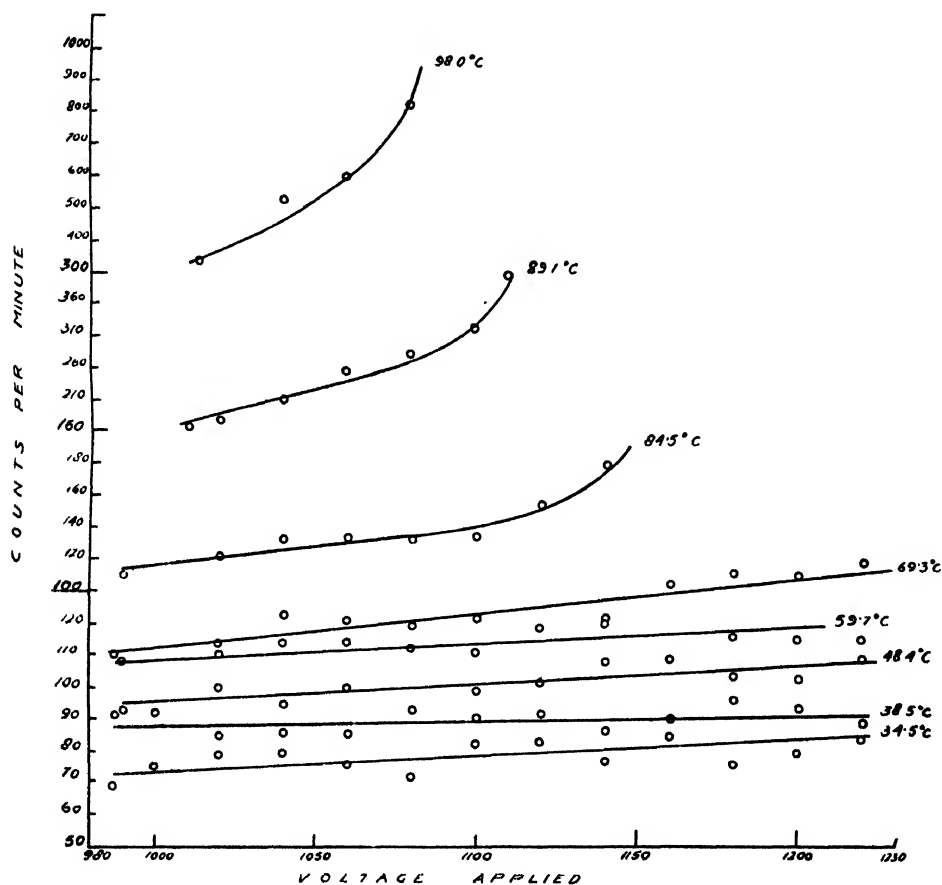


Fig. 2. Plateau characteristics at different temperatures (butane-filled counters) of counter No. 2.

In each of the curves the scale division giving the ordinate has been shifted upwards by one scale division so as to bring out all the changes prominently.

Cosmic radiation served as the source for tracing the plateau characteristics at different temperatures. The total range of temperature variation extended

from 32°C to 150°C, from 34°C to 100°C, and from 27°C to 138°C for counters No. 1, 2 and 3 respectively. Small counting rate was considered preferable to bring out prominently the spuriousness due to temperature variation.

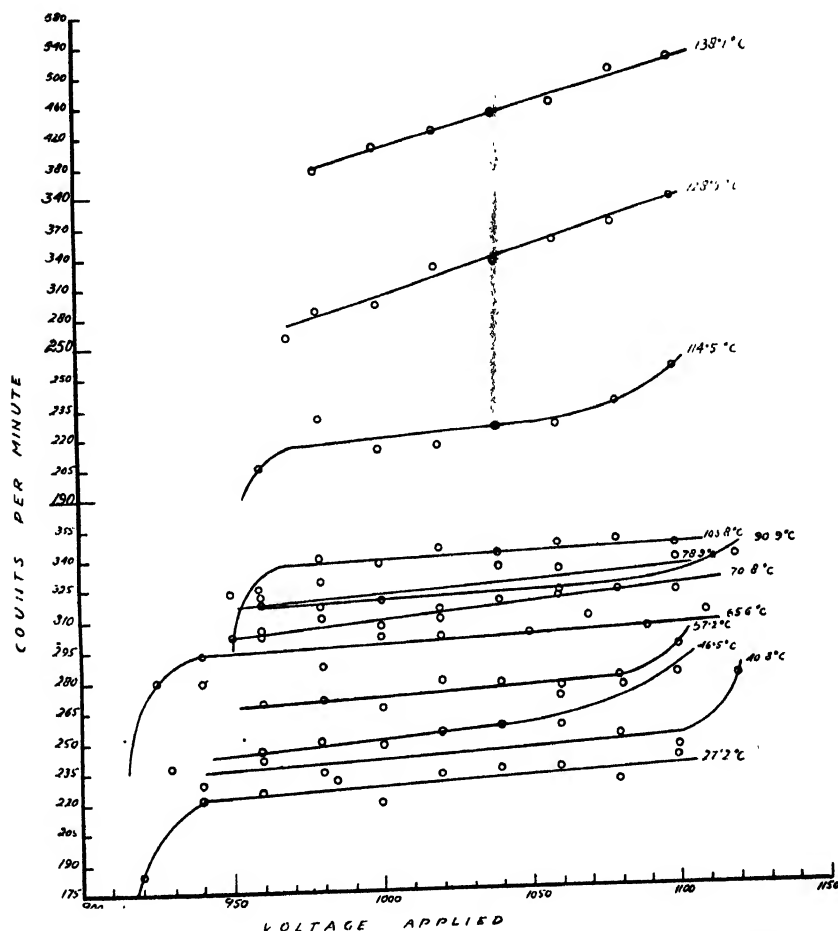


Fig. 3. Plateau characteristics at different temperatures (argon and alcohol filled) of counter No. 3.

In each of the curves the scale division giving the ordinate has been shifted upwards by one scale division so as to bring out all the changes prominently.

OBSERVATIONS AND RESULTS

One by one the counters were placed in the enclosure and characteristic curves at many constant temperatures were obtained. Each characteristic curve was taken after the counter had been kept at a given temperature for about four hours. Such an interval was considered sufficient for any changes, which might set in at that temperature. After completing the observations at higher temperatures

the characteristic curves at room temperature were again obtained to see if there remained any permanent effect on the counters after heating. The data obtained are shown in curves of figures 1, 2 and 3 for the three counters used. The slopes in percent per 100 volts, as calculated from those curves, are shown in Table I

TABLE I

Counter No. 1		Counter No. 2		Counter No. 3	
Temperature in degrees centrigrade	Slope % per 100 volts	Temperature in degrees centrigrade	Slope % per 100 volts	Temperature in degrees centrigrade	Slope % per 100 volts
1. 32.0	0.66	1. 34.6	6.66	1. 27.2	4.17
2. 47.1	1.00	2. 48.4	7.62	2. 40.8	4.17
3. 62.9	3.50	3. 59.7	6.25	3. 57.2	4.5
4. 78.1	2.66	4. 69.3	14.66	4. 70.8	7.16
5. 81.9	6.33	5. 84.0	20.00	5. 78.9	5.9
6. 88.7	4.00	6. 89.1	88.16	6. 90.9	3.12
7. 101.5	16.60	7. 98	142.75	7. 103.8	4.15
8. 108.1	22.50			8. 114.5	6.96
9. 118	37.30			9. 128.5	37.88
10. 125	43.60			10. 138.1	29.0
11. 139	56.00				
12. 148.5	79.50				

The results of these observations may be summed up as follows:

(i) There appears to be a slow progressive rise of the threshold as the temperature is raised showing an abrupt rise near about 125°C for counter No. 1 and near about 90°C for counter No.2.

(ii) Counters 1, 2 and 3 are substantially temperature-independent upto 80°C, 55°C and 105°C respectively. Compared to the internal type of counter, the externally coated cathode counter shows less temperature-dependence.

(iii) There is a decrease in overall width of the plateau at higher temperatures in each case.

(iv) There is a large increase in counting rate at higher temperatures. The visual observations of the pulse shapes on the oscilloscope screen at different temperatures reveal that the pulses are well defined and single, which would mean that they do not originate from earlier discharges. It appears that the high temperature causes the frequency to increase and not the multiplicity of the pulse. The pulses appear to be spontaneous.

(v) There is a sudden deterioration of counters No. 1, 2 and 3 at 100°, 85° and 105°C respectively as shown in Table I

DISCUSSION

Rise of the threshold voltage : The rise of the threshold voltage with temperature is due to the release of polyatomic molecules, which are absorbed on the surface of the cathode at ordinary temperatures. Their partial pressure in the counter increases progressively with temperature, due to greater and greater release of the adsorbed polyatomic molecules. Although the ionization potential of the polyatomic constituent is lower than that of the rare gas, its addition almost invariably raises the threshold voltage. This may be due to the fact that a large portion of the electron energy is dissipated in exciting molecular vibrations at each impact, rather than in ionization. In that case an electron is much less likely to acquire ionization energy over several free paths, with the result that zone of ionization contracts with increase in number of the polyatomic molecules. This results in the increase of the threshold. Such effects have been reported by Trost (1937) and Weisz (1948).

The rise of threshold in case of counter No. 3 as compared to counter No. 1 arises from a greater desorption of polyatomic vapour from the glass surface. The number of molecules leaving unit area of any surface would be

$$n_c dc = A \frac{2k^2 T^2}{m^2}$$

where n_c is the number of molecules with velocity C , T is the temperature of the surface and m , the molecular weight of the adsorbed gas. The number of molecules leaving unit area is inversely proportional to square of molecular weight. The molecular weight being much greater for petroleum ether than for alcohol; the ratio of evolved mass of alcohol to ether is ~ 3.5 at the same temperature. Parkash and Kapur (1950) did not observe any increase of threshold due to the smaller range of temperature employed (8° to 60°C) by them.

As an explanation of these observations we can examine all the possible surface and gas mechanisms.

Hereford (1950) interpreted his shorter recovery times at higher temperatures in the case of parallel plate counters by the help of negative temperature coefficient of high resistivity ($\sim 10^{14}$ ohm-cm) of SiO_2 particles on the cathode, which might be released on baking the counter at 425°C. Two of the counters used in the present investigation have pyrex glass envelopes and the possibility of extracting some SiO_2 particles by baking at 240°C is almost nil.

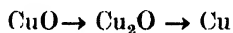
Kimura (1951) observed an increase of spurious counts for the counters whose cathodes had been degassed by high frequency electric furnace, whereas the glass walls were not heated so high.

Oxides of cathode material cannot be responsible for spurious counts because their resistivity ($10^5 \sim \text{ohm-cm}$) is too small to hold the positive charge even for a microsecond (Hereford, 1950).

It has been found by various observers Kutzner (1924), Lewis and Bureham (1936), Wiedenbeck and Crane (1949) and Krammer (1949) that well polished metal surface gives rise to spurious counts in G-M counter which decays gradually with time, and increases again when the tube is heated. Krammer (1949) concludes that electrons are emitted by metals during the exothermal process, after the first discharge. Similar results have also been reported by Loew and Naude (1949). The cathodes used in our counters were oxidized and no electron emission would be expected.

Hereford (1950) has reported shorter recovery times at higher temperatures in the case of parallel plate counter, which he explains on the presence of minute droplets in the gas mixture. Minute droplets only exist at some degree of super-saturation, but in the present case the alcohol content remains unsaturated at all the temperatures. In the case of G-M counter, there cannot be any droplets. Moreover, the weak field strength near the cathode (0.2 volts per mean free path at the cathode) would probably enable the quenching vapour to suppress this mechanism through the well known process of predissociation, (Hereford, 1950).

Parkash (1950) has suggested the reduction of CuO to Cu and the oxidation of $\text{C}_2\text{H}_5\text{OH}$ to CH_3COOH , through the following reactions:



The above explanation seems unwarranted for 150°C is not high enough for either of the above reactions to take place, (Mellor, 1923). H. Moissan found that the decomposition $2\text{CuO} \rightarrow 2\text{Cu} + \text{O}_2$ occurs at 2500°C in the electric arc.

Even the reducing atmosphere of H_2 and CO from the decomposition products of $\text{C}_2\text{H}_5\text{OH}$ will not be favourable for the above reaction. Erzbach (1923) found that the oxide prepared by direct oxidation is reduced at 193°C in a current of H_2 and at 232°C in the case of Cu_2O . Loew noted the reduction of CuO by petroleum ether but only when CuO is red hot, (Mellor, 1923).

The reduction of alcohol into aldehyde by passing over copper oxide occurs at 620°C , (Ipatiev, 1903). No such reduction is therefore possible at 150°C .

Moreover, no permanent change in the characteristics was detected at the end of the investigation.

The large counting rate and greater slope of counting rate *vs* voltage curves in case of internal cathode alcohol-argon counters was attributed to the secondary emission from the cathode by the positive ions of Hg by Parkash (1950).

Mercury vapour, being monatomic, is non-selfquenching vapour and hence will be an impurity in the counter, but will have no bearing on the temperature effect because the number of molecules of Hg remains constant at higher temperatures, provided there is no free mercury in the counter at the time of filling.

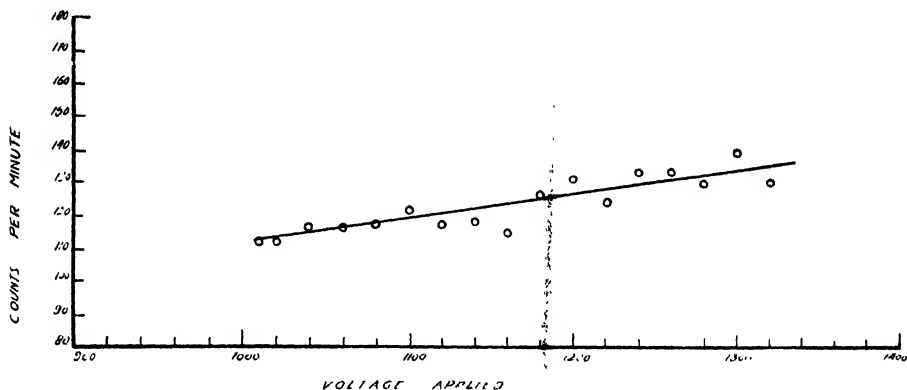


Fig. 4. Plateau characteristics of counter No. 1, after returning to room temperature from the investigation.

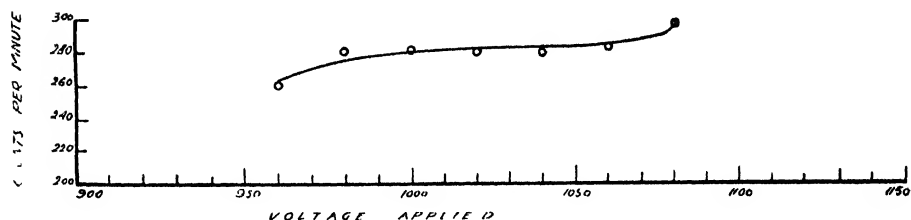


Fig. 5. Plateau characteristics of counter No. 3, after returning to room temperature from the investigation.

Joshi (1953) attributed the deterioration of the plateau characteristics of ether-argon and argon-hydrogen filled counters at 52°C, to the formation of long lived metastables 2^3P_0 states of mercury atoms with life time of 10^{-2} sec. But in a sealed-in counter, no variation of the quantity of mercury vapour can be anticipated with the increase of temperature.

Parkash and Kapur (1950) explained the high counting rates at higher temperatures due to increased secondary emission, because the average energy and the number of positive ions are greater at higher temperatures.

The increase in average energy is $\frac{(3n-6)}{2} kT$, where n is the atomicity

$$= \frac{27 \times 1.38 \times 10^{-16} \times 425}{2 \times 1.6 \times 10^{-12}} \text{ e.v.}$$

$$= 0.385 \text{ e.v.}$$

Thus the increase in energy due to temperature rise is negligible as compared to 200 e.v. the energy due to the intense field

There seems to be no reason to suppose that there is an increase in the positive ions with temperature. On the other hand, at higher temperatures the increase in randomness will increase the probability of charge transfer.

Moreover, the oscilloscopic observation does not show the pulses to be due to secondary emission, for there are no doubles or triples at higher temperatures.

Field emission as a result of the electric double layer at the cathode surface, had been observed by Malter (1936) and Paetow (1939).

Kimura (1951) could expect this effect only in the case of Al cathode, but not with Ni and Fe cathodes. Ni and Fe cannot give trouble as these are neither highly insulating nor show phosphorescence action with ultraviolet frequencies from argon. In our case thicker deposit of CuO on the cathode surface is not amenable to any such trouble (Loeb, 1947).

An explanation of the phenomena by the thermoelectric emission does not seem to play any part since the Richardson plot of the spurious counts does not give a linear fit.

Massey and Burhop (1952) show that an important practical effect of the bombardment of a surface with positive ions consists in the liberation of adsorbed layers of gas on the surface. The adsorbed gas may be liberated from the surface as a negative ion. Sloane and Press (1938) identified the production of negative ions CO^- and C_3H_3^- which they attributed to adsorbed layers on the nickel surface. Evidence of light negative ions produced by positive ion impact on adsorbed layers has also been obtained by Arnot and Beckett (1937). So spurious pulses are probably due to the emission of negative ions, which occurs as the result of the energy freed during elementary exothermic chemical reaction between the impinging molecules and those adsorbed on the cathode.

The importance of formation of a suitable surface layer which prevents spontaneous discharges and electron escape from the cathode was pointed out by Trost (1937). The heat of adsorption being always positive, the amount of adsorbed gas at a given pressure decreases with rise in temperature. The partial pressure of the polyatomic constituent goes on increasing.

The abrupt deterioration of counters No. 1, 2, and 3 at 100°C, 85°C and 105°C respectively, may be explained as follows: In the usual way an adsorbed atom or molecule will vibrate about its position of minimum energy, but should it receive sufficient additional energy to reach the continuous equipotential line, it will be able to travel freely over the surface without requiring any supply of energy and this motion can persist until the particle loses its energy either by colliding with another molecule or by interaction with the solid. The two states of the film are exactly analogous to the solid and liquid states of a three dimensional phase, and we should therefore expect a definite temperature of transition between

the two states, that is, a melting points. Such an explanation has been given by Gregg (1934) in the case of adsorption of H_2 on Ni surface.

ACKNOWLEDGMENT

One of the authors (S.P.P.) acknowledges with pleasure the help of the Union Education Ministry for the award of a Research Scholarship.

REFERENCES

- Arnot, F. L. and Beckett, Clark, 1938, *Proc. Roy. Soc.*, **168**, 103.
 Craggs, J. A. and Jaffe, A. A., 1947, *Phys. Rev.*, **72**, 784.
 Fujioka Goro, Kita, Isao and Minakawa, Osami, 1950, *J. Phys. Soc. Japan*, **6**, 103.
 Gregg, S. J., 1934, "The adsorption of Gases by solids". Methuen's Monographs on chemical subjects.
 Horeford, Frank, L., 1950, *Phys. Rev.*, **77**, 559.
 Joshi, C. P., 1953, *Ind. J. Phys.*, **27**, 48.
 Kimura, Motoharu, 1951, *J. Phys. Soc. Japan*, **6**, 141.
 Korff, S. A., 1948, "Electron & Nuclear Counters". New York: Van Nostrand & Co.
 Korff, S. A., Spatz, W. D. B. and Hilberry, N., 1942, *Rev. Sci. Inst.*, **13**, 127.
 Krammer, J., 1949, *Zeits. f. Physik*, **125**, 739.
 Kutzner, W., 1924, *Zeits. f. Physik*, **23**, 117.
 Lewis, W. B. and Bureham, W. E., 1936, *Proc. Camb. Phil. Soc.*, **32**, 503.
 Loeb, L. B., 1947, "Fundamental Processes of electrical discharges in gases" pp. 500, John Wiley & Sons, Inc.
 Loosemore, W. R., Taylor, Denis, 1950, *Proc. Phys. Soc.*, **63B**, 728.
 Loew, J. D., Naude, S. M., 1949, *Phys. Rev.*, **76**, 571.
 Massey, H. S. W. and Burhop, E. H. S., 1952, "Electronic and ionic impact phenomena", Oxford Clarendon Press.
 Mader, H. J., 1954, *Z. f. Physik*, **137**, No. 2, 216.
 Malter, Louis, 1936, *Phys. Rev.*, **50**, 48.
 Mellor, J. W., 1923, "A comprehensive Treatise on Inorganic & Theoretical Chemistry" Vol. III, Longmas, Green & Co., pp. 133, 137.
 Montgomery, C. G. and Montgomery, D. D., 1940, *Phys. Rev.*, **57**, 1030.
 Paetow, H., 1939, *Z. f. Physik*, **111**, 770.
 Parkash, O, 1946, *Phys. Rev.*, **76**, 568.
 Parkash, O, 1950, *Phys. Rev.*, **80**, 303.
 Parkash, O, 1950, *Curr. Sci.*, **9**, 273.
 Parkash, O, and Kapur, P. L., 1950, *Proc. Phys. Soc.*, **63A**, 453.
 Putman, J. L., 1948, *Proc. Phys. Soc.*, **61**, 312.
 Ramsay, W. E., 1940, *Phys. Rev.*, **57**, 1022.
 Rose, M. E. and Korff, S. A., 1941, *Phys. Rev.*, **59**, 850.
 Seidl, R. and Roubnek, F., 1952, *Czech. J. Phys.*, **1**, 207.
 Sloane, R. H. and Press, R., 1938, *Proc. Roy. Soc.*, **168**, 284.
 Spatz, W. D. B., 1943, *Phys. Rev.*, **64**, 236.
 Stanisiz, O., 1952, *Acta. Phys. Polon.*, **11**, No. 2, 140.
 Tanyel, Besim, 1950, *Phys. Rev.*, **77**, 843.
 Trost, A., 1937, *Z. f. Physik*, **105**, 399.
 Weisz, P. B., 1948, *Phys. Rev.*, **74**, 1807.
 Wiedenbeck, M. and Crane, H. R., 1949, *Phys. Rev.*, **75**, 1268.

DETERMINATION OF ABSOLUTE CROSS-SECTION OF (n, p) REACTION IN S^{32}

N. K. SAHA AND L. KASTURI RANGAN

[PHYSICS DEPARTMENT, UNIVERSITY OF DELHI, DELHI]

(Received for publication, September 12, 1955)

ABSTRACT: The absolute cross-section of (n, p) reaction in S^{32} has been determined by measuring the activity of P^{32} produced by fast neutrons from a 95 mgm. (Ra+Be) source, under cylindrical geometry. The various corrections involved are taken into account. The counter efficiency is determined as $(4.7 \pm 0.5) \%$ by means of a calibrated end-window counter and a thin layer of chemically separated radiophosphorus of high specific activity. An average value of $\sigma_{n,p} = 150 \pm 37$ millibarns is obtained, which compares reasonably well with the estimated value from other workers' results.

STATEMENT OF THE PROBLEM AND THE PRINCIPLE OF THE EXPERIMENT

Nuclear reactions in light and medium heavy nuclei with charged particle emission predominantly take place with fast neutrons (of energy range 0.5 to 10 Mev.). The reason is that for these nuclei the cross-section of (n, γ) reaction is comparatively low on account of the low γ -width. Γ_γ of the compound nucleus and that the fast neutron initiated p or α -particle may have sufficient kinetic energy to leak through the potential barrier with finite cross-section. The Gamow penetration factor G for p and α -particles approaches 1 for these nuclei with fast neutron excitation. This enables exothermic as well as some endothermic reactions of the (n, p) and (n, α) type to take place with fairly large cross-section if the threshold of the reaction falls in the range of the neutron energy.

Experimental determination of such reaction cross-sections in various nuclei is however, possible with reasonable accuracy only relative to the cross-section in a standard nucleus, as only by this method most of the uncertainties present in the absolute determination of the cross-section in the individual cases are largely eliminated. Such relative cross-section determinations have been done by a number of authors for elements like S^{32} , P^{31} , Mg^{24} , Al^{27} , Si^{28} , Fe^{56} etc. [Cohen (1951), Jensen (1944)]. The standard substance which is generally selected for this relative determination is S^{32} producing radiophosphorus P^{32} as the end product. The reaction characteristics for this element are given below:

Reaction	Energy balance Q	Mean half life	Reaction threshold E_t	$E_t + E_0$	Radiations and energy
S^{32} (n, p) P^{32}	0.93 Mev	14.3d	0.96 Mev	5.6 Mev	β^- 1.72 Mev (max.) γ (None)

E_t = threshold of the reaction and B_0 = height of the potential barrier for the outgoing proton of angular momentum $l = 0$.

To obtain the absolute values of the cross-sections for the different nuclei from their relative values, a determination of the absolute cross-section of the sulphur reaction is necessary. The absence of γ -radiation and probably also of resonance capture of neutrons in the sulphur reaction, makes this element most suitable as the standard substance. One such determination of absolute cross-section for the sulphur reaction exists due to Klema and Hanson (1948) in which monochromatic neutrons of known fluxes having energies from 1.6 to 5.8 Mev. were used and the activity of the resulting P^{32} was measured. Similar observations due to Bleuler (1947), Lüscher, Scherrer and others (1950) and more recently due to Hürlimann and Huber (1955) are available. The last one uses the ionisation chamber method and is a work of considerable precision. The results of the earlier workers are, however, not always in accord, as we shall discuss in the last section of this paper. It is moreover clear that the reaction can also be produced quite conveniently by a fairly strong source of $(Ra\alpha + Be)$ neutrons which has almost a continuous energy spectrum between zero and about 11 Mev (Teucher, 1949). Actually, we have recently used the $(Ra\alpha + Be)$ source for the determination of relative (n, p) cross-section in a number of cases [Saha and Choudhury, 1953; Nandi and Saha, 1954] including S^{32} . The energy dependence of the reaction cross-section here would mainly reflect the variations of the Coulomb penetration factor G with energy which approaches 1 in these cases. Hence, below the energy limit $E_t + B_0$ the cross-section is expected to increase monotonously with neutron energy and above this limit remain relatively steady. The interpretation of the cross-section measured in this way therefore becomes possible at the corresponding mean energy of the neutron spectrum. The object of the present work is, therefore, to redetermine the absolute cross-section of the (n, p) reaction in S^{32} using the 100 mgm. $(Ra\alpha + Be)$ neutron source at our disposal, which we have employed in determining the relative cross-sections of reactions in the different elements.

Consider a neutron beam of effective flux F per sec. per cm^2 of the target, passing through the thickness of the target material containing, say, N nuclei/cc. If V be the total volume of the material, a total of NV nuclei are exposed to the neutron source. The cross-section per nucleus is σ cm^2 and therefore $NV\sigma$ is the effective area of the target. On multiplying this by F , the result $NV\sigma F$ gives the number A_0 of the target nuclei in the volume V that have undergone transmutations per sec. The initial rate of disintegration per sec. of the transmuted nuclei would therefore be given by

$$A_0 = NV\sigma F \quad \dots (1)$$

The above formula will be strictly valid for a monochromatic beam of neutrons. In actual practice the neutron beam employed may have a wide energy spectrum

ranging between energies 0 and E_{max} and the reaction cross-section $\sigma(E)$ may be considerably energy-dependent. If $F(E) dE$ be the neutron flux in the energy range E and $E+dE$ and E_s the threshold of the reaction, then the total absolute activity produced would be given by

$$A_0 = NV \int_{E_s}^{E_{max}} \sigma(E) F(E) dE \quad \dots (2)$$

The integral can be evaluated only if the form of the energy-dependence of the reaction cross-section and the energy distribution function of the neutrons are known. As these are not always possible to know one can obtain only the average reaction cross-section $\bar{\sigma}$ for the total fast neutron flux per unit area f_0 as

$$A_0 = N\bar{\sigma}V \int_{E_s}^{E_{max}} F(E) dE \approx N\bar{\sigma}Vf_0 \quad \dots (3)$$

assuming that the neutron flux is negligibly small between 0 and E_s . Only in case of a resonance capture of fast neutrons at a definite energy E_r , the integral in (2) reduces to a single term with $\sigma(E) = \sigma_r$, the resonance capture cross-section. The neutron flux F_r at E_r , must however, be known in this case.

Using a thick target of sulphur (32) under 'poor geometry' we determine the initial rate of disintegration of radiophosphorous (32) by means of a thin-walled β -ray tube counter under a standard geometry of counting. A determination of A_0 from this observation necessitates a measurement of the absolute efficiency of the counter used. We propose to determine the tube-counter efficiency by comparing the activity of a thin layer of chemically concentrated active P^{32} source as recorded by the counter with that by a calibrated end-window β -counter. The effective neutron flux F in the above equation is a factor of considerable uncertainty in most of the determination of absolute cross-sections. F has to be estimated either by monitoring the fast neutrons by a standard indicator like silver or by comparison with a standard neutron source. We have, however, determined the total neutron flux from the (Ra α +Be) source by the method of thermalisation (Saha and Rangan, 1953) and make use of the result obtained in calculating the cross-section in the present case. The use of the thermalised neutron-flux may not be absolutely free from objection, since a low energy part is also associated with the natural spectrum of the (Ra α +Be) neutrons, which cannot be separated from the thermalised fast neutrons. It is, however, estimated that the contribution of the natural slow neutrons would be small, not exceeding 1% of the total. The inaccuracy due to this would then be far out-weighted by the uncertainties involved in some other factors used in the determination.

2. DESCRIPTION OF THE EXPERIMENT

A saturation mass (407 gm., sufficient to give the maximum or saturation value of total activity), of pure reprecipitated flower of sulphur was exposed to neutrons from the 100 mgm. (Ra α +Be) source filtered through about 1 mm of cadmium for 94 hours. After irradiation, the exposed material was mixed thoroughly and a part of it packed in the form of a hollow cylinder which can be placed coaxially with the β -ray tube counter of thin wall (~ 0.1 mm). The cylinder was supported on the inside by very thin paper (0.6 mg/cm 2). The thickness of the sample material corresponded to the maximum thickness for saturation activity and weighed 90 gm. The saturation mass and saturation thickness were found by a number of separate experiments. The final sample cylinder was 8.9 cm. high, 1.04 cm. thick and 4.25 cm. in inner diameter. The cylinder was slipped over the counter and the activity followed for 31 days. The semi-log plot of the nett activity is shown in figure 1. The initial activity of 367 counts/2 min. was corrected for the following: (1) a factor of 1.05

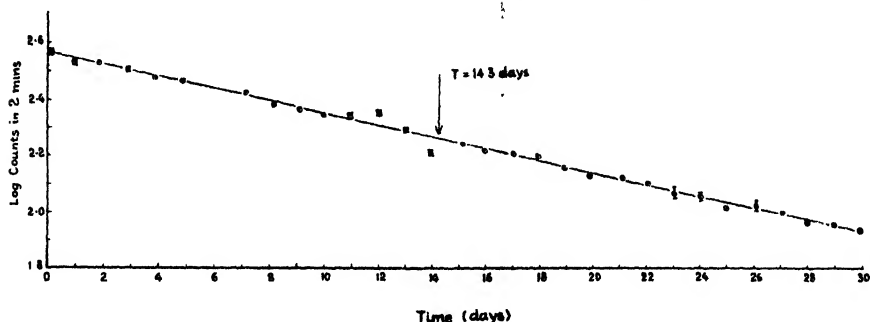


Fig. 1. Decay curve of P^{32} due to fast neutron irradiation of sulphur.

for isotopic content of S^{34} , (2) self-absorption : 23%, (3) non-saturation neutron exposure time giving a correction factor 5.7. The corrected initial activity for the sample cylinder of mass 90 gm as measured by the tube counter amounts to 79 ± 8 c/sec. In order to convert this activity into absolute number of disintegrations per gram of the sample, the efficiency of the tube counter was determined.

3. EFFICIENCY OF THE TUBE COUNTER

A standardised end window counter was set up in which the extent of the effective counting area in two mutually perpendicular directions and the directional efficiency of the counter were carefully determined by means of a narrow, well-collimated RaD β -ray source. This counter was used by us for the absolute determination of β -ray counting rate from a chemically concentrated P^{32} source. Two such active samples of known masses were then prepared. One of these was counted by the standardised end-window counter (under a well defined geometry) and the other by the thin-walled β -ray tube counter whose efficiency was

to be found. In the latter case the source was mounted in the same form and with the same amount of absorber backing as the samples in the previous tube counter measurements. As the neutron irradiated sulphur samples could not give good activities in thin layers under the end-window counter, chemically concentrated P^{32} sample was used. This was prepared as follows: Following a method due to Goaverts (1938) 4 pounds of pure carbon disulphide was taken in a 2 litre round bottom flask. Dipping inside the liquid were two clean thin sheets of copper ($2" \times 1"$) electrodes kept parallel to each other and with an electric field of $100V/cm$ between them, as in figure 2.

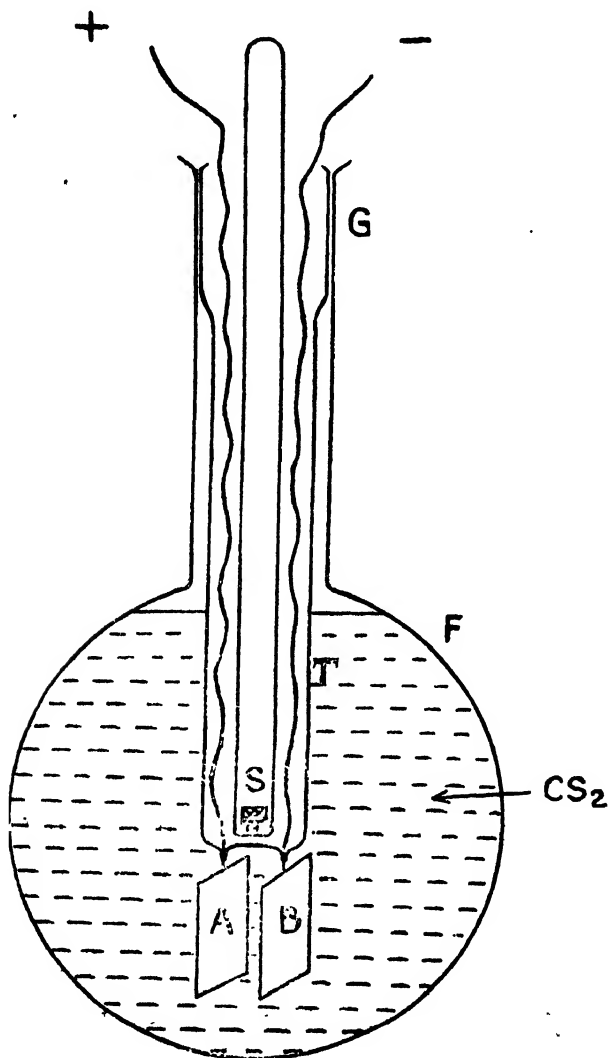


Fig. 2. Arrangement for neutron irradiation of carbon disulphide (S =neutron source, A, B —copper electrodes, T —glass tube, G —ground joint, F —glass flask.)

The neutron source covered with 1 mm. cadmium was kept at the centre of the solution through a glass tube and the liquid was thus exposed for 10 days. As originally reported by Goaverts, the active P^{32} was found to get deposited on both the positive and the negative copper electrodes in the ratio $\sim 3:2$. The copper plates were then removed and digested in concentrated nitric acid, all the copper removed as copper sulphide, carrier phosphorous added in the form of sodium-dihydrogen-phosphate and finally precipitated as magnesium-ammonium-phosphate. This gave a P^{32} phosphate sample of fairly high specific activity (roughly 5000 c/min/mg. after correcting to 4π geometry and other sources of errors) as measured by the calibrated end-window counter. Details of the subsequent measurements are given below. To obtain a suitable activity for measurement, part of the above sample was diluted with pure flower of sulphur. A weighed quantity (15.8 mgm) of this diluted sample was uniformly spread on the sticky side of a 'cellotape' sheet, which was rolled into a cylinder of the same dimension and with the same thin paper support as in the tube counter measurements. This was slipped over the tube counter and the initial disintegration rate (153.5 ± 2.5 c/min.) counted by following the activity for 22 days. Simultaneously a weighed quantity (6.0 mg) of the active phosphate was spread as a thin layer on a rigidly mounted source holder of the standardised end-window counter and the activity again followed for the period of 22 days. An initial disintegration rate of 213.8 ± 2.5 c/min. was recorded for the sample. The two decay curves are shown in the semi-log plot in figure 3.

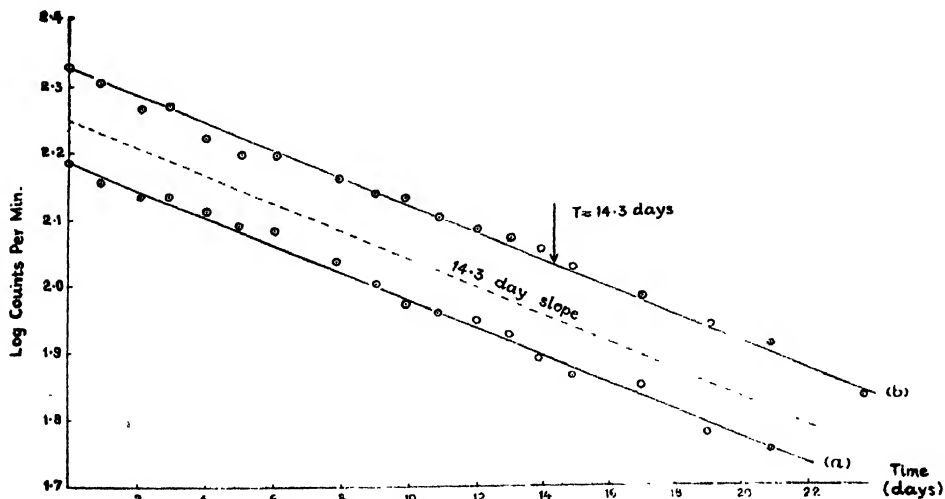


Fig. 3. Decay curve of chemically separated P^{32} sample as measured by (a) the tube-counter and (b) the end-window counter.

A subsidiary experiment was performed for finding out the self-absorption of β -rays in the active source-layer under the end-window counter by measuring

the counting rates with absorbers over the source, and applying the usual formula for zero source thickness. A factor of 0.85 was obtained as correction. A correction factor of 0.9 was applied for back-scattering by the sample holder as determined by us earlier (Saha and Rangan, 1953) and a factor of 5.3 for correction to 4π geometry and the planar nature of the source. Thus the corrected absolute rate of disintegration for the sample comes out to be 208 ± 18 disintegrations/min/mgm. of the sample. This value, compared with the initial rate of disintegration per milligram of the sample as measured by the tube counter, viz. 9.7 counts/min./mgm., gives directly the efficiency of the tube counter $\epsilon = 9.7/208 = (4.7 \pm 0.5)\%$ under the experimental conditions.

4. CALCULATION OF ABSOLUTE CROSS-SECTION

In our activation experiment, a "poor geometry" arrangement has been used, where an approximately spherical neutron source of diameter "2b" giving a total flux F_0 neutrons/sec. is surrounded by a thick spherical shell of the material of diameter "2a" (see figure 4). The neutron

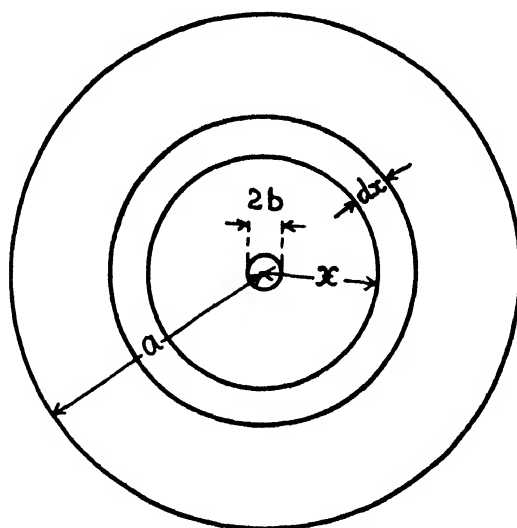


Fig. 4.

flux over an elementary shell of radius r and a small thickness " dr " would be $\bar{F} = F_0/4\pi r^2$ and the shell volume would be $dV = 4\pi r^2 dr$. From (3) the number of activated nuclei in this shell would be $dA_0 = N\bar{\sigma} \bar{F} dV$. Integrating over the spherical volume we get

$$A_0 = \int_b^a F_0 N \bar{\sigma} dr = F_0 N \bar{\sigma} (a - b) \quad (4)$$

assuming zero attenuation of the neutron flux for the activated material shell between radii b and a . We thus get

$$\bar{\sigma} = \frac{A_0}{F_0 N(a-b)} \quad \dots (5)$$

A_0 is given by the corrected activity as measured by the tube counter for the total amount of the original sulphur sample exposed (407 gm.) divided by the efficiency of the tube counter. This comes to:

$$A_0 = \frac{407 \text{ gm.}}{90 \text{ gm.}} \cdot \frac{79 \text{ cps}}{0.047} = 7.6 \times 10^3 \pm 10\%$$

disintegrations per second.

F_0 , as mentioned earlier, has been taken as our measured value of the total neutron flux from the source and is $F_0 = 1.3 \times 10^7 \pm 23\%$, $(a-b) = 5.1$ cm. and $N = 7.7 \times 10^{21}$ atoms/cc, as calculated from the packing density of the sulphur powder in our arrangement of exposure. Substituting these in relation (5) we get

$$\sigma_{(n,p)} S^{32} = 150 \times 10^{-27} \text{ cm}^2 \pm 25\%$$

5. DISCUSSION

Weisskopf and Blatt (1950) have shown from a statistical theory of nuclear reactions with fast neutrons that the cross-section of (n, p) reactions can be represented by

$$\sigma_n(n, p) = \pi r^2 f_p / (f_n + f_p) \approx \pi r^2 f_p / f_n$$

where f_p and f_n are the relative probabilities of the compound nucleus decaying by emission of a proton and a neutron respectively. Methods of calculating these factors have been given by these authors. Cohen (loc. cit) has shown the results of calculation of $\sigma(n, p)$ on the various assumptions of the values of r_0 occurring in the nuclear radius $r = r_0 A^{1/3} \cdot 10^{-13}$ cm. and also for various nuclear temperatures. He considers his calculated cross-section for S³² reaction in fair agreement with the experimental value ($285 \pm 5\%$ millibarn) obtained from Klema and Hanson's (loc. cit) determination (probably after correcting for the energy spread of his neutron beam). Since the density of nuclear levels generally changes with excitation energy, correction to cross-section for reduction to zero threshold is necessary. Cohen, however, comes to the conclusion that the last correction is unimportant for light nuclei and that the statistical theory of nuclear reaction provides no further than a general basis for the calculation of the reaction cross-section, with considerable variation to be expected in individual cases.

The reaction cross-section for S³² (n, p) P³² was observed by Bleuler (1947) and later by Klema and Hanson (1948) and Lüscher and others (1950) from the activity measurements of P³². More recently Hürlimann and Huber (1955) have

measured the same reaction cross-section with great care using an ionisation chamber method. These authors have also found the variation of the reaction cross-section with neutron energy upto 4 to 6 Mev. Klema and Hanson have observed a monotonous increase in the reaction cross-section from 1.3 mb. to 300 mb. as the neutron energy increases from 1.6 to about 5 Mev., further on the cross-section remaining steady upto ~ 5.8 Mev. The last two groups of authors, on the other hand, have obtained results showing the same general trend as those of Klema and Hanson, but their observed variation of cross-section with energy is marked with a number of close-lying sharp resonance peaks between 2.2 and 4 Mev neutron energy. If the resonance peaks are, however, averaged over their mean energies, the absolute values of the cross-section come out somewhat lower than those of Klema and Hanson. This can be seen from curves (b) and (c) in figure 5 where the cross-section curve of Klema and Hanson (curve b) and that of Hürlimann and Huber (curve c) are reproduced on the same scale.

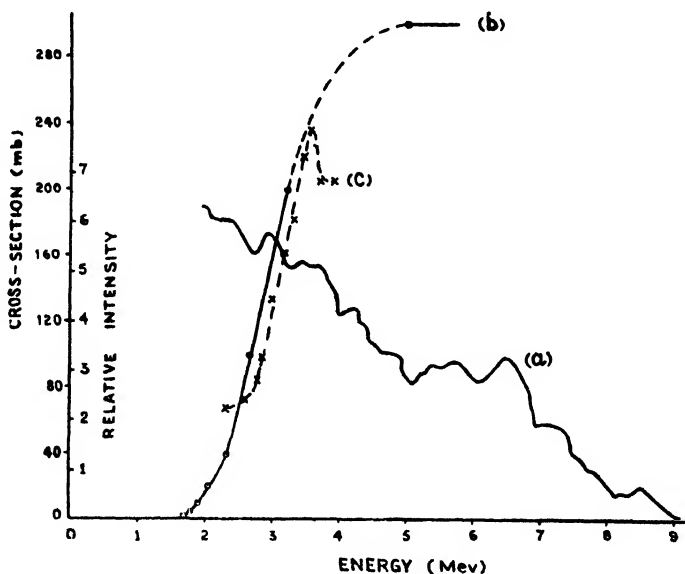


Fig. 5. (a) Energy spectrum of neutrons from a (Ra α + Be)—source due to Schmidt-Rohr (1953); Energy variation of σ_{np} (S) due to (b) Klema and Hanson (1948), (c) Hürlimann and Huber (1955) (averaged).

In our case, the (Ra α + Be) neutrons have a wide energy spectrum, on the precise nature of which considerable uncertainty still exists. In recent years careful measurements of the energy spectrum have been made by Teucher (*loc. cit.*) and still later by Schmidt-Rohr (1953). Excepting in details the results of the two different investigators more or less agree.

Even then, since the energy distribution function of the neutrons and the energy-dependence of the cross-section are not analytically known, we cannot

evaluate the integral under equation (2). However, by combining graphically the results of Schmidt-Rohr with the observations of cross-section variation with energy (Klema and Hanson) an approximate estimate of the mean $\bar{\sigma}_{n,p}$ for the $(Ra+Be)$ -neutron spectrum may be attempted. In figure 5, curve (a), the energy spectrum of $(Ra+Be)$ -neutrons obtained by Schmidt-Rohr is reproduced for this purpose. The neutron spectrum referred to can be considered to consist of the following features. (a) The spectrum starting at ~ 2 Mev with a relative intensity of nearly 6 falls off more or less linearly (with several small changes in slope) up to 5 Mev where the relative intensity is nearly 3. (b) From 5 to 6.7 Mev the spectrum is almost flat with the relative intensity of 3. (c) Beyond 6.6 Mev, the relative intensity falls off quite rapidly and becomes practically insignificant at about 8 to 9 Mev. (d) There is a fine structure superposed on the general run of the distribution throughout. On the basis of this energy distribution the weight factor of the neutrons in any part of the spectrum (i.e. for a given energy interval) can be estimated by multiplying the mean relative spectral intensity over this part by its energy interval. Now, looking closely into Klema and Hanson's cross-section $\sigma(n, p)$ [curve (b), figure 5] at various neutron energies, we can split it into a number of linear portions as shown in the table below:

TABLE I

Linear energy intervals (Mev)	2-3.5	3.5-4	4-4.5	4.5-5	5-6.6	6.6-8
Mean $\sigma(n,p)$ in millibarns	120	273	295	298	300	300
Neutron intensity weight factor.	8.5	2.4	2.1	1.7	5.6	2.3

The corresponding spectral weight factors for the various energy intervals estimated as above are given in 3rd row of the table. The mean $\bar{\sigma}(n, p)$ for the whole neutron spectrum therefore calculates out to be 220 mb.

This result, obtained as an extrapolation of Klema and Hanson's observations, seems to be somewhat higher than our experimental value 150 ± 37 mb. Of course, we have done the extrapolation upto the maximum neutron energy on the assumption that the cross-section remains constant at ~ 300 mb. from ~ 5 Mev upward. This assumption may not be justified, since at high neutron energies, reactions like $(n, 2n)$, (n, α) etc. are likely to ensue and produce a rapid fall in the cross-section of (n, p) reaction by competition. This view seems to be supported by the observations of the reaction cross-section by Hürlimann and Huber (curve c) where the smoothed out cross-section curve shows a monotonous increase with energy upto ~ 3.5 Mev, beyond which the curve shows a sharp fall. The absolute values of the mean cross-sections obtained from this curve are also appreciably lower

than Klema and Hanson's values at the same energy. An estimate of the mean cross-section $\bar{\sigma}_{np}$ for the (Ra α +Be) neutron spectrum can also be carried out with Hurlimann and Huber's cross-section curve in the same manner as we have done with Klema and Hanson's curve. The mean $\bar{\sigma}_{np}$ obtained in this way comes out to be ~ 138 mb taking the neutrons of energies upto 4 Mev only. This value is a better approach to our experimental value.

It may be further pointed out that there are several factors of uncertainty, e.g., the value of the fast neutron flux, the large correction factors etc., involved in our determination, giving a large probable error in our value. The method of extrapolation used above to estimate the average cross-section for the (Ra α +Be) neutrons is also far from satisfactory, since some uncertainty still exists both in the energy-dependence of the reaction cross-section σ_{np} as well as in the energy distribution of the (Ra α +Be) neutrons. A further refinement of our measurements is also possible. An improved series of determination of σ_{np} where the large correction factors mentioned above are almost completely eliminated is under way.

ACKNOWLEDGMENTS

Our sincere thanks are due to Prof. D. S. Kothari and Prof. R. C. Majumdar, for their constant encouragement and for allowing us the facilities for the work, and also to Dr. K. R. Kar of the Chemistry Department for helping us in the chemical separations. The work was carried out under the financial support of the Department of Atomic Energy, Government of India.

REFERENCES

- Blouler, E., 1947. *Helv. Phys. Acta*, **20**, 519.
 Cohen, B. L., 1951. *Phys. Rev.*, **81**, 184.
 Goaverts, 1938. *Nature*, **141**, 871.
 Hürlimann, T. and Huber, P., 1955. *Helv. Phys. Acta.*, **28**,
 Jensen, P., 1944. *Zeit. f. Phys.*, **122**, 387.
 Klema, E. D. and Hanson, A. O., 1948. *Phys. Rev.*, **73**, 106.
 Lüscher, E., Ricamo, R., Scherrer, P. and Zunti, 1950. *Helv. Phys. Acta.*, **23**, 561.
 Nandi, S. K. and Saha, N. K., 1954. *Ind. Jour. Phys.*, **28**, 396.
 Saha, N. K. and Choudhury, M., 1953. *Ind. Jour. Phys.*, **27**, 244.
 Saha, N. K. and Rangan, L. K., 1953. *Ind. Jour. Phys.*, **27**, 18.
 Schmidt-Rohr, U., *Zeit. f. Natur.*, 1953. **8a**, 470.
 Teucher, M., 1949. *Zeit. f. Phys.*, **126**, 410.

DIELECTRIC PROPERTIES OF 2, 4-DINITROFLUOROBENZENE

D. V. G. L. NARASIMHA RAO

PHYSICS DEPARTMENT, ANDHRA UNIVERSITY, WALTAIR.

(Received for publication, January 3, 1956)

ABSTRACT. The dipole moment of 2, 4-dinitrofluorobenzene is determined in solution in benzene at 30°C. and the value obtained 3.56 D is found to be in exact agreement with that calculated using the general method given by the author previously. The absorption of the molecule at 3 cm., is also studied in the same solvent and a value of 3.30 D for the dipole moment and 5.3×10^{-11} sec., for the relaxation time are obtained. It is expected from the value of the relaxation time that the molecule will show maximum absorption near about 10 cm.

INTRODUCTION

A general method for the calculation of the dipole moments of 1:2:4 tri-substituted benzenes was given by the author (1955a) previously. The method was applied in the first instance to a few compounds for which data on the dipole moments were available. It is noticed that the discrepancy between the calculated and the observed values increases in the group of molecules—2:4 dinitro-chlorobenzene, 2:4 dinitro-bromobenzene and 2:4 dinitro-iodobenzene—the deviation increasing as we pass from chloro to bromo to the iodo compound (cf. Table I below).

TABLE I

Compound	μ (calculated)	μ (observed)
2, 4-Dinitro-fluoro* benzene	3.56D	3.56
2, 4-Dinitro-chloro benzene	3.19	3.0 \pm .1 3.29
2, 4-Dinitro-bromo benzene	3.54	3.1 \pm .1
2, 4-Dinitro-iodo benzene	4.29	3.4 \pm .1

Hence we may expect a fair agreement in the case of the fluoro compound. A reference to the existing literature indicates that there is no published record of the dipole moment of this molecule. It is thought worthwhile to calculate the

* Present investigation, briefly reported in *Curr. Sci.*, 1955, 24, 497.

moment of the compound using the general equation and also to carry out an experimental investigation on the molecule.

Further, it may be of interest to study the microwave absorption of the molecule which also gives the value of the dipole moment. The monosubstituted benzenes—fluoro and nitro-benzenes—have wavelengths of maximum absorption near about 3 cm. In the case of this molecule the region of maximum absorption may shift to longer wavelengths due to the increased size as a result of the three substituted radicals.

CALCULATION

The moments of the monosubstituted compounds are assumed as $m_{e1} = 1.45$ and $m_{e2} = m_{e3} = 3.90$. The polarizability of the NO_2 group is the same as used previously and that of $-\text{F}$ is taken as 0.57×10^{-24} obtained from the value of the refraction of HF (Syrkin and Dyatkina 1950). As a result of the application of Equation (5) of the previous article (1955a) the moment turns out to be 3.64 D. When the correction for the dielectric constant of the internuclear space is also effected, this reduces to 3.56 D. It is easily seen that the simple vectorial addition gives a value of 3.42D for the moment of the molecule.

EXPERIMENTAL RESULTS

The method of measurement of the dipole moment in dilute solution was described in a previous communication (1955b). For the measurement of the dielectric constant an improved set up is used. This is a Franklin-oscillator wavemeter combination operated at a fixed frequency of 1 Mc/s similar to the one described by Le Fevre *et al* (1950). The results are given in Table II, in which the symbols have the usual significance (author, 1955b).

TABLE II

Temperature = 30°C.
Density of benzene = 0.8704 gm/c.c.

w	ϵ_{12}	$\Delta\epsilon$	$\Delta\epsilon/w$	n_{12}	n^2_{12}	Δn^2	$\Delta n^2/w$
	2.2640	—	—	1.49354	2.23065	—	—
0.01901	2.4065	0.1425	7.498	1.49522	2.23569	0.00504	0.265
0.03162	2.4922	0.2282	7.216	1.49575	2.23727	0.00662	0.209
0.05017	2.6158	0.3518	7.013	1.49636	2.23909	0.00844	0.168
0.07084	2.7583	0.4943	6.977	1.49757	2.24273	0.01208	0.171
0.10240	2.9651	0.7011	6.844	1.49783	2.24350	0.12855	0.125
0.11952	3.1083	0.8443	7.068	1.49797	2.24391	0.01326	0.111

$$(\Delta\epsilon/w)_{w \rightarrow 0} = 7.470$$

$$(\Delta n^2/w)_{w \rightarrow 0} = 0.256$$

$$(\Delta/w)_{w \rightarrow 0} = 7.214$$

$$P_d = 254.1 \text{ c.c.}$$

$$\mu = 3.55 \text{ D. (graphical)}$$

Details of the microwave measurements at 3 cm. are described elsewhere (1955c). The values of the orientation polarisation (P_d) and the relaxation time (τ) are calculated using the equations

$$P_d = \frac{P_i^2 + (P_0 - P_r)^2}{P_0 - P_r} \text{ and } \tau = I' \omega \cdot \frac{P_0 - P_r}{P_i}$$

since in this case $\omega\tau > 1$. The value of the total polarisation (P_0) at infinite dilution obtained from the r.f. measurements described above by adding the molecular refraction (obtained from bond refractions) to the value of P_d . Benzene is used as the solvent in both cases. The results are tabulated below.

TABLE III
Frequency 9515 Mc/s.
Temperature 30°C.

ω	ϵ'	ϵ''	D	p_r	p_i
0.02810	2.36	0.0623	0.8884	0.3514	0.01106
0.04076	2.40	0.1029	0.8932	0.3567	0.01785
0.05927	2.45	0.1301	0.8978	0.3625	0.02197
0.07767	2.48	0.1572	0.9086	0.3640	0.02587
0.09018	2.49	0.1851	0.9122	0.3652	0.03013
0.10212	2.51	0.2053	0.9152	0.3668	0.03308

Extrapolated values $P_r = 95.0$ c.c.

$P_i = 62.5$ c.c.

$P_0 = 293.0$ c.c

$(P_d = 254.1 + R_D = 38.9 - \text{r.f.measurements})$

$\mu = 3.30$ D.

$\tau = 5.3 \times 10^{-11}$ sec.

It will be seen from the value of the moment of the molecule obtained by the simple vector addition of the group moments and that derived using the detailed calculation of the general method that the induced contribution to the value of the moment is not considerable, whereas in the case of the similar iodo compound it is appreciable. This may be attributed to the difference in the polarizability values of the two radicals. Thus for fluorine with the least value of the polarizability the correction term is least. The observed value of the moment 3.55D is in good agreement with the calculated value of 3.56D. When the small correction term of Palit (1952) to the Guggenheim equation used in deriving the value of the moment from the observed data is also considered, the moment turns out to be 3.56D in exact agreement with the calculated value.

The absorption measurements at 3cm. give a value of 3.30D for the dipole moment of the molecule which agrees within about 8% with the r.f. measurements. The relaxation time obtained is fairly higher than that of the mono substituted benzenes; this may be due to the increased size of the molecule. From the value of the relaxation time obtained in this investigation, the wavelength of maximum absorption is expected at about 10 cm. It would be of interest if the absorption in this region is examined for this molecule.

ACKNOWLEDGMENTS

The author is deeply indebted to Prof. K. R. Rao for his kind and invaluable guidance throughout the progress of the work. He is grateful to the Union Government for the award of a Senior Research Scholarship.

REFERENCES

- Le Fevre, R. J. W., Ross, I. G. and Smythe, B. M., 1950, *Jour. Che. Soc.*, 276.
Narasimha Rao, D. V. G. L., 1955a, *Ind. Jour. Phys.*, **29**, 49.
" 1955b, *Ibid.*, **29**, 398.
Palit, Santi R., 1952, *Jour. Am. Chem. Soc.*, **74**, 3952.
Radhakrishna Murty, Ch. and Narasimha Rao, D. V. G. L., 1955c, *Jour. Sci. Ind. Res.*,
(Communicated).
Syrkin, Y. K. and Dyatkina, M. E., 1950. *Structure of Molecules and the Chemical Bond.*,
Interscience Publishers Inc., New York, page 199.

Letter to the Editor

STRUCTURE OF THE SPECTRUM OF SINGLY IONISED BROMINE

Y. BHUPALA RAO

PHYSICS DEPARTMENT, ANDHRA UNIVERSITY, WALTAIR

(Received for publication, November 12, 1955)

The line spectrum of singly ionised bromine (Br II) was investigated by Bloch and Lacroute (1934), Lacroute (1935), and Rao and Ramanadham (1944); the term values known till now are collected by Moore (1952). Still several strong lines in the spectrum remain unclassified, and the analysis is far from complete. An extensive study of the spectrum has been made over the range from λ 9000Å to λ 400Å with spectrographs of small and large dispersion. Several levels have been newly determined by which about 250 additional lines are classified. The new levels with their designations and J values are given in table below in ascending order of magnitude calculated with respect to the ground level $4p^4 \ ^3P_2$ as zero; the notation is that adopted by Moore.

Details of the analysis will be published shortly.

TABLE I

Designa- tion	J	Level	Designa- tion	J	Level	Designa- tion	J	Level
$4p^4 \ ^1D$	2	12098	$5p^4 \ ^3P_2$	1	142839.9	$5d^4 \ ^1G^\circ$	4	156963.8
$4p^4 \ ^1S$	0	27876	$5p^4 \ ^3P_1$	0	143148.1	$5d^4 \ ^3P^\circ$	3	157226.9
$4p^4 \ ^3P^\circ$	2	96439.4*		1	145601.6		1	157369.7
	1	98807.3*		2	145921.5		2	157632.8
	0	100242.2	$5p^4 \ ^1P_1$	0	143486.4		3	157806.3
$4d^4 \ ^3D^\circ$	4	104097.9	$5p^4 \ ^1D_2$	1	144517.7	$5d^4 \ ^3D^\circ$	2	158327.4
	3	104044.6	$5p^4 \ ^1D_1$	2	145370.0	$5d^4 \ ^1F^\circ$	3	158414.5
	2	104087.2	$4f^4 \ ^3F_4$	5	145931.6	$5d^4 \ ^3P^\circ$	0	
	1	104152.3		4	145929.9		1	159778.4
	0	104206.6		3	145934.0		2	159910.8
$4p^4 \ ^1P^\circ$	1	113342.8		2	145937.9	$5d^4 \ ^3D^\circ$	2	160449.7
$4d^4 \ ^3P^\circ$	2	117744.6		1	145941.6			

TABLE I (Contd.)

Designation	<i>J</i>	Level	Designation	<i>J</i>	Level	Designation	<i>J</i>	Level
4d' ³ F	3	118509.1	4f' ³ F	2	146087.5	4f' ³ G	3	160884.4
	4	119432.1		3	146081.3		4	
							5	
4d' ¹ G	4	122191.9		4	146095.6			
4d' ¹ F	3	122720.7	6s' ³ D°	1	151357.8	5d' ¹ D°	2	160887.7
				2	151502.3	4f' ³ F	2	161132.8
5s" ¹ P°	1	125058.7		3	152380.6	4f' ¹ H	5	161289.7
4d' ³ D°	1	126788.2	6s' ¹ D°	2	152832.3	4f' ¹ D	4	161526.4
	2	127687.7				4f' ¹ G	2	161896.2
	3	127940.6	5d' ¹ P°	1	155148.0			
4d' ¹ D°	2	128890.5	5d' ³ G°	3	156116.1*	4f' ³ F	4	162210.2
5p" ³ D	1	142095.3		4	156152.3*		3	162255.9
	2	142854.1		5	156756.6		2	162313.9
	3	143704.8	5d' ³ G°	1	156512.2			
4f' ³ D	3	162344.0	6s" ³ F°	2	166487.2	5d" ³ F°	2	169676.2
	2	161169.1						
	1	162395.7	6s" ¹ P°	1	167439.0	5d" ³ D°	2	169768.9
						or	3	
4f' ¹ F	3	162364.6	5d" ³ F°	2	169127.6	5d" ¹ D°	2	170703.1
				or				
				3				
6s" ³ P°	0		5d" ³ H°	2		5d" ¹ P°	1	170827.4
	1	165329.3		or	169368.1			
				3				
	2							

*Identified in previous investigations.

REFERENCES

- Bloch, L., Bloch, E., and Lacroute, 1934. *Compt. Rend.*, **199**, 41.
 Lacroute, 1935. *Ann. de. Phys.*, **3**, 3.
 Moore, C. E., 1952. *Atomic Energy Levels*, Vol. II, 161.
 Rao, K. R. and Ramanadham, R., 1944. *Ind. J. Phys.*, **18**, 317.

REVIEW

LIGHT CALCULATIONS AND MEASUREMENTS—By H. A. E. Keitz. Pp. I-XVI+413.
Philips Technical Library, Eindhoven, Holland, 1955. Price not given.

As mentioned in the preface, the book is written avoiding as far as possible higher mathematics, so that beginners having little knowledge in higher mathematics can follow the subject easily. The book is divided into two parts, Part I dealing with light calculations and Part II with measurement of light. Of the twelve chapters in Part I the first two chapters deal with some properties of light and measurement of solid angle, and the next chapter with the units and calculations of luminous flux, luminous intensity and quantity of light. The fourth and fifth chapters deal with methods of diagrammatic representation of light distribution around a source of light. The units of illumination, luminance and luminous emittance and methods of calculating these quantities have been explained in detail in the next three chapters. The properties of extended sources of various shapes have been discussed in Chapter IX, and the next chapter deals with the influence of reflection, absorption and transmission of light in illuminating engineering. A fairly long chapter is then devoted to geometrical optics and luminance of images formed by optical systems. The last chapter of Part I deals with photometric measuring units and their dependence on the sensitivity of the eye to different wavelengths in the visible region.

In the second part various types of apparatus used for measurement of the quantities which have been defined in Part I have been described in detail and methods of measurement have been explained. Appendices containing several useful tables and also diagrams showing light distribution and zonal luminous flux in a few typical light fittings have also been included.

Although the book is intended for beginners, frequent references to original papers have been included in it to help illuminating engineers engaged in research work in this line. The volume can be used as a text book in this subject and wide circulation of this book among professional illuminating engineers in India and other countries in which new types of artificial light have been introduced only in recent years will no doubt result in the economic use of such sources of light.

S. C. S.

A TIME OF FLIGHT NEUTRON VELOCITY SELECTOR USING SCINTILLATION COUNTER*

A. P. PATRO

INSTITUTE OF NUCLEAR PHYSICS, CALCUTTA.

(Received for publication, November 11, 1955)

ABSTRACT. A method of selecting neutrons of different energies in the range 1 Kev to 30 Kev is described. The method utilises scintillation counters for the detection of neutrons, and neutron energies are measured from the time elapsing in its travel from one scintillating phosphor to a second phosphor. It is shown that the method is capable of greater resolution than the usual time of flight methods and various improvements are suggested. Measurements of transmission curves ($\sim \sigma_t$) have been made in the above energy range for vanadium, manganese and bismuth. The evidence of resonances for these elements is found and discussed.

INTRODUCTION

The investigations of interaction of neutrons of different energies with nuclei of elements requires the production of neutrons of definite energies or selection of neutrons of definite energies from a spectrum of neutrons of different energies. Bombardments by charged particles of suitable targets yield neutrons of known energies which can be utilised in the high energy regions or diffracting crystals can be used to separate neutrons of different energies according to Bragg relation in the low energy range. In another method utilised for slow and intermediate neutrons, the neutron velocities are measured by noting the time taken by the neutron to travel a given distance. In this time of flight method neutrons are generated in short pulses and the time elapsing between its generation and arrival at the detector is measured. The velocity v and consequently energy E can be obtained from the relations

$$v = 10^6/t, \quad E = 52.3 \times 10^2/t^2, \quad t = 72.3/E^{1/2} \quad (1)$$

where t = flight time per metre in $\mu\text{sec}/\text{metre}$. At low energies pulses of neutrons have been obtained from reactors by regularly interrupting a continuous beam mechanically by means of absorbing shutters. Pulsed cyclotrons have been successfully used as accelerating agents for neutron spectrometers and the experiments with the system described by Rainwater and Havens (1946) have been the

* This work is a part of the D.Phil (Science) dissertation submitted to the Calcutta University by the author in April, 1955.

most fruitful source of published data. Recently, linear accelerators have been used for producing bursts of neutrons by (γ , Be) reaction from γ -rays produced from the linear accelerator. Results of these time of flight methods can be obtained from the works of Rainwater and Havens (1946), Melkonian (1949), Havens and Rainwater (1951), Brill and Lichtenberger (1947), Selove (1951), Seidl *et al* (1954), and Goulding *et al* (1954).

THEORY

The theory for obtaining the resolution is the same in all these methods. If x is the flight distance and t the flight time, then $v = x/t$ and resolution

$$\frac{\Delta E}{E} = 2 \left(\frac{\Delta x}{x} + \frac{\Delta t_1 + \Delta t_2}{t} \right) \quad (2)$$

where Δx is the uncertainty in flight distance and Δt_1 , Δt_2 are uncertainties in time of production and detection.

The resolution can be improved only by reducing $\Delta x/x$ and $(\Delta t_1 + \Delta t_2)/t$. Δx is fixed by the length of detector and the flight path x is fixed by the intensity of the source. Consequently resolution can only be improved by reducing $(\Delta t_1 + \Delta t_2)/t$. Here $t = x/v$ and is fixed by the energy of the neutrons that are being selected. Δt_1 and Δt_2 are the neutron pulse-widths at the source and detector. The minimum time resolution obtained so far is $1.4 \mu\text{sec}$ by Seidl *et al* (1954). This figure is obtained because of the uncertainties in time of the production and detection of the neutron. If one can consider the actual time of formation and detection of the neutron, this time can be very much reduced.

After the development of scintillation counters, it was found that detection times of the order of $1/100$ th of a μsec . can easily be attained and these detectors have been widely used for detection and measurement of short half-lives of metastable states of nuclei. Scintillation counters have also been used for detection of neutrons and if one uses a scintillating phosphor containing very high percentage of hydrogen it can also be used for measuring the neutron energy by measuring the energy transferred to the recoil proton. An instrument based on the above principle has been developed by Draper (1954). Draper has used his energy selection on the fact that if the scattered neutron is emitted at an angle of 90° with respect of the incident neutron, then by keeping that angle fixed by means of a second detector, the proton pulses will give the incident neutron energies. The proton pulses are delayed artificially by a time equal to the average time of flight of the recoil neutron to the second detector. The delayed proton pulses which are in coincidence with the neutron pulses are subjected to pulse height analysis and their spectrum is directly related to the energy spectrum of the incident neutrons. In the above method the energy distribution of the neutron source is utilised. In an alternative method one can measure the time elapsing between the detection by means of proton recoil in the first detector and the

detection of the scattered neutron in a second detector. This time together with the distance between the two detectors will give the energy of the neutron. In this method the neutrons of various energies are created, so to speak, inside the first detector, and can be selected by inserting different delays between the two detector pulses. The advantages of a scintillation counter are that the two detector pulses are of the order of 10^{-9} to 10^{-7} sec. depending on the phosphors and following electronic circuits used and time measurements between the two can be reduced to that accuracy. The detectors being solids have high efficiencies and Δx can be small. This method of selecting out neutron energies has been employed and a time of flight neutron velocity selector has been developed.

EXPERIMENTAL

The experimental arrangement is shown in figure 1. *A* is the neutron source, *B* is an organic crystal and *C* is a LiI(Cu) crystal. Fast neutrons from *A* fall on the crystal *B*. The photomultiplier *B'* detects scintillations due to proton recoil in *B*. The scattered neutrons travelling in the direction of the second crystal *C* are detected by the photomultiplier *C'*. The output pulses from the two photomultipliers are passed through two pulse shapers to produce pulses of definite duration. Figure 2 shows the schematic diagram of the experimental arrange-

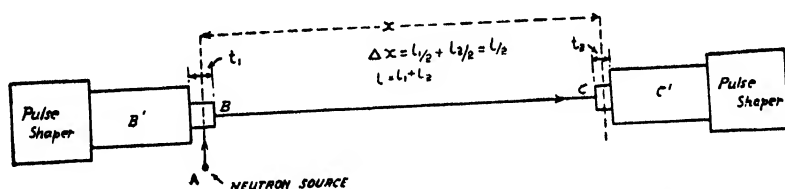


Fig. 1. Experimental arrangement of the neutron velocity selector.

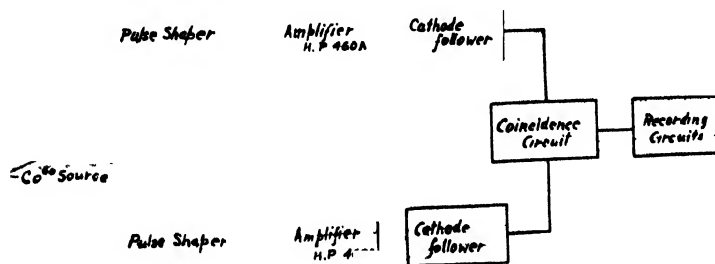


Fig. 2. Block diagram of the experimental arrangement.

ment. The shaped pulses are amplified by distributed amplifiers (Hewlett-Packard 460A) and are fed to the coincidence circuit by a cathode follower and

RG7/U cables. By changing the length of the RG7/U cables, various delays can be introduced in any one of the channels. The details of the apparatus is described elsewhere, (Patro, 1955).

RESULTS

From the delay versus count curve one can determine the velocity or energy spectrum, knowing the distance between the two crystals. Such a plot is shown in figure 3, where the abscissa gives the delay as well as the energy. Coincidence peak at zero delay is caused by the fast neutrons as well as by the gamma's. The variation in the neutron intensity is due to the variation in intensity of the source and variation of detection efficiency with energy in the second crystal.

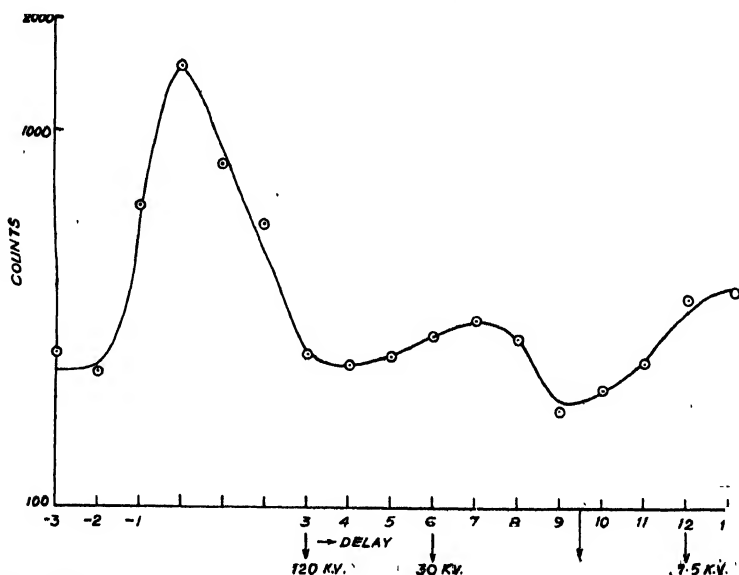


Fig. 3. Neutron energy spectrum obtained with the neutron velocity selector.

The resolution is given by (2) where Δx is half the sum of the thickness of the two crystals and $\Delta t_1 + \Delta t_2$ is the width of the coincidence peak. The resolution obtained in an experimental set up along with those of the Harwell linear accelerator (Goulding *et al*, 1954) are given below.

Energy Kev.	$\Delta E/E$ Harwell	$\Delta E/E$ Present experimental set up
1	1/2.5	1/1
2		1/1.5
4		1/1.2
6.5	1/1	
7.5		1/1

From this comparison it can be concluded that in this region with the present set up the resolution is not bad compared to the linear accelerator. This figure is preliminary and can easily be improved upon.

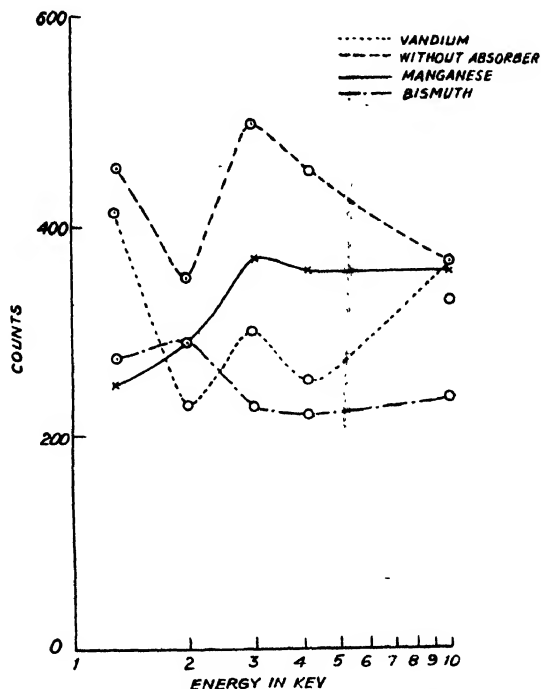


Fig. 4. Neutron spectrum selected by the velocity selector without absorber and with absorbers.

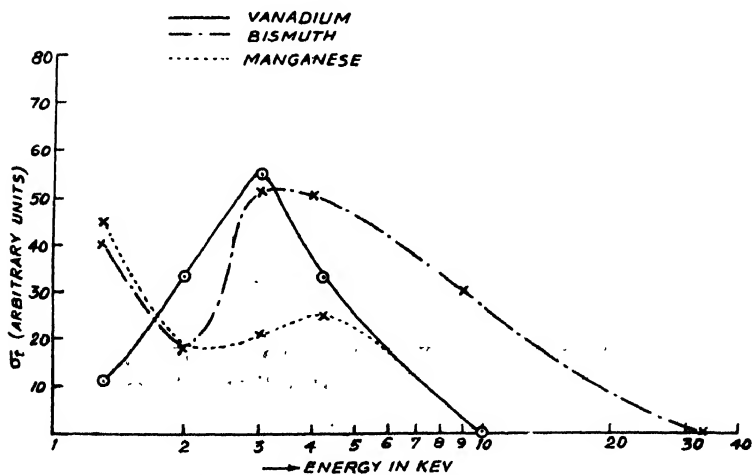


Fig. 5. Variation of ' σ_t ' with energy for manganese, bismuth and vanadium. ' σ_t ' scale is arbitrary and is different for different absorbers.

Transmission experiments performed with the set up for vanadium, manganese and bismuth are given in figure 4. Figure 5 gives the variation of σ_t with energy in the region investigated, where,

$$\sigma_t = \frac{\text{Counting rate without absorber} - \text{counting rate with absorber}}{\text{Counting rate without absorber}}$$

Manganese shows a peak in σ_t in the region 2.5 Kev to 7 Kev. This may well be due to the smearing effect due to poor resolution. Vanadium shows a peak at 3 Kev with half-width of 3 Kev. This indicates resonance levels in this region. Bismuth has also been studied and it shows strong absorption in the region 3 to 4 Kev.

DISCUSSION

An improved apparatus was set up to study neutron cross-sections in the region of 2.5 to 10 Kev. The latter apparatus was used to check known values of manganese and sodium and increased resolution was obtained. It seems entirely feasible to increase the resolution ten times.

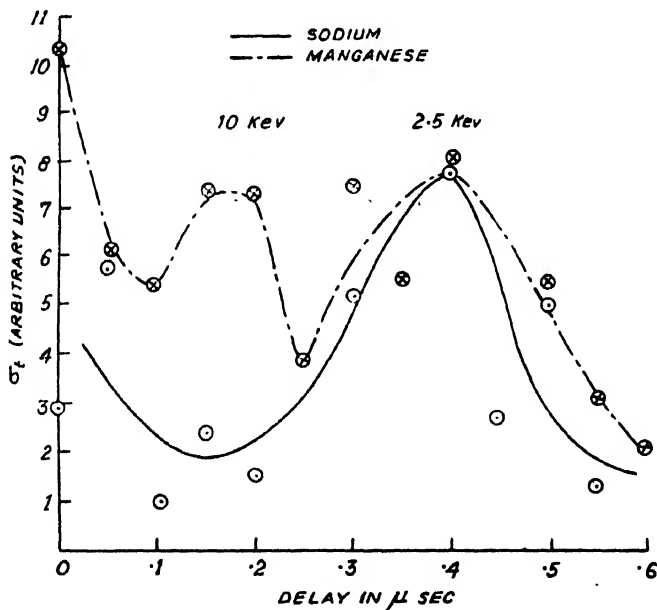


Fig. 6. Variation of ' σ_t ' with energy for manganese and sodium.
' σ_t ' scale is arbitrary and different for sodium and manganese.

Recent compilation of total cross-section data (Hughes and Harvey, 1955) confirm all the above features and reveal many other resonances in the region investigated.

The poor resolution of the experimental set up is due to the weak neutron source (8mc. RaD—Be neutron source) and consequent use of large phosphors and small flight paths. By using small crystal 1 cm thick and keeping the flight path to one metre and using a coincidence circuit of $1\mu\text{sec}$ resolving time, it is possible to obtain a resolution of $< 5\%$ even up to 0.5 Mev.

There is a further advantage that the method can be applied to measure variation of (n, γ) cross-section by having the sample near the second crystal which in that case will be a gamma detector. The work is being continued.

ACKNOWLEDGMENTS

The author wishes to express his gratitude to Prof. M. N. Saha, F.R.S. for his keen interest and encouragement and to Prof. B. D. Nag Chaudhuri for guidance throughout the work. The author wishes to thank Sri B. Basu for the help rendered during the work.

REFERENCES

- Brill, T. and Lichtenberger, H. V., 1947, *Phys. Rev.*, **72**, 585.
Draper, J. F., 1954, *R.S.I.*, **25**, 558.
Goulding, F. S., *et al*, 1954, *Proc. I.E.E.*, **101**, 248.
Havens, W. W. and Rainwater, J., 1951, *Phys. Rev.*, **83**, 1123.
Hughes, D. J. and Harvery, J. A., 1955, *B.N.L.*, 325.
Jones (Jr.), W. B., 1948, *Phys. Rev.*, **74**, 364.
Melkonian, E., 1949, *Phys. Rev.*, **76**, 1750.
Patro, A. P., 1955, D.Phil. Thesis, Calcutta University.
Selove, W., 1951, *Phys. Rev.*, **84**, 869.
Seidl *et al*, 1954, *Phys. Rev.*, **95**, 476.
Rainwater, J. and Havens, W. W., 1946, *Phys. Rev.*, **70**, 136.

ULTRAVIOLET ABSORPTION SPECTRA OF α -METHYL NAPHTHALENE AND β -METHYL NAPHTHALENE IN THE LIQUID AND SOLID STATES*

S. B. BANERJEE

OPTICS DEPARTMENT, INDIAN ASSOCIATION FOR THE CULTIVATION OF SCIENCE, JADAVPUR, CALCUTTA.

(Received for publication January 14, 1956)

ABSTRACT. The near ultraviolet absorption spectra of α -methyl naphthalene and β -methyl naphthalene have been studied for the liquid and solid states at low temperatures and the results have been compared with those for the vapour state reported by previous authors. Both the substances yield two systems of bands.

In the case of α -methyl naphthalene, in the first system of bands the 0-0 band is at 31192 cm^{-1} for the liquid state and is displaced by 976 cm^{-1} towards the longer wavelength side from its position in the vapour state. The 0-0 band in the solid state is at 31285 cm^{-1} and shows only a small displacement of 93 cm^{-1} with respect to that in the liquid state. Thus the major change in the 0-0 band of this system takes place with the liquefaction of the vapour. In the second system, on the other hand, the major change in the excited electronic state occurs when the liquid is solidified and cooled to -180°C . It was found necessary to assume that the electronic energy level is split up due to strong intermolecular field resulting from the formation of virtual bonds between neighbouring molecules in the solid state at -180°C in order to assign the bands satisfactorily.

In the case of β -methylnaphthalene, in the first system the 0-0 bands for the liquid and solid states are at 31202 and 31114 cm^{-1} respectively, while that for the vapour state is at 31593 cm^{-1} . Thus with the liquefaction of the vapour and the subsequent solidification of the liquid the 0-0 band shifts towards longer wavelengths by 391 and 479 cm^{-1} respectively. The 0-0 band of the second system due to the liquid undergoes a large shift of 1584 cm^{-1} towards longer wavelengths from its position in the case of the vapour. With solidification of the liquid there is a further shift of 234 cm^{-1} of the 0-0 band towards longer wavelengths. But in this case no splitting of energy level is observed with solidification and lowering of temperature. The results have been discussed and compared with those obtained by previous authors for the frozen solution of β -methylnaphthalene in 3-methyl pentane rigid glass solvent at 77°K .

INTRODUCTION

The ultraviolet absorption spectra of α -chloronaphthalene and α -bromonaphthalene in the vapour, liquid and solid states at low temperatures were studied by Deb (1954) in this laboratory. Both the substances showed two systems of absorption bands in the near ultraviolet. It was observed by him

*Communicated by Prof. S. C. Sirkar.

that the ν_0 -bands of the two systems shift towards longer wavelengths with the liquefaction of the vapour. These results clearly suggest that the excited electronic energy state is lowered by the influence of the intermolecular field in the liquid phase of these compounds, as observed also in the case of many substituted benzenes (Swamy, 1952a, 1953; Deb, 1952, 1953). The absorption spectra of *o*-dichlorobenzene and *m*-chlorotoluene, however, show that a splitting of the electronic energy levels takes place with solidification and lowering of temperature to -180°C . (Sirkar and Swamy, 1952; Swamy, 1952b, 1953). No such splitting was observed in the case of α -chloro- or α -bromonaphthalene.

The ultraviolet absorption spectra of α -methylnaphthalene and β -methyl naphthalene in the vapour state were studied by de Laszlo (1925). These substances also exhibit bands in two distinct regions extending from 3000 \AA to 3200 \AA and from 2500 \AA to 2900 \AA respectively. Recently, the absorption spectra of β -methylnaphthalene in 3-methyl pentane rigid glass solvent at 77°K were studied by McConnell and Tunnicliff (1955) who obtained two systems of bands with the ν_0 -bands at 31412 cm^{-1} and 34410 cm^{-1} respectively. It is not known, however, whether the bands undergo major changes with solidification of the pure liquids. The present investigation was undertaken to study the absorption spectra of α -methylnaphthalene and β -methylnaphthalene in the liquid state and in the solid state at low temperatures and to compare the results with those for the vapours. It was also intended to compare the results for the pure crystals of β -methyl naphthalene at -180°C with those of the solid solution in 3-methyl pentane at 77°K .

EXPERIMENTAL

The liquids used were of chemically pure quality and were supplied by Eastman Kodak Co. They were repeatedly distilled under vacuum before use. With films of thickness of the order of a few microns the bands in the region $2500\text{--}2900 \text{ \AA}$ were fairly intense, while considerably thicker films showed other weaker bands in the region $3000\text{--}3200 \text{ \AA}$. A hydrogen discharge tube running at 3 KV served as the source of continuous spectrum. Spectrograms were taken on Ilford HP 3 films with a Hilger E I spectrograph having a dispersion of 3 A.U. in the region 2600 \AA . As the continuum from the hydrogen discharge tube contained a number of intense emission bands of nitrogen in the region $3000\text{--}3200 \text{ \AA}$ there was a little difficulty in identifying the absorption bands of α -methyl naphthalene falling in that region. To remove this difficulty a spectrogram of the liquid was obtained using a tungsten-ribbon lamp in silica bulb as the source of continuous radiation and a Hilger medium quartz spectrograph. Microphotometric records of the spectrograms were taken with a Kipp and Zonen type

self-recording microphotometer. Iron arc spectrum was recorded on each spectrogram as a comparison.

In order to find the wavelengths of the absorption peaks accurately from the microphotometric records, a suitable iron arc line was chosen in each spectrogram and a linear scratch was made on the absorption spectrum in the position of this line to serve as a reference line. A microphotometric record of the iron arc spectrum was then taken from the same film. The wavelengths of the absorption peaks in the record for the absorption spectrum were then determined by measuring the distances of the peaks from the reference line and finding out the wavelength on the record due to iron arc spectrum at this distance from the same reference line. The wavelengths of sharp bands could be measured with an accuracy of about 1.0 A.U. by this method.

RESULTS

The microphotometric records of the absorption spectra are reproduced in figures 1, 2, 3 and 4. The frequencies in cm^{-1} of the bands and their assignments are given in Tables I and II. Assignments for the second system of bands in the region 2500 \AA – 2900 \AA of α -methylnaphthalene in the solid state at -180°C have been made on the assumption that the electronic energy level is split up into three components; otherwise the bands could not be assigned properly. No such splitting was, however, observed in the case of β -methylnaphthalene in the solid state at -180°C .

The spectra of the compounds in the vapour state were not studied, as they had already been reported by de Laslo (1925) who, however, could not assign the bands properly, probably because the Raman effect had not been discovered at that time. The frequencies of the absorption bands were determined from the absorption curves for vapour reproduced in his paper and assignments were made. These assignments have been included in the Tables I and II for comparison.

DISCUSSIONS

It can be seen from figures 1, 2, 3 and 4 as well as from Tables I and II that the absorption spectrum of either α -methylnaphthalene or β -methylnaphthalene consists of two groups of bands. The relative intensities of the bands in the two groups clearly indicate that they constitute two distinct systems. The feeble group of bands on the longer wavelength side was called Part I by de Laszlo (1925) while the other group was called Part II by him. In this paper they are designated as the first system and the second system of bands respectively. The changes observed with liquefaction of the vapours and with solidification of the liquids are discussed below.

α -Methylnaphthalene

I. Bands of the first system

As the first band of the first system of α -methylnaphthalene at -180°C is very strong this is taken as the ν_0 -band. Consequently, the third strong band in the curve reproduced by de Laszlo is taken as the ν_0 -band, the other two bands on the longer wavelength side being assigned as those due to $\nu \rightarrow 0$ transition. The frequency differences 708 and 1125 cm^{-1} agree fairly well with the Raman

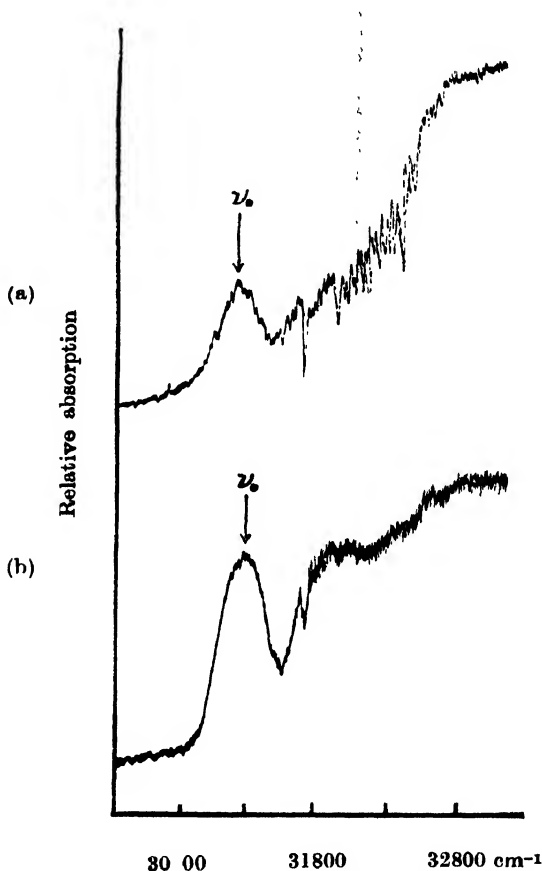


Fig. 1. Microphotometric records of the ultraviolet absorption spectra of α -methyl naphthalene (First System).

a) Liquid at 34°C .

(b) Solid at -180°C .

shifts 700 cm^{-1} and 1141 cm^{-1} observed by Ziemecki (1932). If the ν_0 -band is taken at 32168 cm^{-1} we get bands at distances 387, 872 and 1264 cm^{-1} respectively from the ν_0 -band. These are evidently some vibration frequencies in the excited state. In the case of the liquid these frequencies are not observed,

but the bands can be assigned satisfactorily by assuming excited state frequencies, 434, 615, 1041, 1224 and 1467 cm^{-1} respectively, while the the solid state these are changed to 421, 664, 1078, 1278 and 1470 cm^{-1} respectively. The

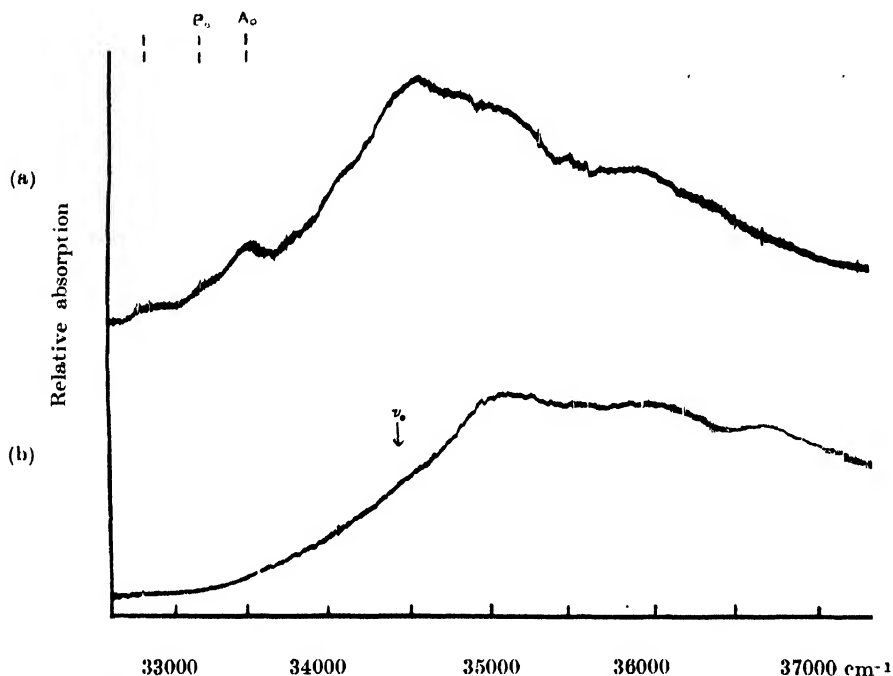


Fig 2. Microphotometric records of the ultraviolet absorption spectra of α -methyl naphthalene (Second system).
(a) Solid at -180°C . (b) Liquid at 34°C .

ν_0 -bands in the liquid and solid states are at 31192 cm^{-1} and 31285 cm^{-1} respectively. Thus with the liquefaction of the vapour the ν_0 -band of this system shifts by 976 cm^{-1} towards the longer wavelengths. It is thus evident that the excited electronic levels are lowered by the intermolecular field in the liquid state and also some of the excited state frequencies are changed.

II. Bands of the second system.

From the absorption curve published by de Laszlo (1925) the absorption spectra of α -methylnaphthalene in the vapour state is found to have four bands in the second system of which the first and the most intense band at 34940 cm^{-1} on the longer wavelength side can be taken as the ν_0 -band. In the liquid state the compound shows six broad bands, the first band on the longer wavelength side being weaker than the other bands. In order to identify the ν_0 -band it was found indispensibly necessary to study the absorption spectrum in the solid state. In the spectrum of the solid, the first intense band is at 33463 cm^{-1} ,

TABLE I

 Absorption bands of α -methylnaphthalene

Vapour de Laszlo, 1925		Liquid at 34°C. Present author		Solid at -180°C Present author	
Wave number (cm ⁻¹) and Int.	Assignment	Wave number (cm ⁻¹) and Int.	Assignment	Wave number (cm ⁻¹) and Int.	Assignment
1st system		1st system		1st system	
31043 (vw)	$\nu_0 - 1125$	31192 (vs)	ν_0	31285 (vs)	ν_0
31460 (m)	$\nu_0 - 708$	31626 (w)	$\nu_0 + 434$	31706 (m)	$\nu_0 + 421$
32168 (vs)	ν_0	31807 (ms)	$\nu_0 + 615$	31949 (ms)	$\nu_0 + 664$
32555 (ms)	$\nu_0 + 387$	32233 (w)	$\nu_0 + 1041$	32363 (s)	$\nu_0 + 1078$
33040 (s)	$\nu_0 + 872$	32416 (s)	$\nu_0 + 1224$	32563 (s)	$\nu_0 + 1278$
33432 (vs)	$\nu_0 + 1264$	32659 (w)	$\nu_0 + 1467$	32755 (w)	$\nu_0 + 1470$
2nd system		2nd system		2nd system	
34940 (vs)	ν_0	34460 (m)	ν_0	32766 (w)	C_0
35262 (w)	$\nu_0 + 322$	35127 (s)	$\nu_0 + 666$	33141 (w)	B_0
35540 (s)	$\nu_0 + 600$	35555 (s)	$\nu_0 + 1095$	33463 (m)	A_0
36420 (vs)	$\nu_0 + 1480$	35947 (s)	$\nu_0 + 1487$	33756 (m)	$C_0 + 990$
		36221 (s)	$\nu_0 + 1095$ + 666	33854 (m)	$C_0 + 1088$
		36659 (w)	$\nu_0 + 2 \times$ 1095	34131 (s)	$A_0 + 668$ $B_0 + 990$
				34228 (s)	$B_0 + 1088$
				34454 (vs)	$A_0 + 990$
				34550 (vs)	$A_0 + 1088$
				34881 (s)	$A_0 + 1418$
				35126 (s)	$A_0 + 668 +$ 990
				35532 (s)	$A_0 + 1088 +$ 990
				35646 (m)	$A_0 + 2 \times 1088$
				35973 (m)	$A_0 + 1088 +$ 1418
				36432 (w)	$A_0 + 3 \times 990$

TABLE II

Absorption bands of β -methylnaphthalene

Vapour de Laszlo, 1925		Liquid at 37°C Present author		Solid at -180°C Present author	
Wave number (cm ⁻¹) and Int.	Assignment	Wave number (cm ⁻¹) and Int.	Assignment	Wave number (cm ⁻¹) and Int.	Assignment
1st system		1st system		1st system	
31065 (vw)	$\nu_0 - 528$	31202 (vs)	ν_0	31114 (vs)	ν_0
31593 (vs)	ν_0	31596 (w)	$\nu_0 + 394$	31526 (w)	$\nu_0 + 412$
31932 (ms)	$\nu_0 + 339$	31939 (ms)	$\nu_0 + 737$	31876 (s)	$\nu_0 + 762$
32333 (s)	$\nu_0 + 740$	32521 (ms)	$\nu_0 + 1319$	32500 (ms)	$\nu_0 + 1386$
32959 (vs)	$\nu_0 + 1366$	32680 (ms)	$\nu_0 + 2 \times 737$	32638 (w)	$\nu_0 + 2 \times 762$
33418 (w)	$\nu_0 + 2 \times 740 + 339$	33257 (w)	$\nu_0 + 737 + 1319$	33059 (w)	$\nu_0 + 2 \times 762 + 412$
33753 (s)	$\nu_0 + 2 \times 740 + 2 \times 339$				
34332 (vs)	$\nu_0 + 2 \times 1366$				
2nd system		2nd system		2nd system	
35250 (vw)	$\nu_0 - 500$	34166 (m)	ν_0	33932 (s)	ν_0
35750 (s)	ν_0	34556 (ms)	$\nu_0 + 390$	34342 (vs)	$\nu_0 + 410$
36220 (s)	$\nu_0 + 470$	35263 (s)	$\nu_0 + 1097$	35016 (ms)	$\nu_0 + 1084$
37005 (vs)	$\nu_0 + 1256$	35500 (s)	$\nu_0 + 1334$	35263 (vs)	$\nu_0 + 1331$
37160 (ms)	$\nu_0 + 1410$	35883 (s)	$\nu_0 + 1334 + 390$	35671 (ms)	$\nu_0 + 1331 + 410$
37624 (vs)	$\nu_0 + 1410 + 470$	36273 (w)	$\nu_0 + 1334 + 2 \times 390$	36339 (w)	$\nu_0 + 1331 + 1084$
38091 (s)	$\nu_0 + 1410 + 2 \times 470$	36835 (ms)	$\nu_0 + 2 \times 1334$	36605 (w)	$\nu_0 + 2 \times 1331$

This band is accompanied by two faint satellites, both being on the longer wavelength side of it. These fainter bands cannot be due to $\nu \rightarrow 0$ transition as at -180°C the number of molecules present in the excited state in this mode of vibration is negligible. It is also found from the microphotometer records (figure 1) that each of the other two principal bands at 34454 cm⁻¹ and 34550 cm⁻¹ is accompanied on the longer wavelength side by two companions which are

much feebler than the main band. It can, therefore, rightly be concluded that the electronic energy level is split up into three components in the case of this substance in the solid state at -180°C . Such splitting of energy level was also demonstrated in the case of *o*-dichlorobenzene (Sirkar and Swamy, 1952; Swamy, 1953) and *m*-chlorotoluene (Swamy, 1952b). This phenomenon may be due to the influence of strong intermolecular field brought into play by the formation of virtual bonds between the molecules in the solid state at -180°C . The assignments given in Table I are made on this assumption. The first band at 33463 cm^{-1} is designated as A_0 and its two satellites at 33141 and 32766 cm^{-1} as B_0 and C_0 respectively. This assignment and a comparison of the relative intensities of the bands due to the solid with those due to the liquid leads to the selection of the weak band at 34460 cm^{-1} as the ν_0 -band in the case of the liquid. Thus with solidification of the liquid the ν_0 -band shifts by about 1000 cm^{-1} towards longer wavelength besides being split up into three components. The shift of 480 cm^{-1} of the ν_0 -band of the liquid towards longer wavelengths with respect to that in the vapour state is again due to the intermolecular field lowering the excited electronic energy state in the condensed phase of the substance. In the spectra of the liquid the bands obtained are broad and the excited state vibrational frequencies 666 cm^{-1} , 1095 cm^{-1} , 1487 cm^{-1} and their combinations are observed. This broadening of the bands in the liquid state may be due to the fluctuation of intermolecular field caused probably by thermal fluctuation of density.

β -Methylnaphthalene

I. Bands of the first system.

In the first system six bands have been observed for both the liquid and solid states of β -methylnaphthalene. The strong bands at 31202 cm^{-1} and 31114 cm^{-1} are taken as the ν_0 -bands respectively for the liquid and solid states. In the case of the vapour, the strongest band on the longer wavelength side is at 31593 cm^{-1} as given in the absorption curve for vapour reported by de Laszlo (1925). This is to be taken as the ν_0 -band, because the band at 31065 cm^{-1} is very weak. The bands of the vapour can then be assigned satisfactorily as shown in Table II. With the liquefaction of the vapour and with the solidification of the liquid the ν_0 -band shifts towards longer wavelengths by 391 cm^{-1} and 479 cm^{-1} respectively with respect to the ν_0 -band in the vapour state. The other bands in the liquid state correspond to the fundamental excited state frequencies 394 , 737 and 1319 cm^{-1} and their harmonics and combinations. These are slightly different from the frequencies observed in the case of the vapour. The frequencies change to 412 , 762 and 1386 cm^{-1} respectively with the solidification of the substance. Thus the excited state frequency 339 cm^{-1} increases to 394 and 412 cm^{-1} respectively with liquefaction and solidification of the substance. The other two frequencies are not affected so much with

solidification, but the frequency 1366 cm^{-1} seems to diminish a little with liquefaction.

In the spectra of β -methylnaphthalene dissolved in 3-methyl pentane rigid glass solvent at 77°K , McConnell and Tunnicliff (1955) observed the ν_0 -band at 31412 cm^{-1} and seven other bands corresponding to frequencies 430, 710, 960 and 1410 cm^{-1} and their harmonics and combinations. They attributed the

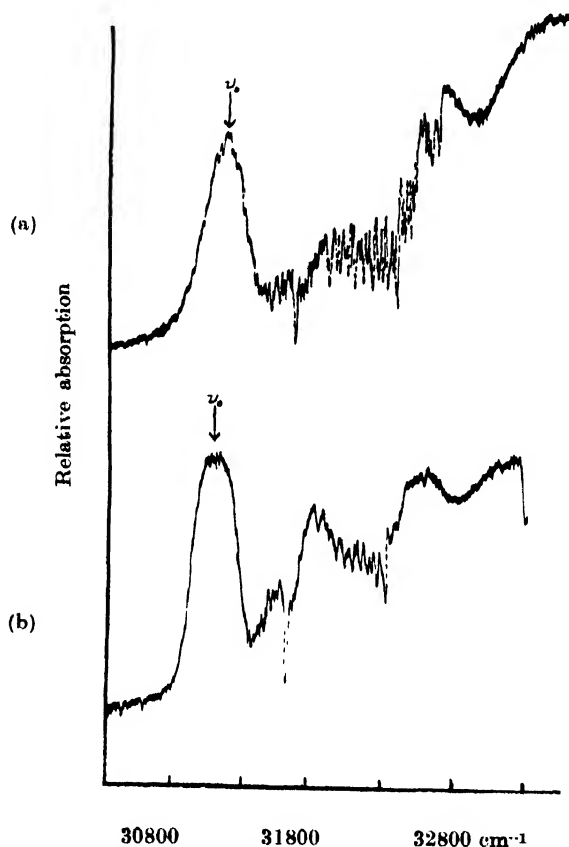


Fig 3. Microphotometric records of the ultraviolet absorption spectra of β -methyl naphthalene (First system).

(a) Liquid at 37°C .

(b) Solid at -180°C .

absorption bands to the single molecules of β -methylnaphthalene. A comparison of this result with that obtained for pure β -methylnaphthalene in the solid state at -180°C reveals that the ν_0 -band for the pure substance lies at a distance of 298 cm^{-1} towards longer wavelengths with respect to the ν_0 -band of the frozen solution spectra. This difference can be explained on the assumption

that the electronic energy level is perturbed by the intermolecular field and that this field in the pure substance is different from that in the solvent. The change in the frequency of ν_0 -band with liquefaction supports this conclusion. As the

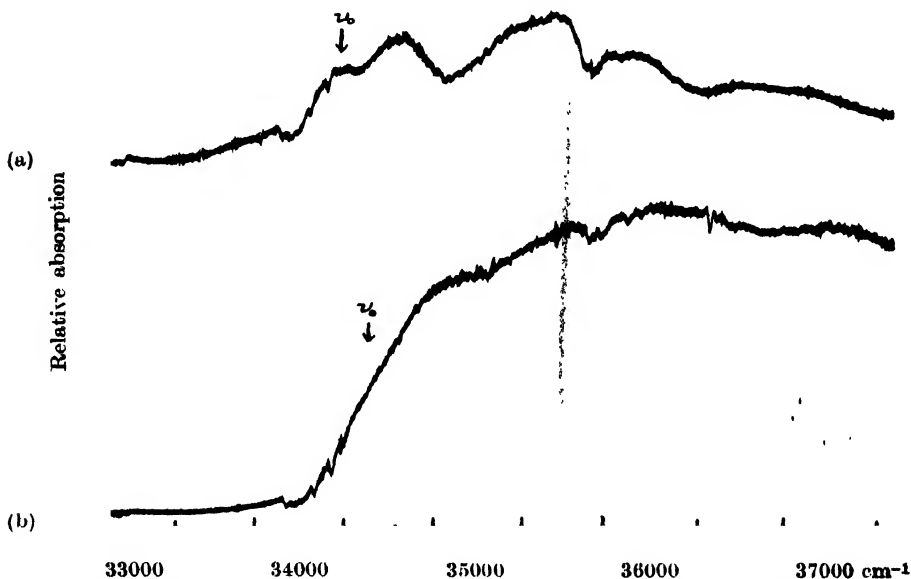


Fig. 4. Microphotometric records of the ultraviolet absorption spectra of β -methylnaphthalene (Second system).

(a) Solid at -180° .

(b) Liquid at 37° .

ν_0 -band tends to shift towards its position in the vapour state when the molecules are dispersed in the 3-methyl pentane glass, it might be inferred that breaking up of associated groups in the solution are responsible for this shift.

II. Bands of the second system.

In this system the substance exhibits seven absorption bands in both the liquid and solid states. The ν_0 -band due to the liquid is at 34166 cm^{-1} and that due to the solid is at 33932 cm^{-1} . Taking the strong band at 35750 cm^{-1} as the ν_0 -band due to the vapour state from de Laszlo's curve for the vapour, it is seen that the ν_0 -band is displaced by 1584 cm^{-1} towards longer wavelength when the vapour is liquefied, while the band shifts still towards longer wavelengths by 234 cm^{-1} when the liquid is solidified and cooled to -180°C . No such large shift in the ν_0 -band takes place in the case of the first system. Thus in this case the intermolecular field has much greater influence on the second system than on the first system. If these results for β -methylnaphthalene are compared with those obtained in the case of α -methylnaphthalene it is observed that the influence of intermolecular field in the former case is quite different

from that in the latter case, because in the case of α -methylnaphthalene a major change in the first system takes place with liquefaction of the vapour and further, very large changes take place in the second system with solidification of the liquid. The position of the substituent thus determines the influence of intermolecular field on the electronic energy states.

This large shift of 1584 cm^{-1} of the ν_0 -band in the case of β -methylnaphthalene may be due to formation of strongly associated groups of molecules. The other bands of β -methylnaphthalene due to the liquid can be expressed in terms of three fundamental frequencies 390 , 1097 and 1334 cm^{-1} . These are changed to 410 , 1084 and 1331 cm^{-1} in the solid state.

In the frozen solution of β -methylnaphthalene in 3-methyl pentane glass solvent at 77°K , McConnell and Tunnicliff (1955) observed seven bands which were not assigned properly. If the first band at 34410 cm^{-1} is taken as the ν_0 -band, it is seen that the ν_0 -band of the pure substance at -180°C is displaced towards longer wavelengths by 478 cm^{-1} with respect to the frozen solution spectra. This probably indicates that the intermolecular field in the pure substance in the solid state at -180°C is stronger than that in the solution in 3-methyl pentane at 77°K and therefore, even in the case of single molecules dispersed in the glass, the ν_0 -band is displaced towards longer wavelengths by about 1100 cm^{-1} from its position in the vapour state.

ACKNOWLEDGMENT

The author's thanks are due to Prof. S. C. Sirkar, D.Sc., F.N.I. for his kind interest and helpful guidance during the progress of the work.

REFERENCES

- de Laszlo, H. G., 1925, *Zeits. f. Phys. Chem.*, **118**, 369.
- Deb, A. R., 1952, *Ind. J. Phys.*, **26**, 201.
- Deb, A. R., 1953, *Ind. J. Phys.*, **27**, 183.
- Deb, A. R., 1954, *Ind. J. Phys.*, **28**, 21.
- McConnell, H. M. and Tunnicliff, D. D., 1955, *J. Chem. Phys.*, **23**, 927.
- Sirkar, S. C. and Swamy, H. N., 1952, *J. Chem. Phys.*, **20**, 1177.
- Swamy, H. N., 1952a, *Ind. J. Phys.*, **26**, 119.
- Swamy, H. N., 1952b, *Ind. J. Phys.*, **26**, 445.
- Swamy, H. N., 1953, *Ind. J. Phys.*, **27**, 55.
- Ziomecki, S., 1932, *Z. Physik*, **78**, 123.

ANALYSIS OF THE NEAR ULTRAVIOLET ABSORPTION SPECTRUM OF ORTHOCHLOROANISOLE

V. SURYANARAYANA AND V. RAMAKRISHNA RAO

PHYSICS DEPARTMENT, ANDHRA UNIVERSITY, WALT AIR

(Received for publication, November 12, 1955)

Plate III

ABSTRACT. About 66 bands were recorded in the absorption spectrum of ortho-chloro-anisole in the region 2873 to 2503 A.U. and interpreted on the basis of 8 fundamentals in upper state and 4 fundamentals in lower state. In the light of Raman frequencies and their depolarisation factors, the ultra-violet fundamentals are correlated and assigned to various modes of vibration. The molecule is assumed to belong to the point group C_s .

INTRODUCTION

The absorption spectra of many disubstituted benzenes remain to be studied and interpreted. In order to understand the vibrational frequencies a systematic investigation of a series of molecules of the type $X-C_6H_4-OCH_3$ (substituted anisoles) has been taken up, with 'X' being halogens or (OH) or (CH_3) units. Work has been finished and preliminary reports appeared on (1) ortho-chloro-anisole (2) para-chloro-anisole and (3) para-fluoro-anisole (Rao and Suryanarayana, 1955) while investigations are in progress on para-bromo-anisole, the methoxy phenols and methoxy toluenes. In the following pages, our detailed results on the near ultraviolet absorption spectrum of *o*-chloro-anisole ($1, 2, OCH_3 - C_6H_4 - Cl$) are reported.

The Raman spectrum and depolarisation data of the molecule have been reported by Herz (1946). The frequency data were obtained by us also and checked. The present work appears to be the first investigation on the ultra violet absorption spectrum. Our attempts to obtain the fluorescence spectrum under various conditions were not fruitful. It is probable that the molecule does not fluoresce.

EXPERIMENTAL

The substance *o*-chloro-anisole is obtained from B.D.H. Its boiling point is $195^\circ-196^\circ C$ at 760 mm. pressure. This is purified by distilling three times in vacuum sealed tubes in the temperature range $70^\circ-80^\circ C$ and this distilled product is used for further work.

The absorption tube (figure 1) is an all-quartz one of various lengths (A) with fused plane windows. The side limb B is for containing the liquid while C is a quartz to pyrex graded seal. To this pyrex end, component D is attached. The end E is connected to a vacuum pump and the whole tube is evacuated continuously with intermittent heating so as to degas the tube. After 36 hours the tip F is broken and the liquid is introduced into D and F is sealed off again. Immersing D in a low temperature bath (-18°C) evacuation is repeated for half an hour and the tube is sealed near E. About 1 c.c. of the liquid in D is distilled into

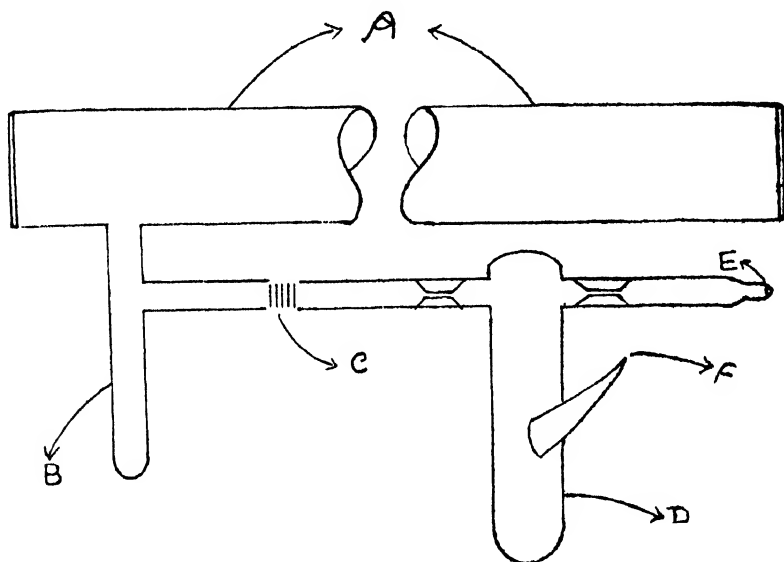
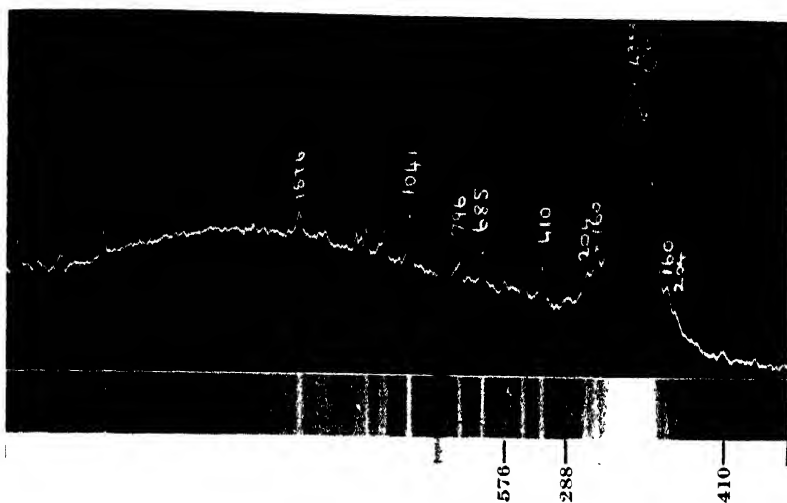
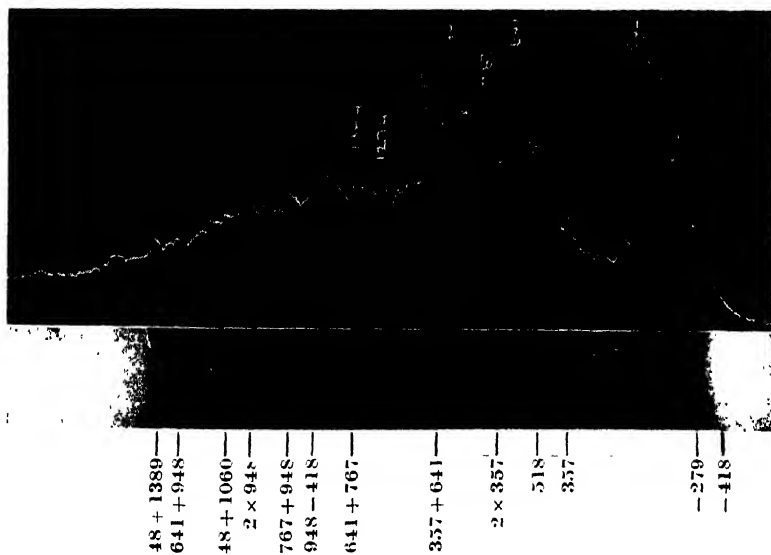


Fig. 1. Absorption tube.

B and the tube is sealed off between C and D. Under these conditions the substance in the absorption tube exists at about its saturated vapour pressure which depends on the temperature of the container B. This is regulated to any desired value by changing the temperature of B.

For temperatures higher than the room temperature the main body of the absorption tube has to be kept at about 10°C higher than the temperature of the container. This is achieved by keeping the absorption tube in an asbestos furnace with attached quartz windows and a nichrome heating element. The container protrudes out of the lower surface of the furnace through a hole and is immersed in a suitable temperature bath in a silvered thermos flask to acquire any desired temperature.

Of the various path-lengths used (10, 25, 50 and 75 cms), the 75 cms tube operated in the temperature range -18°C to 160°C is found most suitable. To develop the bands on the long wavelength side of the (0,0) band, a 150 cms tube

Fig. 2. Raman spectrum of *o*-chloroanisole.Fig. 3. Ultraviolet absorption spectrum of *o*-chloroanisole.

is used in the temperature range 20°C to 60°C . The nature of the spectrum depends on two factors (1) the path length (2) the temperature of the liquid container. The spectrum obtained with 75 cms tube at 28°C is found to be similar to that obtained with 150 cms tube at a temperature of 0°C . Thus on account of the greater path length the ground state frequencies are obtained at a lower temperature before the continuous absorption sets in.

Hilger hydrogen lamp run on stabilised direct current hydrogen lamp supply unit FL 16 is used as a source of continuum. Spectrograms were taken on Hilger small quartz, medium quartz and quartz Littrow spectrographs. The quartz Littrow pictures were taken only at the condition where the maximum number of bands developed. The other studies were confined to the other two instruments. Exposures were two minutes with baby quartz and 5 to 10 minutes on medium quartz and about 2 hours on quartz Littrow. Ilford Special Rapid plates were used. Measurements of wavelengths were made with a Higher comparator and with reference to standard iron lines. Each band is measured at least four times from all the plates and the mean value is given for the wavelength. Intensities are visual estimates in the scale 0 to 10 and are relative within the small regions that develop under various conditions.

To obtain the Raman data, about 5 cc of the specimen was used in a small Raman tube with a modified Woods set up using two mercury arcs of pyrex glass made in our laboratory. The exciting radiation was the λ 4358 of mercury filtered through the Rohdamine 5GDN extra, a Du Pont dye, in para-nitro-toluene in ethyl alcohol solution. With the narrowest slit an exposure of twelve hours was given to obtain a good Raman spectrum, (Plate III).

RESULTS

With the 75 cms pathlength, about 60 bands were recorded in the region 2826 to 2600 A.U. in various stages of the nearly saturated vapour pressures corresponding to the temperatures -18°C to 160°C . There is a region of continuous absorption below 2250 A.U. which spreads to longer wavelengths at higher vapour pressures finally merging into the first region.

At the saturated vapour pressure corresponding to -18°C only one band was recorded at 2795.6 A.U. This helps us to fix up the (0, 0) band at 2795.6 A.U. As the temperature of the container is increased in units of about 10°C , more and more bands are developed to the short wavelength side of 2795 A.U. The maximum number of discrete bands are recorded when the container is kept at 28°C (figure 3). At higher temperatures, the absorption in this region grows stronger and becomes continuous, a few bands were recorded on the long wavelength side of 2795 and in the region below 2640 A.U. This study is pursued until all the bands disappear in continuous absorption. With a 75 cms path length no band was recorded on the long wavelength side of 2828.7 A.U. Using a 150 cms path length and container temperatures in the region 0°C to 60°C , we could record five

bands in the region 2828.7 and 2873.3 A.U. Beyond this temperature these bands again merge in continuous absorption.

The bands in general appear to be red-degraded. While they are not diffuse there appears to be a certain breadth of the bands. The maximum intensity of absorption appears to be in the region 2746 to 2715 A.U. Next in order, follow the regions 2828 to 2818 and 2700 to 2685 A.U. The long wavelength bands developed with 150 cms path length are very weak. The wavelength, wave number and intensity data were given in Table I. The intensities were only relative and at the path lengths mentioned.

DISCUSSION AND ANALYSIS OF THE SPECTRUM

The band at 2795.6 A.U. is obviously the (0, 0) band. Frequency shifts of various bands from (0, 0) band are given in column 4 of Table I. The identified fundamentals in both the states with corresponding Raman data and assignments were given in Table II. The strong bands with shifts 641, 767, 948 and 1060 cm^{-1} (figure 3) are easily identified as fundamentals in the upper state. Of these 641 and 948 appear to be stronger than the others. Less obvious are the fundamentals 357, 518, 1274 and 1389 cm^{-1} . In the ground state four fundamentals could be identified with reasonable certainty with values 279, 418, 565 and 690 cm^{-1} . The band at 887 cm^{-1} may possibly be a fundamental, it does not find much support in combination bands. The fundamentals 641, 767 and 948 occur as overtones and combinations within themselves and with other lower and upper state fundamentals. Of the 65 bands recorded only about 7 are left uninterpreted on the basis of these fundamentals. Some theoretical considerations for the analysis and discussion of the assigned fundamentals are given below.

If we treat (OCH_3) group as one unit, this molecule $\text{O-Cl-C}_6\text{H}_4\text{OCH}_3$ (*o*-chloro-anisole) at best belongs to the point group C_s with only the molecular plane σ_z perpendicular to *Z*-axis as the element of symmetry. Only two types of electronic and vibrational levels are possible: the A' and α' respectively symmetric to the plane of the molecule and A'' and α'' antisymmetric to the same. The selection rules are given in Table III.

A molecule $\text{X-C}_6\text{H}_4\text{-Y}$ will have 30 vibrations out of which 21 are of α' type and 9 α'' type. Both are allowed in Raman and infrared spectra. Considering the molecule as X-OCH_3 where X is the rest of the phenyl radical, we expect 12 modes of vibration thus accounting for the total of 42 vibrations to be expected for the general molecule *o*-chloroanisole.

In benzene the near ultraviolet absorption spectrum is due to a forbidden $A_{1g} \rightarrow B_{2u}$ transition. The present system is obviously its corresponding transition. Both the above states become A' states in C_s point group and this transition $A' \rightarrow A'$ is allowed: the transition moment lies in the molecular plane.

TABLE I
Bands of ortho-chloro-anisole

Wave-lengths (λ)	Inten- sity	Wave- numbers (ν)	Shift from (0, 0) band ($\Delta\nu$) Obs.value	Assignment	$\Delta\nu$ Calc. value	Difference between observed and calculated values
150 Cms. path length.						
2873.3	$\frac{1}{2}$	34793	— 967			
2866.7	2	34873	— 887	0—887		
2862.5	$\frac{1}{2}$	34924	— 836	0—2 \times 418	— 836	0
2850.6	2	35070	— 690	0—690		
2840.5	1 $\frac{1}{2}$	35195	— 565	0—565		
75 Cms. path length.						
2828.7	$\frac{1}{2}$	35342	— 418	0—418		
2824.8	1	35390	— 370			
2817.6	3	35481	— 279	0—279		
2810.5	6	35570	— 190	0—2 \times 418+641	— 195	5
2803.5	7	35659	— 101	0—2 \times 690 2 \times 641 0—2 \times 690+1274	— 98 — 106	3 5
2799.6	1	35709	— 51	0—690+641	— 49	2
2795.6	9	35760	— 0	(0, 0) band		
2790.9	1	35820	+ 60	0 948—887	+ 61	1
2788.1	3	35856	+ 96	0+518—418	+ 100	4
2781.5	3	35941	+ 181	0 1060—887?	+ 173	8
2775.5	0	36019	+ 259	0 948—690 0 357—2 \times 641—2 \times 690	+ 258 + 259	1 0
2770.9	1	36079	+ 319	0+357—51	+ 306	13
2768.0	3	36117	+ 357	0 357		
2764.4	0	36164	+ 404			
2760.0	1	36221	+ 461			
2755.7	4	36278	+ 518	0 518		
2751.3	1	36336	+ 576	0+641+357—418	+ 580	4
2746.4	8	36401	+ 641	0+641		
2740.3	2	36482	+ 722	0+2 \times 357 0+641+767—690	+ 714 + 718	8 4

TABLE I (contd.)

Wave-lengths (λ)	Inten- sity	Wave- numbers (ν)	Shift from (0, 0) band. ($\Delta\nu$) Obs. value	Assignment	$\Delta\nu$ Calc. value	Difference between observed and calculated values
2736.9	7	36527	+ 767	0 + 767		
2729.9	1	36621	+ 861	0 + 1274 - 418	+ 856	5
2723.4	7	36708	+ 948	0 + 948		
2719.4	3	36762	+ 1002	0.641 + 357	+ 998	4
2715.1	6	36820	+ 1060	0 + 1060		
2709.8	$\frac{1}{2}$	36892	+ 1132	0 + 767 + 357	+ 1124	8
2704.8	1	36960	+ 1200	0 + 2 \times 948 - 690	+ 1206	6
2699.4	3	37034	+ 1274	{ 0 + 2 \times 641 0 + 1274	+ 1282	8
2696.0	1	37081	+ 1321			
2691.1	2	37149	+ 1389	0 + 1389		
2689.1	3	37176	+ 1416	{ 0 + 641 + 767 0 + 1060 + 357 0 + 1060 + 767 - 418	{ + 1408 + 1417 + 1409	{ 8 1 7
2684.9	$\frac{1}{2}$	37234	+ 1474	0 + 2 \times 948 - 418	+ 1478	4
2680.8	0	37291	+ 1531	0 + 2 \times 767	+ 1534	3
2678.2	$\frac{1}{2}$	37327	+ 1567			
2677.0	1	37344	+ 1584	0 + 641 + 948	+ 1589	5
2675.9	1	37360	+ 1600	0 + 1060 + 948 - 418	+ 1590	10
2672.7	$\frac{1}{2}$	37404	+ 1644	{ 0 + 2 \times 641 + 357 0 + 1389 + 948 - 690	{ + 1639 + 1647	{ 5 3
2667.2	2	37481	+ 1721	0 + 767 + 948	+ 1715	6
2663.8	$\frac{1}{2}$	37529	+ 1769	{ 0 + 357 + 641 + 767 0 + 1060 + 2 \times 357	{ + 1765 + 1774	{ 4 5
2659.7	1	37587	+ 1827	0 + 1060 + 767	+ 1827	0
2653.9	2	37669	+ 1909	{ 0 + 2 \times 948 0 + 1274 + 641	{ + 1896 + 1915	{ 13 6
2650.1	1	37723	+ 1963			
2646.3	$1\frac{1}{2}$	37777	+ 2017	0 + 1060 + 948	+ 2008	9
2642.0	0	37839	+ 2079			
2639.4	0	37876	+ 2116	0 + 2 \times 1060	+ 2120	4

TABLE I (contd.)

Wave-lengths (λ)	Inten- sity	Wave- numbers (ν)	Shift from (0, 0) band. ($\Delta\nu$) Obs. value	Assignment	$\Delta\nu$ Calc. value	Difference between observed and calculated values
2636.3	0	37921	+2161	$\{0 + 2 \times 767 + 641$ $\{0 + 1389 + 767$	+2175 +2156	14 5
2631.4	1	37991	+2231	$0 + 2 \times 641 + 948$	+2230	1
2628.0	$\frac{1}{2}$	38040	+2280	$0 + 357 + 641 + 1274$	+2272	8
2623.9	2	38100	+2340	$\{0 + 1389 + 948$ $\{0 + 1060 + 1274$ $\{0 + 1060 + 2 \times 641$	+2337 +2334 +2342	3 6 2
2618.8	—	38174	+2414	$0 + 1389 + 767 + 948 - 690$	+2414	0
2613.5	$\frac{1}{2}$	38252	+2492	$0 + 2 \times 767 + 948$	+2482	10
2609.7	$\frac{1}{2}$	38307	+2547	$\{0 + 2 \times 948 + 641$ $\{0 + 2 \times 1274$	+2537 +2548	10 1
2606.3	$\frac{1}{2}$	38357	+2597	$0 + 1060 + 948 + 1274$ — 690	+2592	5
2601.0	1	38435	+2675	$\{0 + 2 \times 948 + 767$ $\{0 + 641 + 1274 + 767$	+2663 +2682	12 7
150 Cms. path length.						
2588.0	2D	38628	+2868	$0 + 641 + 948 + 1274$	+2863	5
2571.5	$\frac{1}{2}$ D	38876	+3116	$0 + 1389 + 767 + 948$	+3104	12
2559.8	2D	39054	+3294	$0 + 1060 + 948 + 1274$	+3282	12
2550.0	1v.D	39203	+3443	$0 + 2 \times 767 + 2 \times 948$	+3430	13
2538.2	1D	39387	+3627	$0 + 1060 + 2 \times 641 + 1274$	+3616	11
2525.0	1v.D	39593	+3833	$0 + 3 \times 1274$	+3822	11
2503.6	$\frac{1}{2}$ v.D	39930	+4170	$0 + 1389 + 767 + 948$ + 1060	+4164	6

D means that the band is diffuse.

v.D means that the band is very diffuse.

TABLE II

Identified frequencies and their assignment

Raman data	U.V. absorption data		Assignment
	Lower state	Upper state	
288 ?	279
410	418	357	{Components of ϵ_g^+ vibration in benzene.
576	565	518	
685	690	641	C-OCH ₃ valence
793	..	767	C-Cl valence
1041	..	948	{C-C valence (totally symmetric vibrations).
1183 ?	..	1060	
..	..	1274	CH ₃ bending
..	..	1389	O-CH ₃

TABLE III

Types of electronic and vibrational levels of group C_s ortho-chloro-anisole

Symmetry type	Essential elements of symmetry σZ	Number of vibrations	Selection rules	
			Raman	Infra-red
A'	+	21 T _x T _y	+	+
A''	-	9 T _z	-	-

As the transition is allowed, we expect a strong (0,0) band and numerous fundamentals, progressions and combinations of totally symmetric vibrational frequencies occurring on the short wavelength side of the (0,0) band. On the long wavelength side of the (0,0) band we can expect ground state fundamentals of totally symmetric vibrations and a v - v transition of low frequency vibrations. In spite of the large number of totally symmetric fundamentals not many are usually recorded. About six fundamentals in the upper state are found adequate to explain most of the bands. Correspondingly in the ground state only three vibrations could be identified with certainty.

The ϵ_g^+ vibration in benzene (606 cm⁻¹) splits into two totally symmetric components in the reduced symmetry of C_s point group. One of these two would change considerably in its value from 606 cm⁻¹, the other keeping near to it. The

medium intense band at 357 cm^{-1} from the (0, 0) band (35760 cm^{-1}) can be definitely assigned to the upper state value of the much reduced component of ϵ_g^+ in benzene. It is easily correlated with the 418 cm^{-1} frequency in the ground state which occurs so prominently in the analysis. In the Raman spectrum the corresponding value seems to be 410 cm^{-1} . This Raman line is strong and broad and has a depolarisation factor of 0.18. This undoubtedly represents a totally symmetric vibration. From the Raman spectrum it can be seen that 410 occurs weakly as an antistokes line too. This shows that even the liquid at room temperatures can exist in this singly excited vibrational level. If so, it is by far easier for the vapour to exist in that condition at room temperatures. This explains how the 418 cm^{-1} frequency occurs in the ground state at 20°C and also in combination with various bands at other temperatures. As the temperature of the container increases this frequency gains in intensity as it is to be expected. It is also to be observed that the 357 frequency in the upper state is able to explain a large number of bands by occurring in combination with various other fundamentals. We might take this as an indication that the ϵ_g^+ vibrational mode in benzene continues to play an important role in the production of the spectrum in this case. Thus we might conclude that 410 , 418 and 357 cm^{-1} represent in Raman effect and the ground and upper electronic states, one of the components of ϵ_g^+ vibrational mode of benzene.

The other component changes much less in magnitude and is possibly identified at 565 cm^{-1} in the ground state and 518 cm^{-1} in the upper state. The corresponding Raman line is a weak broad one at 576 cm^{-1} and is very weakly polarised. It may be added that in a mono-substituted benzene belonging to the point group C_{2v} , this is actually a non-totally symmetric type of vibration. The above frequencies do not occur frequently in the analysis. The assignment may only be treated as a possibility.

The frequency 641 cm^{-1} in the upper state is represented by the second strongest band of all the fundamentals (figure 3). It is found to occur in combination with a large number of other fundamentals in both the states. In the ground state its counterpart may be the band at 690 cm^{-1} . The corresponding Raman line is 685 cm^{-1} , a strong and highly polarised ($\rho = 0.15$) line. In anisole (Sreeramamurthy, 1950) a strong band was identified at 755 cm^{-1} with a ground state frequency of 786 cm^{-1} and the Raman frequency 781 cm^{-1} . An assignment of this set of frequencies has not been suggested by Sreeramamurthy. However, if we compare with the substituted anisoles, we might conclude that the above set in anisole represents the totally symmetric $C_{aromatic} OCH_3$ valence vibration. On further substitution in anisole we expect this frequency successively to decrease with increasing molecular weight of the substituted atom. Taking the upper state frequencies only, the corresponding values appear to be 720 , 699 and 641 cm^{-1} in para-fluoro, para-chloro and *o*-chloro anisoles respectively. These behave according to the above expectation and thus may be attributed to the

vibration common to all these molecules, namely C-OCH_3 . The unit OCH_3 has a molecular weight of about 31 which is very near the atomic weight of chlorine and so the C-OCH_3 and the C-Cl frequencies can be of the same order of magnitude in chloro-anisoles. Thus in *o*-chloro anisole we have a choice between 641 and the equally prominent frequency 767 for assignment to the C-COH_3 vibration. Fixing in anisole 755 as this frequency and comparing with some other substituted anisoles as above we could definitely establish that 641 and (690 and 685 cm^{-1}) represent the C-OCH_3 fundamental frequency in the upper and lower electronic states respectively.

The frequency 767 cm^{-1} in the upper state is also very prominent explaining a very large number of bands. A corresponding ground state frequency could not be identified with any reasonable certainty. The Raman frequency 796 cm^{-1} is highly polarised ($\rho = 0.18$) and possibly corresponds to this upper state frequency. We find this Raman line is slightly less intense than the Raman line at 685 cm^{-1} discussed earlier. In the ultraviolet also 767 is definitely less intense than 641 cm^{-1} . The C-Cl frequency in mono-chloro benzene has been identified by Sponer (1941) at 670 cm^{-1} . It is possible that 767 (u.v.) and 793 (Raman) in *o*-chloro-anisole may represent the totally symmetric C-Cl valence vibration.

Two frequencies at 948 cm^{-1} and 1060 cm^{-1} are represented by two strong bands in the u.v. spectrum. Of these the 948 cm^{-1} is slightly more intense than the 641 cm^{-1} . Corresponding to these the ground state frequencies could not be obtained even with the 150 cm tube. The strongest Raman line 1041 cm^{-1} may correspond to 948 cm^{-1} in the upper state. This Raman line is also highly polarised ($\rho = 0.12$). There are two Raman lines at 1162 and 1183 cm^{-1} of which the latter is polarised and possibly this corresponds to the 1060 in the upper state. These two pairs 1041, 948 and 1183, 1060 may represent the lower and upper state frequencies respectively of two totally symmetric (α') C-C valence vibrations.

The upper state frequency 1274 cm^{-1} is of particular interest. It is represented by a medium intensity band in the u.v. spectrum. It is found that 2×641 (1282) is very nearly equal to 1274 and this caused a slight confusion in our early attempts, as to whether to treat this 1274 as a fundamental or an overtone of 641. On comparison with other substituted anisoles, where such accidental coincidence does not occur, it was found that a frequency in this region is a characteristic of anisole and its products. The values are 1267, 1274, 1299 and 1297 in anisole, para-chloro-anisole, para-fluoro-anisole, and para-dimethoxy benzene (Sreeramamurty, 1950) respectively. The obvious conclusion is that this frequency corresponds to a vibration that is common to all these molecules. In the Raman spectrum also frequencies are found at 1298, 1291, 1297, 1261 in the above order of molecules. All these lines are strongly polarised. It can be seen that there is not much variation between the upper state frequencies and the lower state frequencies. From this we are led to the observation that probably they represent a totally symmetric vibration outside the phenyl radical and common to all. We

are thus left with a choice between the C-O vibration and the CH_3 (bending) vibration. To decide between these two we studied the analyses of toluene and its substitutions which do not contain the C-O unit but contain the CH_3 unit. In fluoro-toluene (Cave and Thompson, 1950) for instance, we find bands with frequencies of this order of magnitude. This is also the case in toluene, and dimethyl benzenes (Cooper and Sastri, 1952). The above authors either did not treat the corresponding bands as fundamentals (Cave and Thompson) or assigned them to some C-C vibrations in the phenyl radical (Cooper and Sastri). On a comparative study of all the spectra we came to the conclusion that these frequencies in substituted anisoles and toluenes represent a mode of vibration that is common to all these molecules, namely the CH_3 bending, a totally symmetric vibration. This view is further strengthened by a similar observation made by Kohlrausch (1946) from the Raman spectra of various substituted benzenes containing a methyl radical. Thus we conclude that 1274 cm^{-1} frequency in O-Cl anisole represents the totally symmetric CH_3 bending vibration.

A few bands could be explained on the basis of still another fundamental 1389 cm^{-1} in the upper state. The fundamental itself is diffuse and is of medium intensity. It is found to combine with the frequencies 767, 948 etc. A corresponding ground state frequency is not obtained and among the Raman lines as well a polarised line with probable correspondence could not be found. A frequency similar to this was found in para-fluoro-anisole at 1367 cm^{-1} and probably in para-chloro-anisole at 1345 cm^{-1} . In anisole a similar frequency was not identified by Sreeramamurty, however, there are two bands at 1328 and 1386 cm^{-1} from the (0,0) band left unexplained. Of these the former is slightly more intense than the latter. It is possible that one of these may represent a fundamental probably 1328 cm^{-1} . Assuming the fundamentals given by Sreeramamurty, we also find that this 1328 combines with six of them explaining some uninterpreted bands and giving a reasonable alternative to the original assignments. From this we are encouraged to treat these bands as due to fundamentals in all these molecules and common to all of them. A possible assignment therefore is to associate with the O-C vibration in the OCH_3 unit. Thus we may suggest this assignment to the 1389 cm^{-1} in *o*-chloroanisole.

Lastly we take up a possible lower state fundamental 279 cm^{-1} . No reasonable explanation could be found for this band. An assignment of this intense band could not be obtained. Similar bands are also obtained in *p*-fluoro and *p*-chloro anisoles

ACKNOWLEDGMENTS

This work was taken up under the C. S. I. R. scheme on "The Fluorescence and Absorption Spectra of Organic Molecules" granted to one of us (V. R. Rao). Our thanks are due to Prof. K. R. Rao for his interest in the work.

REFERENCES

- Cave, W. T. and Thompson, H. W 1950. A General Discussion of the Faraday Society in on Spectroscopy and Molecular Structure and Optical Methods of Investigating Cell Structure, Pages 35 to 46.
- Copper, C. D and Sastri, M L. N., 1952. *Jour. Chem. Phys.*, **20**, 607.
- Herz, E., 1946. *Monat. Fur. Chemie*, **76**, 22.
- Kohlrausch, K. W. F., 1946. *Monat. Fur. Chemie.*, **76**, 231.
- Ramakrishna Rao, V. and Suryanarayana, V., 1955. *Journ. Sci. Indus. Res.*, **14B**, 479.
- Sponer, H. and Wollman, S. H., 1941. *Jour. Chem. Phys.*, **9**, 816.
- Sreeramamurty, K., 1950. *Ind. Jour. Phys.*, **24**, 421.
- Sreeramamurty, K., 1950. D.Sc. Thesis submitted to the Andhra University.
- Suryanarayana, V. and Ramakrishna Rao, V., 1955. *Jour. Sci. Indus. Res.*, **14B**, 36.
- Suryanarayana, V. and Ramakrishna Rao, V., 1955. *Jour. Sci. Indus. Res.*, **14B**, 128.

BEHAVIOUR OF SATURABLE REACTORS IN MAGNETIC AMPLIFIERS

P. N. DAS

B. E. COLLEGE, SIBPORE, HOWRAH

(Received for publication, October 26, 1955)

ABSTRACT. The exact behaviour of saturable reactors when used in a magnetic amplifier, depends not only on the nature of material of the core and the magnitudes of d.c. and a.c. excitations used, but it also depends, to a great extent, on the external circuit conditions. Even with an idealised core and with the optimum values of d.c. and a.c. excitations for the given magnetic amplifier, its behaviour depends on a number of other factors namely on the number of cores used, on the nature of d.c. source and the way in which a.c. and d.c. windings are connected.

Its exact behaviour in a number of different cases has been studied and explained from fundamental considerations. These cases are . 1. A single core with the d.c. source of (i) infinite and (ii) low impedance. 2. Two cores series connected with the d.c. source of (i) infinite and (ii) low impedance. 3. Two cores parallel connected with the d.c. source of (i) infinite and (ii) low impedance. The B - H loop described becomes unsymmetrical in certain cases but symmetrical in others. Similarly the a.c. wave becomes flat-topped in certain cases but peaky in others. The flux density and the current through the d.c. winding also vary differently in different cases. All these differences in behaviour in different cases have been explained and some important results have been deduced. The movement of the working point in the B - H curve with the applied a.c. voltage has been determined in different cases and it has been shown that the average value of alternating current is zero in each case. The relation of the rectified average value of alternating current to direct current has also been found out in different cases and it has been shown that the fundamental formula for amplification in the case of a magnetic amplifier has to be modified in accordance with external circuit conditions.

INTRODUCTION

A large amount of work on magnetic amplifiers has been done in the last years and many experimental results have been published ; but no satisfactory explanations of their behaviour seem to have been given. The exact behaviour of saturable reactors under simultaneous d.c. and a.c. excitations depends not only on the magnetic properties of the material of the core and on the magnitudes of d.c. and a.c. excitations, but it also depends, to a large extent, on external circuit conditions, namely the number of cores used, the nature of d.c. source and the way in which a.c. and d.c. windings are connected. The object of this paper is to find out the exact behaviour of magnetic amplifier with an ideal core and with optimum values of d.c. and a.c. excitations in different cases of external circuit conditions.

An ideal material for the core of a magnetic amplifier should have its $B-H$ curve vertical in the unsaturated region and horizontal in the saturated region and should pass abruptly from one region to the other; for then it would be possible for the a.c. winding to have a very large impedance in the unsaturated region and a very low impedance in the saturated region and, therefore, it would be possible to get a very high amplification in a.c. when the working point moves from unsaturated to saturated region by the presence of a d.c. signal. In the case of some materials, like *mu*-metal, these are approximately true but we shall assume an ideal core in our investigations. The optimum value of a.c. voltage will be the maximum value which will keep the working point confined in the unsaturated region in the absence of any d.c. signal and the optimum value of d.c. signal will be that which will move the working point in to the saturated region such that it traverses both the saturated and unsaturated regions in the presence of both d.c. and a.c. excitations. We shall assume such optimum values of d.c. and a.c. excitations to be present in our investigations. Since the behaviour under steady conditions will be the same irrespective of whether we apply a.c. or d.c. first, we shall assume that d.c. is applied before a.c. for the sake of convenience of explanations, although in actual practice, d.c. is applied after a.c.

While studying the behaviour under such ideal and optimum conditions, the following fundamental points have been kept in mind.

1. When the a.c. voltage is zero in its cycle, the position of the working point while in the saturated region, is determined by the d.c. excitation applied.
2. When the a.c. voltage is zero in its cycle while the working point is in the unsaturated region, there must not be any change of flux. This will take place when the working point will reverse its path in the $B-H$ curve and so it must be in the farthest position from the saturated region when the a.c. voltage is zero.
3. If the decrease of flux produces a positive voltage, an increase of flux must produce a negative voltage. The magnitude of induced voltage either positive or negative must be equal to the rate at which the flux decreases or increases.

4. The magnitude of induced e.m.f. is given by $e = -N \frac{d\phi}{dt} \cdot 10^{-8}$ volts.

$$\therefore \int e \cdot dt = -N \cdot 10^{-8} \cdot \int d\phi, \quad \text{or} \quad \int e \cdot dt = -N \cdot 10^{-8} \phi.$$

Thus when a change of flux ϕ takes place, the voltage point in the voltage-time curve describes an area which is equal to $N \cdot 10^{-8} \phi$.

5. The current through the a.c. winding at any instant is determined not only by the position of the working point at that moment, but also by the magnitude of d.c. excitation at the moment.

We shall consider in the present paper the behaviour in the following different cases :

1. Single core having a d.c. source of infinite impedance.
2. Single core having a d.c. source of low impedance.
3. Two cores series connected with d.c. source of infinite impedance.
4. Two cores series connected with d.c. source of low impedance.
5. Two cores parallel connected with d.c. source of infinite impedance.
6. Two cores parallel connected with d.c. source of low impedance.

The different figures and curves in diagrams I to VI give a full picture of the behaviour in the different cases respectively.

CASE 1.

In this case there are two windings, one meant for a.c. and the other for d.c. signal both wound on the same core and the impedance of the signal source is infinitely large. Figures 1 and 2 in diagram 1 indicate the nature of $B-H$ curve and of $B-H$ loop described and figures 4, 5, 6, 7, and 8 indicate the path of the working point along the $B-H$ curve, the sinusoidal applied a.c. voltage, the nature of alternating current, the nature of flux variation, and the nature of alternating current through the d.c. winding respectively, all referred with respect to the voltage variation curve of figure 5.

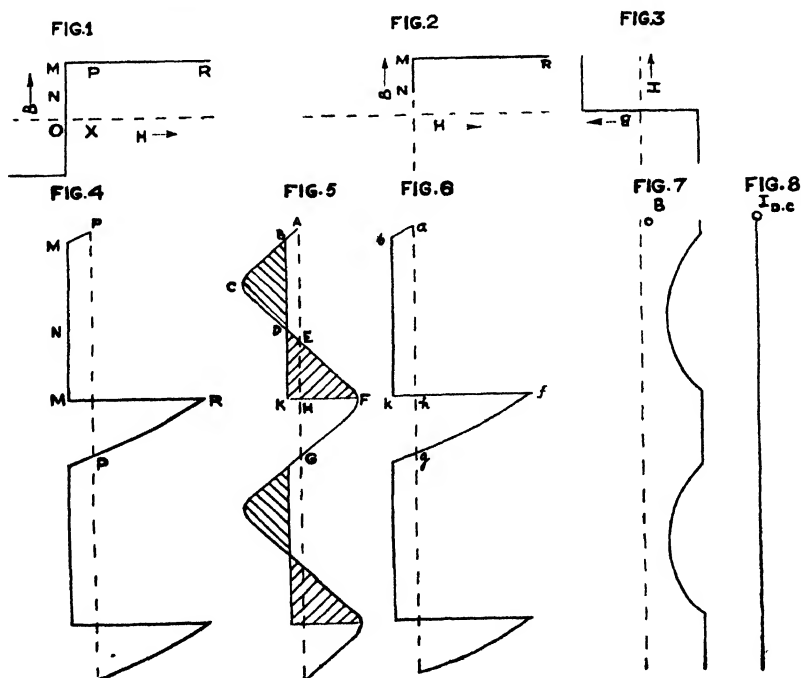


Diagram 1.

As the d.c. circuit has an infinitely large impedance, no current can flow through it by the voltage induced in it due to any flux change in the core. Therefore, the d.c. excitation OX due to the signal remains constant throughout the cycle, as shown by the dotted line in figure 4. The working point will be at P (figure 1) in the saturated region when the a.c. voltage is zero at A in the presence of d.c. signal. The working point moves from P to M as the voltage point moves from A to B say, and the current increases sinusoidally from a to b as shown in figure 6, and its magnitude at any instant is given by $E \sin \omega t / R$ where $E \sin \omega t$ is the a.c. voltage applied and R is the resistance of the a.c. winding. When the working point reaches M , it enters the unsaturated region and there can not be any further increase in current. As the voltage increases further, a change of flux takes place and the working point moves downwards in the unsaturated region at such a rate that the induced voltage due to the change of flux, will balance the increase in applied voltage. The working point will go on moving downwards and the change of flux will continue to take place in the same direction till the voltage point reaches D where its magnitude is the same as that at B . The area of the voltage-time curve between the points B and D , as shown by the hatched portion, is proportional to the total change of flux taking place when the working point moves from M to N . As the voltage point moves beyond D , it becomes positive with respect to the point D and so to balance the voltage now, there must be change of flux in the opposite direction and so the working point moves upwards from N towards M . The working point will come back to M when the voltage point reaches F where the voltage time area between points D and F , as shown by the hatched portion, is equal to the former hatched area. When the point M is reached, there can not be any further change of flux. So the working point suddenly moves from M to R in the saturated region and the current, which was so long constant and negative, suddenly become positive and reaches such a value that this current multiplied by the resistance R becomes equal to the voltage at F . After that, the working point being in the saturated region, the current varies sinusoidally with the voltage and the working point comes back to P and so the current is zero when the voltage becomes zero at G . This is repeated similarly in subsequent cycles. The current curve is shown by $abkhfg$ in figure 6, and the nature of variation of B by the curve in figure 7. The $B-H$ loop described will be as shown in figure 2.

In voltage-time curve, the area BCD = the area DKF . So the area $ABKH$ = the area HFG . It follows, therefore, that in current-time curve in figure 6, the area $abkh$ is equal to the area hfg . Therefore, the average value of alternating current is zero. The average value of rectified alternating current will be given by the average value of height of either of these two areas. The average value of height from area $abkh$ is given by $I_a(av)/N_a = OX$.

But $I_c N_c = OX$. $\therefore I_a(av) = I_c N_c / N_a$.

There is hardly any such practical case in which the signal source produces a current due to the signal, but at the same time offers an infinitely large impedance to the voltage induced in the d.c. winding due to change of flux. A practical case arises when there is no d.c. winding at all and the d.c. excitation due to the signal is applied from a large current passing through a single conductor or when the d.c. excitation is furnished by a magnet.

CASE 2

In this case the impedance of the d.c. source is low, so whenever there will be any change of flux in the core, the voltage that is induced in the d.c. winding, will produce a current through it and so the d.c. excitation furnished by the d.c. signal will change, as shown by the dotted curve in figure 4, in diagram II in such a direction that it would tend to oppose the change of flux due to which it is produced. This happens when the working point enters unsaturated region at

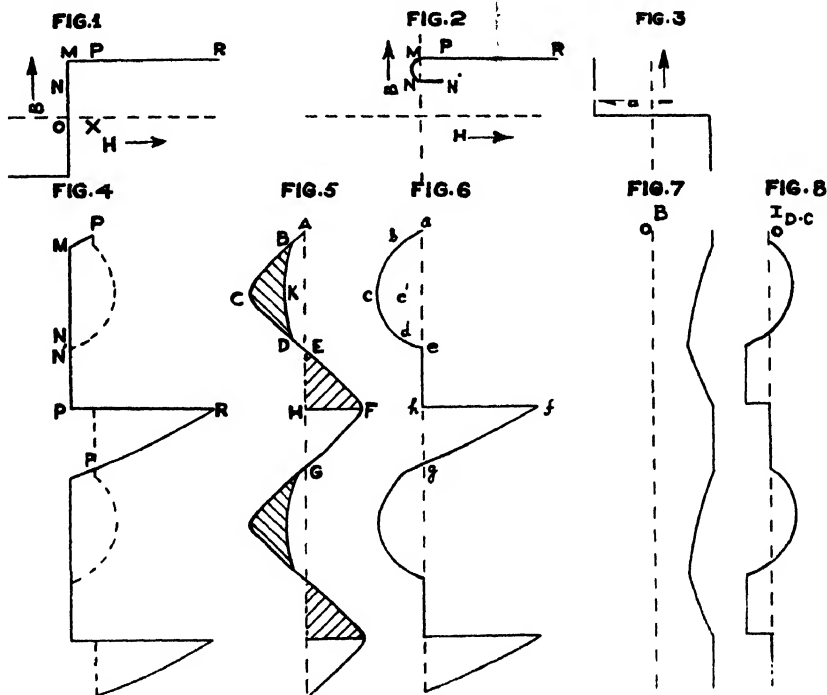


Diagram II.

M (figure 1) and a larger current flows through the a.c. winding which produces larger ohmic drop and so a lesser change of flux is necessary to balance the lesser voltage time area as shown by the hatched portion $BCDK$ (figure 5) than in the former case. When the voltage point reaches D , the working point reaches the extreme end of its path N . As the voltage point moves beyond D , it becomes positive with respect to D and a change of flux in opposite direction is necessary to balance the voltage. But any change of flux in this direction will produce

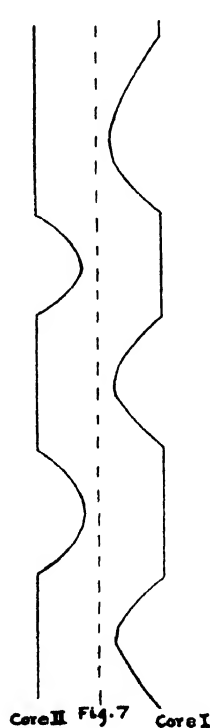
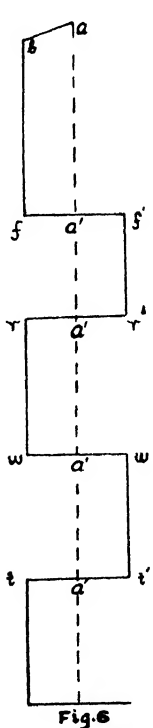
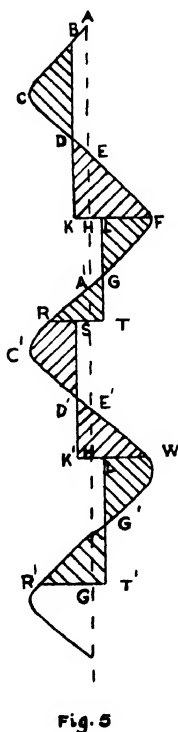
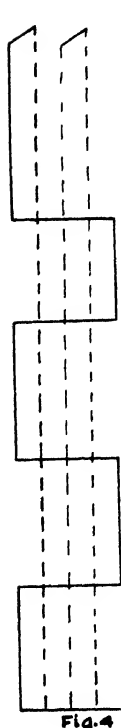
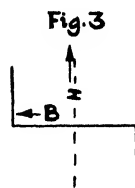
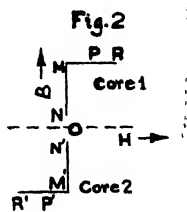
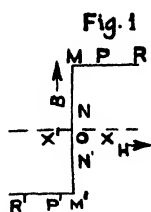
a current through the d.c. winding in the opposite direction and it will affect the d.c. excitation in the opposite direction till it becomes zero. When the total d.c. excitation becomes zero, there can not be any further change in it; as it would now act as a transformer whose secondary is short-circuited and there will be appreciable change of flux to balance out the voltage. This change of flux in the opposite direction may be assumed to take place practically when the voltage is zero at E , as the change of flux necessary to bring the total d.c. excitation to zero, is small. The working point will come back to M when the voltage point reaches F where the voltage time area EFH is equal to the area $BCDK$. When the voltage point reaches E from D , the resultant d.c. excitation becomes zero and therefore, although the working point remains fixed at N , the current through the a.c. winding becomes zero. In the $B-H$ loop (figure 2.) it will appear as if the working point has moved from N to N' . When the working point moves from N to M (figure 1), the current is still zero due to the resultant d.c. excitation being zero and it will appear, therefore, that the working point moves along $N'P$ in figure 2. The behaviour in the saturated region will be same as in case 1. The whole operation will be repeated in subsequent cycles. Thus the nature of $B-H$ loop described will be as shown by $NN'PRPM$ in figure 2. and the nature of current variation is shown by $abcde$ and hfg in the two half cycles. As the area $BCDK$ — the area EFH , the area $ABKDE$ = the area HFG in the voltage-time curve. Therefore, the resultant alternating current is zero. The average value of rectified current will, therefore, be the average value from area $abcde$. It is clear that the value of this area will depend on the impedance and number of turns of the d.c. winding circuit. This area will be greater for lower impedance and larger number of turns of the d.c. circuit. If this area be equal to the area $abc'de$, then the average value will be given by I_a (av). $N_a = OX$. But $OX = I_c.N_c$. $\therefore I_a(\text{av}) = I_c.N_c/N_a$. As this area is always greater than the area $abc'de$, I_a is always greater than $I_c.N_c/N_a$. So I_a/I_c is always greater than N_c/N_a . The nature of variation of B and of current due to flux change through the d.c. winding are shown in figure 7 and 8 respectively and the $B-H$ loop traced will be as shown by $NN'PRPM$ of figure 2.

CASE 3

When two cores are series connected, the a.c. windings are connected in series and the d.c. windings are connected in series opposition. The object of connecting the d.c. windings in series opposition is that when flux changes in both the cores at the same rates, the resultant induced e.m.f. in the d.c. windings is zero. The effect of connecting two a.c. windings in series is that the same current must always flow through both the windings and, therefore, the current through any winding can not abruptly increase to a very high value when one of the cores becomes saturated. When flux changes in one core only, the voltage is induced in its d.c. winding only and though it can not be balanced by the

voltage in the d.c. winding of the other core, it can not produce any current through the d.c. winding due to the infinitely large impedance of the d.c. source. Therefore, the d.c. excitation remains constant throughout as shown by the dotted line in figure 4 in diagram III.

In figure 1, $ONMPR$ and $ON'M'P'R'$ are the $B-H$ curves for the two cores. As d.c. windings are oppositely connected, current through them will produce d.c. excitation, as given by OX and OX' in the two cores. When the working point in core I reaches M as the voltage point reaches B from A , the same in core II reaches R' . When the working point in core I, has reached M , there will be



gram III.

change of flux in it before current can increase any further; and so the working point in core II, although in saturated region, can not move beyond R' when the voltage increases. The voltage is entirely balanced by the induced e.m.f. in core I by change of flux in it and the current remains constant. This change of flux continues until the voltage point reaches D where the voltage is of the same magnitude as at B . When the voltage point moves further, it becomes positive with respect to D and so change of flux begins to take place in the opposite direction. This change of flux in opposite direction continues to take place till the working point in core I, reaches back to M when the voltage point reaches F such that the area $BC'D =$ the area DFK . Now there can not be any further change of flux in core I, and so the working points in both the cores will move abruptly from M to R and from R' to M' in the saturated regions respectively and current point will move suddenly from f to f' , as shown in figure 6. This current can balance a portion HL of the voltage and to balance the remaining portion of voltage, there must be a change of flux in core II as the working point in core II has reached M' in the unsaturated region and there can not be any further change of current. This change of flux continues to take place till the voltage point reaches G where its magnitude is same as that at L . As the voltage point moves beyond G , it becomes negative with respect to G and so the working point in core II must move in the opposite direction to produce an opposite change of flux. This change of flux continues till the working point in core II reaches M' at the voltage point R such that the area $LFG =$ the area GRT . Throughout this time the current remains constant at the same previous value but in the opposite direction. When the working point reaches M' in core II, the working points will move again from R to M and from M' to R' and the new current will balance a portion of voltage, the remaining portion being balanced by change of flux produced this time by core I.

It follows that the area $a'rw'a' =$ the area $a'w't'a'$ in the current-time curve in figure 6. Therefore, the resultant current through the a.c. winding is zero and the average value of rectified current is given by $I_a(av).N_a = OX = I_c.N_o$. $\therefore I_a(av) = I_c.N_c/N_a$. Figure 7 shows the variations of flux in the two cores and figure 2, shows the nature of $B-H$ loops in the two cores.

CASE 4

This is the most important case so far as practical magnetic amplifiers are concerned. This is similar to case 3 except that the d.c. source is of low impedance; so the resultant induced voltage across the d.c. windings must be zero. Therefore, $N_c \left(\frac{d\phi_1}{dt} \right) + N_c \left(\frac{d\phi_2}{dt} \right)$ must be zero and $\left(\frac{d\phi_1}{dt} \right) = - \left(\frac{d\phi_2}{dt} \right)$. So if there be any change of flux in one core, there must also be a simultaneous change in the other core under steady conditions and the rate of change must also be the same in both the cores when number of turns is the same in them. If simultaneous

flux change is not possible initially in both the cores due to one core being in the saturated region, a large current will flow through the d.c. winding due to flux change in one core and this will adjust conditions in such a way that flux will change simultaneously in both the cores under steady conditions.

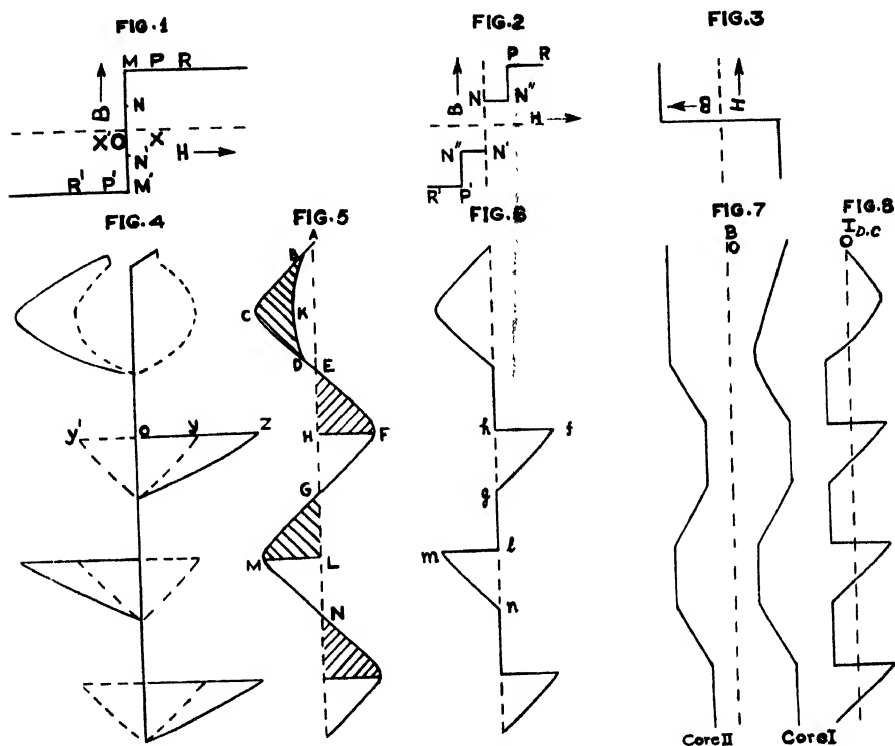


Diagram IV.

In this case the change of flux that takes place in core I after the voltage point goes from *A* to *B*, induces a voltage in the d.c. winding of core I which produces a current through it and the d.c. excitation varies as shown by the dotted lines in figure 4, in diagram IV and so the current through the a.c. winding increases and the change of flux necessary to balance the increase in voltage becomes smaller as the area of voltage-time curve which has to be balanced, becomes smaller and equal to *BCDK* as shown in figure 5. This change of flux continues to take place until the voltage point is at *D* where the voltage is of same magnitude as at *B*. As the voltage point goes beyond *D*, it becomes positive with respect to *D* and a change of flux in opposite direction is necessary to balance the voltage. But any tendency to change the flux in this direction will produce a current through the d.c. winding in the opposite direction, and the resultant d.c. excitation will change till it will become zero in both the cores. This will take place just after the voltage point crosses *D* before there is any appreciable

change of flux depending on the d.c. winding and the d.c. source. As the change of flux necessary is negligible, the working points will be practically at N and M' when the voltage point reaches zero at E ; but as d.c. excitation has decreased, it will appear that the working point in core I has moved from N to N'' (figure 2). As the voltage increases now, the cores will behave as having their secondaries shorted and there will be change of flux in both the cores at the same rate till the working point in core I reaches saturation region at M when the voltage point is at F such that the area $EFH =$ twice the area $BCDK$. There can not be any further change of flux as core I reaches saturation and also the working point at M can not move horizontally as such, since the working point in core II is at N' in the unsaturated region. But the voltage at F can not be balanced as such and will tend to produce a change of flux in core II. But this tendency to produce change of flux will produce a current in the d.c. winding and the d.c. excitations in the two cores will change from O to OY and OY' respectively. So, although the working point in core II remains at N' , a current flows through its winding and the working point in core I moves to Z (figure 4) such that the same current flows through its winding also. The d.c. excitations change in such a way that the current corresponding to OY' or YZ , can balance the voltage at F . As the voltage point goes beyond F , the d.c. excitations change in such a way that the current balances the voltage always till the voltage point comes to zero at G when the total d.c. excitation in the two cores will be again zero. The working point in core I reaches M again and that in core II remains at N' . As the voltage point goes beyond G , there is again change of flux in the cores till the working point reaches M' in the saturated region in core II when the voltage point reaches M such that the area $GML =$ the area EFH . The same operation is repeated in subsequent cycles. It is clear that the average value of current in each half cycle is same and so the resultant current is zero. The average value of rectified current is proportional to the average value of area hfg or lmn in current curve of figure 6. Now the area HFG in the voltage-time curve $=$ the area $ABCDE$ —twice the area $BCDK$ $=$ the area $ABKDE$ —the area $BCDK$ and if this is equal to the area $ABDE$, then $I_a(av) = I_c N_c / N_a$ as before. This happens when the area $BCDK =$ the area BKD . If the impedance of d.c. circuit is not very low, the area $BCDK$ will be greater than the area BKD and $I_a(av)$ will be less than $I_c N_c / N_a$. Figure 7 shows the variation of flux in both the cores and it is clear that change of flux takes place simultaneously in them. Figure 8 shows the nature of current through the d.c. winding due to change of flux and figure 2 gives the nature of $B-H$ loops described as $NN''PR$ and $R'P'N'''N'$ in two cores.

CASE 5

In this case the two a.c. windings are connected in parallel and the impedance of the d.c. source is infinitely large. So, though there may be a voltage induced

in the d.c. windings when there is change of flux in one core only, no current can flow through it due to very high impedance of the d.c. source. Therefore, the d.c. excitations in the two cores will remain constant throughout. It is just equivalent to two single cores with d.c. source of infinitely large impedance (case 1) connected in parallel. The current through the a.c. winding of any core in one half cycle will be just the image opposite of the current in the winding of the other core in the other half cycle. Thus curve $abcdef$ (figure 6) in diagram V gives the nature of current through one winding and the curve $a'b'c'd'e'f'$ gives the nature of current through the other winding. The resultant current

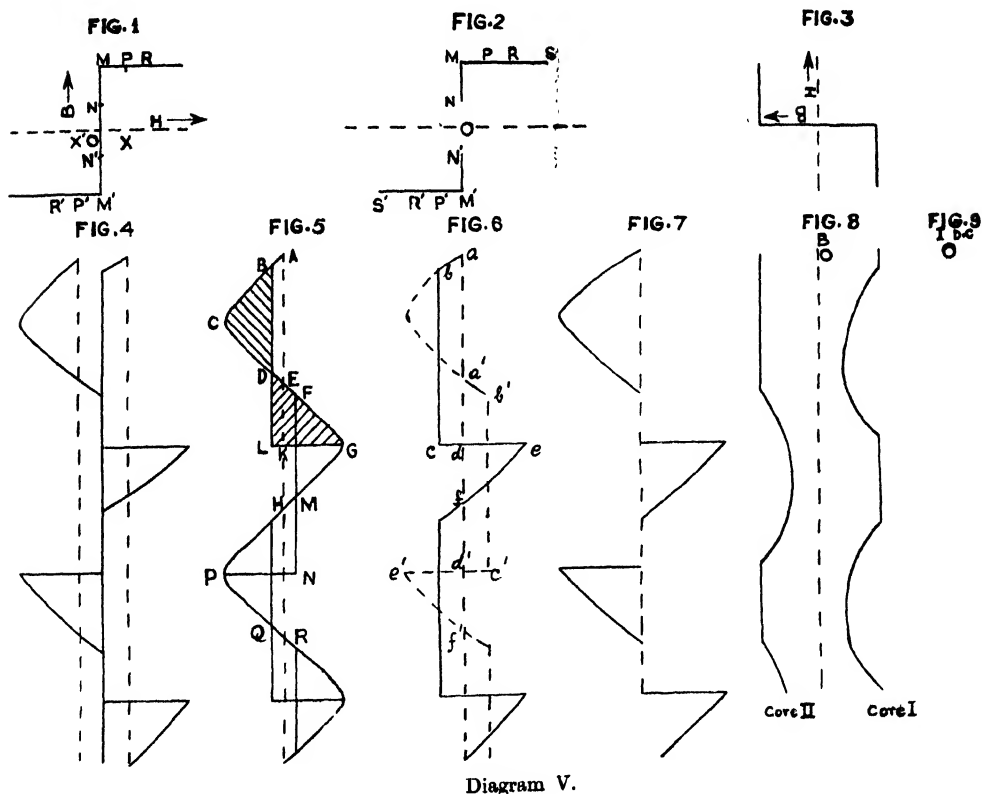


Diagram V.

which will be the sum of the currents through the two cores is shown in figure 7. It is clear that the resultant current will be zero and the average value of rectified current will be double the value given by a single core with d.c. source of infinitely large impedance. Therefore, the average value is given by $I_a(av) = 2 I_c N_c / N_a$. The nature of variation of B is shown by figure 8 and the nature of $B-H$ loops in the two cores will be as shown by $NMPRS$ and $N'M'P'R'S'$ in figure 2.

CASE 6

In this case the a.c. windings are connected in parallel and the d.c. source is of low impedance. When the working point in core I enters the unsaturated region with the increase of voltage, there is change of flux in it as before, but current in core II goes on increasing as shown in figure 6. in diagram VI, the working point being in the saturated region. The change of flux in core I induces

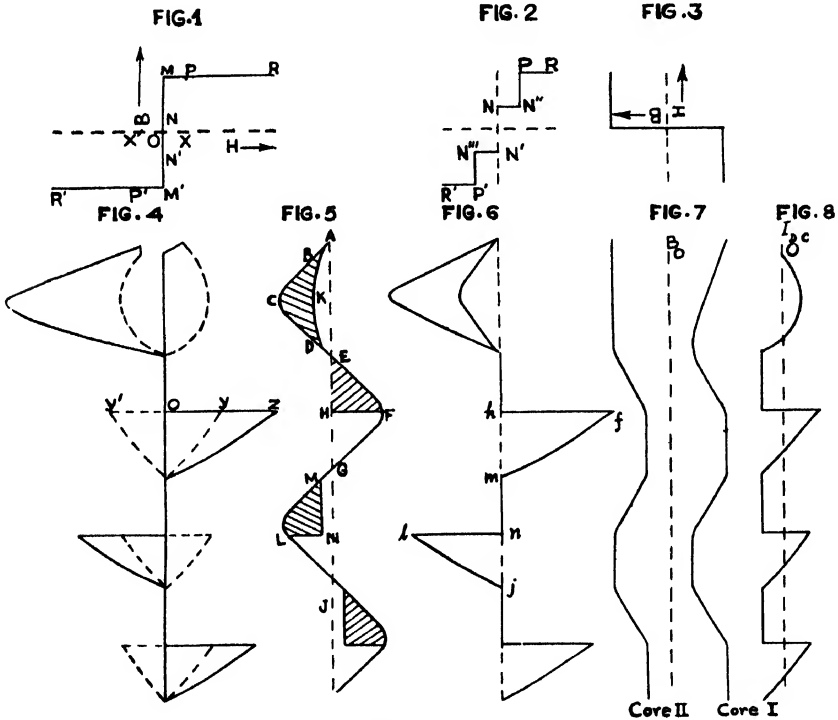


Diagram VI.

a voltage in its d.c. winding and a current flows through it which changes the d.c. excitations in the two cores as shown by the dotted lines in figure 4. This change of flux continues until the voltage point reaches D where the voltage is of the same value as at B . Then there will be a flux change in core I in the opposite direction to balance the voltage which becomes positive. As the d.c. winding is of low impedance, a current flows through it in opposite direction before any appreciable change of flux takes place and the resultant d.c. excitations in the two cores becomes zero when the voltage is zero at E , as in previous cases. So when the voltage is zero at E , the working points will be at N and M' and there will be change of flux in both the cores to balance out the applied voltage. When the working point in core I reaches at M at the voltage point F such that the area $EFH =$ the area BCD (figure 5), there can not be any further change of flux

in core I. The working point in core I will move to Z in the saturated region and there will be abrupt increase of current to balance the applied voltage at F in the core winding. In core II there will be a tendency to undergo a further change of flux to balance out the voltage and this will induce a voltage in the d.c. winding which can not be opposed by a similar voltage in the other d.c. winding and so a direct current will flow and the d.c. excitations will be changed, as shown by the dotted lines. The d.c. excitations will be changed in such a way that the currents in the two cores which will be given by YZ and $Y'O$, will individually balance the voltage at F . As the voltage changes, the working point in core I moves along the saturated region and that in core II remains fixed at N' and the d.c. excitations vary in such a way that the currents balance the voltage at each point till the voltage point is at M when the working point in core I reaches M (figure 1). Now there will be change of flux in both the cores to balance the applied voltage till the working point in core II reaches M' at the voltage point L where the area MLN = the area EHF . The working point in core II moves in the saturated region and that in core I remains fixed at N and the d.c. excitations change as before and the cycle is repeated.

The current I_1 or I_2 will be practically equal and their average values will be proportional to the area HFG . Therefore, their resultant current which will be $I_1 + I_2$, will be proportional to twice the area HFG . But the area HFG = the area $ABKDE$. Therefore, it is clear that the average value of current will always be greater than $I_c N_c / N_a$ and the amount by which it will be greater, is given by the area BKD . The lower the impedance of the d.c. source, the greater will be this area and hence greater will be the amplification. The nature of variation of B and of current through the d.c. winding due to change of flux are given by figures 7 and 8 and the nature of $B-H$ loops described, are given by $NN''PR$ and $N'N'''P'R'$ in figure 2.

EXPERIMENTAL OBSERVATIONS AND CONCLUSION

The behaviour of the saturable reactor under above conditions was experimentally verified with the help of a C.R.O. tube and was found to be very much like the cases under idealised conditions as given above. As mentioned above, it is very difficult to get a d.c. source of infinite impedance. An approximate condition was reached by connecting a choke of high value in series with the d.c. source of high value. Two ring cores of μ -metal, each having 500 a.c. turns and 1,550 d.c. turns, were used. In the case of a single core with d.c. source of low impedance, the current amplification was found to be approximately equal to 7; but in the case of two cores series connected with the d.c. source of low impedance, it was found to be of the order of 3.8. The value of B was measured by means of an integrating circuit connected in a separate winding.

Therefore, it is clear that when the d.c. source is of infinitely large impedance which is a very rare case, we can use a single core and get the same amplification

and hence the same advantage as two cores connected in series. If they are connected in parallel, however, we can get the double amplification. If the source is of very low impedance, although a single core can give the same amplification as two cores, a single core can not be used in practice due to the fact that, generally, when the d.c. signal is absent, the low impedance connected to the d.c. winding is still present and this produces a d.c. excitation even in the absence of the d.c. signal. Under these circumstances, therefore, the two cores with either series or parallel connection are used. From the point of consideration of low value of time constant, series connection is, however, more frequently used than the parallel connection.

ACKNOWLEDGMENTS

The author gratefully acknowledges the invaluable guidance and help received from Dr. H. Rakshit, Head of the Department of Physics and Communication, Bengal Engineering College, Sibpore.

REFERENCES

- Miles, J. G., 1951. 'Bibliography of Magnetic Amplifier Devices and the Saturable Reactor Art,' Proc. A. I. E. E., 70.
- Say, M. G., 'Magnetic Amplifiers and Saturable Reactors', Newnes Electrical Engineering Progress Series, London.
- Geyger, W. A. 'Magnetic Amplifier Circuits', McGraw-Hill Book Co. Inc., New York, N.Y.

ON THE FLUORESCENCE OF PARACHLOROTOLUENE IN THE SOLID STATE AT LOW TEMPERATURE*

D. C. BISWAS

OPTICS DEPARTMENT, INDIAN ASSOCIATION FOR THE CULTIVATION OF SCIENCE, JADAVPUR,
CALCUTTA.

(Received for publication, January 16, 1956)

Plate IV

ABSTRACT. The fluorescence spectra of pure *p*-chlorotoluene in the solid state at -30°C and -180°C have been investigated using filtered Hg radiation and the spectrum has been compared with those due to frozen solutions of the substance in benzene, *n*-heptane, methyl cyclohexane, methyl alcohol, carbon tetrachloride, tetrachloroethylene and carbon disulphide of different concentrations. Altogether eight bands are produced by the pure substance and these diminish in intensity abruptly as the temperature of the solidified mass is raised from -180°C to -30°C . The bands persist with undiminished intensity even in the case of a 2% solution of the substance in benzene, carbon tetrachloride and tetrachloroethylene at -180°C . In the case of solution in methyl cyclohexane, *n*-heptane and methyl alcohol at -180°C , strong new bands appear in the fluorescence spectra. When the substance is dissolved in carbon disulphide and the solution is frozen and cooled to -180°C , the bands persist upto 15% concentration, but the intensities of the bands diminish rapidly and the bands almost disappear as the concentration is reduced to 5%. The results have been explained on the assumption that the formation of virtual links between the chlorine and hydrogen atoms of the *p*-chlorotoluene molecule respectively with hydrogen and chlorine atoms of the neighbouring molecules in the solidified mass is responsible for the production of the metastable states giving rise to the observed fluorescence. It is pointed out that the absence of fluorescence in very dilute frozen solutions in carbon disulphide corroborates this hypothesis.

INTRODUCTION

While studying the Raman spectra of ortho- and para-chlorotoluene at low temperatures, Sanyal (1953) first observed that either of these two compounds produces fluorescence in the visible region in the solid state at -180°C . Later, the present author (Biswas, 1954, 1955a, 1955b) observed that many substituted benzene compounds give rise to similar fluorescence in the visible region when the substances are solidified and cooled down to -180°C . The experimental arrangements in these cases were not, however, suitable for studying the fluorescence spectra at low temperatures, as the mercury lines in the near ultraviolet region were largely absorbed by the glass condensers used in these experiments and also other mercury lines were overexposed. The fluorescence

*Communicated by Professor S. C. Sirka .

bands reported by these authors were therefore, probably incomplete. It would be of interest to find out the complete spectrum and the influence of environment on it, because such data might throw some light on the origin of these fluorescence spectra. The investigation of the fluorescence of some frozen substituted benzenes was, therefore, undertaken and the results obtained in the case of *p*-chlorotoluene are discussed in the present paper.

EXPERIMENTAL

Para chlorotoluene used in the present investigation was supplied by Eastman Kodak Co., N.Y. and it was of chemically pure quality. The liquid was again repeatedly fractionated in vacuum before exposure. The purity was also tested by studying the Raman spectrum of the liquid and it was observed that there were no extra feeble Raman lines and the background was clear.

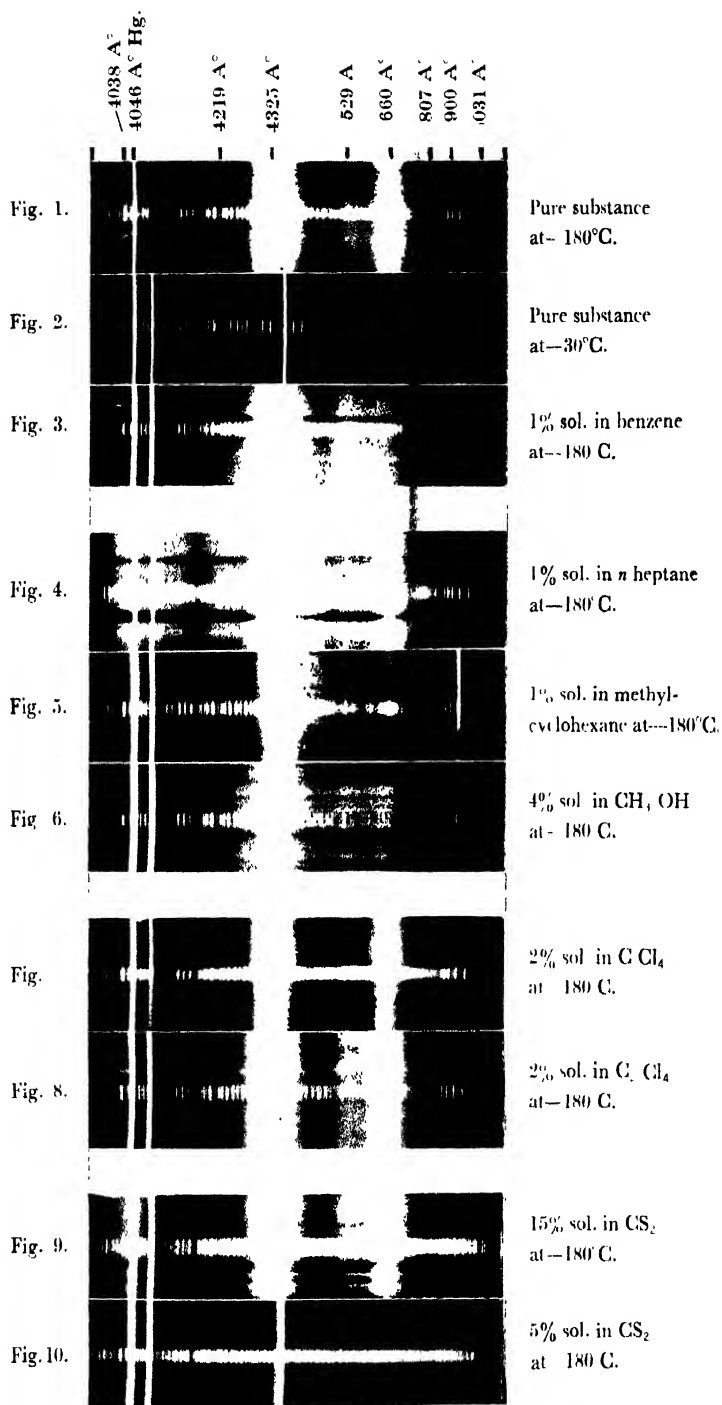
The incident beam, which is generally used for illuminating the sample in studying Raman spectra at low temperature, was slightly modified in the present case. A light filter transmitting the 3600 Å group of Hg-lines and almost cutting off the other mercury lines of longer wavelengths was placed in the path of the incident light from a mercury arc. It was observed in the preliminary investigation that after the introduction of this filter it becomes practically immaterial whether we use containers of fused silica or of pyrex glass. So, pyrex glass containers were used in the final investigation. The samples were solidified by dipping the container in liquid oxygen. Besides the fluorescence spectra of the frozen liquid at different low temperatures those of the solutions of the substance in benzene, *n*-heptane, methyl cyclohexane, carbon tetrachloride, tetrachloroethylene and carbon disulphide of concentrations varying from 15% to 1% were also investigated. All these solutions of strengths below 10% appear as homogeneous solid mass when frozen by liquid oxygen and the mass is almost transparent throughout its entire volume.

The spectra were photographed on Ilford Zenith plates using a Fuess glass spectrograph of dispersion about 11 Å in the 4046 Å region. On each spectrogram an iron arc spectrum was superposed for comparison.

As the bands were observed to be very broad a slit width varying from 0.3 to 0.6 mm. was used to reduce the time of exposure.

RESULTS AND DISCUSSION

The positions, approximate widths, estimated relative intensities and the successive distances of the fluorescence bands exhibited by pure *p*-chlorotoluene in the solid state at -180°C and -30°C and those due to a 1% solution in benzene at -180°C are given in Table I. The relative intensities are indicated as very strong (v.s), strong (s) etc., in the tables. The spectra due to 5% and

Fluorescence spectra of *p*-chlorotoluene.

10% solutions in benzene were found to be practically identical with that of the 1% solution.

The fluorescence bands given by 1% solutions of *p*-chlorotoluene in *n*-heptane and in methyl cyclohexane and also the bands given by a 4% solution in methyl alcohol cooled down to -180°C are similarly shown in Table II. A 5% solution of the substance in *n*-heptane also gives the same spectrum as the 1% solution.

Similar data for 2% solutions of *p*-chlorotoluene in carbon tetrachloride and tetrachloroethylene are given in Table III. A 5% solution of this substance in CCl_4 gave exactly the same spectrum as the 2% solution. The fluorescence bands due to a 15% and a 5% solution of *p*-chlorotoluene in carbon disulphide are given in Table IV. Some of the spectrograms are reproduced in Plate IV.

TABLE I
Fluorescence spectra

Substance	Position of the band in A.U.	Width of the band in A.U.	Position of the band in cm^{-1}	Successive differences in cm^{-1}
<i>p</i> -Chlorotoluene at -30°C .	4325 (w)	106	23115	1662
	4660 (w)	80	21453	
	4038 (s)	77	24758	1062
	4219 (m)	80	23696	581
<i>p</i> -Chlorotoluene at -180°C .	4325 (v.s.)	122	23115	1041
	4529 (s)	81	22074	621
	4660 (v.s.)	120	21453	656
	4807 (v.w.)	35	20797	395
	4900 (w)	60	20402	531
	5031 (v.w.)	38	19871	
	4048 (m)	100	24697	1001
	4219 (s)	85	23696	484
1% solution of <i>p</i> -chlorotoluene in benzene at -180°C .	4307 (v.s.)	70	23212	293
	4362 (m)	64	22919	845
	4529 (s)	80	22074	621
	4660 (s)	135	21453	626
	4800 (w)	—	20827	

TABLE II
Fluorescence spectra

Substance (frozen and cooled down to -180°C)	Position of the band in A.U.	Width in A.U.	Position of the band in cm^{-1}	Successive differences in cm^{-1}
1% solution of <i>p</i> -chlorotoluene in <i>n</i> -heptane	4025 (s)	83	24838	
	4132 (m)	44	24195	643
	4219 (m)	80	23696	499
	4316 (v.s.)	91	23163	533
	4439 (s)	34	22521	642
	4529 (m)	75	22074	447
	4660 (v.s.)	124	21453	621
	4807 (w)	37	20797	656
	4900 (?)	—	20402	395
	5031 (w)	38	19871	531
1% solution of <i>p</i> -chlorotoluene in methyl cyclohexane	4032 (m)	59	24795	
	4143 (m)	28	24130	665
	4219 (m)	90	23696	434
	4325 (s)	85	23115	581
	4454 (m)	19	22445	670
	4529 (w)	50	22074	371
	4667 (s)	24	21421	653
	4712 (m)	87	21216	205
	4817 (m)	51	20754	462
	5040 (v.w.)	45	19836	918
4% solution of <i>p</i> -chlorotoluene in methyl alcohol	4030 (m)	28	24807	
	4142 (w)	25	24136	671
	4186 (w)	27	23882	254
	4220 (v.w.)?	—	23690	192
	4273 (m)	15	23396	294
	4323 (s)	30	23126	270
	4406 (m)	36	22690	436
	4529 (m)	40	22074	616
	4660 (s)	142	21453	621
	4800 (w)	35	20827	626

TABLE III

Fluorescence spectra

Substance (frozen and cooled down to -180°C)	Position of the band in A.U.	Width in A.U.	Position of the band in cm^{-1}	Successive differences in cm^{-1}
2% solution of <i>p</i> -chlorotoluene in carbon tetrachloride	4038 (m)	77	24758	1062
	4219 (w)	80	23696	581
	4325 (v.s.)	122	23115	1041
	4529 (m)	81	22074	621
	4660 (v.s.)	120	21453	1051
	4900 (v.w)	55	20402	531
	5031 (v.w)	35	19871	
2% solution of <i>p</i> -chlorotoluene in tetrachloroethylene	4038 (w)	70	24758	1062
	4219 (w)	74	23696	581
	4325 (v.s)	120	23115	1041
	4529 (m)	75	22074	621
	4660 (s)	116	21453	656
	4807 (v.w)	—	20797	926
	5031 (v.w)	35	19871	

TABLE IV

Fluorescence spectra

Substance (frozen and cooled to -180°C)	Position of the band in A.U.	Width in A.U.	Position of the band in cm^{-1}	Successive differences in cm^{-1}
15% solution of <i>p</i> -chlorotoluene in carbon disulphide	4038 (m)	70	24758	1062
	4219 (m)	72	23696	581
	4325 (v.s)	116	23115	1041
	4529 (s)	75	22074	621
	4660 (v.s)	118	21453	656
	4807 (v.w)?	—	20797	395
	4900 (v.w)	—	20402	531
	5031 (v.w)	32	19871	
5% solution of <i>p</i> -chlorotoluene in carbon disulphide	4325 (v.w)		23115	1662
	4660 (v.w)		21453	

It is found from Table I that when the solidified mass of *p*-chlorotoluene is cooled down to -30°C only two weak fluorescence bands are observed at 4325 and 4660 Å respectively. When the temperature of the solid is lowered to -180°C , the intensity of fluorescence increases enormously and besides the two bands mentioned above six more weaker bands are observed. Table I further shows that when the substance is dispersed in frozen benzene the fluorescence bands undergo some changes. The bands at 4219 and 4529 Å become stronger while the broad band at 4325 Å appears to be split up into two components at 4307 and 4362 Å respectively. The three weaker bands at 4807, 4900 and 5031 Å seem to merge into one another to form a broad and weak band at 4800 Å.

Table II shows that the fluorescence spectrum is altered appreciably if the substance is dispersed in frozen *n*-heptane, methyl cyclohexane or methyl alcohol, the change depending on the nature of the solvents. In the case of the solution of *n*-heptane each of the strong bands at 4038 and 4325 Å splits up into pairs at 4025 and 4132 Å, 4316 and 4439 Å respectively. The wave number difference between the components in each pair is about 642 cm^{-1} . Further, the band at 4807 Å seems to become stronger and that at 4900 Å becomes weaker when the substance is dispersed in frozen *n*-heptane. In the case of solution in methyl cyclohexane also each of the three strong bands breaks up into two components which are at 4032 and 4143 Å, at 4325 and 4454 Å and at 4667 and 4712 Å respectively while the band at 4807 Å shifts to 4817 Å and becomes stronger. In the case of the solution in methyl alcohol either of the bands at 4038 and 4219 Å breaks up into a pair of components while the strong band at 4325 splits up into three components at 4273, 4325 and 4406 Å respectively. Amongst the three weak bands on the longer wavelength side, only one diffuse band can be observed at 4800 Å in this case.

Table III on the other hand shows that when the molecules of *p*-chlorotoluene are dispersed in carbon tetrachloride or tetrachloroethylene in the solid state the fluorescence spectrum is only slightly altered. In the former case the band at 4807 Å disappears and in the latter case the relative intensities of some of the bands undergo slight changes.

Table IV shows that the nature of the fluorescence spectrum is not at all altered when *p*-chlorotoluene is dissolved in carbon disulphide, but the intensity of fluorescence diminishes rapidly with lowering of concentration of *p*-chlorotoluene in carbon disulphide. The fluorescence spectrum is observed to be intense in the case of a 15% solution of *p*-chlorotoluene in carbon disulphide,

but the fluorescence tends to disappear when the strength of the solution is reduced from 15% to 5% by volume.

The appearance of fluorescence in *p*-chlorotoluene in the solid state at low temperature and also the rapid increase in its intensity with lowering of temperature of the solidified mass suggest that the fluorescence is due to the influence of intermolecular field which seems to increase rapidly with lowering of temperature. In order to understand whether this intermolecular field is to be identified with the lattice field of the crystalline substance or it is due to the formation of small groups of associated molecules, the fluorescence spectra of the substance in dilute solutions in a number of solvents are to be examined carefully. The results given in Tables I—III show that the fluorescence persists even in very dilute solutions of the substance in benzene, *n*-heptane, methyl cyclohexane, methyl alcohol, carbon tetrachloride and tetrachloroethylene. When *p*-chlorotoluene is dissolved in small quantities in these solvents and the solutions are frozen, the molecules remain dispersed homogeneously in the frozen mass and the solute does not separate out in the form of small crystals. Further, to prevent the fluorescence coming out from any such separated crystallites from entering into the spectrograph, fluorescence from the upper portions of the frozen solutions was studied in the case of solvents lighter than the substance and in the case of heavier solvents the lower portions of the solidified solution were used, so that there was very little chance for the fluorescence of such separated crystals to fall on the slit of the spectrograph. Hence the fluorescence exhibited by the frozen solutions cannot be due to lattice field in the pure substance. It appears, therefore, that when the molecules of *p*-chlorotoluene come very close to each other, they probably form small groups amongst themselves and the distortion produced in the molecules in these groups in the solid state at low temperature leads to the production of metastable states responsible for this fluorescence.

It is observed that different solvents have different influence on the fluorescence spectrum of this substance. The influence is the least in the case of benzene used as the solvent, but the other aliphatic solvents alter the spectra appreciably.

These results can be interpreted on the following assumptions. In the case of the pure substance in the solid state whenever virtual bond is formed between the chlorine atom of one *p*-chlorotoluene molecule and the hydrogen atom of a neighbouring molecule, the metastable states are produced. When the molecules are dispersed in benzene, the chlorine atom of the *p*-chlorotoluene molecule probably forms such virtual bond with the hydrogen atom of a neighbouring benzene molecule and again almost the same metastable state is produced. So even in the case of 1% solution the fluorescence persists without diminution in intensity. When the aliphatic solvents are used, the chlorine atom of the *p*-chlorotoluene atom again forms virtual bonds with the hydrogen atoms

of the CH_2 groups, but the metastable states produced in this way are different from those produced by similar attachment of the chlorine atom to the hydrogen atom of the benzene ring. Hence the fluorescence persists with undiminished intensity even in the case of 1% solutions although the spectrum is altered appreciably. When the solvent molecule does not contain any hydrogen atom but contains chlorine atoms, the hydrogen atoms of the *p*-chlorotoluene molecule can be attached to the chlorine atoms of the neighbouring solvent molecules and even then nearly the same metastable states are produced as in the case of the pure substance. It appears that the bands at 4325 \AA and 4660 \AA are due to such attachment of the chlorine atom of the solvent molecule to the ring of the *p*-chlorotoluene molecule while the bands at 4038 \AA and 4529 \AA are produced by attachment of hydrogen atom of the solvent molecule to the chlorine atom of the *p*-chlorotoluene molecule because these latter two bands become weaker when the substance is dispersed in solidified C_2Cl_4 .

The results obtained using carbon disulphide as the solvent seem to support the assumption mentioned above. It has been observed that the fluorescence persists in the case of 15% solution of the substance in frozen CS_2 , but it almost disappears abruptly when the concentration is reduced to 5%. The times of exposure and the width of the slit of the spectrograph were suitably adjusted to verify this conclusion. Also, the spectrum of the light coming only from the lower portion of the frozen solution was recorded. It appears that in the case of the 15% solution some of the molecules of *p*-chlorotoluene exist as dimers or in small associated groups giving rise to the metastable state, while such groups break up into monomers at lower concentrations.

It can be clearly seen that the abrupt disappearance of the fluorescence with the change of concentration from 15% to 5% can not be due to the quenching by CS_2 molecules, because if a quenching effect would exist, no fluorescence could be observed in the case of the 15% solution. Further, the fluorescence spectrum is in the visible region while the longest electronic absorption band of the CS_2 molecule lies in the region between 3400 \AA to 800 \AA , and therefore, the fluorescence cannot be quenched by carbon disulphide molecules.

The results thus furnish new evidence for the formation of strongly associated groups of molecules in the solid state of such substituted benzene molecules. Investigations with other compounds are in progress.

ACKNOWLEDGMENT

The author is indebted to Professor S. C. Sirkar, D.Sc., F.N.I. for his kind interest and constant guidance during the progress of this work.

REFERENCES

- Sanyal, S. B., 1953, *Ind. J. Phys.*, **27**, 447.
Biswas, D. C., 1954, *Ind. J. Phys.*, **28**, 423.
Biswas, D. C., 1955a, *Ind. J. Phys.*, **29**, 257.
Biswas, D. C., 1955b, *Ind. J. Phys.*, **29**, 503.

Letter to the Editor

THE ULTRAVIOLET ABSORPTION SPECTRUM OF META-FLUOROCHLOROBENZENE

S. L. N. G. KRISHNAMACHARI

PHYSICS DEPARTMENT, ANDHRA UNIVERSITY, WALTAIR

(Received for publication, January 24, 1956)

In continuation of the work on the ortho-fluoro-chlorobenzene (author, 1955), the ultraviolet absorption spectrum of meta-fluorochlorobenzene in the vapour state was studied, the only previous investigation on the absorption of this molecule being in hexane solution by Conrad-Billroth (1936). The spectrum was photographed with path lengths 15, 50 and 75 cms and at different temperatures ranging from -80°C to about $+100^{\circ}\text{C}$.

Two regions of absorption were observed :

(1) a continuous one below 2150 \AA and (2) a discrete one in the region $2850\text{--}2350 \text{ \AA}$. These two regions merge together at higher vapour pressures. The bands in the discrete region are red degraded and about 200 of them were measured. This system could be interpreted as due to the electronic transition $A'-A'$. In accordance with this a strong 0,0 band and progressions and combinations of many totally symmetrical vibrations were observed. The strong band at 37026.5 cm^{-1} was chosen as the 0,0 band of the system. Most of the bands were interpreted in terms of five upper state and four lower state frequencies. These, together with other data, are presented in Table I.

TABLE I

Ground and excited state frequencies of $m\text{-C}_6\text{H}_4\text{F.Cl}$

Raman data (Kohlrausch, 1935)		U.V. absorption data		Tentative assignment
	Int.	Ground state	Excited state	
683	7	688	636 (st)	C-Cl stretching
880	2	895	846 (m)	
1002	10	1007	966 (vst)	Carbon ring breathing
1060	4	..	1023 (s)	
1217	4	1229	1218 (ms)	C-F stretching

On the red side of each of the strong bands, satellite bands were observed with frequency separations of 42 and 78 cm^{-1} , the latter being more pronounced. These bands were interpreted as the $v-v$ transitions of some of the low lying vibrations. All strong bands also exhibit a double-headed structure with a separation of 6 cm^{-1} . These double heads are most probably rotational fine structure. A portion of the spectrum is reproduced in figure 1.

A detailed discussion of the analysis will be published shortly.



Fig. 1. Part of the U.V. absorption spectrum of *m*-fluorochlorobenzene

ACKNOWLEDGMENTS

The author is grateful to Dr. G. C. Finger of the Illinois State Geological Survey for the gift of the sample and to the Govt. of India for the award of a senior research scholarship. The author is deeply indebted to Prof. K. R. Rao for his valuable guidance.

REFERENCES

- Krishnamachari, S. L. N. G. 1955, *Ind. J. Phys.* **29** 603.
 Conrod-Billroth, H. and Forster, G., 1936. *Zeit. F. Phys. Chem. B.*, **33**, 311.
 Kohlraush *et al.*, 1935. *Monats. Fur. Chem.*, **65**, 199-204.

GEOMAGNETIC ACTIVITY AND SOLAR M-REGIONS FOR THE CURRENT EPOCH OF THE SUNSPOT MINIMUM

J. N. TANDON

DEPARTMENT OF PHYSICS, UNIVERSITY OF DELHI, DELHI

(Received for publication January 28, 1956)

ABSTRACT. The analysis of geomagnetic activity has been made for the period 1950-54 and four sequences of annual variations have been detected. It has been shown that the most predominant effect of M-regions is observable only on particular dates separated at an interval of 27 days. In the last section the possibility of the association of M-regions with various solar features has been discussed and it is found that they can be identified with unipolar magnetic regions which may also be the seat of low coronal line intensities.

I. INTRODUCTION

The moderate geomagnetic storms showing 27-day recurrence tendency were supposed to last for the duration of seven to eight rotations only, forming the so called *M*-sequences, due presumably to the existence of some *M*-regions (Bartels, 1932). In a recent paper Naqvi and Bhargava (1954, hence forth referred to as Paper I) have shown the presence of two very long *M*-sequences, showing annual variations against the six-monthly variations discussed by Bartels. The most probable cause of this annual variation was described to be tilt of solar axis of rotation to the ecliptic and is referred to as "axial hypothesis" in Paper I. In a more recent paper Naqvi and Tandon (1955) have given the results of the analysis of geomagnetic activity for the period 1930-34 and detected three very long sequences showing annual variations. The longest sequence in this period lasts for about 58 rotations.

In the present paper, the sample of data for the period 1950-54 has been re-examined and four sequences (*A*, *B*, *A*₁, and *B*₁) have been obtained. The first two sequences are essentially of the same nature as referred to in Paper I while the last ones apparently show six-monthly variations. A close examination of *A*₁ and *B*₁ sequences has indicated the presence of the real annual variation and thus strongly favours the axial hypothesis which is also supported by the analysis of geomagnetic activity in regard to their association with regions of coronal emission lines (Bell and Glazer, 1954). It has further been shown that the most predominant effect of *M*-regions is observable on particular dates which are separated from one another at an interval of 27 days and that these regions live for

about 30-50 rotations. In the last section the possibility of identifying these *M*-regions with various solar features has been discussed and is shown that *M*-regions can be identified with the newly observed 'unipolar' magnetic regions.

II. ANALYSIS OF THE GEOMAGNETIC ACTIVITY

(a) *Method of Analysis* :—The three days running means of the daily *C*-figure of the geomagnetic activity is plotted for the period 1950-54 and the sequences of recurrent activity with a period of 27 days are constructed. The sequences are considered to be continuing during the next year, even after six or seven rotations of low activity, if the high activity repeats during that year. It has been verified that this process of three days running means essentially does not affect the variation of the activity within a sequence except slightly reducing the large maxima and slightly increasing the minima or shifting the date of maximum activity by one day on either side.

To study the variation of geomagnetic activity within a particular sequence five different sets of curves are plotted as follows;

(i) *Mean day activity curve*: The *C*-figure after every 27 days starting from certain selected dates, determined on the basis of the plots of the three days running means of the daily *C*-figure. These curves show a well marked periodicity of annual nature.

(ii) The *C*-figure after every 27 days starting one day earlier than in the case of the mean day activity curve.

(iii) The *C*-figure after every 27 days starting one day later than in the case of the mean day activity curve.

The purpose of the second and the third set of curves is to check the appropriateness of the particular dates chosen for the first set. The periodicity in the later sets is found to be less marked than in the mean day activity curves. This was expected in view of the fact that moderate geomagnetic storms last for about 2-4 days only. To illustrate this departure we consider *A*-sequence in figure 1 which shows the mean day activity curve by thick lines while the second and the third set of curves by thin lines superimposed over the thick curve. A close examination of this figure clearly indicates the departure in the periodicity of the second and the third set of curves from the mean day activity curves, referred to as above.

(iv) *Mean activity curve*: The three day running means centered around the selected dates used in the mean day activity curves at an interval of 27 days; this, indeed, is a composite effect of the first, the second and the third set of curves and shows a well marked periodicity as good as in the case of the first set of curves.

There are theoretical difficulties to account for the behaviour of the set of curves 2 and 3 and the mean day activity curves as regards to their periodicity

and can probably, be explained on the assumption of narrow beam of particles. We will not enter into the cause of such peculiar behaviour of these sets of curves because we have not investigated the theories of magnetic storms here. The same properties of M-storms have also been found by the author in the analysis of the geomagnetic activity for the period 1920-24 and 1930-34.

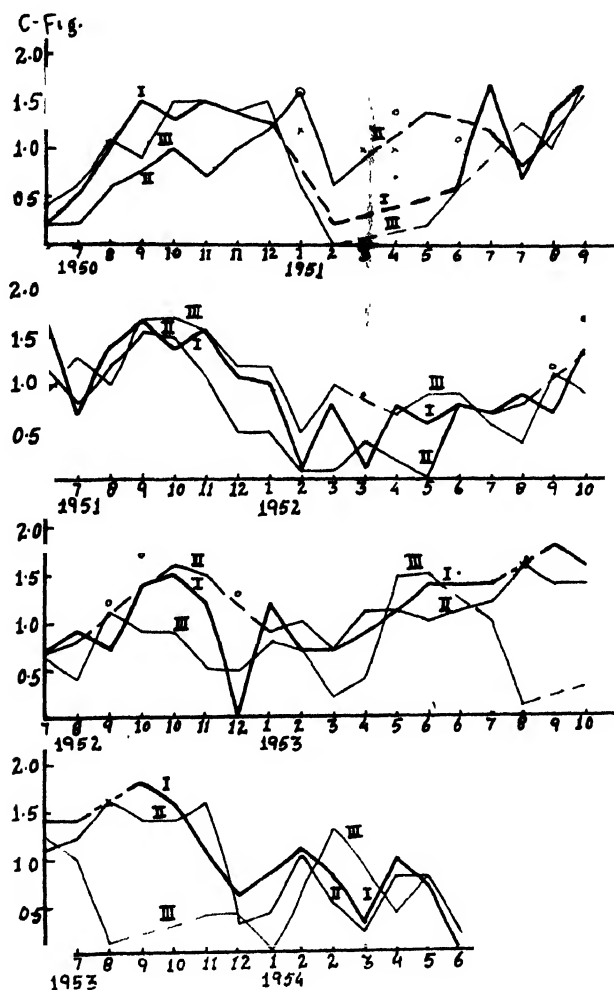


FIG. 1

Curve I—(Thick line)—The mean day activity curve.

Curve II—(Medium thick line)—The one day earlier curve.

Curve III—(Thin line)—The one day later curve.

Cross—Values of C-fig. for the S.S.C type storm for curve I.

Circle—Values of C-fig. for the S.S.C. type storm for curve II.

Dot—Values of C-fig. for the S.S.C. type storm for curve III.

(v) *The maximum activity curve:* This set of curves is plotted by picking the highest value of C-figure around the selected dates with a departure of only

± 1 day from the 27 days periodicity. The annual variation of the sequence is sufficiently marked but not as good as in the case of the mean day activity curves. This set of curves is essentially the same as discussed in Paper I, differing only in minor details which are given below along with the discussion of *A* and *B* sequences.

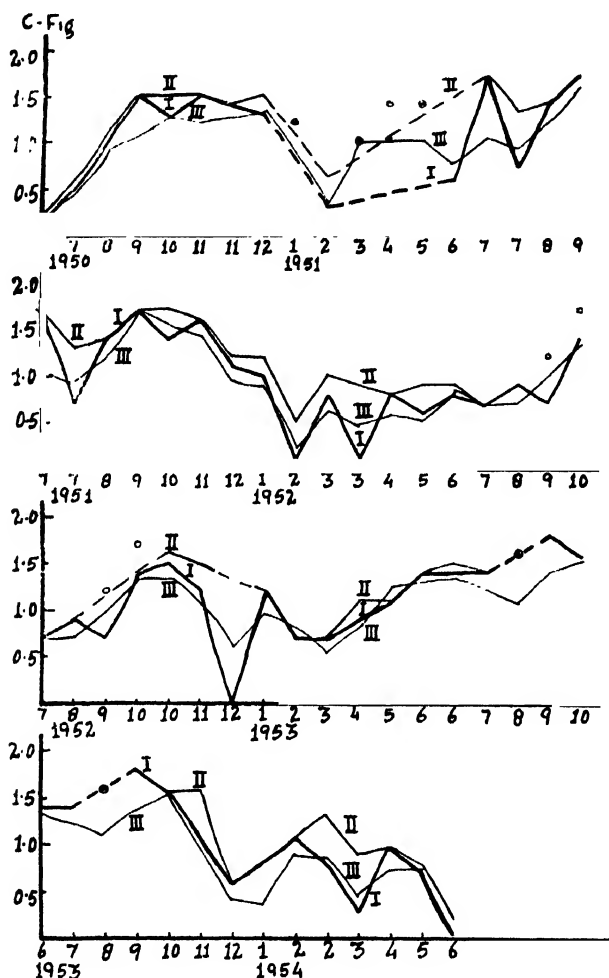


FIG. 2

Curve I (Thick line)—The mean day activity curve.
 Curve II (Medium thick line) —The maximum activity curve.
 Curve III (Thin line)—The mean activity curve.
 Cross—Values of C.fig. for the S.S.C. type storms for curve I.
 Circle—Values of C.fig. for the S.S.C. type storms for curve II.

(b) *Discussion of Sequences*:—The data for the analysis have been taken from the Journal of Geophysical Research. The sudden commencement type of

storms considered here are those marked as S.S.C. type of storms. This analysis of geomagnetic activity for the period Jan. 1950 to June 1954 has led to the four sequences (called A , B , A_1 and B_1) showing annual variations. The A and B sequences are essentially of the same nature as discussed in Paper I, while A_1

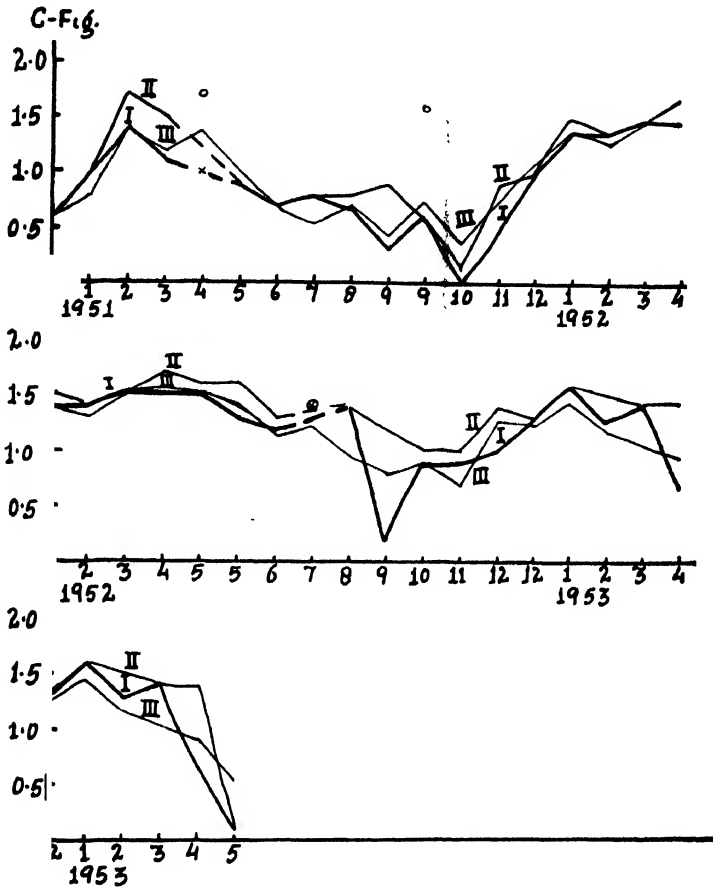


FIG. 3

Curve I (Thick line)—The mean day activity curve.
 Curve II (Medium thick line)—The maximum activity curve.
 Curve III (Thin line)—The mean activity curve.
 Cross—Values of C-fg. for the S.S.C. type storms for curve I.
 Circle—Values of C-fg. for the S.S.C. type storms for curve II.

and B_1 sequences refer to the new sequences which apparently show six-monthly variation and are discussed in detail below. These four sequences are shown in figures 2 to 5 respectively. The days and months in these figures are represented by the numerical numbers from 1 to 12, corresponding to the activity belonging to the months from January to December, respectively. The mean activity

and maximum activity curves are shown superimposed over the mean day activity curves in these figures. The data for these curves are tabulated in Tables II to V. Column 1 gives the dates of the sequences while columns 2 and

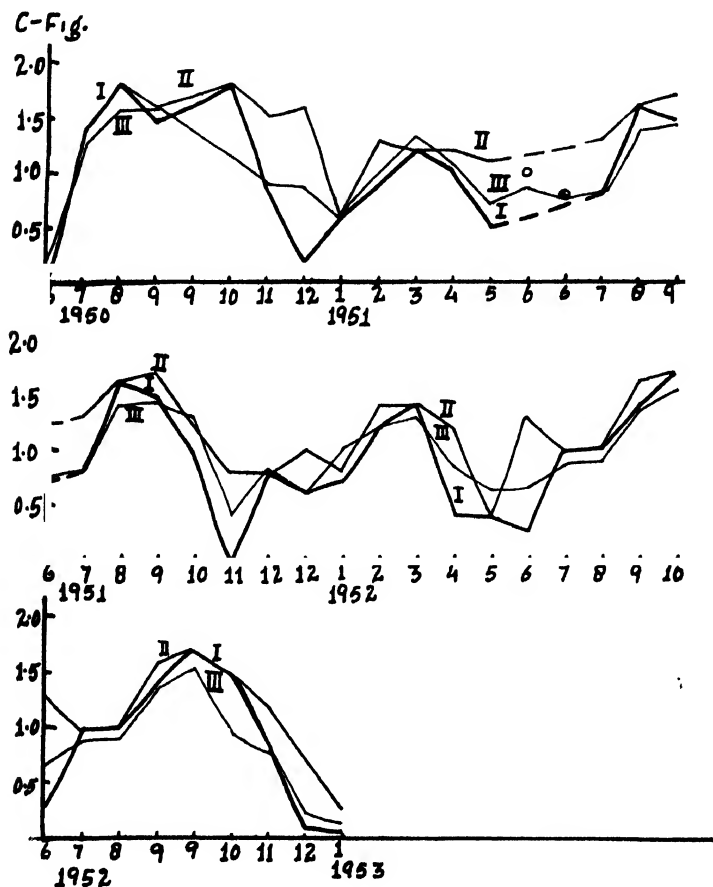


FIG. 4

Curve I (Thick line)—The mean day activity curve.

Curve II (Medium thick line)—The maximum activity curve.

Curve III (Thin line)—The mean activity curve.

Cross—Values of C-fig. for the S.S.C. type storms for curve I.

Circle—Values of C-fig. for the S.S.C type storms for curve II.

4 represent the values of *C*-figures for the mean day activity and maximum activity curves. Column 3 gives the 3-day running means of the *C*-figures for the mean activity curves and in column 5 the interval of recurrence for the maximum activity curves is given. In the last column of Tables II and IV, the dates of *M*-sequences of Bell and Glazer are given for comparison. To summarize these results

we have given the approximate dates of beginning and of the end, the number of rotations and the probable latitude of the *M*-regions in Table I. The longitude

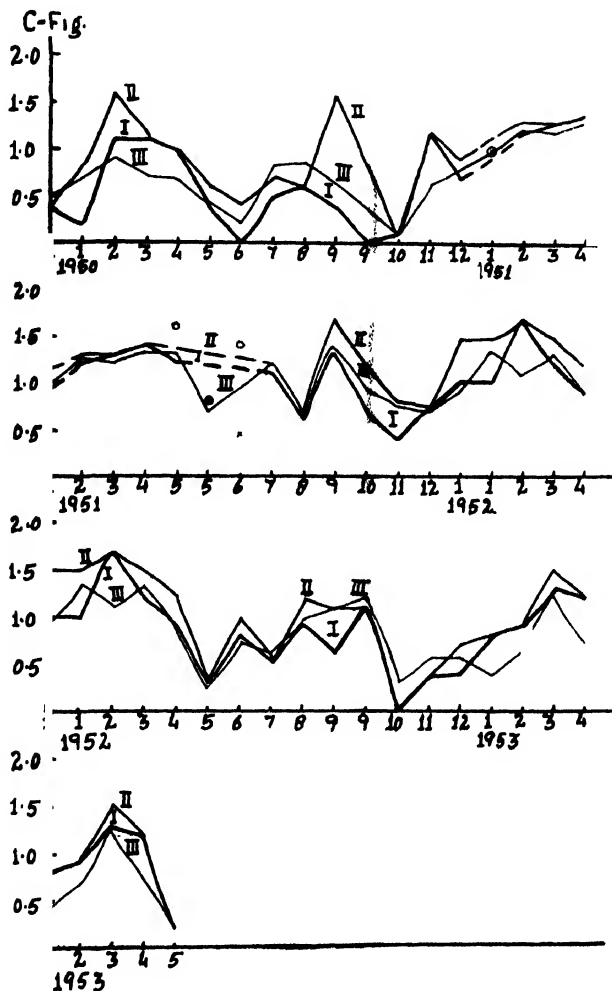


FIG. 5

Curve I (Thick line)—The mean day activity curve.

Curve II (Medium thick line)—The maximum activity curve.

Curve III (Thin line)—The mean activity curve.

Cross —Values of C-fig. for the S.S.C. type storms for curve I.

Circle—Values of C-fig. for the S.S.C. type storms for curve II.

difference of the A_1 ; the *A* and the *B M*-regions (called after the respective sequences) with respect to the B_1 *M*-region are about 27° , 80° and 175° respectively.

TABLE I

	<i>A</i> -sequence	<i>B</i> -sequence	<i>A</i> ₁ -sequence	<i>B</i> ₁ -sequence
The approximate date of beginning	19 Jun. 1950	1 Jan. 1951	15 Jun. 1950	2 Jan. 1950
The approximate date of end	—	14 May 1953	15 Jan. 1953	1 May 1953
Month of max. activity	Sept.	Mar.	Sept.	Mar.
Month of min. activity	Marc.	Sept.	Mar.	Sept.
No. of rotations	54	32	35	45
Periodicity	12 month	12 month	12 month	12 month
Position of <i>M</i> -region(Latitude) above 7°.2.N.	below 7°.2.S.	above 7°.2.N.	below 7°.2.S.	

A and *B* sequences :—The *A* and *B* sequences are supposed to begin respectively from the 19th June 1950 and the 1st Jan. 1951 rather than from the 15th June 1950 and 22nd Nov. 1951 as reported in Paper I, where the authors have departed by ± 3 days from the mean day activity by taking consecutive rotations of 26 or 28 days and hence the beginning part of their *A* sequence belongs to our *A*₁-sequence. In the present analysis we have restricted ourselves to a ± 1 day shift only from the dates chosen for the mean day activity curve. The two sequences last for about 54 and 32 rotations respectively. The *M*-regions (*A* and *B*) responsible for these sequences are found to be separated with a difference of about 95° in longitude and lie above 7°.2 and below 7°.2 in the northern and southern solar hemispheres respectively.

TABLE II

S. No.	Date	C-flg.	Three times the values of the running mean	Max. C-flg.	Interval days	Date for Bell and Glazer sequences.
1	19- 6-50	0.2	0.8			
2	16- 7-50	0.5	1.3	0.6	26	
3	12- 8-50	1.0	2.7	1.1	27	
4	8- 9-50	1.5	3.2	1.5	28	
5	5.10.50	1.3	3.8	1.5	26	
6	1-11-50	1.5	3.7	1.5	27	
7	28-11-50	1.4	3.8	1.4	27	
8	25-12-50	1.3	4.0	1.5	27	
9	21- 1-51	1.2	3.4	1.2	28	
10	17- 2-51	0.3	0.9	0.6	28	
11	16- 3-51	1.0	2.9	1.0	26	
12	12- 4-51	1.0	3.1	1.4	28	
13	9- 5-51	1.4	3.0	1.4	27	
14	5- 6-51	0.6	2.3	1.1	27	

TABLE II (contd.)

S. No.	Date	C-fig	Three times the values of the run- ning mean	Max C-fig	Interval days	Date for Bell and Glazer sequences
15	2- 7-51	1.7	3.1	1.7	26	1- 7-51 ^(c)
16	29- 7-51	0.7	2.8	1.3	26	28- 7-51
17	25- 8-51	1.4	3.6	1.4	28	24- 8-51
18	21- 9-51	1.7	5.0	1.7	27	20- 9-51
19	18-10-51	1.4	4.6	1.7	26	17-10-51
20	14-11-51	1.6	4.3	1.6	27	12-11-51
21	11-12-51	1.1	2.8	1.2	27	8-12-51
22	7- 1-51	1.0	2.7	1.2	27	
23	3- 2-52	0.1	0.7	0.5	27	
24	1- 3-52	0.8	1.9	1.0	27	
25	28- 3-52	0.1	1.4	0.9	27	
26	24- 4-52	0.8	1.7	0.8	28	
27	21- 5-52	0.6	1.5	0.9	26	
28	17- 6-52	0.8	2.5	0.9	27	
29	14- 7-52	0.7	2.0	0.7	28	
30	10- 8-52	0.9	2.1	0.9	27	
31	6- 9-52	0.7	2.0	1.2	28	7-9-52 ^(f)
32	3-10-52	1.4	4.0	1.7	27	3-10-5
33	30-10-52	1.5	4.0	1.6	27	30-10-52
34	26-11-52	1.2	3.2	1.5	27	26-11-52
35	23-12-52	0.0	1.8	1.3	27	24-12-52
36	19- 1-53	1.2	2.9	1.2	26	
37	15- 2-53	0.7	2.4	1.9	28	
38	14- 3-53	0.7	1.6	0.7	27	
39	10- 4-53	0.9	2.4	1.1	27	10-4-53 ^(h)
40	7- 5-53	1.1	3.7	1.1	27	6 5-53
41	3- 6-53	1.4	3.9	1.4	26	2- 5-53
42	30- 6-53	1.4	4.0	1.5	27	29- 6-53
43	27- 7-53	1.4	3.6	1.4	27	26- 7-53
44	23- 8-53	1.6	3.3	1.6	27	23- 8-53
45	19- 9-53	1.8	4.2	1.8	27	19- 9-53
46	16-10-53	1.6	4.6	1.6	27	15-10-53
47	12-11-53	1.	3.	1.6	27	
48	9-12-53	0.6	1.3	.06	27	
49	5- 1-54	0.8	1.2	0.8	27	
50	1- 2-54	1.1	2.7	1.1	27	
51	28- 2-54	0.8	2.6	1.3	26	
52	27- 3-54	0.3	1.4	0.9	26	
53	23- 4-54	1.0	2.2	1.0	29	
54	20- 5-54	0.7	2.3	0.8	27	
55	16- 6-54	0.0	0.4	0.2	26	

TABLE III

S. No.	Date	C.-fig.	Three times the values of run- ning mean	Max. C. fig.	Interval days
1	1- 1-51	0.6	1.8		
2	28- 1-51	1.0	2.4	1.0	27
3	24- 2-51	1.4	4.1	1.7	26
4	23- 3-51	1.1	3.6	1.5	27
5	19- 4-51	1.0	4.1	1.7	27
6	16- 5-51	0.9	2.9	0.9	28
7	12- 6-5	0.7	2.1	0.7	27
8	9- 7-51	0.8	1.7	0.8	27
9	5- 8-5	0.7	3.1	0.8	26
10	1- 9-5	0.3	1.3	0.9	27
11	28- 9-51	0.6	2.3	1.6	27
12	25-10-51	0.0	1.1	0.	27
13	21-11-51	0.5	2.3	0.9	27
14	18-12-51	1.0	3.2	1.0	27
15	14- 1-52	1.4	4.	1.5	27
16	10- 2-52	1.4	3.9	1.4	28
17	8- 3-52	1.5	4.5	1.5	27
18	4- 4-51	1.5	4.6	1.7	26
19	1- 5-52	1.5	4.5	1.6	27
20	28- 5-52	1.3	4.2	1.6	27
21	24- 6-52	1.	3.4	1.3	27
22	21- 7-52	1.4	3.6	1.4	28
23	17- 8-52	1.4	2.8	1.	27
24	13- 9-52	0.2	2.4	1.2	27
25	10-10-52	0.9	2.7	1.0	27
26	6-11-52	0.9	2.1	1.0	27
27	3-12-52	1.0	3.8	1.4	27
28	30-12-52	1.3	3.7	1.3	26
29	26- 1-53	1.6	4.3	1.6	27
30	22- 2-52	1.3	3.5	1.5	28
31	21- 3-53	1.4	3.2	1.4	28
32	17- 4-53	0.7	2.8	1.4	26
33	14- 5-53	0.1	1.6	0.1	28

A₁ and B₁ Sequences :—The *A₁* and *B₁* sequences begin from the 15th June 1950 and the 2nd January, 1950 respectively. The difference in longitude between the two *M*-regions (*A₁* and *B₁*) responsible for these sequences is about 27°. The two *M*-regions are to be situated above 7.2° and below 7.2° in the northern and the southern solar hemisphere respectively.

TABLE IV

S. No.	Date	C-fig.	Three times the values of the run- ning mean	Max. C-fig.	Interval days	Date for Bell and Glazer sequences
1	15- 6-50	0.0	0.6			
2	12- 7-50	1.4	3.8	1.4	27	11- 7-50
3	8- 8-50	1.8	4.7	1.8	27	7- 8-50
4	4- 9-50	1.5	4.7	1.6	28	3- 9-50
5	1-10-50	1.6	4.1	1.7	27	1-10-50
6	28-10-50	1.8	3.5	1.8	26	28-10-50
7	24-11-50	0.9	2.7	1.5	28	25-11-50
8	21-12-50	0.2	2.6	1.6	27	22-12-50
9	17- 1-51	0.5	1.8	0.5	27	
10	13- 2-51	0.9	2.9	1.3	26	
11	12- 3-51	1.2	4.0	1.2	27	
12	8- 4-51	1.0	3.2	1.2	27	
13	5- 5-51	0.5	2.2	1.1	27	
14	1- 6-51	1.0	2.6	1.0	28	
15	28- 6-51	0.8	2.3	0.8	27	
16	25- 7-51	0.8	2.4	1.3	28	
17	21- 8-51	1.6	4.2	1.6	26	
18	17- 9-51	1.5	4.3	1.7	26	
19	14-10-51	1.0	3.9	1.2	27	
20	10-11-51	0.0	1.2	0.8	27	
21	7-12-51	0.8	2.5	0.8	28	
22	3- 1-52	0.6	1.8	1.0	28	
23	30- 1-52	0.7	3.0	0.8	27	
24	26- 2-52	1.2	3.6	1.4	27	
25	24- 3-52	1.4	3.9	1.4	26	
26	20- 4-52	0.4	2.6	1.2	26	
27	17- 5-52	0.4	1.9	0.4	28	
28	13- 6-52	0.3	2.0	1.3	28	
29	10- 7-52	1.0	2.6	1.0	26	
30	6- 8-52	1.0	2.7	1.0	27	
31	2- 9-52	1.4	4.1	1.6	26	
32	29- 9-52	1.7	4.6	1.7	28	
33	26-10-52	1.5	2.9	1.5	27	
34	22-11-52	0.9	2.4	1.2	26	
35	19-12-52	0.1	0.8	0.7	27	
36	15- 1-53	0.1	0.5	0.3	26	

TABLE V

S. No.	Date	C-fig.	Three times the values of the run- ning mean	Max. C-fig.	Interval days
1	2- 1-50	0.4	1.5		
2	29- 1-50	0.2	2.0	0.8	26
3	25- 2-50	1.1	2.7	1.6	27
4	24- 3-50	1.1	2.1	1.1	28
5	20- 4-50	1.0	2.0	1.0	27
6	17- 5-50	0.4	1.2	0.6	26
7	13- 6-50	0.0	0.6	0.4	27
8	16- 7-50	0.5	2.5	0.7	27
9	6- 8-50	0.6	2.6	0.6	28
10	2- 9-50	0.4	2.0	1.6	28
11	29- 9-50	0.0	1.1	0.8	27
12	26-10-50	0.1	0.3	0.1	26
13	22-11-50	1.2	1.9	1.2	27
14	19-12-50	0.7	2.4	0.9	26
15	15- 1-51	1.0	2.8	1.0	28
16	11- 2-51	1.2	3.7	1.3	28
17	10- 3-51	1.3	3.6	1.3	26
18	6- 4-51	1.4	3.9	1.4	27
19	3. 5-51	1.2	3.9	1.6	26
20	30- 5-51	0.8	2.1	0.8	28
21	26- 6-51	0.6	2.8	1.4	26
22	23- 7-51	1.1	3.6	1.2	27
23	19- 8-51	0.6	2.1	0.6	28
24	15- 9-51	1.3	4.1	1.7	28
25	12-10-51	0.7	2.8	1.2	27
26	8-11-51	0.4	2.2	0.8	27
27	5-12-51	0.7	2.1	0.7	26
28	1- 1-52	1.0	2.7	1.5	26
29	28- 1-52	1.0	4.0	1.5	27
30	24- 2-52	1.7	3.3	1.7	28
31	22- 3-52	1.2	4.0	1.5	28
32	18- 4-52	0.9	2.7	1.2	27
33	15- 5-52	0.3	0.8	0.3	26
34	11- 6-52	0.8	2.2	1.0	26
35	8- 7-52	0.5	1.9	0.5	28
36	4- 8-52	0.9	2.9	1.2	26
37	31- 8-52	0.6	3.3	1.1	27
38	27- 9-52	1.1	3.6	1.1	27
39	24-10-52	0.0	0.9	0.0	27
40	20-11-52	0.4	1.7	0.4	38
41	17-12-52	0.4	1.7	0.7	26
42	13- 1-53	0.8	1.2	0.8	26
43	9- 2-53	0.9	1.9	0.9	27
44	6- 3-53	1.3	3.7	1.5	28
45	4- 4-53	1.2	2.2	1.2	26
46	1- 5-53	0.2	0.9	0.2	27

The study of these sequences on the basis of the maximum activity curves shows marked six-monthly periodicity which is not so predominant, if one considers the mean day activity curves. It is quite apparent from the study of the A and B -sequences of the present analysis (see figures 1, 2 and 3) that the main features of the M -sequences are markedly seen on the mean day activity curves. This effect has also been observed by the author, while analysing the samples of data for the two other periods viz. 1920-24 and 1930-34. Further, it is seen that the secondary maxima of the two sequences (A_1 and B_1) are not as much pronounced as the primary ones. From these one can very well judge the reality of the annual variations of these sequences.

Keeping in view the fact that the moderate geomagnetic storms last for about 2 to 4 days, this six-monthly periodicity of A_1 and B_1 sequences can very well be accounted for from the hypothesis of Bhargava and Naqvi (1954, see also Paper I) by assuming that the two M -regions responsible for these sequences are lying in the opposite hemispheres and have a longitude difference of about 27° . The A_1 and the B_1 M -regions were active for about 35 and 45 rotations respectively.

III. SOLAR FEATURES AND M-REGIONS

The annual variation of geomagnetic activity for the period 1930-34 (Naqvi and Tandon) and 1950-54 (Paper I) related to solar M -regions has given some clue to the probable position of these regions. The cause associated with these annual variations viz., the tilt of solar axis of rotation to the ecliptic has already been discussed in detail in Paper I (see also Bhargava and Naqvi 1954). This explanation (axial hypothesis) further receives support from the study of geomagnetic variation associated with regions of weak coronal line emission (Bell and Glazer, 1954).

Several attempts have been made to identify the M -regions on the basis of visible phenomena occurring in the solar corona and on the disc. There are two different views, one relating the source of the M -regions responsible for the moderate geomagnetic storms with the solar ultraviolet radiations and the other relating them with the solar corpuscular radiations. Wulf and Nicholson (1948) and Richardson (1951) considered the first possibility, by relating the M -regions activity with the bright hydrogen and calcium flocculi which emit ultraviolet radiations. It has now been tentatively decided that these M -sequences are due to the effect of the corpuscular radiation coming from some hypothetical M -regions. Allen (1944) and Kiepenheuer (1952) ascribed the M -regions to an increase in the filament area near the central meridian of the sun. The present analysis indicates that the storms related to coronal streamer observed at the eclipse of 25th Feb. 1952 (Von Klüber, 1952) and discussed by Kiepenheuer, do not belong to any of the four sequences considered above.

Maxwell (1952) has discussed the first few rotations of A_1 sequence which also forms a part of the A -sequence of Paper I. He ascribed this M -sequence

to a coronal region overlying a sunspot group with intense radio emission in the metre wave band. The M -region associated with A_1 sequence lie in the northern hemisphere while this sunspot group is situated at a latitude of 18° south.

Waldmeier (1939, 1946, 1950) has found that in some cases, M -regions may be identified with the solar C -regions—those small areas of the corona associated with a brightening of the green coronal line at $\lambda = 5303\text{\AA}$ —and he has also shown that the M -regions and the C -regions have the same statistical properties. Shapely and Roberts (1946) have also associated the C -region with M -regions. Trotter and Roberts (1952) and Muller (1953) have also reached the same conclusions for the current epoch of the sunspot minimum.

On the other hand, Bell and Glazer have reported nine M -sequences (a to i) during the years 1950-53 and associated the M -storms of these sequences with the regions of weak coronal line ($\lambda = 5303\text{\AA}$) intensities located on the same side of the solar equator as the earth. These conclusions were drawn previously by Bruzek (1952) and Smith (1952).

While comparing the M -sequences of Bell and Glazer with our four sequences we find that their M -sequences (c , f and h) forms the part of our A -sequence and one of them (a) belongs to our A_1 sequence (see Tables II and IV). Thus it is clear that the A -sequence is mostly associated with the regions of weak coronal line intensities.

In the recent papers Babcock and Babcock (1955, a , b) have reported the presence of unipolar magnetic (UM) regions over the solar disc and associated one of them* with the M -sequence and with the regions of weak coronal line (5303) intensities (1955b). The M -sequence considered by them forms a part of our A -sequence which is also associated with regions of weak 5303 intensities. It has further been found that there is only one UM-region quite active during the period 1953 and is situated at a latitude of about 15°N . From our analysis it is also clear that there is only one M -region (A) which was active during the year 1953 while the rest (B , A_1 and B_1) M -regions have died early in 1953 and further this M -region should be situated at a latitude above $7^\circ.2\text{N}$. Thus one can very well conclude that the M -regions which are associated with regions of weak 5303 intensities may be identified with the Babcock's UM-regions. To confirm our findings we hope to investigate the behaviour of others M -sequences (B , A_1 and B_1) in regard to their association with UM-regions and with the regions of weak 5303 intensities as soon as the data will be available to us.

The emission of particles from the M -regions is supposed to be associated with spicule activity. Rush and Roberts (1954) suggested a mechanism in which they considered the cone of the particles to be formed due to the magnetic field of the

*The author is grateful to Dr. H. W. Babcock for informing him, in advance of the dates when this, most prominent, UM-regions of 1953 crossed the central meridian.

sunspot groups. Babcock and Babcock are of the opinion that the ejection of the particles from the *M*-regions due to spicule activity is associated with the magnetic field of the UM-regions. The particles will come out more or less radially from these regions, without pronounced collisions, and hence will not be strong radio flux generators. As far as the author is aware there are not much evidences about the *M*-sequences associated with strong radio emission. However, Das and Bhargava (1953) have shown such a possibility by accounting the short duration radio noise of Aug. 24 and Aug. 25, 1953 with the *M*-storms of Naqvi and Bhargava. On the basis of our analysis, we can postulate that this short duration radio noise and also the one observed on Aug. 29, 1953 may not be associated with *M*-region and it needs further investigations before one can really associate *M*-regions with radio flux emission. Hence in our opinion the UM-regions, unassociated with radio noise, may turn out to be identical with the *M*-regions which may further be associated with regions of weak 5303 intensities. Further evidences, in its support have very recently been put forward by Simpson, Babcock and Babcock (1955). They have associated the UM-regions with changes of primary cosmic ray intensities and also with the recurrent geomagnetic storm and have proposed a mechanism to account for such peculiar behaviours of UM-regions. The unpublished results of an independent study of the magnetic maps of solar disc (Magnetogram records of H.W. and H.D. Babcock) by Miss Marion B. Wood of High Altitude Observatory, Colorado, have recently been brought to the notice of the author by Dr. Walter Orr Roberts. They appear to differ from our findings of UM-regions.

In conclusion, we can only say that there is a large probability of identifying *M*-regions with these newly observed UM-regions but the confirmation of these results needs further observational data.

A C K N O W L E D G M E N T S

The author is indebted to Dr. D. S. Kothari, to Dr. Ali M. Naqvi, to Dr. P. K. Sen Gupta and to Dr. Walter Orr Roberts for their continued interest and help in the preparation of this work. He also expresses his thanks to Miss Marion B. Wood for placing her unpublished results at his disposal and to the Ministry of Education, Government of India for the award of senior research scholarship.

R E F E R E N C E S

- Allen, C. W., 1944, *M. N.* **104**, 13.
 Babcock, H. W. and Babcock, H. D. 1955a, *Nat.* **175**, 296; 1955b, *Ap. J.* **121**, 349.
 Bartels, J., 1932, *Terr. Magn.* **37**, 1.
 Bell, B and Glazer, H., 1954. Scientific, Report No. 17, Harvard University, Solar Department of Harvard College Observatory.
 Bhargava, B. N. and Naqvi, A. M., 1954, *Nat.* **173**, 498.
 Bruzek, A., 1952, *Z. Natur f.* **7a**, 708.

- Das, A. K. and Bhargava, B. N., 1953, *Nat.*, **172**, 885.
- Kiepenheuer, K. O., 1952, *J. Geophys. Res.*, **57**, 113.
- Maxwell, A., 1952, *Observatory.*, **72**, 22.
- Muller, R., 1953, *Observatory.*, **73**, 75.
- Naqvi, A. M. and Bhargava, B. N., 1954, *Ind. J. Met. Geophys.*, (Sp. Wo) **5**, 195.
- Naqvi, A. M. and Tandon, J. N., 1955, *Ind. J. Met. Geophys.*, **6**, 251.
- Reichardson, R. S., 1951, *Trans. Amer. Geophys. Union.*, Pt. II, 454.
- Rush, J. H. and Roberts, W. O., 1954, *Trans. I.R.E.*, Vol. C.S. 2 No. 1..**103**.
- Shapley, A.H. and Roberts W.O., 1946, *Ap. J.*, **103**, 257.
- Simpson, J. A., Babcock, H. W. and Babcock, H. O., 1955, *Phys. Rev.*, **98**, 1402.
- Smyth M. J., 1952, *Observatory.*, **72**, 236.
- Trother, D. E. and Roberts, W. O., 1952, *Rep. HAQ. NBS*, 10, High Altitude Obs. Colorado. U.S.
- Waldmeier, M., 1939, *Z. F. Astrophys.*, **19**, 21.; (1946, *Terr. Magn.*, 51, 537.; (1950) *Z. F. Astrophys.* **37**, 42.
- Wulf, O. R. and Nicholson, S. B., 1948, *Pub. Astr. Soc. Pacific.*, **60**, 37.
- Von Klüber, H., 1952, *Observatory.*, **73**, 207.

STUDIES ON THE MAGNETIC SUSCEPTIBILITY OF THE Cr^{+3} ALUMS IN THE RANGE 300°K to 100°K.

S. K. DUTTA ROY

INDIAN ASSOCIATION FOR THE CULTIVATION OF SCIENCE, CALCUTTA.

(Received for publication, January 28, 1956)

ABSTRACT The results of some accurate measurements of the magnetic susceptibility of a series of Cr^{+3} double sulphate, sulphato-selenate and selenate alums in the range 300°K to 100°K have been discussed in the present paper. Analysis of the mean square moments shows the existence of an appreciable contribution from Van Vleck's high frequency paramagnetism and an orbital contribution to the Curie term comparable to the high frequency term, over and above the spin contribution. The Weiss term due to spin separation by the anisotropic crystalline field, is, however, negligibly small in the Cr^{+3} alums in our temperature range. In most of the alums an appreciable temperature dependence of the h.f. and Curie term is observed, stimulating the effect of a Weiss term. This temperature dependence is reversible and may be better represented by two sets of h.f. and Curie coefficients, one for upper and the other for the lower range of temperature, and evidently arises from the thermal expansion of the alum lattice and very probably also from the variation with temperature in the proportion of the two coexisting phases of the α , β and γ alums or the thermal conversion from one phase to another, and the consequent changes in the crystalline electric field acting on the Cr^{+3} ion.

Taking the spin orbit coupling to be not very different from the free ion value of $+87 \text{ cm}^{-1}$, optical absorption and paramagnetic resonance results have been compared with the magnetic susceptibility data and an estimate of the covalency factor and cubic separation of the orbital levels made.

INTRODUCTION

The magnetic behaviours of chromium alums are apparently very simple. The single crystals of the alums being of the cubic class show no magnetic anisotropy. The mean susceptibility of the Cr^{+3} alums has been found to obey very closely a Curie law of temperature variation (de Haas and Gorter, 1930; Serres, 1932), with a value of the magnetic moment very nearly equal to the "spin only" value, which has made the alums eminently suitable for the production of extremely low temperatures by the method of adiabatic demagnetisation (de Klerk, Steen-land and Gorter, 1949). But a limit is set to the low temperature obtained, by a small twofold splitting of the spin levels of the Cr^{+3} ion, evidently caused by a small departure from cubic symmetry of the crystalline electric fields in the alums. This also should cause a slight departure of the susceptibility from the Curie law, and a small anisotropy of the Cr^{+3} ion.

The Cr^{+3} alums have been recently the subject of extensive investigations by the paramagnetic resonance method (Bleaney *et al*, 1951), which directly gives the value of the spin splittings of the individual Cr^{+3} ion. But the optical absorption spectra do not show any level corresponding to the splitting of the orbital levels by the anisotropic field. Also several anomalies and uncertainties have been observed at low temperatures in the paramagnetic resonance observation, the causes of which are not very clear. The structural data also indicate that in some of the alums at least the Cr^{+3} ions are under the influence of a non-cubic crystalline electric field due to the surrounding charges and dipoles.

We have therefore undertaken an extensive series of accurate measurements of the susceptibility of a large number of Cr^{+3} alums, between the range 300°K to 100°K , expecting to throw more light upon these problems, the results of which are discussed in the present paper.

DETAILS OF THE EXPERIMENTAL METHOD

(a) *Preparation of the sample:*

The chromium alums have the general formula, $\text{Cr A}(\text{XY}_4)_2, 12\text{H}_2\text{O}$, where $\text{A} = \text{K}, \text{NH}_4, \text{Rb}, \text{Tl}, \text{Cs}, \text{NH}_2\text{OH}$ etc. and $(\text{XY}_4)_2 = (\text{SO}_4)_2, (\text{SeO}_4)_2$ or $(\text{SO}_4)(\text{SeO}_4)$. They crystallize commonly in the form of deep violet octahedra and are in many cases easily obtainable as large single crystals by the slow evaporation of a nearly saturated aqueous solution of the component salts in equimolecular proportion. For example, in the case of sulphates and sulphato-selenates the corresponding component salts (of analytical quality of Kahlbaum, Merck or Malinckrodt) are dissolved in double distilled water, crystallized several times to purify them and finally crystallized in a quiet dust free and vibration-proof chamber by moderately slow evaporation of the nearly saturated solution, kept in flat-bottom crystallizing dishes. The temperature of the chamber is not allowed to fluctuate much during crystallization, by suitable lagging of the chamber. In several cases the component salts were prepared by ourselves using analytical quality of the hydroxides or carbonates of the metals and the desired acids. The analytical purity of the final materials were always carefully checked. It was found in some cases that while exposed to air for free evaporation for sometime, particularly if the room temperature remained above about 30°C , as happens during the hot weather, the aqueous solution turned green, no doubt due to formation of complexes by the Cr^{+3} ion, with the anions. Even then, in some cases the crystals came out as violet octahedra as usual. But in such cases there is some likelihood of contamination of the alum by the green complex. We have therefore taken precaution not to use crystals out of such crops. We have prevented such occurrences in future by putting the dishes of the solutions to be crystallized in a vacuum desiccator with a suitable desiccant and the whole thing within a double walled ice-box, in which the temperature

may be maintained at 20°C by putting in it a suitable amount of ice, replenishing it as necessary.

The tendency for the green complex formation in the alums is so marked in the sodium sulphate alum, that the solution even from the moment of preparation was dark green and in spite of many trials became treacly on evaporation and never crystallized, but dried up into a green conglomerate mass. The same tendency is also very marked in the selenate alums in general and we could prepare only two of them (NH_4 and Rb alums) adopting a somewhat different technique. About 4.000 grams of $\text{Cr}(\text{NO}_3)_3$ and 3.582 grms of $(\text{NH}_4)_2\text{SeO}_4$ (or Rb_2SeO_4 as the case may be) are separately dissolved in ice cold double distilled water and the two solutions are mixed together keeping the mixture always below 5°C using an ice bath and with constant stirring. Precooled acetic acid is added drop by drop and the alum is precipitated as fine shower of violet microcrystals. The precipitate is washed with acetone to free it from acetic acid and is again dissolved in double distilled water and reprecipitated with acetone, all the processes being carried out at low temperature. The purified precipitate is again dissolved in ice cold water and left for crystallization in the ice-box controlling its temperature below 5°C , with large blocks of ice. Large violet octahedral crystals thus obtained are once again crystallized in the same manner for use in magnetic measurements.

The best of the crystals free from distortion and of as nearly possible symmetric shape were chosen from each crop, firstly with a magnifying glass and then under a polarising microscope, stored in a dry clean test tube (stopper of which is sealed with wax) and indexed. But in several cases where the crystals have a tendency to dehydrate, melt or decompose quickly, the sample on removal from the mother liquor and cleaning, is coated with an extremely thin layer of collodion or durofix by momentarily dipping it in a dilute solution of these substances and immediately used for magnetic measurements.

(b) *Method of Magnetic Measurements*

As we have already mentioned alums being of the cubic class, the magnetic measurement consists only in finding the mean susceptibility of the crystals at different temperatures. For this reason our information about the magnetic behaviour of Cr^{+3} ion derived from such measurements are necessarily more limited, than could be obtained from those on crystals of lower than cubic symmetry, e.g the hydrated salts of Cu^{+2} and Ni^{+2} ions (Bose, Mitra and Datta, in course of publication). It has been pointed out however, that the effect of the anisotropic crystalline electric field may vary from alum to alum and thus manifest itself even in the mean susceptibility (Bose and Mitra, 1952), when refined techniques of measurement are adopted for a large number of these salts. The mean susceptibility might have been obtained by using the powdered crystals in glass ampoules, but apart from the tediousness of the process of packing of the powder in the

ampules, errors are likely to arise due to uncertainty in the density of packing. A further drawback is that while finely powdering and packing, most of the crystals, which are highly hydrated, are found to loose some water or decompose. So we have preferred to use single crystals of suitable size. They are also chosen to be of very regular shape to avoid errors due to demagnetizing coefficient. A trial with different shapes of crystals not very much departing from an octahedron or cube, was carried out in this laboratory to observe this effect which was found to be not more than 1 part in 1000 even at 100°K (Datta, 1954). Since the crystals of the alums are isotropic, it is not necessary to set them in the field in any preferred direction of orientation.

A refined Curie balance and a liquid air cryostat are used for the measurements, firstly to find out accurately the values of the absolute susceptibility of the crystals at room temperature (300°K) by comparison with a chrome potassium alum crystal standardised against a standard NiCl_2 solution. Magnetic forces on the sample, mounted at the end of the horizontal balance arm, placed in a vertical magnetic field with a horizontal gradient, is balanced accurately by twisting the vertical quartz fibre from which the balance beam is suspended. The forces at the other constant temperatures down to 100°K, are then compared with that at room temperature, retaining all other conditions e.g. suspension, magnetic field etc, the same as at room temperature. The details of the balance and the cryostat, the method of measurement and avoiding or correcting the various errors, are fully discussed in an earlier paper by the author (1955) and need not be repeated here. Some remarks, however, should be made here about the probable limits of error in the present measurements and the final treatment of the results of observation for the purpose of discussion.

As is indicated in our earlier paper the overall error in the susceptibility measurement at room temperature is about 0.2 % including the uncertainty of temperature measurement and slight differences in the value for different crystals, to reduce which the mean value for 3 or 4 such crystals is taken. With the fall of temperature the susceptibility increases and the accuracy of measurement increases. The values at low temperatures relative to that at room temperature have even greater accuracy, of about 0.1 %, since all other conditions of the experiment remain practically the same, though this is somewhat offset by the slightly increased inaccuracy in temperature measurement. There is a chance that during a series of measurements a crystal might undergo some permanent change physically or chemically. To detect this effect, two series of measurements with the same crystal *in situ* were carried out, one going from room temperature down to the lowest and the other back again. In case of any irreversible changes occurring, two such susceptibility curves would be more or less different. We could not observe any such appreciable difference, (except in the case of ammonium selenate alum), which shows that in our conditions of measurements most of these alums are more or less stable, particularly when most of the time

they are kept below room temperature. As we have noted, several of the crystals slowly tend to dehydrate or decompose at or above about 300°K , to avoid which we had to start low temperature measurement very soon after preparation. Again in one or two cases in e.g., K and NH_4 sulphate alums, we had observed slow surface dehydration occurring on prolonged exposure to the dry air of the experimental chamber at liquid air temperature. In the NH_4 selenate alum similarly a slight melting of the crystal was observed after the run back to the room temperature was completed. A coating of collodion or durofix helped to check these. Our entire series of measurements at low temperature were finished before appreciable change in susceptibility curve could occur. A large number of readings, at the interval of 15° to 20°K or even closer, where thought necessary from a preliminary run, are taken to follow the susceptibility curve very closely, to see whether it contained any changes in slope or any other singularity which may be reversible with temperature. This was found to occur in most of the crystals.

From the temperature variation measurement of the angle of torsion, say α , of the quartz fibre required to balance the sample against the magnetic force, a graph of $\alpha \cdot T$ against absolute temperature T is prepared, which is a line with a small slope against T axis and a small curvature. From this curve intrapolated values of α 's may be obtained at 300°K and at other temperatures at 20°K interval down to 100°K . Knowing the susceptibility at 300°K , the values at other temperatures may be calculated from the formula,

$$\frac{F_T}{F_\theta} = \frac{\chi_T}{\chi_\theta} \left[1 + \frac{k_{a\theta}}{k_\theta} (1 - \gamma\theta) \left(1 - \frac{\theta}{T} \right) \right] \quad \dots (1)$$

where χ_T and χ_θ are the gram-molecular susceptibilities of the crystal at temperature T and 300°K respectively, and F_T and F_θ are the forces acting on the crystal at these temperatures, $k_{a\theta}$ and k_θ are the volume susceptibilities of air and that of the crystal at 300°K , and γ the coefficient of thermal volume expansion of the crystal.

The above method of graphical intrapolation is very sensitive to experimental scatter and we have found that all our points for a given crystal lie on a smooth curve within the limit of our accuracy of about 0.2%. This method of treating the results is also better for our ultimate discussion of the results in terms of the squares of the mean effective moments which are very nearly proportional to $\alpha \cdot T$'s. From the values of the mean gm. molecular susceptibility χ_M (after correcting for diamagnetism of the molecule) thus obtained at different temperatures, the square of the mean effective magnetic moment p_f^2 in Bohr magnetons is calculated from the formula.

$$p_f^2 = \frac{3k\chi_M T}{N\beta^2} = 7.995\chi_M T^*, \quad \dots (2)$$

in which the other symbols have the usual meanings.

*The latest values of physical constants $k = 1.38032 \times 10^{-16}$ ergs. deg $^{-1}$, $N = 6.0243 \times 10^{23}$, $\beta = .92731 \times 10^{-20}$ erg. gauss $^{-1}$ (Dumond and Cohen, 1948) are used.

TABLE IX

$\text{Cr}_2(\text{SO}_4)_3, \text{Rb}_2(\text{SeO}_4)_2, 24 \text{ H}_2\text{O}$			
Temp°K	$\chi_M \times 10^6$	pf^2	
		Obs.	Calc.
300	6125	14.65	14.69
280	6541	14.65	14.65
260	7028	14.61	14.62
240	7598	14.58	14.58
220	8276	14.57	14.57
200	9098	14.55	14.55
180	10120	14.56	14.56
160	11395	14.56	14.56
140	13010	14.55	14.56
120	15175	14.55	14.56
100	18220	14.56	14.56

TABLE X

$\text{Cr}_2(\text{SO}_4)_3, \text{Cs}_2(\text{SeO}_4)_2, 24 \text{ H}_2\text{O}$			
Temp°K	$\chi_M \times 10^6$	pf^2	
		Obs.	Calc.
300	6116	14.67	14.67
280	6546	14.65	14.65
260	7037	14.62	14.62
240	7611	14.61	14.59
220	8287	14.58	14.57
200	9104	14.55	14.55
180	10093	14.52	14.52
160	11380	14.55	14.57
140	13080	14.63	14.63
120	15250	14.63	14.61
100	18240	14.59	14.59

TABLE XI

$\text{Cr}_2(\text{SeO}_4)_3, (\text{NH}_4)_2, (\text{SeO}_4)_2, 24 \text{ H}_2\text{O}$			
Temp°K	$\chi_M \times 10^6$	pf^2	
		Obs.	Calc.
300	6050	14.51	14.51
280	647	14.51	14.51
260	6981	14.51	14.51
240	7563	14.51	14.51
220	8255	14.51	14.50
200	9070	14.50	14.50
180	10075	14.50	14.50
160	11369	14.55	14.55
140	13000	14.55	14.55
120	15166	14.55	14.55
110	16555	14.55	14.55
104	17060	14.46	—
100	18064	14.45	—

TABLE XII

$\text{Cr}_2(\text{SeO}_4)_3, \text{Rb}_2 \text{ SeO}_4, 24 \text{ H}_2\text{O}$			
Temp°K	$\chi_M \times 10^6$	pf^2	
		Obs.	Calc.
300	6141	14.72	14.72
280	6570	14.71	14.71
260	7060	14.70	14.70
240	7650	14.68	14.68
220	8339	14.67	14.67
200	9160	14.66	14.66
180	10180	14.64	14.65
160	11440	14.63	14.63
140	13060	14.62	14.62
120	15220	14.60	14.60
100	18260	14.60	14.60

DISCUSSION OF THE RESULTS

(1) Variation of the p_f^2 from salt to salt and with temperature.

It will be seen immediately from the values given in tables, that p_f^2 is in general appreciably different from the 'spin only' value of 15 Bohr magnetons for Cr^{+3} ion and is also different from salt to salt. The values of p_f^2 for NH_4 and Tl sulphate and NH_4 selenate alums are seen to be appreciably smaller than the others. It will be seen further that p_f^2 values do not obey the Curie law very well i.e. are not constant with temperature but go on changing appreciably and in a manner characteristic of the given salt. However, certain general features may be observed. In Rb and Cs sulphate and Rb selenate alums, the values of p_f^2 go on falling more or less systematically with temperature; the values become practically constant below about 140°K. For Rb sulphato-selenate salt there is a small decrease down to about 200°K and then it is very nearly constant. For K sulphate and NH_4 sulphato-selenate the initially falling curves rise up rather quickly between about 200°K-160°K, and 220°K-180°K respectively, and then start falling again. In NH_4 and Tl sulphate and K and Cs sulphato-selenate, the value decreases down to about 220-180°K and then rises more or less slowly except for the last salt which shows a fall again below 140°K. In (NH_2OH) sulphate, the value, being nearly constant down to about 200°K, rises down to 140°K and then starts falling. In NH_4 selenate alum p_f^2 remains practically constant down to 180°K, rises fairly suddenly between this temperatures and 160°K, remains about steady and then sharply falls down below 106°K. Thus it will be seen that in several of the alums a distinct change in the slope of the curve occurs somewhere about the middle of our temperature range, extending over about 20-40 degrees, perhaps even more. *Actually, a similar change in the slope was indicated in the Leiden data of de-Haas and Gorter (1930; see also Dutta Roy, 1955) for K sulphate alum e.g. 14.92 at 290°K, 14.88 at 143.6°K and 14.91 at 77.7°K. However they did not put any significance to this departure from linearity in their curves and smoothed the susceptibility data to accord to the formula,

$$p_f^2 = 14.92 + \frac{1.32}{T} \quad (3a)$$

On a rigorous analysis of their data it has been found that between 290°K and and 14°K these obey the following formula, much better.

$$p_f^2 = -.0002693T + 14.91 + \frac{1.867}{T} \quad \dots (3b)$$

It has been already mentioned that the change in the curvature of the p_f^2-T , curves are generally exactly reversible and reproducible with falling and rising

*In our earlier paper (Dutta Roy, 1955) all the p_f^2 should be reduced by a factor 7.995/8.061 owing to correction for the latest value of physical constant.

temperature, so that they can not be attributed to possible changes in the structures due to decomposition or dehydration as referred to earlier, except in the case of NH_4 selenate alum below 110°K .

To compare our results with the existing theories and to explain the various peculiarities observed, it would be better to try to analyse the data with an empirical three-constant formula of the form,

$$p_f^2 = AT + B + \frac{C}{T} \quad \dots (3c)$$

in which the terms are evidently those corresponding to temperature independent, Curie and Weiss terms respectively, in susceptibility. The constants A , B , C , are determined from the experimental data by the method of least squares. It was, however, found that though in several alums such a formula would fit reasonably well with experimental values at both the higher and lower sides of the temperature range, it gave a wide systematic deviation in all the others beyond experimental errors, from the experimental values in the medium temperature range, where singularities are usually observed in the experimental curves. These deviations are such that the addition of T^2 and $1/T^2$ terms though improving the fit with experimental values would unduly complicate the situation. On the other hand, it was found that the observed values on *either side* of the singularity might be made to fit very well with a simple formula of the type $p_f^2 = AT + B$, with different values of the constants (A_1, B_1) , (A_2, B_2) . The values of p_f^2 calculated back from these two sets of constants are given in Tables (I—XII) side by side with the experimental values for comparison. The horizontal lines in the last column indicate the range of applicability of each formula. One or two values in the intermediate range not fitting with either formula individually, give, however, a fairly good fit with a formula with mean A and B values. All this evidently means that in this region the A and B values are changing more or less continuously (of course reversibly) from one set of values to another as the temperature changes. The values of A and B for upper and lower ranges of temperature for the individual salts are given in Table XIII.

It will be seen from this table that A_1 values are small in all cases, their contributions to p_f^2 being not more than about 4 % of the total at room temperature, falling to less than 2 % near the middle of the range. On passing through this region, as A_1 changes to A_2 , the contribution of this term at the beginning of the lower range rises again to about 4 % and then decreases again by about the same amount at the bottom of the range in the cases where A_2 is found to be positive. It is obvious, however, that these values may not be correct to more than about 10 to 25 % ; particularly in the cases where calculations are made from the variations of p_f^2 , small and confined to only a few temperatures. B -values are correct to about 0.2 % and contribute the bulk of the moment, about 96 %. The significance of A and the leading term B and its variations in the different temperature

ranges and from salt to salt will be discussed more fully in a later section with reference to the structure of the alum and the crystalline field theory.

(b) *Structure of the alums.*

All the alums belong to the cubic class of crystals with four molecules in the unit cell. From the analysis of the structures of the alums (Beever and Lipson, 1935; Lipson, 1935; Klug 1940), it appears that the alums are not strictly isomorphous, and may be divided into three classes α , β , and γ , with reference to the size of the monovalent cation and the differences in the symmetry and orientations of the different groups of atoms, in the unit cell. In all the alums the trivalent cation is immediately surrounded by an octahedron of water molecules. In the α -class the water octahedron is found to be slightly distorted along its trigonal axis which lies along a body diagonal of the unit cell, and the octahedron axis makes a small angle with the (unit cell) cube axis. In the β -class the octahedron is found to be perfectly regular (at least in the Al^{+3} alums), its axes coinciding with the cube axis. About the γ -class, of which the only representative is sodium sulphate alum, no information is available regarding orientations. Though the Al^{+3} alums containing K, NH_4 , Rb and Tl belong to α -class, and those containing Cs and NH_3CH_3 to the β -class (Beever and Lipson, 1935; Klug, 1940), on changing over to Cr^{+3} alums both those containing Rb and Tl (almost of similar ionic radius) go over to the β -class. Rb seems to grow in both α and β classes and therefore is a link between the two. All these refer to SO_4 alums at room temperature.

(c) *Crystalline electric fields in the Cr^{+3} alums.*

Siegert (1936), Van-Vleck (1939), and Broer (1942) have postulated the existence of a predominantly cubic field, with a small superimposed trigonal field in all the alums. Though the X-ray structure of the β -alums seems to indicate a regular octahedron of water molecules about the Cr^{+3} ion, the adiabatic demagnetisation, paramagnetic absorption and resonance experiments all indicate a small separation of the spin levels and Van-Vleck (1939) has shown that a separation of this order arises with a distortion of the water octahedron by as little as $\sim 10^{-10}$ cm, which is below the margin of errors in X-ray measurements. Under the influence of the cubic field with a positive sign, as exists about the octahedrally coordinated Cr^{+3} ion in the alums (Gorter, 1932), the ground $3d^3\ ^4F_{3/2}$ -state of the Cr^{+3} ion splits up into an orbital singlet and two orbital triplets above it separated from one another to the order of 10^4 cm^{-1} . Each triplet under the influence of the uniaxial field and spin orbit coupling breaks up into two sublevels separated to $\sim 10^{+2}\text{ cm}^{-1}$ and 10^{+3} cm^{-1} . Of the four-fold spin degeneracy, only two-fold is removed to $\sim 10^{-2}\text{ cm}^{-1}$ by the asymmetric field and the spin-orbit coupling λ , the other two-fold being of the Kramers' type remains unaffected by the crystalline field, unless magnetic, exchange or other types of interaction intervene.

The principal susceptibilities of the Cr^{+3} are given by Schlapp and Penney (1932); Abragam and Pryce (1951), Griffith and Owen (1952) as:

$$K_i = \frac{15N\beta^2}{12kT} g_i^2 \left\{ 1 - \frac{12}{5} \cdot \frac{X_i}{3kT} \right\} - 15N\beta^2 \alpha_i \quad \dots (4)$$

in which the splitting factor $g_i = 2\gamma(1 + 4\lambda\alpha_i)$, α_i is a crystalline field constant used by Schlapp and Penney, i denotes either \parallel (parallel) or \perp (perpendicular) to the trigonal axis, $\gamma = 1.00115$ (Owen, 1955) the anomaly factor of the magnetic moment of electron (Kusch *et al.*, 1952).

$$X_{\parallel} = 4\lambda^2(\alpha_{\parallel} - \alpha_{\perp}), \quad X_{\perp} = -2\lambda^2(\delta(\alpha_{\parallel} - \alpha_{\perp}))$$

Then the square of the mean effective moment for the Cr^{+3} ion is obtained as:

$$\begin{aligned} p_f^2 &= \frac{3kT}{N\beta^2} \left(\frac{K_{\parallel}}{3} + \frac{2K_{\perp}}{3} \right), \\ &= 15 \left(\frac{g^2}{4\gamma^2} - 3kT\alpha - \frac{128}{15} \frac{\lambda^3}{kT} \left\{ (\alpha_{\parallel} - \alpha_{\perp})^2 \right\} \right) \end{aligned} \quad (5)$$

(neglecting the terms of the order of $\lambda^4\alpha^3$), in which

$$\alpha = \frac{1}{3}(\alpha_{\parallel} + 2\alpha_{\perp}), \text{ and} \quad \dots (6)$$

$$g^2 = \frac{1}{3} (g_{\parallel}^2 + 2g_{\perp}^2) = 4\gamma^2(1 + 4\lambda\alpha) \quad \dots (7)$$

The first term in equation (5) is the Curie terms containing the contributions from the spin moment and from the orbital moment due to admixture of the upper orbital levels with the lowest, through spin-orbit coupling, the second term is the high frequency term of Van Vleck (1932) and the third arises from interaction of the spin levels with the orbital.

Equation (5) is equivalent to an experimental three-constant formula (3c) if we take:

$$A = -45k\alpha \quad \dots (8)$$

$$B = +\frac{15}{4\gamma^2} g^2 \quad \dots (9)$$

$$C = -128 \frac{\lambda^3}{k} (\alpha_{\parallel} - \alpha_{\perp})^2 \quad \dots (10)$$

and the values of the three unknown quantities λ , α and $\alpha_{\parallel} - \alpha_{\perp}$ in the theoretical equation may be found out approximately from the above three equations, from the experimental values of A , B and C , if the results can be so represented.

We may try to ascertain whether the last term in equation (4) is sufficiently important to contribute any experimentally appreciable C term. The values of λ for the free Cr^{+3} ion is $+87 \text{ cm}^{-1}$ (Laporte, 1928) and this is probably not appreciably different from that in the solid state as will be discussed later. The value of $\alpha_{||} - \alpha_{\perp}$ could have been accurately known if an anisotropic class of Cr^{+3} salts similarly constituted as the alums could be measured. This being not the case we have used the value of $\alpha_{||} - \alpha_{\perp}$, obtained from the recent very accurate anisotropy measurements on $\text{NiSO}_4 \cdot 6\text{H}_2\text{O}$ by Datta (1954), which should not be very different from that for Cr^{+3} alums, in view of the similarity in the Stark pattern for Ni^{+2} and Cr^{+3} ions. The value of $\alpha_{||} - \alpha_{\perp}$ for Ni^{+2} ion, is obtained from,

$$K_{\perp} - K_{||} = \frac{8N\beta^2}{3kT} \left(8\lambda - 3kT - \frac{2\lambda^2}{kT} \right) (\alpha_{\perp} - \alpha_{||}) \quad (11)$$

to a fairly good degree of approximation (Schlapp and Penney, 1932), in which $\lambda = -335 \text{ cm}^{-1}$ (Laporte, 1928), $K_{\perp} - K_{||} = 348 \times 10^{-6} \text{ c.g.s.e.m.u.}$ at 300°K (Datta, 1954), so that, $\alpha_{||} - \alpha_{\perp} \approx +24.0 \times 10^{-6}$

Since in equation (9) the last term, $(\alpha_{||} - \alpha_{\perp})^2$ is involved, the sign of $\alpha_{||} - \alpha_{\perp}$ will not matter though this is evidently $-ve$ in Cr^{+3} alums (Van Vleck, 1939). The magnitude may also be somewhat different but since the term is small, a rough estimate will be enough for our purpose. We then find for Cr^{+3} , the value of this term to be 2.3×10^{-4} at 300°K and 7.0×10^{-4} at 100°K , which is much smaller than the magnitude of errors in our experimental values. The Curie temperature corresponding to this term in equation (5) is $\sim 0.005^\circ\text{K}$ which is of about the same order of magnitude as $.004^\circ\text{K}$ (Leiden, 1949) and $.011^\circ\text{K}$ (Oxford, 1954) for Cr^{+3} alum found by adiabatic demagnetisation. It is interesting to note that if this term has been appreciable compared to other terms in equation (5) in the alums, we could have calculated $\alpha_{||} - \alpha_{\perp}$ the anisotropic field constant from equation (10), referring to even the mean square moments. Since we are justified in neglecting this term in equation (5) in our temperature range, arising from the theory in case of Cr^{+3} alums, if from susceptibility measurements a C term be still found to exist in the experimental results it must then be ascribed mainly to variations in g and α in equation (5) with temperature caused by thermal expansion of the alum lattice. This thermal expansion of the lattice directly affects very little the octahedron of water molecules immediately surrounding and firmly bound to the Cr^{+3} ion, but may considerably change the positions of the atoms outside the octahedron and thus indirectly affect the field due to the octahedron appreciably (Van Vleck, 1939; Bose, Mitra and Datta unpublished; Bose and Mitra, 1951). Indeed, as has been earlier noted, in the present case the thermal variations of g and α are of such a nature that instead of using a C/T term, the experimental data have to be represented in two-constant

form with different values (A_1, B_1), (A_2, B_2) above and below the singularity region found to occur more or less continuously between 220°K and 160°K in most cases. In three cases one single two-constant formula is found to hold good over the entire range showing that the thermal variation of g and α is negligible.

Using the experimental values of B_1 and B_2 it is possible to calculate g' and g'' , the values of the mean splitting factor g in the two temperature ranges, with a high degree of accuracy from equation (9). The high frequency term A has been predicted by Van Vleck (1932) to arise from the non-diagonal matrix elements of the magnetic moment corresponding to transitions to the upper levels, but was neglected in the treatment of Schlapp and Penney (1932), for Cr^{+3} ion to suit the earlier results of de Hass and Gorter. But we find that in many cases this term is quite appreciable, and has a positive sign. This is to be expected since in equation (8) α should have a negative sign for octahedrally coordinated Cr^{+3} ion (Van Vleck 1932, Gorter, 1932) and its magnitude is not very far from that of $\text{NiSO}_4 \cdot 6\text{H}_2\text{O}$ (Mookherji, 1946) namely -8×10^{-5} cm. It will be seen that in several cases the h.f. term tends to become practically zero or even negative, especially on passing to the low temperature region. Though in such cases a part of this anomaly may be due to the large errors in estimating this term and also, to a small extent the diamagnetic corrections, the major part of this must be ascribed to other reasons to be explained in the later sections.

(d) *The splitting factor g in Cr^{+3} alums.*

It will be seen that in all the chrome alums the values of g are always less than $2\gamma (=2.0023)$ in both the high and low temperature ranges. This is always as it should be since in the formula $g = 2.0023 (1 + 4\lambda\alpha)$, λ is positive and α is negative. It is to be remarked that in all the cases, except NH_2OH alum, g has appreciably higher value in the low temperature range, and in two cases, e.g. Tl sulphate and K sulphato-selenate, it approaches to within about 0.7 % of the spin only value. It should be seen that in these last two cases the high frequency term has a negative value in the low temperature range which according to (8) should have been positive. This negative value then indicates that g value is probably still varying with temperature in this range in such a direction as to mask the +ve value of the high frequency term and which hence may not be the true values independent of temperature. Indeed, one should regard with caution the absolute values of g and also of the h.f. term in such cases. The anomalous change of g in the NH_2OH alum, i.e. a decrease in the low temperature region, is also presumably to be ascribed to a similar reason, since the high frequency term in the high temperature range is found to be abnormally low and that in the low temperature range is also not very accurately determined. The negative and unusually small positive values of the high frequency term in several cases e.g. NH_4 sulphate, Rb sulphato-selenate in the low temperature range and NH_4 selenate also no doubt suffer from similar masking of the term. The general increase of g in all other cases on passing

from high to low temperature range, is indicative of the fact that α decreases more or less quickly from α' to α'' while passing through the intermediate temperature range indicated earlier; since it is not probable that λ can decrease with temperature.

TABLE XIII
Double sulphate series

	K	NH ₄	Rb	Cs	Tl	NH ₂ OH
$A_1 \times 10^4$	18.5	5.0	10.2	8.0	10.0	0.0
B_1	14.36	14.29	14.49	14.40	14.22	14.68
g'	1.960	1.954	1.968	1.962	1.952	1.980
$-\alpha' \times 10^5$	6.03	6.8	4.90	5.70	7.1	3.45
in cms.	(6.0)	(2.0)	(3.3)	(2.7)	(3.2)	(0.0)
$A_2 \times 10^4$	12.5	-5.0	10.2	8.0	-15.4	16.0
B_2	14.66	14.61	14.49	14.40	14.77	14.65
g''	1.979	1.975	1.968	1.962	1.987	1.978
$-\alpha'' \times 10^5$	3.3	4.0	4.90	5.70	2.2	3.2
in cms.	(4.0)	(-ve)	(3.3)	(2.7)	(-ve)	(5.0)

(SO ₄) (SeO ₄) series					(SeO ₄) ₂ series	
	K	NH ₄	Rb	Cs	NH ₄	Rb
$A_1 \times 10^4$	10.2	12.0	12.5	12.5	1.1	6.45
B_1	14.56	14.31	14.30	14.30	14.48	14.53
g'	1.973	1.956	1.955	1.955	1.968	1.970
$-\alpha' \times 10^5$	4.2	6.60	6.75	6.75	4.90	4.60
in cms.	(3.3)	(3.9)	(4.0)	(4.0)	(1.2)	(2.4)
$A_2 \times 10^4$	-1.7	10.0	0.0	10.0	0.0	6.45
B_2	14.80	14.59	14.56	14.49	14.55	14.53
g''	1.988	1.974	1.973	1.968	1.972	1.970
$-\alpha'' \times 10^5$	2.85	4.02	4.2	4.9	4.33	4.60
in cms.	(-ve)	(3.2)	(0.0)	(3.2)	(0.0)	(2.4)

In the few cases, e.g. Rb, Cs sulphates and Rb selenate no change in g is observed over the entire range and the g values are very close to each other showing that they not only belong to the same class of alums but the crystalline fields in them are also very nearly the same and are practically constant in the entire temperature range. Rb and Cs sulphato-selenates though showing a considerable change

in g values in passing through the medium temperature range, have g values in the low temperature region very close to the previous three salts and to K sulphato-selenate and NH_4 selenate in the high temperature region and hence all these may be supposed to belong to the same class, in the respective range of temperatures [*class* (1)]. K, NH_4 and Tl sulphates NH_4 , Rb and Cs sulphato-selenates, all at the high temperatures have distinctly smaller g values than the previous salts. The g 's as also the high frequency terms being very similar, these alums should have similar crystalline fields (varying similarly with temperature) and belong to *class* (2). Apparently, K, NH_4 , NH_2OH sulphates, NH_4 sulphato-selenate and NH_4 selenate have g values at low temperatures very close to each other and belong to *class* (3), but the high frequency terms in NH_4 sulphate and selenate are anomalous, and small changes in g values may have to be made on extending the temperature range. Tl sulphate and K sulphato-selenate at low temperatures have also negative high frequency terms and the high g values in them may have to be similarly even more reduced so that they may also be put amongst the last class. NH_2OH sulphate in high temperature range, for a similar reason belongs to *class* (1).

It would be worthwhile to compare our g values with the resonance experiments in this connection. Unfortunately the available data are given to be same for all sulphate salts = $1.98 \pm .02$ (Bleaney, Bagguley and Griffith, 1951) so that the margin of error covers our observed variations of g . On the other hand, the nature of spin splitting from these measurements is appreciably different for the two classes of alums (Bleaney, 1951), (a) Rb, Cs, NH_3CH_3 alums having spin separations 0.165 cm^{-1} , 0.145 cm^{-1} , 0.165 cm^{-1} at room temperature show only very little decrease in the splittings which become practically constant below 90°K , (b) K and NH_4 alums have values near 0.12 cm^{-1} and 0.135 cm^{-1} at room temperature, but these splittings change enormously and in a complicated manner with temperature, falling to 0.055 cm^{-1} and 0.035 cm^{-1} near about 90°K , after which some sort of transition occurs and the salts consistently show an increased double value for the spin splitting about (0.32 cm^{-1} , 0.24 cm^{-1}) and (0.27 cm^{-1} , 0.15 cm^{-1}) for NH_4 and K alums respectively down to 20°K . The salts after transition are put in class (c) by Bleaney. The transition phenomena is similar to the findings of Kraus and Nutting (1941) from the studies of absorption spectra, though the classification of the alums from this and resonance measurements do not agree well.

It will be found from a consideration of our g values that our class (2) of alums having the largest departure of g from spin only value is identical with the class (b) of Bleaney (1951) and α class of Klug (1940). Our class (1) having a moderate departure of g value from spin only value is the same as the class (a) of Bleaney (1951) and β alums of Klug (1940). Our class (3) to which belong NH_4 , NH_2OH , Tl sulphate and K and NH_4 sulphate-selenate, NH_4 selenate at low temperature has the highest value of g .

The considerable narrowing of the spin splitting in K and NH_4 sulphate alums in the range 300°K and 90°K shows that the anisotropic crystalline field is decreasing very much. The change in the anisotropic field with temperature may conceivably be accompanied by changes in the average value of the field and hence of g as observed by us in these and similar alums. The spin splittings change very little in Rb and Cs sulphate alums in which we correspondingly find no appreciable change in g . A recent accurate value of g ($= 1.976 \pm .002$) from paramagnetic resonance (Bleaney and Bowers, 1951) not bound in the light refers to the K selenate alum diluted to 5 % concentration with Al-K selenate alum, and the temperature is not given but it seems to have about the g value as our class (1) alums.

The double splittings observed by the resonance experiments when class (2) of alums is cooled below 90°K , i.e. in class (c) of Bleaney, are probably due to coexistence in this region of two crystal phases of different space groups but of the same composition and cubic crystal class as the alums. The large changes in spin splittings (Bleaney, 1951) and in g values of this class above 90°K i.e. our class (2), observed by us as mentioned above are then no doubt precursors of the actual transitions to class (c) below this temperature. It is very probable that in all cases where we find a change of g value with temperature in our range, there is a continuous process of transition from $\alpha \rightarrow \beta$ or γ and $\beta \rightarrow \gamma$ phases of the alums. Apparently the electric fields are stronger in the β and γ alums since g values tend to increase towards the spin only value owing to greater quenching of the orbital moments. Further, during such a progressive change over, without change in the space group, taking place through a small rotation of the octahedral Cr^{+3} ionic group, as may quite possibly be due to anisotropic thermal expansion of the crystals, the magnetic properties may very well change in a continuous but non-linear manner as we observe. The irreversible transitions of Bleaney occur outside our temperature range, and in some cases do not probably take place at all even if it is near the bottom of our temperature range, since owing to methods of slow cooling of the specimen, strains set up are never enough to shatter our crystals as we observed and supercooling very probably takes place. In one case only, that of $(\text{NH}_4)_2\text{SeO}_4$ alum, a rather sharp and irreversible change has been observed in magnetic moment near about 106°K as will be found from the p_f^2 value at the bottom of the temperature range given in Table XII. This is more or less in agreement with Kraus and Nutting's observation.

(e) *Calculation of the spin-orbit coupling constant.*

From the equation :

$$\frac{p_1^2 - n^2}{8\lambda - 3kT_2} \quad \dots \quad (12)$$

(derived from equation 5, neglecting the terms involving $\lambda^2\alpha^2$, and $\lambda^3(\alpha_{\parallel} - \alpha_{\perp})^2$ which are very small) i. e. the ratio of the excess of the p_f^2 over the spin only

value at two extreme temperatures, for any given alum, eliminating α , taking to be constant, we may calculate the value of λ . In view of (1) the small value of the above excess, (2) the uncertainty in the high frequency term due to changes in g with temperature in many cases (3) the fact that α is not constant, also (4) that in the medium temperature range the temperature variations can not be made to fit with the theoretical formula, the calculation of λ has to be done preferably from the rather limited upper range of temperatures; the value of $\lambda \approx +100 \text{ cm}^{-1}$ for K, Rb, Cs salts so calculated is to be considered satisfactory.

A slightly better way of calculation is from the g value from which α is eliminated using (Eq. 7), since this gives due weight to all the experimental points in the given temperature range. Of course the values g' and α' in the upper range should be used here also. λ comes out to be between $+54$ and $+120 \text{ cm}^{-1}$ for most of the salts, giving a mean value $+84 \text{ cm}^{-1}$ as against $+87 \text{ cm}^{-1}$ in the free ion. The differences between individual salts are due to uncertainties in the experimental determination of the g' and α' values, due to reasons already mentioned.

That λ should be more or less the same in the solid state and free ion has been verified by the measurement of Krishnan and Bose (1938), Bose, Mitra and Datta (unpublished); Bose (1948) for Ni^{+2} salts. Owen (1952) and Bleaney (1951) have recently shown from theoretical considerations that λ should be practically the same for the free ion value and in the solid state, though others (Van den Handel and Siegert, 1937; Abragam and Pryce, 1951; Griffiths and Owen, 1952) have claimed a decrease in λ as large as 30-40 % in the solid. It appears from these investigations that owing to a partial sharing of the $3d$ electrons of the central paramagnetic ion by the surrounding eight oxygen atoms of the water octahedron, both g and the high frequency terms are affected, so that these are really given by,

$$A = -45 k\alpha f$$

$$g = 2\gamma(1+4\lambda\alpha f),$$

instead of equations (8) and (7) where f is the 'covalency factor'.

Our calculation of λ (incidentally of Krishnan and Bose also) is then still valid and gives us the actual value of λ in the solid state (or for free ion), since what we have eliminated is really the *effective* value of the field constant, $\alpha_f = \alpha.f$ inclusive of the covalency factor f . The lower value of λ obtained by the other authors are due to their method of calculation which includes f in the value of λ .

(f) *Calculation of the effective field constant and covalency factor*

In view of the large errors in the calculation of α_f in many cases directly from the high frequency term, particularly in the low temperature region where several of these terms are abnormally small or even negative, it would be better to calculate them from the g value $= 2\gamma(1+4\lambda\alpha_f)$, where λ is known. From what has been

said in the earlier section, the value of λ calculated, suffers much from not only errors in the A and B terms but also from the variations in the value of α_f due to thermal expansion of the lattice and transitions from one phase to another. It would be then better to assume $\lambda = +87 \text{ cm}^{-1}$, the free ion value in all cases. The values of α_f thus calculated from g as also from high frequency term, where possible, are actually those given as α' and α'' in Table XIII. It would be seen for all the alums of NH_4 sulphate class, the α -class, the mean value of α_f is about $6.7 \times 10^{-5} \text{ cm}$, for Rb sulphate class presumably the β -class, the mean value is about $5.0 \times 10^{-5} \text{ cm}$, which are somewhat smaller than the value $8.0 \times 10^{-5} \text{ cm}$ in $\text{NiSO}_4 \cdot 6\text{H}_2\text{O}$. For the last class to which belong K and NH_4 sulphates and several other alums at low temperature, the mean value is $3.5 \times 10^{-5} \text{ cm}$. Very probably these values are much closer to each other perhaps about 6, 5.5, and 5.0 for the three classes respectively, in view of large uncertainty in the experimental values; and one has to be satisfied only with a qualitative discussion of the results. The values of α_f from h.f. terms where possible to estimate with sufficient certainty, also support this conclusion.

It is known from the theory of Owen (1952) that $-1/\alpha$ and $-1/7\alpha$ (in which α is the *actual* value of the field constant) are the separations of the mean centres of the lower and upper orbital triplets respectively, from the lowest singlet in the Stark pattern of Cr^{+3} alum. But since the values of α found from our measurements are the *effective* ones inclusive of the covalency factor what we obtain from these are only the effective separations. It would be worth while to compare these separations with the extensive optical absorption data on the Cr^{+3} alums by Kraus and Nutting (1941) and on Cr^{+3} chloride solutions by Tsuchida and Kobayashi (1938) quoted by Hartmann and Schlafer (1951). Their results differ considerably, the former giving near about 15000 cm^{-1} differing by a few hundred cm^{-1} at most from alum to alum, the latter 17500 cm^{-1} , as the first absorption level, of which evidently the former value is more appropriate to the present discussion on Cr^{+3} alums. Our mean *effective* separations for the three classes of alums corresponding to above absorption level are roughly about 16600, 18200 and 20000 cm^{-1} respectively. The ratio of the *actual* (optical) to *effective* separation gives us the shared $3d$ electrons of the Cr^{+3} ion spend correspondingly longer fractions of time in the σ orbitals (and possibly π orbitals also) of each of the oxygen atoms of the water octahedron for the three classes. The value quoted by Owen for this is 0.6 calculated from the g value for highly diluted Cr^{+3} selenate alum, 1.976 given by resonance method (Bleaney and Bowers, 1951), and Hartmann and Schlafer's value of actual separation for Cr^{+3} chloride solution (which is normally a green solution in which the Cr^{+3} complex constitution is surely different from the alums). Our values show that in the alums the covalency factor is probably larger than estimated by Owen, i.e. the bonds are more ionic. The mean centre of the upper level taking these values of f comes out to be at about 21000 cm^{-1} , as the mean for the three classes, but for this, data are not available for Cr^{+3} alums, and for

the chloride solution mentioned the value is 24500 cm^{-1} . The difference from the mean value for the individual salts indicate, though qualitatively, the differences in "actual" crystalline field in them. The differences arise evidently from the variation in the long range structures of the alums, due to replacement of one monovalent cation or divalent anion by others and by the disturbing influence of the temperature, and their indirect action on the size and shape of the $(\text{Cr}^{+3}, 6\text{H}_2\text{O})$ octahedron, according to the theory of Van Vleck (1939).

ACKNOWLEDGMENTS

The author expresses his sincerest thanks to Dr. A. Bose, D.Sc, for suggesting the problem and for his keen interest throughout the progress of the work.

REFERENCES

- Abraham, A. and Pryce, M. H. L., 1951, *Proc. Roy. Soc. A.*, **205**, 135.
 Bose, A., Mitra, S. C. and Datta, S. K. (In course of publication).
 Bose, A. and Mitra, S. C., 1952, *Ind. J. Phys.*, **8**, 393.
 Bose, A., 1948, *Ind. J. Phys.*, **22**, 276.
 Baggeley, D. M. S. and Griffith, J. H. E., 1951, *Proc. Roy. Soc. A.*, **204**, 188.
 Bleaney, B. and Bowers, K. D., 1951, *Proc. Phys. Soc. A*, **64**, 1135.
 Bleaney, B., 1951, *Proc. Roy. Soc. A.*, **204**, 203.
 Broer, L. J. F., 1942, *Physica*, **9**, 547.
 Broer, L. J. F., 1947, *Physica*, **13**, 353.
 Beevers, C. A. and Lipson, H., 1935, *Proc. Roy. Soc. A.*, **148**, 664.
 Daniels, J. M. and Kurti, N., 1954, *Proc. Roy. Soc. A.*, **221**, 243.
 Datta, S. K., 1954, *Ind. J. Phys.*, **28**, 239.
 Dumond, J. W. M. and Cohen, E. R., 1948, *Rev. Mod. Phys.*, **20**, 82.
 Dutta Roy, S. K., 1955, *Ind. J. Phys.*, **29**, 429.
 Griffiths, J. H. E. and Owen, J., 1952, *Proc. Roy. Soc. A.*, **213**, 459.
 de Haas, W. J. and Gorter, C. J., 1929-30, Comm. Leiden. no. 208c.
 Hartmann, H. von. and Schlafar, H. L., 1951, *Z. Naturf.*, **6a**, 760.
 Koenig, S., Prodell, A. G. and Kusen, P., 1952, *Phys. Rev.*, **88**, 191.
 Kraus, D. L. and Nutting, G. C., 1941, *J. Chem. Phys.*, **9**, 133.
 Krishnan, K. S. and Mookherji, A., 1938, *Phil. Trans. Roy. Soc. A.*, **237**, 135.
 de Klerk, D., Steenland, M. J. and Gorter, C. J., 1947-52, Comm. Leid. No. 278c.
 Klug, H. P., 1940, *Journ. A. Chem. Phys.* 2992.
 Laporte, O., 1928, *Zeits. f. Krist.*, **47**, 761.
 Lipson, H., 1935, *Proc. Roy. Soc.*, **151**, 347.
 Schlapp, R. and Penney, W. G., 1932, *Phys. Rev.*, **42**, 666.
 Seigert, A., 1936, *Physica*, **3**, 85.
 Serres, A., 1932, *Ann. der. Phys.*, **17**, 1.
 Van-Vleck, J. H., 1932, *Phys. Rev.*, **41**, 208.
 Van-Vleck, J. H., 1939, *J. Chem. Phys.*, **7**, 61.

IONOSPHERIC PREDICTION METHODS AND THE PROBABLE SOURCES OF ERROR*

S. S. BARAL

INSTITUTE OF RADIO PHYSICS AND ELECTRONICS, CALCUTTA UNIVERSITY

(Received for publication February 6, 1956)

ABSTRACT. The various sources of error in the prediction of foE , foF_1 , foF_2 and $(M3000)$ F_2 are discussed. It is shown that the deviations of the foE and medium-latitude foF_1 predictions are to be ascribed to inaccuracy in sunspot number prediction. The deviations of high and low latitude foF_1 predictions are to be ascribed to deviation from $\sqrt{\cos \chi}$ law.

Deviations of foF_2 and $(M3000)F_2$ predictions are caused by the insufficient knowledge of the diurnal and seasonal trends of these parameters.

Interpolation errors of foF_2 and $(M3000)F_2$ are due to incomplete knowledge of the geographical distribution of these parameters. The law of geomagnetic control, on which the predictions are based, is different for different hours of the day. For instance, during equinox months, the geomagnetic latitude distribution of foF_2 values shows a cusp near the geomagnetic equator for hours for which the F-layer is separated into F_1 and F_2 and a single maximum near the geomagnetic equator for hours for which the layer is not so separated.

It has been found that the inaccuracy in MUF prediction cannot be completely accounted for by the inaccuracies of fo and M predictions taken together.

Study of the day to day dispersion of foF_2 values from their monthly median shows that the dispersion is low for low values of the solar zenith angle. No such generalisation can, however, be made in the case of the dispersion of $(M3000)F_2$ values.

INTRODUCTION

For efficient maintenance of long distance radio communication it is essential that the maximum usable frequency (MUF) between the communicating stations at different hours of the day and in different seasons of the year be known well in advance. Ionospheric prediction services have therefore been established in the different parts of the world. The foremost amongst these are those conducted by (1) the Radio Research Board, England, (2) the Service des Previsions Ionospheriques Militaires, France, (3) the Central Radio Propagation Laboratory, Bureau of Standards, Washington, U.S.A., and (4) the Ionospheric Prediction Service, Australia.

The ionospheric predictions are based upon the vertical incidence ionospheric data collected by the vertical incidence pulse technique mainly from the records of $h'-f$ curves and obtaining therefrom monthly mean or median hourly values of the critical frequencies (fo 's) of the various ionospheric regions, and the MUF

* Communicated by Prof. S. K. Mitra.

factors (M 's) for various distances of propagation. For the latter, it has been internationally agreed to publish only the factors for 1500km transmission *via* region E, ($M1500$)E and 3000km *via* region F₂, ($M3000$)F₂.

Unfortunately, the accuracy of these predictions is still far from the desired standard. The predicted monthly mean ionospheric parameters are therefore constantly checked with their actual values and efforts are being made to increase the accuracy of the predictions. The expected range of day-to-day dispersion of the values of the parameters from their monthly mean or median is also of interest because, long distance transmission at a particular hour is assured only when the frequency of transmission is lower than the actual value of the MUF at the hour. However, when the median value is predicted, success for 50% of the days is assured.

In the present paper the magnitude and the nature of the errors that occur in the predictions of foE , foF_1 , foF_2 , ($M3000$)F₂ and MUF will first be assessed. The causes that are likely to contribute to these errors will then be discussed. Finally, study will be made of the temporal variation in the fluctuation of the daily values of the ionospheric parameters from the monthly mean.

2. RESUME OF THE METHODS OF PREDICTION OF MONTHLY MEAN IONOSPHERIC CHARACTERISTICS

Since long range associations between the variations of ionospheric parameters and sunspot numbers are known more or less accurately from past data, the first step in the prediction work is to estimate the mean sunspot number for the future epoch under consideration. This may be done by the method of Waldmeir (1944), or of Gleissberg (1942, 1949), and is obtained as a mean yearly value centred on the epoch. The second step is to predict the mean yearly value of the ionospheric parameter for a particular hour (say, noon) from a knowledge of its past relation with the mean yearly sunspot number. The mean yearly noon-time value being thus determined, the third step is to determine the mean *monthly* noon-time value of the parameter from a knowledge of its seasonal trend obtained from past data. Finally, the mean diurnal variation for the particular month is obtained either from the knowledge of hourly coefficients for the particular month with reference to noon values or by repeating the second and third steps for other hours of the day.

It is evident from the above, that prediction is possible only for stations for which past ionospheric records are available. But in actual radio communications, it is, more often than not, necessary to make predictions of fo and M for places for which there are no ionospheric records. For such cases a knowledge of the law of geographical variation of the parameters to be predicted (fo and M) is necessary. For regions E and F₁ the law of variation is simple and for routine prediction, it is assumed that longitude and time can be interchanged for these

regions for all places situated in the same latitude. For latitude variation, the law is taken as $K \cos^n \chi$ where χ is the zenith angle of the sun, K is considered constant depending on sunspot number only, and the index n is usually taken as 0.25. Thus, the predictions of E and F₁-region parameters for any place are made on the basis of the values of the parameters for any other place. This simplified method of predicting E and F₁-region characteristics, however, leads to some errors. (The errors involved and their sources have been discussed later in this paper). The MUF factor M is considered as constant and is calculated once for all for the E-layer height of 100km and F₁-layer height of 200km.

For the F₂ region, however, there is considerable longitude effect as both f_o and M vary in a complicated manner with λ and depend upon $\lambda - \phi$, (λ is the geomagnetic and ϕ is the geographic latitude). Data from a large number of stations are therefore, necessary and the values at intermediate points can only be obtained by interpolation. The current practice is therefore to make world predictions for F₂-region parameters in three sections of the earth's surface, it being assumed that $\lambda - \phi$, and hence the longitude effect within each of the sections is small.

The methods adopted by the different prediction services for obtaining future values of f_o and M are almost identical for regions E and F₁ but differ considerably from one another for region F₂. We now describe briefly the methods for prediction of F₂ region parameters by the different prediction services :

Radio Research Board (RRB), England :—The mean diurnal variation curve for the month of prediction is obtained by extrapolating mean hourly values of the ionospheric parameters for the same month in previous years, the guiding trend in this extrapolation being obtained from the latest available data. The curve is then adjusted to allow for the trend of solar activity near the time of prediction. The monthly average value so obtained for each hour is then checked by finding the corresponding yearly average with this value and those for the previous eleven months. For correct prediction, this yearly value must approach that obtained from the relation between the yearly average sunspot number and the yearly average ionospheric parameter for a probable value of the former near the time of prediction.

For making world prediction the above procedure is repeated for all the stations for which the data are available and with the values so predicted for each parameter, contour curves are drawn separately for the three zones: east zone (50°E–170°E), west zone (130°W–10°W), and intermediate zones (10°W–50°E and 170°E–130°W).

Central Radio Propagation Laboratory (CRPL), Bureau of Standards, Washington, U.S.A.—The annual running average sunspot number expected near the time of prediction is first estimated. The monthly median ionospheric parameter for different hours is then read off from a nomogram constructed for the month of

prediction on the basis of a linear relationship between the sunspot number and the ionospheric parameter.

The procedure is repeated for all world stations for which data are available and world prediction is made on three charts as explained in the previous case.

Service des Previsions Ionospheriques Militaires (SPIM), France.—The 24-hour average of the monthly mean $(foF_2)^2$ for a given month (denoted by Q) is determined from the relation $Q = \bar{Q}JU$, where \bar{Q} is the twelve month running average value of Q obtained from a long term comparison of Q and mean sunspot number R (predicted value). Thus,

$\bar{Q} = mR + n$ (where $m = 0.883 - 0.00833i$, $n = 64 - 0.743i$, and i is the magnetic inclination),

$J = Q/\bar{Q}$ for the given month,

and $U =$ the irregularity factor $\div 1$

With the value of Q so obtained, the mean diurnal variation of foF_2 is calculated from a knowledge of the mean foF_2 variation for the same month in the previous years. For $(M3000)F_2$ prediction, a graphical method such as that of the Radio Research Board, England, is followed.

For world prediction a new zonal division has been adopted by this organization on the ground that F_2 -region characteristics over Asia and Africa correspond closely to those of Europe: east zone, $10^\circ E$ to $160^\circ E$, west zone, $40^\circ W$ to $100^\circ W$, and the rest, intermediate zones.

Ionospheric Prediction Service (IPS) Australia.—A 24-hour mean monthly value of the ionospheric parameter is predicted, first, by studying the numerical

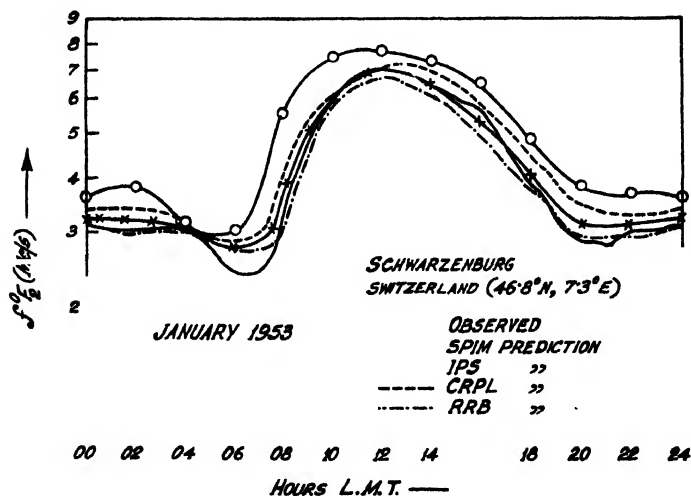


Fig. 1

differences observed between successive monthly means and, then by comparing the variations in ionospheric parameters with variations in mean sunspot numbers. Next, the hourly values which make up the monthly mean of the parameter under

consideration are predicted from a family of curves of the same for the particular month in all previous years plotted in the same sheet. A diurnal curve is thus built up. The mean hourly values from this curve when averaged, should correspond to the monthly mean already obtained.

For world prediction, the same procedure is repeated for all stations for which data are available and three charts are prepared as in the case of the RRB and the CRPL.

The predicted mean diurnal variation curves for the month of January 1953 for the station Schwarzenberg, Switzerland as obtained by the different methods are shown in figure 1, together with the observed curves, for comparison.

3. COMPARISON OF THE PREDICTED VALUES OF f_o AND M WITH THE VALUES OBTAINED FROM IONOSPHERIC DATA AND ORIGIN OF THE DEVIATIONS

To compare the relative accuracy of the predictions by the different methods as discussed in the last section we shall draw observed and predicted diurnal variation curves of f_oE , f_oF_1 , f_oF_2 and $(M3000)F_2$ for stations representative of low, intermediate and high latitudes, e.g., Trinidad (10.6°N), Washington (39°N) and Oslo (60°N). The sources of error that are common to predictions for all the regions are:

- (1) Inaccuracy of sunspot number predictions.
 - (2) Approximations made regarding laws of variation of f_o with
 - (a) solar zenith angle ($f_o = K \cos^n \chi$, where χ is the zenith angle of the sun, $n = 0.25$ and K is a constant for a given value of sunspot number)
 - and (b) solar radiation intensity ($f_o = a + bR$ where 'a' and 'b' are constant and R is the mean sunspot number).
 - (3) Inaccuracy in the interpolation for different latitudes and longitudes.
- (a) f_oE and f_oF_1

Figure 2 shows the percentage deviation in noon f_oE prediction during the period December 1950 to October 1951. It will be seen from the figure that during the period considered, the predictions were more accurate in summer than in winter and less so at high and low latitudes than at intermediate ones.

Figure 3 compares the observed values of f_oF_1 with those predicted by RRB England, for the periods December 1950 and June 1951. It will be seen that in the winter months, the region itself was not observed at Washington and at Oslo and, during summer months, the deviations from predicted values are greater at Oslo and Trinidad than at Washington.

The sources of these deviations must lie in the deviation of the exponent n from the Chapman value and/or in errors in the prediction of the sunspot numbers.

The latter will affect the prediction of the f_o values of all the ionospheric regions, and this it should do similarly and to the same degree.

From what follows it will, however, be seen that for f_oE and for the intermediate latitude f_oF_1 only, the errors in ionospheric predictions are comparable with and are similar to errors in sunspot number predictions. The errors in the prediction f_oF_1 for high and low latitudes, are often much greater than what errors in sunspot number predictions warrant and are not correlated in any way with the same.

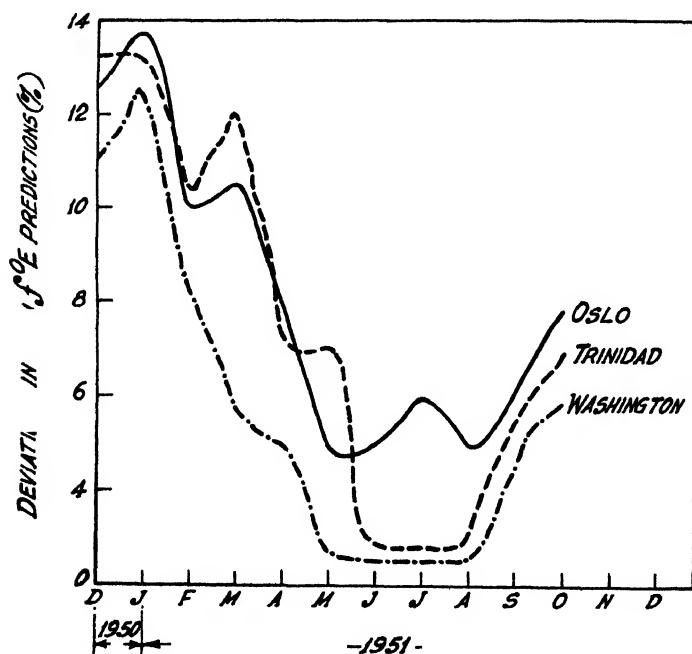


Fig. 2

Regarding the law of variation with the solar zenith angle it has been found that n deviates from the Chapman value 0.25. Such deviations of n have been studied by Harnischmacher (1951), Scott (1952) and Saha (1953). They have found that n ranges from 0.26 in winter to 0.30 in summer. Errors due to deviation of n from the Chapman value would thus affect predictions in such a way that the summer values will be more in error than the winter values. For instance, for the latitude of Washington, this means that the errors will vary from about 3% in winter to as much as 16% in summer. But, it will be seen from figure 2 that actually the reverse is the case. The errors have varied from about 12% in winter to about 3% in summer in the period Dec. 1950- Dec. 1951. Deviation of n from the value 0.25 cannot, therefore, account for the observed error on f_oE predictions.

Regarding the variation of f_o with the sunspot number, it has been shown by Naismith (1942) that the variation of E-region character figure $(f_oE)^4/\cos \chi$ is correlated to within 4% with the variation of sunspot number. This means that lack of correlation between K and sunspot number does not also account for the observed errors in f_oE predictions. It has, however, been found that while the errors of f_oE predictions show no correlation with errors in n or K values, they do show a strong correlation with the errors in sunspot number prediction.

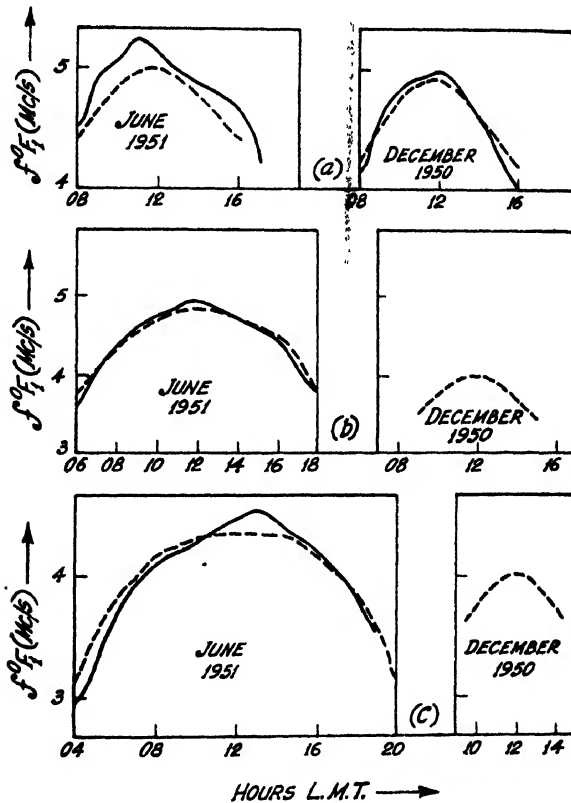


Fig. 3. Comparison of the predicted and observed diurnal variations of foF_1 for high, low and intermediate latitude stations for December 1950 and June 1951. (a) Trinidad (b) Washington (c) Oslo.

Similar consideration shows that at intermediate latitudes, the errors in foF_1 predictions, are strongly affected by those in the estimation of the sunspot numbers. At low and high latitudes, however, the deviation of foF_1 variation from $\cos \chi$ law itself is large (figure 3) particularly during periods of high solar activity, and the inaccuracy in foF_1 prediction in these latitudes is ascribed to this cause alone.

(b) foF_2 and $(M3000)F_2$

Figure 4 compares the observed values of foF_2 and $(M3000)F_2$ at Washington in June 1950 with those predicted by RRB England. Figure 5 compares

the observed values of foF_2 at Trinidad and Oslo with those predicted by CRPL, Washington, and the observed values of $(M3000)F_2$ at these places with those predicted by the RRB, England for December 1950. It will be seen that the errors

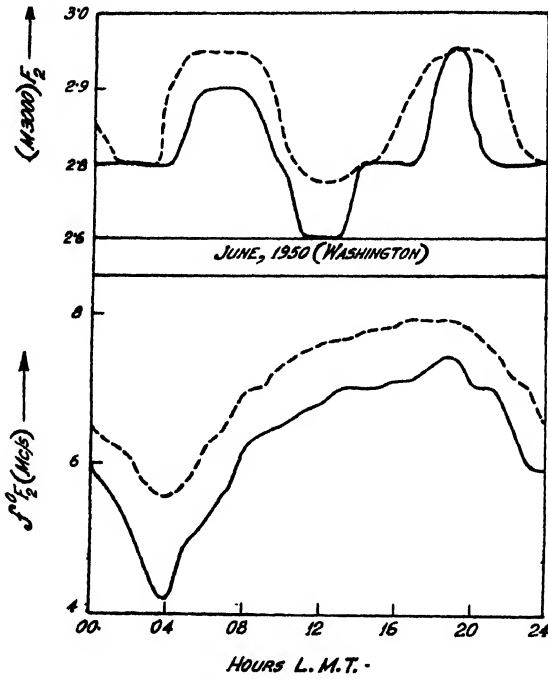


Fig. 4

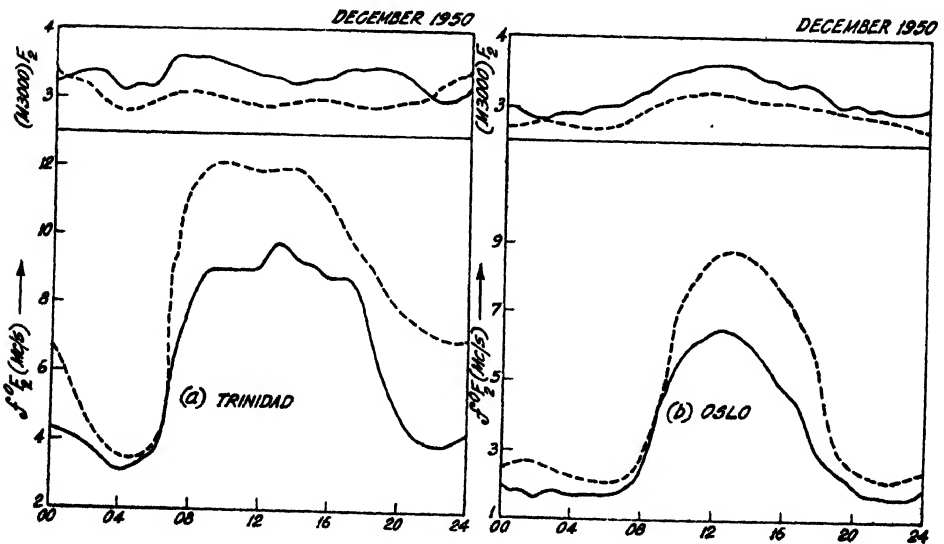


Fig. 5

in prediction are quite large and, the percentage differences are often higher for the hours at night than those for the daylight. No definite latitudinal variation in the errors of prediction of foF_2 and $(M3000)F_2$ has been observed.

Predictions of foF_2 values, besides being subject to the errors listed for the case of the E and F_1 -regions are affected by errors due to the complex nature of the longitude effect, and, in so far as the monthly mean values are concerned, to the uncertainty regarding the average number of quiet days in the month of prediction. Further, error is introduced due to the lack of homogeneity of scaling and interpretation of data from different stations during interpolation of foF_2 values.

We first note that the assumed linear relation between fo and the sunspot number ($foF_2 = a + bR$) holds only very approximately for the F_2 -region, there being large scatter round the mean straight line. This scatter is greater for the hour at night than for daylight hours, showing that the linearity of the relation is less rigorous at night (figure 6). Deviations due to this cause, therefore, make the predictions for the hours at night more inaccurate than those at daytime.

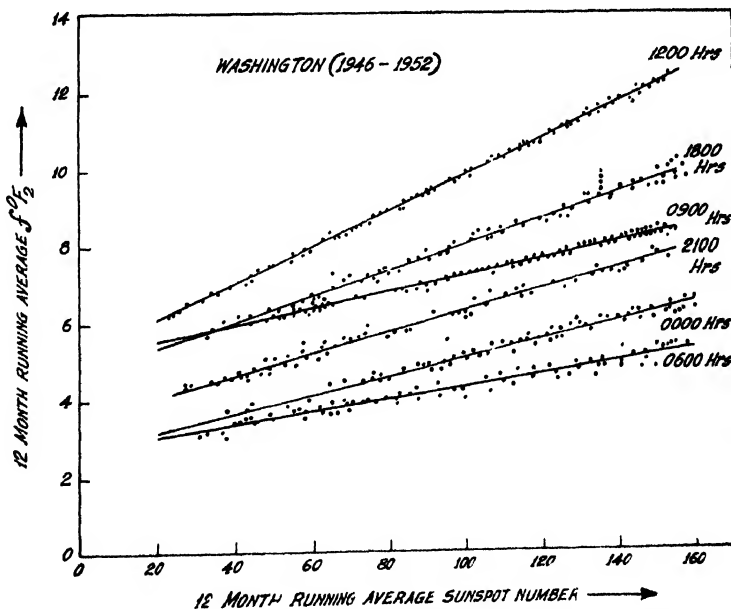


Fig. 6. Running average foF_2 vs. running average sunspot numbers for Washington for different hour of the day. It will be seen that the plotted points show more scatter for the hours at night (0000, 2100) and near sunrise and sunset (0600 and 1800) than for the day light hours (0900, 1200 hrs).

Also, it is to be noted that for the same value of R , the value of foF_2 depends upon whether the solar activity is increasing or decreasing (figure 7) and in course of the solar cycle the same seasonal variation is not repeated from year to year (figure 8) nor is the nature of the diurnal variation curve identical for the same

month in different years (figure 7). All these mean that the computed monthly coefficients or the extrapolated monthly trends will be inaccurate.

Further, the solar activity change of foF_2 is not the same for all stations. This is proved by the fact that the foF_2 vs sunspot number curves do not possess the same slope at the same local time at all latitudes (figure 9). Such curves are, therefore, to be drawn separately for each station before constructing the world chart for foF_2 prediction.

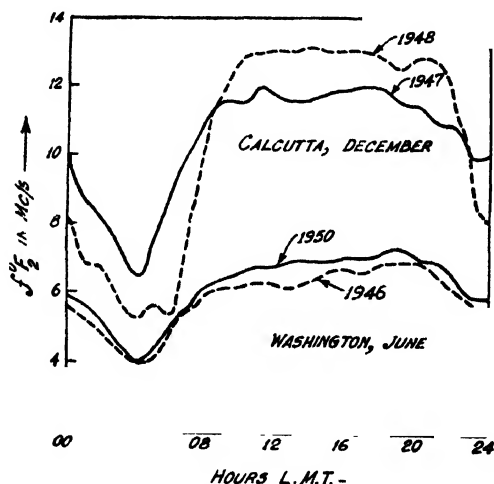


Fig. 7. Diurnal variation of foF_1 for the same month for the same mean value of the sunspot number at different phases of the solar activity (e.g. December in 1947 and 1948 and June in 1946 and 1950).

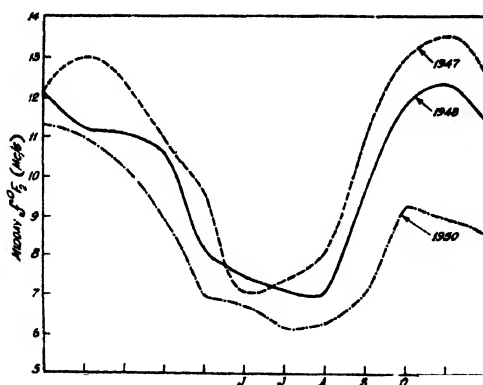


Fig. 8. Seasonal variation of midday foF_2 for the years 1947, 1948 and 1950. The lack of accord is to be noted. The seasonal minimum occurred in June in 1947, in July in 1950 and August in 1948.

In the interpolation of foF_2 values inside each of the E- W- or I-zones on the earth's surface it is assumed that inside the zone $\lambda-\phi$ is negligible and hence longitude and time can be interchanged along the same latitude. But it is found

that at certain stations in the same zone and on nearly the same latitude, the shapes of the diurnal variation curves are not at all similar (figure 10). This shows that longitude and time cannot always be interchanged for all places on the same zone. This is because, the geomagnetic control, which is responsible for the longitude effect, is not the same for all hours of the day for any

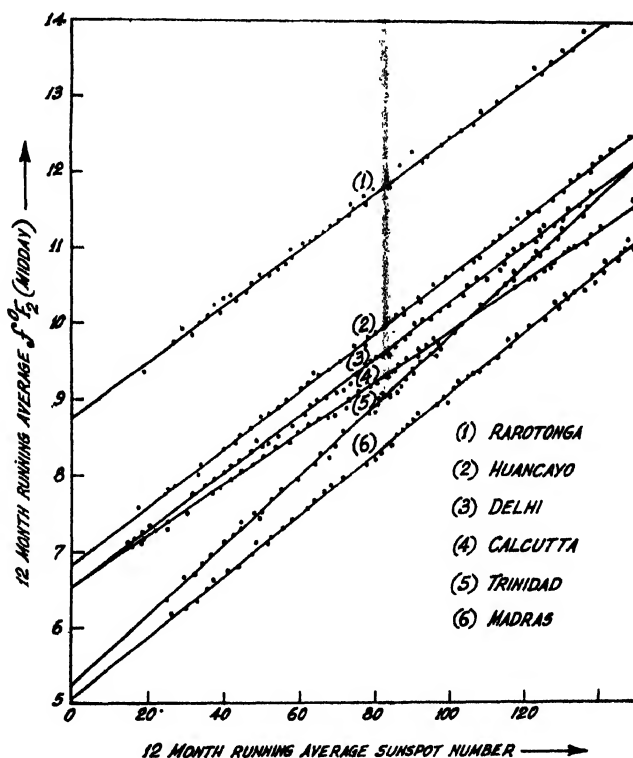


Fig. 9. 12 month running average value of midday f_oF_2 plotted against 12 months running average value of sunspot number for a few stations in low latitudes in both the hemispheres. It will be seen that the variation (as given by the slope) is not the same for all the stations.

particular season. The pronounced equinoctial midday dip in the low latitude f_oF_2 distribution with geomagnetic latitude changes gradually to a pronounced midnight maximum near the geomagnetic equator showing a complete oscillation in 24 hours (figure 11) Appleton 1954; Baral, 1954)

All the sources of error listed in the case of f_oF_2 prediction also affect the prediction of $(M3000)F_2$ and more so because of the paucity of recorded data for this parameter. There is still a great deal of uncertainty in our knowledge of the diurnal, seasonal and solar cycle variation of M as also its latitudinal variation. The accepted law of variation of M viz., M is high when χ is low and low when the solar activity is high, does not hold universally, particularly for

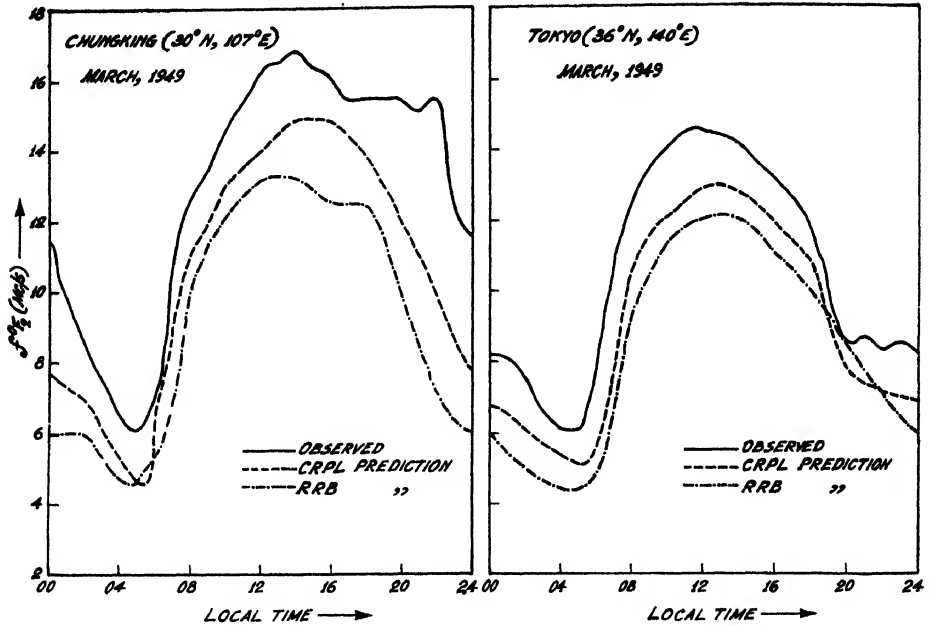


Fig. 10. Comparison of the observed equinox values of f_oF_2 with the values as predicted by the CRPL and RRB methods for two stations in the East zone at nearly the same latitude.

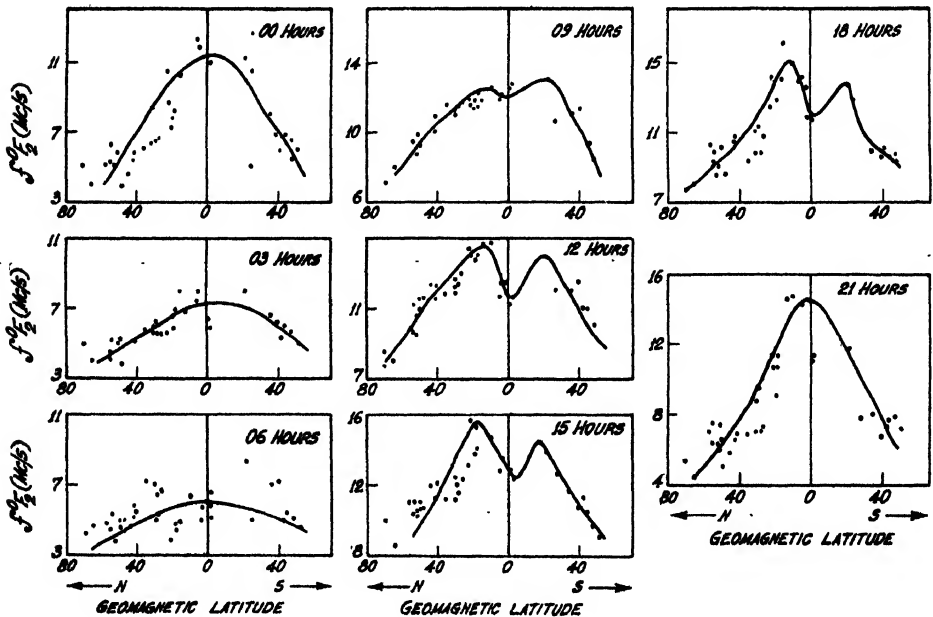


Fig. 11. Geomagnetic control of the equinox f_oF_2 values at different hours of the day. It will be noted that near the geomagnetic equator the dip in the midday curve is retained for most of the daylight hours. For the hours at night this dip disappears and there is a single maximum instead of two. This maximum occurs near the geomagnetic equator.

equatorial latitudes. The world variation of M cannot also be very simply represented either with respect to the geographical or to the geomagnetic equator causing difficulty in interpolation. Inaccurate interpolation is also caused by the inhomogeneity in the M values obtained from different stations using recorders of different sensitivity and scaling records by different methods.

All the methods of determining M suffer from a common error, namely, that due to the factor M being determined from the ordinary ray trace of the $h'-f$ curve. It is assumed that this trace is unaffected by the earth's magnetic field, but this is true only for strictly transverse propagation. The methods cease to be accurate when applied to vertical incidence ionospheric data from stations far from the geomagnetic equator. However, the effect of the earth's magnetic field can be approximately taken into account in the final MUF calculation by taking $MUF = pfH + f_0M$ where p is a fraction, and fH , the gyro-frequency at the point of reflection (Tremellen and Cox, 1947).

(c) *MUF*

Errors in the final prediction of the MUF values obviously depend on the inaccuracy in the predictions of f_0 and M . Minnis and Wilkins (1951) have assigned a deviation of 18-20% of the predicted MUF's from the observed ones. Of this deviation, 4-10% is due to f_0 -error and 4% due to M -error, both arising out the 'zone error'. The rest has been ascribed to causes such as uncertainty regarding the mode of propagation along the great circle path resulting mainly from the neglect of the earth's magnetic field, disregard of abnormal propagation, etc. The magnitudes of the errors due to all these causes vary widely and no typical figure can be given unless direct oblique incidence observations are made regularly to determine them. Unfortunately, the check on MUF prediction can only be based upon commercial service data which give only a limited range of frequencies and time for study. For instance, these services seldom utilise frequencies as high as 30-50 Mc/s which are the common MUF values during high solar activity.

For transmission distances greater than 4000 kms, the ionosphere at the midpoint of the transmission path does not control the MUF. On the other hand, the MUF is the lowest of the MUF's predicted from the ionospheric characteristics at 2000 km for each end of the path. No examination of the ionosphere along the rest of the route is made. The control point method of predicting long distance MUF's is based upon the observed behaviour of commercial circuits in terms of conditions near their end points. The reason for this is yet to be found out, as the method is entirely empirical.

Again, for very long distance propagation, it is often found that the major arc rather than the minor arc of the great circle path determines the MUF and sometimes it is not easy to determine the actual path followed by the wave, e.g. the number of hops, etc.

It will appear from what has been said about the predicted values of MUF, that the product of the values of f_0 and M may not always represent the actual value of the MUF. Errors in MUF prediction are sometimes too large to be accounted for by errors in the predictions of f_0 and M taken together (Minnis and Wilkins, 1951).

The MUF on some particular hour may also be entirely at variance with the mean value. It is known that the daily values of f_0 and M undergo fluctuations about the monthly mean and the probability that successful communication may be made on a given frequency may be determined from systematic study of these fluctuations. This we proceed to do in the next section for three chosen stations, representative of high, low and medium latitudes. It will be seen that the amplitudes of the fluctuations vary with season, hour and latitude.

4. VARIATIONS IN THE SCATTER OF f_0 AND M VALUES

The dispersions in the daily f_0 and M values about the monthly mean have been studied from hourly data of the three stations, College (Alaska), Huancayo and Washington. As already mentioned, these are chosen to represent high, low and medium latitudes stations. The ionospherically quiet days only were selected for the analysis.

For region E there is no appreciable diurnal or seasonal variations in the scatter for any station. However, the late afternoon values at low latitude stations and the early morning values at high latitude stations show larger scatter than the midday value. This seems to be associated with the frequent occurrence of E's.

For region F₂ the amount of scatter of f_0 values shows definite seasonal and diurnal variations. The measure of the scatter is taken to be $\frac{\sqrt{\Sigma \Delta f_0^2/n}}{f_0}$ and is expressed as a percentage (n = number of days chosen, f_0 mean value of the critical frequency, Δf_0 = deviation from mean). The scatter is least near midday and greatest at sunrise and sunset times (figure 12). Study of the seasonal variation of the scatter for any given hour shows that it is least in summer months and greatest in equinox months (figure 13). It may be recalled, in this connection, that marked peaks occur in equinox months in the annual distribution of geomagnetic disturbances (Allen, 1944).

If we consider the scatter of values for a given hour at different latitudes we find that the scatter is less at low than at high latitudes.

From the above we may conclude that the scatter of f_0 values is small for small values of the solar zenith angle.

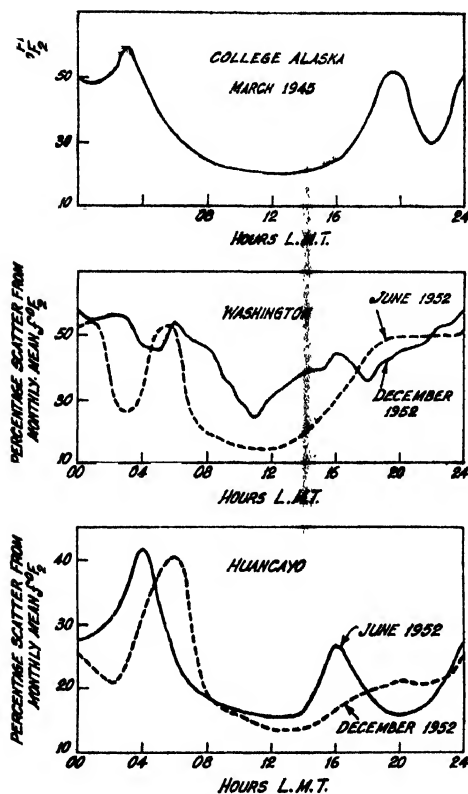


Fig. 12. Diurnal variation of the percentage scatter of daily values of f_oF_2 from their monthly mean at stations representative of high, low and medium latitudes. It will be noted that the scatter is low for low value of solar zenith angle.

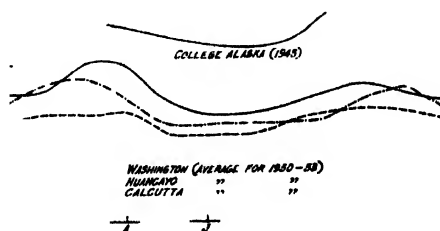


Fig. 13. Seasonal variation of the scatter of mean midday f_oF_2 values at stations representative of high, low and intermediate latitudes. The larger scatter during equinox months may be noted.

The dispersion of $(M3000)F_2$ values have also been considered in the light of the existing data. Although no definite variation can be attributed to the

distribution of the scatter, yet the smoothed curves (figure 14) definitely show low values during daytime. The scatter of M values is, however, much less than

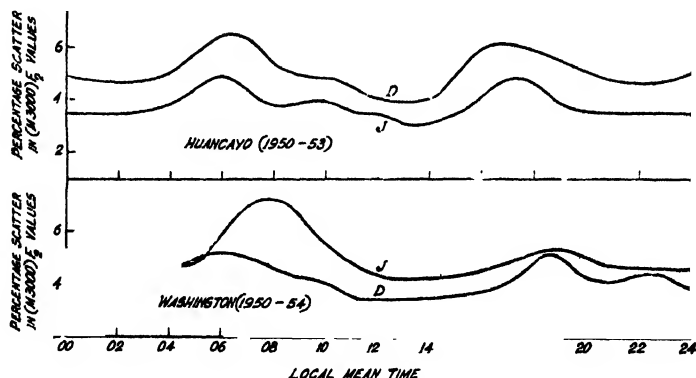


Fig. 14. Diurnal variation in the scatter of $(M\ 3000)F_2$ values at Washington and Huancayo for June and December 1950. As in case of f_oF_2 (figure 12) the scatter is greatest during sunrise and sunset hours.

the scatter of f_o values. The scatter of MUF values may, therefore, be supposed to be predominantly due to the latter.

5. CONCLUDING REMARKS

The systematic errors that are found to occur in the predicted values of f_o and M for the various regions are due to, (1) error in forecasting the sunspot numbers, (2) error in the assumed laws of diurnal, seasonal and solar cycle variations of the characteristics and (3) errors due to the imperfect knowledge of the geographical variation of the characteristics. Accurate sunspot number forecasting will remove the errors in f_oE and medium latitude f_oF_1 predictions. More precise knowledge of diurnal, seasonal and solar cycle variations of the characteristics will remove most of the errors in the prediction of f_oF_1 in high and low latitudes. f_oF_2 and $(M3000)F_2$. As a determination of an exact law of variation, taking all the factors into account has not yet been possible, it is preferable to adopt the method of extrapolation of the trends rather than that of computation. In the interpolation of f_oF_2 and M values, one should consider in detail the longitude effect, viz the different geomagnetic control at different hours of the day and the exact shape of the mean diurnal variation curve for any given month at the different stations in the same zone of prediction at the same latitude. In this connection the recent work of Minnis (1952) in which, it is recommended that predictions be made in G.M.T. rather than L.M.T., deserves special mention.

It is also emphasised that in the extension of the F_2 -layer prediction from one place to another for the preparation of the world charts, the data utilised from

existing ionospheric observatories should be made homogeneous. This means that the method of reduction and scaling of records as well as the methods of predicting the vertical incidence characteristics for all the stations should be standardized. New observatories should also be established to make the distribution of same even throughout the world. For instance, the north Pacific regions and most of the southern hemisphere possess the lowest density of ionospheric observatories and interpolation is difficult in these regions.

ACKNOWLEDGMENT

The work forms part of the programme of the Radio Research Committee of the Council of Scientific and Industrial Research, Government of India.

The author is indebted to Professor S. K. Mitra for helpful discussions and advice during the progress of the work.

He is also indebted to the Council of Scientific and Industrial Research for financial assistance and to Dr. A. P. Mitra, Senior Scientific Officer of the National Physical Laboratory for some stimulating discussions.

REFERENCES

- Allen, C. W., 1944. *Mon. Not. Roy. Astr. Soc.*, **104**, 13.
Appleton & Beynon, 1940, *Proc. Phys. Soc.*, **52**, 518; 1947, *Ibid*, **59**, 58.
Appleton, 1954, *Jour. Atmos. Terr. Phys.* **349**.
Baral, S. S., 1954, D. Sc. Thesis, Calcutta University.
Gleissberg, W., 1942, *Astrophys. Jour.*, **96**, 234.; 1949, *Ibid*, **110**, 90.
Hanischmacher, E., 1951, *C. R. Acad. Sci. Paris*, **230**, 1301.
Minnis, C. M., 1952, *Jour. Atmos. Terr. Phys.*, **2**, 261.
Naismith, R., 1942, Paper No. RRB/C75, DSIR, England.
Saha, A. K., 1953, *Ind. Jour. Phys.*, **27**, 431.
Scott, J. C. W., 1952. *Jour. Geo. Res.* **56**, 396.
Tremellen, K. W. & Cox, J. W., 1947, *Jour. Inst. Elec. Engrs.*, Pt. III, **94**, 200.
Waldmier, M., 1944. *Mon. Not. Roy. Astr. Soc.*, **104**, 602.
Wilkins, A. & Minnis, C. M., 1951, *Ppoc.Inst. Elec. Engrs.*, **98**, 209.

CALCULATION OF DIPOLE MOMENTS OF THE TETRA-SUBSTITUTED BENZENES. PART I

K.V. GOPALA KRISHNA

MICROWAVE LABORATORY, ANDHRA UNIVERSITY, WALTAIR

(Received for publication February 21, 1956)

ABSTRACT. A general method is given for the calculation of dipole moments of 1, 2, 3, 4-tetra-substituted benzenes taking into account the dielectric constant of internuclear space in the field equations as suggested by Frank. The calculated value is given for 1, 2, 3, 4-tetra-chloro benzene for which the observed value is available and from a comparison between the calculated and the observed values it is seen that the agreement will be considerably improved when calculations are made using the field equations of Frank instead of the field equations of Smallwood and Herzfeld applied for the disubstituted compounds.

INTRODUCTION

The dipole moments of disubstituted benzenes are computed by Smallwood and Herzfeld (1930) taking into account the induced effects in the substituents; the method has led to values in better agreement with the experimental values than by the simple vectorial addition of the group moments. The same method was extended by Narasimha Rao (1955) for tri-substituted benzenes, and the agreement with the observed values was improved considerably by introducing a correction factor $(\epsilon+2)/3\epsilon$, as suggested by Lefevre and Lefevre (1936, 1937) to the total induced moment, ϵ being the dielectric constant of the internuclear space. A better approach to the calculation will be by introducing the factor ϵ directly in the field equations, as given by Frank (1935). This method is adopted in the present paper for calculation, in the case of 1, 2, 3, 4-tetra-substituted benzenes.

METHOD OF CALCULATION

The resultant moment of a tetra-substituted benzene is regarded as comprising of (i) the vector sum of the moments of the primary dipoles, (ii) the mutual induction of the four primary dipoles on one another and (iii) the moments induced in the unsubstituted $-\text{CH}$ groups and $-\text{C}-\text{C}$ bonds.

Figure 1 represents the positions of the primary dipoles of a 1, 2, 3, 4-substituted compound. The distances and various angles may be understood from the figure. The notation used is that of Smallwood and Herzfeld. $\xi_1, \xi_2, \xi_3, \xi_4$ represent the X -components, and $\eta_1, \eta_2, \eta_3, \eta_4$ the Y -components of the actual group moments m_{01}, m_{02}, m_{03} , and m_{04} respectively.

Using the field equations suggested by Frank (1935) which account for the dielectric constant of the internuclear space, the actual group moment m_0 of a dipole

which differs from that of the experimentally observed mono-substituted compound (m_s) due to the induced effects in the -C-C bonds and in the five unsubstituted -CH groups, can be given by

$$m_s = 1.843m_o$$

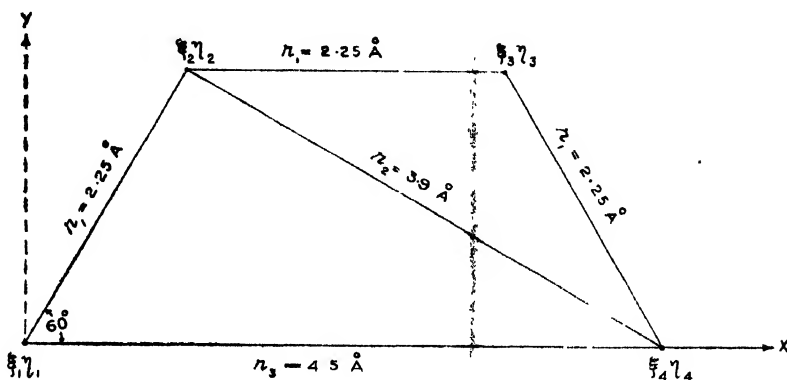


Fig. 1

The value of ϵ , as given by Lefevre and Lefevre (1937), is taken as 2.4 in the calculation.

The interaction of the four primary dipoles on one another gives the following relations.

$$\begin{aligned} \xi'_1 + 0.1528 a_1 \xi'_2 - 0.7939 a_1 \eta'_2 - 0.764 a_2 \xi'_3 - 0.7939 a_2 \eta'_3 - 1.223 a_3 \xi'_4 &= \xi_1 \\ \eta'_1 - 0.7939 a_1 \xi'_2 - 0.764 a_1 \eta'_2 - 0.7939 a_2 \xi'_3 + 0.1528 a_2 \eta'_3 + 0.6112 a_3 \eta'_4 &= \eta_1 \\ \xi'_3 + 0.1528 b_1 \xi'_1 - 0.7939 b_1 \eta'_1 - 0.764 b_2 \xi'_4 + 0.7939 b_2 \eta'_4 - 1.223 b_1 \xi'_3 &= \xi_2 \\ \eta'_2 - 0.7939 b_1 \xi'_4 - 0.764 b_1 \eta'_1 + 0.6112 b_1 \eta'_3 + 0.7939 b_2 \xi'_4 + 0.1528 b_2 \eta'_4 &= \eta_2 \\ \xi'_3 - 0.764 c_2 \xi'_1 - 0.7939 c_2 \eta'_1 - 1.223 c_1 \xi'_2 + 0.1528 c_1 \xi'_4 + 0.7939 c_1 \eta'_4 &= \xi_3 \\ \eta'_3 - 0.7939 c_2 \xi'_1 + 0.1528 c_2 \eta'_1 + 0.6112 c_1 \eta'_2 + 0.7939 c_1 \xi'_4 - 0.764 c_1 \eta'_4 &= \eta_3 \\ \xi'_4 - 1.223 d_3 \xi'_1 - 0.764 d_2 \xi'_2 + 0.7939 d_2 \eta'_2 + 0.1528 d_1 \xi'_3 + 0.7939 d_1 \eta'_3 &= \xi_4 \\ \eta'_4 + 0.6112 d_3 \xi'_1 + 0.7939 d_2 \xi'_2 + 0.1528 d_2 \eta'_2 + 0.7939 d_1 \xi'_3 - 0.764 d_1 \eta'_3 &= \eta_4 \end{aligned}$$

where

$$\begin{array}{lll} \alpha_1/r_1^3 = a_1 & \alpha_1/r_2^3 = a_2 & \alpha_1/r_3^3 = a_3 \\ \alpha_2/r_1^3 = b_1 & \alpha_2/r_2^3 = b_2 & \alpha_2/r_3^3 = b_3 \\ \alpha_3/r_1^3 = c_1 & \alpha_3/r_2^3 = c_2 & \alpha_3/r_3^3 = c_3 \\ \alpha_4/r_1^3 = d_1 & \alpha_4/r_2^3 = d_2 & \alpha_4/r_3^3 = d_3 \end{array}$$

$\alpha_1, \alpha_2, \alpha_3, \alpha_4$, represent the polarisabilities of the four substituent groups.

In the above equations for the interaction of the four primary dipoles, the fields of the induced moments are also considered since it is written that $\xi^1 = \xi + \xi_i$ and $\eta^1 = \eta + \eta_i$. The numerical values for ξ^1 and η^1 for each dipole can be obtained by solving the eight equations.

The induced moments by primary dipoles in -C-C bonds and in the remaining -CH groups at 5, 6 are calculated from Frank's field equations, using the angles and distances in Tables I and II respectively.

TABLE I

Group		1	2	3	4	5	6
I	r	1.3	2.6	3.438	3.438	2.6	1.3
	v	30°	30°	10°54'	-10°54'	-30°	-30°
II	r	1.3	2.6	3.438	3.438	2.6	1.3
	v	-30°	-30°	-49°6'	-70°54'	-90°	-90°
III	r	1.3	2.6	3.438	3.438	2.6	1.3
	v	-90°	-90°	-109°6'	-130°54'	-150°	-150°
IV	r	1.3	2.6	3.438	3.438	2.6	1.3
	v	-150°	-150°	-169°6'	169°6'	150°	150°

TABLE II

Group		5	6
I	r	3.9	2.25
	v	-30°	-60°
II	r	4.5	3.9
	v	-60°	-90°
III	r	3.9	4.5
	v	-90°	-120°
IV	r	2.25	3.9
	v	-120°	-150°

The total induced effect in the -C-C bonds and the remaining -CH groups is obtained as

$$\begin{aligned}\Sigma \xi_i + \xi'_i &= 0.8257 \xi'_1 - 0.05432\eta'_1 + 0.06343\xi'_2 - 0.4415\eta'_2 + 0.6794\xi'_3 + 0.4415\eta'_3 \\ &\quad + 0.8257\xi'_4 + 0.0543\eta'_4 \\ \Sigma \eta_i + \eta'_i &= -0.05432 \xi'_1 - 0.1382\eta'_1 - 0.4415 \xi'_2 + 0.5936\eta'_2 + 0.4415 \xi'_3 + 0.5936\eta'_3 \\ &\quad + 0.0543 \xi'_4 - 0.112\eta'_4\end{aligned}$$

Hence the resultant moment of the molecule is given as

$$M = \{M_x^2 + M_y^2\}^{1/2} \quad \dots (3)$$

where

$$\begin{aligned}
 M_x &= 1.8257\xi'_1 - 0.05432\eta'_1 + 1.0634\xi'_2 - 0.4415\eta'_2 + 1.6794\xi'_3 + 0.4415\eta'_3 + 1.8257\xi'_4 \\
 &\quad + 0.0543\eta'_4 \\
 M_y &= -0.05432\xi'_1 + 0.8618\eta'_1 - 0.4415\xi'_2 + 1.5936\eta'_2 + 0.4415\xi'_3 + 1.5936\eta'_3 \\
 &\quad + 0.0543\xi'_4 + 0.888\eta'_4
 \end{aligned}$$

RESULTS

The final result for 1, 2, 3, 4 tetra-chloro benzene, together with the experimentally observed values, is presented in Table III.

TABLE III

Compound	M_{expt}	$M_{\text{eqn(3)}}$	M'	M''	M_{vec}	m_e value
1, 2, 3, 4-Tetrachloro benzene	1.90	1.97	2.19	2.39	2.70	1.56

The value in column M_{expt} is due to Smyth and Lewis (1940). The value of m_e is also taken from their observations on monochloro benzene. The value under $M_{\text{eqn(3)}}$ is the value obtained by calculation from (3). M' represents a value obtained when the dielectric constant of the internuclear space is not taken into account in the calculation as done by Smallwood and Herzfeld (1930). M'' represents the value of the moment obtained by taking $(\epsilon + 2)/3\epsilon$ as a correction factor in the final value of the induced moment as done by Narasimha Rao (1955) in the calculation of tri-substituted benzenes. The value in column M_{vec} is obtained by simple vectorial addition of the group moments. The computed value is seen to agree well with the experimental observation when the dielectric constant of internuclear space is taken in the field equations, as done by this author.

ACKNOWLEDGMENTS

The author is highly indebted of Prof. K. R. Rao for his constant guidance throughout the progress of the work.

REFERENCES

- Frank, F. C. 1935, *Proc. Roy. Soc., A*, **152**, 174.
 Lefevre and Lefevre, 1936, *Jour. Chem Soc.* 1134; 1937, *Ibid*, 196; 1937, *Ibid*, 1088
 Narasimha Rao, D. V. G. L., 1955. *Ind. Jour. Phy.* **38**, 53.
 Smallwood and Herzfeld, 1930, *Jour. Am. Chem. Soc.* **52**, 1919.
 Smyth C. P. and Lewis, G. L. 1940. *Ibid*, **62**, 721.

A NUCLEAR MAGNETIC RESONANCE APPARATUS

A. K. SAHA, B. M. BANERJEE, T. P. DAS,* D. K. ROY,
S. K. GHOSH ROY AND T. GHOSE†

INSTITUTE OF NUCLEAR PHYSICS, CALCUTTA

(Received for publication February 12, 1956)

ABSTRACT. Following in the main Gutowsky's model, a nuclear magnetic resonance apparatus has been set up in this laboratory. It includes both Purcell's double bridge and marginal oscillator circuit for the detection of nuclear resonance signal. A Bloch head arrangement also, has recently been set up. Detailed account of the instrumentation is presented. Some records of the signal obtained by different techniques are also given.

INTRODUCTION

For the detailed study of the structure of solids and liquids and the nature of motion existing in them, a nuclear magnetic resonance apparatus is one of the most important tool in the hands of physicists and chemists now-a-days. The principle of the nuclear resonance experiments, from the classical point of view, is the detection of the Larmor precession of the magnetic nuclei about a strong magnetic field H_z . Due to the dissipation of energy of these magnetic nuclei to the surroundings, this Larmor precession would by itself be damped down. But by applying an oscillating field with frequency equal to that of the Larmor precession, at right angles to the steady magnetic field, the energy transferred to the surroundings is continually restored and a "resonance" precession of the magnetic nuclei occurs. This precessional motion is detected either by the voltage it induces in a separate "receiver" coil at right angles to the "transmitting" coil producing the *rf*-magnetic field or by the effect it produces on the transmitting coil itself. These two alternative detection techniques termed the "crossed-coil" and "single-coil" techniques have also come to be known as the Stanford and Harvard techniques respectively; the first mainly developed by Bloch *et al* (1946) and the second by Purcell *et al* (1948). The sample may also be put directly in the inductance arm of an oscillator circuit and whenever there is a resonance absorption of energy the voltage level will change in the tank circuit which can be amplified and detected. This is the main principle of marginal oscillator technique. The quantum mechanical point of view regards the *rf*-field as providing the requisite energy for transitions between successive Zeeman levels

*Now at Cornell University, Ithaca, U.S.A.

†Holder of A. E. C. Fellowship (Junior).

in the steady magnetic field, this energy being given by $\gamma\hbar H_z$ corresponding to the Larmor frequency $\omega_z = \gamma H_z$, where γ is the magnetogyric ratio $\frac{\mu}{\hbar}$, μ and I being respectively the magnetic moment and spin of the nuclei in question. Two pictures are thus equivalent.

The interaction of the nuclei with surrounding nuclei and atomic electrons gives rise to splitting, broadening and shift of the Zeeman levels, leading to corresponding splitting, broadening and shifts of the resonance line. The measurement of these effects require very good resolving power and can yield valuable information about the molecular and crystal structure of the surrounding lattice in which the nuclei are contained as well as the extent of internal motions within it. The magnetic dipolar interaction between a nucleus and surrounding nucleus is termed "spin-spin interaction", the order of which is denoted by a parameter T_2 , the spin-spin relaxation time. The interaction between nuclei might fluctuate due to the thermal motions in the lattice, in which the nuclear system is situated, leading to "spin-lattice interaction". This is taken into account by T_1 , the spin-lattice relaxation time. The different methods developed for measuring all these parameters have their own advantages, but for work involving high resolving power, the *rf*-bridge technique of Purcell *et al* is the most convenient and has been used by most workers interested in chemical investigations. An apparatus of this type has been set up in this laboratory, basing on the early design of Purcell and his collaborators. Suitable modifications have been made for tackling the problem of noise. An autodyne circuit has also been used for the continuous and longtime observations of weak signals. This whole apparatus is very similar to that of Gutowsky and his collaborators in many aspects. Recently a Bloch head arrangement, primarily set up for spin-echo experiments, has also been used for steady experiments.

This paper deals with the details of the instrumentation and some of the observational results. Section I gives a short sketch of classical theory of Bloch and the steady state solutions. The conditions have also been stated under which the steady state pattern of the nuclear resonance signal can be visualised. The theories of measuring relaxation times by different methods have also been shortly discussed. Section II deals with a detailed account of the different parts of the final set up of the apparatus. Records of performance of the apparatus including the magnetic moment of F^{19} are given in Section III.

SECTION I

A SHORT SKETCH OF THE THEORY INVOLVED

The classical theory of nuclear induction phenomena, as has been first given by Bloch, is as follows: The nuclear magnets contained in the sample is placed under the action of a steady magnetic field H_x in the z -direction and a rotating

or oscillating radio frequency field in the XY -plane. The equation of motion of the macroscopic magnetisation of the sample due to nuclear magnets will be given by

$$\frac{d\vec{M}}{dt} + \vec{i} \frac{M_x}{T_2} + \vec{j} \frac{M_y}{T_2} + \vec{k} \frac{M_z - M_0}{T_1} = \gamma \vec{M} \times \vec{H} \quad \dots (1)$$

$\vec{i}, \vec{j}, \vec{k}$ are the unit vectors along X, Y and Z direction respectively. γ is the magnetogyric ratio of the nuclei concerned. T_1 and T_2 are the two relaxation times introduced phenomenologically by Bloch to take into account the interaction of the nucleus with other nuclei and the surrounding lattice. T_1 is called the spin-lattice relaxation time and denotes the time in which the Z -component of the nuclear moment vector comes to the equilibrium value M_0 . T_2 is called the spin-spin relaxation time and is equal to the inverse of the line width. It measures the local field produced at a particular nucleus, due to neighbouring nuclei. If the field inhomogeneity produced over the sample be appreciable then T_2 is replaced by T_2^* the total transverse relaxation time.

The oscillating radio-frequency field along X -direction say, will be equivalent to two rotating radio-frequency fields polarised in opposite directions. Depending on the sign of γ , only one of these will be effective in producing resonance. Thus for γ positive, clockwise field is effective, and converse is the case for γ negative.

Initially, in the absence of the rf -field, \vec{M} points in the direction of the Z -field. With the switching on of the rf -field there will occur for some time a damped oscillatory and a periodic motion of \vec{M} . In this particular experimental set up, we are interested in the steady state motion of \vec{M} and not in its transient behaviour. The steady state solution of Bloch equation is given by

$$\left. \begin{aligned} U &= \frac{\omega_1 T_2^{*2} \Delta\omega}{1 + (T_2^* \Delta\omega)^2 + \omega_1^2 T_1 T_2^*} \\ V &= - \frac{\omega_1 T_2^*}{1 + (T_2^* \Delta\omega)^2 + \omega_1^2 T_1 T_2^*} \\ W &= \frac{1 + (T_2^* \Delta\omega)^2}{1 + (T_2^* \Delta\omega)^2 + \omega_1^2 T_1 T_2^*} \end{aligned} \right\} \quad \dots (2)$$

where U, V and W are the components of the unit vector parallel to \vec{M} in the rotating coordinate system.

$$\Delta\omega = \gamma H_z - \omega$$

$\omega_1 = \gamma H_1$, where H_1 is the amplitude of the rf -field.

The nature of variation of U and V components (the inphase and out-of-phase components of the rotating rf -field) are shown in figures (1.1a) and (1.1b).

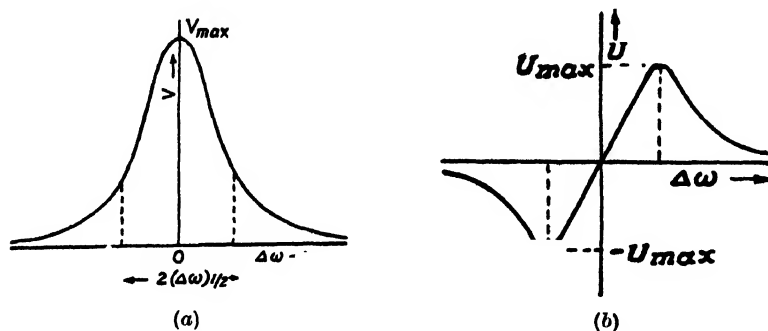


Fig. 1.1. Change of U and V with $\Delta\omega$

It can be easily shown that V reaches a maximum at $\Delta\omega = 0$, which is the condition of exact resonance. U is zero here but reaches maximum values on the two sides of it at

$$\Delta\omega = \pm \frac{1}{T_2^*} (1 + \omega_1^2 T_1 T_2^*)^{\frac{1}{2}}$$

As the amplitude of the rf -field is increased the maximum value of V increases continuously to the limit $\frac{1}{2} \left(\frac{T_2^*}{T_1} \right)^{\frac{1}{2}}$ at $\omega_1^2 T_1 T_2^* = 1$, and after that it starts to decrease. This condition is called the “saturation” condition.

In actual experiments the entire shape of the quantities U and V are obtained by modulating the Z -field at a slow audiorate about the resonance value. Under this condition these Bloch solutions do not strictly hold but Bloch has shown that when the speed of the modulation is sufficiently slow so that one can assume conditions of equilibrium at every stage of passage through resonance, then the solutions may be still correct. This is called the “slow adiabatic passage” the mathematical condition for which are

$$\left. \begin{aligned} \frac{d(\Delta\omega)}{\omega_1 dt} &\ll \frac{1}{T_1} \text{ \& \& } \frac{1}{T_2^*} \\ \frac{d(\Delta\omega)}{\omega_1^2 dt} &\ll 1 \end{aligned} \right\} \dots \quad (3)$$

The effects of rotation of the nuclear magnets can be looked at from two points of view: (i) they induce by their rotation, an alternating voltage with frequency equal to the Larmor frequency, in the transmitting coil itself in the Purcell experiment, or in another receiving coil as in the Bloch experiment, (ii) or it can

be considered as an absorption of power from the transmitter coil or transfer of power to the receiving coil, which appear as induced signals. The power P absorbed per unit volume by the sample can be shown to be equal to

$$P = \omega H_1 V = \frac{\gamma \omega H_1^2 T_2^* M_0}{1 + \gamma^2 H_1^2 T_1 T_2^* + (\Delta \omega T_2^*)^2} \quad \dots (4)$$

In the Purcell technique which has been followed here, there will be a fall in Q of the tuning coil oscillator circuit due to this power absorption and this will appear as a voltage signal

$$\delta V = - \frac{V_0 Q_0}{Q} = - \frac{P_0 \epsilon V_c}{(P_0/Z_0)^{1/2}} \quad \dots (5)$$

where

V_0 —value of the V at resonance

Q_0 —value of Q at resonance

ϵ —filling factor

V —volume of the sample

P_0 —power absorbed at resonance

Z_c —volume of the impedance at resonance.

From the shape, size and position of the resonance signal one can determine γ , T_1 and T_2 . γ is obtained from the relation $\omega = \gamma H_2$. The exact value of the steady magnetic field for which resonance occurs, together with a knowledge of ω , will give γ . Conversely, if γ is known, one can determine the magnetic field H_2 . T_2 the spin-spin relaxation time or T_2^* the total transverse relaxation time has to be determined from the line width measurement, the relations being given by

$$(\Delta \omega)_1 = \frac{2\sqrt{Z}}{T_2^*}$$

T_1 can be obtained from the saturation condition.

SECTION II

AN ACCOUNT OF THE INSTRUMENTATION

Work began in this laboratory following Purcell's double-bridge arrangement for detecting nuclear resonance signal. A block diagram of Purcell's arrangement is shown in the figure (2.1).

Rf-power is fed from a signal generator into a unit containing phase shifting arrangement, a *rf*-double-bridge and a pre-amplifier, the sample coil of the bridge being contained in a probe which is placed in the magnetic field. The main magnetic field is modulated by two coils of Helmholtz proportions. The signal

after amplification by the preamplifier is fed into a receiver where it is further amplified and detected. The detected signal is applied to vertical plates of an oscilloscope, to the horizontal plates of which is fed a voltage in phase with the applied modulating field. Power for field modulation is derived from a low-frequency sine-wave generator. With low amplitude modulation i.e. with modulation amplitude less than the line width, the detected output from the receiver is analysed by a "lock-in" amplifier and mixer circuit, the output of which will give a derivative of the original signal and it is recorded by a pen-recorder. The use of slow sweep circuit avoids the transients which distort the line shape.

This is in short the mechanism of Purcell's technique. In the original set up of the apparatus in this laboratory, Purcell's arrangement was more or less followed. Modifications were made in the use of a preamplifier in the bridge box itself and a phase-shifting arrangement for *rf*-input to the two arms of the double bridge done by a transformer instead of coaxial cable of requisite length as done by Purcell.

The main difficulties encountered in the progress of the work can be summarised as follows:

- (1) Microphonics,
- (2) Electrical noise,
- (3) Field-inhomogeneity problem,
- (4) Field stabilization problem.

Microphonics were produced mainly by mechanical disturbances. These led to vibrations of the bridge components, coils and capacitors, giving rise to corresponding electrical output, the bridge and the receiver amplifier system acting almost like a microphone. So there were regular vibrations of the signal pattern on the oscilloscope screen. Initial attempts in eliminating these disturbances were made by constructing a rigid platform for holding the bridge box. Microphonics were reduced somewhat but not eliminated. Then the magnet was placed on a sand-bed foundation. Finally the whole equipment was shielded from all sides by placing it inside a specially built room constructed of aluminium and lined with cellotex and rubber.

The next important problem was the minimization of electrical noise. Purcell's theoretical analysis shows that the signal-to-noise ratio, apart from external noises, depends upon the constants of the detecting arrangement and the applied field in the following manner, viz.

$$\frac{A_s}{A_n} \propto \frac{V_c^{2/3} \epsilon N_0 H_z^{1/4}}{B^4} \left(\frac{T_2^*}{T_1} \right)^{1/2} \quad \dots (6)$$

A_s and A_n being the signal and noise amplitudes and

V_c —volume of the coil

ϵ —filling factor of the sample

N_0 —number of nuclei in the sample

H_z —value of the steady magnetic field

T_2^* —total transverse relaxation time, given by the relation $\frac{1}{T_2^*} = \frac{1}{T_2} + \gamma\Delta H$,

(T_2 representing the natural spin-spin relaxation time and ΔH the inhomogeneity of the field over the sample.)

T_1 —spin-lattice relaxation time

B —band width of the receiver.

Now considering the case where there is no field inhomogeneity i.e. the entire width of the resonance line is due to natural causes alone, it is evident that one can enhance the signal-to-noise ratio in the following way. If ϵ be same for a certain number $\epsilon V_c N_0$ of nuclei the signal to noise ratio is proportional to $V_c^{-1/3}$ as V_c is changed; so the smaller the coil volume the better, which automatically implies a larger filling factor. Secondly, one can work at a higher frequency and a corresponding larger value of field viz. H_0 .

In the case where the field inhomogeneity dominates the contribution to the line width, the above considerations get modified. From the expression just cited, the signal-to-noise ratio is proportional to $\left(\frac{T_2^*}{T_1}\right)^{1/2}$ and T_2^* is reduced from the natural value T_2 , in the presence of field inhomogeneity, leading to a consequent reduction in signal to noise ratio. In such a case, an increase of field H_z is likely to contribute to the inhomogeneity linearly and the signal-to-noise depends on H_z in the ratio $H_z^{3/4}$ only, as pointed out by Gutowsky (1953). Further, increase of sample size is also not likely to enhance the signal-to noise ratio as it may lead to greater inhomogeneity and hence smaller T_2^* . In such a case the best procedure is to go on decreasing the sample volume till the width of the signal is as close to the natural width as possible. The signal strength will not suffer much, as the loss in signal strength due to the reduction in V_c could be compensated by the increase in T_2^* due to smaller inhomogeneity. The procedure has been followed here by regularly decreasing the sample volume. The results will be reported later on.

The equation (6) gives values of signal-to-noise ratio only if internal Johnson and shot noise are reckoned with and there is no pick up of stray external noises. In actual practice, as has already been pointed out, the apparatus picks up considerable amount of external noises of both electrical and mechanical origin and this causes a great decrease in signal-to-noise ratio from that given by equation (6). This has been eliminated to a great extent by using a preamplifier in the bridge itself and putting the whole equipment in a shielded room.

The electrical power input into all the apparatus such as the signal generator (G.R. 805C), receiver (Hammerland BC 779B) and the cathode ray oscilloscope (DuMont 304A) was fed through isolating transformers with *rf*-filters at input. It was found that the cables pick up considerable amount of electrical disturbance inspite of their shields and of all conceivable grounding arrangements for them. The use of preamplifier makes the signal sufficiently strong before being put in the cable.

The procedure that was next followed for increasing the signal to noise ratio and for obtaining better resolutions of signal line, was to increase the homogeneity of the magnetic field over the sample volume. The smaller magnet was found to be inconvenient to be further plane-polished. So a big magnet with pole diameter 12" and separation 2" with a double yoke was designed and constructed. The signal pattern obtained with this magnet is shown in figure (2.28) Due to

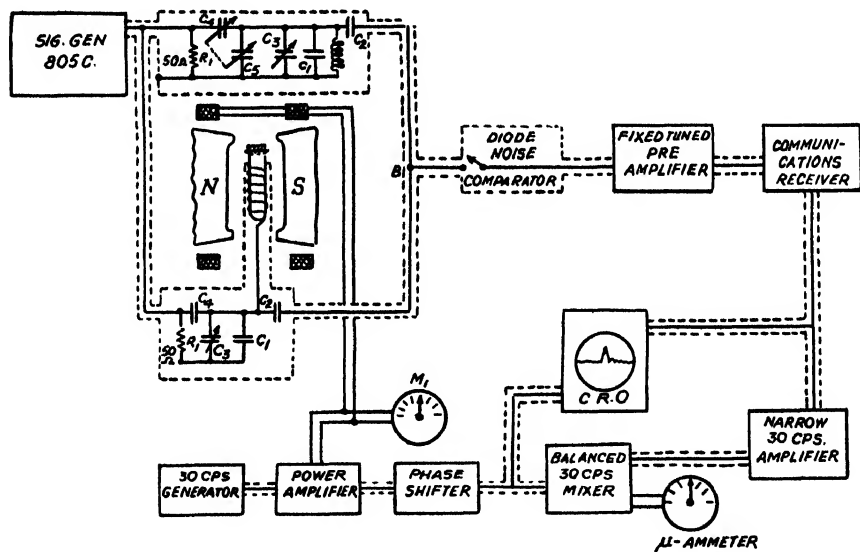


Fig. 2.1. Block diagram of Purcell bridge arrangement.

better homogeneity, wiggle patterns appear even with 25 cycle field modulation. The patterns appear whenever there is violation of Bloch's slow passage condition and greater homogeneity over the sample. As these transient patterns sometimes create difficulties in actual measurements of line shape, these are to be avoided and steady pattern restored. This was done by using a slow sweep modulation of the field so that slow passage condition was always maintained. The rate of passage can be determined from the relation $a T_2^* \ll 1/2$, where $a = \gamma \left(\frac{dH_z}{dt} \right)$. Moreover, this arrangement has the advantage of suppressing noise by limiting

amplified *rf*-voltage is fed to the transmitting coil by a coupling link as shown in figure (2.3). Necessary shielding arrangements have been made to prevent

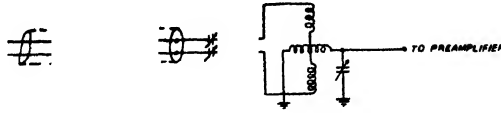


Fig. 2.3. Inducting coupling link.

the receiver from the direct pick-up from the transmitter. The transmitter has a high frequency stability and does not inject electrical noise.

Magnet : As mentioned before, earlier experiments were carried out with a small magnet with pole faces vertical to the pole diameter being 4" and the pole-gap being adjustable. The magnet gave a field of about 1100 gauss per ampere, the dependence on current being linear upto about 6 amperes. The magnet had a yoke only on the lower side. At the best position there was an inhomogeneity

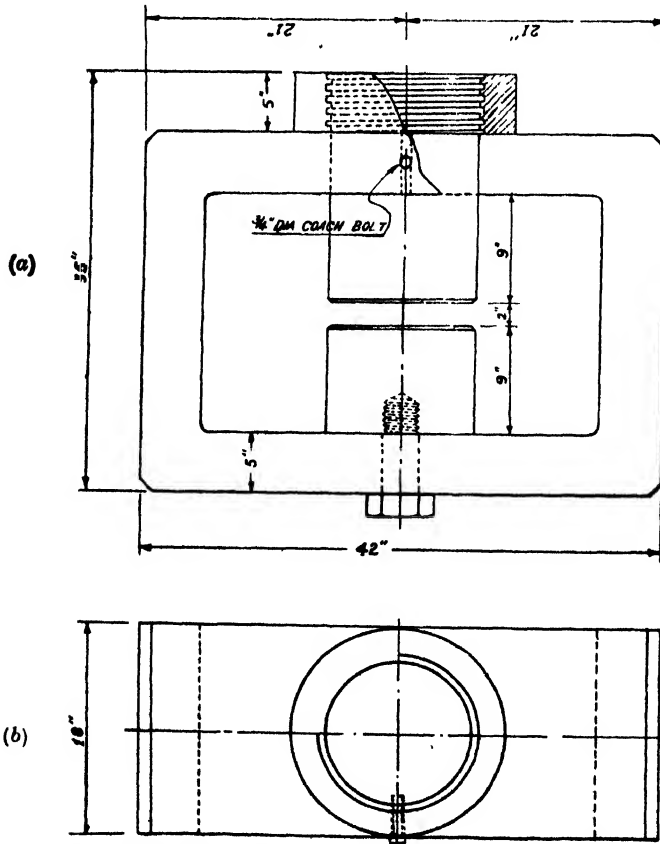


Fig. 2.4. Plan of the big magnet. Bottom shows the elevation.

of about 0.5 gauss per cm. at 3500 gauss. The modulating coils were wound on a pair of brass rings which were fixed rigidly to the pole-faces. The separation between the two was about 1 " and each contained about 500 turns of enamelled SWG 30 copper wire. The modulating field was measured both by the voltage induced in a pick-up coil and also by monitoring the magnet current to move the signal from one end of the sweep to the other; the field was found to be about 3.5 gauss per 100 mA. The magnetic field was measured at different values of the magnetising circuit and compared with crystal measurements, using Krishnan's theory. The big magnet is shown in plan in figure (2.4) and after assembly in figure (2.5). The pole-pieces are of cast steel having very low carbon content, each 9" long and 12" in diameter, with faces horizontal, the distance between

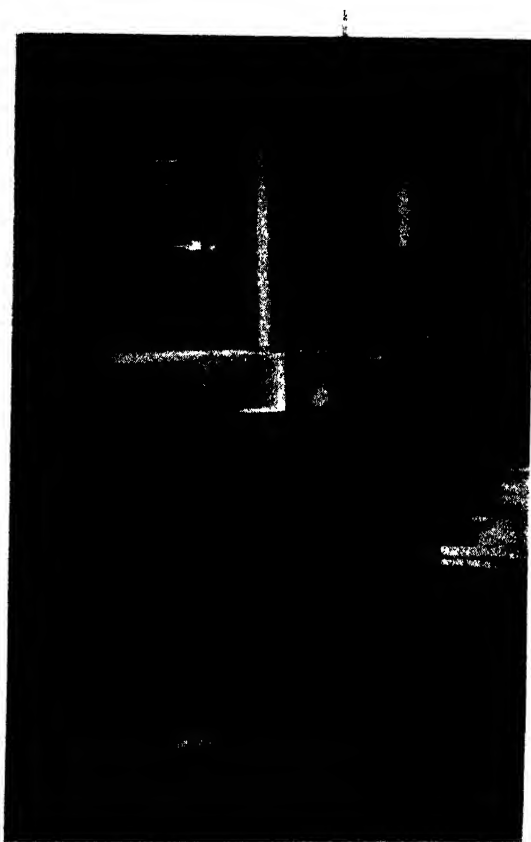


Fig. 2.5. Assembly of the big magnet.

the two being adjustable from 2" to 4" by moving the upper pole-piece, but work is mainly done with minimum separation i.e. 2". The yoke is rectangular—of size 16" \times 20" and about 5" thick. It is also of low carbon content but of cheaper

material than the pole pieces. The magnet has been cast by the Bhartia Electric Steel Co. and pole faces were worked to a parallelism correct to $1/20,000''$ over the entire pole-gap by Mr. G. C. Mondal of the Institute. The magnet gives a field of about 1000 gauss per ampere at 2" pole separation and the dependence of field on the magnetising current has been tested to be linear up to 10 amperes. The coils for either pole-piece are built of 3 cakes, each of 667 turns of SWG 12 enamelled D.C.C. copper wire. They were fabricated by the Associated Electrical Industries (India) Ltd.

The modulating field is produced by a pair of coils of Helmholtz proportions fixed to the probe. The formers are of perspex with a diameter of 3" and separation of about 1.5". About 15 turns of enamelled SWG 30" wire has been employed. That the modulating field itself does not produce much inhomogeneity has been tested by observing that the signal width remains sensibly constant for different values of the modulating field.

The measurement of the field contour has been done by both audio mixer record and slow sweep record of actual signal width with glycerine sample whose natural width is almost 5 milli gauss. The results of these measurements are discussed in the next section. The inhomogeneity has been found to be 25 milli-gauss at 3500 gauss i.e. 1 in 1.4×10^5 over the central region of the pole faces. The measurements of field contours at different vertical planes show that the pole faces are plane-parallel.

The Rf-bridge Unit: The next component of the apparatus is a composite unit incorporating the *rf*-transformer, Purcell's bridge and a *rf*-preamplifier. The bridge and the preamplifier are contained in a brass box of dimensions $8'' \times 4'' \times 3''$ with wall thickness $3/16''$. It is divided into three equal sections along the length. In the two extreme sections the condensers of the two arms of the bridge are incorporated. In the middle section is placed the preamplifier unit, the power to which is fed through a twin coaxial cable from the power supply of the receiver; cable also serves the purpose of transmitting the amplified signal to the receiver.

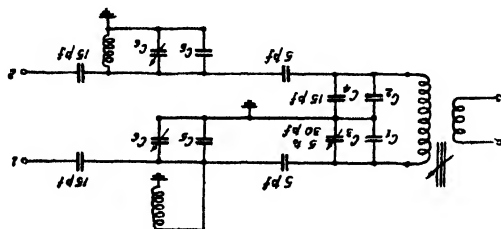


Fig. 2.6. Purcell's double bridge arrangements.

The transformer is enclosed in a separate brass box of length and breadth 4" and 2" respectively and height about 1" with wall thickness about $1/16''$.

This box is fixed on the top of the main box and its output is led through two holes in the lid of the box to the two arms of the bridge. The circuit diagrams for the *rf*-transformer and Purcell bridge are shown in figure (2.6). The *rf*-transformer consists of an untuned primary and tuned secondary. The inductances of the primary and secondary are respectively $0.1\mu h$ and $1.7\mu h$, the turns ratio being 1:8. The secondary has a *Q*-factor of 105 at 7.9 Mc/s. The out-puts at the two arms of the secondary are equalised by the variable air condenser variable from 5 to 30 μf . C_1 and C_2 are fixed ceramic condensers of 100 μf and C_4 is a fixed ceramic condenser about 15 μf . The ratio of the input voltage at the primary and output at the secondary terminals is about 1:3. The two arms of the *rf*-bridge circuit are nearly identical as far as the inductance and capacities involved are concerned.

The inductance part is contained inside two probes—one dummy and the other for holding the sample. Details of them are discussed later on. The outputs of the two arms of the bridge is led to the 2 poles, 1 and 2, of 3-pole 3-way band switch. This band-switch can either feed the two outputs of the two arms individually or together into the grid of 6AK5 preamplifier tube.

The preamplifier consists of two sections shown in figure (2.7). The last section is incorporated in the bridge and second section in a small brass box at

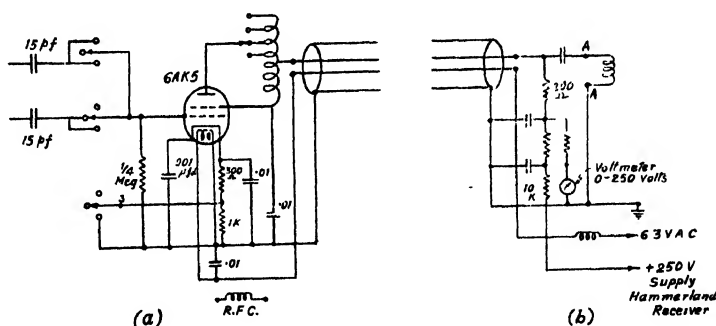


Fig. 2.7. Circuit diagram of the preamplifier.

the end of the Hammerland receiver. The preamplifier is of low noise design and has nearly a constant amplification factor, over a band of frequency of 2 Mc/s. The output of the plate of the preamplifier is led out through one conductor of the shielded twin cable which also carries the plate voltage from the receiver power supply. The other conductor of the cable feeds the filament of the 6AK5 tube. The amplified signal is taken through a condenser from the plate to the antenna terminal of the Hammerland receiver.

The Probe Arrangement:

There are two probes attached to the two arms of the bridge one for holding the sample and the other containing dummy coil. The probe system used in ini-

tial experiments is shown in figure (2.8). The length of the sample probe which

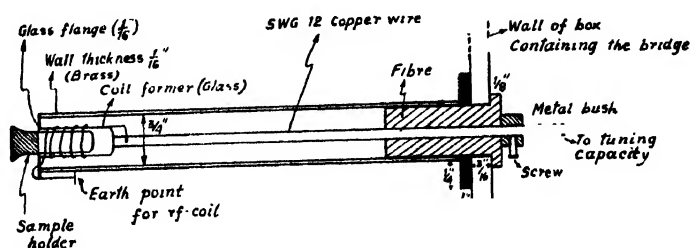


Fig. 2.8. Diagram of the old probe arrangements.

is introduced in the magnetic field is 20" while that of the dummy probe is about 6". These are made up of brass. The coil former is made up of glass.

Specifications for the *rf*-coils used in the two bridges are as follows:

$$5.7 \text{ Mc/s} \quad 11\mu H$$

$$14 \text{ Mc/s} \quad 1.86\mu H$$

With the progress of work it was felt necessary to reduce the sample volume in order to diminish the field inhomogeneity. The subsequent sample holder was made up of perspex, a diagram of which is shown in the figure (2.9). The volume of the sample was then 0.1 c.c. Gradually it was diminished upto 9 mm³. In order to increase the filling factor immersion type *rf*-coils were used. The *rf*-coils being put directly inside the sample hole. All these procedures did not diminish the signal amplitude to any marked extent. So the only conclusion is that loss in signal amplitude due to smaller volume of the sample is compensated by the gain due to smaller field inhomogeneity over the sample volume.

The sample holder was then made of the plug-in type so that it might easily be detachable from the bridge. A diagram is shown in figure (2.10). A brass

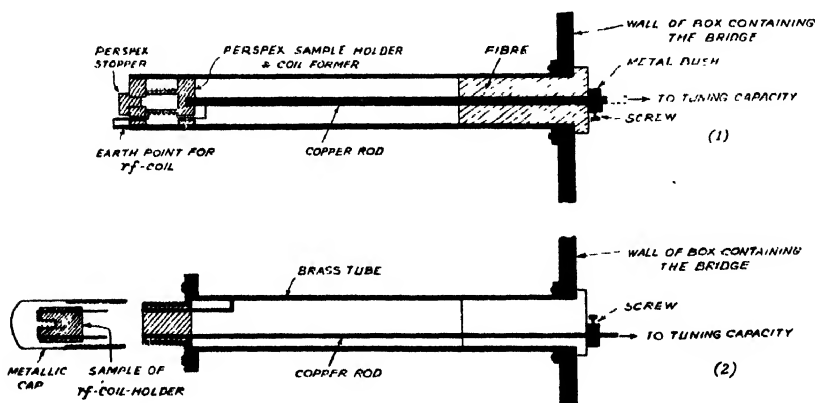


Fig. 2.9. Perspex sample holder. (Top). Fig. 2.10. Detachable sample holder (Bottom).

cap was used to cover up the mouth of the container. Strangely enough it was found that the cap produces a large amount of inhomogeneity so that the wiggle pattern vanished and a broad signal was observed. This led to the idea that there might be some magnetic impurity in the material of the brass used. A chemical analysis showed the presence of .1% of Fe—somewhat greater than the imported brass usually have. So to eliminate the possibility of any inhomogeneity being produced by the magnetic impurity, the probe inside the magnet was constructed of pure electrolytic copper.

Receiver: The receiver used for Purcell's bridge arrangement is a Ham-merland BC779B. It has a maximum gain at the second detector stage of about 10^5 at the frequencies used. The tuning of the receiver is not very stable and needs adjustment very often when the minimum band-width is used. The output to the oscillo- scope is taken directly from the 2nd detector stage, as the audioamplifier stages distorts the signal shape. The receiver used for Bloch arrangement has a band width of 100 Kc/s at 14 Mc/s. It is superheterodyne receiver having inter- mediate frequency of 5 Mc/s. The receiver has a low noise figure and has a maxi- mum amplification of 10^4 .

Oscilloscope: The oscilloscope is a DuMont 304A. Its special feature is the D.C. amplifier in the Y-plate circuit which can amplify signal voltages as low as 0.1 volt without any distortion in the signal shape. There is provision for ampli- fication of the input voltage to the X-plate also. A linear sweep circuit is also provided which can give frequencies of sweep as low as 2 cycles/sec. By the use of an external condenser the external sweep can be reduced upto 0.5 c.p.s. which is being used here during the slow sweep modulation circuit.

25-Cycle generator: A 25 cycle generator is used to provide power for audio modulation of the field. 25 cycle being a sub-harmonic of the mains frequency (50 cycles) the spurious mains noises are being avoided. The use of smaller frequency has been preferred in this laboratory due to these reasons:

First, the use of higher frequency will make the wiggle and other transients more prominent thus vitiating the signal shape measurements.

Secondly, the use of smaller frequency will make the signal amplitude stronger as the moment vector will then have more time between successive passages through resonance.

Thirdly, the use of higher frequency produces other spurious effects like eddy current, the removal of which is difficult and troublesome.

The circuit (figure (2.11)) is based mainly on the design of the 30 cycle generator used by Bloembergen *et al.* The only difference lies in the use of 25-cycle twin-T filters instead of 30-cycle filters. The circuit consists of four stages, the first stage is a multivibrator which oscillates locked at half the mains frequency

Phase-shifter Circuit: The circuit diagram is shown in figure (2.13). It is necessary to synchronise the phase of the input voltage to the *X*-plates of the oscilloscope with the signal voltage on the *Y*-plates; (the latter follows the phase of the modulating current), otherwise the signal on the oscilloscope splits into

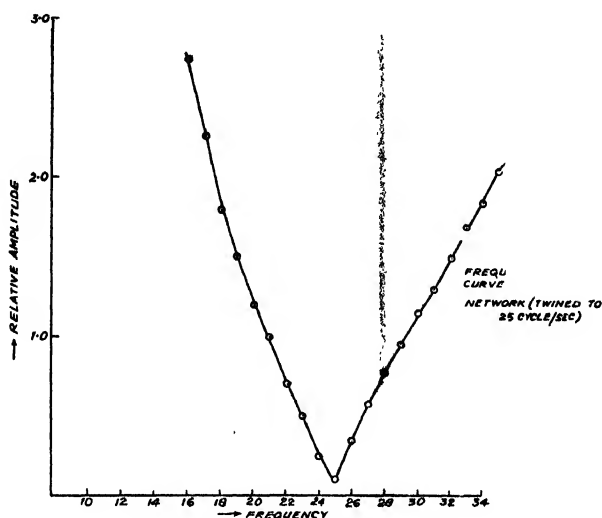


Fig. 2.12. Characteristic curve of twin T network.

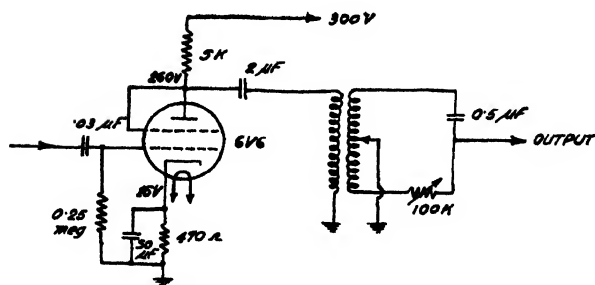


Fig. 2.13. Phase shifter circuit.

two as shown in figure (2.14). The circuit consists of an audio amplifier employing 6V6 tube which amplifies the output from the 25-cycle generator and a

RC phase shifting arrangement. The phase can be controlled by varying the resistance of the variable potentiometer. The audio amplifier is used to get sufficient output of 25 cycle voltage required for the mixer circuit.

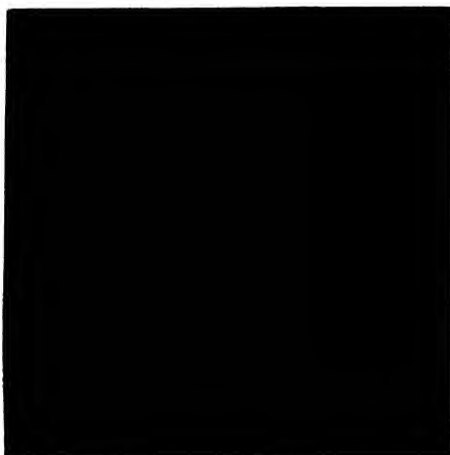


Fig. 2.14. Splitting of the signal (H in glycerine) due to phase difference.

The "Lock-in" amplifier and Mixer circuit:

Two such circuits have been set up here on employing valve-mixing (figure (2.15) and the other transformer mixing figure (2.16) properties. The basic

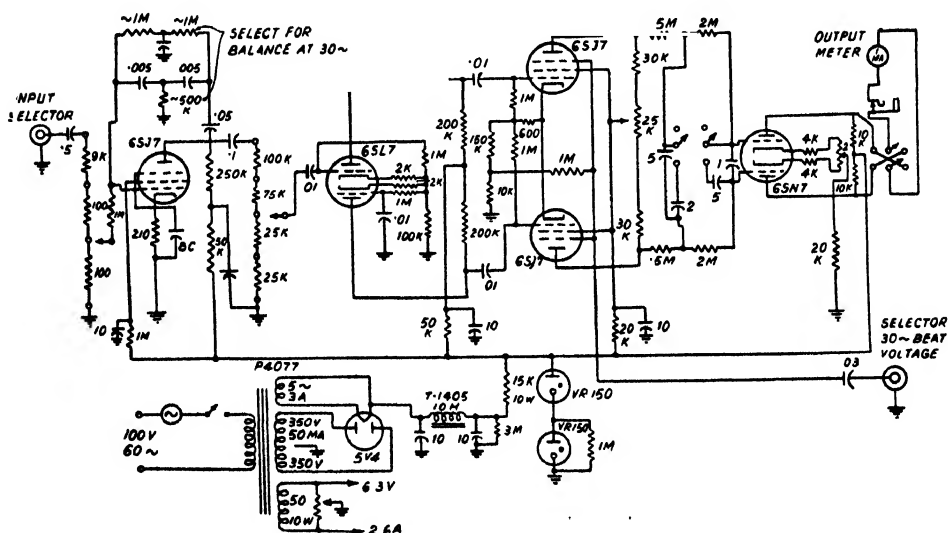


Fig. 2.15. Valve mixer circuit.

principle of this method of detection is as follows: If the Z-field is modulated by a 25-cycle sinusoidal wave having amplitude equal to a small fraction of the line

width then a 25 cycle sinusoidal output will be obtained as shown in figure (2.17), proportional to the slope of the signal at the point where the d.c. field is maintained.

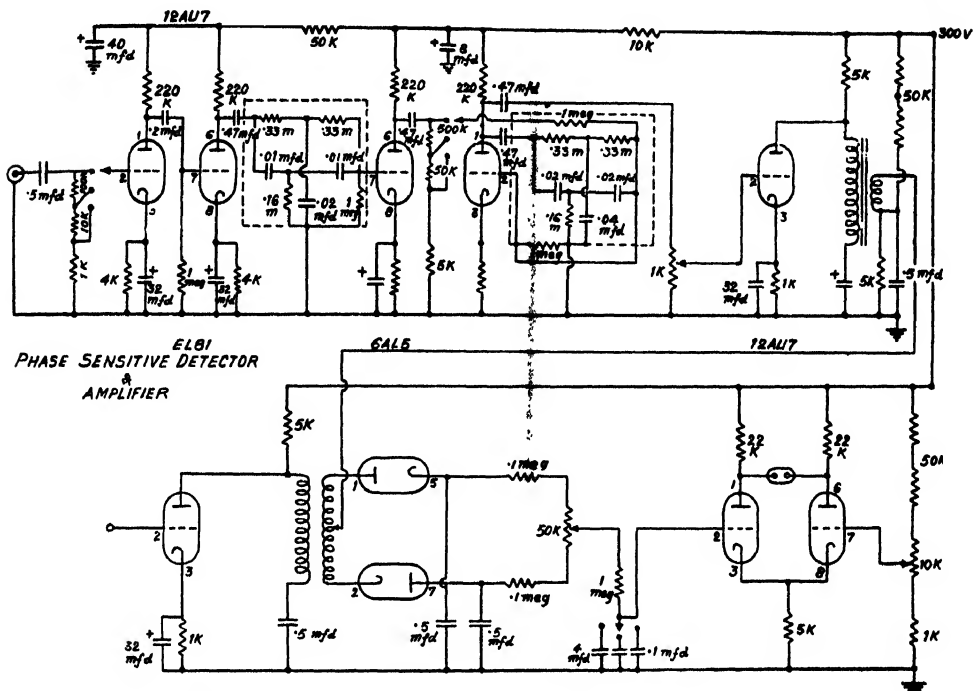


Fig. 2.16. Lock in amplifier (transformer mixing) circuit.

now the d.c. field is slowly varied, the amplitude of the 25 cycle output will give a curve as shown in figure (2.18). So a circuit has to be devised which gives

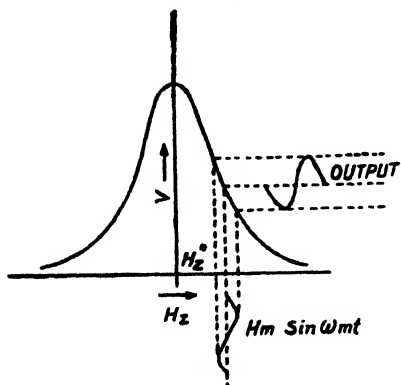


Fig. 2.17. 25~small amplitude modulation of the signal.

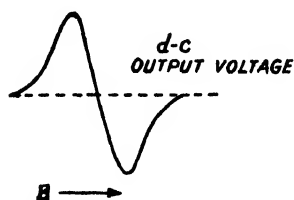


Fig. 2.18. Derivation curve of the absorption signal.

sufficient d.c. output proportional to the amplitude and phase of the above 25 cycles output. The distance between the two maxima of the derivative curve will give the line width directly.

The "lock-in" amplifier circuits have been constructed to serve the above purpose. The mixer consists of three stages—amplifier stage, mixer stage and d.c. amplifier stage. In the valve mixer circuit, two 6SJ7 tubes in push-pull arrangement, with beat voltage to the suppressor grid and signal voltage fed to the two control grids in opposite phases, gives the d.c. output proportional to the amplitude of the signal voltage. This d.c. voltage output is then fed into a d.c. amplifier which drives the pen of the Esterline Angus recorder. There is a long time-constant integrating R.C. network after the mixer part which averages the output signal and thereby eliminates most of the noise fluctuation.

In order to make the circuit behaviour more stable and to get a wide range of linearity, a transformer mixer has recently been set up. A comparative study of the two mixer circuits is made in Table I.

Slow-sweep Circuit: The circuit used to obtain a linear modulating current for the modulating coils with a minimum sweep frequency 0.5 c.p.s is shown in figure (2.19). The sweep voltage occurring at the terminals of the external capacitors of 8 mfd., that must be connected to the DuMont model 304A scope, is applied to a cathode follower stage which is one half of the 6SN7 tube. A stage

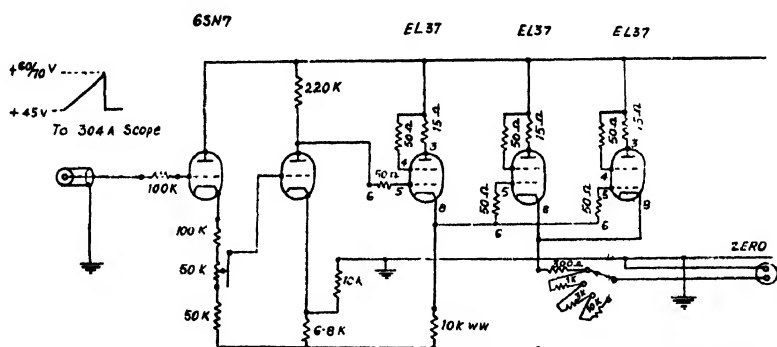


Fig. 2.19. Slow sweep circuit.

of d.c. amplification is provided by the other half of the 6SN7 tube. This is followed by an EL37 tube acting as a cathode follower driving two EL37 tubes, in parallel which provide the requisite output current. The value of the output current is adjustable by the resistance chain in the cathodes of the power amplifier stages. Out-put of the order of 100 mA can easily be obtained with this arrangement. Records of actual signal shapes obtained with slow sweep technique are shown in figure (2.20). The transients have been completely avoided and the signal to noise ratio has also considerably increased.

Low frequency function Generator: This is a Hewlett Packard model 202A. It gives output of sinusoidal, triangular and square waves, over a frequency range

of .01 to 1200 cycles. The output of this circuit is fed directly to the slow sweep circuit which gives the required current output for modulating the magnetic field.



Fig. 2.20. H' signal (in glycerine sample) obtained with slow sweep technique.

Thus z -field modulation of a wide frequency range can be done with this arrangement.

D.C. amplifier for driving pen-recorder with the signal output obtained by a slow variation of the D.C. field:

This circuit is employed to record the signal shape by varying the magnetic field synchronously with a pen recorder as described above. The circuit diagram is shown in figure (2.21). It consists essentially of two successive difference amplifier stages. At the first stage, the difference between the rectified signal voltage

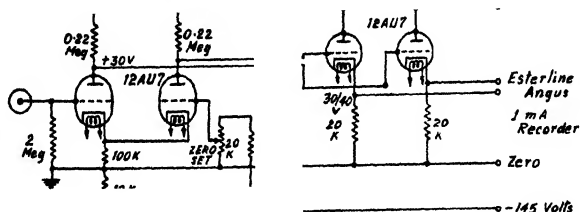


Fig. 2.21. Circuit diagram of the D.C. amplifier.

from the receiver and a standard reference voltage is amplified and fed to the grid of another difference amplifier stage. The output current from the cathodes

of this last difference amplifier stage is recorded on the Esterline Angus recording milliammeter.

Helipot arrangement for varying the magnetic field:

In order to vary the magnetic field synchronously with the pen recorder for audio mixer record, a helipot is run by the motor of the pen recorder itself. The helipot has a resistance of 50K and consists of 15 turns of helically wound wire. The potential tapped from a dry battery changes as the helipot is varied. This voltage variation is then put to the input of the slow-sweep circuit which feeds the requisite current to a separate pair of coils over the modulating coils.

Marginal Oscillator Circuit: There are two main disadvantages of the bridge circuit—first, the bridge balance does not remain steady for a long time and there is a continual change of V mode to U mode. So for a long time scanning, the pen-recorder records of derivative of the signal shape give an erroneous result, and the interpretation of the data becomes difficult. Secondly, the electrical noise from the signal generator makes the signal to noise ratio poorer with the bridge arrangement. The marginal oscillator circuit records only absorption signal and also dispenses with the signal generator. The first built for this purpose is a very simple one employing a simple 6AK5 tube. The circuit diagram is shown in figure (2.22). The sample is placed in the inductance part

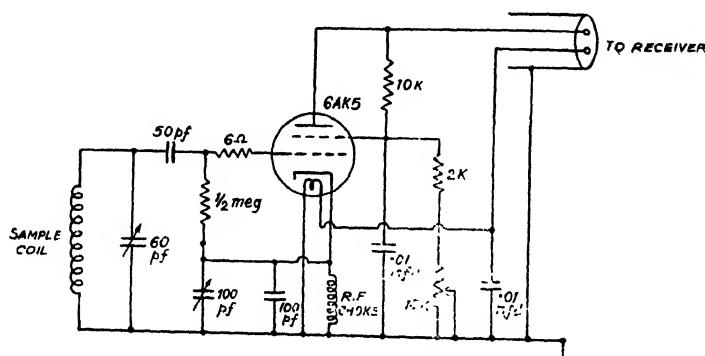


Fig. 2.22 Marginal oscillator circuit.

of the oscillator itself. The oscillator is a modified Colpitt's circuit. The design is similar to that of Hopkins with some modifications. The output is taken directly from the plate to the antenna of the receiver which further amplifies the signal. This is then displayed on the oscilloscope screen. Signals obtained with this circuit are shown in figure (2.23). The operation point has to be critically set in order to obtain maximum signal-to-noise ratio.

In order to avoid the use of the receiver, a new marginal oscillator employing a pre-amplifier and audio-amplifier is now being set up.

Further a Wang's type of spectrometer for quadrupolar work using the autodyne technique is now under construction.

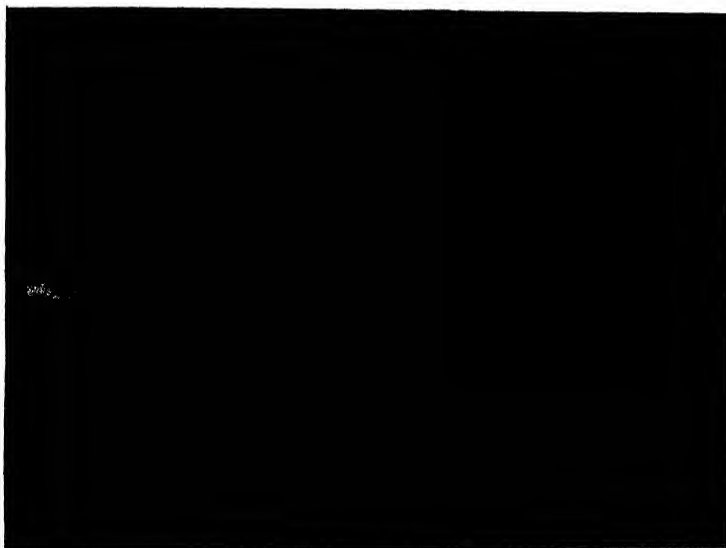


Fig. 2.23 H' signal in glycerine with the autodyne detector

Cryostat Arrangement: For the study of relaxation times at low temperature, a cryostat giving a temperature upto liquid air temperature has been set up in this laboratory. The design is shown in figure (2.24). It essentially consists

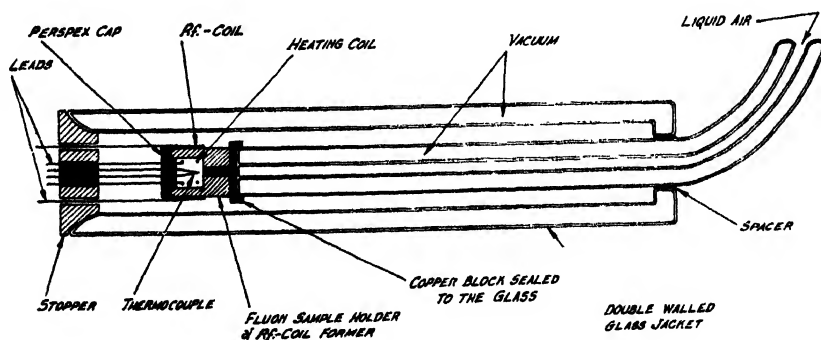


Fig. 2.24 Design of the cryostat.

of two parts—one part containing the sample, *rf*-coil, thermocouple and the heater element, and the other the Dewar vessel part. Care has been taken to minimise loss of heat as far as possible. The Dewar vessel part consists of an inner double-walled glass vessel containing the liquid air and an outer double-walled vessel

to shield the whole arrangement. Liquid air is poured into the vessel through one funnel at the extreme corner. A copper disc with a small copper rod is sealed by araldite cement to the other end of the Dewar vessel. The small copper rod is attached to the sample holder made up of fluon over which *rf*-coil is wound. A thermocouple element and wire which can be heated up by passing current through it are introduced within the sample. By controlling the current in the heater coil the temperature inside the sample can be conveniently controlled. Arrangements for automatic recording of the temperature on the signal record chart by a double pen recorder is now being made.

The Bloch Head:

The Bloch head of our arrangement is somewhat like that of Protector and Yu's. The transmitting and the receiving coils are housed in a copper box of dimension $3\frac{1}{2}'' \times 3\frac{1}{2}'' \times 1\frac{1}{2}''$. A block diagram is given in the figure (2.25). The

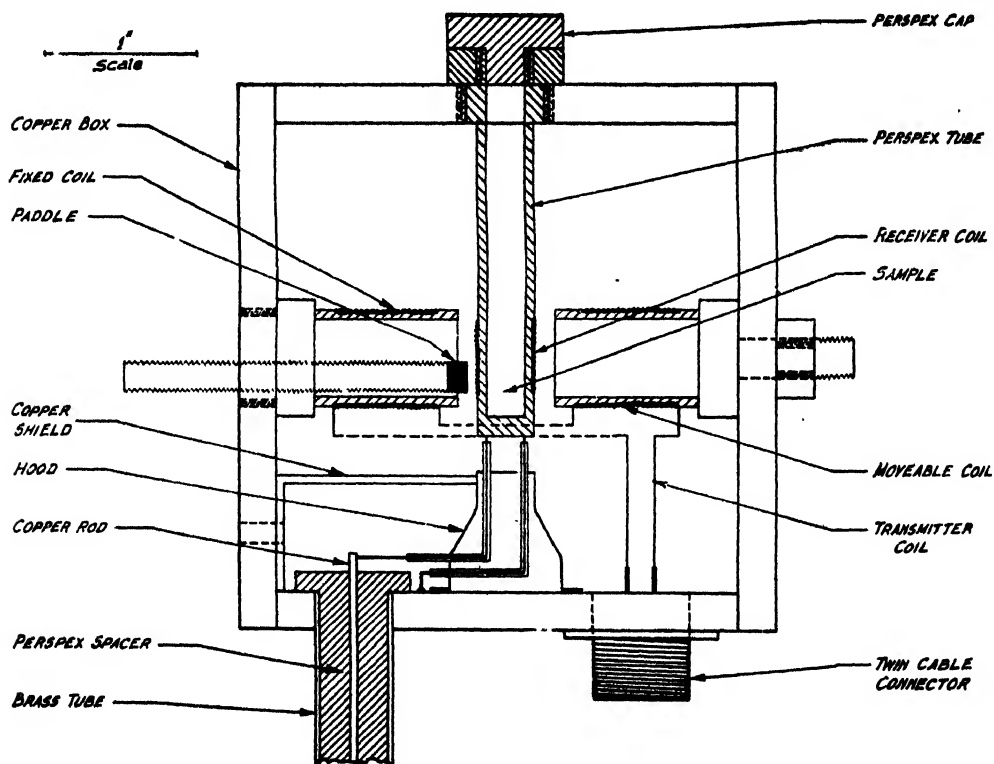


Fig. 2.25. Diagram of the Block head.

transmitter coils are wound in Helmholtz proportion on two perspex rods, made hollow partially. One of them is held fixed by screwing itself to one wall of the box and the other fixed to the opposite wall having some play for the sideways

movement. In between the two sections of the transmitting coil is placed the receiving coil wound on a perspex cylinder placed at right angles to the former. Inside the cylinder the sample is placed. Through the fixed section of the transmitting coil holder passes a small threaded perspex rod eccentrically, carrying a small copper disc of $3/16$ " diameter, at its end for the fine V-mode control. For the U-mode control the transmitter coil is series resonated with two condensers (mentioned earlier) at its ends, so that the *rf*-voltage at the centre of the transmitting coil can be brought near the earth potential and the voltage induced in the receiving coil due to capacitative coupling is minimised to a large extent. By this arrangement we have achieved a voltage reduction of the order of 1 in 10^5 . Two coils in the Helmholtz proportions were placed over the Bloch head for the modulation of the steady field.

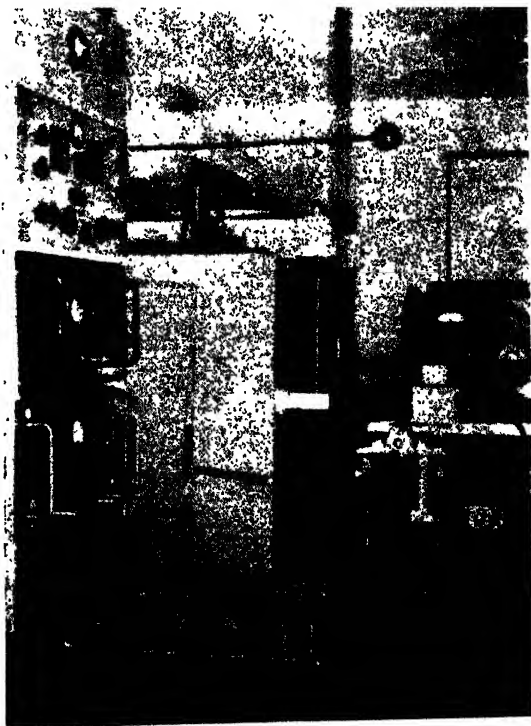


Fig. 2.26. Assembly of the whole apparatus.

Assembly of the Apparatus: The whole assembly is shown in figure (2.26). The most important points to remember are that all parts of the apparatus must

be properly shielded, they must have a common ground and all connections must be made with shielded coaxial cables of the shortest possible lengths, to avoid stray noise pick up. To avoid microphonics and electrical noise pick ups, as mentioned before, the entire apparatus is being shielded by keeping it inside a room with aluminium walls lined with cellotex and with rubber and aluminium flooring.

SECTION IV

RECORDS OF THE WORKING ON THE APPARATUS

Photographs of signals obtained with the smaller magnet are shown in figure (2.27). Preliminary experiments were done with this magnet for calibrating the steady field of the magnet and for standardising the fluxmeter and other measuring

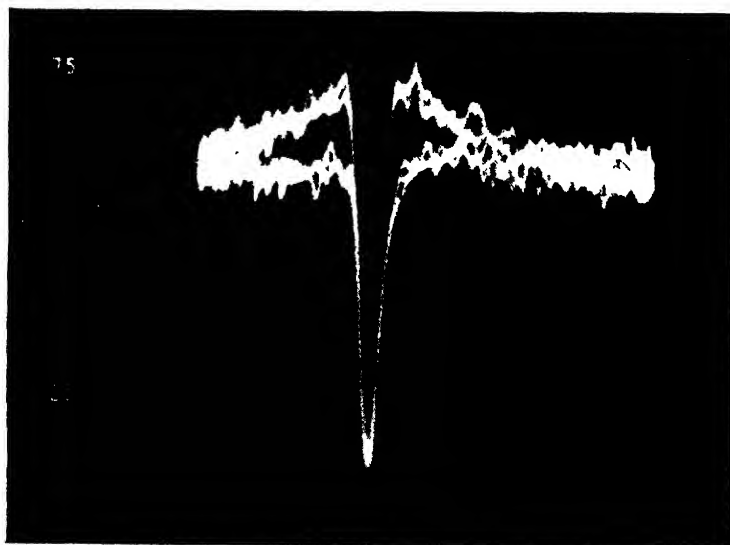


Fig. 2.27. H' signal in FeNO_3 solution in water with the smaller magnet.

instruments. The line width is determined wholly by the inhomogeneity and there is no wiggle.

With the new magnet the wiggles become very prominent even at 25 cycle modulation as shown in figure (2.28). Wiggles were avoided by the slow sweep



Fig. 2.28. H' signal in glycerine obtained with the new magnet. Wiggles are very prominent.

and audio mixer techniques, photographs of the records of which are shown in figure (2.29) and (2.30). The inhomogeneity at different points of the pole face

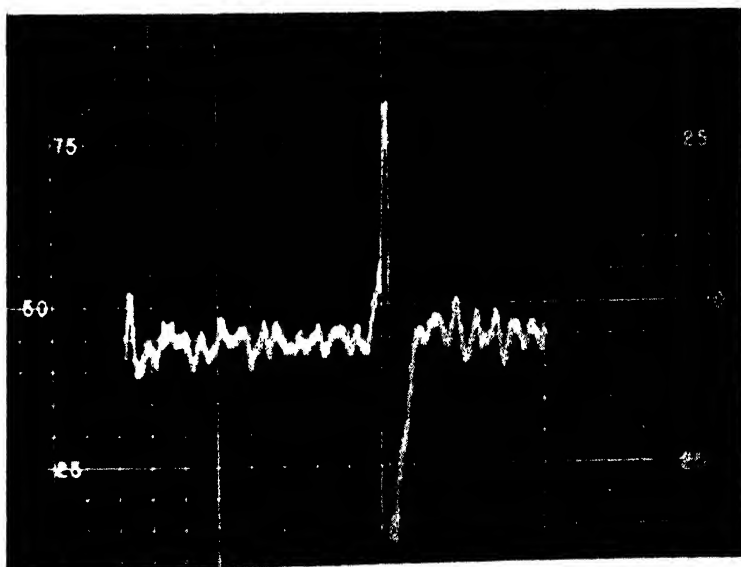


Fig. 2.29. Slow sweep signal of F in trifluorobenzene. (Dispersion signal).

area was measured by the audio mixer technique as follows: The magnetic field was kept slightly above the resonance value and the mixer circuit was run on. The field was continuously decreased at a very slow rate and the mixer traced the derivative curve as the field crossed the resonance value. Now the frequency

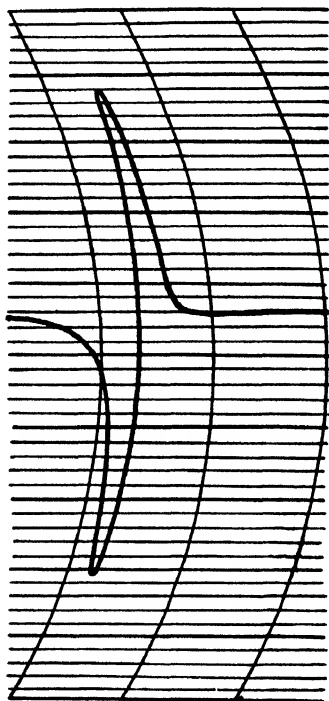


Fig. 2.30. Derivative signal of H' in glycerine obtained with lock-in amplifier circuit.

of the signal generator was tuned down by .02%; when the field value again satisfied the resonance condition $\omega = \gamma H$, there will be another tracing of the derivative curve. So the interval between the two curves is directly calibrated in terms of frequency i.e., in terms of field. The line width i.e. the distance between the two peaks of a derivative curve, can then be easily measured. Some records of these readings are shown in figure (2.31).

Records of signals obtained with the autodyne technique and the Bloch technique are shown in figures (2.23) and (2.32). Two cases of Bloch signals are given—one with *rf*-leakage voltage greater than the signal voltage and the other with smaller leakage voltage.

Magnetic moment of F^{19} has been measured by this instrument using a sample which can be obtained in the liquid state at room temperature. Current, rather the voltage across the standard resistance in the main current circuit, can be

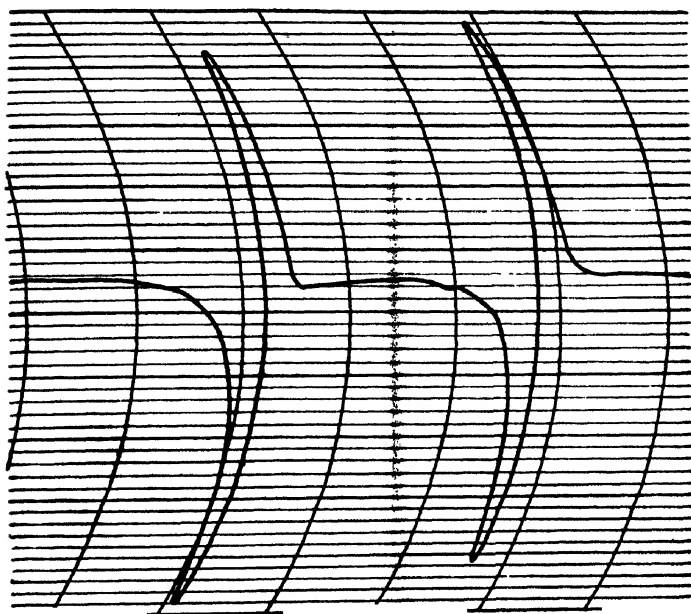


Fig. 2.31. Derivative signal of H' in glycerine obtained with 0.02 % frequency change at 1Mc/s.

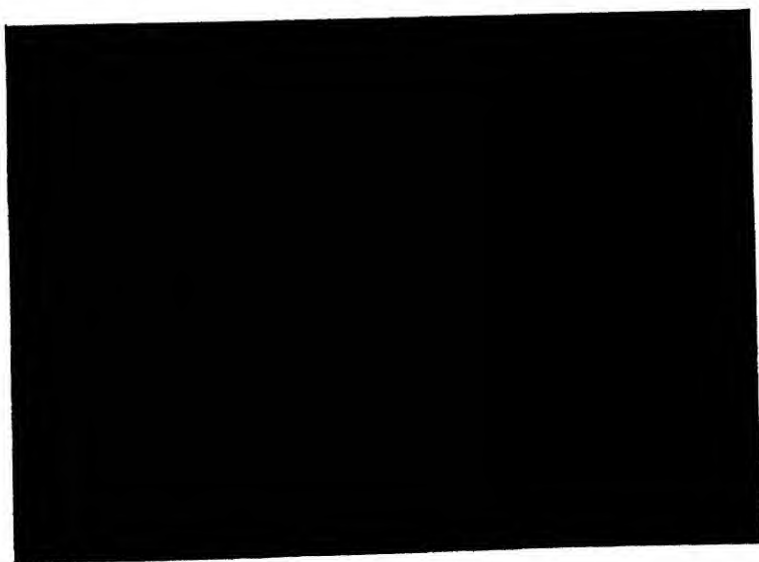


Fig. 2.32 (a). H' signal in glycerine obtained in the Bloch's arrangement.
Rf-leakage smaller than the signal voltage.

accurately determined upto sixth decimal place with the help of vernier potentiometer. From the ratio of two currents required for centering the proton and

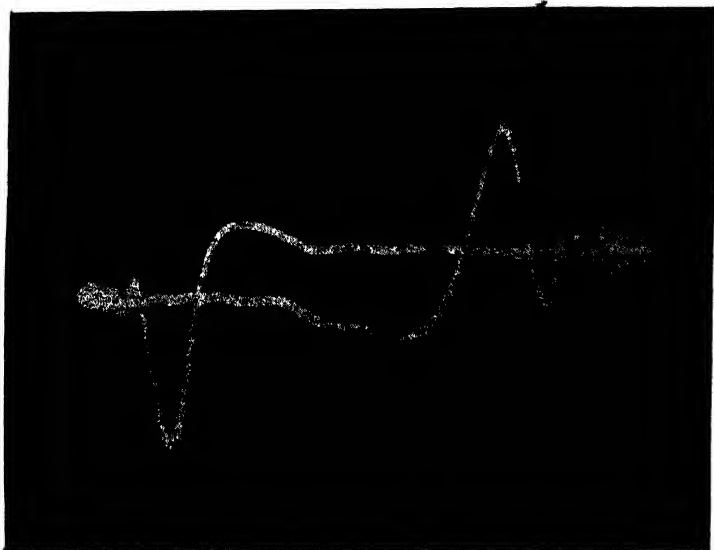


Fig. 2.32 (b). H' signal in glycerine obtained with Bloch's arrangement. Rf-leakage greater than the signal voltage.

fluorine signals in the oscilloscope screen, the ratio of magnetic moments can be accurately determined and hence γ for fluorine can be calculated, provided γ for H^1 is known. The value of $\mu_{F^{19}}$, uncorrected for diamagnetic and second order paramagnetic effect, was found to be 2.6117 in case of benzo-trifluoride.

CONCLUSION

Instrumentation of the steady technique is now complete for systematic study of relaxation time and nature of motions existing in solids and liquids. The condition of homogeneity of magnetic field is not so stringent for this class of experiments. For $J\delta$ -coupling experiments, homogeneity of the order of 1 milligauss is required which is 10 times more than what has been achieved as yet. Attempts are now being made to reach this limit by using two highly polished auxiliary pole pieces and a sample spinner arrangement. One disadvantage of the magnet set up here, is that the pole pieces are horizontal and therefore not easily approachable by hand. So required polishing cannot be done. For this purpose auxiliary pole pieces that are detachable from the main pole pieces are now being set up. The sample spinner is an arrangement where the sample rotates at a high speed inside the magnetic field, thus averaging the inhomogeneity over the sample

area. Bloch and others have reached a limit of .01 milligauss in 7000 gauss by this technique.

A comparative study of the different methods of measuring relaxation times—steady and transient—will be done by the authors in the near future.

ACKNOWLEDGMENT

The authors are grateful to Prof. M. N. Saha for his encouragement during the progress of the work and for providing requisite funds for the above programme of work.

REFERENCES

- Bloch, F., 1946, *Phys. Rev.*, **70**, 460.
Bloch, F., Hansen, W., and Packard, M., 1946, *Phys. Rev.*, **70**, 471.
Gutowsky, H. S., Meyer, L. H. and McClure, R. E., 1953, *Rev. Sci. Instr.*, **24**, 644.
Hopkins, N. J., 1949, *Rev. Sci. Instr.*, **20**, 401.
Purcell, E. M. Bloembergen, N., and Pound, R. V., 1948, *Phys. Rev.*, **73**, 69.
Proctor, W. G. and Yu, F. C., 1950, *Phys. Rev.*, **77**, 716.
Wang, T. C., 1955, *Phys. Rev.*, **99**, 566.

ON THE CRYSTAL STRUCTURE OF PARA DICHLORO-BENZENE AT DIFFERENT TEMPERATURES*

G. S. R. KRISHNA MURTI AND S. N. SEN

OPTICS DEPARTMENT, INDIAN ASSOCIATION FOR THE CULTIVATION OF
SCIENCE, JADABPUR, CALCUTTA

(Received for publication March 20, 1956)

Plate V

ABSTRACT. The dependence of the structure of crystals of para-dichlorobenzene on temperature has been investigated by taking Debye-Scherrer photographs at different temperatures. It has been observed that the structure of the crystal is triclinic when the polycrystalline mass is kept at 40°C without ever allowing it to cool down below 40°C and this structure is identical with that reported by Jeffrey and McVeagh (1955) for the single crystal at 40°C. The transformation from triclinic to monoclinic system is observed to take place when the crystal at 40°C is cooled down to 28°C. It is pointed out that as the low frequency Raman lines do not undergo any change with the change of structure these lines are not connected with the lattice. It has been further observed that in place of the two spacings 1.882 A.U. and 1.839 A.U. of the crystal at the room temperature, only one spacing 1.870 A.U. is shown by the crystal at -180°C and that the two spacings 4.282 A.U. and 3.542 A.U. of the crystal at room temperature increase respectively to 4.333 A.U. and 3.616 A.U. at -180°C, which indicates a slight increase in the length of the edge b of the unit cell at -180°C. It is pointed out that this may be due to reorientation of the molecules at low temperatures and that the sharpening of the ultraviolet absorption bands observed by Swamy (1953) and the increase in the frequencies and number of the Raman lines observed by Ray (1951) with lowering of temperature of the crystal, may be connected with this reorientation of the molecules at low temperatures.

INTRODUCTION

The crystal structure of para-dichlorobenzene was first determined by Hendricks (1933) who observed that at the room temperature the crystal belongs to the space group C_{2h}^3 with $a = 14.83$ A.U., $b = 4.10$ A.U., $c = 5.88$ A.U. and $\gamma = 112^\circ 30'$. Here c -axis was the axis of two-fold rotation. The structure was reinvestigated by Bua and Scatturin (1951), Croatto, Bezzi and Bua (1952) who also got the same results with slight modification in the dimensions of the unit cell, the values given by them being $a = 14.80$ A.U., $b = 5.78$ A.U., $c = 3.99$ A.U., $\beta = 113^\circ$. It was observed by Vuks (1936) that the low frequency lines in the Raman spectra of the crystals of p -dichlorobenzene undergo a change in position with the change of temperature of the crystal from about 40°C to about 32°C and an attempt was made by Sirkar and Gupta (1937) to find out whether

*Communicated by Prof. S. C. Sirkar.

the Laue pattern of the crystal changes with the change of temperature mentioned above. They could not detect any change in the Laue pattern with this change of temperature.

The Raman spectra of the crystals at different temperatures were reinvestigated by Ray (1951) who observed that the intensities and positions of the low frequency lines do not change when the temperature of the crystal is changed from 45°C to 28°C but when the crystal is once cooled to -180°C and brought back to room temperature the number of the low frequency lines increases and changes in their frequencies also take place. The frequencies of these lines change again when the substance is cooled to -180°C, and kept at that temperature. It is not known whether any change in the structure takes place with the change of temperature mentioned above. It has been recently reported by Jeffrey and McVeagh (1955) that the lattice of the single crystal changes from monoclinic to triclinic when the temperature of the crystal is raised to above 40°C and they called the monoclinic and triclinic forms the α - and β -forms of the crystal respectively. They reported that $\beta \rightarrow \alpha$ transformation takes place only when the β -form is cooled below 0°C. They got single crystals of both the forms by sublimation of the substance at about 40°C and allowing the sublimate to crystallise on a cooler surface.

It is not known, however, whether the β -form predominates the polycrystalline mass obtained by melting the substance and cooling it to about 40°C, and in case such a predominance of the β -form actually exists whether $\beta \rightarrow \alpha$ transformation takes place with gradual lowering of the temperature to room temperature. It was therefore thought worthwhile to study the Debye-Scherrer patterns of the *p*-dichlorobenzene crystals under all the conditions mentioned above in order to find out whether any change in the spacings takes place with these changes of temperature of a polycrystalline mass of the substance obtained from the melt.

EXPERIMENTAL

Pure para-dichlorobenzene was melted and was allowed to solidify and cool down to the particular temperature at which the Debye-Scherrer pattern was to be photographed. As the substance is extremely volatile powdered sample was prepared by packing it in a narrow cellophane paper tube of diameter about 1mm and length about 1 cm. Different samples were prepared under the following conditions:

(a) The melt was solidified in a glass tube immersed in a hot water bath kept at about 40°C and was transferred to a heating chamber maintained at 40°C. The sample was powdered in a mortar kept in the same heating chamber for a long time and the cellophane paper tube was filled with the powdered substance inside the heating chamber. The sample was then transferred to a test tube kept in a hot water bath maintained at 40°C. The Debye-Scherrer camera was heated

to maintain the temperature near its axis at 40°C and the sample was quickly transferred to its position in the camera from the test tube.

(b) The melt was solidified in a glass tube and allowed to cool down to the room temperature. Then it was powdered and a tube was filled with the powder.

(c) The melt was solidified in a glass tube and allowed to cool down once below 0°C . It was brought back to the room temperature and a cylindrical specimen was prepared in the same way as in the case of the specimen at the room temperature.

(d) The sample obtained by solidifying the molten mass was powdered and the specimen was prepared by packing the powder in a glass tube of diameter about 0.8 mm. The specimen was placed in its position in the low temperature camera which is described below and a diagram of which is given in figure 1. The

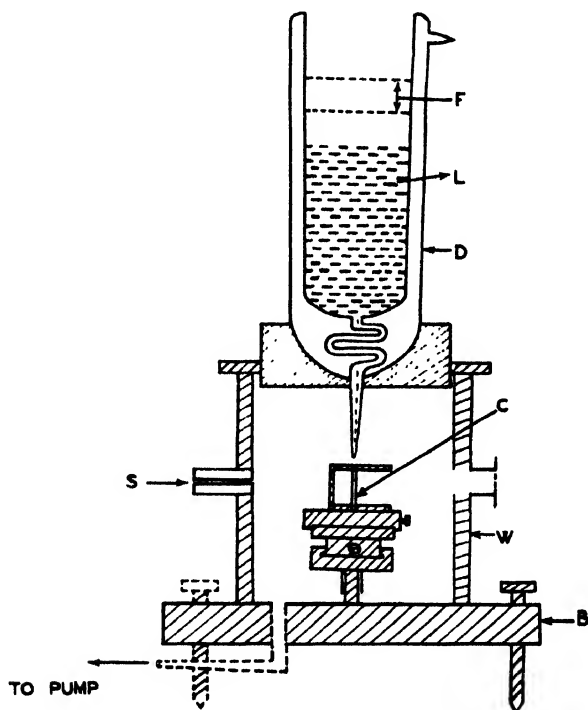


Fig. 1

C—Specimen, W—Cylindrical camera, B—Base, S—Slit, D—Dewar flask, L—liquid oxygen, F—filter.

camera was provided with an outlet tube for pumping out air from the region inside the camera. Liquid oxygen came out of the nozzle at the bottom of the pyrex Dewar vessel *D* as a very narrow stream formed just above the specimen. But the jet was so narrow that it evaporated almost immediately. The specimen

was thereby cooled to about -180°C but only a weak pattern due to liquid oxygen was observed.

(e) The Dewar vessel containing liquid oxygen fitted to the low temperature camera was removed and the specimen of the powdered crystal irradiated at low temperature was allowed to attain the room temperature. The camera was loaded again and another Debye-Scherrer pattern of the same specimen at room temperature was photographed.

A Seifert X-ray tube running at 26 ma, 32KV was used to photograph the patterns. An exposure of about $2\frac{1}{2}$ hrs was enough to get the patterns recorded with moderate densities. The total angular divergence of the X-ray beam incident on the specimen was about 2° but the rings were very sharp because the total diameter of the cylindrical specimen excluding cellophane paper tube was about $\frac{1}{2}$ mm. The X-ray tube was provided with a copper target and a nickel filter was used to cut off the $K\beta$ lines. Two cylindrical cameras were used. The distance from the specimen to the film was measured accurately by recording the Debye-Scherrer pattern of rocksalt. For the smaller camera the distance was 2.920 cms and for the low temperature camera it was 5.20 cms. Several photographs under the same conditions were taken for each specimen to verify genuineness of the results. Spacings were calculated from the diameters of the rings which could be measured correct to about 0.1 mm.

RESULTS AND DISCUSSION

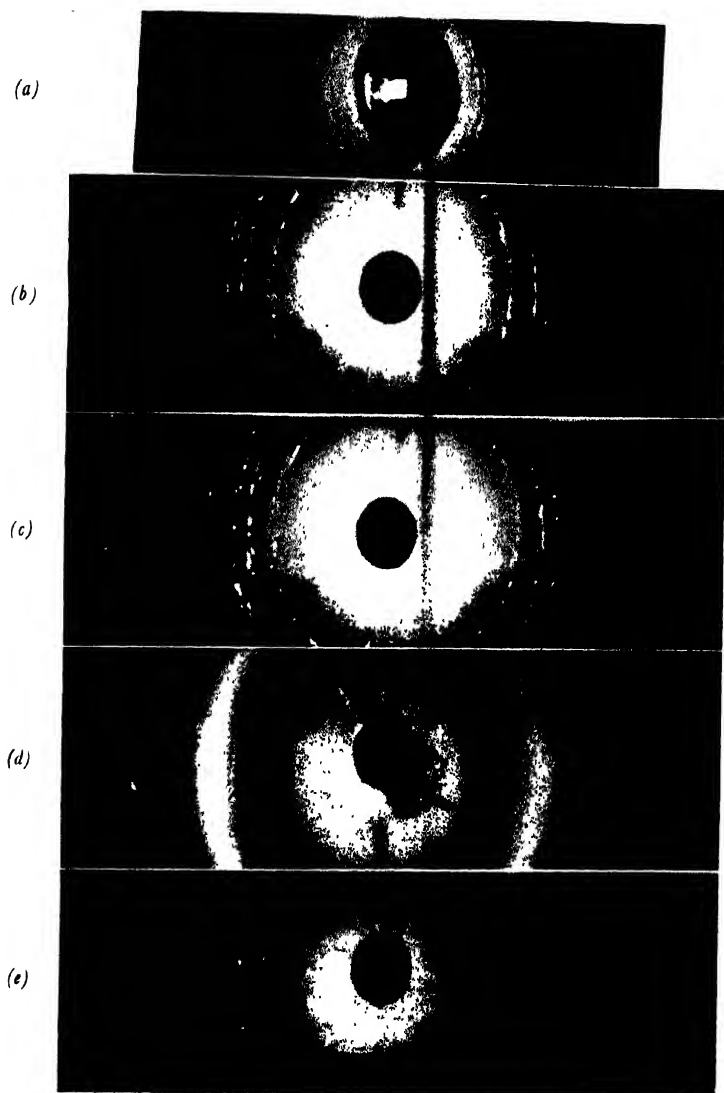
The spacings calculated from the Debye-Scherrer rings obtained under the different conditions mentioned above, are given in Table I in which the spacings calculated from the structure reported by Bua and Scatturin (1951) and also those for the triclinic structure reported by Jeffrey and McVeagh (1955) are also included in the first and the last column respectively for comparison. The intensities are indicated as very strong (vs), strong (s), medium (m), weak (w) and very weak (vw). Some of the representative photographs of the Debye-Scherrer patterns are reproduced in Plate V.

It can be seen from Table I that the spacings observed for the specimen kept at 40°C as described above under (a) agree with those calculated for the triclinic structure reported by Jeffrey and McVeagh (1955). The spacings, of course, are very near to those observed for the monoclinic structure at room temperature (28°C); but the difference between the two structures is indicated by the complete absence of the spacings 3.58 A.U., 2.802 A.U. in the case of triclinic structure at 40°C . It is quite clear from the patterns reproduced in Plate V that the two spacings 1.882 A.U. and 1.839 A.U. observed in the case of monoclinic structure are replaced by only one spacing 1.869 A.U. in the case of triclinic structure. Similarly for the spacing 2.240 A.U. in the case of monoclinic structure two spacings 2.345 A.U. and 2.195 A.U. are observed in the triclinic structure. So it is conclu-

ded that the structure of the polycrystalline mass at 40°C is identical with that of the β -form reported by Jeffrey and McVeagh (1955) in the case of the single crystal at the same temperature.

TABLE I
Spacings in A.U. of crystals of para-dichlorobenzene

From the data of Bua and Scat- turin (1951)		at 28°C	Cooled below 0°C and brought back to 28°C	at - 180°C	Cooled to - 180°C and brought back to 32°C	at 40°C	From the data of Jeffrey and McVeagh (1955)	
Planes	Spacings						Spacings	Planes
100	13.62							
200	6.81						6.759	100
010	5.78						5.950	010
110	5.321							
300	4.540							
210	4.408	4.384(s)	4.384(s)	4.407(m)	4.442(s)	4.342(s)	4.364	110
001	3.673						3.931	001
310	3.572	3.580(vs)	3.580(vs)	3.621(m)	3.680(s)	3.637(s)	3.643	10 $\bar{1}$
400	3.405							
21 $\bar{1}$	3.255	3.253(s)	3.253(s)	3.229(m)	3.325(s)		3.379	200
101	3.243							
011	3.099	3.129(w)	3.129(w)	(masked in liquid oxy- gen halo.)	3.232(w)	3.247(s)	3.233	011
410	2.935	2.941(m)	2.941(m)		3.022(m)	3.172(vw)	3.193	101
020	2.890					2.951(w)	2.975	020
111	2.828						2.880	210
120	2.828	2.802(m)	2.802(m)		2.834(m)			
201	2.807							
500	2.724					2.758(w)	2.759	111
220	2.661						2.676	120
211	2.525							
510	2.465							
301	2.429				2.420(vw)		2.390	201
021	2.272					2.345(w)	2.336	021
600	2.270							



Debye-Scherrer Patterns of p-dichlorobenzene.

- (a) Specimen at 40°C (Radius of Camera ≈ 2.90 , cms).
- (b) Specimen at 28°C (Radius of Camera ≈ 5.20 , cms).
- (c) Specimen cooled below 0°C and brought back to 28°C
[Radius of the Camera ≈ 5.2 cms].
- (d) Specimen at -180°C . [Radius of the Camera ≈ 5.2 cms]
- (e) Specimen cooled to -180°C and brought back to 32°C .
[Radius of the Camera ≈ 5.2 cms].

TABLE I (contd.)
 Spacings in A.U. of crystals of para-dichlorobenzene

From the data of Bua and Scat- turin (1951)		at 28°C	Cooled below 0°C and brought back to 28°C	at -180°C	CoolWed to -180°C and brought back to 32°C	at 40°C	From the data of Jeffrey and McVeagh (1955)
Planes	Spacings						Spacings Planes
311	2.253	2.240(w)	2.240(w)	2.229(w)	2.252(w)		2.253 300
420	2.204					2.195(w)	2.182 220
121	2.158						2.178 211
401	2.118				2.123(w)		2.125 121
610	2.118						
221	2.098	2.086(w)	2.086(w)	2.087(w)		2.079(w)	2.074 310
411	1.989						1.983 030
							1.965 002
030	1.927				1.923(w)		1.923 130
130	1.907	1.882(w)	1.882(w)				
501	1.846			1.870(w)	1.876(w)		
710	1.845	1.839(w)	1.839(w)			1.869(w)	1.849 012
002	1.836						1.838 30±1
330	1.774				1.772(w)		

It can be seen from Table I that the spacings of the crystals for the two specimens (b) and (c) agree completely with the spacings calculated for the monoclinic structure reported by Bua and Scatturin (1951). Powders of single crystals also gave the same results. So, no change in structure takes place with the lowering of the temperature of the crystal below 0°C and raising it again to 28°C. The actual volumes of the unit cell at 28°C and at 40°C have been calculated and the values are found to be 315.2×10^{-24} c.c. and 160.3×10^{-24} c.c. respectively. It is seen that the volume at 40°C is almost half of that at 28°C. If we remember that the value of a in the triclinic system is just half that in the monoclinic system and take a unit cell with $2a$ as the primitive translation along a -axis in the case of triclinic system, we see that no remarkable contraction of volume takes place with the change from the triclinic to the monoclinic system, the actual contraction being only 2%.

It has been reported by Jeffrey and McVeagh (1955) that the transition from $\beta \rightarrow \alpha$ form cannot take place unless the crystal is cooled below 0°C. It is found

in the present investigation, however, that in order to bring about the transformation it is not necessary to cool the crystal below 0°C , and the triclinic form changes to monoclinic form even when the crystal at 40°C is gradually cooled down to the room temperature (28°C). When the specimen is cooled below 0°C and again brought back to 28°C no further change in the structure of the crystal takes place.

It has been reported by Sirkar and Gupta (1936) and Ray (1951) that no changes in the number and positions of the low frequency Raman lines take place when the temperature of the crystal is changed from about 45°C to about 28°C . As mentioned above it has been found that the spacings actually change with change of temperature. So, this change in the structure does not bring about any change in the low frequency Raman lines.

The Raman spectrum in the low frequency region undergoes a slight change when the crystal is once cooled below 0°C and brought to about 28°C (Sirkar and Gupta, 1936). But it is observed in the present investigation that no change in the structure takes place after the crystal is subjected to this treatment. So, the observed changes in the Raman spectra are not connected with the structure of of the crystal at all.

It can be seen from Table I that the spacings obtained for the crystal at -180°C agree fairly well for the crystal at room temperature. The first two spacings, however, are slightly larger than those for the crystal at 28°C and also in the place of the two spacings 1.882 A.U. and 1.839 A.U. observed in the latter case, only one spacing 1.87 A.U. is observed in the case of the crystal at -180°C . The results indicate a slight increase in the length of the edge b of the unit cell at -180°C . This increase is caused probably by reorientation of the molecules in unit cell at low temperatures. The correctness of this hypothesis can be tested only by taking the rotation photograph about b -axis at -180°C and an attempt is being made to test this hypothesis. Such a rotation in the molecules may be due to formation of new virtual bonds which may be responsible for the sharpening of ultraviolet absorption bands observed by Swamy (1953) and for the increase in the frequency-shifts of Raman lines observed by Ray (1951) with the lowering of temperature of the crystal to -180°C .

The data entered in column 6 indicate that such a change persists when the crystal is brought back to 32°C from -18°C . But due to the thermal expansion of the crystal the distance between the molecules increases slightly resulting in the increase of the dimensions of the unit cell. This explains why the spacings observed in the case of the crystal brought back to 32°C from -180°C are slightly larger than those for the untreated crystal at 28°C . These changes in the distances between molecules probably accounts for the changes in the frequencies of the Raman lines observed by Ray (1951) with the change in the temperature from -180°C to 32°C .

ACKNOWLEDGMENT

The authors are indebted to Professor S. C. Sirkar, D.Sc., F.N.I. for his kind help and guidance throughout the progress of this work.

REFERENCES

- Bua, E. and Scatturin, V. . 1951, *Gazz. Chem. ital*, **81**, 351.
Croatto, U., Bezzi, S., and Bua E., 1952, *Acta cryst.*, **5**, 825.
Hendricks, S. B., 1933, *Z. Cryst.*, **84**, 85.
Jeffrey, G. A., and McVeagh, J., 1955, *J. Chem. Phys.*, **23**, 1165.
Ray, A. K., 1951, *Ind. J. Phys.*, **25**, 459.
Sirkar, S. C. and Gupta, J., 1936, *Ind. J. Phys.*, **10**, 473.
Sirkar, S. C., and Gupta, J., 1937, *Ind. J. Phys.*, **11**, 283.
Swamy, H. N., 1953, *Ind. J. Phys.*, **27**, 55.
Vuks, M., *Compt. Rend. Acad. Sci. U.R.S.S.*, **1**, 73.

DEPENDENCE OF LIMIT OF RESOLUTION ON BACKGROUND INTENSITY, DETECTING INSTRUMENT AND STAGE OF RESOLUTION IN X-RAY SPECTRA.

D. C. PURKAYASTHA

DEFENCE SCIENCE LABORATORY, MINISTRY OF DEFENCE, NEW DELHI

(Received for publication January 20, 1956)

ABSTRACT. Ditchburn has suggested that a combination of stage of resolution desired and the detecting instrument is characterized by C , the ratio of the minimum to maximum of resultant intensity pattern of two spectral lines, for optimum resolution. If k is the ratio of background intensity to the intensity of two-X-ray spectral lines of half width b , the limit of resolution is given by

$$\Delta\lambda_r = b \left[\frac{\{5k(1-C) - 6C + 8\} + \sqrt{\{3k(1-C) - 2C + 8\}^2 - 32C}}{2\{C - k(1-C)\}} \right]^{1/2}$$

A table giving the values of $b/\Delta\lambda_r$ for various values of k and C has been constructed.

INTRODUCTION

Sodha (1954) has discussed the effect of background intensity on the resolving power of optical instruments. He has also discussed the case when the instrumental width is negligible, the intensity distribution being governed by Doppler effect. His discussion is based on the Rayleigh criterion for resolution of spectral lines.

Ditchburn (1930) has emphasized the fact that the resolving power also depends on the detecting instrument and the stage of resolution desired. A given combination of detecting instrument and stage of resolution is characterized by the value C of I_{\min}/I_{\max} for optimum resolution of two spectral lines, where I_{\min} and I_{\max} denote the minimum and maximum of the resultant intensity pattern. Ditchburn has given the following values of C for three main stages of resolution when microphotometer is used as a detecting instrument.

Stage of resolution	C
(i) Detection of inhomogeneity in radiation	0.98
(ii) Partial resolution (approximate measurement of wavelength separation)	0.8
(iii) Complete measurement (measurement of wave length separation and relative intensities)	0.4

Sharma and Sodha (1954) and Mitra (1954) have discussed the dependence of resolving power of prism, grating, reflecting echelon, Fabry-Perot etalon and

Lummer Gehrcke plate C. Sodha (1954a) has also discussed the case when the lines have an intensity distribution, governed by Doppler effect.

In this paper the author has discussed the effect of background intensity, detecting instrument and the stage of resolution desired on the limit of resolution of two X-ray spectral lines. An explicit expression for the limit of resolution has been obtained in terms of half-width, C and k the ratio of background intensity to the intensity of the spectral line.

INTENSITY CONSIDERATIONS

The intensity distribution of an X-ray spectral line is best represented by Hoyt (1932)

$$I_1 = \frac{I_0}{1 + \{(\lambda - \lambda_0)/b\}^2}$$

where b is the half-width of the line. The intensity distribution of another line of equal intensity separated by $\Delta\lambda$ is

$$I_2 = \frac{I_0}{1 + \{(\lambda - \lambda_0 - \Delta\lambda)/b\}^2}$$

If the background intensity is kI_0 the resultant intensity pattern of the two lines is given by

$$I/I_0 = \frac{I_1 + I_2}{I_0} = \frac{1}{1 + X^2} + \frac{1}{1 + (X - a)^2} + k \quad \dots (1)$$

Neglecting shrinkage effect the intensity maxima ($x \approx 0$ or a) and minimum ($x = \frac{a}{2}$) are given by

$$I_{max}/I_0 = k + 1 + \frac{1}{1 + a^2} \quad \dots (2)$$

$$I_{min}/I_0 = k + \frac{2}{(1 + a^2/4)} \quad \dots (3)$$

LIMIT OF RESOLUTION

We have

$$I_{min} = C \times I_{max} \quad \dots (4)$$

which gives

$$a = \left[\frac{\{5k(1-C) - 6C + 8\} + \sqrt{\{3k(1-C) - 2C + 8\}^2 - 32C}}{2\{C - k(1-C)\}} \right]^{\frac{1}{2}} \quad \dots (5)$$

$$\Delta\lambda_r = b \left[\frac{\{5k(1-C) - 6C + 8\} + \sqrt{\{3k(1-C) - 2C + 8\}^2 - 32C}}{2\{C - k(1-C)\}} \right]^{\frac{1}{2}} \quad \dots (6)$$

where $\Delta\lambda_r$ is the limit of resolution, meaning the smallest wavelength difference, resolvable. The resolving power is given by

$$R = \frac{\lambda}{\Delta\lambda_r} = \frac{\lambda}{b} \left[\frac{\{5k(1-C) - 6C + 8\} + \sqrt{\{3k(1-C) - 2C + 8\}^2 - 32C}}{2\{C - k(1-C)\}} \right]^{-\frac{1}{2}} \quad \dots (7)$$

Table 1 gives the value of Rb/λ for various values of k and C ; where $0 < k < C/(1-C)$.

Figures 1 and 2 illustrate the variation of Rb/λ with k and C .

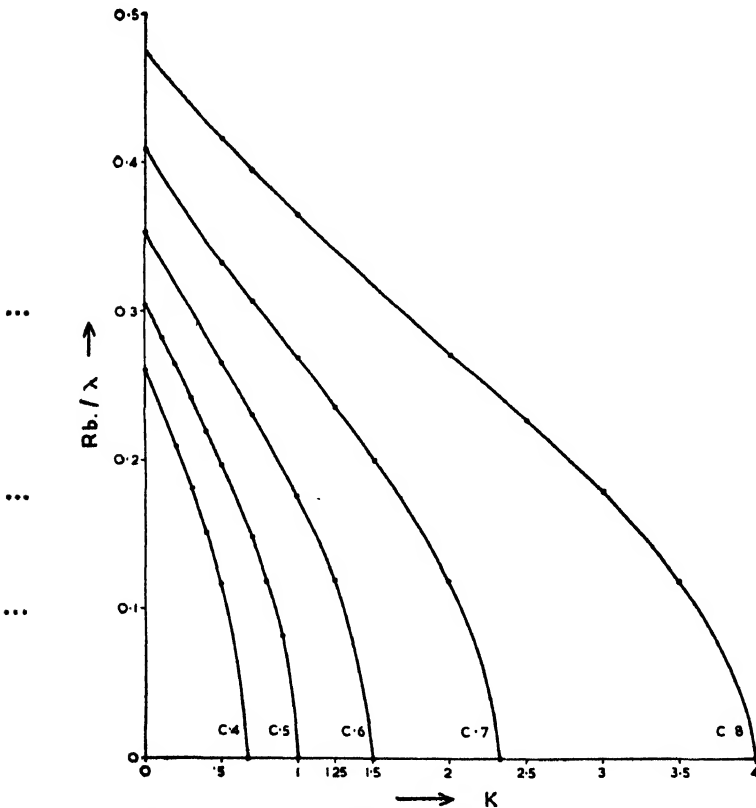


Fig. 1. Variation of Rb/λ with k . ($0.4 \leq C \leq 0.8$)

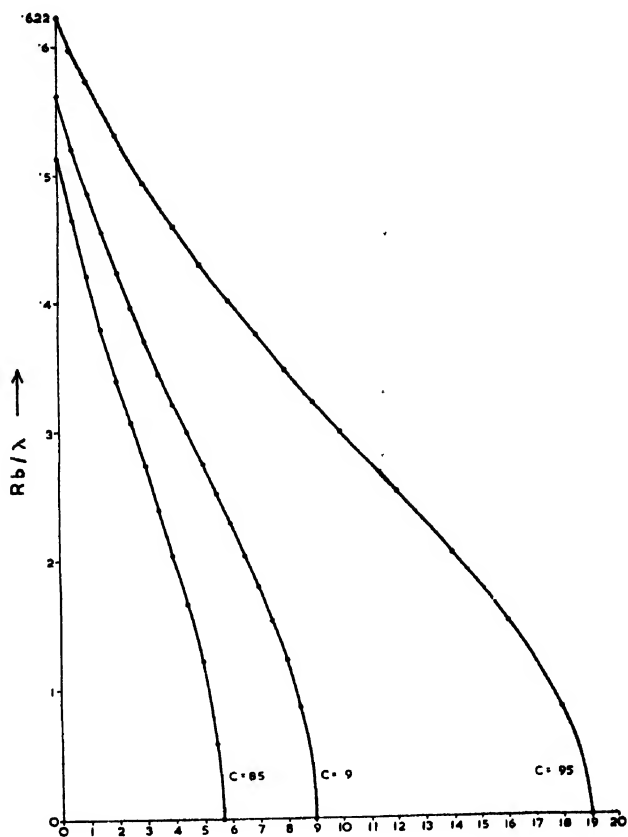


Fig. 2. Variation of Rb/λ with k . ($0.85 \leq C \leq 0.95$).

TABLE I
Value of Rb/λ

$C \backslash k$.4	.5	0.6	0.7	0.8	0.85	0.9	0.95
0	.260	.305	.353	.408	.474	.514	.562	.622
.1	.235	.284	—	—	—	—	—	—
.2	.209	.265	—	—	—	—	—	—
.3	.181	.241	—	—	—	—	—	—
.4	.152	.219	—	—	—	—	—	—
.5	.118	.197	.265	.331	.416	.464	.522	.596
.66	0	—	—	—	—	—	—	—
.7	—	.148	.222	.301	—	—	—	—

TABLE I (contd.)

.8	—	.119	—	—	—	—	—	—
.9	—	.083	—	—	—	—	—	—
1	—	0	.175	.268	.364	.42	.485	.572
1.25	—	—	.12	.235	—	—	—	—
1.5	—	—	0	.201	.317	.38	.454	—
2	—	—	—	.12	.27	.34	.424	.530
2.5	—	—	—	—	.226	.307	.396	—
3	—	—	—	—	.178	.273	.37	.493
3.5	—	—	—	—	.122	.238	.345	—
4	—	—	—	—	0	.203	.321	.459
4.5	—	—	—	—	—	.166	.300	—
5						.122	.274	.429
5.5						.059	.251	—
6							.228	.400
6.5							.204	—
7							.179	.375
7.5							.153	—
8							.123	.348
8.5							.086	—
9							0	.323
10								.300
12								.253
14								.205
16								.153
18								.085
19								0

ACKNOWLEDGMENTS

The author is highly grateful to Dr. M. S. Sodha for suggesting the problem and for valuable guidance. He is also thankful to Prof. D. S. Kothari and Dr. H. Nath for their kind encouragement. Thanks are also due to Dr. A. R. Varma for making helpful comments.

REFERENCES

- Ditchburn, 1930, *Proc. Roy. Irish. Acad.*, 39, 58.
 Hoyt, 1930, *Phys. Rev.*, 40, 477.
 Mitra, S. S. 1954, *Ind. J. Phys.*, 28, 543.
 Sharma and Sodha, M. S., 1954, *Ind. Phys.*, 28, 437.
 Sodha, M. S., 1954, *Ind J. Phys.*, 28, 141.
 Sodha, M. S. 1954a, Ph.D. Thesis, Allahabad University.

ON THE DEPENDENCE OF THE INTENSITY OF FLUORESCENCE OF FROZEN *p*-CHLOROTOLUENE ON THE WAVELENGTH OF THE EXCITING RADIATION*

D. C. BISWAS

OPTICS DEPARTMENT, INDIAN ASSOCIATION FOR THE CULTIVATION OF SCIENCE,
JADAVPUR, CALCUTTA 32.

(Received for publication, March 5, 1956)

Plate VI.

ABSTRACT. The dependence of the intensity of fluorescence of frozen *p*-chlorotoluene on the wavelength of the exciting radiation is investigated. It is observed that the group of Hg-lines at 3650Å and other lines of shorter wavelength are responsible for the production of this fluorescence spectrum.

INTRODUCTION

It has been recently observed by Sirkar and Biswas (1956) and by Biswas (1956) that the radiations from a quartz or a pyrex mercury arc filtered through ultraviolet light filter can excite strong fluorescence in solidified parachlorotoluene when the substance is cooled down to -180°C . The above filter transmits the 3650Å group of Hg-lines almost with undiminished intensity and the other mercury lines longer than 3100 Å are also transmitted with slightly diminished intensities. The lines in the visible region and the continuous background are, however, absorbed heavily so that the fluorescence bands can be recorded on clean background.

The 0,0 band of solid *p*-chlorotoluene at -180°C (Swamy, 1952) is at 2760 Å and therefore it is surprising that radiation of wavelengths much longer than 2760Å can excite strong fluorescence in the substance in the solid state at 180°C . It is not known, however, whether the fluorescence persists if the 3650Å group of Hg-lines is completely cut off and such an information would indicate the position of the absorption band responsible for the excitation of this fluorescence. So, in order to find out the maximum wavelength which can excite the fluorescence spectrum, filters of aqueous solutions of NaNO_2 crystals in different concentrations have been used in the present investigation to cut off shorter wavelengths in the near ultraviolet region of the spectrum of mercury arc in gradual steps and the intensities of the fluorescence spectra excited by the filtered radiations have been compared with each other. The results are discussed in this paper.

*Communicated by Prof. S. C. Sirkar

EXPERIMENTAL

Pure *p*-chlorotoluene supplied by Eastman Kodak Co. and distilled in vacuum was used in the investigation. The experimental set up was almost the same as that described earlier by Biswas (1956). The light from a mercury arc in pyrex tube filtered through the ultraviolet light filter was focussed with a cylindrical pyrex tube of diameter 40 mm filled with aqueous solution of NaNO_2 . The concentrations 2.5%, 5% and 10% of the solution were used to cut off the ultraviolet lines step by step. The fluorescence spectra were photographed with a Fuess glass spectrograph of dispersion of about 11\AA per mm in the 4046\AA region while the absorption of the different Hg-lines in the near ultraviolet region was studied with the help of an Adam Hilger medium quartz spectrograph. The fluorescence spectrum excited by the mercury arc lines not filtered through the NaNO_2 solution was also recorded under similar conditions for comparison of intensities. The time of exposure in this case was 40 minutes while that for the spectra excited by filtered radiation was 4 hours, the width of the slit of the spectrograph in the two cases being 0.25 mm and 0.70 mm respectively.

RESULTS AND DISCUSSION

The spectrograms showing the fluorescence bands excited under different conditions of excitation are reproduced in figure 1, Plate VI and those showing the transmission of the different Hg-lines through the different filters are shown in figure 2, Plate VI. On comparing the intensities of the fluorescence bands in figure 1(a) and figure 1(b), it is seen that the intensities of the bands are drastically reduced when the 3650\AA group of mercury lines are absorbed partially by a 2.5% aqueous solution of NaNO_2 and all the lines of shorter wavelengths are completely absorbed. When the strength of the NaNO_2 filter is increased to 5% the intensity of the transmitted 3650\AA group of lines is reduced still more and a consequent reduction in the intensity of the fluorescence excited by radiations filtered through the 5% solution of NaNO_2 can be observed. When the strength of the NaNO_2 filter solution is further increased to 10%, the intensity of fluorescence becomes negligibly small. From the results given above it is clear that the 3650\AA group of Hg-lines and other lines of shorter wavelengths are effective in producing the fluorescence in solid *p*-chlorotoluene at -180°C .

The excitation of fluorescence in *p*-chlorotoluene by the 3650\AA group of Hg-lines indicates that parachlorotoluene should exhibit some absorption band on the longer wavelength side of this region in the solid state at -180°C . Swamy (1952) observed that the 0,0 band of the solidified *p*-chlorotoluene at -180°C is at 2760\AA . The excitation of fluorescence in this substance under the present condition, therefore, shows that in the solid state at low temperature *p*-chlorotoluene probably gives rise to some new absorption region on the longer wave length

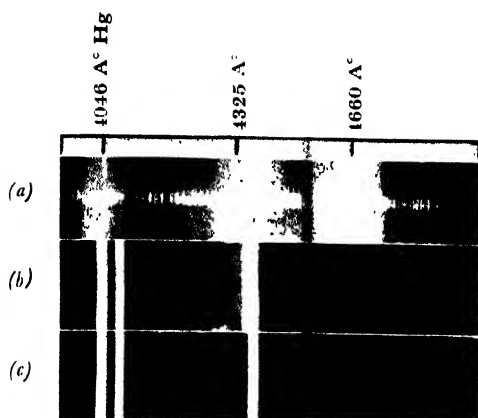


Fig. I
Fluorescence of *p*-chlorotoluene at -180°C

- (a) Incident light filtered through ultraviolet light filter + H_2O
 (b) " " " " " " " + 2.5% aqueous sol. of NaNO_2 .
 (c) " " " " " " " + 5% aqueous sol. of NaNO_2 .

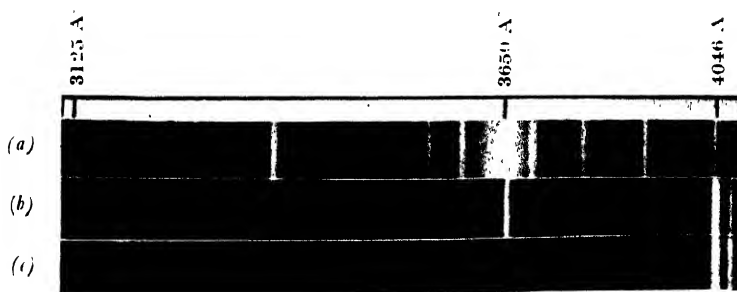


Fig. II
Transmission of Hg lines through different filters.

- (a) Ultraviolet light filter + H_2O .
 (b) " " " " + 2.5% aqueous sol. of NaNO_2 .
 (c) " " " " + 5% " " " " " "

side of 3650 Å which has been overlooked earlier. Instead of giving rise to any well defined absorption band in this region the substance at the low temperature may also exhibit some diffuse absorption extending to some extent beyond the 3650 Å towards the longer wavelength side. As the original band system of the molecule does not undergo drastic changes with solidification excepting slight shift of the system towards shorter wavelengths the new absorption region may be due to the presence of new energy levels in the associated group of molecules formed in the solid state at low temperature. Formation of such groups was indicated by the disappearance of the fluorescence in the case of solution of the substance in CS₂.

ACKNOWLEDGMENT

The author is indebted to Professor S. C. Sirkar, D.Sc., F.N.I. for his kind interest and helpful guidance during the progress of the work.

REFERENCES

- Biswas, D. C., 1956, *Ind. J. Phys.*, **30**, 143.
Sirkar, S. C. and Biswas, D. C., 1956, *J. Chem. Phys.*, **24**, 470.
Swamy H. N., 1952, *Ind. J. Phys.*, **26**, 445.

Letters to the Editor

The Board of Editors will not hold itself responsible for opinions expressed in the letters published in this section. The notes containing reports of new work communicated for this section should not contain many figures and should not exceed 500 words in length. The contributions must reach the Assistant Editor not later than the 15th of the second month preceding that of the issue in which the Letter is to appear. No proof will be sent to the authors.

1. BOILING POINT AND OTHER PHYSICAL PROPERTIES OF THE HALOGENS AND HALIDES

G. R. SOMAYAJULU

INDIAN ASSOCIATION FOR THE CULTIVATION OF SCIENCE, CALCUTTA-32

(Received for publication April 2, 1956)

Some regularities have been already observed for many physical properties of halides. We have, however, found that most of the physical properties of halogens and of halides can be treated from a common basis. It has been found that in a sequence of compounds of the general formula RX_n , where X stands for any halogen and R is any atom (may be a halogen itself) or a group of atoms, many physical properties are linearly related to the sum of the effective atomic numbers of the halogen atoms in RX_n ; in other words, there exists a relationship of the type

$$P = a\Sigma(Z-S) + b = a\Sigma Z' + b$$

where P is the property in question, a and b are constants for any particular series of molecules, and Z' is the effective atomic number of X, the summation being carried over all the X's; Z' is equal to $Z-S$ where Z is the atomic number, and S is a constant characteristic for each halogen (the significance of which is not yet quite clear) and has the value 0 for fluorine and chlorine, 13 for bromine and 23 for iodine.

We first illustrate the above relationship from available boiling point data. Taking R to be a halogen itself, the boiling points of all compounds of the type X_2 , viz., F_2 , FCI , Cl_2 , $ClBr$, Br_2 , ICl , IBr and I_2 , have been plotted in figure 1 against the summation of the effective atomic numbers of the two atoms constituting the X_2 molecule and it would be seen that all the points fall in a straight line. Similar behaviour is also exhibited (figure 1) by twenty-one tetrahalides of silicon and also by twelve tetrahalides of carbon for which data are available.

An exactly similar relation is also obtained with the same Z' values for halogens for the boiling points of a multitude of other sequences, viz., monohalides

of H (with the exception of HF), R (alkyl or aryl), Si H₃, etc., dihalides of CH₂, C₂H₄, SiR₂, Hg, etc., trihalides of B, N, P, As, Sb, (excepting SbF₃), Bi, PO, PS, CH, SiH, SiR, etc. tetrahalides of Ti, Ge, Sn (excepting TiF₄ and SnF₄), etc., and so on.

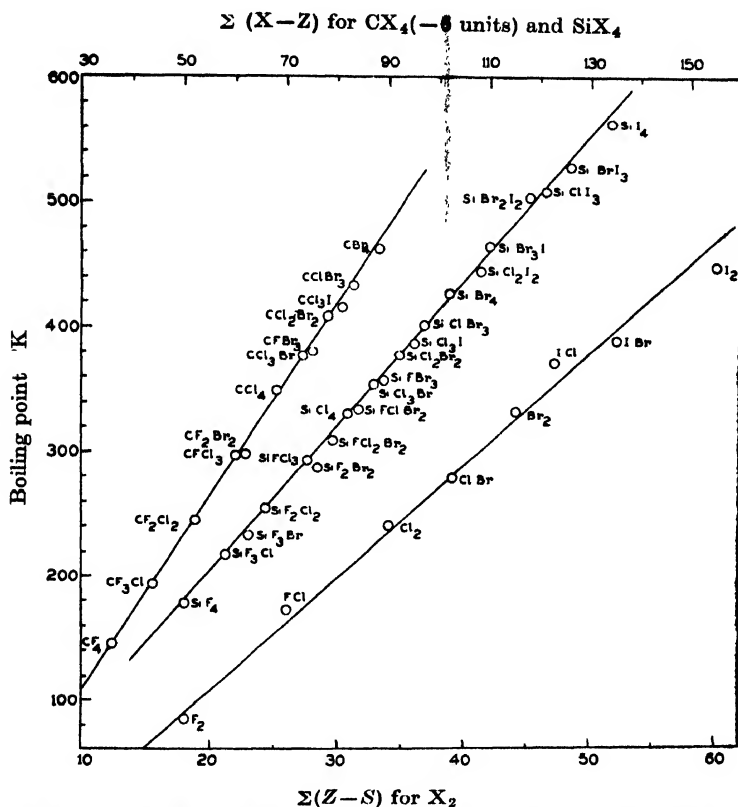


Fig. 1. Boiling point vs. summation effective atomic number diagram.

Linear relationships have also been found to exist between several other properties such as polarisability, refractivity, square of atomic covalent radius (*vide* the other note appearing herewith), van der Waals volume, atomic volume, parachor, Pascal's constant, etc., on the one hand and Z' on the other for halogens. In fact, all sequences, of the type RX_n we have tried so far and which are

too numerous to mention here, have shown this regularity and we present in figure 2 a few typical illustrations for halogens.

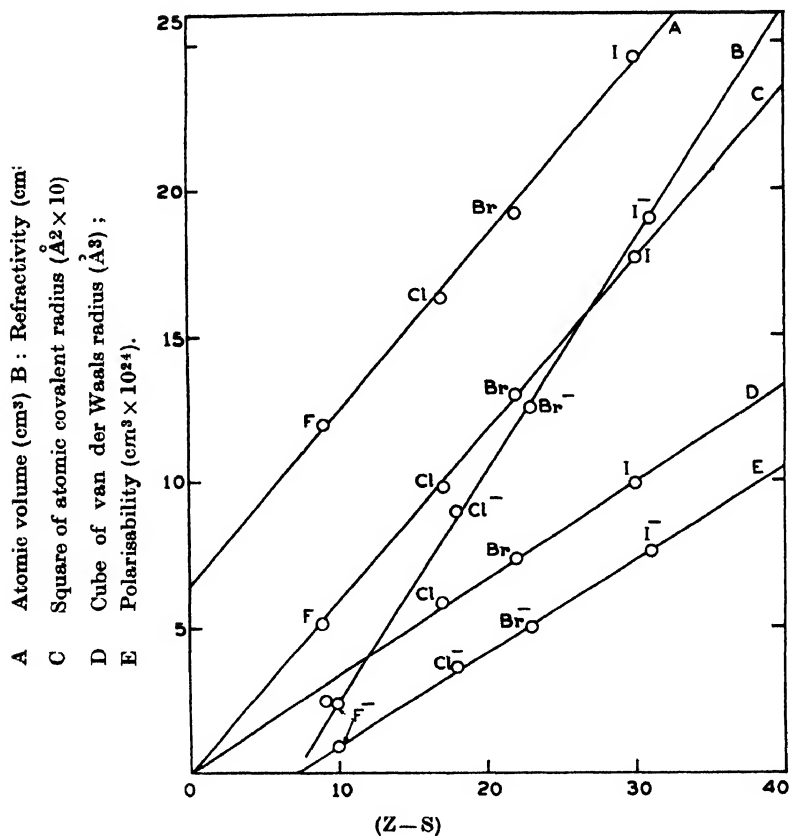


Fig. 2. Plots of some physical properties of halogens and their ions *vs.* $(Z-S)$.

The regularities reported above for halogens also apply to other similar sequences of elements and the most surprising thing is that practically the same set of S -values as found for F, Cl, Br and I has also been found to hold good for corresponding elements in the following sequences, viz., (i) O, S, Se and Te, (ii) N, P, As and Sb, (iii) C, Si, Ge and Sn, (iv) B, Al, Ga and In, (v) Mg, Ca, Sr and Ba, (vi) Na, K, Rb and Cs and (vii) Ne, Ar, Kr and Xe, with respect to at least

some physical properties of these elements and their compounds. A few typical illustrations are shown in figure 3.

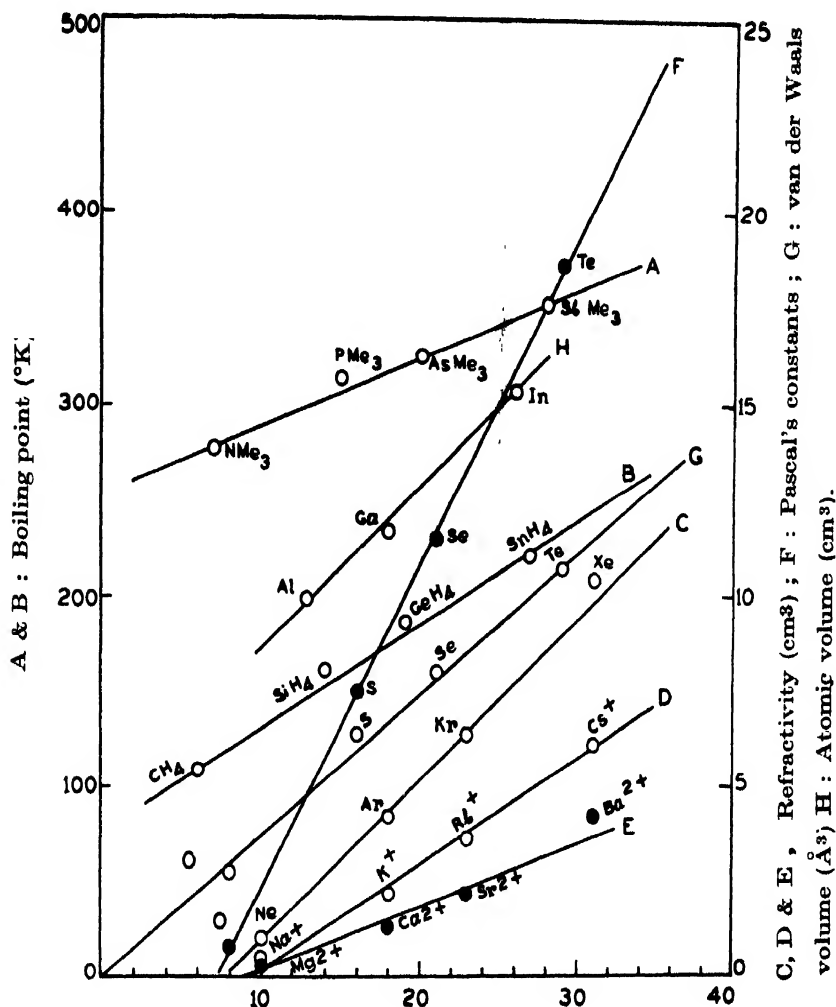


Fig. 3. Plots of some physical properties vs. $(Z-S)$ for various sequences.

A detailed account of the above relationships will appear elsewhere.

The author expresses his indebtedness to Prof. Santi R. Palit for his kind interest and helpful suggestions and thankfully acknowledges the help of the Council of Scientific and Industrial Research, Govt. of India, for financial aid.

2. BOILING POINT AND ATOMIC SIZE

G. R. SOMAYAJULU AND SANTI R. PALIT

INDIAN ASSOCIATION FOR THE CULTIVATION OF SCIENCE, JADAVPUR, CALCUTTA

(Received for publication April 2, 1956)

One of the authors (G.R.S.) has discovered a simple relation¹ (Somayajulu, 1956) that the boiling points and quite a few other properties of halogens and also of a series of analogous halogen compounds, are linear with the sum of the effective atomic number, Z' where $Z' = Z - S$, Z being the atomic number of the halogens in the molecule and S is a screening constant whose value is zero for F and Cl, 13 for Br and 23 for I. Following on the above clue it has been found,

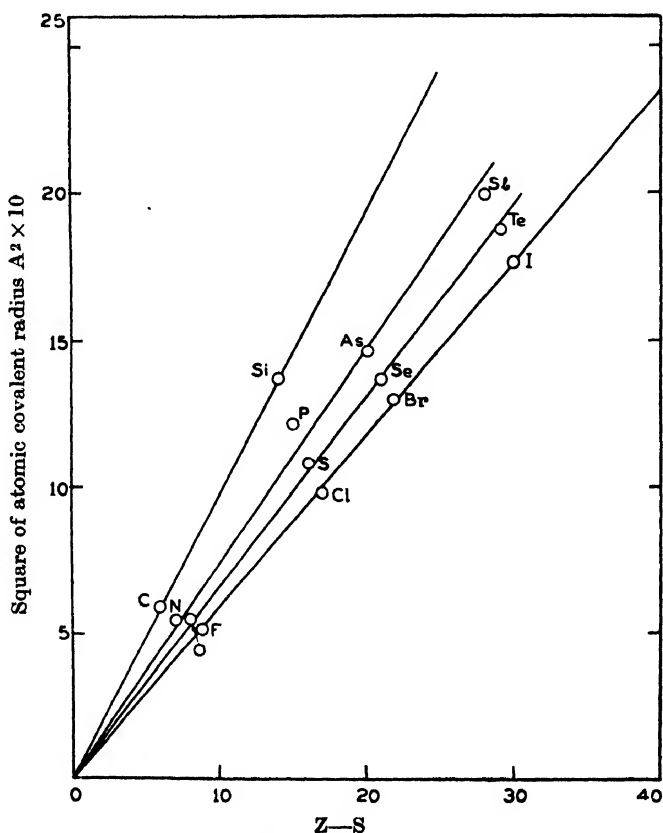


Fig. 1. Plots of square of atomic covalent Radii vs. $Z-S$.

as shown in figure 1, that the squares of the covalent radii are also linear with Z' for the following sequences, (i) F, Cl, Br and I, (ii) O, S, Se and Te and (iii) N, P, As and Sb, using the same sequence of values of S as given by Soma-

yajulu for all the above three groups of four elements. The most striking feature of these straight lines is that they pass through the origin which leads to a few rather unexpected conclusions as discussed below. All data for covalent radii, r , have been taken from the latest compilation by Schomaker and Stevenson (1941).

Size of the Covalent Atom:—Assuming that the effective atomic number, Z' represents the net nuclear charge of the atom in so far as it determines the physical properties as described by Somayajulu (1956), the most obvious conclusion is that the normal induction per unit surface area for all atoms in the same group of the periodic table is the same and increases with increase in group number or electro-negativity within the same period. It thus appears that the covalent size of an atom is predominantly determined by its effective nuclear charge, $Z'e$

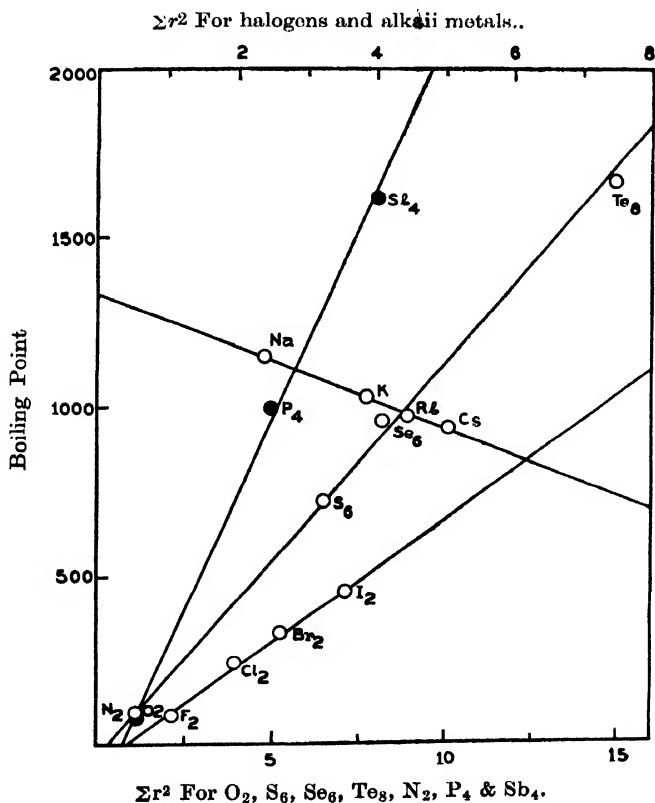


Fig. 2. Plots of boiling point vs. $p\Sigma r^2$.

such that it attains the same effective normal induction per unit area for all members of the same group. Alternatively, since eZ'/r^2 is the field strength on the surface of an atom due to its effective nuclear charge, we can as well say that all atoms of the same group have on their surface the same effective field strength owing to their nuclear charge, and the field strength increases with

increasing group number. This is a rather unusual conclusion whose full significance, particularly with reference to the electronegativity scale is yet to be elucidated.

Boiling Point and Atomic Size—Combining figure 1 with Somayajulu's findings, as summarised in the opening paragraph, we immediately see that the boiling point of the halogens and similar halogen compounds should be linear with the sum total of the surface area of the halogens in the molecule. This is shown in figure 2 curve A for halogens. It would be seen that an excellent straight line is obtained. The obvious conclusion is that the boiling points of similar halogen compounds are determined by the sum of the surface area of the constituent atoms. This is further corroborated by plotting the available data for other groups. Thus, curve B shows that O_2 , S_8 and Se_8 being the states in which they occur near their boiling points, also give a good straight line. Curve C shows that the relationship is also valid for N_2 , P_4 and Sb_4 (datum for As is not available). It thus appears established that the boiling points of elements are simply related to the sum total of the surface area of the constituent atoms in the molecule.

The above relationship also holds good fairly well (curve D) for the alkali metal sequences Na, K, Rb and Cs; but here the slope is reversed. This interesting behaviour is however, understandable from figure 2. From curves A, B and C we find that the slope increases with decreasing periodic group number and so, in this case the slope has become much more than a right angle. In fact, we can reasonably expect from the above trend that somewhere around the middle groups of the periodic table these B. P. versus r^2 curves may be just steeper than a right angle as a result of which the first members are likely to show very high boiling points. This is in agreement with the well-known occurrence of high boiling elements, viz., B, Si, etc., in this region. It is thus seen that the trend in boiling points in various groups of the periodic table, though apparently irregular, forms part of a common plan depending on the size and nuclear charge for the whole periodic table; an explanation of the whole plan itself however, is yet to be found.

Schomaker V. and Stevenson, D. P. 1941, *J. Amer. Chem. Soc.* **63**, 37.

Somayajulu, G. R. 1956. *Ind. Jour. Phys.* **30**, 258, the foregoing note.

COMPTON SCATTERING OF LIGHT BY ELECTRON

D. BASU AND D. P. SURAL

DEPARTMENT OF THEORETICAL PHYSICS, INDIAN ASSOCIATION FOR THE CULTIVATION OF
SCIENCE, CALCUTTA.*(Received for publication, April 12, 1956)*

ABSTRACT. In this paper the relative importance of the influence of spin and relativity on the decrease of the Compton scattering cross section with increasing photon energy has been studied in the semirelativistic approximation. A semirelativistic Hamiltonian in which the influence of spin can be treated with the Pauli theory has been constructed and the total scattering cross section determined by the second order perturbation method. The terms due to relativity and spin have appeared separately in the final result; the spin tends to increase the cross section so that the influence of relativity effect is predominant in making the Compton scattering cross section decrease with increasing energy.

INTRODUCTION

It is well-known that the quantum mechanical cross section for Compton scattering of light by free electron, as calculated by the second order perturbation method agrees with the Thomson formula in the nonrelativistic limit but differs appreciably from it even for energies slightly higher than the nonrelativistic limit. The cross section, first derived by Klein and Nishina, comes out to be the same whether one uses the Dirac one electron theory in which the negative energy states are unoccupied or the Dirac hole theory where all the negative energy states are initially filled up. It is of some interest to study the relative importance of the influence of spin and relativity on the decrease of the scattering cross section from the Thomson formula when energy begins to increase. The exact relativistic equation of motion of an electron in a specified electromagnetic field based on the classical theory has been given by Dirac (1938); but he has calculated the scattering cross section in the limit of very low energy, thus getting only the Thomson formula corrected by the damping effect. On the other hand, Dirac's quantum theory of the electron incorporates spin and relativity in an inseparable way, that is why it is not possible to separate the two influences in the Klein-Nishina formula. We shall therefore try to approach the problem from the semirelativistic Hamiltonian in which the influence of spin can be treated with the Pauli spin theory. In this method the corrections due to relativity and spin

appear separately, as such the method would fulfil our purpose but it has the limitation that it cannot be pushed to high relativistic energies. In the region where our semirelativistic approach is valid, it will be seen that the effect of the spin is to increase the scattering cross section. The calculation of Booth and Wilson (1940) shows that the cross section of scattering of light by vector meson is larger than that by spinless scalar meson; further the curve for the Klein-Nishina correction lies above that due to scalar meson scattering. All these indicate that the spin of the particle tends to increase the scattering cross section. So we are led to conclude that the decrease of the Klein-Nishina cross section with energy is due to relativity, the exact effect of which, however, has not been taken into account in the calculations based on the classical theory of Dirac.

2. SCATTERING CROSS SECTION

The Hamiltonian of the electron-radiation system is the sum of the Hamiltonian of the transverse radiation field and the Hamiltonian of the electron which includes the electron-radiation interaction. To express the latter in our semirelativistic approximation we start with the Dirac Hamiltonian which satisfies the equation

$$\{H - \beta\mu - \vec{\alpha} \cdot (\vec{p} - e\vec{A})\}\psi = 0 \quad \dots (1)$$

where μ and \vec{p} are the mass and momentum of the electron in energy units and the other symbols have their usual meaning. \vec{A} is only the transverse part of the vector potential satisfying $\text{div } \vec{A} = 0$. Multiplying the above by $H + \beta\mu + \vec{\alpha} \cdot (\vec{p} - e\vec{A})$ from the left we obtain the well-known relation

$$H'\psi = \left\{ \frac{1}{2\mu} (\vec{p} - e\vec{A})^2 - \frac{e\hbar c}{2\mu} (\vec{\sigma} \cdot \vec{H}) - \frac{ie\hbar}{2\mu} \vec{\alpha} \cdot \frac{\partial \vec{A}}{\partial t} - \frac{H'^2}{2\mu} \right\} \psi \quad \dots (2)$$

where $H' = H - \mu$, $\sigma_3 = -i\alpha_1\alpha_2$ etc., and the magnetic field $\vec{H} = \text{curl } \vec{A}$. We neglect the term involving $\vec{\alpha} \cdot \frac{\partial \vec{A}}{\partial t}$ on the same ground as Dirac has done. Further the last term $H'^2/2\mu$ is regarded as very small so that in it we can take for H' the approximate value

$$H' = \frac{1}{2\mu} (\vec{p} - e\vec{A})^2 - \frac{e\hbar c}{2\mu} (\vec{\sigma} \cdot \vec{H}).$$

We then obtain

$$H'\psi = \left[\frac{1}{2\mu} (\vec{p} - e\vec{A})^2 - \frac{e\hbar c}{2\mu} (\vec{\sigma} \cdot \vec{H}) - \frac{1}{2\mu} \left\{ \frac{1}{2\mu} (\vec{p} - e\vec{A})^2 - \frac{e\hbar c}{2\mu} (\vec{\sigma} \cdot \vec{H}) \right\}^2 \right] \psi \quad \dots \quad (3)$$

In our approximation we treat the σ matrices as Pauli's two-by-two matrices.

In the Hamiltonian in (3) the part due to free electron is $\frac{1}{2\mu} p^2 - \frac{1}{8\mu^3} p^4$; if we neglect the effect of the second term the eigen functions may be taken as $u_p e^{i\vec{p} \cdot \vec{r} / \hbar c}$ where u_p is the usual two component column-symbols. The other terms give the interaction of radiation with the electron. Since the Compton effect is a two quanta process and since calculations will be confined to second order approximation only, we shall retain in the interaction Hamiltonian the terms that are linear or quadratic in \vec{A} . Further, for an electron initially at rest the interaction terms having the operator \vec{p} at the extreme right will have no contribution to the matrix element and hence these terms are left out. The interaction Hamiltonian then becomes

$$\begin{aligned} H^{int} = & \frac{e^2}{2\mu} A^2 - \frac{e^2}{8\mu^3} \vec{p} \cdot \vec{p} A^2 - \frac{e^2 \hbar^2 c^2}{8\mu^3} H^2 - \frac{e^2 \hbar c}{8\mu^3} (\vec{p} \cdot \vec{A} + \vec{A} \cdot \vec{p}) (\vec{\sigma} \cdot \vec{H}) \\ & - \frac{e\hbar c}{2\mu} (\vec{\sigma} \cdot \vec{H}) + \frac{e\hbar c}{8\mu^3} p^2 (\vec{\sigma} \cdot \vec{H}). \end{aligned} \quad \dots \quad (4)$$

We consider the case of a photon of energy K_0 and momentum \vec{K}_0 (in energy units) colliding with an electron at rest ($\vec{p}_0 = 0$). After scattering the energy and momentum of the photon become K and \vec{K} respectively and those of the electron become E and \vec{p} . The differential cross section for the process is given by

$$d\phi = \frac{2\pi}{\hbar c} \rho_F \left\{ \frac{1}{2} \sum \Sigma \left| H_{F/i}^{int} \right|^2 \right\} \quad \dots \quad (5)$$

where $H_{F/i}^{int}$ is the scattering matrix element calculated from the interaction Hamiltonian (4), the summations are over both spin directions of the electrons before and after the scattering process and ρ_F , the density function of the final state is given by

$$\rho_F = \frac{d\Omega K^2}{(2\pi\hbar c)^3} \frac{EK}{\mu \vec{K}_0} \quad \dots \quad (6)$$

The first four terms in (4) will give rise to direct transitions, the corresponding matrix elements being

$$\frac{e^2}{\mu} \frac{2\pi\hbar^2 c^2}{\sqrt{K_0 K}} \left[\cos \Theta (u_p^* u_{p_0}) - \frac{1}{4\mu^2} (K_0^2 + K^2 - 2K_0 K \cos \alpha) \cos \Theta (u_p^* u_{p_0}) \right. \\ \left. - \frac{1}{4\mu^2} K_0 K \cos \theta (u_p^* u_{p_0}) + \frac{1}{4\mu^2 i} \left\{ K^2 \cos \left(\overset{\wedge}{\vec{e}_0 \vec{K}} \right) (u_p^* \sigma_\mu u_{p_0}) \right. \right. \\ \left. \left. + K_0^2 \cos \left(\overset{\wedge}{\vec{e} \vec{K}_0} \right) (u_p^* \sigma_\lambda u_{p_0}) \right\} \right] \dots \quad (7)$$

where

Θ = the angle between \vec{e}_0 and \vec{e} the unit vectors in the direction of polarisation of incident and scattered photon respectively,

α = the angle of scattering,

θ = the angle between the vectors $[\vec{k} \times \vec{e}_0]$ and $[\vec{k} \times \vec{e}]$, and $\sigma_\mu, \sigma_\lambda$ are the components of $\vec{\sigma}$ in the direction of the vectors $[\vec{K} \times \vec{e}]$ and $[\vec{K}_0 \times \vec{e}_0]$ respectively.

The fifth and sixth term in (4) will give rise to transitions only through the two types of intermediate states.

- I. \vec{K}_0 is first absorbed by the electron which gains the momentum \vec{K}_0 . In the transition to the final state \vec{K} is emitted, the momentum of the electron becoming $\vec{p} = \vec{K}_0 - \vec{K}$.
- II. \vec{K} is first emitted by the electron which gains the momentum $-\vec{K}$. In the transition to the final state \vec{K}_0 is absorbed.

The matrix element of $-\frac{e\hbar c}{2\mu} (\vec{\sigma} \cdot \vec{H})$ will be

$$\frac{e^2}{\mu} \frac{2\pi\hbar^2 c^2}{\sqrt{K_0 K}} \frac{K_0 K}{4\mu} \left[\frac{(u_p^* \sigma_\mu \sigma_\lambda u_{p_0})}{K_0 - \frac{1}{2} K_0^2 / \mu} + \frac{(u_p^* \sigma_\lambda \sigma_\mu u_{p_0})}{-K - \frac{1}{2} K^2 / \mu} \right] \dots \quad (8)$$

In the denominators, terms of order higher than K_0^2 / μ^2 have been neglected.

The matrix element of the term $\frac{e\hbar c}{8\mu^3} p^2 (\vec{\sigma} \cdot \vec{H})$ will be omitted because its contribution is of order higher than $\frac{e^2 2\pi\hbar^2 c^2}{\mu} \frac{K_0^2}{\sqrt{K_0 K} \mu^2}$.

The sum of the expressions (7) and (8) gives the scattering matrix element H_{fi}^{int} whence the value of $\frac{1}{2} \sum \Sigma |H_{fi}^{int}|^2$ can be calculated out by a direct spur calculation. Remembering that $\sigma_\mu \sigma_\lambda + \sigma_\lambda \sigma_\mu = 2 \cos \theta$ and using (5) and (6) we get the differential scattering cross section for the process as

$$d\phi = \frac{e^4}{\mu^2} d\Omega \frac{E}{\mu} \frac{K^2}{K_0^2} [B_1^2 + B_2^* B_2 + B_2'^* B_2' + B_3^2 + B_4^2 + 2B_1 B_3 \cos \theta + 2B_1 B_4 \cos \theta + 2B_2^* B_2' \cos \theta + 4B_3 B_4 \cos^2 \theta - 2B_3 B_4] \quad \dots (9)$$

where $B_1 = \cos \Theta - \frac{K_0^2 + K^2 - 2K_0 K \cos \alpha}{4\mu^2} \cos \Theta - \frac{K_0 K}{4\mu^2} \cos \theta$

$$B_2 = \frac{K^2 \cos(\vec{e}_0, \vec{K})}{4i\mu^2}, B_2' = \frac{K_0^2 \cos(\vec{e}, \vec{K}_0)}{4i\mu^2}, B_3 = \frac{K}{4\mu \left(1 - \frac{1}{2} \frac{K_0}{\mu}\right)}, B_4 = -\frac{K_0}{4\mu \left(1 + \frac{1}{2} \frac{K}{\mu}\right)}.$$

Using now the Compton relation

$$\left. \begin{aligned} K &= \frac{K_0}{1 + \frac{K_0}{\mu}(1 - \cos \alpha)} \\ E &= K_0 + \mu - K \end{aligned} \right\} \quad \dots (10)$$

the factors $\frac{K}{K_0}$, $\frac{K}{\mu}$ and $\frac{E}{\mu}$ occurring in (9) are expanded in powers of $\frac{K_0}{\mu}$.

Retaining terms up to order K_0^3/μ^2 we obtain

$$d\phi = \frac{e^4}{\mu^2} d\Omega \left\{ 1 - 2 \frac{K_0}{\mu} (1 - \cos \alpha) + 3 \frac{K_0^2}{\mu^2} (1 - \cos \alpha)^2 + \frac{K_0^2}{\mu^2} (1 - \cos \alpha) \right\} \times \\ \left[\cos^2 \Theta + \frac{1}{4} \frac{K_0^2}{\mu^2} - \frac{K_0^2}{4\mu^2} \cos^2 \theta - \frac{K_0^2}{\mu^2} (1 - \cos \alpha) \cos^2 \Theta - \frac{K_0^2}{2\mu^2} \cos \Theta \cos \theta + \right. \\ \left. \frac{K_0^2}{2\mu^2} \cos \alpha \cos \Theta \cos \theta \right] \quad \dots (11)$$

In the square bracket above the first term comes from the term $\frac{e^2}{2\mu} A^2$ in the interaction Hamiltonian which, in the nonrelativistic limit, would alone give the Thomson formula. The second and third terms are due to the spin part $-\frac{e\hbar c}{2\mu} (\vec{\sigma} \cdot \vec{H})$. The fourth term arises from $\frac{e^2}{2\mu} A^2$ and $-\frac{e^2}{8\mu^3} p^2 A^2$, the correction due to semirelati-

vistic velocities considered by us. The fifth term is the contribution of $\frac{e^2}{2\mu} A^2$ and $-\frac{e^2 \hbar^2 c^2}{8\mu^3} H^2$ and the last term results from both $\frac{e^2}{2\mu} A^2$ and the spin term $-\frac{e\hbar c}{2\mu} (\vec{\sigma} \cdot \vec{H})$. The terms in the curly bracket includes the effect of the density function ρ_F expanded in power series of $\frac{K_0}{\mu}$. In our approximation they combine with the contribution of the interaction $\frac{e^2}{2\mu} A^2$ to give the first four terms in the differential cross section (12) below. But the rest of the interaction Hamiltonian contributes to the differential cross section in combination with only the first term in the curly bracket. The differential cross section thus becomes

$$d\phi = \frac{e^4}{\mu^2} d\Omega \left[\left\{ 1 - 2 \frac{K_0}{\mu} (1 - \cos \alpha) + 3 \frac{K_0^2}{\mu^2} (1 - \cos \alpha)^2 + \frac{K_0^2}{\mu^2} (1 - \cos \alpha) \right\} \right. \\ \left. \cos^2 \Theta + \frac{1}{4} \frac{K_0^2}{\mu^2} - \frac{K_0^2}{4\mu^2} \cos^2 \theta - \frac{K_0^2}{\mu^2} (1 - \cos \alpha) \cos^2 \Theta - \frac{K_0^2}{2\mu^2} \cos \Theta \cos \theta + \right. \\ \left. + \frac{K_0^2}{2\mu^2} \cos \alpha \cos \Theta \cos \theta \right] \dots \quad (12)$$

Choosing now for \vec{e} two directions, one perpendicular to \vec{K}, \vec{K}_0 plane and other in the \vec{K}, \vec{K}_0 plane, it can be easily shown that

$$(\perp) \quad \cos \Theta = \sin \phi, \quad \cos \theta = \cos \alpha \sin \phi$$

$$(\parallel) \quad \cos \Theta = \cos \alpha \cos \phi, \quad \cos \theta = \cos \phi$$

where ϕ is the angle between \vec{K}_0, \vec{e}_0 and \vec{K}, \vec{K}_0 plane.

For unpolarised primary radiation, we are to average over ϕ and then

$$d\phi = \overline{d\phi_{\perp}} + \overline{d\phi_{\parallel}} \\ = \frac{1}{2} \frac{e^4}{\mu^2} d\Omega \left[\left\{ 1 - \frac{2K_0}{\mu} (1 - \cos \alpha) + \frac{3K_0^2}{\mu^2} (1 - \cos \alpha)^2 + \frac{K_0^2}{\mu^2} (1 - \cos \alpha) \right\} \right. \\ \left. (1 + \cos^2 \alpha) + \frac{K_0^2}{\mu^2} - \frac{K_0^2}{4\mu^2} (1 + \cos^2 \alpha) - \frac{K_0^2}{\mu^2} (1 - \cos \alpha) (1 + \cos^2 \alpha) \right. \\ \left. + \frac{K_0^2}{\mu^2} \cos \alpha + \frac{K_0^2}{\mu^2} \cos^2 \alpha \right] \dots \quad (13)$$

Integrating over all angles the total scattering cross section becomes

$$\begin{aligned}\phi &= \phi_0 \left[1 - 2 \frac{K_0}{\mu} + \frac{26}{5} \frac{K_0^2}{\mu^2} + \frac{3}{4} \frac{K_0^2}{\mu^2} - \frac{K_0^2}{\mu^2} \right] \\ &= \phi_0 \left[1 - \frac{2K_0}{\mu} + \frac{99}{20} \frac{K_0^2}{\mu^2} \right]\end{aligned}\quad (14)$$

where $\phi_0 = \frac{8\pi}{3} \frac{e^4}{\mu^2}$ is the Thomson cross section.

3. DISCUSSIONS

The total cross section according to Klein-Nishina formula when expanded in powers of $\frac{K_0}{\mu}$, gives only the first three terms of the expression in the right of

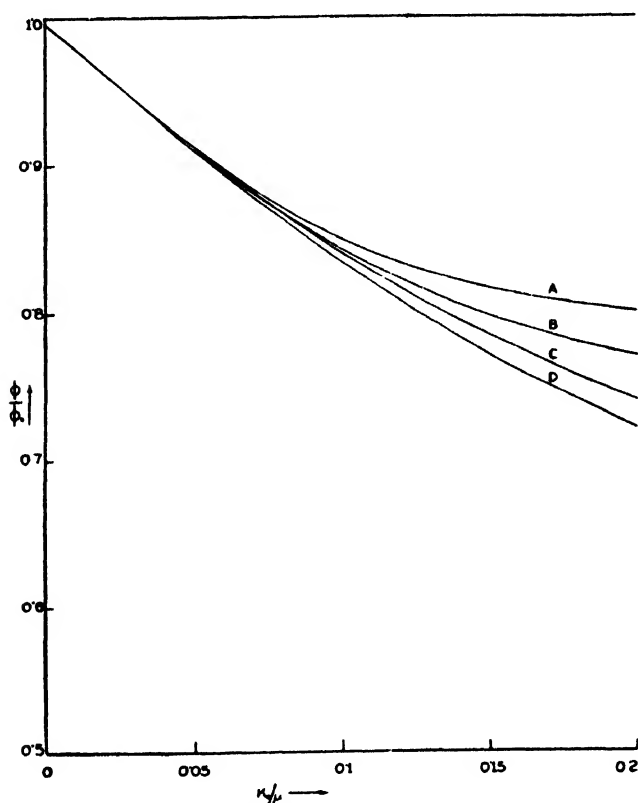


Fig. 1. Variation of scattering cross section with incident photon energy.

- A—Our value including spin correction.
- B—Our value excluding spin correction.
- C—Klein-Nishina formula,
- D—Booth-Wilson formula for scalar meson.

equation (14). In the relation (6) for the density function if we use the relation (10) and expand in powers of $\frac{K_0}{\mu}$ we obtain, from the interaction term $\frac{e^2}{2\mu} A^2$, exactly the second and third terms in (14) as correction to the Thomson formula. The last term is a further relativistic correction, whereas the fourth term is due to spin of the electron. Up to this approximation the influence of the term $-2 \frac{K_0}{\mu}$ is predominant in making the Compton scattering cross section decrease with increasing energy. The spin term $\frac{3}{4} \frac{K_0^2}{\mu^2}$, though small compared to the relativity contributions, has a definite effect and it tends to increase the scattering cross section. In the figure 1 below ϕ/ϕ_0 has been plotted against K_0/μ . Curve *A* is based upon (14) and the curve *B* is obtained from (14) excluding the spin term. The curve *C* gives the scattering cross section according to the exact Klein-Nishina formula. The curve *D* shows the cross section for scattering of light by spinless scalar mesons (μ in this case denoting the meson mass in energy units) as calculated by Booth and Wilson. It is clear that the Klein-Nishina cross section due to spinning electron lies above the Booth-Wilson cross section due to spinless mesons for a particular value of $\frac{K_0}{\mu}$. The separation of the spin and relativity term in (14) has thus been rightly effected at least up to this semirelativistic approximation.

REFERENCES

- Booth, F. and Wilson, A. H., 1940, *Proc. Roy. Soc. A.*, **175**, 483.
 Dirac, P. A. M., 1938, *Proc. Roy. Soc. A.*, **167**, 148.

ON WAVE NATURE OF MATTER. PART II.

BRAHMANANDA MISHRA

PHYSICS DEPARTMENT, RAVENSHAW COLLEGE, CUTTACK

(Received for publication, January 31, 1956)

Plate VII

ABSTRACTS. Investigation on the diffraction of a molecular beam by apertures of different shapes and sizes has been carried out and it is observed that straight slits produce a pair of fringe-like deposits with a minimum at the centre, the width of the fringe being smaller in the case of the wider slit.

In the case of circular apertures, circular deposits are formed at the centre, the radius of the central disc being smaller for the larger aperture.

INTRODUCTION

It was reported previously (Mishra, 1951) that when vapours of some organic compounds are allowed to pass through slits in an evacuated chamber and to be deposited on an ice-cooled metallic surface the deposit appears to consist of several systems of fringes. It was not known at the time how the whole pattern as well as the width of the fringes depend on the dimensions of the aperture. The investigation has therefore been repeated using apertures of different shapes and sizes and also vapours of substances having high melting points at moderately low temperatures.

EXPERIMENTAL ARRANGEMENT

The experimental arrangement is shown in figure 1, where K is a calibrated thermo-junction for recording temperatures, H is an electric heater, T is a resistance

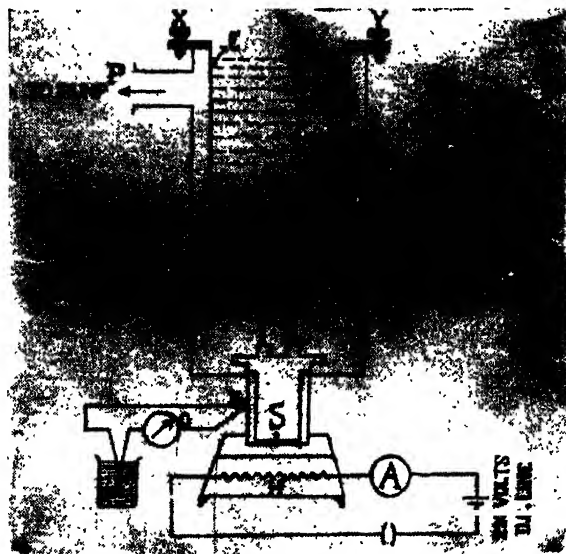


Fig. 1. Experimental arrangement.

which forms one arm of a Pirani gauge, A_1 and A_2 are two capillary tubes of bores, 0.36 mm. and 0.61 mm. respectively or two tunnel slits of widths 0.4 mm. and 0.8 mm. The distance between A_1 and A_2 was approximately 2 inches. The length of the capillary tubes or height of the tunnel slits was more than 10 cms. The apertures A_1 and A_2 were at a distance of 4 mm from the cold collecting surface.

P is the pumping system which is an Edward's Speedivac Model F 203 pump, consisting of an oil diffusion pump backed by a rotary pump. There were three valves in the pumping circuit, called baffle valve, isolation valve and backing valve. By operating the valves, one could conveniently produce either static vacuum or dynamic vacuum in the chamber. The minimum pressure attainable with our present arrangement was 0.020 mm. of mercury. S is a thin film of para-nitrobenzoic acid.

EXPERIMENTAL RESULTS

The patterns obtained with the vapour of para-nitrobenzoic acid at 40°C using the circular apertures of diameters 0.36 mm and 0.61 mm and long slits of widths 0.4 mm and 0.8 mm are reproduced in figures 2 and 3, Plate VII

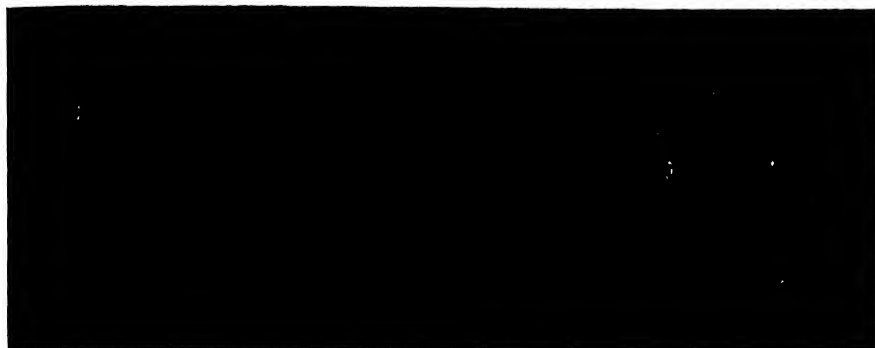
As the tubes or channels were each about 10 cms long the molecular beam just before reaching the apertures was almost parallel, the total divergence being about 15' of arc.

It is seen from figure 2 that in the case of the circular apertures of diameters 0.36 mm and 0.61 mm the pattern is circular. In each case there is a circular deposit at the centre, the diameter of the deposit being larger for smaller aperture. This deposit is surrounded by a blackened annular area, the diameter of which is smaller in the case of the smaller aperture.

In the patterns due to the two slits (figure 3) there is practically no deposit at the centre. The central portion, however, appears as black, probably due to chemical action of a very thin deposit of the compound with brass surface. On each side of the central minimum there is a fringe-like deposit in both the cases. The central black fringe is wider in the case of the wider slit, but the width of the fringe formed by the deposit of the compound is larger in the case of the narrower slit. The actual widths are shown in Tables I and II.

TABLE I
Straight slit

Slit width in mm.	Width of the fringe in mm.
0.40	5.20
0.80	3.00



(a)

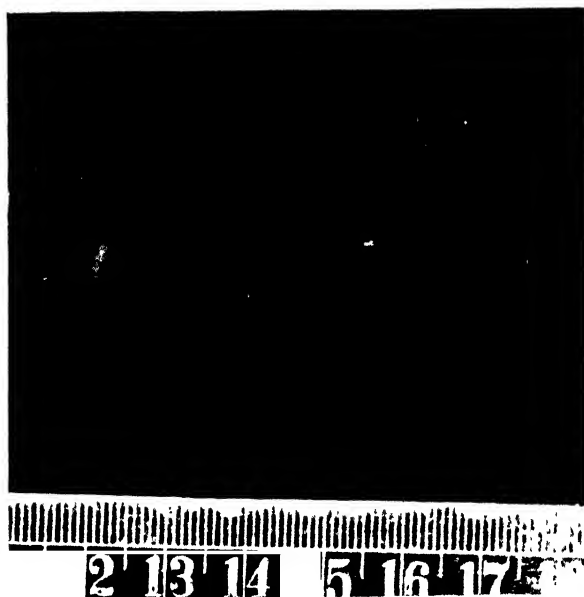
(b)

Fig. 2.

Patterns formed by *p*-nitrobenzoic acid by two capillary tubes.

(a) Diameter of capillary bore = 0.36 mm.

(b) Diameter of capillary bore = 0.61 mm.



(a)

(b)

Fig. 3

Patterns formed by *p*-nitrobenzoic acid by two slits.

(a) Width of slit = 0.8 mm.

(b) Width of slit = 0.4 mm.

TABLE II
Circular aperture

Diameter of the bore in mm.	Diameter of the central disc in mm.
0.36	3.6
0.61	2.2

DISCUSSION

It will be noted that in both figures 2 and 3, the widths of the minima show irregularities which may be due to the spreading of chemical action of minute quantities of *para*-nitrobenzoic acid on brass surface. For the actual material deposits of benzoic acid on brass surface, it is evident from the results given in Tables I and II, that the width of the fringe-like deposit is larger in the case of the narrower slit and also the diameter of the circular deposit is smaller for the larger circular aperture. These results show that the deposit is not formed by a beam of molecules travelling along the axis of the beam, but after emerging from the aperture their path is bent in opposite directions like diffraction of waves. These results are obtained with the chamber once evacuated and kept hermetically sealed or with a chamber which was being evacuated continuously by the pumping system. The reproduction of the pattern in both static and dynamic vacuum indicates the phenomenon to be a molecular one. The deposit was formed very slowly in about 80 hours at a temperature moderately above room temperature and it appears that the patterns are formed only when the molecules are collected one by one.

REFERENCE

Mishra, B., 1951, *Ind. J. Phys.*, **25**, 57.

ULTRAVIOLET ABSORPTION SPECTRA OF FROZEN SOLUTIONS OF *o*-, *m*- AND *p*-CHLOROTOLUENE^{*} IN ISOBUTYL ALCOHOL^{*}

S. B. ROY

OPTICS DEPARTMENT, INDIAN ASSOCIATION FOR THE CULTIVATION OF SCIENCE, JADAVPUR,
CALCUTTA-32

(Received for publication, April 25, 1956)

ABSTRACT. The ultraviolet absorption spectra of solutions of *o*-, *m*- and *p*-chlorotoluene in isobutyl alcohol in the liquid and solid states at -180°C have been investigated. The results obtained have been compared with those reported by previous workers for the pure liquid and for solid state at -180°C . It has been observed that in case of the solutions in the solid state no splitting of electronic energy level of either *o*-chlorotoluene or *m*-chlorotoluene molecule takes place although in the case of the pure substances in the solid state splitting of the band was observed by previous workers.

In the case of *p*-chlorotoluene, the position of the 0, 0 band due to the pure liquid, solution in isobutyl alcohol and the solution frozen and cooled to -180°C is almost the same but it shifts much when the pure substance is frozen and cooled to -180°C .

Probably the presence of permanent electric moment in the molecules of the ortho- and the meta-compound facilitates formation of virtual bonds between neighbouring molecules in the solid phase of the pure substances. Formation of such bonds may be responsible for splitting of the energy level.

INTRODUCTION

The ultraviolet absorption spectra of *o*-, *m*- and *p*-chlorotoluene in liquid and solid states were investigated by Swamy (1952) and it was shown by him that in all these cases the principal bands in the liquid state shift towards shorter wavelengths on solidification of the liquids. In the case of both *o*- and *m*- chlorotoluene in the solid state, the electronic energy level was found to be split up into three components. In the case of *p*-chlorotoluene on the other hand, no such splitting was observed. It was concluded by him that this splitting of the electronic energy level may be due to the strong intermolecular field, which may be produced by the formation of virtual bonds between neighbouring molecules in the solid state.

Wolf and Harold (1931) studied the ultraviolet absorption spectra of *o*-, *m*- and *p*-chlorotoluene dissolved in heptane. They observed a larger number of bands in the case of the solution than in the case of the pure liquid (Swamy, 1952). In the case of *o*- and *m*-chlorotoluene, the 0,0 band shifts towards shorter wavelengths by 100 to 200 cm^{-1} from its position in the case of the pure liquid,

* Communicated by Prof. S. C. Sirkar.

whereas in the case of *p*-chlorotoluene, the shift is towards the longer wavelengths and it is only by about 30 cm^{-1} .

McConnell and Tunnicliff (1955) studied the ultraviolet absorption spectra of β -methyl naphthalene in rigid glass medium of 3-methyl pentane at 77°K . As the molecules were in a dispersed state, the absorption bands were attributed by them to single molecules. Recently, Banerjee (1956) studied the ultraviolet absorption spectra of pure α - and β -methyl naphthalene in the solid state at -180°C . He found that the 0,0 band due to pure β -methyl naphthalene in the solid state at -180°C is at a distance of 300 cm^{-1} on the longer wavelength side with respect to the position of 0,0 band due to the frozen solution of the substance in 3-methyl pentane reported by McConnell and Tunnicliff (1955). He concluded that the association of the molecules in the pure substance in the solid state might be responsible for this shift of the 0,0 band. The object of the present investigation was to compare the absorption spectra of pure *o*-, *m*- and *p*-chlorotoluene at -180°C with those of the frozen solutions of the substances in a suitable solvent in order to find out whether the intermolecular field has any marked influence on the absorption spectra.

EXPERIMENTAL

The experimental arrangement was the same as that used by Swamy (1951), but instead of the Hilger quartz E 1 spectrograph used by him an Adam Hilger medium quartz spectrograph, having a dispersion of $10\text{\AA}/\text{mm}$ in the 2600\AA region was used in the present investigation.

The absorption cell consists of two plain parallel quartz discs cemented with Araldite cement to a ring-shaped distance piece of brass of thickness 1.4 mm. The inner diameter of the annular brass ring is about 8 mm. A groove cut across the annular ring, parallel to its radius facilitates the introduction and removal of liquids with the help of a hypodermic syringe.

The cell was mounted in a brass frame provided with a long vertical rod which was held by a clamp. The cell was suspended in a transparent Dewar vessel made of fused silica and first the spectrum of the solution contained in the cell was photographed. Next, liquid oxygen was introduced in the Dewar vessel and the solution was frozen and cooled to about -180°C by suddenly immersing the cell in the liquid oxygen. When the solution was frozen into a transparent mass, the brass frame was raised a little, so that the cell was above the surface of the liquid oxygen, but the lower end of the brass frame was still immersed in the liquid oxygen and the ultraviolet absorption spectra of the frozen solution was photographed. The level of the liquid oxygen was kept constant during the exposure. The solvent used was isobutyl alcohol which was found to exhibit no absorption in the region under consideration either in the liquid state or in the solid state at -180°C . Very dilute solutions of *o*-, *m*- and *p*-chlorotoluene in isobutyl alcohol yielded homogeneous transparent mass when frozen at -180°C .

The experimental liquids were of chemically pure quality and were repeatedly distilled in vacuum before use. The proper strength of the solutions was determined by trial.

Ilford HP3 films were used for photographing the absorption spectra. The continuum was given by a hydrogen discharge tube. The time of exposure in each case was a few minutes only. Microphotometric records of these spectra were taken with a Kipp and Zonen type self-recording microphotometer. Iron arc spectrum was recorded on each spectrogram as a comparison.

The frequencies of these bands were measured with the help of these microphotometric records of the absorption spectra in which records of two known iron lines were taken as reference lines, and the records of the iron arc spectrum photographed as comparison.

RESULTS

The microphotometric records of the spectra are reproduced in figures 1, 2 and 3 and the wave numbers of the bands and their probable assignments are given in Tables I, II, III, IV, V and VI.

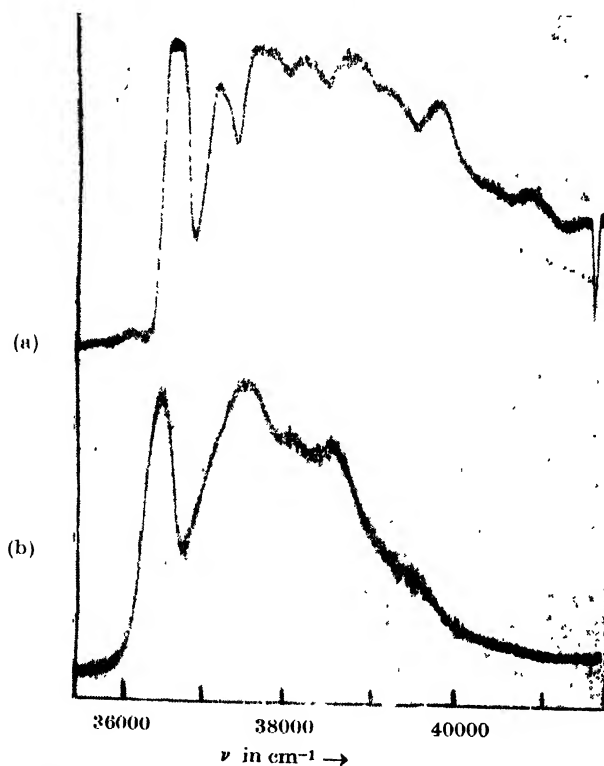


Fig. 1. Microphotometric records of the ultraviolet absorption spectra of solutions of *o*-chlorotoluene in isobutyl alcohol.

(a) Frozen solution at -180°C .

(b) Solution at 25°C .

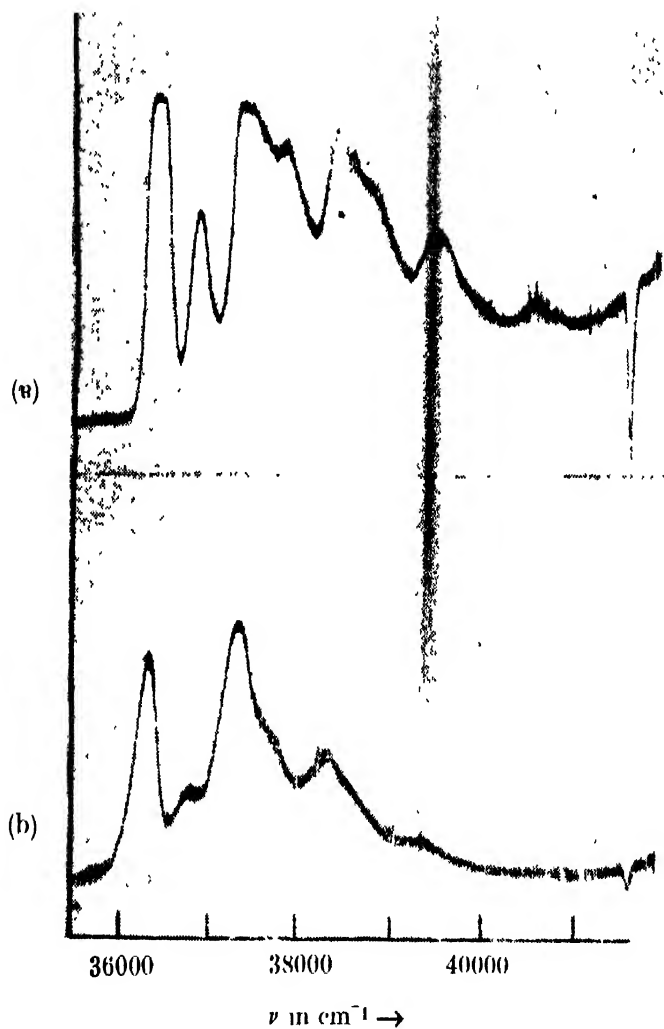


Fig. 2. Microphotometric records of the ultraviolet absorption spectra of *m*-chlorotoluene in isobutyl alcohol.

(a) Frozen solution at -180°C

(b) Solution at 25°C

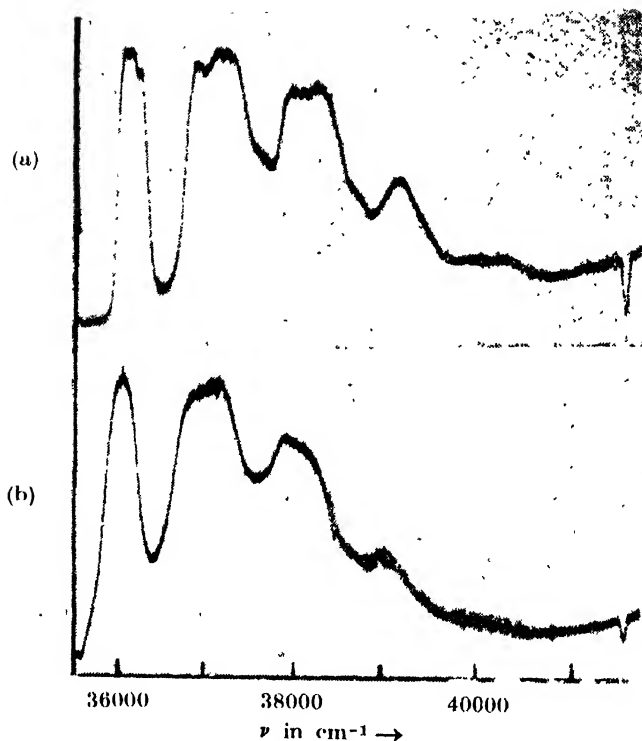


Fig. 3. Microphotometric records of the ultraviolet of absorption spectra of solution of *p*-chlorotoluene in isobutyl alcohol. Curve (a) Frozen soln. at -180°C . Curve (b) Soln. at 25°C .

DISCUSSION

TABLE I

Absorption spectra of *o*-chlorotoluene

Pure liquid (Swamy, 1952)		Solution in heptane (Wolf and Harold, 1931)		Solution in isobutyl alcohol (Present author)	
ν in cm^{-1}	Assignment	ν in cm^{-1}		ν in cm^{-1}	Assignment
36381 (vs) (broad)		ν_0		36499 (vs)	ν_0
		36560 (s)		37012 (m)	$\nu_0 + 513$
37396 (s) (broad)	$\nu_0 + 1015$	37550 (m)		37512 (vs)	$\nu_0 + 1013$
38413 (w)	$\nu_0 + 2 \times 1015$			38011 (m)	$\nu_0 + 513 + 1013$
		38750 (s)		38538 (s)	$\nu_0 + 2 \times 1013$
		39500 (m)			
		40550 (w)		39529 (w)	$\nu_0 + 3 \times 1013$

TABLE II

 Absorption spectra of *o*-chlorotoluene

Pure solid at -180°C (Swamy, 1952)		Frozen solution in isobutyl alcohol at -180°C (Present author)	
ν in cm^{-1}	Assignment	ν in cm^{-1}	Assignment
		36156 (w)	$\nu_0 - 513$
		36672 (vs)	
36830 (m)	B_0		
37122 (vs)	A_0	37177 (s)	$\nu_0 \pm 505$
37420 (m)	C_0		
37840 (vs)	$\{B_1$ $\{B_0 \pm 1010$	37710 (vs)	$\nu_0 \pm 1038$
38130 (s)	$\{A_1$ $\{A_0 \pm 1010$		
38428 (ms)	$\{C_1$ $\{C_0 \pm 1008$	38214 (vs)	$\nu_0 \pm 505 \pm 1038$
38849 (m)	$\{B_2$ $\{B_1 \pm 2 \times 1010$	38748 (vs)	$\nu_0 \pm 2 \times 1038$
		39235 (s)	$\nu_0 \pm 2 \times 1038 \pm 505$
		39781 (m)	$\nu_0 \pm 3 \times 1038$
		40294 (w)	$\nu_0 \pm 3 \times 1038 \pm 505$
		40820 (w)	$\nu_0 \pm 4 \times 1038$

It can be seen from Tables I and II that in the case of solution of *o*-chlorotoluene in isobutyl alcohol the absorption bands can be assigned to progression of excited state frequencies 513cm^{-1} and 1013cm^{-1} . When the solution is frozen and cooled to -180°C the bands can again be classified in the same way, the excited state frequencies now being changed respectively to 505cm^{-1} and 1038cm^{-1} . Thus the splitting of the energy levels observed in the case of the pure substance in solid state (Swamy, 1952) does not take place when the molecules are dispersed in the forezen isobutyl alcohol. A comparison of the positions of the 0,0 band observed in the case of the substance in different environments shows that the influence of solvent molecules causes the 0,0 band to shift towards shorter wavelengths from its position in the spectrum due to pure liquid. The shift is, however, less than 200cm^{-1} , but the influence of intermolecular field increases very much when the liquid is solidified to form a polycrystalline mass, so that the 0,0 band shifts by about 740cm^{-1} towards shorter wavelengths and also the band is split up into three components. Thus it is quite evident that when the molecules are surrounded by similar molecules in the solid state, the influence of intermolecular field is the largest. This indicates that probably, some virtual bonds are formed between the molecules when the liquid is solidified and cooled to -180°C .

TABLE III
Absorption spectra of metachlorotoluene

Pure liquid (Swamy, 1952)		Solution in heptane (Wolf and Herold, 1931)	Solution in isobutyl alcohol (Present author)	
ν in cm^{-1}	Assignment	ν in cm^{-1}	ν in cm^{-1}	Assignment
36315 (vs) (broad)	ν_0	36400 (s)	36353 (s)	ν_0
36742 (vw)	$\nu_0 + 427$		36794 (w)	$\nu_0 + 441$
37310 (vs) (broad)	$\nu_0 + 995$	37400 (s)	37330 (vs)	$\nu_0 + 977$
38297 (m)	$\nu_0 + 2 \times 995$	38350 (m)	37767 (vw)	$\nu_0 + 441 + 977$
		39350 (w)	38318 (ms)	$\nu + 2 \times 977$
			39280 (w)	$\nu_0 + 3 \times 977$

TABLE IV
Absorption spectra of metachlorotoluene

Pure solid at -180°C (Swamy, 1952)		Frozen solution in isobutyl alcohol at -180°C (Present author)	
ν in cm^{-1}	Assignment	ν in cm^{-1}	Assignment
36120 (m)	C_0	36405 (vs)	ν_0
36630 (s)	B_0	36862 (s)	$\nu_0 + 457$
37015 (vs)	A_0		
37150 (w)	C_1	37386 (vs)	$\nu_0 + 981$
37656 (s)	B_1	37839 (s)	$\nu_0 + 457 + 981$
38040 (s)	$\begin{Bmatrix} \text{A}_1 \\ \text{A}_0 + 1025 \end{Bmatrix}$		
38175 (m)	C_2	38376 (s)	$\nu_0 + 2 \times 981$
38680 (w)	B_2	38823 (ms)	$\nu_0 + 2 \times 981 + 457$
39065 (s)	$\begin{Bmatrix} \text{A}_2 \\ \text{A}_0 + 2 \times 1025 \end{Bmatrix}$		
39200 (vw)	C_3	39358 (ms)	$\nu_0 + 3 \times 981$
		39813 (vw)	$\nu_0 + 3 \times 981 + 457$
		40343 (w)	$\nu_0 + 4 \times 981$

TABLE V
 Absorption spectra of *p*-chlorotoluene

Pure liquid (Swamy, 1952)		Solution in heptane (Wolf and Harold, 1931)	Solution in isobutyl alcohol (Present author)	
ν in cm^{-1}	Assignment	ν in cm^{-1}	ν in cm^{-1}	Assignment
36059 (vs,b)	ν_0	36030 (s)	36038 (vs)	ν_0
		36930 (s)	36862 (s)	$\nu_0 + 824$
37071 (vs,b)	$\nu_0 + 1012$		37136 (s)	$\nu_0 + 1098$
		37400 (w)		
		37990 (s)	37953 (mb)	$\nu_0 + 824 + 1098$
38075 (m)	$\nu_0 + 2 \times 1008$	38760 (s)		
		39650 (w)	39051 (wb)	$\nu_0 + 824 + 2 \times 1098$

 TABLE VI
 Absorption spectra of *p*-chlorotoluene

Pure solid at -180°C (Swamy, 1952)		Frozen solution in isobutyl alcohol at -180°C (Present author)	
ν in cm^{-1}	Assignment	ν in cm^{-1}	Assignment
36240 (vs)	ν_0	36064 (vs)	ν_0
36992 (s)	$\nu_0 + 768$	36875 (s)	$\nu_0 + 811$
37282 (s)	$\nu_0 + 1058$	37177 (vs)	$\nu_0 + 1113$
37756 (w)	$\nu_0 + 2 \times 768$	37681 (m)	$\nu_0 + 2 \times 811$
38048 (s)	$\nu_0 + 768 + 1058$	37982 (s)	$\nu_0 + 811 + 1113$
38344 (m)	$\nu_0 + 2 \times 1058$	38288 (s)	$\nu_0 + 2 \times 1113$
		38793 (w)	$\nu_0 + 2 \times 811 + 1113$
		39096 (m)	$\nu_0 + 2 \times 1113 + 811$
39118 (m)	$\nu_0 + 2 \times 1058 + 768$	39908 (vw)	$\nu_0 + 2 \times 1113 + 2 \times 811$
		40229 (vw)	$\nu_0 + 3 \times 1113 + 811$

As the unit cell is anisotropic, the nature of such linkages in three different directions in the lattice, may be different from each other and this difference may be responsible for producing the three components of the energy states indicated by the splitting of the bands. The bands observed in the case of *m*-chlorotoluene under different conditions show that the intermolecular field in the liquid state, has only a small influence on the position of the bands irrespective of whether

the molecules are surrounded by those of the same type, as in the case of the pure liquid, or of different types as in the case of solutions. Even when the solution in isobutyl alcohol is frozen the 0,0 band shifts only by about 50 cm^{-1} towards shorter wavelengths. On the other hand, when the pure liquid is frozen, the 0,0 band shifts by about 700 cm^{-1} and the bands indicate splitting of the excited state energy level into three components. Thus in this case also, similar molecules in the solid state exert much greater influence on the electronic state than molecules of other types and this may be due to formation of virtual linkage between adjacent molecules in the lattice as in the case of *o*-chlorotoluene. The excited state frequencies 441 and 977 cm^{-1} observed in the case of the solution in the liquid state are not altered much when the solution is frozen as in the case of the ortho compound.

In the case of *p*-chlorotoluene the 0,0 band given by the pure liquid, solutions in heptane and in isobutyl alcohol and frozen solution in isobutyl alcohol, is almost at the same position but this position, is shifted from that of 0,0 band due to vapour (Viswanath, 1952) by about 250 cm^{-1} towards longer wavelengths. When the pure liquid is solidified the 0,0 band tends to return to its position observed in the case of the vapour. This shows that when the two substituents are in the para position and the molecules are arranged regularly in the lattice, the intermolecular fields due to different neighbouring molecules cancel each other and also the value of the permanent electric moment being small, the chance of the formation of associated molecules is much less in this case than in the case of *o*- and *m*- compounds. So, the absence of the splitting of the energy level indicates that no such association of molecules takes place in solid state in this particular case. These results thus confirm the view expressed above that in the case of *o*- and *m*- compounds, the splitting of the energy level is caused by formation of associated molecules. A comparison of the absorption spectra of the frozen solutions of these three compounds with those of the pure substances in the solid state thus leads to the conclusion that in the case of the *o*- and *m*- compounds owing to the presence of permanent electric moment, the molecules become strongly associated with each other through virtual linkages in the solid state and such association causes splitting of the energy state.

ACKNOWLEDGMENT

The author's grateful thanks are due to Professor S. C. Sirkar, D.Sc., F.N.I. for kindly suggesting the problem and guidance throughout the progress of the work.

REFERENCES

- Banerjee, S. B., 1956, *Ind. J. Phys.*, **30**, 106.
- McConnell, H. M. and Tunnicliff, D. D., 1955, *J. Chem. Phys.*, **23**, 927.
- Swamy, H. N., 1952, *Ind. J. Phys.*, **26**, 445.
- Viswanath, G., 1952, *Ind. J. Phys.*, **26**, 263.
- Wolf, K. L. and Harold, W., 1931, *Z. f. Phys. Chem.*, **B13**, 201.

ORIGIN OF THE ZODIACAL LIGHT AND THE VARIATIONS OF ITS BRIGHTNESS

PRABHAT K. SENGUPTA

METEOROLOGICAL OFFICE, SAFDARJUNG AIRPORT, NEW DELHI, INDIA

(Received for publication, March 15, 1956)

ABSTRACT. It has been suggested that the zodiacal light originates from the scattering of photospheric radiation by electrons and interplanetary dust particles lying within an ellipsoidal volume in the interplanetary space with the sun at its centre. The corpuscles in the solar corpuscular stream, leaving the sun with velocities less than the velocity of escape and carrying the interplanetary dust particles with them, form the ellipsoidal volume with the rotation of the sun, and account for the lenticular shape of the zodiacal light and the varying inclinations of its light axis with the plane of the ecliptic in different seasons. The variations of the intensities during magnetic storms and with the advent of meteor swarms are satisfactorily explained with the help of the above picture, as due to the augmentations in the number of electrons in the solar corpuscular stream and the number of dust particles respectively.

I

According to the planetary theory (Mitra, 1952) of the zodiacal light, the phenomenon is manifested as a result of scattering of sunlight by a cloud of interplanetary dust particles of meteoric origin. The characteristic conical shape of the light is attributed to a concentration of the dust particles in the plane of the ecliptic in the form of a colossal lens having the sun at its centre. The particles are supposed to be rather small bodies but large enough not to be repelled by solar radiation pressure.

On the hypothesis that the outer corona of the sun is an extension of the zodiacal light and manifested in a similar manner, van de Hulst (1947) estimated the radii of the scattering particles to be of the order of .01 to .03 cm., and suggested a thickness of the order of 0.1 A.U. for the lenticular dust cloud. Allen (1946) from similar considerations, but assuming a non-homogeneous distribution of the dust particles, deduced the radii of the particles to be of the order of .001 cm. with density varying as r^{-1} , where r is the distance from the sun.

The observed polarization and brightness in the zodiacal light may be ascribed either to scattering by electrons or to reflection from interplanetary dust particles consisting of pulverized minerals like lava, basalt and granite, etc. (Whipple and Gossner, 1949). The first suggestion according to the estimates of Whipple and Gossner gives an upper limit of the density of electrons at 1 A.U. as 1000 cm^{-3} .

In view of Mie's theory of scattering, Siedentopf *et al* (1953) and Elsässer (1954) did not consider it possible for the dust particles to contribute materially to the polarized component of zodiacal light which they ascribed to scattering by electrons the brightness of zodiacal light was associated mainly with the scattering by dust particles. On this basis they deduced from photoelectric observations, the various densities of electrons and dust particles at different distances from the sun, the values being 600 cm^{-3} and $1.2 \times 10^{-15} \text{ cm}^{-3}$ respectively at 1 A.U. Generally the observations on the outer corona do not extend beyond 1° elongation from the sun, while those on the zodiacal light commence from 30° elongation, leaving a region between 1° to 30° elongations missing. But during the eclipse of February 25, 1952 at Khartoum, Pietenpol and Rense's (1953) observations covered the region between 5° and 15° elongations and confirmed that the zodiacal light is accounted for by the presence of a lenticular meteoric dust cloud having density falling off as r^{-1} (Jackson and Rense, 1953).

II

Of special interest to us are the variations of the intensity of the zodiacal light observed from time to time. The seasonal variations are well marked. There are other variations, which according to some observers (Elvey, 1937; Hulburt, 1930), occur during meteoric showers or geomagnetic disturbances. Hulburt (*loc. cit*) pointed out that no planetary theory could account for the rapid variations in the brightness of the zodiacal light during geomagnetic disturbances and hence suggested an atmospheric theory based on the action of the molecules and ions formed in the upper atmosphere of the earth by solar ultraviolet light. It appears to the present writer that some of the magnetic storms mentioned by Hulburt were M-storms having a 27-day recurrence tendency suggesting a relationship between the zodiacal light and the solar corpuscular streams responsible for the geomagnetic disturbances. In fact, Whipple and Gossner (*loc. cit.*) had hinted a possible contribution to the luminosity of the zodiacal light from the scattering of sunlight by a high concentration of free electrons in the solar corpuscular streams. In this paper an attempt has been made to explain the variations of the brightness of zodiacal light, from a consideration of the behaviour of the material responsible for the phenomenon.

III

Allen (1944, 1946) identified the solar corpuscular streams with the coronal streamers through which coronal matter is supposed to be forced out in the form of a jet, containing electrons and positive ions (mostly protons) in equal numbers so as to make the streamers neutral. The streamer becomes luminous as a result of the scattering of sunlight by the electrons in the streamer, the scattering due to protons being negligible. The visible portion of the streamer has been so far

lines in figure 1 (in which the depression at the centre represents diminished activity at the higher latitudes of the sun beyond 40°). A few interplanetary dust particles are likely to be swept with the corpuscular stream and will behave in a similar manner. However, the probability of encounters with dust particles will be extremely small and negligible, unless the stream density is sufficiently high. The volume in figure 1 contains mostly protons, electrons and a few interplanetary dust particles. As the corpuscular stream diverges like a jet, the density will fall as r^{-2} . Temperature diffusion may be neglected unless the temperature is of the order of 10^5 °K or more.

Group II. *Velocity of emission at the surface of the sun, smaller than 616 Km/sec.*

The emission of corpuscles having these velocities is likely to be a persistent feature even when the sun is quiet. The corpuscles describe Kepler orbits with the centre of force located in the sun's centre. It may be mentioned that Bredechin and Schaeberle (see van de Hulst, 1953) also believed such elliptical orbits to exist when they proposed a mechanical theory to explain the form of the streamers. The major and minor axes for a few cases are given in the following table in terms of R the radius of the sun. For comparison the sun-earth distance may be taken as equal to $200 R$ approximately.

TABLE I

Velocity Km/sec.	$2a$	$2b$
500.0	2.9	2.8
600.0	19.5	8.6
614.0	154.2	24.8
614.5	206.1	28.6
615.0	308.3	36.1

It is seen that when the velocities approach the velocity of escape from the sun, the orbits become highly elongated and extend beyond the ecliptic. As the long coronal streamers emerge from the equatorial regions of the sun, we may infer that the more elongated ellipses have their major axes nearly parallel to the plane of the ecliptic. The planes of these ellipses will, however, be slightly inclined to the plane of the ecliptic so that with the rotation of the sun these elliptical jets will describe a volume having a section given by the broken line in figure 2 normal to the plane of the ecliptic. Interplanetary dust particles caught in these corpuscular streams will have a tendency to concentrate within the volume. It may be mentioned that as the density of the corpuscles in these streams is not sufficiently high and the density of dust particles in interplanetary space is extremely small, the number of encounters will be very few and far between of the order of one in 10^5 years (Öpik, 1954). However, since the

birth of the sun about 10^{12} years ago (Jeans, 1938), the number of encounters would be about 10^7 . We may therefore regard the formation of the volume, as an evolution of the system with the solar system. It is suggested that the *zodiacal light is caused by the scattering of photospheric radiation by the electrons and dust particles within this volume*. Slower corpuscles associated with diminished solar activity at the higher latitudes would give rise to the depressed parts in the volume to the north and the south of the sun. Except for the depressions, which will not be noticeable from the earth the appearance of the volume is almost lenticular and accounts for the conical shape of the zodiacal light and its orientation along the plane of the ecliptic. The minor axes of the ellipses, with limiting values of the order of $30 R$ or so, determine the thickness of the lenticular cloud. Due to the inclination of the planes of the ellipses to the plane of the ecliptic, the thickness of the cloud in figure 2 is likely to be about half this value, that is, $15 R$ or about $.08A.U.$ If we allow for the divergence of the jets, which constitute these orbits, at the boundaries the thickness of this cloud will be slightly greater and comparable with the estimate of van de Hulst (loc. cit). The dilution of electrons in the elliptical jet stream may be taken as proportional to $1/vr^2$, that is, the fall in density due to divergence will be partly compensated by the increase in density with diminishing velocity v towards the aphelion. If at the aphelion at $1 A.U.$ (is $200 R$) of an elliptical stream, the density of electrons is taken as 600 cm^{-3} , the densities at the aphelions of smaller ellipses may be calculated and compared with those deduced by Behr and Siedentopf (1953) from photometric observations, as follows:

TABLE II

Distance from Sun	Density $\propto 1/vr^2$	Density as deduced by Behr and Siedentopf along the plane of the ecliptic
200 R	—	600 cm^{-3}
180 R	666 cm^{-3}	780 „
160 R	750 „	900 „
120 R	1000 „	1030 „
100 R	1200 „	1070 „

According to the second column, the density is found to vary as r^{-1} . A further fall in density due to temperature diffusion may be neglected as in the case of Group I of the corpuscles. It has already been stated that the most elongated ellipses extend along the sun's equatorial plane. From qualitative considerations the smaller ellipses, with axes inclined to the sun's equatorial plane may be taken to be confined within the dotted line. Hence the densities given in column 2 above will be found to occur in spherical shells having the respective radii given

in column 1 of Table 2 and limited by the dotted line of figure 2. However, due to the preponderance of largest number of elliptical streamers with their major axes almost parallel to the sun's equatorial plane, there will be a tendency for the density of electrons to be highest near the sun's equatorial plane diminishing towards the north and south. According to Elsässer (loc. cit.) the electrons are distributed in ellipsoidal shells with the axis of rotation passing through the sun's centre perpendicular to the plane of the ecliptic.

In the present treatment, the density distribution of the dust particles is supposed to be subject to encounters with the electrons and positive ions of the solar corpuscular stream. With every impact, the dust particles swept towards the earth will accumulate towards the aphelion with the result that there is a piling up of the dust particles in the vicinity of the earth. The above consideration also shows that we need not take into account much higher velocities of Group II, as the dilution of electrons in the stream associated with the highly elongated orbits may be too great to enable the scattered light to contribute materially to the luminosity. The transit from the aphelion back to the sun brings about a reversal of the above process. The stream converges and the density of the electrons increases until the sun is reached. However, due to the increasing velocities of the stream, the density of the dust particles swept with it, may first diminish, and thereafter increases towards the perihelion. *In this manner the interplanetary dust particles may be carried with the solar corpuscular stream into the sun, and provide at least partially, the energy, which causes the high temperature of the corona.* In the immediate vicinity of the sun, within a distance of about 0.1 A.U. the space is devoid of dust particles which are vaporized by the high temperature of the sun (van de Hulst, loc. cit.).

Unlike the fast corpuscles of Group I, which cover the distance from the sun to the earth in 1 to 4 days (Sen Gupta and Mitra, loc. cit.), the slow corpuscles of the Group II would take several weeks in transit to cover the same distance. It has already been suggested that the evolution of the volume in figure 2 containing Group II corpuscles (electrons) and interplanetary dust particles account for the unvarying shape of the zodiacal light. The effect of Group I corpuscles due to solar flares and M-region activity is superimposed on the above augmenting the number of free electrons in the volume (figure. 2), with the result that the zodiacal light becomes brighter at the same time when geomagnetic disturbances occur. In a similar manner the advent of meteor swarms in the interplanetary space augments the number of dust particles and thereby brings about an intensification of the zodiacal light. Figure 2 represents conditions on September 5 when the earth has the highest heliographic latitude 7.3° . As may be seen from figure 2, the light axis of the phenomenon, which may be taken to coincide with the sun's equatorial plane, is inclined at this time about 7.3° to the south of the ecliptic plane.

ACKNOWLEDGMENTS

The author is deeply indebted to the late Professor M. N. Saha for encouragement and interest. He is also thankful to Dr. D. E. Blackwell for helpful comments and to Sri B. K. Banerjee of Defence Science organisation, New Delhi, for Table I.

REFERENCES

- Allen, C. W., 1944, *Mon. Not. Roy. Astro. Soc.*, **104**, 13.
- „ 1946, *Ibid.*, **106**, 137.
- Behr, A., and Siedentopf, H., 1953, *Zeit. f. Ap.*, **32**, 19.
- Bredschin and Schaeberle, See Article by H. C. van de Hulst in 'The Sun', p. 392, (Chicago, 1953, edited by G. P. Kuiper).
- Champan, S. and Bartels, Geomagnetism, Vol. II, p. 804 (Oxford, 1940).
- Elsässer, H., 1954, *Zeit. f. Ap.*, **33**, 274.
- Elvey, C. T., 1937, *Astrophys. J.*, **86**, 84.
- Hewish, A., 1955, *Proc. Roy. Soc. Lond. A.*, **228**, 238.
- Hulburt, E. O., 1930, *Phys. Rev.*, **35**, 1098.
- Jackson, J. M., and Rense, W. A., 1953, *Ibid.*, **90**, 345.
- Jeans, J., 1938, *The Universe Around Us*, Cambridge, p. 202.
- Mitra, S. K., 1952, *The Atmosphere*, p. 497 (The Asiatic Society, Calcutta).
- Öpik, E. J., 1954, *Zeit. f. Ap.*, **35**, 48.
- Pietenpol, W. B. and Rense, W. A., 1953, *Phys. Rev.*, **90**, 345.
- Sen Gupta, P. K. and Mitra S. N., 1954, *Nature*, **173**, 814.
- Siedentopf, H., Behr, A., and Elsässer, H., 1953, *Nature*, **171**, 1066.
- Van de Hulst, H. C., 1947, *Astrophys. J.*, **105**, 471.
- Whipple, F. L. and Gossner, J. L., 1949, *Astrophys. J.*, **109**, 380.

POLARISATION IN p-p SCATTERING

C. C. BANERJEE

DEPARTMENT OF THEORETICAL PHYSICS,
INDIAN ASSOCIATION FOR THE CULTIVATION OF SCIENCE, JADAVPUR, CALCUTTA-32*(Received for publication, April 10, 1956)*

ABSTRACT. The paper attempts to investigate the polarisation and asymmetry in proton-proton scattering with the assumption that the particles obey Dirac equation. The results obtained explain qualitatively the main aspects of experimental observations.

INTRODUCTION

Recent experiments on proton-proton scattering show that a beam of unpolarised protons, after being scattered by a target consisting of unpolarised protons, become partially polarised in a direction normal to the scattering plane. This polarisation can be detected if we allow this beam to suffer a similar second scattering, then the differential cross section shows azimuthal dependence—left to right asymmetry. Various attempts have been made to find out what sort of spin-dependent potential would explain the occurrence of polarisation of an unpolarised beam of protons when they are scattered by themselves. Goldferb and Feldman (1952) have compared the theoretical values of the asymmetry as calculated from the potentials of Christian and Noyes (1950), Case and Pais (1950) and Jastrow (1951). It has been found that the value of asymmetry with the tensor force of Christian-Noyes comes out to be 13% with L. S. model of Case-Pais 30% and the hard core of Jastrow gives 0.5%, whereas the experimental value of the asymmetry is $9.6 \pm 3.5\%$. It has also been observed experimentally that the polarisation effects in p-p scattering increase with energy and at moderate energies one obtains an asymmetry of the type $\sin \theta \cos \theta$, deviations from which, however, are noticeable at higher energies. In some of the theoretical studies to explain polarisation, a complex potential, a part of which is spin dependent, has been used. Breit (1955) has worked out an expression for the polarisation in terms of the phase shifts δ_L^{\pm} using a Hamiltonian with implicit dependence on the interaction between spins and coordinates. The expression takes up a simplified form if only S and P wave scatterings are assumed to contribute to the process. But his method of calculation of phase shifts does not suggest the explicit form of spin orbit dependence in the potential.

In this paper the author calculates the asymmetry from a real potential using Dirac equation in a way similar to that adopted by Mott (1932) in electron scattering. Our method gives a value 6.5% for the asymmetry and it explains broadly the different aspects of the polarisation data.

SCATTERING CROSS SECTION FROM DIRAC EQUATION

The wave function ψ describing the scattering of particles which obey Dirac equation has four components which have the asymptotic forms

$$\psi_\lambda = a_\lambda e^{ikz} + \frac{e^{ikr}}{r} u_\lambda(\theta, \phi), \quad (\lambda = 1, 2, 3, 4) \quad \dots (1)$$

The corresponding differential cross section is given by

$$\sigma(\theta, \phi) d\omega = \frac{\sum_1^4 |u_\lambda(\theta, \phi)|^2}{\sum_1^4 |a_\lambda|^2} d\omega = \frac{|u_3|^2 + |u_4|^2}{|a_3|^2 + |a_4|^2} d\omega \quad \dots (2)$$

We have neglected here the contributions of ψ_1 and ψ_2 which are small unless the energy of the colliding particles is comparable with the rest energy.

The asymptotic forms of ψ_3 and ψ_4 for antiparallel spins are

$$\psi_3 = \sum_{n=0}^{\infty} \{ (n+1)e^{i\eta_n} G_n + n e^{i\eta_{-n-1}} G_{-n-1} \} i^n P_n(\cos \theta). \quad \dots (3a)$$

$$\psi_4 = \sum_{n=0}^{\infty} \{ -e^{i\eta_n} + e^{i\eta_{-n-1}} \} i^n P_n^1(\cos \theta) e^{i\phi} \quad \dots (3b)$$

where G_n and G_{-n-1} represent the radial part of the solution for ψ_3 and ψ_4 obtained by Darwin (1928) and they have the asymptotic forms

$$G_n \sim \frac{1}{r} \sin \left(kr - \frac{n\pi}{2} + \eta_n \right) \quad \dots (4a)$$

$$G_{-n-1} \sim \frac{1}{r} \sin \left(kr - \frac{n\pi}{2} + \eta_{-n-1} \right) \quad \dots (4b)$$

If we set, $G_n = \frac{\sqrt{\alpha}}{r} g_n$ where $\alpha = \frac{1}{\hbar c} (W - \epsilon V + mc^2)$ it is found that g_n satisfies an equation of the Schrödinger form given by

$$\frac{d^2 g_n}{dr^2} + \left\{ k^2 - \frac{n(n+1)}{r^2} - U_n(r) \right\} g_n = 0 \quad \dots (5)$$

where $k^2 = \frac{W^2 - m^2 c^4}{\hbar^2 c^2} \quad \dots (6)$

and
$$U_n(r) = -\frac{2W\epsilon V}{\hbar^2 c^2} + \frac{\epsilon^2 V^2}{\hbar^2 c^2} + \frac{n+1}{r} \frac{\alpha'}{\alpha} - \frac{3}{4} \left(\frac{\alpha'}{\alpha} \right)^2 + \frac{1}{2} \frac{\alpha''}{\alpha} \dots \quad (7)$$

A similar result would be obtained for g_{-n-1} replacing n by $-n-1$.

The corresponding expressions for scattered amplitudes for antiparallel spins are,

$$f_1(\theta) = \frac{1}{2ik} \sum_{n=0}^{\infty} \left\{ (n+1)(e^{2i\eta_n} - 1) + n(e^{2i\eta_{-n-1}} - 1) \right\} P_n(\cos \theta) \quad \dots \quad (8a)$$

$$= f(\theta) \quad (\text{say})$$

$$g_1(\theta, \phi) = \frac{1}{2ik} \sum_{n=0}^{\infty} \left\{ -e^{2i\eta_n} + e^{2i\eta_{-n-1}} \right\} P_n^1(\cos \theta) e^{i\phi} \quad \dots \quad (8b)$$

$$= g(\theta) e^{i\phi} \quad (\text{say})$$

where η_n denotes the phase shift of the scattered wave which is given by

$$\eta_n = -\frac{1}{k} \int_0^{\infty} G_n^2 U_n(r) dr \quad \dots \quad (9)$$

G_n being the solution of equation (5) with $U_n(r) = 0$. Similarly, the scattered amplitudes for parallel spins would be given by

$$f_2(\theta) = f(\theta) \quad \text{and} \quad g_2(\theta) = -g(\theta) e^{-i\phi} \quad \dots \quad (10)$$

The equations (8) show that the scattered amplitude not only depends on θ but also on ϕ and if the beam which has undergone scattering on a target, is allowed to be incident on a second target, the intensity of scattering will not be the same for a fixed value of scattering angle in different azimuths i.e. for the same value of the scattering angle the intensity of scattering will be different for left and right sides.

The relative polarisation which has been developed as a consequence of the first scattering is conventionally expressed by relative polarisation,

$$P(\theta) = \frac{I_0 - I_{180}}{I_0 + I_{180}} = \frac{AB^* + A^*B}{AA^* + BB^*} \quad \text{where } I_0 \text{ and } I_{180} \text{ are intensities of scattering at}$$

azimuthal angles 0° and 180° . Now, from the equations (8), we derive below the expressions for the intensity at the first scattering and relative polarisation.

We can write down the expressions for scattering amplitudes $f(\theta)$ and $g(\theta, \phi)$ neglecting terms involving η_n^2 since it will in general be small at high energies particularly for values of n greater than zero, as such, we obtain

$$f_1(\theta) = \frac{1}{2ik} A \quad \text{and} \quad g_1(\theta, \phi) = \frac{1}{2ik} B e^{i\phi}$$

where $A = 2i \sum \{(n+1)\eta_n + n \eta_{-n-1}\} P_n(\cos \theta) \dots (11)$

and $B = 2i \sum (\eta_{-n-1} - \eta_n) P_n^1(\cos \theta)$

Similar calculations would give analogous expressions for $f_2(\theta)$ and $g_2(\theta, \phi)$ for the second scattering.

Therefore, the intensity of scattering for antiparallel spins for first scattering is given by

$$\begin{aligned} I_1 &= |f_1(\theta) + g_1(\theta, \phi)|^2 \\ &= \frac{1}{k^2} \left\{ [\sum \{(n+1)\eta_n + \eta_{-n-1}\} P_n(\cos \theta)]^2 + [\sum (\eta_{-n-1} - \eta_n) P_n^1(\cos \theta)]^2 \right. \\ &\quad \left. + \sum_n \sum_m \{(n+1)\eta_n + \eta_{-n-1}\} \{\eta_{-m-1} - \eta_m\} P_n(\cos \theta) \cdot P_m^1(\cos \theta) \cos \phi \right\}. \end{aligned} \quad \dots (12a)$$

Similarly the intensity of scattering for parallel spins for the first scattering is given by

$$\begin{aligned} I_2 &= \frac{1}{k^2} \left\{ [\sum \{(n+1)\eta_n + \eta_{-n-1}\} P_n(\cos \theta)]^2 + [\sum (\eta_{-n-1} - \eta_n) P_n^1(\cos \theta)]^2 \right. \\ &\quad \left. - \sum_n \sum_m \{(n+1)\eta_n + \eta_{-n-1}\} \{\eta_{-m-1} - \eta_m\} P_n(\cos \theta) P_m^1(\cos \theta) \cos \phi \dots \right\} \end{aligned} \quad (12b)$$

Hence the intensity of scattering for both parallel and anti-parallel spins is

$$\begin{aligned} I(\theta, \phi) &= \frac{1}{4} I_1(\theta, \phi) + \frac{3}{4} I_2(\theta, \phi) \\ &= \frac{1}{k^2} \left\{ [\sum \{(n+1)\eta_n + \eta_{-n-1}\} P_n(\cos \theta)]^2 + [\sum (\eta_{-n-1} - \eta_n)]^2 \right. \\ &\quad \left. - \frac{1}{2} \sum_n \sum_m \{(n+1)\eta_n + \eta_{-n-1}\} \{\eta_{-m-1} - \eta_m\} P_n(\cos \theta) P_m(\cos \theta) \cos \phi \right\}. \end{aligned} \quad \dots (13)$$

According to Pauli's exclusion principle in proton-proton scattering only 1S , 3P , 1D and 3F states would be present. Since contribution to polarisation for the S -state is zero we can assume that the polarisation is mainly due to triplet P scattering. The contributions of the D and F states would be small at the energies considered. For the S state therefore no polarisation would be exhibited. For the P -state ($n = 1$) and also for the high r states (1D , 3F etc) the phase shifts are small and can be evaluated from the expression for η_n given in equation (7).

Since $G_n(r) = \sqrt{\frac{\pi k r}{2}} J_{n+\frac{1}{2}}(kr)$

therefore $\eta_n = -\frac{\pi}{2} \int_0^{\infty} U_n(r) \{J_{n+\frac{1}{2}}(kr)\}^2 r \, dr \quad \dots \quad (14a)$

Similarly,

$$\eta_{-n-1} = -\frac{\pi}{2} \int_0^{\infty} U_{-n-1}(r) \{J_{-n-\frac{1}{2}}(kr)\}^2 r \, dr \quad \dots \quad (14b)$$

The expression for $U(r)$ given by (7) may be simplified as below before substituting it into (14a) or (b) for integration. The radial potential $V(r)$ used in the expression for $U_n(r)$ has been taken to be exponential which of course has been obtained by Bhabha (1950) from meson field theory. Taking the interaction potential of the type $-\chi e^{-\lambda r}$ we have for the expressions of $U(r)$ with the approximation

$$\frac{\alpha'}{\alpha} = \frac{-\epsilon V'(r)}{W + mc^2 - \epsilon V(r)} = \frac{-\epsilon V'(r)}{W + mc^2}$$

$$U_n(r) = ae^{-\lambda r} + be^{-2\lambda r} - (n+1)c \frac{e^{-\lambda r}}{r} \quad \dots \quad (15a)$$

and $U_{-n-1}(r) = ae^{-\lambda r} + be^{-2\lambda r} + \frac{nc}{r} \cdot e^{-\lambda r} \quad \dots \quad (15b)$

where $a = \frac{2W\epsilon^2\chi}{\hbar^2 c^2} + \frac{1}{2} \frac{\epsilon^2\chi^3}{W+mc^2}$; $b = \frac{\epsilon^4\chi^2}{\hbar^2 c^2} - \frac{3}{4} \frac{\epsilon^4\chi^4}{(W+mc^2)^2}$

and $c = \frac{g^2\chi^2}{W+mc^2}$. ($g^2/\hbar c = .08$)

Substituting the value of $U_n(r)$ given by (15a) in the integral for η_n in 14(a) we have

$$\begin{aligned} \eta_n &= -\frac{\pi}{2} \int_0^{\infty} \left\{ ae^{-\lambda r} - C(n+1) \frac{e^{-\lambda r}}{r} \right\} \{J_{n+\frac{1}{2}}(kr)\}^2 r \, dr \\ &= \frac{a\chi}{2k^3} Q' \left(\frac{\chi^2 + 2k^2}{2k^2} \right) + \frac{c(n+1)}{2k} Q_n \left\{ \frac{\chi^2 + 2k^2}{2k^2} \right\} \quad \dots \quad (16a) \end{aligned}$$

(neglecting the contribution of the second term of (15) which is small)

when Q_n is the Legendre function of the second kind and Q'_n is its first derivative. Similarly

$$\eta_{-n-1} = \frac{a\chi}{2k^3} Q'_n \left(\frac{\chi^2 + 2k^2}{2k^2} \right) - \frac{cn}{2k} Q_n \left(\frac{\chi^2 + 2k^2}{2k^2} \right) \quad \dots \quad (16b)$$

Exactly similar calculations may be made for calculating the values of phase shifts η'_n and η'_{-n-1} for the second scattering and the value of relative polarisation may be calculated from a similar expression as given by equation (9) with η'_n and η'_{-n-1} substituted for η_n and η_{-n-1} respectively. If $P(\theta_1)$ and $P(\theta_2)$ denote the relative polarisation in the two cases and if $P(\theta_1) = P(\theta_2)$ the asymmetry $2e$ which is expressed as twice the product of the two values of relative polarisation is given by

$$2e = 2P(\theta_1) P(\theta_2) = 2P^2(\theta) \\ = 2 \left[2 \cdot \frac{\{(n+1)\eta_n + \eta_{-n-1}\}\{\eta_n - \eta_{-n-1}\} P_n(\cos \theta) P'_n(\cos \theta)}{\{(n+1)\eta_n + \eta_{-n-1}\}^2 P_n^2(\cos \theta) + \{\eta_n - \eta_{-n-1}\}^2 P_n'^2(\cos \theta)} \right]^2 \quad \dots \quad (17)$$

Since the value of relative polarisation for the S -state would become zero due to the zero value of the factor involving associated Legendre polynomial for $n = 0$ let us calculate the value of the asymmetry for the P -state. The contribution to asymmetry for higher states may be neglected in view of the energy considered.

EVALUATION OF THE PHASES AND CALCULATIONS OF RELATIVE POLARISATION AND ASYMMETRY, IN THE STATE AT 230 MEV.

In the state, $n = 1$, therefore the equation (17) for asymmetry becomes,

$$2e = 2 \left[\frac{2\{2\eta_1 + \eta_{-2}\}\{\eta_1 - \eta_{-2}\} \cos \theta \sin \theta}{\{2\eta_1 + \eta_{-2}\}^2 \cos^2 \theta + \{\eta_1 - \eta_{-2}\}^2 \sin^2 \theta} \right]^2 \quad \dots \quad (18)$$

Now from (16) we can evaluate η_n and η_{-n-1} whose values are as follows :

$$\eta_n = 2.2 \quad \text{and} \quad \eta_{-n-1} = 1.7$$

and hence the values of $P(\theta)$ and $2e$ are (for 230 Mev and 19° scattering angle in the laboratory system)

$$= .18 \text{ (or } 18\%)$$

$$2e = 2\{P(\theta)\}^2 = .065 \text{ (or } 6.5\%).$$

DISCUSSION

It appears from the investigation given above that the third term in the expression for $U(r)$ involving n is most significant in giving a non-zero value of the polarisation. If the magnitude of polarisation is calculated for individual terms of the expression for $U(r)$ we get the value of polarisation to be zero for all

other terms excepting the third. If the calculations are carried out with the third term only the magnitude of the polarisation comes out very high and is independent of energy of the incident particle. The effect of the other terms, therefore is to lower down the magnitude of polarisation and to make it dependent on the energy of the colliding particles in the C.M. system. It appears from the expressions for polarisation and asymmetry given above that they increase with the increase of energy and this agrees with the observations. Further, the $\sin \theta \cos \theta$ symmetry which is observed experimentally is also apparent from the expression for polarisation. Thus the investigation explains qualitatively the principal aspects of polarisation observed in proton-proton scattering experiments. The radial potential considered in this paper is a short range potential of the exponential type which has been obtained by Bhabha (1950) from field theoretical considerations of higher order meson field equations. The trend of the calculations exhibit that a spin dependent radial potential might increase the value of the polarisation and asymmetry a little higher and thus bring their theoretical values in close agreement with observations. The calculations for the asymmetry and polarisation with spin dependent potentials like tensor forces are in progress and will be reported when ready.

ACKNOWLEDGMENT

The author wishes to express his thanks to Prof. D. Basu, Ph. D. for suggesting the problem and for his valuable discussions throughout the progress of the work.

REFERENCES

- Breit, G., 1955, *Phy. Rev.*, **97**, 1091.
Case, K. M. and Pais, A., 1950, *Phy. Rev.*, **80**, 263.
Christian, R. S. and Noyce, H. P., 1950, *Phy. Rev.*, **79**, 85.
Jastrow, R., 1950, *Phy. Rev.*, **81**, 165.
Mott, 1932, *Proc. Roy. Soc.*, A **135**, 429.
Darwin, 1928, *Proc. Roy. Soc.*, A **118**, 654.
Goldferb and Feldman, 1952, *Phys. Rev.*, **88**, 1099.

TEST OF THE WORKABILITY OF LOTMAR'S POTENTIAL ENERGY FUNCTION.

N. R. TAWDE AND N. V. GEJJI

DEPARTMENT OF PHYSICS, KARNATAK UNIVERSITY, DHARWAR

(Received for publication, April 3, 1956)

ABSTRACT. Lotmar, while examining some potential energy functions, found that the function of Rosen and Morse was better than those of Morse and of Poschal and Teller. He, however, improved upon the function of Rosen and Morse. The condition for the workability of this improved function of Lotmar has been derived in this paper and it has been tested in the case of certain molecules.

Kronig (1935) has suggested that when the Morse expression is inadequate, the potential energy in the case of a diatomic molecule can be expressed by a more general expression like that of Rosen and Morse (1932). While Morse expression, which has been generally accepted as satisfactory for many purposes and has been experimentally verified as such, no data is on record on the performance of the Lotmar's (1935) expression, which is based upon that of Rosen and Morse. It is proposed to examine the workability of Lotmar's expression in the case of some molecules where the necessary accurate experimental data are available.

Lotmar (1935) has examined the function of Morse, Rosen and Morse and of Pöschl and Teller in the case of molecules HgH, CdH and O₂ and has concluded that the curves of Rosen and Morse are comparatively nearer the truth than those of the other two. On the basis of this conclusion, he started to improve upon the expression of Rosen and Morse, by introducing more constants and it is this improved form of the function of Rosen and Morse that is attributed to Lotmar.

The expression due to Rosen and Morse has the form:

$$V(r/d) = A \tan^2(r/d) - C \sec^2(r/d) \quad \dots (1)$$

while that due to Lotmar as noted by Kronig is

$$V(\rho) = - \tanh \left(\frac{\rho + c}{d} \right) = b \operatorname{sech}^2 \left(\frac{\rho + c}{d} \right) \quad \dots (2)$$

Lotmar's expression contains four arbitrary constants a , b , c and d instead of the three constants A , C and d of Rosen and Morse's expression.

The constants in (2) above, can be evaluated by using the quantities ω_e , $\omega_e x_e$, B_e , ρ_e , α_e , and M , experimentally determinable from the band spectrum analysis.

Comparing Lotmar's expression with the following potential energy function of a diatomic molecule in power series, viz:

$$V = \frac{K_2}{2!} (\rho - \rho_e)^2 + \frac{k_3}{3!} (\rho - \rho_e)^3 + \dots \quad \dots \quad (3)$$

relations have been obtained for ω_e , $\omega_e x_e$, etc., in terms of the constants of this expression. Using (2) above, and going through the derivatives of various order, Kronig obtained the following results

$$\tanh \frac{\rho_e + c}{d} = a/2b \quad \text{when } \rho = \rho_e \quad \dots \quad (4)$$

$$\omega_e = \frac{4b^2 - a^2}{4\pi d(2\pi b^3)^{\frac{1}{3}}} \quad \dots \quad (5)$$

$$\omega_e x_e = \frac{h}{8\pi^2 M d \left(1 + \frac{3a^2}{4b^2} \right)} \quad \dots \quad (6)$$

$$\alpha = - \left[\frac{6B_e^2}{\omega_e} - 24 \left(\frac{B_e}{\omega_e} \right)^3 \cdot \frac{\rho_e^3}{h} \cdot \frac{a}{d^3} \left(1 - \frac{a^2}{4b^2} \right)^2 \right] \quad \dots \quad (7)$$

$$\text{and } D_e = \left(\frac{a - 2b}{4b} \right)^2 \quad \dots \quad (8)$$

Using relations (4) to (7), one obtains

$$d^2 \left[8\pi^2 M \omega_e x_e - \frac{3}{4} h^3 \left\{ \frac{\alpha \omega_e + 6B_e^2}{48\pi^2 M B_e^3 \rho_e^3} \right\}^2 \right] = h \quad \dots \quad (9)$$

$$8\pi^2 M d^2 \omega_e x_e = h(1 + \frac{3}{4} x^2) \quad \dots \quad (10)$$

$$b = \frac{32\pi^2 d^2 M \omega_e^2}{(4 - x^2)^2} \quad \dots \quad (11)$$

where

$$x = a/b.$$

From relations (9), (10) and (11), the constants a , b and d are determined. The value of c is obtainable from equation (4). It is, however, determinable only if $(a/2b) < 1$, as $\tanh \left(\frac{\rho + c}{d} \right) < 1$. Hence it follows that Lotmar's expression is workable for plotting the potential energy curves for only such states of molecules, where the above condition $(a/2b < 1)$ is satisfied.

For putting the above condition of the expression to test in actual cases, the molecules C_2 and N_2 were chosen as the spectral data on these for the various electronic states is at present in a crystallised state.

Applying the condition $a/2b < 1$, it was found that it could not be satisfied for all the electronic states. Only where the above condition holds that the $V(\rho)$ value could be actually determined and the potential energy curves defined. But for many band systems, both the curves involved in transition were not obtainable. in order to determine the course of maximum transition probabilities for verification with experimental observations. Hence the workability was examined in terms of the dissociation energy D_e . It was possible, by use of the expression (8) derived from Lotmar's function, to estimate D_e and compare it with approximate values such as those obtained by extrapolation or other more precise data, wherever available. The following table is drawn up for the known electronic states of C_2 and N_2 , giving cases where the condition $a/2b < 1$ holds, with the values of the dissociation energy derived from the expression (8) and the corresponding available values.

TABLE I

Molecule	State	Test of condition $a/2b < 1$	Value of D_e derived from expression (8) in e.v.	Extrapolated value $D_e = \omega_e^2/4\omega_e x_e$ in e.v.	Available values of D_e	
C_2	$X^3\pi_u$	X	7.48	7.15	4.95, ⁽²⁾	4.2, ⁽⁴⁾ ~5 ⁽¹⁾
	$A^3\pi_g$	*	4.9]	6.03		
	$B^3\pi_g$	*	0.78	0.93		
	$a^1\Sigma_g^+$	*	7.25	7.59		
	$b^1\pi_u$	X	—	6.6		
	$c^1\pi_g$	*	5.72	6.42		
	$d^1\Sigma_u^+$	X	—	7.43		
N_2	$X^1\Sigma_g^+$	X	13.48	11.93	9.76, ⁽¹⁾	7.37 ⁽³⁾
	$A^1\Sigma_u$	*	3.81	4.76	8.8, ⁽⁵⁾	3.67 ⁽⁶⁾
	$B^3\pi_g$	X	—	6.44	4.76 ⁽⁶⁾	
	$C^3\pi_u$	*	7.20	7.52	2.29 ⁽⁶⁾	

* indicates workability;

X indicates non-workability

(1) Gaydon, A. G., (1947).

(2) Brewer, Giles and Jenkins, (1948).

(3) Hangstrum, (1951).

(4) Tawde, (1949).

(5) Hendric, (1954).

(6) Tables De Constantes (Union Internationale de Chimie) No. 4, 1950, p. 204.

A further test is applied for Lotmar's expression in terms of the dissociation energy data in ground states, where they are available from either the thermochemical or atomic fluorescence methods for those molecules where the required spectroscopic constants are known. These are recorded in Table II.

TABLE II

Molecule	Extrapolated value $D_e = \omega_e^2/4\omega_e x_e$ in e.v.	D_e by T.C. and A.F. methods in e.v.	Workability of condition $a/2b < 1$	D_e in e.v. according to Lotmar equation (8)
C ₂	7.15	3.6, 3.85 and round about 5.	X	7.48
CO	10.85	8.8 to 9.1	X	11.45
Cl ₂	2.47	—	X	imaginary
HCl	5.33	4.43	X	6.08
HI	4.16	2.76	*	3.64
HBr	4.81	3.6 ± .05	X	5.26
N ₂	11.93	9.704	X	13.48
O ₂	6.41	—	X	6.93
S ₂	5.74	4.4	X	6.14
SiO	7.91	7.7	*	6.05

* indicates workability;

X indicates non-workability.

T.C. = Thermo-chemical method;

A.F. = Atomic fluorescence method.

(Gaydon, A. G., 1947).

It appears from the study given above that Lotmar's expression has its limitations, viz., (1) it is applicable only in cases where the condition $a/2b < 1$ holds, (2) it requires the knowledge of six molecular constants as against four of Morse. Hence it is not as universally usable as Morse's expression. In the few cases where it satisfies the basic condition $a/2b < 1$, it leads to values of dissociation energy, which are nearer to true values than those based on methods of extrapolation ($D_e = \omega_e^2/4\omega_e x_e$). This happens only in a few cases as evident from Tables I and II, which also show that the expression succeeds better in excited states than in the ground states. In the latter states, only two cases are met with among those examined, which satisfy the condition $(a/2b) < 1$. In other cases (i.e. where the condition $a/2b < 1$ is not satisfied), the derived values of D_e are far away and appear to be almost imaginary. Thus the expression has a very limited scope for application.

REFERENCES

- Brewer, Giles and Jenkins, 1948, *J. Chem. Phys.*, **797**, 60.
 Gaydon, A. G., 1947, *Dissociation Energies and Spectra of Diatomic molecules*, (Chapman and Hall, p. 206).
 Hangstrum, 1951, *Rev. Mod. Phys.*, **185**, 23.
 Hendric, 1954, *J. Chem. Phys.*, 1503, 23.
 Kronig, R. De L., 1935, "The Optical Basis of the Theory of Valency, Camb. U. Press, p. 88,
 Lotmar, W., 1935, *Zeit. f. Phys.*, **93**, 528.
 Rosen, N. and Morse, P. M., 1932, *Phys. Rev.*, **42**, 210.

SPECTROSCOPIC CONSTANTS OF MOLECULES. V SIMILARITIES IN CONSTANTS OF DIFFERENT GROUPS

Y. P. VARSHNI AND K. MAJUMDAR

DEPARTMENT OF PHYSICS, ALLAHABAD UNIVERSITY, ALLAHABAD

(Received for publication, November 11, 1955)

ABSTRACT. It is shown that ω_e of diatoms of $4b-7b$ groups are linear with ω_e of corresponding diatoms of $4b-6b$ group. Other constants viz., $\omega_e x_e$, r_e and D_0 are also found to give similar results. The resemblances between the vibration frequencies of corresponding halides of different groups have been pointed out.

INTRODUCTION

The band spectral constants of a diatom are, to a very large extent, governed by the forces due to the valence electrons of its constituent atoms. Consider a diatom XY formed out of two atoms X and Y . Let us replace Y by another atom Z , whose closed shell structure is the same as that of Y , and the number of valence electrons does not differ much from that of Y . If we consider a series of molecules of XY and XZ type, it is quite probable that the constants of the two series may be inter-related. Recently, Walsh (1951) has plotted the force constants of the diatoms of the $4b-6b$ group against the corresponding diatoms of the $4b-7b$ group ($7b$ group element having atomic number greater by unity than that of $6b$ group element). He obtained a straight line passing through the origin, indicating that the force constants are proportional. However, numerical calculations by Varshni (1953) showed that the ratio seems to vary as $V^{3/4}$, where V is the ionization potential of the $4b$ group element. Mitra (1954) has studied the force constants of $3b-7b$ and $4b-7b$ groups on analogous lines.

Parallel results are obtained if we investigate other constants. The plot of ω_e ($4b-7b$) against ω_e ($4b-6b$) yields a good straight line, not passing through the origin (figure 1). r_e and $\omega_e x_e$ show a similar behaviour (figures 2 and 3). Only approximate values for dissociation energies are available, which have been plotted in figure 4.

The numerical results for ω_e , $\omega_e x_e$ and r_e are recorded in Tables I, II and III. The equations for the corresponding lines are

$$\omega_e(4b-7b) = .662 \omega_e(4b-6b) + 25 \quad \dots (1)$$

$$\omega_e x_e(4b-7b) = .6785 \omega_e x_e(4b-6b) + .1290 \quad \dots (2)$$

$$r_e(4b-7b) = .929 r_e(4b-6b) + .22 \quad \dots (3)$$

For dissociation energies the spread of points is rather wide and it was not thought worthwhile to make the numerical comparison.

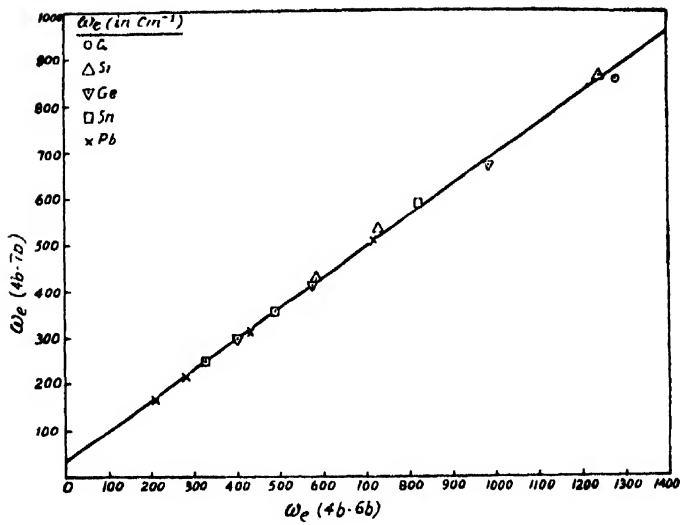


Fig. 1

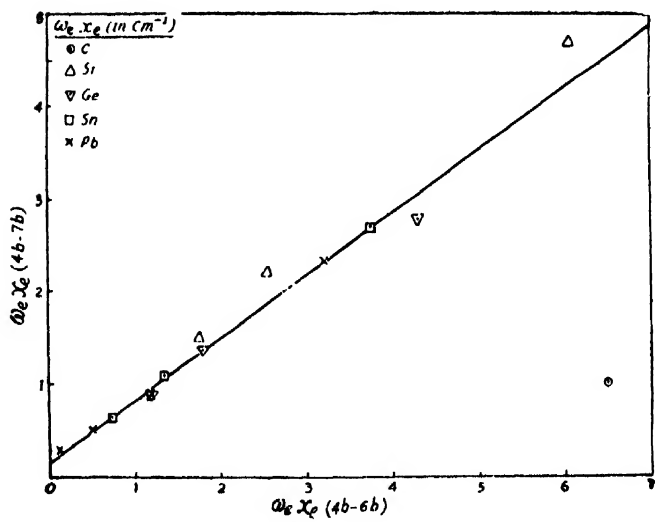


Fig. 2

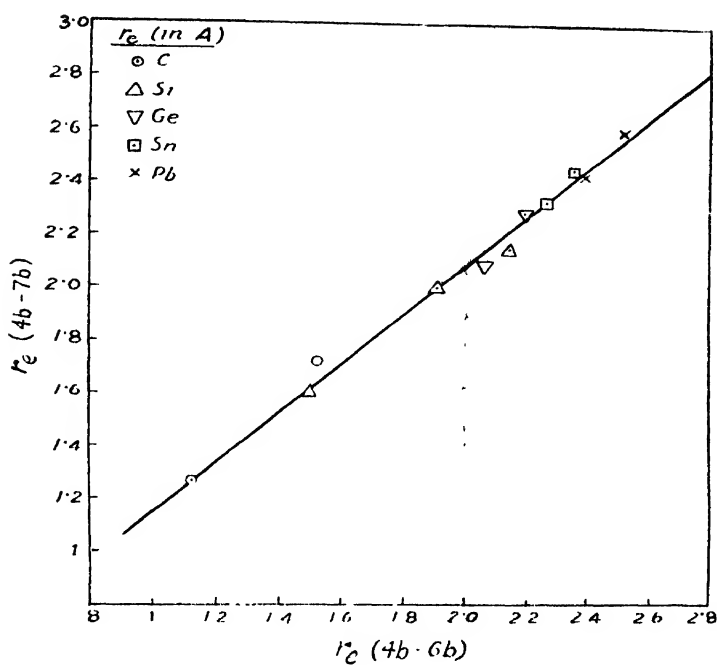


Fig. 3

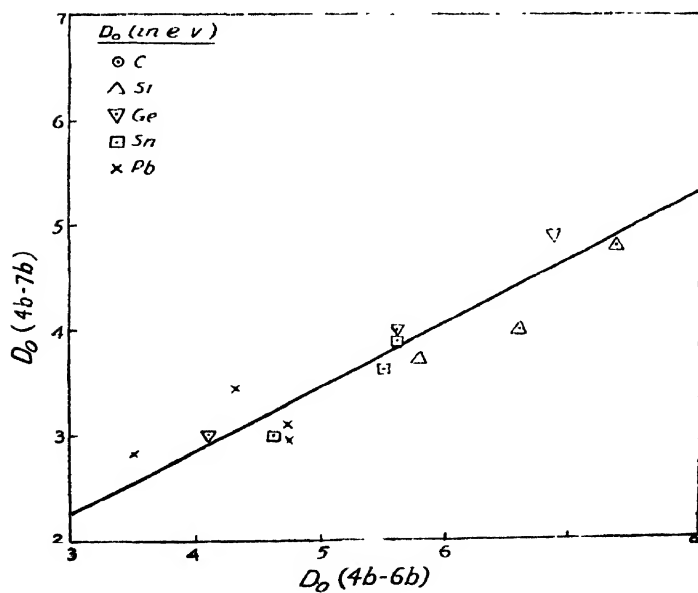


Fig. 4

DATA

Sources same as in Part III, excepting where otherwise indicated below the tables.

TABLE I

4b-6b group	ω_e obs.	4b-7b group	ω_e obs.	ω_e calc.	Percentage error
CO	2170.2	CF	1308	1461.7	(+ 11.5)
CS	1285.1	CCl	846	875.8	+ 2.8
CSe	1036	CBr		710.8	
CTe	~875	CI		~604.1	
SiO	1242	SiF	856.7	847.1	- 1.0
SiS	749.5	SiCl	535.4	521.1	- 2.5
SiSe	580	SiBr	425.4	409	- 3.5
SiTe	481.2	SiI		343.6	
GeO	985.7	GeF	665.2	676	+ 1.6
GeS	575.8	GeCl	407.6	406.2	- .3
GeSe	406.8	GeBr	296.6	294.3	- .8
GeTe	323.4	GeI		239.1	
SnO	822.4	SnF	582.9	569.4	- 2.1
SnS	487.68	SnCl	352.5	347.8	- 1.3
SnSe	331.2	SnBr	247.7	244.2	- 1.4
SnTe	259.5	SnI		196.8	
PbO	721.8	PbF	507.2	502.9	- .8
PbS	428.14	PbCl	303.8	308.4	+ 1.5
PbSe	277.6	PbBr	207.5	208.8	+ .6
PbTe	211.8	PbI	160.5	165.2	+ 3.0
Average					± 1.6

TABLE II

4b-6b group	$\omega_e x_e$ obs.	4b-7b group	$\omega_e x_e$ obs.	$\omega_e x_e$ calc.	% error
CO	13.46	CF	10.86	9.262	- 14.7
CS	6.5	CCl	1.0	4.539	(+ 353.9)
CSe	4.8	CBr		3.385	
CTe		CI			
SiO	0.047	SiF	4.7	4.231	- 9.9
SiS	2.56	SiCl	2.20	1.866	- 15.2
SiSe	1.78	SiBr	1.5	1.337	- 10.9
SiTe	1.30	SiI		1.01	
GeO	4.30	GeF	2.79	3.05	+ 9.2
GeS	1.80	GeCl	1.36	1.35	- .7
GeSe	1.2	GeBr	.9	.943	+ 4.8
GeTe	.75R ₁	GeI		.638	
SnO	3.73	SnF	2.69	2.659	- 1.2
SnS	1.34	SnCl	1.06	1.038	- 2.1
SnSe	.736	SnBr	.62	.627	+ 1.1
SnTe	.50	SnI		.468	
PbO	3.70	PbF	2.30	2.639	+ 14.8
PbS	1.20	PbCl	.88	.943	+ 7.2
PbSe	.51	PbBr	.50	.475	- 5.0
PbTe	.12	PbI	.25	.210	- 16.0
Average					± 8.1

TABLE III

4b-6b group	r_e obs.	4b-7b group	r_e obs.	r_e calc.
CO	1.128	CF	1.271	1.268
CS	1.534	CCl	1.73 EG ₁	1.64
CSe	1.735 eG ₁	CBr		1.83
CTe	1.935 eG ₁	CI		2.02
SiO	1.510	SiF	[1.603]	1.62
SiS	1.929	SiCl	2.00 EG ₁	2.01
SiSe	2.14 eG ₁	SiBr	2.15 EG ₁	2.21
SiTe	2.34 eG ₁	SiI		2.39
GeO	1.651	GeF		1.75
GeS	2.06 eG ₁	GeCl	2.08 EG ₁	2.12
GeSe	2.19 eG ₁	GeBr	2.29 EG ₁	2.25
GeTe	2.39 eG ₁	GeI		2.44
SnO	1.838	SnF		1.93
SnS	2.26* eR ₁	SnCl	2.32 EG ₁	2.32
SnSe	2.37 eG ₁	SnBr	2.44 EG ₁	2.42
SnTe	2.57 eG ₁	SnI		2.61
PbO	1.922	PbF		2.0
PbS	2.395	PbCl	2.43 EG ₁	2.44
PbSe	2.53 eG ₁	PbBr	<2.60 EG ₁	2.57
PbTe	2.73 eG ₁	PbI		2.76

* The reported experimental value is 2.06. However this seems to be too low (Rosen, 1951).

e—estimates

E—electron diffraction values

G₁—Guggenheimer (1946)

R₁—Rosen (1951).

DISCUSSION

Excepting CF, the agreement between the observed and calculated values of ω_e is good. The average percentage error, excepting CF, is 1.6. However, for the prediction of ω_e of heavier molecules, this exception need not concern us greatly. No experimental determination of ω_e of CBr, CI, SiI, GeI, and SnI have been made. The predicted values are given in the table.

The average percentage error in case of $\omega_e x_e$ is larger, being 8.1 (excepting CCl). This is understandable. Usually the $\omega_e x_e$ values are not known with the accuracy that the ω_e values are known, specially in cases where only a limited number of bands have been observed. Further it should be remembered that the given errors are due to errors in both 4b-6b group and/or 4b-7b group. The observed value for CCl undoubtedly seems to be in error.

Very limited spectroscopic data for r_e are available. Most of the values are either from electron diffraction studies or only estimates. Nevertheless these values and the calculated values are quite close.

In view of the fact that some of the dissociation energies may be in large errors, no definite conclusions can be drawn from the graph, though there are

indications of the linear relationship. The given figure has been plotted from Herzberg's values, which have been mostly obtained from Birge-Sponer linear extrapolation. Gaydon (1950) has pointed out that often this method gives much too high values. If the values recommended by Gaydon are used, however, the character of the inter-relation essentially remains the same.

So far we have only considered the $4b-6b$ and $4b-7b$ groups. Very similar results are obtained for other groups for which data are available. The case of halides is very interesting. If we compare the ω_e of corresponding halides of $1b$, $2a$, $2b$, $3b$, $4b$ and $5b$ groups, we find that there are close resemblances in their vibration frequencies. Table IV gives the relevant data. We can also make predictions by these comparisons.

It is evident that if the vibration frequencies of one of the groups are plotted against corresponding vibration frequencies of another group, straight lines with slope very nearly equal to unity will be obtained.

TABLE IV. ω_e values

1b-7b	Groups				
	2a-7b	2b-7b	3b-7b	4b-7b	5b-7b
	BeF 1265.6		BF 1399.8	CF 1308	NF (1400)e, (1300)eeeV ₅
	BeCl 846.6		BCl 839.12	CCl 846	NCl (900)eeeV ₅
	BeBr 670eV ₄		BBr 684.31	CBr 667eV ₁ , 670eV ₂ , 710eV ₆	NBr (693)
	BeI ≤ 580eV ₄		BI 570eV ₄	CI 563eV ₁ , 570eV ₄ , (604)eV ₆	NI 600eV ₅
	BeAt 490e		BAt 480eV ₅	CAt 500eV ₅	NAt 500eV ₅
	MgF 717.6		AlF 814.5	SiF 856.7	PF (900)e, (950)eeV ₅
	MgCl 465.4		AlCl 481.3	SiCl 535.4	PCl (580)e, (700)eeV ₅
	MgBr 373.8		AlBr 378	SiBr 425.4	PBr (460)e, (550)eeV ₅
	MgI (312)		AlI 316.1	SiI 340eV ₄ , 360eV ₅ , 344eV ₆	PI 370eV ₅

TABLE IV—Continued.

	MgAt		AlAt	SiAt	PAI
	280ee		285eV ₅	300eV ₅	310eV ₅
CuF	CaF	ZnF	GaF	GeF	AsF
622.6	587.1	(630)	623.8	665.2	(700)eV ₅
CuCl	CaCl	ZnCl	GaCl	GeCl	AsCl
416.9	369.8	390.5	365	407.6	430eeeV ₅
CuBr	CaBr	ZnBr	GaBr	GeBr	AsBr
314.1	285.3	280eV ₄	263	296.6	310e
		(220)			270eeeV ₅
CuI	CaI	ZnI	GaI	GeI	AsI
264.8	242	223.4	216.4	230eV ₄	240e
				240eV ₅	225eeV ₅
				239eV ₆	
CuAt	CaAt	ZnAt	GaAt	GeAt	AsAt
~200ee	~200ee	180eV ₅	185eV ₅	200eV ₅	200eV ₅
AgF	SrF	CdF	InF	SnF	SbF
525eV ₄	500.1	(535)	534.7	582.9	614.2
AgCl	SrCl	CaCl	InCl	SnCl	SbCl
343.6	302.3	330.5	317.4	352.5	369
AgBr	SrBr	CdBr	InBr	SnBr	SbBr
247.72	216.5	230	221	247.7	255e
					225eV ₄
AgI	SrI	CdI	InI	SnI	SbI
206.18	173.9	178.5	177.1	195eV ₁	200e
				190eV ₄	175eV ₄
				197eV ₆	
AgAt	SrAt	CdAt	InAt	SnAt	SbAt
~150ee	~140ee	130eV ₅	145eV ₅	160eV ₅	160eV ₅
AuF	BaF	HgF	TlF	PbF	BiF
500e	468.9	490.8	475	507.2	510.7
AuCl	BaCl	HgCl	TlCl	PbCl	BiCl
382.8	279.3	292.61	287.47	303.8	308
AuBr	BaBr	HgBr	TlBr	PbBr	BiBr
230e	193.8	186.25	192.1	207.5	203.34
AuI	BaI	HgI	TlI	PbI	BiI
170e	150e	125.6	150	160.5	163.9
	160eV ₄				
AuAt	BaAt	HgAt	TlAt	PbAt	BiAt
~130eee	~120eee	90eeV ₅	125eeV ₅	130eeV ₅	130eeV ₅

NOTES ON TABLE IV :

If there are 'n' number of 'e', this signifies that the given estimated value depends on (n-1) previous estimations. 'e' not followed by any reference indicates that the value has been estimated by the method described in this paper.

V₁—Varshni (1953).

V₄—Varshni and Majumdar (1955 III).

V₅—Varshni and Majumdar (1955 IV).

V₆—Table I or II of this paper.

TABLE V. $\omega_e x_e$ values.

Groups					
1b—7b	2a—7b	2b—7b	3b—7b	4b—7b	5b—7b
	BeF		BF	CF	NF
	9.12		11.3	10.86	
	BeCl		BCl	CCl*	NCl
	5.11		5.11	1.0,	
				4.54eV ₆	
	BeBr		BBr	CBr	NBr
			3.52	3.87eV ₆	5
	BeI		BI	CI	NI
	MgF		AlF*	SiF	PF
	3.84		8.1	4.7	
	MgCl		AlCl	SiCl	PCl
	2.05		1.95	2.20	
	MgBr		AlBr	SiBr	PBr
	1.34		1.28	1.5	
	MgI		AlI	SiI	PI
			1.0	1.01eV ₆	
CuF	CaF	ZnF	GaF	GeF	AsF
3.95	2.74	(3.5)	3.4	2.79	
CuCl	CaCl	ZnCl	GaCl	GeCl	AsCl
1.57	1.31	1.55	1.1	1.36	
CuBr	CaBr	ZnBr	GaBr	GeBr	AsBr
.865	.86		.81	.9	
CuI	CaI	ZnI	GaI	GeI	AsI
.71	.64	.75	.5	.64eV ₆	
AgF	SrF	CdF	InF	SnF	SbF
	2.21		2.56	2.69	2.77
AgCl	CrCl	CdCl	InCl	SnCl	SbCl
1.163	.95	1.2	1.01	1.06	.92
AgBr	SrBr	CdBr	InBr	SnBr	SbBr
.6795	.51	.50	.65	.62	
AgI	SrI	CdI	InI	SnI	SbI
.4327	.42	.625	.4	.47eV ₆	
AuF	BaF	HgF*	TlF	PbF	BiF
	1.79	4.05	1.89	2.30	2.05
AuCl	BaCl	HgCl*	TlCl	PbCl	BiCl
1.30	.89	1.602	1.24	.88	.96
AuBr	BaBr	HgBr*	TlBr	PbBr	BiBr
	.42	.975	.39	.50	.468
AuI	BaI	HgI*	TlI	PbI	BiI
		1.09		.25	.31

* Anomalous

See notes below Table IV.

Notice the anomalous $\omega_e x_e$ reported values of CCl and AlF. These undoubtedly seem to be wrong. Mercury halides $\omega_e x_e$ are also too high. However, these abnormal values seem to be real and indicate some special characteristic of mercury halides potential energy curves. The abnormal behaviour of $\omega_e x_e$ of mercury halides has also been observed in connection with a relation between $\omega_e x_e$ and ω_e which will be discussed in a later paper.

In this paper and the previous two (Parts III and IV), we have investigated various regularities in vibration frequencies and found it possible to estimate them for molecules which have not been investigated so far, by several methods. In a way the different methods are complementary. We can make a good estimate of an unknown vibration frequency by comparing the predicted values by the different methods, giving due weight to the accuracy of each method. This may be illustrated by a few examples.

CBr—The predicted values by the various methods are as follows:

Walsh-Varshni (Varshni 1953)	667
Part III	670
Part V (Table I)	710

Iso-electronic considerations (Part IV) support any value near these.

Thus, considering the spread of the values, 690 would be a fair estimate.

BaI—	Part III	160
	Part V (Table IV)	150

From force constant considerations we expect that

$$k_e(\text{BaI}) < k_e(\text{BaBr})$$

$$k_e(\text{BaI}) < k_e(\text{SrI})$$

The value 160 does not satisfy both the inequalities, while the value 150 does. Hence it is to be preferred.

SnI—Walsh-Varshni	195
Part III	190
Part V (Table I)	197

Here the estimated values by the three methods are very close, and we can expect that the correct value would not be far from 195.

Thus we can draw up a critical list of unknown vibration frequencies. This would be given in a forthcoming paper in another connection. Before concluding, a word of caution is necessary regarding the estimated values. These values depends on the values of other molecules which have been investigated. In some cases the observed values may be modified by later experiments and consequently the estimated values will also have to be changed. Some of the estimated values

depend on values which themselves have been obtained by one or two previous estimates. Obviously in such cases the errors would be larger. Roughly speaking we may assign the following average probable errors:

'First' estimated value (e)	5%
'Second' estimated value (ee)	7%
'Third' estimated value (eee)	10%

ACKNOWLEDGMENT

The authors are thankful to the Council of Scientific and Industrial Research for the financial assistance.

REFERENCES

- Gaydon, A. G., 1950, *Dissociation Energies and Spectra of Diatomic Molecules*, (Dover Publications, Inc., New York).
- Guggenheimer, K. M., 1946, *Proc. Phys. Soc.*, **58**, 456.
- Mitra, S. S., 1954, *J. Chem. Phys.*, **22**, 2097.
- Rosen, B., 1951, "Donnees Spectroscopiques concernant les molecules Diatomiques" (Hermann and Cie, Depositaires, Paris V^e).
- Varshni, Y. P., 1953, *Curr. Sci.*, **22**, 199.
- Varshni, Y. P. and Majumdar, K., 1955, III, *Ind. J. Phys.*, **29**, 38.
- Varshni, Y. P. and Majumdar, K., 1955, IV, *Ind. J. Phys.*, **29**, 285.
- Walsh, A. D., 1951, *Proc. Roy. Soc.*, **A207**, 13.

RAMAN SPECTRA OF FROZEN SOLUTIONS OF TOLUENE AND BENZENE IN ALIPHATIC SOLVENTS*

G. S. KASTHA

OPTICS DEPARTMENT, INDIAN ASSOCIATION FOR THE CULTIVATION OF SCIENCE, JADAVPUR,
CALCUTTA-32

(Received for publication, April 16, 1956)

Plate VIII A & B

ABSTRACT. The Raman spectra of frozen solutions of toluene in ethyl alcohol of strengths 81.5% and 35.4% and of benzene in solutions of ethyl alcohol (35.5%), cyclohexane (18%) and cyclohexanol (32%) at -180°C have been studied. In the first two cases the spectra show a continuous wing accompanying the Rayleigh line, there being a strong band at 95 cm^{-1} in the first case. It has been pointed out that the band at 95 cm^{-1} in case of solution of strength 81.5% is probably formed by the coalescence of the two discrete lines at 86 cm^{-1} and 108 cm^{-1} found in the spectrum due to pure toluene in the solid state at -180°C and that these lines are due to vibrations in groups of toluene molecules formed by virtual linkages amongst neighbouring molecules some of which break up into single molecules when the strength is reduced to 35.4% and that the continuous wing may be due to oscillations in groups formed by association of toluene molecule with ethyl alcohol molecules.

In all the spectra due to the frozen solutions of benzene in different solvents at -180°C , the new low frequency lines appear with the same intensities and at the same positions as in the case of pure benzene in the solid state at -180°C . From considerations of the relative densities of the solvents and of the solute, the solubility and the persistence of the low-frequency Raman lines with undiminished intensity in the spectra of these frozen solutions, it has been concluded that these lines are due to oscillations in small groups of molecules which are always present in concentrated solutions of the aromatic molecules in the solvents mentioned above.

INTRODUCTION

The Raman spectra of frozen solutions of carbon disulphide in methyl cyclohexane and other aliphatic solvents at -180°C were first studied by Sirkar and Kastha (1955) and Kastha (1955). In the Raman spectra of these frozen solutions except in that due to the solution in methyl cyclohexane of strength about 20%, the new low frequency lines at 70 cm^{-1} and 81 cm^{-1} appear with intensities almost the same as in the case of pure carbon disulphide in the solid state. These two lines, however, were found to be totally absent in the Raman spectrum, due to 20% solution of carbon disulphide in methyl cyclohexane

* Communicated by Prof. S. C. Sirkar.

in the solid state (Sirkar and Kastha, 1955). It was concluded from these results that these two new lines cannot be due to angular oscillations of the molecules in the lattice of pure carbon disulphide crystals, because in the 20% solution also such oscillations with some other frequencies might take place and these would produce new lines at some other positions, but actually no such lines are observed. They further concluded from the observed results that these two lines are produced by oscillations in small groups of carbon disulphide molecules and that these groups break up completely in the 20% solution.

It is well known that benzene and many substituted benzene compounds in the solid state yield strong new lines in the neighbourhood of the Rayleigh line. These new Raman lines of solid benzene were reported first by Gross and Vuks (1935) and they were studied under different conditions later by Sirkar (1936) and Sirkar and Ray (1950). It was pointed out by Sirkar (1936) that the lines might be due to oscillations in associated groups of molecules in solid benzene. Later he pointed out (Sirkar, 1937) that, in the case of crystals, of which the unit cell possesses a centre of symmetry, lattice oscillations involving translations are forbidden, and therefore, the new lines cannot be due to any such lattice oscillations. Lattice oscillations of angular type, of course, might produce these lines as supposed by Kastler and Rousset (1941) and Bhagavantam (1941) but from a study of the dependence of the intensities and position of these lines on temperature, Sirkar and Ray (1950) concluded that as the intensities of most of the lines of benzene do not diminish appreciably at lower temperature the lines cannot be attributed to such angular oscillations. Such a hypothesis can, however, be tested by studying the Raman spectra of frozen solutions of these compounds in suitable solvents.

With this object in view, a programme has been undertaken to study the Raman spectra of frozen solutions of substituted benzenes in different solvents and the results obtained in the case of such solutions of benzene and toluene have been discussed in the present paper.

EXPERIMENTAL

The arrangement for photographing the Raman spectra of frozen solutions of benzene in different solvents, pure benzene and pure toluene in the solid state at low temperature was the same as that used by Majumdar (1949). The Raman spectra of frozen solutions of toluene in ethyl alcohol and of pure ethyl alcohol at -180°C were photographed by using the arrangement described earlier (Kastha, 1954).

The solvents used in case of benzene, were ethyl alcohol, cyclohexane and cyclohexanol, while in case of toluene only ethyl alcohol was used as a solvent. All these chemicals were of chemically pure quality and they were distilled

repeatedly in vacuum before use. The solutions of benzene were sealed under vacuum in cylindrical pyrex glass containers. The Raman spectrum was photographed in each case keeping the container always immersed in liquid oxygen during the exposure. The Raman spectra of pure benzene and pure toluene in the solid state at -180°C were also photographed under similar conditions.

The solutions of toluene in ethyl alcohol of strength 35.4% and 81.5%, when frozen in sealed long containers of pyrex glass, were found to form transparent homogeneous masses. The lower portion of the container was immersed in liquid oxygen contained in a transparent Dewar vessel of pyrex glass, the bottom of the container being blown flat to serve as the exit window. The container was held vertically and was illuminated by two vertical mercury arcs. The scattered light coming out through the window at the bottom was reflected by a right-angled prism and focussed on the slit of the spectrograph. The Raman spectrum of pure ethyl alcohol in the solid state at -180°C was also photographed in the same way. A Fuess glass spectrograph having a dispersion of $11\text{\AA}/\text{mm}$ in the region λ 4047 \AA and Ilford Zenith plates were used to photograph the Raman spectra.

RESULTS AND DISCUSSION

The spectrograms due to pure toluene in the solid state and of frozen solutions of toluene in ethyl alcohol are reproduced in figures 1, 2 and 3, Plate IA. The spectrum due to pure ethyl alcohol in the solid state is also reproduced in figure 4, Plate IA. The spectrograms due to pure benzene in the solid state and frozen solutions of benzene in different solvents are given in figures 5—8, Plate VIIIB.

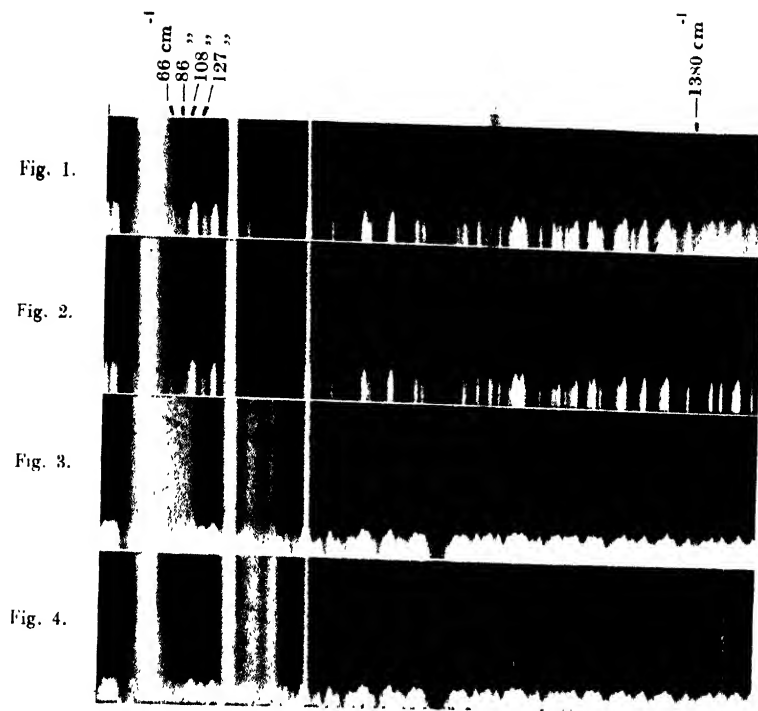
The spectrogram due to pure ethyl alcohol at -180°C (figure 4) does not show any modified line or wing in the region between the Hg lines 4047 \AA and 4077 \AA . But it is seen from figure 2 that there is a continuous wing in this region with a strong band at a distance of about 95 cm^{-1} in the case of 81.5% solution but in the spectrum due to the 35.4% solution (figure 3) only a continuous wing is present.

It is well known and can be seen from figure 1 also that in the Raman spectrum of pure toluene at -180°C there are discrete lines at 66, 86, 108 and 127 cm^{-1} (Ray, 1950). The intensity of these lines are of the same order of magnitude as that of the line at 1380 cm^{-1} . As the frozen solutions of toluene appeared to be transparent, it is quite unlikely that crystals of pure toluene remained dispersed in frozen alcohol in the frozen solutions mentioned above. Hence the band observed in the case of 81.5% solution at -180°C cannot be due to lattice oscillation in pure toluene crystals. Since in the case of pure alcohol in the

solid state no modified scattering is observed in the neighbourhood of the Rayleigh line, the band at 95 cm^{-1} cannot be due to oscillation of the alcohol lattice. Also the band is found to be stronger than the line 1380 cm^{-1} due to the toluene molecule. From a comparison of the intensities of the lines 86 and 108 cm^{-1} and 1380 cm^{-1} in the Raman spectra of frozen toluene at -180°C it is found that the first two lines are slightly stronger than the line 1380 cm^{-1} . Hence it can be concluded that in the spectrum due to the frozen solution of strength 81.5% the band at 95 cm^{-1} is produced by the coalescence of the two lines 86 and 108 cm^{-1} of undiminished intensity, owing to increase in the width of the individual lines. These lines are therefore due to groups of toluene molecules formed by virtual linkages among neighbouring molecules. When the strength of the solution is diminished to 35.4% , some of these groups break up and the band disappears but a continuous wing persists. This wing may be due to groups formed by association of toluene molecules with ethyl alcohol molecules. These groups of molecules, unlike small crystals, do not produce inhomogeneity in the refractive index of the solutions and hence these solutions appear to be transparent.

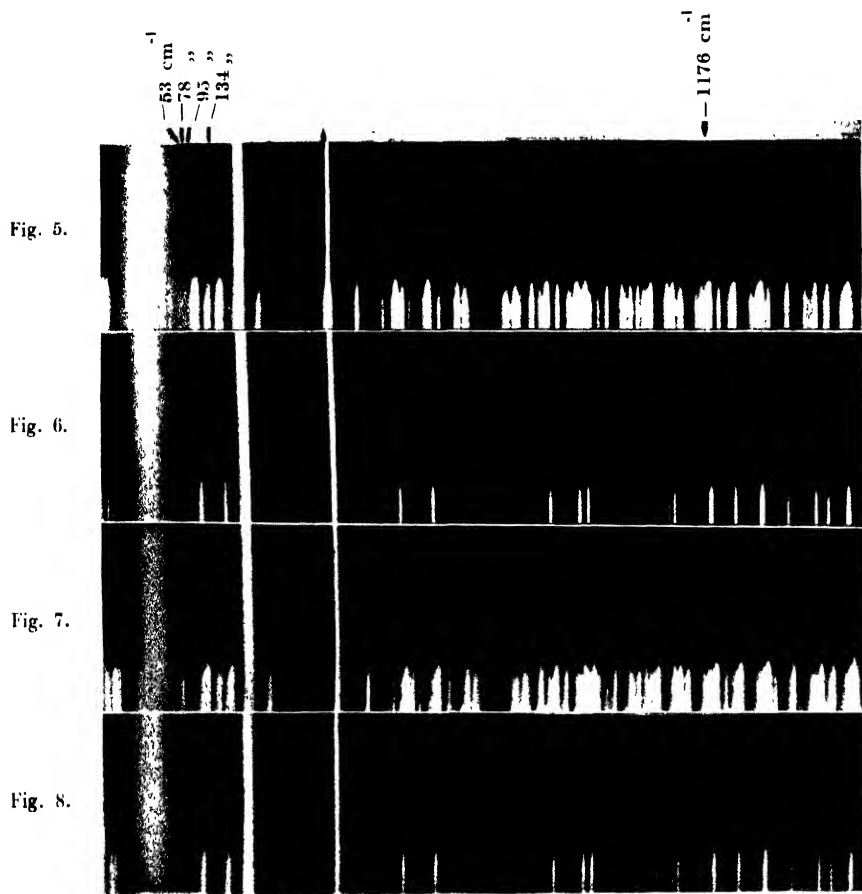
The Raman spectrum of frozen solution of 35.5% benzene in ethyl alcohol at -180°C (figure 6) shows that the prominent new lines at 53 , 78 , 95 and 134 cm^{-1} of crystalline benzene have all appeared with almost undiminished intensity, although the spectrum of the light scattered only from the upper half of the frozen mass was photographed. This fact indicates the presence of benzene molecules in the upper half of the frozen solution. But it is evident that these molecules did not form small crystals, because such crystals would have settled down at the bottom of the container before the solvent was completely frozen. So the appearance of the new low frequency lines in the spectrum of this solution in the solid state suggest that these lines are produced by vibrations in small associated groups of benzene molecules as pointed out by Sirkar (1936). The alcohol molecules apparently are not able to break up these associated groups of benzene molecules as in the case of 81.5% solution of toluene in alcohol in the solid state. The fact that in the frozen state the solutions of toluene appear to be transparent while those of benzene form white mass, probably indicates that in the former case the associated groups are very small, while in the latter case, the molecules of benzene being smaller the groups are larger and cannot be broken easily by the solvent molecules owing to closer packing.

The alternative interpretation of these results that when the 35.5% solution of benzene in ethyl alcohol was frozen, some of the benzene molecules were separated out in the form of crystals is improbable, because the solubility of benzene in ethyl alcohol being very high even at low temperatures at least a portion of the solution would remain dispersed in the frozen solvent and in that case the new lines in the low frequency region would be much weaker than those due



Raman spectra of solid toluene and its frozen solutions in different solvents.

- Fig. 1. Raman spectra of pure toluene in the solid state at -180°C
 Fig. 2. " " " 81.5% solution of toluene in ethyl alcohol at -180°C
 Fig. 3. " " " 35.4% " " " " " " " "
 Fig. 4. " " " pure ethyl alcohol in the solid state at -180°C



Raman spectra of solid benzene and its frozen solutions in different solvents.

Fig. 5. Raman spectra of pure benzene in the solid state at -180°C

Fig. 6. " " " 35.4% solution of benzene in ethyl alcohol at -180°C

Fig. 7. " " " 18% " " " in cyclohexane at -180°C

Fig. 8. " " " 32% " " " in cyclohexanol at -180°C

to pure benzene in the solid state. Actually, it is found that the new lines due to the frozen solution are not weaker than those due to the pure benzene as can be seen from a comparison of the intensities of these lines with that of the line 1176 cm^{-1} .

The frozen solutions of benzene in cyclohexane of strengths 18% and 28% at -180°C are found to form translucent white masses. On comparing the Raman spectra due to 18% solution of benzene in cyclohexane (figure 7) and 32% solution in cyclohexanol (figure 8) with the spectrum due to pure benzene in the solid state at -180°C (figure 6) it is found that all the prominent lines in the low-frequency region persist in the spectra of the frozen solutions at -180°C . It has also been observed that the intensities and positions of the low frequency lines in the Raman spectra of 25% solution of benzene in cyclohexane at -180°C and 18% solution in cyclohexane at -100°C are the same as those observed in the spectrogram due to pure benzene in the solid state at corresponding temperatures. The freezing points of benzene and cyclohexane are 5.5°C and 6.5°C respectively and therefore it is improbable that when a dilute solution of strength about 18% was frozen all the benzene molecules crystallised out of the solution. Since the solution was gradually cooled, benzene would have crystallised out first and in that case the upper portion of the frozen solution would have contained very few benzene molecules. The spectrum scattered by this portion of the frozen mass does not reveal any change in the relative intensities of the new lines as compared to those in the case of pure benzene in the solid state. Hence, it is probable that in this case also the benzene molecules might have been present in associated groups rather than in form of small crystals. Similar arguments can be put forward also to explain the results obtained in the case of the frozen solution of benzene in cyclohexanol. Apparently, in these solutions as in the solution in ethyl alcohol the intermolecular field in the solvents is not able to break up the associated groups formed by benzene molecules.

Thus these results furnish strong evidence in support of the view that these aromatic molecules exist in small groups in the liquid state, these groups break up only in suitable solvents at low concentrations.

ACKNOWLEDGMENT

The author is indebted to Professor S. C. Sirkar, D. Sc., F. N. I. for his keen interest and helpful guidance during the progress of the work.

REFERENCES

- Bhagavantam, S., 1941, *Proc. Ind. Acad. Sc.*, **18A**, 543.
Gross, E. and Vuks, M., 1935 *Nature*, **135**, 100, 998.

- Kastha, G. S., 1954, *Ind. J. Phys.*, **28**, 329.
 ,, 1955, *Ind. J. Phys.*, **29**, 474.
Kastler, A. and Rousset, A., 1941, *Compt. Rend.*, **212**, 645.
Majumdar, N. C., 1949, *Ind. J. Phys.*, **23**, 253.
Ray, A. K., 1950, *Ind. J. Phys.*, **24**, 111.
Sirkar, S. C., 1936, *Ind. J. Phys.*, **10**, 189.
 ,, 1937, *Ind. J. Phys.*, **11**, 343.
Sirkar, S. C. and Kastha, G. S., 1955, *J. Chem. Phys.*, **23**, 2439.
Sirkar, S. C. and Ray, A. K., 1950, *Ind. J. Phys.*, **24**, 189.

Letters to the Editor

The Board of Editors will not hold itself responsible for opinions expressed in the letters, published in this section. The notes containing reports of new work communicated for this section should not contain many figures and should not exceed 500 words in length. The contributions must reach the Assistant Editor not later than the 15th of the second month preceding that of the issue in which the Letter is to appear. No proof will be sent to the authors.

THE ULTRAVIOLET ABSORPTION SPECTRUM OF PARA FLUOROCHLOROBENZENE.

S. L. N. G. KRISHNAMACHARI

PHYSICS DEPARTMENT, ANDHRA UNIVERSITY, WALTAIR

(Received for publication, April 23, 1956)

In continuation of the work on the ortho- and meta-fluorochlorobenzenes (author, 1955, 1956), the ultraviolet absorption spectrum of para-fluorochlorobenzene in the vapour was studied. There is no previous report on the ultraviolet absorption of this compound. The spectrum in the present investigations was photographed with path lengths of 25, 50 and 75 cms. and at different temperatures ranging from -80°C to about $+100^{\circ}\text{C}$.

Two regions of absorption were observed : (1) a continuous one below 2150Å and (2) a discrete one in the region 2940-2375Å. These two regions merge together at higher vapour pressures. About 275 bands were measured in this discrete region. This system could be explained as due to the allowed electronic transition A_1-B_1 . In accordance with this, a strong 0,0 band and overtones and combinations of many totally symmetrical vibrations were observed. The strong band at 36276 cm^{-1} was chosen as the 0,0 band. Most of the bands were interpreted in terms of 5 upper state and 5 ground state frequencies. These, together with other data, are presented in the following table. On the red side of each of the strong bands, satellite bands were observed with frequency separations of 33 and 90 cm^{-1} , the former being more pronounced. The absorption spectrum

obtained with a path length of 50 cm and at -10°C is reproduced in the adjoining figure 1.

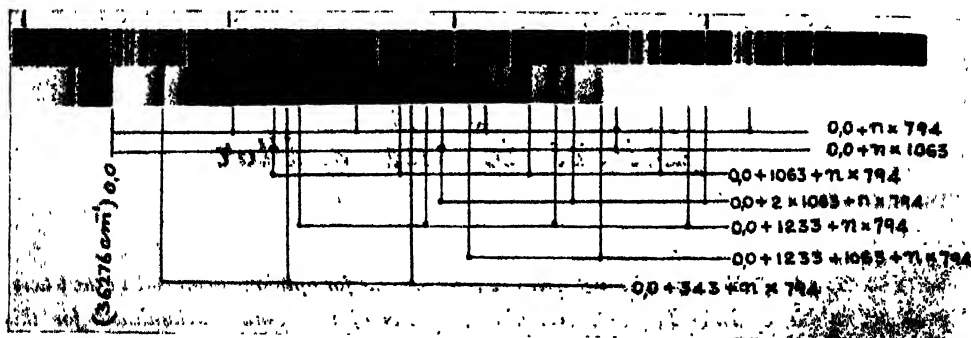


Fig. 1. Ultraviolet absorption spectrum of *p*-fluorochlorobenzene.

A detailed discussion of the analysis will be published shortly.

Ground and excited state frequencies of *p*-F.C₆H₄.Cl.

Raman data (Kohlrausch, 1947)			U.V. absorption data		Tentative assignment
λ^{ν}	Int	* ρ	Ground state	Excited state	
379	st	.42	370	343 (m)	one of the ϵ^{ν}_g com- ponents of C ₆ H ₆
634	ms	.64	637	563 (w)	
817	vs	.19	815	794 (st)	C-C vibration
1094	st	.22	1090	1063 (ms)	C-C vibration
1227	mw	.38	1239	1233 (m)	C-F stretch

*Determined in the present investigations.

The author is grateful to Dr. G. C. Finger of the Illinois State Geological Survey for the gift of the sample and to the Govt. of India for the award of a senior research scholarship. The author is deeply indebted to Prof. K. R. Rao for his valuable guidance.

REFERENCES

- Krishnamachari, S. L. N. G., 1955, *Ind. J. Phys.*, **29**, 603.
 „ 1956, *Ind. J. Phys.*, **30**, 151.
 Kohlrausch, et al., 1947, *Mh. Fur. Chem.*, **76**, 200-14.

ULTRAVIOLET ABSORPTION SPECTRA OF PHENYL ACETONITRILE, PHENYL ACETATE, PHENYL SALICYLATE AND MONOMERIC STYRENE IN THE LIQUID AND SOLID STATES*

S. K. SEN

OPTICS DEPARTMENT, INDIAN ASSOCIATION FOR THE CULTIVATION OF SCIENCE,
JADAVPUR, CALCUTTA-32

(Received for publication April 21, 1956)

ABSTRACT. Absorption spectra of phenyl acetonitrile, phenyl acetate, phenyl salicylate and monomeric styrene in the liquid and solid states at low temperatures have been investigated and the results have been compared with those for vapours and for solutions of these substances. Absorption spectrum of phenyl salicylate in the vapour state has also been studied and the prominent bands have been assigned.

In the liquid state phenyl acetonitrile gives five broad bands with the 0,0 band at 37844 cm^{-1} , while in the vapour state the 0,0 band is at 38010 cm^{-1} . In the solid state at -180°C the 0,0 band shifts to 37917 cm^{-1} and the excited electronic state is found to be split up into two components.

Phenyl acetate in the liquid state yields four broad bands with the 0,0 band at 37554 cm^{-1} . The bands do not seem to undergo any change with changes of state except that the bands become a little sharper at the low temperature.

Phenyl salicylate in the liquid state gives a very broad band with the absorption edge on the longer wavelength side at 31306 cm^{-1} taken as the 0,0 band. The 0,0 band due to the vapour state has been found at 36342 cm^{-1} . Thus major change is found to occur on the liquefaction of vapour. In the solid state at -180°C the spectrum gives four narrower bands with the 0,0 band at 31046 cm^{-1} .

The liquid state of monomeric styrene yields five broad bands with the 0,0 band at 34228 cm^{-1} while that for the vapour state is at 34761 cm^{-1} . In the solid state at -180°C , the 0,0 band shifts to 34215 cm^{-1} and the excited electronic state is found to be split up into two components giving rise to thirteen bands. It has been suggested that two types of molecules formed by two types of associated groups of molecules in the crystal may give rise to the splitting of electronic energy level.

INTRODUCTION

In a previous investigation (Sen, 1955) it was observed in the case of *o*- and *p*-tolunitriles ($\text{CN C}_6\text{H}_4\text{CH}_3$) that $\text{C} \equiv \text{N}$ as a substituent in the aromatic ring

* Communicated by Prof. S. C. Sirkar.

has got an influence on the electronic energy levels of the molecules in the state of aggregation different from that observed in the case of molecules having halogen atom as a substituent (Swamy 1952, 1953). It was observed that major change in the absorption spectra occurs with the liquefaction of vapours of both the nitriles and the 0,0 band shifts towards longer wavelengths with the solidification of the liquids and lowering of temperature to -180°C , further shift towards longer wavelengths was observed in the case of the ortho compound, but no such shift takes place in the case of para compound. In tolunitrile the $\text{C} \equiv \text{N}$ group is attached to the benzene ring. The influence of the introduction of $\text{C} \equiv \text{N}$ group in CH_3 group of toluene on the ultraviolet absorption spectra of the compound in the state of aggregation is not known. Therefore, the ultraviolet absorption spectra of phenyl acetonitrile ($\text{C}_6\text{H}_5\text{CH}_2\text{CN}$) in the liquid and solid states have been studied in the present investigation. The results have been compared with those for vapour state reported by Imanishi and Kanda (1949) and with those for other substituted toluenes reported by Swamy (1952, 1953).

The ultraviolet absorption spectra of esters of benzoic acid in the liquid and solid states were studied by Deb (1951, 1953). It was observed by him that although in the case of halogen substituted benzenes the bands become sharp when the liquids are frozen and cooled to -180°C , in the case of alkyl benzoates the bands remain almost as broad as in the case of the liquid state when the liquids are frozen and cooled to -180°C . These benzoates may be regarded as substituted benzenes in which the substituent is attached to the benzene ring through a C-C bond. It was thought worthwhile to compare these results with those for esters of aliphatic acids containing CH_3 group and for esters containing two substituted benzene rings. Phenyl acetate and phenyl salicylate have been chosen for this purpose in the present investigation. The ultraviolet absorption spectra of phenyl acetate in the liquid and solid states have been investigated and compared with those for the vapour and the solution in ether reported by Kato and Someno (1938).

The absorption spectra of phenyl salicylate in the vapour state was not studied by any previous worker. So, the spectra of the compound in all the three states have been studied and the results have been discussed in the present paper.

The ultraviolet absorption spectra of monomeric styrene in the liquid and solid states were studied by Nikitana (1953) and he reported three bands in the liquid state which split up into twelve narrow bands in the solid state at -195°C , the continuous spectrum being resolved into seven wide bands. The original Russian journal being not available, it is not also known whether the results of absorption spectra of the liquid and solid states have been compared with those

for the vapour state in order to find out whether in the case of this substituted benzene containing a $C \equiv C$ group in the substituent, the influence of intermolecular field is the same as in other substituted benzenes in the solid state at low temperature. So the absorption spectra of monomeric styrene in the liquid and solid states have been reinvestigated and the results have been compared with those for the solution in cyclohexane reported by Robertson, Music and Matsen (1950) and that of vapour state reported by Morgan (1953).

EXPERIMENTAL

Chemically pure samples of phenyl acetonitrile and phenyl acetate supplied by Fisher Scientific CO., (U.S.A), phenyl salicylate supplied by E. Merck (Germany) and styrene monomer supplied by the Department of Physical Chemistry of this Association*, were distilled four times under reduced pressure before being used in the present investigation.

The experimental set up is the same as that employed in an earlier investigation by the author (Sen, 1955). Spectrograms were taken on HP 3 films with a Hilger E1 quartz spectrograph having a dispersion of 3 ÅU per mm in the region 2600 Å. The absorption spectrum of phenyl salicylate in the vapour state was photographed using an absorption tube of length 50 cm and diameter 14 mm, quartz windows being cemented to the tube with Araldite. An exposure of 10 minutes was required to record the spectra for the liquid, while that for the spectra of the solid at -180°C was one hour. The spectrum of phenyl salicylate in the vapour state was recorded with an exposure of one and a half hours. In the case of liquid and solid states thin films of thickness less than .01 m.m. were used.

Iron arc was photographed on each spectrogram as comparison. Microphotometric records were obtained with a self-recording microphotometer supplied by Kipp & Zonen. The frequencies of the bands were measured from these records in which the record of two known iron lines were taken as reference lines. The microphotometric record of the iron lines was used as comparison.

RESULTS

The spectrogram of the vapour state of phenyl salicylate is reproduced in figure 1.

The microphotometric records of the spectrograms due to the substances in the liquid and solid states are given in figures 2, 3, 4 and 5. The frequencies of the bands are given in the Tables I, II, III, IV and V with approximate relative intensities indicated as strong, medium, weak etc.

*The author's thanks are due to Professor S. R. Palit for supplying the monomer after purifying it.

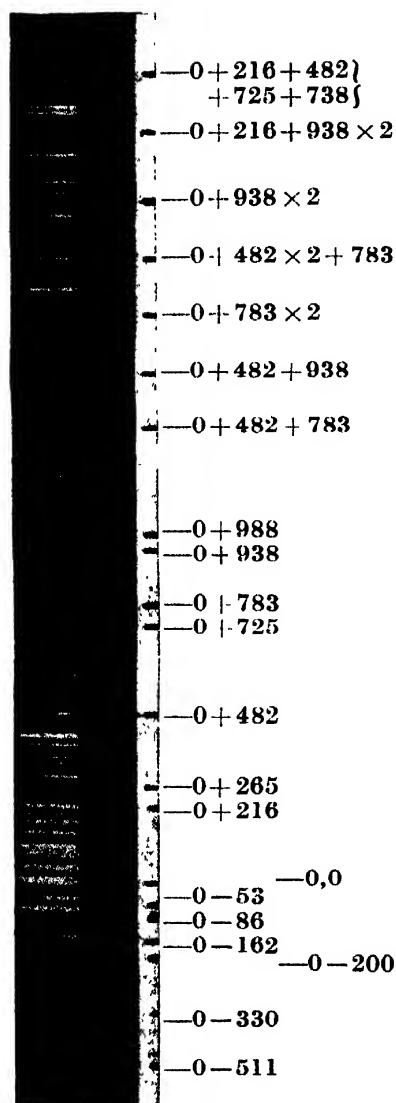


Fig. 1.
Ultraviolet absorption spectrum of
phenyl salicylate vapour at 50°C.

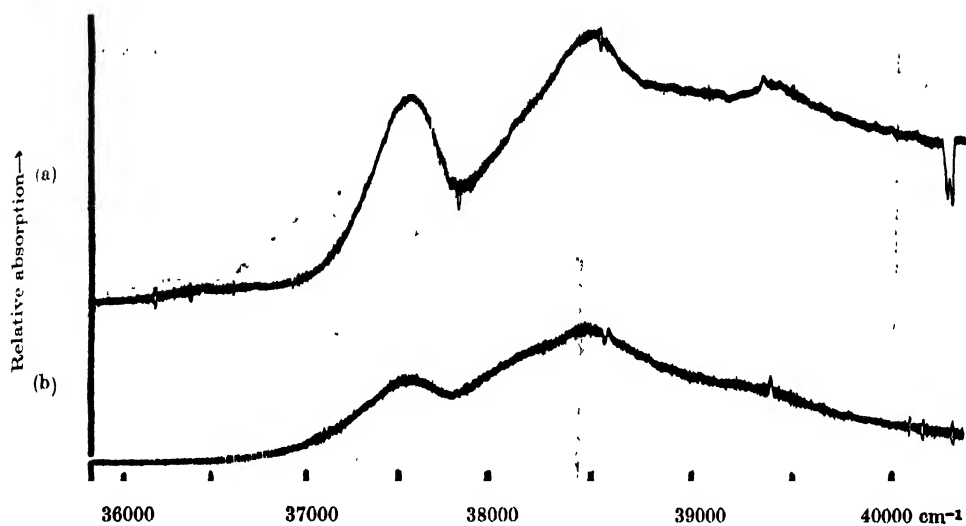


Fig. 2. Microphotometric records of the ultraviolet absorption spectra of phenyl acetate.
Curve (a)-Solid at -180°C . Curve (b)-Liquid at 30°C .

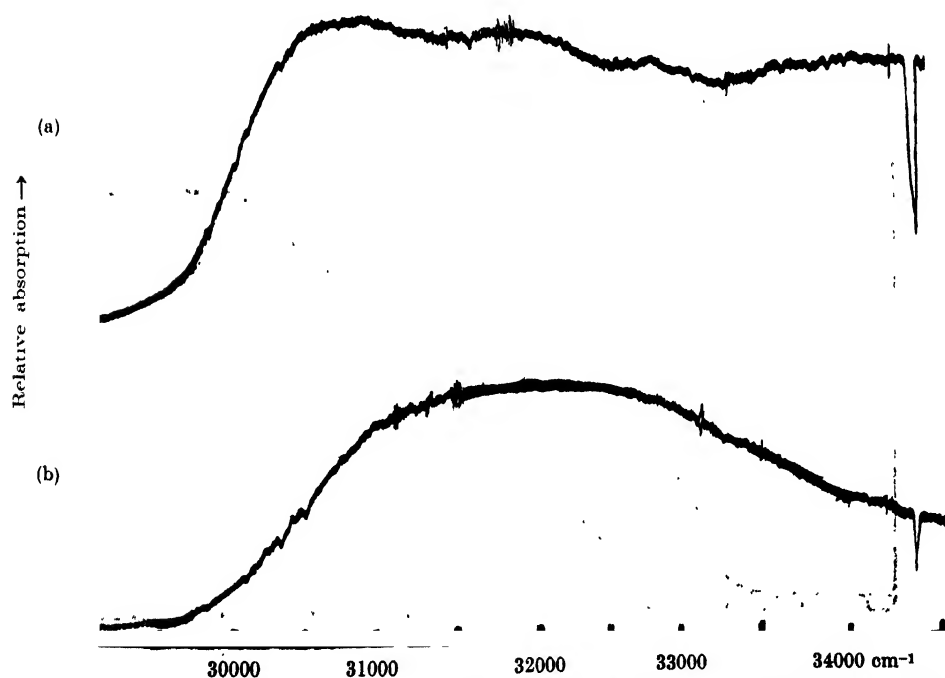


Fig. 3. Microphotometric records of the ultraviolet absorption spectra of phenyl salicylate.
Curve (a)-Solid at -180°C . Curve (b)-Liquid at 42°C .

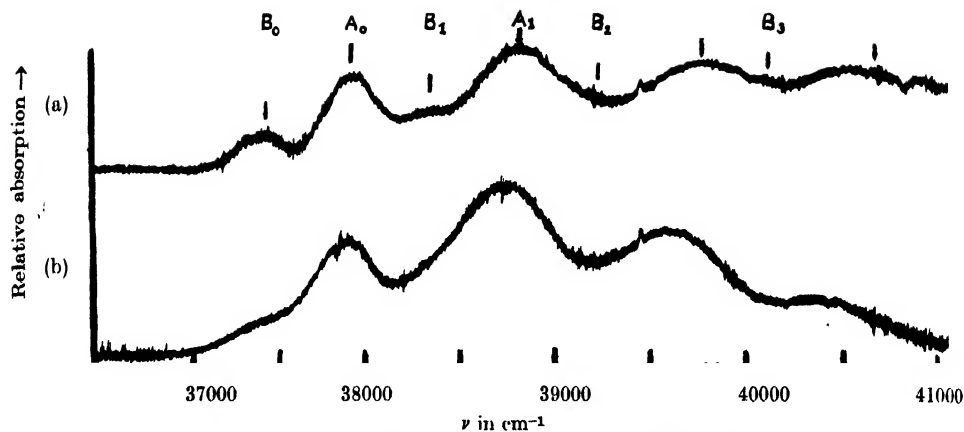


Fig. 4. Microphotometric records of the ultraviolet absorption spectra of phenyl acetonitrile.

Curve (a)-Solid at -180°C .

Curve (b)-Liquid at 32°C .

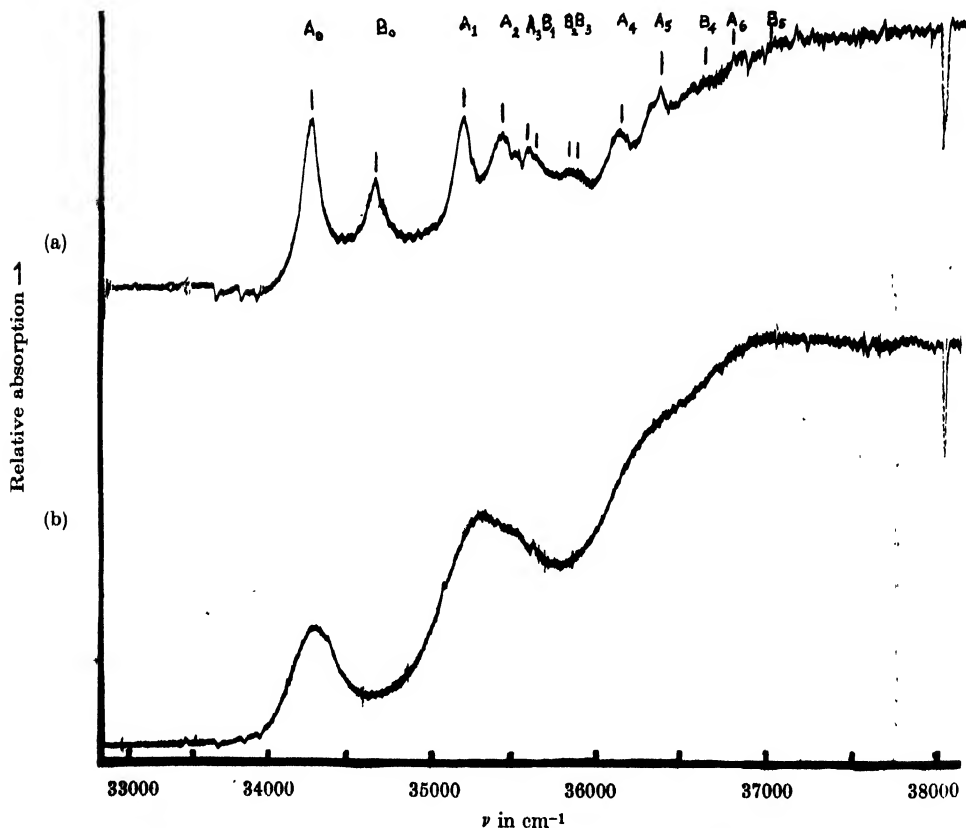


Fig. 5. Microphotometric records of the ultraviolet absorption spectra of monomeric styrene.

Curve (a)-Solid at -180°C .

Curve (b)-Liquid at 30°C .

TABLE I

Absorption bands of phenyl acetonitrile in the liquid and solid states

Liquid at 32°C			Solid at -180°C		
Wave No cm ⁻¹	Difference from 0,0 band	Assignment	Wave No in cm ⁻¹	Designation	Assignment
37316 (vw)	-528	0-528			
			37404 (ms)	B ₀	
37844 (s,b)		0,0			513
			37917 (s)	A ₀	
38713 (vs,b)	869	0 + 869	38313 (w)	B ₁	B ₀ + 909
39590 (s,b)	1746	0 + 2 × 869	38826 (s,b)	A ₁	A ₀ + 909
40452 (ms, b)	2608	0 + 3 × 869	39219 (w)	B ₂	B ₀ + 909 × 2
			39727 (s, b)	A ₂	A ₀ + 909 × 2
			40138 (w)	B ₃	B ₀ + 909 × 3
			40634 (ms)	A ₃	A ₀ + 909 × 3

TABLE II

Absorption bands of phenyl acetate in the liquid and solid states

Liquid at 30°C			Solid at -180°C		
Wave No cm ⁻¹	Difference from 0,0 band	Assignment	Wave No cm ⁻¹	Difference from 0,0 band	Assignment
37554 (s, vb)		0,0	37556 (s, b)		0,0
38244 (w, vb)	690	0 + 690	38247 (w, b)	691	0 + 691
38494 (s, vb)	940	0 + 940	38496 (s, b)	940	0 + 940
38938 (w, vb)	1384	0 + 690 × 2	38939 (w, b)	1383	0 + 691 × 2
39435 (w, vb)	1881	0 + 940 × 2	39426 (w, b)	1870	0 + 940 × 2

TABLE III

Absorption bands of phenyl salicylate in the vapour state at 50°C

Wave No cm ⁻¹	Difference from 0,0 band	Assignment	Wave No cm ⁻¹	Difference from 0,0 band	Assignment
35831 (w)	-511	0-511	37125 (s)	783	0+783
36012 (w)	-330	0-330	37280 (s)	938	0+938
36142 (w)	-200	0-200	37330 (s)	968	0+988
36180 (w)	-162	0-162	37618 (ms)	1276	0+482+783
36256 (ms)	-86	0-86	37758 (ms)	1416	0+482+938
36289 (ms)	-53	0-53	37917 (ms)	1575	0+783×2
36342 (s)		0,0	38083 (w)	1741	0+482×2+783
36558 (ms)	216	0+216	38219 (w)	1877	0+938×2
36607 (ms)	265	0+265	38313 (w)	1971	0+988×2
36824 (s)	482	0+482	38433 (w)	2091	0+216+938×2
37067 (ms)	725	0+725	38556 (w)	2214	0+216+482+725 +783

TABLE IV

Absorption bands of phenyl salicylate in the liquid and solid states

Liquid at 42°C	Wave No cm ⁻¹	Difference from 0,0 band	Assignment
Broad band extending from	31046 (s)		0,0
3199.5 Å (31245 cm ⁻¹) to	31897 (ms)	851	0+851
3021 Å (33092 cm ⁻¹). The absorption edge on	32755 (w)	1709	0+851×2
the longer wavelength side at 3193.3 Å	33595 (w)	2549	0+851×3
(31306 cm ⁻¹) taken as the 0,0 band.			

—Transmission in the region between 2981Å

(33536 cm⁻¹) and 2666Å (37498 cm⁻¹) and continuous absorption thereafter.

TABLE V

Absorption bands of monomeric styrene in the liquid and solid states

Liquid at 30°C			Solid at -180°C		
Wave No cm ⁻¹	Difference from 0,0 band	Assignment	Wave No cm ⁻¹	Designation	Assignment
34228 (s)	—	0,0	34215 (vs)	A ₀	
35224 (s)	996	0+996	34637 (s)	B ₀	422
35475 (ms)	1247	0+1247	35172 (s)	A ₁	A ₀ +957
36223 (w)	1995	0+996×2	35434 (s)	A ₂	A ₀ +1219
36726 (w)	2498	0+1247×2	35509 (ms)	A ₃	A ₀ +1294
			35589 (ms)	B ₁	B ₀ +957
			35854 (w)	B ₂	B ₀ +1219
			35934 (w)	B ₃	B ₀ +1294
			36123 (ms)	A ₄	A ₀ +957×2
			36399 (ms)	A ₅	A ₀ +957+1219
			36549 (w)	B ₄	B ₀ +957×2
			36646 (w)	A ₆	A ₀ +1219×2
			36821 (w)	B ₅	B ₀ +957+1219

DISCUSSION

 Phenyl acetonitrile (C₆H₅CH₂CN)

The ultraviolet absorption spectrum of phenyl acetonitrile in the vapour state was studied by Imanishi and Kanda (1949) and the bands were classified according to the following series:

$$\nu = 38010 + 930u' + 395v' - (765w'' + 145x'')$$

The intense band at 38938 cm⁻¹ was not taken by them as the 0,0 band but it was assigned to 1,0 transition. In the present investigation, the liquid state yields five broad bands with the first band at 37316 cm⁻¹. This band is probably due to a $\nu \rightarrow 0$ transition; if this weak band is taken as the 0,0 band, succeeding bands cannot be assigned properly. So the band at 37844 cm⁻¹ is taken as the 0,0 band and a progression of excited state frequency 869 cm⁻¹ is observed. The 0,0 band is found to be shifted by 166 cm⁻¹ towards longer wavelengths from its position in the vapour state, probably due to formation of virtual bonds which lowers the excited electronic energy state. The excited state frequency 930 cm⁻¹ observed in the case of the vapour corresponds to the frequency 869 cm⁻¹

in the excited state in the case of the liquid. In the case of the solid at low temperature eight bands are observed of which the first band on the longer wavelength side at 37404 cm^{-1} is weaker than the second one. It is found that all the bands cannot be assigned properly by taking this band as the 0,0 band, but if both the first and the second band are taken as the 0,0 band, all the bands are assigned and we get a progression of excited state frequency 909 cm^{-1} . Thus in this case the excited state energy level is split up into two components. The cynogen group is thus responsible for this splitting, but the 0,0 band does not shift very much with solidification of the liquid.

The weak band on the long wavelength side of the principal band marked. A_0 (figure 4) is at a distance of 513 cm^{-1} . The latter weak band cannot be due to $v \rightarrow 0$ transition as the large distance does not permit of molecules present in the excited state to have this mode of vibration. Also there is no strong band in the vapour state corresponding to this transition. The excited state frequency 909 cm^{-1} found in the case of the solid at -180°C , is larger than 869 cm^{-1} observed in the case of liquid. While the frequency 395 cm^{-1} observed in the case of the vapour is completely absent in the spectra due to the liquid and solid states, the aromatic ring vibration frequency seems to predominate in the excited state. Splitting of electronic energy level into three components was observed in the case of *o*-, *m*-chlorotoluenes, *o*-dichlorobenzene and *o*-bromotoluene by Swamy (1952, 1953). One of the two weak components was found to be on the longer wavelength side of the principal band in the case of *o*-chlorotoluene and *o*-dichlorobenzene just as the weak component in the present case, but in the case of *m*-chlorotoluene and *o*-bromotoluene both the weak components were on the longer wavelength side of the principal band.

Phenyl acetate ($\text{CH}_3\text{COO C}_6\text{H}_5$).

The absorption spectrum of phenyl acetate in the vapour state was studied by Kato and Someno (1938). With the 0,0 band at 37500 cm^{-1} , the principal bands were assigned to progression of excited state vibration frequency 963 cm^{-1} . The bands were found to be broad and diffuse. In the present investigation the liquid state yields five broad bands represented by progression of excited state frequencies 690 cm^{-1} , 940 cm^{-1} . The 0,0 band of the liquid is at 37554 cm^{-1} . So the 0,0 band does not shift very much with liquefaction of vapour. This indicates that the intermolecular field has very little influence on the electronic energy state in this case. The frequency 963 cm^{-1} found in the vapour state corresponds to excited state frequency 940 cm^{-1} in the liquid state. In the solid state at -180°C , the substance yields almost the same spectrum as in the liquid state except that the bands become a little sharper at low temperatures. The rotational freedom of the $0 - \text{C} = \text{CH}_3$ group about the C—O bond may be responsible for the broadening of the bands in the vapour and liquid states.

In the case of solution of phenyl acetate in ether, three bands were reported by Kato and Someno (1938), the bands being at $37,700\text{ cm}^{-1}$, $38,500\text{ cm}^{-1}$ and $39,300\text{ cm}^{-1}$ with the frequency difference of 800 cm^{-1} between successive bands. If this band at $37,700\text{ cm}^{-1}$ is taken as the 0,0 band, it is shifted by 146 cm^{-1} towards shorter wavelengths from its position for the liquid phase. This shift and the change in the excited-state vibration frequency show that the intermolecular field of the solvent exerts some influence on the electronic state of the molecule.

If these results are compared with those due to esters of benzoic acid (Deb, 1951, 1953), it is found that in the latter case the shift of the 0,0 band with change of state is much larger. Thus it appears that when the substituent in the benzene ring is connected through a C-C bond to the ring, the intermolecular field in the state of aggregation has a large influence on the electronic state but when it is connected through a C-O bond, the influence is small.

Phenyl salicylate ($\text{HOC}_6\text{H}_4\text{COOC}_6\text{H}_5$)

The absorption spectrum of phenyl salicylate in the vapour state has not been reported by any previous worker. In the spectrum of the vapour obtained in the present investigation the intense band at 36342 cm^{-1} has been taken as the 0,0 band and assignments have been made only of the prominent bands. On the longer wavelength side of the 0,0 band there are some weak bands represented by transitions $0-162$, $0-200$, $0-330$, $0-511\text{ cm}^{-1}$. These vibrational frequencies correspond respectively to the Raman frequencies $163, 191, 326, 504\text{ cm}^{-1}$ (Magat, 1936). The two bands on the longer wavelength side of the 0,0 band represented by transitions $0-53$, $0-86\text{ cm}^{-1}$ are due to $v \rightarrow v$ transitions. The bands have been assigned to progression of excited state vibration frequencies $216, 265, 482, 725, 783, 938, 988\text{ cm}^{-1}$ and their combinations. The liquid state yields a very broad band extending from 31245 cm^{-1} to 33092 cm^{-1} . Further, the spectrum due to the liquid shows transmission in the region between 33536 cm^{-1} and 37498 cm^{-1} and thereafter continuous absorption. If the absorption edge on the longer wavelength side at 31306 cm^{-1} is taken as the 0,0 band, the spectrum shows that the 0,0 band shifts by 5036 cm^{-1} towards longer wavelengths from its position in the vapour state. Such a large shift towards longer wavelengths shows that owing to very strong association of molecules in the state of aggregation, there is a huge change in the excited electronic energy state. When the liquid is frozen and cooled to -180°C , the broad band exhibited by the liquid state splits up into four narrower bands and the 0,0 band shifts further by 260 cm^{-1} towards longer wavelengths from its position in the liquid state. As the excited state frequency 851 cm^{-1} is observed in the spectrum of the solid in place of 938 cm^{-1} for the vapour state, the intermolecular field has greater influence on this frequency in the solid state than in the liquid state.

Thus we find that in the case of the ester containing two substituted benzene rings the influence of intermolecular field on the positions and the widths of the bands and on the excited state vibration frequency is very large.

Monomeric styrene ($\text{C}_6\text{H}_5-\text{CH}=\text{CH}_2$)

The ultraviolet absorption spectrum of monomeric styrene in the vapour state was studied by Morgan (1953). The 0,0 band was observed to be at 34761 cm^{-1} and the bands were assigned to progression of excited state vibration frequencies 148, 478, 746, 948, 959, 1024, 1209, 1300, 1486 cm^{-1} . The liquid state, in the present investigation, yields five broad bands. The 0,0 band is at 34228 cm^{-1} and the successive bands are represented by progression of excited state frequencies 996 cm^{-1} and 1247 cm^{-1} . Evidently, the two bands at 959 cm^{-1} and 1024 cm^{-1} become broad and merge into one another to form the broad band at 996 cm^{-1} in the case of the liquid. Similarly the frequency 1247 cm^{-1} may be the mean of the two frequencies 1209 cm^{-1} and 1300 cm^{-1} observed in the case of the vapour. The 0,0 band of the liquid state is at a distance of 533 cm^{-1} towards longer wavelengths from its position in the vapour state

The bands in the spectrum of the solution of the substance in cyclohexane reported by Robertson and others (1950) are at 34354 , 35387 and 36485 cm^{-1} . If the 0,0 band of the spectrum is assumed to be at 34354 cm^{-1} , it is found to be shifted towards shorter wavelengths by 126 cm^{-1} from its position in the spectrum of the pure liquid. The successive bands of the spectrum of the solution can be assigned as $\nu_0 + 1033$, $\nu_0 + 2 \times 1033$ whereas frequencies observed in the pure liquid spectrum are 996 cm^{-1} and 1247 cm^{-1} . The shift of the bands and the change in excited state frequencies mentioned above furnish strong evidence for the existence of strong influence of the solvent molecules on the energy state of the molecule.

With the solidification and lowering of temperature to -180°C the 0,0 band of the pure substance shifts from 34228 cm^{-1} to 34215 cm^{-1} and it is split up into two components of unequal intensities. The weaker component marked B_0 is on the shorter wavelength side of the principal band marked A_0 (figure 5). Assignments have been made on the assumption that electronic energy level is split up into two components. Accordingly, as mentioned above, in place of five bands given by substance in the liquid state, thirteen bands are observed in the case of the solid state at -180°C . The splitting of the 0,0 band is probably due to the formation of virtual bonds between neighbouring molecules in the solid state. The very appearance of the two components suggests that two different types of molecules produce the two components and these two types of molecules are probably produced by formation of the two types of associated groups of molecules in the crystal. It cannot be indicated clearly how such different types of associated molecules are formed unless the crystal structure is

determined accurately. The excited state frequencies observed in the solid state are 957, 1219 and 1249 cm^{-1} and correspond to the frequencies 959, 1209 and 1300 cm^{-1} respectively found in the spectrum due to the vapour state. So, these frequencies do not undergo much change with change of state in this case.

Four low frequency Raman lines were reported by Roy (1954) in the solid state of the monomer at -180°C . The appearance of these low-frequency Raman lines may be explained by assuming them to be due to vibrations in associated groups of molecules mentioned above.

ACKNOWLEDGMENT

The author is indebted to Professor S. C. Sirkar, D. Sc., F.N.I. for his kind interest and guidance throughout the progress of the work and to Government of India, Ministry of Scientific Research for the sanction of a scholarship.

REFERENCES

- Deb, A. R., 1953a, *Ind. J. Phys.*, **27**, 183.
" 1953b, *Ind. J. Phys.*, **27**, 458.
" 1951a, *Ind. J. Phys.*, **25**, 237.
" 1951b, *Ind. J. Phys.*, **25**, 433.
Imanishi, Sunao, Kanda Yoshiya, 1949, *Journal of the Scientific Research Inst. (Tokyo)*, **43**, 10.
Kato, S., Someno, Fujiko., 1938, *Sci. Papers Inst. Phys. Chem. Res. (Tokyo)*, **34**, 905.
Morgan, John V., 1953, *J. Am. Chem. Soc.*, **75**, 5055.
Magat, M., 1936, Numerical data on Raman Effect.
Nikitana, A. N., 1953, *Izvest. Akad. S.S.S.R. Ser. Fiz.*, **17**, 728.
Robertson, W. W., Music, J. F., Matsen, F. A., 1950, *J. Am. Chem. Soc.*, **72**, 5260.
Sen, S. K., 1955, *Ind. J. Phys.*, **29**, 561.
Swamy, H. N., 1953a, *Ind. J. Phys.*, **27**, 55.
" 1953b, *Ind. J. Phys.*, **27**, 119.
" 1952, *Ind. J. Phys.*, **26**, 445.

ANALYSIS OF THE ABSORPTION AND FLUORESCENCE SPECTRA OF URANYL SALTS.

(PART I.) URANYL ACETATE (ABSORPTION)

V. RAMAKRISHNA RAO AND K. V. NARASIMHAM

PHYSICS DEPARTMENT, ANDHRA UNIVERSITY, WALTAIR

(Received for publication March 19, 1956)

ABSTRACT. The absorption spectrum of uranyl acetate was analysed as consisting of two systems involving two transitions from two excited states to a common ground state. The separation between these two excited states was found to be ν 1839 cm^{-1} or 0.228 e.v. System I was explained on the basis of a (0,0) band at ν 20589 cm^{-1} and two upper state fundamentals 735 and 36 cm^{-1} and three lower state fundamentals 856, 210 and 30 cm^{-1} . System II was explained on the basis of a (0,0) band at ν 22428 cm^{-1} and the upper state fundamentals 711 and 212 cm^{-1} and the ground state fundamentals 841 and 228 cm^{-1} .

INTRODUCTION

The spectroscopic properties of uranyl salts have been investigated by a large number of workers from time to time. Significant experimental work has come from Nichols and Howes (1919) on both fluorescence and absorption spectra with some suggestions on the regularities in the spectra. Van Heel and Dieke (1925) suggested that the bands arise out of electronic-vibrational transitions in the uranyl radical. Further attempts by Van Heel (1925) for a detailed interpretation were not of much significance. The study of Raman and infrared spectra by Conn and Wu (1938) and Satyanarayana (1942) established three fundamental frequencies in the ground state 860, 930 and 210 cm^{-1} and a bent structure for the uranyl radical (C_{2v} point-group). Pant (1945), analysed the fluorescence spectra of some simple uranyl salts and arrived at the conclusion that the bands arise out of a transition from a single upper electronic state to vibrational levels in two closely lying lower states. Freymann etc. (1946) carried out analysis of uranyl acetate bands and interpreted them as involving only two states. In 1949, Dieke and Duncan have published an extensive report on the spectroscopic properties of uranium compounds in which we do not find some simple uranyl salts like acetate. In 1950, Pant published the analysis of some uranyl salts on the same lines, as in his analysis of the fluorescence bands. He disputed the analysis of Van Heel and Freymann etc. on various experimental grounds. In view of the extremely controversial nature of the analyses of the various workers mentioned above, it was felt worthwhile to investigate these spectra thoroughly and independently, using our own experimental data. Investigations were made on the absorption spectra of uranyl acetate and uranyl nitrate and the data were compared with those of Nichols and Howes, those of Freymann and also those due to Dieke and Duncan (nitrate). We find that our data, in general, are in good agree-

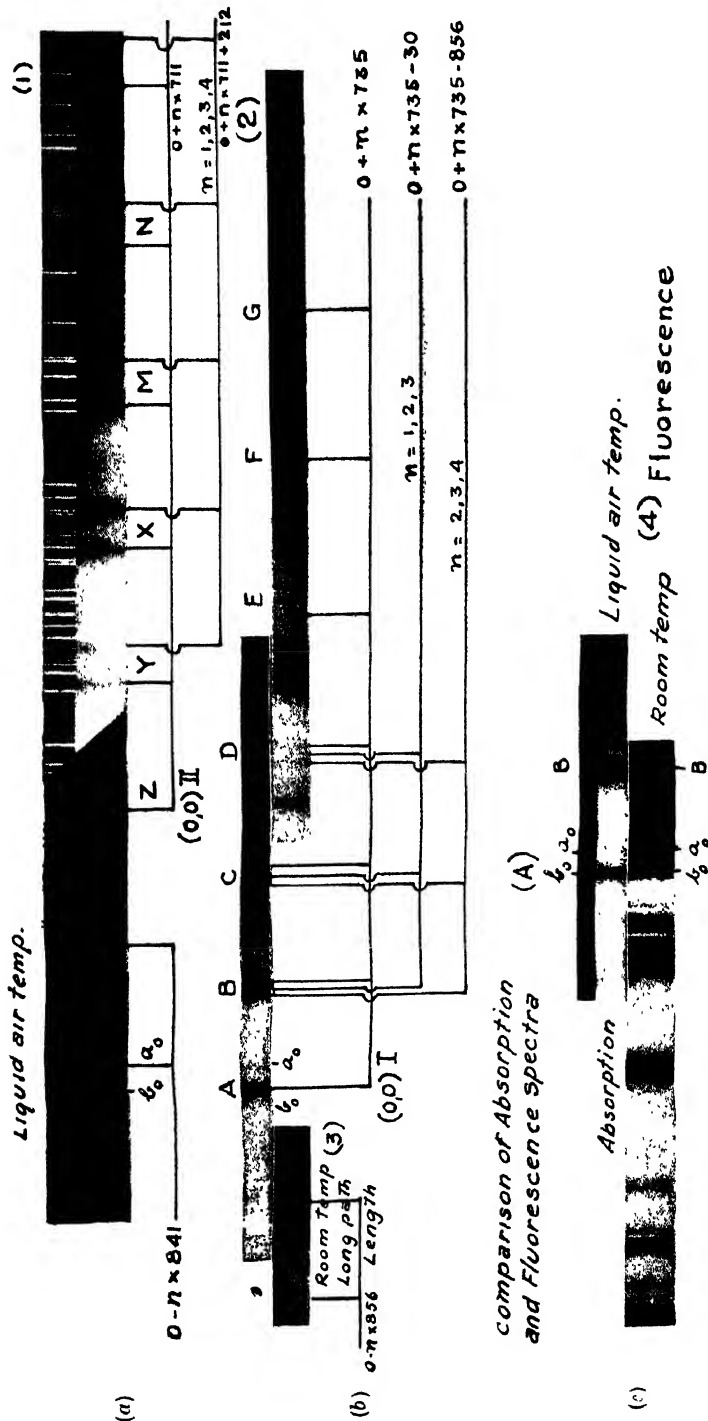


Fig. 1. Absorption spectrum of uranyl acetate.

ment with those of Nichols and Howes and of Dieke and Duncan. The values of Freymann and others are generally found to be slightly higher than ours.

The analysis of these bands has been attempted mainly depending on the features like grouping, intensities, and sharpness of the bands. It is well known in the near ultraviolet absorption spectra of the aromatic molecules, the pattern of the bands plays an important role in the analysis. As a result of this effort on our part, we analysed these bands into two systems, the one with a (0,0) at ν 20589 cm^{-1} and the other (0,0) at ν 22428 cm^{-1} with the possibility of a common ground state. The analysis and its justification and the reasons for our preference of our analysis over others are presented below.

EXPERIMENTAL

Absorption spectra are taken at the liquid air and room temperatures with a variety of path-lengths.

The experimental set-up consists of a brass rod with a rectangular slot in the middle, in which a small glass cell containing the salt is placed tightly. The cell is made of two small rectangular glass plates cut to the size of the slot. Two small holes are bored in the rod at the middle of the slot, one to allow the incident light and the other the transmitted light. The source of continuum is 1000 watt tungsten lamp. The brass rod is suspended by means of a wire into liquid air contained in a transparent Dewar flask. The spectrum is photographed with the help of a Fuess spectrograph (24 A.U. per m.m. at λ 4500) using Ilford Selochrome and Panchromatic plates.

The fluorescence spectra, for the present, are taken only at the room temperatures. Mercury arc was used for the excitation.

Description of the bands (figure 1)

It is well known that the bands of the uranyl salts appear sharp and distinct only at low temperatures. In figure 1 (a), the bands obtained at the liquid air temperature with one path length, are shown. To facilitate description, arbitrary markings like A, B, C, D... and Z, Y, X, M... are adopted. Band A can be seen from figure 1(b) to be a sharp intense band, followed by equally intense bands at B, C, D (see also microphotometer curve in figure 2). These bands B, C, D, on their long wavelength side, are accompanied by two satellite bands which are of much less in intensity. This triplet pattern repeats itself upto D conspicuously. It is not easy to follow this pattern beyond D but at F, on very close examination and at E and G also, on still closer examination, the pattern could be found. What is more conspicuously important in this region is the doublet structure of two broad and diffuse bands marked Y, X, M and N. Their appearance is distinctly different from that of the bands in A, B, C, D. They also definitely resemble the single band at Z which, abruptly presents itself as we study from A, B, C etc. These points are considered to be of much significance

for the analysis. On the longwave length side of A in figure 1(a) there is a definite indication of an abrupt discontinuity in intensity which may be suspected as due to faint absorption. This was established by studying the development of this band at higher temperatures and longer path lengths. Figure 1(b), obtained under

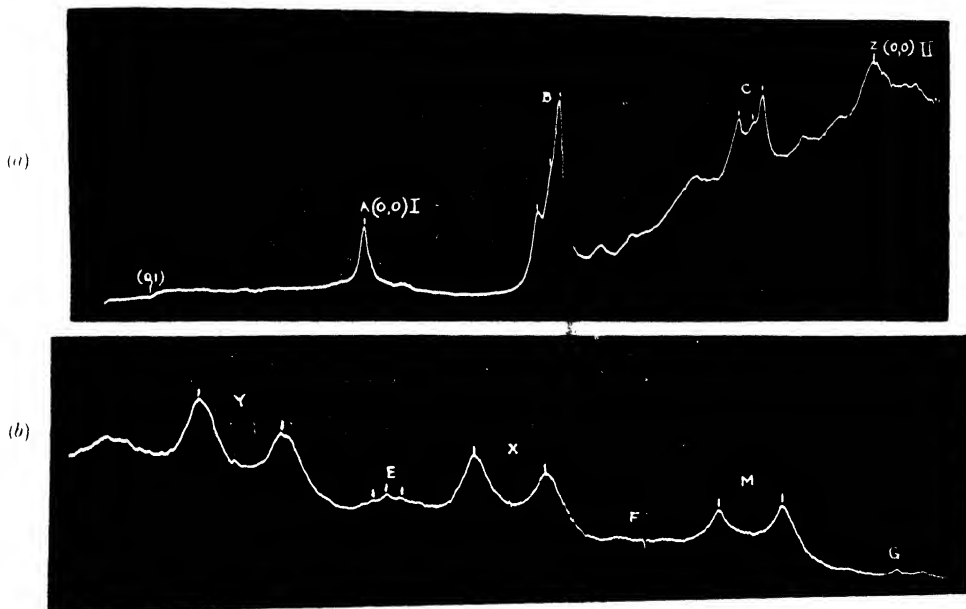


Fig. 2. Microphotometric records of the absorption spectrum of uranyl acetate.

such conditions, definitely establishes this band. A trace of still another band on the long wavelength side of this band is marked in figure 1(b) and it is also found on the negatives corresponding to figure 1(a). The presence of these two bands is of very great importance in the analysis of the spectrum.

In figure 1(a) two bands are marked b_0 and a_0 adopting the nomenclature of Pant. Pant's b_0 is our band A. Between A and B, B and C, and C and D, there are a few weak and diffuse bands which do not form any conspicuous pattern. However, the band a_0 (Pant's terminology) is of crucial importance in our discussion.

In figure 1(c), we have given the fluorescence and absorption spectra side by side taken on the same instrument and to the same scale of enlargement. Earlier authors have reported only four groups of bands in fluorescence starting from ν 20728 cm^{-1} and extending to the long wavelength side. The common region between fluorescence and absorption was only three bands according to earlier workers. They are ν 20746 cm^{-1} , 20625 cm^{-1} and 20587 cm^{-1} in absorption and ν 20732 cm^{-1} , 20627 cm^{-1} and 20588 cm^{-1} in fluorescence. Our picture shows clearly one more group to the short wavelength side obtained on a heavily

exposed plate (exposure 7 hrs.) and this falls in the region of our earlier mentioned B bands. This additional experimental information, we consider, is of great significance in the analysis of the spectra. Detailed work on the fluorescence spectra at various temperatures, is still in progress.

Considerations for the analysis.

It is necessary to examine the reasoning behind the analyses of the earlier workers. Freymann started with the band marked a_0 as the (0,0) and the one marked b_0 (our A) as the (1, 1) transition. He identified a fundamental 720 in the upper state with a similar weak band coming after B and similar bands as the overtones. The strong band b_0 taken as the (1,1) of this frequency and its counterpart in the ground state led to the assignment of similar strong bands as such combination bands. This ultimately led him to the assignment of all strong bands as multiple combinations of various fundamentals in the upper and lower states, the weak bands forming the progression of fundamental 720 (see column 6 of Table I). This is really peculiar and unusual. Besides, his data do not show the bands on the long wavelength side of A while A itself was taken by him as the (1,1) band. This came in for criticism, by Pant on the ground that while the fundamental was itself not found, the difference frequency was found with a very high intensity. In essence, Freymann etc. analysed all the bands as due to one system. Freymann's analysis is conspicuous by the absence of an assignment for the band Z. He gives a wave number of $\nu 22444 \text{ cm}^{-1}$ for this band. Our measurements give an average value of $\nu 22428 \text{ cm}^{-1}$ which agree closely with the value $\nu 22425 \text{ cm}^{-1}$ given by Nichols and Howes. It has already been pointed out that Freymann's data are in general higher than ours and also of Nichols and Howes. So, in the absence of any other band in the neighbourhood of these values, there is no doubt that these two measurements represent the same band which is a very important band. The fact that it does not find an interpretation in Freymann's analysis deserves serious consideration. Besides the above points, we also observe that about five bands in the violet have not been interpreted by them (see Table I, column 6) and the deviations between their observed and calculated values are considerable.

In the analysis of the fluorescence bands, Freymann started with the band a_0 (of Pant) as the (0,0) consistent with his absorption analysis. It is seen that this band is weak in fluorescence as well [figure 1(c)]. Further if we take this band as the (0,0), the new band at B obtained in fluorescence by us and shifted by about 557 cm^{-1} cannot be interpreted in any reasonable manner. This band actually falls in the region of B in absorption, so that, the interpretation of B and this must be identical. We are inclined to consider this as a conclusive evidence against Freymann's analysis.

Pant's analysis was based upon what he considers as experimental facts. The fact that the fluorescence bands are independent of the exciting radiation

TABLE I
Analysis

Wavenum- ber of the band cm^{-1}	System I	System II	Deviation from the observed values cm^{-1}	Freymann etc.	Deviation from their observed values cm^{-1}	D. D. Pant values	Deviation from their observed values cm^{-1}
18855	1	$0-2 \times 856 = 18877$	22				
19733	2	$0-856 = 19733$	0				
20589	8	(0,0)I	0	$0-860+720=20616$	23	$b_0(0,0) \text{ I} = 20593$	0
20625	1	$0+36=20625$	0				
20750	2		4	(0,0) = 20756	0	$a_0(0,0) \text{ II} = 20756$	0
20823	1	$0+36+212 = 20837$	14	$0+2 \times 720-930-2 \times 210=20846$	22	$b_0+220=20813$	11
20891	1	$0+735-2 \times 210=20904$	13	$0+2 \times 720-2 \times 210-860=20916$	13	$a_0+220=20976$	73
21242	6	$0+2 \times 735-856=21203$	39	$0+2 \times 720-930=21266$	16	$a_0+725-235=21246$	4
21293	4	$0+735-30=21294$	1				
21324	10	$0+735=21324$	0	$0+2 \times 720-860=21336$	11	$b_0+725=21318$	3
21477	2		20	$0+720=21476$	17	$a_0+725=21481$	12
21587	2		0	$0-3 \times 720-930-2 \times 210=21566$	18	$b_0+725+220=21538$	46
21641	1	$0+2 \times 735-2 \times 210=21639$	2	$0-3 \times 720-2 \times 210-860=21636$	21	$a_0+725+220=21701$	44
21822	2	$0+2 \times 735-210=21840$	27	$0-3 \times 720-210-860=21846$	20		
21903	6	$0+3 \times 735-856=21938$	25	$0-3 \times 720-930=21986$	42	$a_0+2 \times 725-235=21971$	4
22022	3	$0+2 \times 735-30=22029$	7	$0-3 \times 720-860=22056$	13	$b_0+2 \times 725=22043$	0
22053	8	$0+2 \times 735=22059$	6				
22200	2		0	$0+2 \times 720=22196$	11	$a_0+2 \times 725=22206$	1
22307	2		9	$0+4 \times 720-930-2 \times 210=22286$	18	$b_0+2 \times 725+220=22263$	41
22428	8	(0,0) II	0			$a_0+2 \times 725+220=22426$	18

TABLE I (contd.)

Wavenumber of the band cm^{-1}	Intensity	System I	System II	Deviation from the observed values cm^{-1}	Freymann etc.	Deviation from the observed values cm^{-1}	Pant	Deviation from the observed values cm^{-1}
22578	2	$0 + 3 \times 735 - 210 = 22584$		6	$0 + 4 \times 720 - 860 - 210 = 22566$	21		
22682	4	$0 - 4 \times 735 - 856 = 22673$		9	$0 + 4 \times 720 - 930 = 22706$	22	$a_0 + 2 \times 725 + 2 \times 220 = 22646$	20
22748	2	$0 + 3 \times 735 - 30 = 22764$		16				
22774	5	$0 + 3 \times 735 = 22794$		20	$0 + 4 \times 720 - 860 = 22776$	2	$b_0 + 3 \times 725 = 22768$	6
22928	2		$0 + 711 - 228 = 22911$	17	$0 - 3 \times 720 = 22916$			
23139	10		$0 + 711 = 23139$	0	$0 + 6 \times 720 - 2 \times 860 - 210 = 23146$	28	$a_0 + 3 \times 725 = 22931$	11
23352	6		$0 + 711 + 212 = 23351$	1	$0 + 6 \times 720 - 2 \times 860 = 23356$	4	$a_0 + 3 \times 725 + 220 = 23151$	1
23505	2	$0 + 4 \times 735 = 23529$		24	$0 + 5 \times 720 - 860 = 23496$	6	$a_0 + 3 \times 725 + 2 \times 220 = 23371$	9
23589	2		$0 + 2 \times 711 - 228 = 23622$	1	$0 + 7 \times 720 - 860 - 930 - 2 \times 210 = 23586$	25	$b_0 + 4 \times 725 = 23493$	28
23653	2				$0 - 4 \times 720 = 23636$	13	$a_0 + 4 \times 725 = 23656$	7
23847	8		$0 + 2 \times 711 = 23850$	3	$0 + 7 \times 720 - 2 \times 860 - 210 = 23866$	6	$a_0 + 4 \times 725 + 220 = 23876$	4
24072	6		$0 + 2 \times 711 + 212 = 24062$	10	$0 - 7 \times 720 - 2 \times 860 = 24076$	15	$a_0 + 4 \times 725 + 2 \times 220 = 24096$	5
24277	2	$0 + 5 \times 735 = 24264$		13				
24573	5		$0 + 3 \times 711 = 24561$	12	$0 + 8 \times 720 - 2 \times 860 - 210 = 24586$	2	$a_0 + 5 \times 725 + 220 = 24601$	13
24775	4		$0 + 3 \times 711 + 212 = 24773$	2	$0 + 8 \times 720 - 2 \times 860 = 24796$	1	$a_0 + 5 \times 725 + 2 \times 220 = 24821$	26
25011	2	$0 + 6 \times 735 = 24999$		12				
25283	3		$0 + 4 \times 711 = 25272$	11				
25494	2		$0 + 4 \times 711 + 212 = 25484$	10				
25988	1		$0 + 5 \times 711 = 25983$	5				
26169	1		$0 + 5 \times 711 + 212 = 26195$	4				

was taken by him as indicative of one upper state only. In the overlapping region of fluorescence and absorption, two close lying common bands, named a_0 and b_0 are *sometimes* observed which, at low temperatures, show according to him an interesting relationship. He says that, "in fluorescence, the lower frequency band b_0 is always more intense than the a_0 band while in absorption the reverse is usually the case". These two bands in the case of acetate, are marked in the figure 1, according to his terminology. According to what he says, the band a_0 must be more intense in absorption than b_0 . An examination of the spectrum clearly shows that such is not the case, either in absorption or in fluorescence. As a matter of fact b_0 is by far more intense and sharper in absorption than a_0 in acetate. We examined whether his statement is correct with reference to other simple uranium salts. We tabulate below the results.

TABLE II

Substance	Fluorescence	Absorption
Uranyl acetate	a_0 20728 cm ⁻¹	a_0 20756 cm ⁻¹
	b_0 20583 "	b_0 20593 "
Uranyl chloride	a_0	a_0
	b_0 20535 "	b_0 20534 "
Uranyl fluoride II	a_0 20234 "	a_0 20234 "
	b_0 20082 "	b_0 20082 "
Autunite	a_0	a_0
	b_0 19848 "	b_0 19848 "
Uranyl nitrate	a_0	a_0
	b_0 20584 "	b_0 20591 "

In nitrate, on which we have our own data besides those of Dieke and Duncan, a band corresponding to a_0 is not observed at all, while b_0 is very strong, in absorption. Besides, it is again the starting point for the fluorescence and is strong. In the case of uranyl chloride there is no a_0 band either in fluorescence or in absorption according to his own data. From Van Heel's data, used by Pant, the a_0 band is absent in the case of autunite. It is only in uranyl fluoride II where Pant published a spectrum of both fluorescence and absorption, we find evidence of the presence of these two bands in both and a suggestion of such an exchange of intensities. So we are inclined to consider this two-band-intensity theory, an exception rather than the rule in the case of uranyl salts. In the

fluorescence spectrum as well, the band b_0 is definitely more intense than a_0 (see figure 1(c)). In acetate, both Freymann and Pant considered that they have obtained bands corresponding to a_0 and b_0 . As a matter of fact, Pant assumed the data of Freymann. We made a close examination of this point, by comparing the data of our bands with various workers. The band b_0 (our A) was found by us to be $\nu 20589\text{ cm}^{-1}$, 20587 cm^{-1} by Nichols and Howes and 20593 cm^{-1} by Freymann. A very good agreement can be easily observed. The average value of the absorption band b_0 is $\nu 20590\text{ cm}^{-1}$. In fluorescence, the average value appears to be $\nu 20588\text{ cm}^{-1}$ which is in very good agreement with the absorption value. A similar band was found at $\nu 20725\text{ cm}^{-1}$ by various workers both in fluorescence and absorption. If we compare the average measurements in fluorescence and absorption for this band, we get $\nu 20732\text{ cm}^{-1}$ and 20750 cm^{-1} respectively, with a deviation of at least 18 cm^{-1} between the two measurements. One is inclined to doubt whether really both bands are the same. If they are not, then the views about the intensities require reconsideration. Pant's hypothesis of two lower states, was mainly based on his idea of the a_0 and b_0 bands and their intensity variation. Our experimental evidence definitely shows that there is no such peculiarity in intensity behaviour of these bands and the strong band in absorption is also the strong band in fluorescence. Thus, apart from the additional difficulties of interpreting the origin of two low lying electronic states, the experimental facts do not appear to warrant such a hypothesis.

Figure 1(a) was reproduced from a plate on which we could record the (0,1) band with respect to $\nu 20589\text{ cm}^{-1}$ as (0,0) definitely and possibly (0,2) also with the same path length and temperature as we used for the strong violet bands. This fact was, however, not mentioned by Freymann in his analysis. These two bands gained in intensity with higher temperatures and longer path lengths. This is a clear indication of these bands being associated with vibrational levels, of the ground state. (The usual technique for obtaining the ground state vibrations in the study of the absorption spectra of organic molecules is to obtain the spectra at higher vapour pressures and longer path lengths.)

If we adopt Freymann's (0,0) band, we do not find any interpretation for these two bands except in terms of possibly combinations without fundamentals.

For these various reasons, a detailed and fresh attempt at analysis was found to be desirable. In the actual analysis, steps were taken, on an analogy with the usual requirements in the spectra of organic molecules like substituted benzenes etc.

Our analysis.

It was found in the spectra of the substituted benzenes etc. that the (0,0) band generally corresponds to the strongest band on the long wavelength side of the spectrum for well known reasons. On this analogy, we have chosen the strong

band (A) at $\nu 20589 \text{ cm}^{-1}$ as the (0,0) band and found the shift of other bands from this. On the long wave length side of band A, we found a weak band shifted by 856 cm^{-1} which corresponds to one of the Raman frequencies (860 cm^{-1}) ascribed to the uranyl radical. A still weaker band at $\nu 18855 \text{ cm}^{-1}$ developed in longer path lengths could be interpreted as an overtone of this fundamental. These two long wavelength side bands, demonstrated in our pictures, do not find a place in earlier work. They cannot also be interpreted any other way except by the choice of A, as the (0,0) band. In fact, we are inclined to take these bands as a justification for the choice of our (0,0) band in preference to any other band (c.f. as Freymann's choice). Further, if we take this as the (0,0) band, the weak band B, obtained in fluorescence and shifted by 701 cm^{-1} from our (0,0) band, readily finds an explanation as $0+701$ corresponding to $0+735$ band in absorption (B). The difference of 30 cm^{-1} may be attributed to the weakness of the fluorescence band and a consequent uncertainty in our measurements besides any natural deviation to be expected from fluorescence to absorption data. We consider the observation of this band in fluorescence as a final justification for the choice of our (0,0).

In each of the groups B, C, D etc. the third band (shortest wave length) was found to be the most intense and successive separations of these bands from A i.e. A to B, B to C, C to D etc. are found to be of the order of 735 cm^{-1} . This obviously corresponds to a fundamental in the upper state and taking the A to B value as 735 cm^{-1} , the other bands are explained as the overtones of this fundamental. Upto D i.e. $3 \times 735 \text{ cm}^{-1}$, it is easy to follow this pattern and beyond this point, we are guided by the numerical coincidences up to $6 \times 735 \text{ cm}^{-1}$. A close examination at the point F, in particular, reveals a structure of bands quite similar to the structure of B, C, D and justifies the assignment. The agreement between the calculated and the observed values may be seen from the Table I to be quite satisfactory. Then we attempted an interpretation of the setellite bands of B, C, D etc. The middle band was found to be at -30 cm^{-1} to the 735 band in each case and so, this was interpreted as a difference frequency between the upper state frequency 735 cm^{-1} and a ground state frequency 30 cm^{-1} . This low frequency has already been suggested as a lattice vibration by Freymann (1948). It was found quite useful to adopt this view. Similar bands in C, D, and F are given similar interpretations. The longest wave length bands in the triplets of B, C, D etc. could be interpreted as a difference frequency like $0+n \times 735 - 856 \text{ cm}^{-1}$. This interpretation finds justification from the fact that, we are definitely able to obtain the band $0-856 \text{ cm}^{-1}$.

After the above part of the analysis, we could not make much progress with the other bands notably those at Z, Y, X, M, N, etc. We again had to obtain a clue from the structure of the band pattern. The doublet set Y, X, M, N, etc. were found to have a mean separation of 212 cm^{-1} , which is very suggestive.

It was also found that the separation of the long wavelength band of the doublet from Z was about 711 cm^{-1} . Corresponding bands at Y, X, M, N etc. were found to have a mean separation of 711 cm^{-1} . The appearance of these bands is quite different from those at A, B, C, D. The bands are more diffuse and broader and are obtained distinctly only with extremely thin path-lengths. Band Z, which is extremely intense, does not find an interpretation in the analysis of Freymann, while Pant interpreted as some combination band. We felt that, if we take the band Z as starting another system, we will be able to account for its intensity and also interpret Y, X, M, N as $0+n\times 711$ and $0+n\times 711+212$. Obviously, the 711 is an upper state frequency and 212 cm^{-1} also is to be treated as such. There is another way of interpreting these doublet at Y, X etc. with Z as (0,0) as $0+n\times 930$ and $0+n\times 930-212$. In this kind of interpretation, 930 cm^{-1} corresponds to an upper state frequency, while 212 cm^{-1} corresponds to a lower state frequency. However, we are inclined to reject this possibility for the following reasons. The lower state frequency corresponding to 923 cm^{-1} is the Raman frequency 930 cm^{-1} which is definitely established to represent a non-totally symmetrical vibration. It is not reasonable to obtain a fundamental of a non-totally symmetrical vibration along with its overtones, in what appears to be an allowed kind of transition from intensity considerations. Thus, we are inclined to consider our earlier interpretation on the basis of 711 and 212 cm^{-1} as being more reasonable. 711 cm^{-1} can be taken as corresponding to 735 cm^{-1} in System I. The difference in these two upper state frequencies can be easily understood, if we associate them with two different electronic levels. There is, however, the other frequency 212 cm^{-1} which had to be assumed. The corresponding Raman frequency is 210 cm^{-1} . This means that there is practically no change in the frequency value for both upper and lower states. While normally, we expect a fall in the upper state vibrational frequency compared with the ground state frequency, it is not unusual that, there is no such change particularly with reference to the bending modes of vibration to which actually this value is attributed. It was found in the analyses of a series of substituted anisoles and toluenes from our laboratory that the CH_3 bending frequency which has about 1280 cm^{-1} occurs with practically unchanged values in both the states (Ramakrishna Rao and Suryanarayana 1955).

The choice of the Z band as the (0,0) of the second system, was further justified by the fact that we were able to identify two bands on the long wavelength side shifted by 841 cm^{-1} and $2\times 841\text{ cm}^{-1}$. This value 841 cm^{-1} may be considered as being identical with 856 cm^{-1} , the ground state frequency in System I. The band $0-2\times 841$ (System II) is actually the a_0 band of Pant [figure 1(b)]. This explanation of the a_0 band is preferred by us, instead of its association with the bands of System I. The appearance of this band is more like those of the groups Z, Y, X etc. than those of the groups A, B, C, D. One possible objection

to this interpretation can be the medium intensity with which this band occurs at the liquid air temperatures. It is generally assumed that these high frequency levels are less populated at low temperatures (exponential relationship) and so the bands are expected to be absent. However, we have to remember that this discrete absorption in the uranyl salts makes its presence felt only at such low temperatures. At high temperatures, what we get is some sort of continuous patchy absorption. It is obvious for this reason that we should not attach too much of importance to the population-frequency temperature relationship in this particular case. Further, in System I, we definitely were able to show the bands corresponding to the ground state frequencies. So, there is definitely a certain amount of population of molecules in the 856 and 2×856 vibrational levels. Only the corresponding bands are more intense in the second system than the first. This is possible because the second transition may, as a whole, have a greater intensity than the first transition.

By treating the α_0 band of Pant in this manner as the $0-2 \times 841$ of the second system, we can also understand why it does not occur in certain other uranyl salts, like nitrate, chloride etc. as being only due to the absence of an overtone in some cases. We also hold that this band, at $\nu 20750 \text{ cm}^{-1}$ is not necessarily the same as $\nu 20728 \text{ cm}^{-1}$ obtained in fluorescence.

A band at $\nu 20625 \text{ cm}^{-1}$ (Nichols) was not obtained by us but was found by earlier workers. It is shifted by 36 cm^{-1} to the violet of the (0,0) band of System I. If we can adopt this as the upper state frequency of the crystal lattice vibration, this, like the bending vibration, remains practically unchanged from state to state. This explains the $\nu 20823 \text{ cm}^{-1}$ band also as $0+36+212 \text{ cm}^{-1}$, the value 212 cm^{-1} being borrowed from the second system. This band was not otherwise to be explained. However, our assignment of these two bands is not definite.

For purposes of comparison, we have given in Table I, the observed and calculated values and also the deviation. The last four columns contain similar data for Freymann's and Pant's analyses. The deviations, given, were between these calculated values and their observed values. It can be seen that our analysis shows less deviation from the observed values, apart from the fact, that we are able to interpret all bands.

TABLE III

Upper state		Lower state		Raman and infra- red	Assignment
System I	System II	System I	System II		
—	—	—	—	930	U-O antisymmetrical
735	711	856	841	860	U-O symmetric stretching
—	212	210	228	220	O-U-O symmetric bending
36	—	30	—	—	Crystal lattice vibrational frequency

In the above Table III the probable values of the vibrational frequencies in the three electronic states are given. The non-totally symmetric frequency 930 cm^{-1} does not find a place in our analysis in any of the states, the other frequencies are observed at one stage or another with some modification of values. The totally symmetric (U-0) stretching frequency undergoes a reduction by about 12 percent from the ground state to the upper state values. The other two frequencies (0-U-0 bending and crystal lattice) practically remain unchanged in the various states.

Two systems like this can be further justified on comparison with some spectra of organic molecules. In β - and α -fluoro naphthalenes (Rao and Rao, 1955; Ramamurty and Rao, 1956) for instance, two such systems were definitely found. The system on the long wave length side, consists of sharper bands while the one on the shorter wave length side consists of diffuse bands. The two systems were distinct and separate in the substituted naphthalenes. In the present case also, the difference in the appearance of the bands of the two systems is quite clear. Only, there is an overlap of these two systems. In fact, Dieke 1949, suggested the possibility of more than one transition constituting the absorption of the uranyl salts.

We might finally suggest a tentative energy level diagram for these bands in the following figure 3. Level α represents the common ground state to which transitions take place from the two upper levels β and γ . The shift between the β and γ is 1839 cm^{-1} which corresponds to about 0.228 e.v.

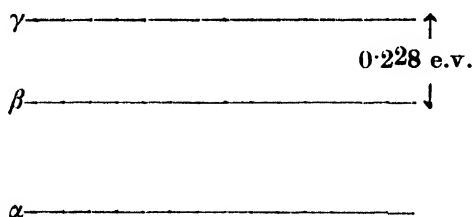


Fig. 3.

At the present stage, we do not consider it useful to discuss the exact nature of the electronic states or the exact types of transition, whether forbidden or allowed. It is our plan to carry out a systematic investigation of the absorption and fluorescence spectra of various uranyl salts, both single and double and arrive at a self consistent schemes of analyses. We may add, however, that we succeeded already, in interpreting the spectrum of uranyl nitrate on similar lines. The results will be published shortly after some confirmatory type of experimental work.

ACKNOWLEDGMENT

Our thanks are due to Prof. K. R. Rao for his kind interest in the work.

Since the publication of this paper, the Department of Atomic Energy, Government of India, has sponsored a Research Project "Spectrographic Investigations of Uranyl Salts" under the direction of the senior author (V. R. Rao). Further work in the series will be conducted under the above scheme.

REFERENCES

- Conn G. K. T. and Wu C. K., 1938, *Trans. Farad. Soc.*, **34**, 1483.
Dieke G. K. and Van Heel, A. C. S., 1925, *Leiden Communications*.. Suppl. No. 55A.
Dieke G. H. and Duncan A. B. F. 1949, *Spectroscopic Properties of Uranium Compounds* (Mcgraw-Hill Publication)
Frey mann M., Guilmart T. and Freymann, R. 1946, *Compt. Rend*, **223**, 573.
Frey mann M., 1948, *Compt. Rend.*, **226**, 332.
Nichols E. L., Howes H. L. and Wick F. G., 1919, *Phys. Rev.*, **14**, 201-221.
Pant D. D., 1945, *Proc. Indian Acad. Sci.*, **A22**, 95.
" 1945, *Ibid* **A22**, 110
" 1950, *Ibid* **31A**, 35.
Rao. V. and Suryanarayana V. R. 1955, *Jour. Sci. Indust. Res.*, **14B**, 479.
Rao, V. R. and Rao, M. J. 1955, *Jour. Sci. Ind. Res.* **14B**, 547.
Rao V. R. and Rao M. 1956, Communicated to *Ind. Jour. Phys.*
Ramamurty S. and Rao. V. R., 1956, Communicated to *Jour. Sci. Indus. Res.*
Satyanarayana, B. S., 1942, *Proc. Ind. Acad. Sci.*, **15A**, 414.
Van Heel A. C. S. 1925, *Leiden Communications*, Suppl. No. 55B.

MEASUREMENT OF SURFACE TENSION BY UNSTABLE PENDANT DROPS

N. R. TAWDE

DEPARTMENT OF PHYSICS, KARNATAK UNIVERSITY, DHARWAR,

AND

K. G. PARVATIKAR

DEPARTMENT OF PHYSICS, RAJARAM COLLEGE, KOLHAPUR

(Received for publication May 17, 1955)

ABSTRACT. A workable experimental technique has been evolved to subject the unstable pendant drops to surface tension measurements, utilising the expression derived earlier. The values calculated from the expression by the use of the observed data on three liquids compare favourably with the known constants on surface tension.

INTRODUCTION

Although the pendant drop method was studied long ago by Worthington (1881) and Fergusson (1912), it remained in disrepute for a considerable time. It is comparatively recently that it has been made useful for precision work as a result of critical study of it by Andreas, Hauser and Tucker (1938). The method has been laid on better foundations by Fordham (1948) by supplying a tabular set of values for the calculation of surface tension from measurements on pendant drops. Brown and McCormick (1948), while working out a new drop-weight method have shown by dimensional analysis that the shapes of all drops forming on a conical tip are similar at the stage of instability.

On this basis one of the present authors (Parvatikar, 1949) derived the following equation giving surface tension ratio γ_1/γ_2 of two liquids in terms of the parameters of the unstable pendant drops:

$$\frac{\gamma_1}{\gamma_2} = \frac{\sigma_1}{\sigma_2} \frac{de_1^2}{de_2^2} \quad \dots (1)$$

where, σ and de are respectively the effective density and equatorial diameter of a drop of the liquids 1 and 2. Thus by measuring the equatorial diameters de_1 and de_2 of the drops of two liquids at the stage of instability, and taking the surface tension of one of the liquids as known, the surface tension of the other can be calculated.

While doing some fundamental work on pendant drops, it was felt worthwhile to test the above equation experimentally, since such a study does not appear to be on record within the knowledge of the present authors. The experimental problem in work of this type, was of measuring the equatorial diameters of drops at the critical stage of instability, when the drops attain similar shapes and it was thought it could be solved by employing a conical tip as in the experiments of Brown and McCormick (1948). According to them a drop detaching from a conical tip is free to adjust its shape and size and consequently at the unstable state, all such drops are similar in shape. The point, however, for correct experimental adjustment is to fix the stage of instability of the drop and to measure its dimension at that state. If sufficient time is allowed for proper development of drops formed at a conical tip, one could follow the changing size of the drop until it just collapses from it. The experimental set-up devised for this purpose and operations involved in measurements are described below.

EXPERIMENTAL AND RESULTS

Drops were formed in air saturated with its own vapour in a thermostat at the tip of a cone. For the formation of drops, the liquid was sucked into a brass tube of external diameter 7 mm. and internal diameter of about 5 mm. One end of the tube was tightly screwed by the conical tip, similar to that of Brown and McCormick (1948), having three holes drilled on it symmetrically, the other end being connected to a glass syringe through a rubber tubing. The set-up is shown in figure 1. The solid cone (figure 2) forming the tip had an angle of 60° . The side of the cone was about 1.2 cms. The three narrow holes having equal bores of about 0.5 m.m. were symmetrically disposed with respect to the tip and had their out-lets almost equally spaced in the middle of the horizontal plane of the inverted cone. The similarity in shapes of the drops at the unstable state is realised in such a conical tip.

The general procedure is to first form a small nucleus of a drop at the conical tip by releasing the liquid to flow through the holes and then allow the drop to grow under gravity. In order to align the drop in the field of view, which was once for all set, the brass tube was inserted rigidly and fixed into a metal tube with its boss-head fitted well into the ceiling of the thermostat case. The conical tip was then screwed tightly at the lower end of the brass tube. By sliding this tube into the metal boss-head, it was possible to move it up and down, as well as slightly sideways, to bring the conical tip into optical alignment. The thermostat has two glass windows into its opposite walls, one for admitting light to illuminate the drop, and the other to observe it for measurements. The thermostat was heated electrically to any desired temperature by electronic temperature control, maintaining the temperature faithfully to within $\pm 0.1^\circ\text{C}$.

The liquid to be investigated is sucked by way of the holes in the conical tip into the brass tube by manipulating the syringe. The rubber tubing connect-

ing the syringe with the metal tube is then squeezed by the screw of the pinch-cock, and then completely detached from the latter. The pinch-cock screw is then gradually loosened to allow air to get in. Through this procedure, a fairly long time of 6 to 7 minutes elapses before the drop develops fully to the point

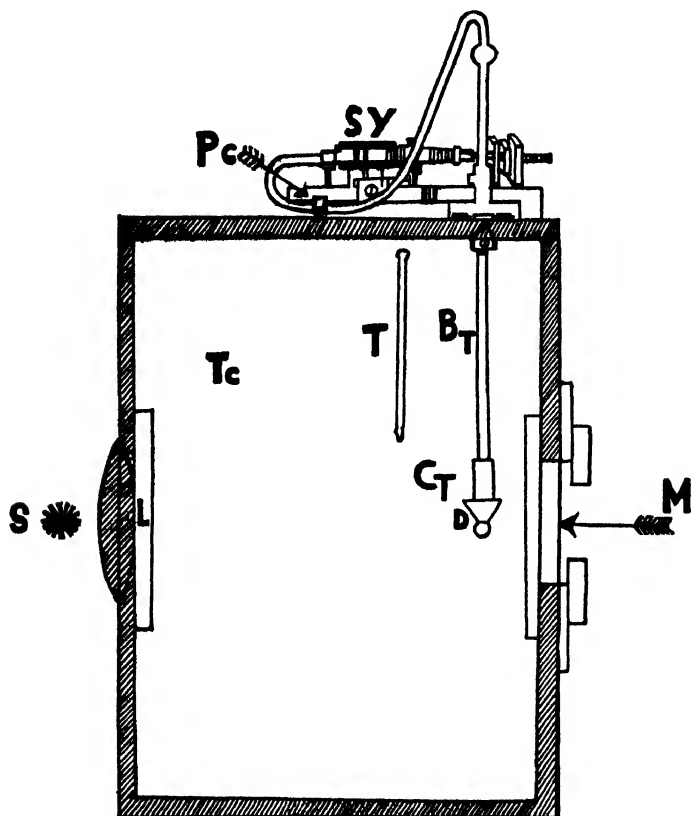


Fig. 1. The experimental assembly.

S - Source	C _T - Conical tip
L - Collimating lens	D - Drop
T _C - Thermostat chamber	M - Microscope
T - Thermometer	SY - Syringe
B _T - Brass tube	P _C - Pinch-cock

of detachment. The drop was observed against diffuse light through a microscope which was provided with a scale having hundred equally spaced divisions (equivalent to approximately 4 m.m.) in its eye-piece. Either the maximum equatorial diameter D , or the maximum equatorial radius R , of the drop, whichever could be accommodated and observed within the extent of the microscope scale, was measured for a number of drops, and the mean of the same was determined. Table I below is a sample set of such observations on water at 30°C.

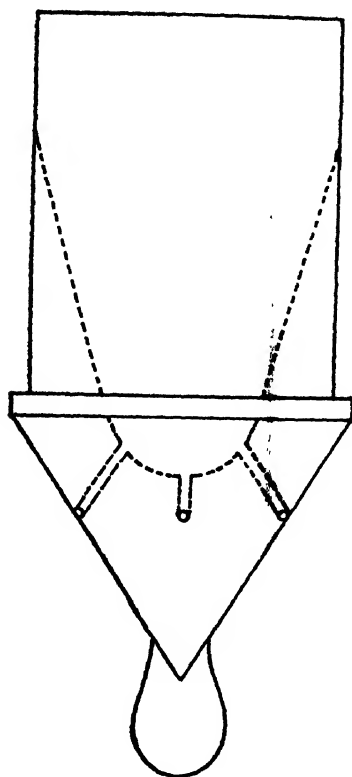


Fig. 2. The conical tip.

TABLE I

Growth of a drop of water at 30°C

Time of formation of the drop			Max. Eq. radius R_e in scale div.
Mins.	Secs.		
0	—	0	—
1	—	0	—
2	—	0	—
3	—	0	—
4	—	0	—
4	—	30	62.0
4	—	50	61.3
5	—	10	60.6
5	—	30	59.8
5	—	50	59.0
6	—	10	58.1
6	—	20	57.2
6	—	30	56.3
6	—	40	55.4
6	—	55	55.2
6	—	56 (detached)	55.0

Without disturbing the microscope set-up, the metal tube with its conical tip was taken out and was thoroughly washed and dried. It was fixed in its original position for taking observations on drops of a liquid of known surface tension. Water was chosen in the present case. The liquids chosen for surface tension measurements were toluene, *m*-xylene, and benzene. Observations were also made on water at high temperatures to explore the capacity of the method to take account of the changes in dimensions of the drops with change in temperature. Assuming the surface tension of water at 30°C to be known, the values of surface tension of the above liquids were calculated from eq. (i). As the primary aim of the investigation was to explore the workability of the method, no attempt was made to obtain the estimate of accuracy of results. However, the observations on the sizes of the drops in Table II are the mean of at least ten independent observations, which did not vary appreciably from each other.

TABLE II

Liquid	Temp. °C	Effective density in gm/c.c.	Measured dimensions		Surface tension in dynes/cm.	
			R_c	D_c	Present work	I.C.T.
Water	30	0.9946	55.0	—	—	(71.18 ± 0.05)
Toulone	30	0.8525	—	73.7	27.3	27.3 ± 0.1
<i>m</i> -xylene	30	0.8530	—	74.4	27.9	27.8 ± 0.1
Benzene	30	0.8622	—	73.8	27.7	27.56 ± 0.05
Water	35	0.9928	54.8	—	70.5	70.38 ± 0.05
Water	45	0.9891	54.2	—	68.7	68.74 ± 0.05
Water	60	0.9822	53.3	—	66.0	66.18 ± 0.05

On comparing the results in the last two columns of Table II, it is apparent that there is a fair agreement of measured values with the accepted constants of surface tension. While the above position is not unsatisfactory, there is scope for improving the technique of the method to obtain better precision in measurements. The method, therefore, seems to have practical potentialities. The work in this direction is proceeding.

REFERENCES

- Andreas, Hauser and Tucker, 1938, *J. Phy. Chem.* **42**, 1001.
 Brown and McCormick, 1948, *Phil. Mag.* **39**, 420.
 Fergusson, 1912, *Phil. Mag.* **23**, 418.
 Fordham, 1948, *Proc. Roy. Soc.*, **194**, 1.
 Parvatikar, 1949, *Curr. Sci.* **18**, 288,
 Worthington, 1881, *Proc. Roy. Soc.*, **32**, 362.

ULTRAVIOLET ABSORPTION SPECTRA OF PHENOL, *o*-BROMOPHENOL AND DIPHENYL ETHER IN DIFFERENT STATES.*

S. B. BANERJEE

OPTICS DEPARTMENT, INDIAN ASSOCIATION FOR THE CULTIVATION OF
SCIENCE, JADAVPUR, CALCUTTA-32

Received for publication May 11, 1956)

ABSTRACT. The ultraviolet absorption spectra of phenol, *o*-bromophenol and diphenyl ether in the different states have been studied. In the spectra of phenol and *o*-bromophenol the main shifts in the ν_0 -bands occur with the liquefaction of the vapours while with the solidification of the liquids and cooling to -180°C practically no further displacements of the ν_0 -bands take place. It has been concluded that for both these compounds the molecules get associated in the liquid state and the strength of the virtual bond remains unaltered even when the liquids are solidified and cooled to -180°C . The changes observed in the case of *o*-bromophenol with change of state are different from those for *o*-chlorophenol reported by previous workers. As the crystal structures of the compounds are expected to be the same it is pointed out that the lattice field is not mainly responsible for the changes observed in these two cases and that the difference in the behaviour of the molecules arises from the difference in the chemical affinity of the chlorine and bromine atoms.

In the case of diphenyl ether in the vapour state the absorption spectrum was found to consist of two overlapping series of bands, the displacement of one series from the other being 242 cm^{-1} , while in the solid state only one series is observed. This is explained by assuming the presence of two types of molecules in the vapour state owing to freedom of rotation about the C-O bonds.

INTRODUCTION

The ultraviolet absorption spectra of *o*- and *p*-chlorophenol were studied by Swamy (1953) who observed that the substances in the liquid and solid states yield broad bands. It was observed that the changes that take place in the spectra with the liquefaction of the vapours and with the solidification of the liquids are different for the two compounds. It is not known how the absorption spectra of phenol is affected by the change of state and it was proposed to study the absorption spectra of phenol in the liquid and solid states and to compare the results with those obtained for the chlorophenols by Swamy (1953).

Swamy (1953) also studied the absorption spectra of bromotoluenes and observed that in the case of ortho bromotoluene the excited energy state is split up into three components when the liquid is frozen and cooled to -180°C while no such change takes place in the case of para bromotoluene. As it would be

*Communicated by Prof. S. C. Sirkar

interesting to find out whether similar changes take place in the spectra when the CH_3 group is substituted by OH group, the absorption spectra of ortho-bromophenol in all the three states have been studied in the present investigation.

Deb (1953a, 1953b) studied the ultraviolet absorption spectra of diphenyl, diphenyl methane and dibenzyl in the liquid and solid states in order to compare the changes which take place with change of state in the spectra of these molecules having more than one phenyl group. He observed in the case of diphenyl in the liquid state structureless absorption in the region $2850\text{--}2300\text{ \AA}$. On the other hand in the case of the other two molecules each having one or two groups of atoms between two phenyl groups he observed a large number of bands which could be assigned properly in progressions of vibration frequencies. It was proposed to study in the present investigation the ultraviolet absorption spectrum of diphenyl ether in different states in order to find out whether the changes which take place in the spectra with the change of state are similar to those observed in the case of either diphenyl methane or diphenyl.

EXPERIMENTAL

The experimental set up was the same as that described in an earlier paper (Banerjee, 1956). The liquids used were of chemically pure quality. Phenol supplied by B. D. H was first fractionated and the proper fractionated portion was redistilled under reduced pressure. Diphenyl ether was supplied by Esarson Co., N.Y., and *o*-bromophenol by E. Merck. The liquids were distilled under vacuum before use. Spectograms were taken on Ilford HP3 films using a Hilger EI spectrograph. Microphotometric records were taken with a Kipp and Zonen type Moll microphotometer. Iron arc spectrum was taken on each spectrogram as a comparison. The frequencies of the absorption bands were determined with the help of the microphotometric records of the bands and the iron lines as described in an earlier paper (Banerjee, 1956).

The absorption spectrum of diphenyl ether vapour was photographed using a tube of length 75 cm. and diameter 14 mm with plane quartz windows cemented at two ends with Araldite. The tube was kept at 50°C and the vapour was introduced from a bulb through a side tube. For studying the absorption spectrum of *o*-bromophenol in the vapour state the tube used was 30 mm long and 14 mm in diameter and the tube was filled with the vapour at saturation pressure at the room temperature.

In the case of the liquid and solid states very thin films had to be used, the thickness being of the order of a few microns. When the liquid was solidified some samples produced pattern due to interference of light passing through the thin film.

RESULTS AND DISCUSSION

The microphotometric records of the absorption spectra are reproduced in the figures 1, 2 and 3. The wave numbers of the bands and their assignments are given in Tables I, II and III.

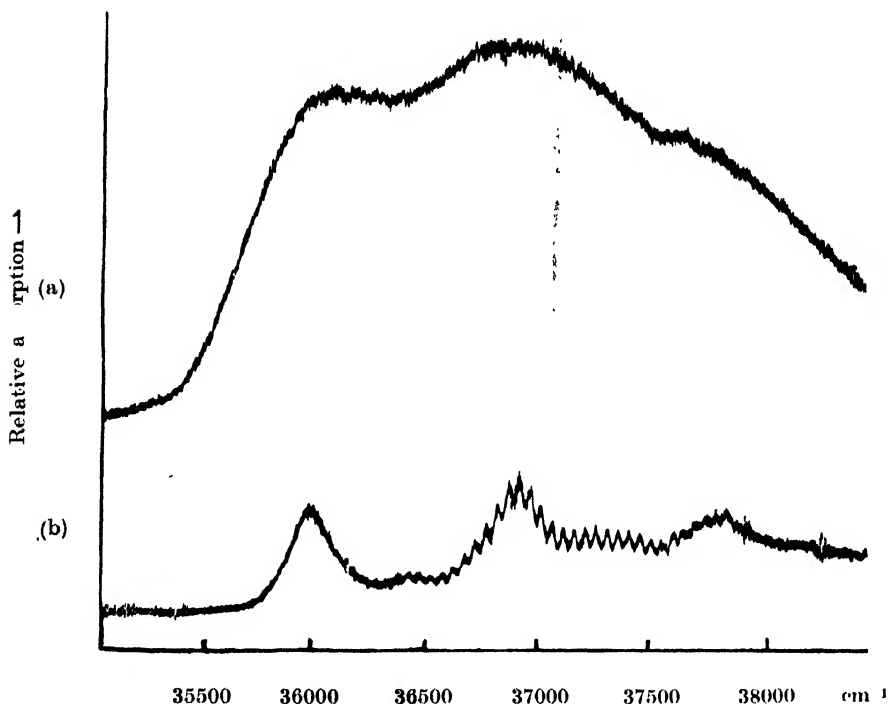


Fig. 1. Microphotometric records of the ultraviolet absorption spectra of phenol
(a) Liquid at 42°C (b) Solid at -180°C .

The bands in the liquid and solid states being, broad, measurements were made of the centres of absorption peaks. In the case of the diphenyl ether in the vapour state the bands could be assigned only by assuming that there are two series of bands separated by 242 cm^{-1} . The results for the three compounds have been discussed respectively in the following paragraphs.

Phenol:

The absorption spectrum of phenol in the vapour state studied by Matsen *et al* (1945) using a three-metre grating consisted of more than 300 bands, the 0-0 transition, the most intense band in the spectrum appearing as a doublet at 36348.6 cm^{-1} and 36351.9 cm^{-1} respectively. In the liquid state phenol exhibits only three broad bands, the centres of the peaks lying at 36051 , 36930 and 37803 cm^{-1} respectively (Table I). Taking the first band as the ν_0 -band it is seen that the

ν_0 -band is shifted by about 300 cm^{-1} towards longer wavelengths from its position for the vapour state. Thus with the liquefaction of the vapour the excited electronic state is lowered due to intermolecular field.

The broadening of the bands in the liquid state is probably due to widening of the energy levels because of the thermal motion of the molecules. This widening of the bands in the liquid state is responsible for the appearance of fewer

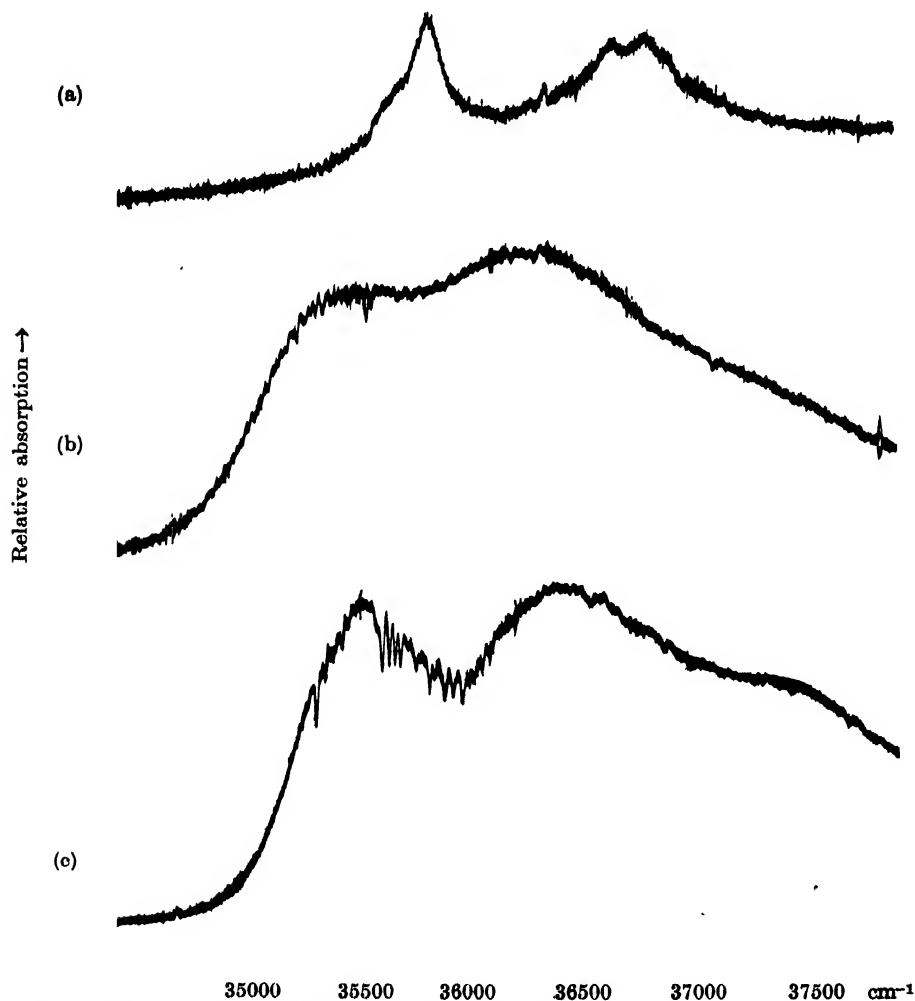


Fig. 2. Microphotometric records of the ultraviolet absorption spectra of *o*-bromophenol.
(a) Vapour at 30°C (b) Liquid at 30°C (c) Solid at -180°C .

bands compared to those corresponding to the nine excited state frequencies observed in the case of the vapour by Matsen *et al* (1945). Probably the band

at a distance of 879 cm^{-1} from the ν_0 -band is produced by the coalescence of the two bands corresponding to vibrational frequencies 935 and 783 cm^{-1} observed

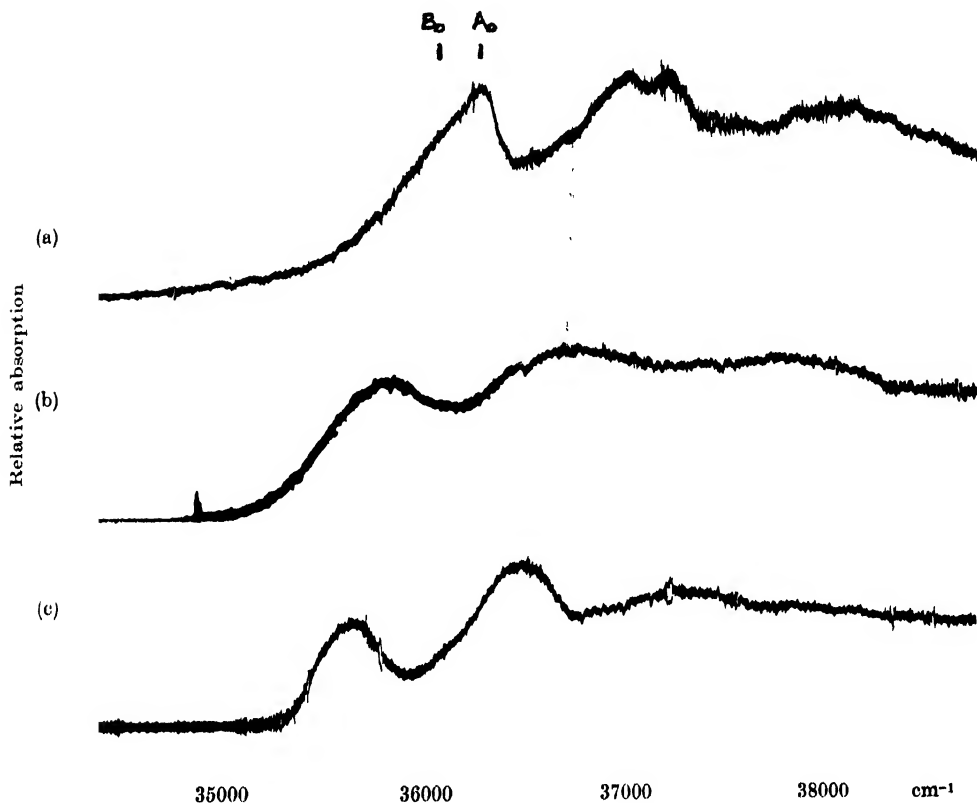


Fig. 3. Microphotometric records of the ultraviolet absorption spectra of diphenyl ether.
(a) Vapour at 50°C (b) Liquid at 32°C (c) Solid at -180°C .

in the case of the vapour. The bands due to other frequencies are not resolved owing to the broadening of the bands in the liquid state.

With the solidification of the liquid there is a very small shift of 52 cm^{-1} of the ν_0 -band towards longer wavelengths. In the case of the solid five bands are observed and the bands are a little sharper. Consequently, the bands corresponding to vibrational frequencies 446 , 936 and 1289 cm^{-1} are resolved. The fundamental excited state frequencies observed in the case of the solid state agree with some of those observed in the case of the vapour.

The sharpening of the bands at -180°C shows that in this case the amplitude of angular oscillation of the molecule taking place in the liquid diminishes greatly with lowering of temperature. The shift of the ν_0 -band with liquefaction and the absence of further shift with solidification indicates that the molecules

TABLE I
Absorption bands of phenol

Vapour* Matsen <i>et al</i> (1945)		Liquid at 42°C Present author		Solid at -180°C Present author	
Wave no. (cm ⁻¹) and intensity	Assignment	Wave no. (cm ⁻¹) and intensity	Assignment	Wave no. (cm ⁻¹) and intensity	Assignment
35351.2 (v _{vw})	$\nu_0 - 999$				
		36051 (s)	ν_0	35999 (s)	ν_0
35524.8					
35528.3 (w)	$\nu_0 - 824$			36445 (w)	$\nu_0 + 446$
35538.3 (v _{vw} B)	$\nu_0 - 811$	36930 (s)	$\nu_0 + 879$	36935 (s)	$\nu_0 + 936$
35822.5		37803 (w)	$\nu_0 + 2 \times 879$	37288 (vw)	$\nu_0 + 1289$
35825.3 (m)	$\nu_0 - 527$			37867 (w)	$\nu_0 + 2 \times 936$
35951.5 (m)	$\nu_0 - 397$				
36105.4					
36106.9 (vw)	$\nu_0 - 245$				
36127.7					
36130.6 (s)	$\nu_0 - 221$				
36287.6					
36290.7 (v _{vs})	$\nu_0 - 61$				
36348.6					
36351.9 (v _{vs})	ν_0				
36389.0					
36391.8 (s)	$\nu_0 + 40$				
36556.8					
36559.4 (ms)	$\nu_0 + 208$				
36722.7					
36725.6 (m)	$\nu_0 + 374$				
36824.9					
36827.2 (vs)	$\nu_0 + 476$				
36911.4					
36914.0 (m)	$\nu_0 + 562$				
37131.5					
37134.7 (v _{vs})	$\nu_0 + 783$				
37284.3					
37286.9 (v _{vs})	$\nu_0 + 935$				
37289.8					
37323.7					
37327.2 (s)	$\nu_0 + 975$				
37622.7					
37625.1 (s)	$\nu_0 + 1274$				
37914.3					
37915.8 (s)	$\nu_0 + 1565$				

*Only the bands corresponding to the fundamental frequencies have been included.

TABLE II
Absorption bands of *o*-bromophenol

Vapour at 30°C		Liquid at 30°C		Solid at -180°C	
Wave no. (cm ⁻¹) and intensity	Assignment	Wave no. (cm ⁻¹) and intensity	Assignment	Wave no. (cm ⁻¹) and intensity	Assignment
35627 (m)	$\nu_0 - 191$	35412 (s)	ν_0	35500 (s)	ν_0
35818 (s)	ν_0	36194 (s)	$\nu_0 + 763$	36432 (s)	$\nu_0 + 932$
36352 (ms)	$\nu_0 + 534$	36971 (m)	$\nu_0 + 2 \times 783$	37372 (m)	$\nu_0 + 2 \times 932$
36639 (s)	$\nu_0 + 821$				
36753 (s)	$\nu_0 + 935$				
37129 (m)	$\nu_0 + 1311$				
37288 (w)	$\nu_0 + 534 + 935$				

TABLE III
Absorption bands of diphenyl ether

Vapour at 50°C		Liquid at 32°C		Solid at -180°C	
Wave no. (cm ⁻¹) and intensity	Assignment	Wave no. (cm ⁻¹) and intensity	Assignment	Wave no. (cm ⁻¹) and intensity	Assignment
36064 (ms)	B_0	35831 (s)	ν_0	35678 (s)	ν_0
36306 (vs)	A_0	36753 (sb)	$\nu_0 + 922$	36103 (m)	$\nu_0 + 425$
36706 (m)	$A_0 + 400$	37681 (msb)	$\nu_0 + 2 \times 922$	36472 (s)	$\nu_0 + 794$
36957 (s)	$B_0 + 892$			37260 (mb)	$\nu_0 + 2 \times 794$
37198 (s)	$A_0 + 892$				
37554 (w)	$A_0 + 1248$				
37853 (m)	$B_0 + 2 \times 892$				
38098 (ms)	$A_0 + 2 \times 892$				

get associated in the liquid state and the strength of the virtual bond is not altered even when the molecules are arranged regularly in the solid state.

o-Bromophenol:

It can be seen from Table II that the absorption spectrum of *o*-bromophenol in the vapour state gives only seven bands. The first band at 35627 cm⁻¹ is assigned to $\nu \rightarrow 0$ transition and the strong band at 35818 cm⁻¹ is taken as the ν_0 -band. The other bands can be expressed by the fundamental excited state frequencies 534, 821, 935 and 1311 cm⁻¹. In the liquid state the substance produces

three broad bands, the centre of the first one being at 35412 cm^{-1} . There is thus a shift of 406 cm^{-1} of the ν_0 -band towards the longer wavelengths on liquefaction, which again suggests a lowering of electronic energy level in the excited state by the intermolecular field in the liquid state. The other bands due to the liquid represent transitions ν_0+783 and $\nu_0+2\times 783$. When the liquid is solidified and cooled to -180°C the ν_0 -band is found to shift towards shorter wavelengths by only 88 cm^{-1} . Thus in this case also the major shift in the ν_0 -band occurs with the liquefaction of the vapour. This behaviour of the compound is different from that of *o*-chlorophenol (Swamy, 1953), because in the latter case the position of the ν_0 -band remains unaltered with liquefaction of the vapour, but it changes when the liquid is solidified. For *o*-bromophenol the bands in the case of the solid are also broad and there is no increase in the number of bands with solidification of the liquid. The bands represent transition ν_0+932 and $\nu_0+2\times 932$.

As the crystal structures are expected to be the same for *o*-chloro- and *o*-bromophenol, the lattice field ought to have similar influence on the electronic state in both the cases. The difference in the behaviour mentioned shows that lattice field is not responsible for the changes observed in these cases. If formation of virtual bonds is assumed to be responsible for the changes observed with change of state, the difference in the behaviour of the two compounds may be attributed to difference in the chemical affinity of the chlorine and bromine atoms. It is well known (Pauling, 1939) that in the *o*-chlorophenol molecule the chlorine atom is attached to the OH group. In the liquid state the chlorine atom cannot form virtual bond with neighbouring molecule and as the ν_0 -band also does not shift with liquefaction of the vapour in this case (Swamy, 1953) the shift observed in the other case is evidently due to formation of such bonds. In the case of *o*-bromophenol some of the molecules may have the bromine atom free and these atoms may form virtual linkage with neighbouring molecules.

It can be seen that in the case of phenol or *o*-bromophenol in the excited state the energy level does not split up into more than one component with solidification unlike the case of *o*-bromotoluene where the energy level is split up into three components when the substance is frozen and cooled to -180°C . This fact supports the conclusion that for phenol or the substituted phenol the strength of the virtual bond remains practically unchanged with solidification and cooling to -180°C .

Diphenyl ether:

In the absorption spectra of diphenyl ether vapour the first strong band is at 36306 cm^{-1} which is accompanied on the longer wavelength side by another band at a distance of 242 cm^{-1} from it. If we take the band at 36306 cm^{-1} to be the ν_0 -band then its companion may be due to a $v\rightarrow 0$ transition. But it can be seen from figure 3 that each of the other principal bands of the vapour also ex-

hibits two peaks separated by about 242 cm^{-1} from each other. Thus it is probable that the absorption spectrum consists of two overlapping series of bands with the ν_0 -bands at 36064 and 36306 cm^{-1} respectively. Assuming this and designating the bands at 36064 and 36306 cm^{-1} as B_0 and A_0 respectively the other bands can be assigned corresponding to transitions B_0+892 , $B_0+2\times 892$ and A_0+400 , A_0+892 , A_0+1248 and $A_0+2\times 892$. The bands corresponding to B_0+400 and B_0+1248 are not observed because these bands are very weak. In the case of the liquid state three very broad bands are observed. The ν_0 -band is at 35831 cm^{-1} . Only one series of bands is found in this case as it is likely that the broadening of the bands in the liquid state causes a coalescence of the two series of bands observed in the case of the vapour. The ν_0 -band of the liquid is displaced by 475 cm^{-1} towards the longer wavelength side of that (A_0) due to the vapour. In the case of the solid the ν_0 -band is displaced towards the shorter wavelengths by 153 cm^{-1} from its position due to the liquid. In the absorption spectra of the solid the bands are a little sharper than those due to the liquid, but in this case also only one series of bands is observed. The bands due to the liquid can be assigned as ν_0+922 and $\nu_0+2\times 922$ while those due to the solid represent transitions ν_0+425 , ν_0+794 and $\nu_0+2\times 794$. Thus the excited state frequency 922 cm^{-1} observed in the case of the liquid is altered to 794 cm^{-1} in the solid state.

A comparison of the absorption spectra of diphenyl ether and diphenyl methane (Deb, 1953a) shows that the spectra exhibited by the two substances in the vapour state are quite different from each other. In the case of diphenyl ether the vapour gives two overlapping series of bands, whereas the other substance yields in the vapour state only one series. In diphenyl ether the two phenyl rings are linked through C—O bonds. Probably the phenyl rings have freedom of rotation about the C—O bond in the vapour state. This rotation of one phenyl group with respect to the other gives rise to a different type of molecule the electronic energy state of which is slightly different from that of the other type. The two series of bands observed in the vapour state may be due to those two types of molecules. In the liquid state there may be rotational oscillation of one phenyl group against the other causing a widening of the bands. In the solid state at -180°C , however, this type of rotatory oscillation ceases completely and all the molecules are probably of one type. In the case of diphenyl methane perhaps the two phenyl rings are connected to the CH_2 group through two bonds making a tetrahedral angle and as they are nearer to each other than in the diphenyl ether molecule free rotation of the rings about the C—C bond is restricted.

The absorption spectra of diphenyl in the vapour state (Seshan, 1936, London, 1945) gives uniform absorption without any structure in the region $2800\text{--}2200\text{ \AA}$. In the liquid state (Deb, 1953b) similar absorption in the region $2850\text{--}2300\text{ \AA}$ is observed. When the liquid is solidified and cooled to -180°C two systems

of bands in the two regions from 2962 \AA to 2800 \AA and from 2783 \AA to 2640 \AA are observed. Since the first system is absent in the spectrum of the vapour it is most probably produced by the perturbation produced by the intermolecular field in the liquid and solid states. This behaviour is different from that observed in the case of diphenyl ether and diphenyl methane because in the spectra of the latter two molecules in the solid state the field in the crystal does not produce any new system.

ACKNOWLEDGMENT

The author is indebted to Professor S. C. Sirkar, D.Sc., F.N.I. for his keen interest and constant guidance during the progress of the work.

REFERENCES

- Banerjee, S. B., 1956, *Ind. J. Phys.*, **30**, 106.
Deb, A. R., 1953a, *Ind. J. Phys.*, **26**, 183.
" 1953b, *Ind. J. Phys.*, **26**, 305.
London, A., 1945, *J. Chem. Phys.*, **13**, 396.
Matsen, F. A., Ginsburg, N. and Robertson, W. W., 1945, *J. Chem. Phys.*, **13**, 309.
Pauling, L., 1939, *The Nature of the Chemical Bond* (Cornell University Press).
Seshan, P. K., 1936, *Proc. Ind. Acad. Sci.*, **3**, 148.
Swamy, H. N., 1953, *Ind. J. Phys.*, **27**, 119.

MASS MEASUREMENTS IN NUCLEAR EMULSIONS BY MULTIPLE SCATTERING AND GAP DISTRIBUTION

INDER SAIN MITTRA

DEPARTMENT OF PHYSICS, MUSLIM UNIVERSITY, ALIGARH

(Received for publication March 16, 1956)

ABSTRACT. A method of identifying singly charged particles in nuclear emulsions with the help of gap distribution and multiple coulomb scattering measurements for the same track is described. A parameter S depending upon scattering parameter α_{100u} and gap distribution parameter g^* is obtained, which is a logarithmic function of the mass. The observed values of S are in good agreement with the calculated ones.

INTRODUCTION

Particle identification in nuclear emulsions, in the case of singly charged particles reduces simply to the determination of the mass of the particles producing the given tracks. Accurate determination of mass has assumed new importance in recent years because of the reported existence of a large number of new particles. The nature of many of these new particles is not very well understood.

In order to find out the mass of an unknown particle producing a track in photographic emulsion, two parameters are necessary, which are functions of velocity and mass. One of them is generally taken to be the ionization produced by the particle. Information of the ionization produced can be had from the measurements of the grain density, blob density, photometric track density, and by studying gap-length distribution.

The other parameter is either the residual range or the mean square angular deviation suffered by the particle as a result of multiple scattering in the emulsion. The last two by themselves are also sufficient to specify the mass.

In a recent paper, Fowler and Perkins (1955), have shown that the distribution of gap-lengths occurring in tracks of ionizing particles is exponential over the entire range of ionization measured and that the coefficient g of this exponential is the most useful measure of the ionization in the track. The normalised value of g is $g^* = g/g_0$ where g_0 corresponds to minimum ionization. g^* is independent of the degree of development of the emulsion. Moreover the value of g^* does not depend on the developed grain size. This method of determination of ionization is as accurate as the photometric method and has the additional advantage of consuming less time.

Multiple coulomb scattering gives a measure of the product of momentum and velocity, i.e. $p\beta$ of the particle. It has been thoroughly investigated both theoretically and experimentally. Recent advances on the "Constant Cell Method" of Fowler (1950) have culminated in the "Constant Sagitta Method" described by Biswas *et al* (1953) and Dilworth *et al* (1954). The constant cell method after the elimination of various kinds of noise, which have been discussed by Menon *et al* (1951) and Biswas *et al* (1955), gives accurate results, especially for fast particles.

In the method developed in this paper the scattering parameter $\bar{\alpha}_{100\mu}$ and the gap distribution parameter g^* are determined for the same track. We have obtained a parameter S which depends upon $\bar{\alpha}_{100\mu}$ and g^* and is a logarithmic function of the mass of the particle. This relation enables us to determine the mass with reasonable accuracy. The values of S calculated according to our relation are in good agreement with those obtained from values of $\bar{\alpha}_{100\mu}$ and g^* given by Glasser (1955) and Fowler and Perkins (1955) respectively.

II. DETERMINATION OF THE RELATIONSHIP BETWEEN $\bar{\alpha}_{100\mu}$ AND g^*

Scattering Parameter $\bar{\alpha}_{100\mu}$:—According to Voyvodic and Pickup (1952), for Ilford G5 emulsions, the mean absolute deflection suffered by a particle undergoing multiple coulomb scattering is given by

$$\bar{\alpha} = Kt^{1/2}/pv \text{ degrees} \quad \dots (1)$$

p , v are the momentum and velocity respectively of the charged particle; t is the cell length in microns and K is referred to as the "scattering constant" in degrees Mev/(100 μ)^{1/2}. K for Ilford G5 emulsion varies from 24 to 29 and is generally taken as 26 Mev degrees/(100 μ)^{1/2} ... (2)

In emulsion work, it has been a useful convention to measure the quantity $\bar{\alpha}_{100\mu}$ which is defined as [Menon and O'Ceallaigh (1953)]

$$\bar{\alpha}_{100\mu} = \frac{1}{B_1 - B_2} \int_{B_2}^{B_1} \bar{\alpha} t^{-1/2} dB \quad \dots (3)$$

where $B = (1 - \beta^2)^{-1/2}$ and B_1 , B_2 are the values of B at the two ends of the section of a track along which multiple scattering is measured.

Using (1) and (3) we get

$$\bar{\alpha}_{100\mu} = \frac{1}{B_1 - B_2} \int_{B_2}^{B_1} K/pv dB \quad \dots (4)$$

*Gap-distribution Parameter g^** :—As mentioned earlier, Fowler and Perkins (1955) have shown that in the tracks produced by ionizing particles, the gap length distribution is exponential over the entire range of ionization. The coefficient g of this exponential is a useful measure of ionization and is given by

$$g = \frac{1}{l_2 - l_1} \ln \frac{H_1}{H_2} \quad \dots (5)$$

where H_1 is the number of gaps exceeding length l_1 and H_2 is the number of gaps exceeding length l_2 . Moreover for values of ionization less than ten times the minimum ionization

$$g \propto \frac{dE}{dR} \quad \dots (6)$$

dE/dR gives the rate of energy loss and is a function of velocity only.

The normalized value of g i.e. g^* is related to the residual range R measured in microns in the case of protons as

$$g_p^* = aR^m \quad \dots (7)$$

$$\text{where} \quad m = -0.42 \quad \dots (8)$$

$$a = 2.93 \times 10^2 \quad \dots (9)$$

The constant of proportionality a in (7) is determined from the g^*--R curve for protons given by Fowler and Perkins (1955).

Range-energy Relation:—The accepted range-energy relation for Ilford G5 emulsions in the case of protons is [Glasser (1955)]

$$R_P = 10.6 E_P^{1.68}$$

$$\text{or} \quad E_P = kR_P^n \quad \dots (10)$$

$$\text{where} \quad k = 0.246 \quad \dots (11)$$

$$n = 0.595 \quad \dots (12)$$

The general range-energy relation for the case of any singly charged particle can be written as

$$E = kM^{1-n} R^n \quad (13)$$

where M is the mass of the particle in proton units.

Determination of S_p : Let us choose a function of $\bar{\alpha}_{100\mu}$ and g^* which will be easily amenable to the theoretical and experimental treatment. After a large number of trials, we arrived at the following function

$$S = \log \bar{\alpha}_{100\mu} - 1.5 \log g^*$$

This function was subsequently slightly modified and we now define S as

$$S = \log \bar{\alpha}_{100\mu} + \frac{n}{m} \log g^* \quad \dots (14)$$

where 'm' and 'n' are given by (8) and (12) respectively.

We can proceed to determine the value of S_p (the value of S for protons) as follows:

Let us rewrite (4) after a little simplification as

$$\bar{\alpha}_{100\mu} = \frac{K}{2\mu(B_1 - B_2)} \log \frac{1 - B_1}{1 - B_2} + \frac{K}{2\mu + (1 + B_2)}$$

μ is the mass of the particle in Mev.

The second term on the right is a small correction term and can be neglected, so that

$$\bar{\alpha}_{100\mu} = \frac{K}{2\mu(B_1 - B_2)} \log \frac{1 - B_1}{1 - B_2}$$

If we put $\bar{B} = (B_1 + B_2)/2$ and $b = B_1 - B_2$, then

$$\begin{aligned} \bar{\alpha}_{100\mu} &= \frac{K}{2\mu b} \log \left[\left(1 - \frac{b/2}{1 - \bar{B}} \right) / \left(1 + \frac{b/2}{1 - \bar{B}} \right) \right] \\ &\approx \frac{K}{2\mu} \frac{1}{\bar{B} - 1} \quad \dots (15) \end{aligned}$$

The range-energy relation (10) can also be expressed as

$$\mu_P [B - 1] = k R_P^n$$

or

$$B - 1 = k \mu_P^{-1} R_P^n$$

Thus

$$B - 1 = k \mu_P^{-1} (R_{P1}^n + R_{P2}^n)/2$$

Let the scattering measurements be made on the faster half of the track so that B_1 and B_2 represent velocities corresponding to ranges R_p and $R_p/2$ respectively. So we have

$$\bar{B} - 1 = k \mu_P^{-1} \frac{2^n + 1}{2 \cdot 2^n} R_P^n \quad \dots (16)$$

Eliminating $(\bar{B} - 1)$ and R_P from (7), (10), and (15) one gets

$$(\bar{\alpha}_{100\mu})_P = \frac{K}{2\bar{K}} g_P^{*-n/m}$$

$$\text{or} \quad \log (\bar{\alpha}_{100\mu})_P + \frac{n}{m} \log g_P^* = \log \frac{K}{2K'} = \text{constant} \quad \dots (17)$$

$$\text{where} \quad K' = k \frac{2^n + 1}{2 \cdot 2^n} a^{-n/m} \quad \dots (18)$$

From (2), (8), (9), (11), (12), and (18), we have

$$\log \frac{K}{2K'} = -1.70$$

$$\text{Hence} \quad S_P = \log (\bar{\alpha}_{100\mu})_P + \frac{n}{m} \log g_P^* = -1.70 \quad \dots (19)$$

Determination of S: — We can find the value of S for any singly charged particle as follows:

If two particles have the same velocity, then their ranges are proportional to their masses. Thus if μ , μ_P represent masses of a singly charged particle and of a proton respectively, in energy units, and R and R_P be the respective ranges, then

$$R_P = (\mu_P/\mu)R \quad \dots (20)$$

Also it follows from (5) and (6) that the value of g and hence of g^* is the same for two particles of the same charge and velocity having different masses. Hence for any singly charged particle we get

$$\begin{aligned} g^* &= a(\mu/\mu_P)^{-n} R^m \\ \therefore a' \mu^{-n} R^m & \end{aligned} \quad (21)$$

$$\text{Taking } \mu_P = 931 \text{ Mev.}, \quad a' = a(931)^m \quad (22)$$

Also general range-energy relation (13) can be written as

$$\begin{aligned} \mu[B-1] &= k(\mu/\mu_P)^{1-n} R^n \\ B-1 &= k' \mu^{-n} R^n \end{aligned} \quad (23)$$

$$\text{Here} \quad k' = k(931)^{n-1} \quad (24)$$

$$\text{As before from (23)} \quad B-1 = k' \mu^{-n} \frac{2^n + 1}{2 \cdot 2^n} R^n \quad (25)$$

Eliminating R and $(B-1)$ from (15), (21), and (25), we have

$$\bar{\alpha}_{100\mu} = \frac{K}{2K''} \mu^{-1} g^{*-n/m} \quad \text{where } K'' = k' \frac{2^n + 1}{2 \cdot 2^n} a'^{-n/m}$$

$$\text{or} \quad \log \bar{\alpha}_{100\mu} + \frac{n}{m} \log g^* = \log \frac{K}{2K''} - \log \mu$$

$$\text{Hence} \quad S = A - \log \mu \quad \dots (26)$$

$$\text{constant } A = \log \frac{K}{2K'}$$

This parameter S depends upon $\bar{\alpha}_{100\mu}$ and g^* by definition. Knowing the values of these two quantities for a given track, we can determine this parameter and hence the mass of the unknown particle from (26). Thus the mass estimate depends upon the experimental determination of the statistical parameter S which is a logarithmic function of the mass. We are to keep in mind that $\bar{\alpha}_{100\mu}$ is determined for the faster half of the track.

Substituting the values of various constants a' , k' , n , m , and K , we obtain $A = 1.36$, so that (26) becomes

$$S = 1.36 - \log \mu \quad \dots (26a)$$

If we substitute for μ for various singly charged particles, we can find the corresponding values for S . We can, thus, have a scale of S -values

$$S_\mu, S_\pi, S_K, S_p, S_D, S_T, \dots$$

for μ -meson, π -meson, K -meson, proton, deuteron, triton etc. Knowing these values and finding the S -value for the unknown particle, we can at once identify it.

III. EXPERIMENTAL VERIFICATION

In order to test the correctness of relations (19) and (26), let us find out the values of S_p and S_π experimentally. For the tracks considered, the values of $\bar{\alpha}_{100\mu}$ and g^* for protons and π -mesons are to be determined.

In the following table the values of $\bar{\alpha}_{100\mu}$ have been taken from the paper by Glasser (1955) wherein an experimental relationship has been found between scattering and range

$$\langle \bar{\eta} \rangle t = (19.0 \pm 0.3)(M_p/M)^{0.303 \pm 0.016} \times (t/50)^{3/2} R^{-(0.607 \pm 0.016)} \quad \dots (27)$$

t is the cell length in microns and M_p , M are masses of proton and any other singly charged particle respectively.

If y_i is the projection of the track on the axis at right angles to the one to which the track is made parallel and y_i is measured after constant cell length t microns, then

$$\langle \eta_i \rangle t = y_i - \frac{1}{2}(y_{i-1} + y_{i+1}) \text{ microns}$$

Usually, we determine the second differences of the projections

$$\begin{aligned} \text{i.e. } \langle D_i \rangle t &= 2y_i - (y_{i-1} + y_{i+1}) \text{ microns} \\ &= 2\langle \eta_i \rangle t \end{aligned}$$

So we have
$$\bar{\alpha}_t = \frac{\langle \bar{D} \rangle_t}{t} \times \frac{180}{\pi} \text{ degrees}$$

and hence
$$\bar{\alpha}_{100\mu} = \frac{2\langle \bar{\eta} \rangle_t}{t} \times \frac{180}{\pi} \times \left(\frac{100}{t} \right)^{\frac{1}{2}} \text{ degrees}$$

$$\text{or } \bar{\alpha}_{100\mu} = 3.24 \langle \bar{\eta} \rangle_{50\mu} \quad \dots (28)$$

$\bar{\alpha}_{100\mu}$ is then determined from (27) and (28) for various values of R .

The values of g_p^* have been determined from the paper by Fowler and Perkins (1955) who have given a curve showing the relationship between g_p^* and R_p . The values of g_π^* have been determined from the corresponding values of g_p^* for the same residual ranges by use of (29) obtained from (7) and (21).

$$g_\pi^* = g_p^* (\mu_\pi / \mu_p)^m \quad \dots (29)$$

The values of S_p and S_π are then determined from (14).

R	g_p^*	g_π^*	$(\alpha_{100\mu})_p$	$(\alpha_{100})_\pi$	S_p	S_π
0.1 cm	14.0	6.29	0.931	1.97	-1.66	-0.84
0.5 cm	8.6	3.86	0.351	0.74	-1.78	-0.96
1.0 cm	6.2	2.78	0.230	0.49	-1.76	-0.94
4.0 cm	3.5	1.57	0.099	0.21	-1.77	-0.96
10.0 cm	2.25	1.01	0.057	0.12	-1.74	-0.93

$$\text{Mean } S_p = -1.74 \text{ and } S_\pi = -0.93$$

The value of S_p from (19) is -1.70 and that of S_π from (26') is -0.88, which are in good agreement with the values obtained above.

IV CONCLUSION

Let us examine (26) critically. First of all we have assumed that A is a constant which amounts to saying that scattering constant K has a fixed value. This, however, is not so, since K depends upon the velocity of the particle and the cell-length employed. Although this dependence is slight and may be neglected in ordinary work, this must be taken into account in precision mass measure-

ments of unknown particles. A correction for the variation in the value of K can be made as done by Menon and O'Ceallaigh (1953).

Secondly, $\bar{\alpha}_{100\mu}$ is measured along the faster half of the track. In general, if B' , B'' measure velocities at residual ranges R' , R'' respectively, then instead of \bar{B} , we should use the value of B_{eff} which corresponds to residual range R_{eff} , which is given by the following relation due to Menon and Rochat (1951)

$$R_{eff} = \left[\frac{1}{R'' - R'} \int_{R'}^{R''} \frac{dR}{R^{2n}} \right]^{-1/n}$$

where ' n ' is given by (12).

Statistical errors in the evaluation of g^* have been discussed by Fowler and Perkins (1955) and the various errors in the measurement of $\bar{\alpha}_{100\mu}$ by Menon *et al* (1951) and Biswas *et al* (1955). Taking an extreme case, if $\bar{\alpha}_{100\mu}$ is measured with an error of 10% and g^* with an error of 5%, then the percentage error in S will be $\approx 12/S$ which in the case of protons is $\approx 7\%$.

ACKNOWLEDGMENTS

The author wishes to express his sincere gratefulness to Professor P. S. Gill for his continuous help and guidance in this work. He is thankful to Dr. K. R. Dixit and Dr. A. N. Mitra for helpful criticism and for making some useful suggestions. The support of the Scientific Research Committee of U.P. for the grant of research assistantship is thankfully acknowledged.

REFERENCES

- Biswas, S., George, E. C. and Peters B., 1953, *Proc. Ind. Acad. Sci.*, **38A**, 418.
 Biswas, S., Peters, B. and Rama, 1955, *Proc. Ind. Acad. Sci.*, **41A**, 154.
 Dilworth, Goldsack and Hirschberg, 1954, *Nuovo Cimento*, **11**, 113.
 Fowler, P. H., 1950, *Phil. Mag.*, **41**, 169.
 Fowler, P. H. and Perkins, D. H., 1955, *Phil. Mag.*, **46**, 587.
 Glasser, R. G., (1955), *Phy. Rev.*, **98**, 174.
 Menon, M. G. K. and O'Ceallaigh, C., 1953, *Phil. Mag.*, **44**, 1291.
 Menon, M. G. K. and O'Ceallaigh, C. and Rochat, O., 1951, *Phil. Mag.*, **42**, 932.
 Menon, M. G. K. and Rochat, O., 1951, *Phil. Mag.*, **42**, 1232.
 Voyvodic, L., and Pickup, E., 1952, *Phy. Rev.*, **85**, 91.

Letters to the Editor

The Board of Editors will not hold itself responsible for opinions expressed in the letters, published in this section. The notes containing reports of new work communicated for this section should not contain many figures and should not exceed 500 words in length. The contributions must reach the Assistant Editor not later than the 15th of the second month preceding that of the issue in which the Letter is to appear. No proof will be sent to the authors.

STRUCTURE OF THE SPECTRUM OF DOUBLY IONISED BROMINE.

Y. BHUPALA RAO

PHYSICS DEPARTMENT, ANDHRA UNIVERSITY, WALTAIR

(Received for publication May 26, 1956)

The first important investigations on the spectrum of doubly ionised bromine (Br III) were done by L. and F. Bloch (1927) and Lacroute (1935) who gave an almost complete list of the lines of Br III. Rao and Krishna Murty (1937) identified some of the quartet terms and gave a tentative identification of the doublet terms independent of the quartet terms. In a later communication Rao (1944) has reported the identification of some intercombination lines and gave the intervals $4p^3\ ^4S^{\circ}_{3/2} - 4p^3\ ^2D^{\circ}_{3/2}$ and $4p^3\ ^2D^{\circ}_{5/2} - 4p^3\ ^2P^{\circ}_1$. Still several strong lines in the spectrum remain unclassified, and the analysis is far from complete and needs confirmation. An extensive study of the spectrum has been made along with that of Br II (Y. B. Rao 1956) over the range λ 10,000Å to λ 400Å. With spectrographs of small and large dispersion. The present investigation has shown that the doublets and intercombinations given by Rao and Krishna Murty (1937) and Rao (1944, an unpublished work) are not correct except for the level $4p^3\ ^2D^{\circ}_{5/2}$. Several levels are newly identified and the intercombinations are definitely established leading to the classification of more than 175 lines. The new levels with their designations and J values are given in Table below in ascending order of magnitude calculated with respect to the ground level $4p^3\ ^4S^{\circ}_{3/2}$ as zero; the notation is that adopted by Moore (1952).

TABLE I

Designation	<i>J</i>	Level	Interval
$4p^3 \ ^2D^\circ$	3/2	15105.0	
	5/2	16300.0	1185.0
$4p^3 \ ^2P^\circ$	1/2	27050.4	
	3/2	28659.7	1609.3
$4p^4 \ ^4P$	5/2	101532.1	
	3/2	104128.7	— 2596.6
	1/2	105379.6	— 1250.9
$4p^4 \ ^2P$	3/2	137531.3	
	1/2	138608.7	— 1077.4
$4d \ ^4F$	3/2	139792.4	
	5/2	142238.8	2446.4
	7/2	144167.1	1928.3
	9/2	145805.5	1638.4
$4d \ ^4D$	1/2	143995.6	
	3/2	145175.4	1179.8
	5/2	145626.3	450.9
	7/2	146252.6	626.3
1	3/2	146164.9	
$4d \ ^4P$	5/2	148868.1	
	3/2	151063.7	— 2195.6
	1/2	152763.8	— 1700.1
2	3/2	149326.8	
$4d \ ^2F$	5/2	149864.8	
	7/2	151625.9	1761.1
$5s \ ^2P$	1/2	150906.3	
	3/2	153845.8	2939.6
3	3/2	152975.8	
$4d \ ^2D$	3/2	153508.3	

TABLE I (contd.)

Designation	J	Level	Interval
$4d\ ^2P$	3/2	153866 ∞	
$5s'\ ^2D$	5/2	160257.4	-935.7
	3/2	161193.1	
$4p^4\ ^2D$	3/2	163641.6	202.1
	5/2	163843.7	
$5p\ ^2S^\circ$	1/2	182006.2	2522.5
$5p^2\ D''$	3/2	182198.0	
	5/2	184720.5	
$5p\ ^2P^\circ$	1/2	183829.9	118.1
	3/2	183948.0	
4	3/2 or 5/2	203261.7	
5	1/2 or 3/2	203465.4	
6	5/2 or 5/2	204247.2	
7	5/2	205162.3	
8	3/2	207243.0	
9	3/2	208561.1	
$5d\ ^4F$	3/2	210602.4	3505.8
	5/2	214108.2	2723.9
	7/2	216832.1	
$5d\ ^4D$	1/2	211713.3	738.3
	3/2	212451.6	1817.4
	5/2	214269.0	2310.4
	7/2	216579.4	
10	3/2	212726.9?	

TABLE I (contd).

Designation	<i>J</i>	Level	Interval
5d ⁴ P	5/2	214703.7	
	3/2	215097.9	-394.2
	1/2	215857.6	-759.7
11	3/2	214882.5	
12	3/2	216397.2	
13	5/2	217173.4	
14	5/2	217923.6?	
15	3/2	218927.1	
16	3/2 or 5/2	219852.9	
17	3/2	220282.6	
18	5/2	220348.9	
19	5/2	221793.8?	
20	1/2 or 3/2	222432.7	
21	3/2	222690.3	
22	3/2 or 5/2	224990.2	
23°	5/2	229823.1	
24°	1/2, 3/2 or 5/2	232442.0	

Details of the analysis will be published shortly.

REFERENCES

- Bhupala Rao, Y., 1956, *Ind. J. Phys.*, **30**, 95.
 Bloch, L. and Bloch, E., 1927, *Ann. de. Phys.*, **7**, 205.
 Lacroute, P., 1935, *Ann de. Phys.*, **3**, 3.
 Moore, C. E., 1952, *Atomic Energy Levels*, Vol. II, 161.
 Rao, K. R. and Krishna Murty, S. G. 1937, *Proc. Roy. Soc. (Lond.)*, A, **161** 38
 Rao, K. R., 1944, *Curr. Sci.*, **13**, 72.

RADIATIONS FROM TWO RADIOACTIVE ISOTOPES OF GOLD†

V. R. POTNIS*

BARTOL RESEARCH FOUNDATION OF THE FRANKLIN INSTITUTE, SWARTHMORE,
PENNSYLVANIA, U.S.A

(Received for publication March 14, 1956)

ABSTRACT. The angular correlation function of the 330kev-358 kev cascade in the decay of Au^{196} has been measured and is in accord with a 2-2-0 sequence of spins for the low lying states of Pt^{196} . The extent of anisotropy at 180° suggests the first emitted gamma transition to be a mixture of E2 in M1. The gamma radiation of the 185-day Au^{195} has been examined by scintillation counting methods and is found to consist of quanta at 31 kev and 99 kev in coincidence and the associated cross-over transition at 130 kev.

INTRODUCTION

Naturally occurring platinum was irradiated by deuterons of energy 15 Mev for 4.1 hours at an average beam current of 75 micro-amperes in the cyclotron at the University of Pittsburgh. The radioactive isotopes of gold so produced were chemically separated from iridium, mercury, and platinum. The gamma-ray spectrum, as measured in NaI(Tl) crystal and two weeks following the cessation of irradiation is shown in figure 1. The apparatus is described in a previous paper, Potnis *et al.* (1956). Photopeaks are in evidence at 65, 158, 350, and 425 kev. The 158 kev gamma ray was identified by its decay period as being emitted in the disintegration of Au^{199} , and the 350 kev and 425 kev quanta could similarly be assigned to Au^{196} . The x-ray energy of 65 kev is characteristic of the region of the noble metals. Calibration points for the spectrometers were obtained at quantum energies of 31.4, 87, 279, and 661 kev. The radiations of these energies were obtained from monoenergetic gamma ray emitters such as Cd^{109} , Hg^{203} , and Cs^{137} . The 31.4 kev x-rays were those of Ba^{137} which are emitted following conversion of the 661 kev gamma ray.

GOLD 196

Au^{196} decays to Pt^{196} by orbital electron capture and the subsequent emission of a 330 kev—358 kev gamma-ray cascade. The radionuclide also decays

† Communicated by Dr. C. E. Mandeville.

* Permanent address, Gwalior (M.B.) India

Assisted by the joint programme of the Office of Naval Research and the U.S. Atomic Energy Commission.

by negatron emission followed by the gamma ray at 425 kev. The angular correlation function of the gamma-ray cascade in Pt^{196} has been previously measured by Steffen (1951, 1953). His results indicated a spin assignment of 2 to the first and second excited states of Pt^{196} and a scheme of 2-2-0 with the first emitted gamma-ray transition, a mixture of 95 percent E2 in M1. Sources in the form of a dilute solution of AuCl_3 as well as in the form of solid AuCl_3 imbedded in gold gave within the statistical errors, the same correlation function.

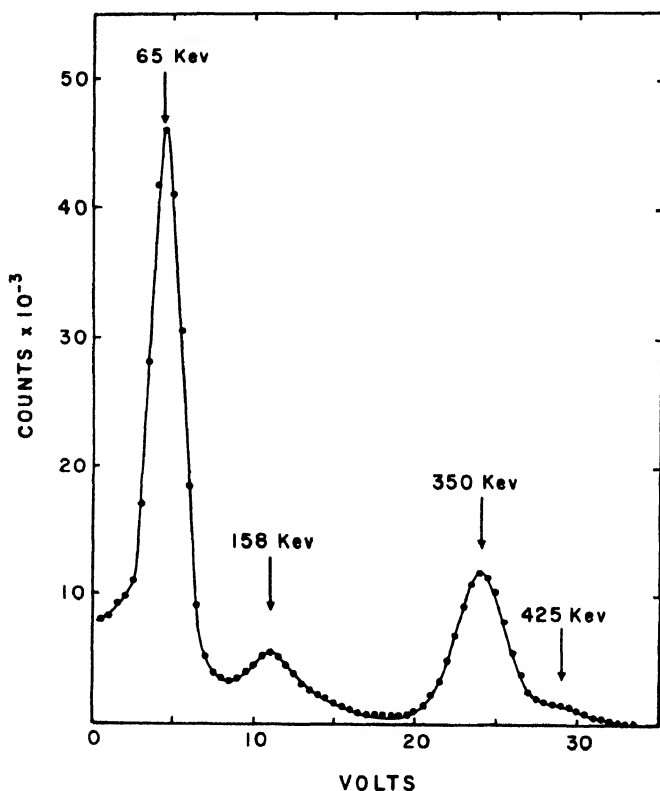


Fig. 1. Energy spectrum of gamma rays from isotopes of gold.

The correlation function of the 330 kev—358 kev cascade has been measured in the present investigation. Pulse height selection was employed in either channel, each being set at the photopeak appearing at ~ 350 kev shown in figure 1 and opened to a width of four volts. The resolving time of the coincidence circuit was 0.2 microsecond. The source was in the form of metallic gold contained in a carbon cylinder. The distance of the source from the face of either crystal was 13 cm, and the half-angle of the detecting system was 7.5 degrees as measured by the coincidence rate of the annihilation radiation of Na^{22} . An initial test of the proper function of the apparatus was carried out by measuring the anisotropy

of the gamma-gamma coincidences of $\text{Co}^{60} \xrightarrow{\beta} \text{Ni}^{60}$. Measurements were performed at five different angles, the moving counter being placed at intervals of 22.5 degrees between the angles of 90 and 180 degrees with the axis of the fixed counter. Coincidences were accumulated at each angle for a period of five minutes at a time. This range of settings was traversed repeatedly so that any decay correction was eliminated. Approximately 10,000 counts were obtained at each angle.

The results of the measurements are presented in figure 2 where the observed

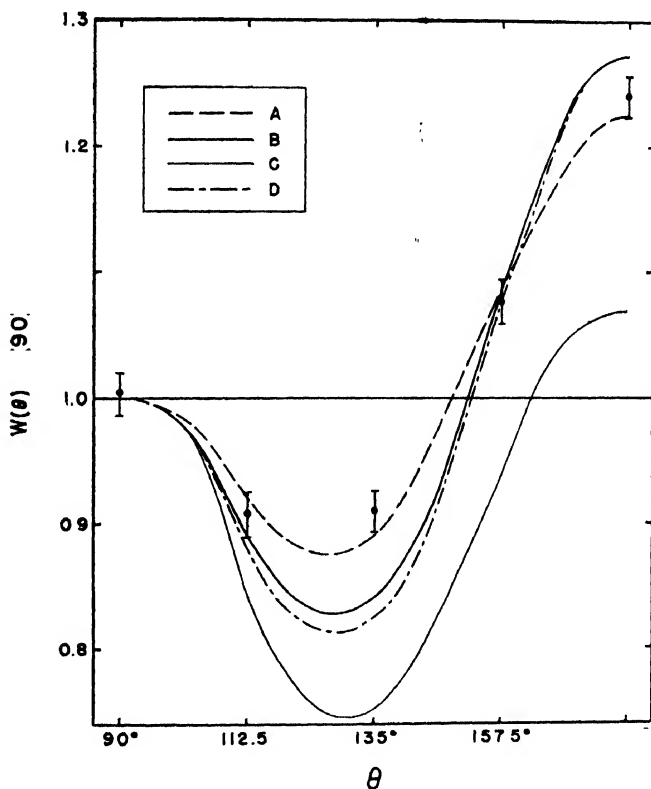


Fig. 2. Angular correlation function of the 330 kev—358 kev cascade in the de-excitation of Pt^{196} . Observed points are shown with statistical errors. Curve A—Least square fit of the data. Curve B—Curve A corrected for angular resolution of the detectors. Curve C—Theoretical correlation function for decay scheme 2(E2); 2(E2); 0. Curve D—Expected for a decay scheme 2(E2, M1); 2(E2); 0.

points are shown together with their respective statistical errors. A "least square" fit of the data yielded the function

$$W(\theta) = 1 - 0.66 \cos^2 \theta + 0.88 \cos^4 \theta$$

where the probable errors of the coefficients of the terms in $\cos \theta$ are about three

percent. When the function is modified for the finite angular resolution of the apparatus, it becomes

$$W(\theta) = 1 - 0.90 \cos^2 \theta + 1.17 \cos^4 \theta.$$

This latter curve is also plotted in figure 2 along with the theoretically expected distribution for a 2—2—0 spin sequence and both transitions pure electric quadrupole. The observed anisotropy at 180 degrees is 0.27 which is larger than would be expected for the pure cascade. A theoretical distribution function with the first emitted quantum a mixture of 96.7 per cent E2 in M1 is also plotted and agrees well with the observed function corrected for angular resolution. Thus is indicated the fact that the first transition occurs as a mixture with the above mentioned intensity ratio. The sign of the ratio of the matrix elements of the two types of transition was found to be positive, corresponding to a phase difference of 180°. Data available with regard to the internal conversion coefficients of the gamma rays are consistent with the condition that both transitions be electric quadrupole in character. The correlation observations of the present investigation are in essential agreement with those already obtained by Steffen (1951, 1953). Thus the spin assignments support the shell model predictions for an even-even nucleus like Pt¹⁹⁶.

GOLD 195

After a time of decay of about three months, the source previously employed in the study of Au¹⁹⁶ was used to measure the radiations of Au¹⁹⁵.

Gold (195) is known to decay to excited states of Pt¹⁹⁵ by orbital electron capture. The radiations emitted in this process have been examined in magnetic spectrometers and coincident Geiger counter arrangements, and several energy level schemes for Pt¹⁹⁵ have been proposed. Steffen *et al.* (1949) found two non-coincident gamma rays with energies of 95 and 129 kev. De-Shalit *et al.* (1952) reported 29 and 97 kev gamma rays in cascade and a cross-over transition at 126 kev. Gillon *et al.* (1954) have observed conversion lines corresponding to the gamma-ray energies of the cascade but did not detect any cross-over transition.

The pulse-height distribution of the gamma rays of Au¹⁹⁵, as measured in a scintillation spectrometer, is shown in figure 3. Photopeaks are in evidence at quantum energies of 32, 65, 99 and 130 kev. The 32 kev photopeak is actually a composite one formed by the 37 kev escape peak of the 65 kev x-rays of Pt and the 31 kev gamma ray. When the pulses of this peak were absorbed in copper, two slopes were obtained corresponding to energies of approximately 31 and 65 kev, showing the presence of photoelectric pulses of a 31 kev gamma ray as well as those of the escape peak of the x-rays. These data are shown in the absorption curves of figure 4. From the counting rates at zero absorber thickness, it is estimated that 14 per cent of the pulses in the peak arise from the 31 kev

gamma ray itself. The pulses of the 131 kev peak were similarly absorbed as is also plotted in figure 4, and the slope of the curve suggests an energy of 130 kev. Thus is eliminated the possibility that this peak arose from the simultaneous detection of the 31 kev and 99 kev gamma rays which are in cascade. Thus, in addition to the x-rays of platinum, it has been shown that three gamma rays are present in the decay of Au^{195} , the cascade, and the associated cross-over

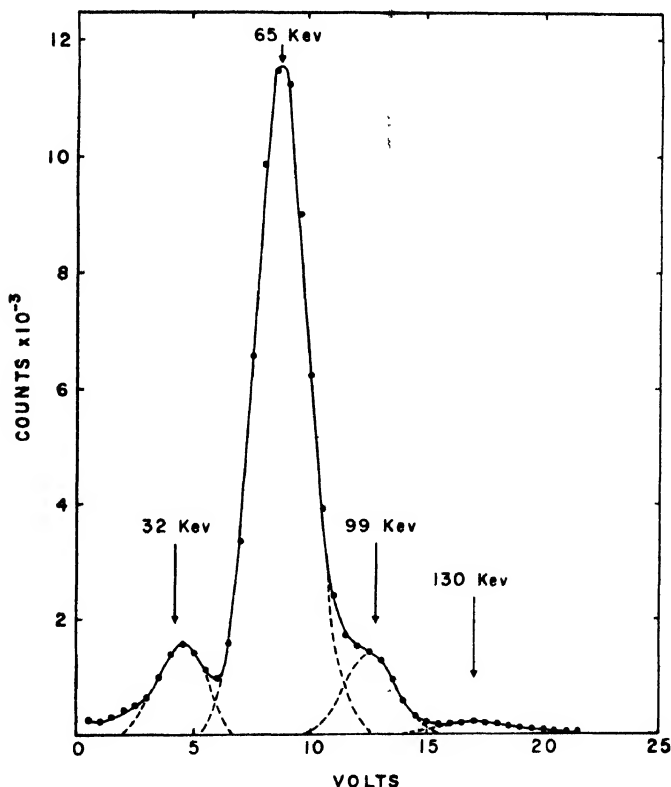


Fig. 3. Energy spectrum of gamma rays from Au^{195} .

transition. The 100 and 130 kev gamma rays are also observed in the proton and alpha-particle bombardment of natural Pt and assigned to Pt^{195} by Stelson and McGowan (1955). Gamma rays of energies 29, 98, 128, 210 and 240 kev have been observed in the electric excitation of Pt^{195} by Bernstein and Lewis (1955). The relative intensities of the unconverted quantum radiations can be

estimated from the areas under the photopeaks of figure 2. They are 1, 12, and 2 in order of ascending energy. In making this estimate, corrections were applied for variation of the detection efficiency of the crystal with energy and the similar variation of the photopeak to Compton cross-section ratio.

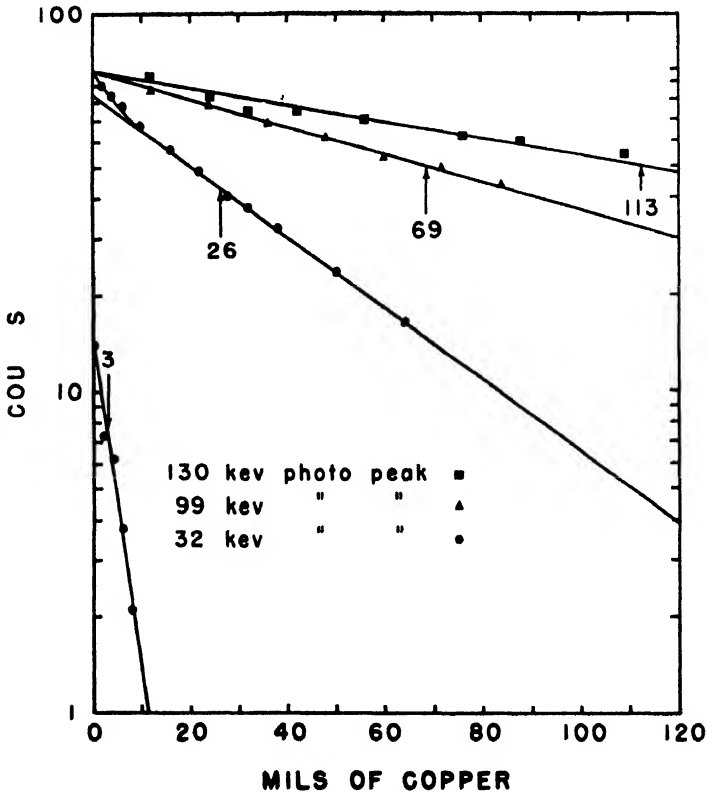


Fig. 4. Absorption of photopeaks of figure 3 in copper. Arrows indicate half-value thickness in mils of copper. Values 113, 69, 26, and 3 mils of copper correspond to gamma rays of 130, 99, 65, and 31 keV.

Coincidences between the gamma rays were measured, and the results are shown in figure 5. With one channel fixed at 99 keV., the data of figure 5A were obtained showing no detectable coincidences between the 99 keV gamma ray and any radiation of energy 130 keV. This shows that 130 keV gamma ray is

a cross-over transition of the 31 and 99 kev gamma-ray cascade. With one channel fixed at the x-ray peak, the data of figure 5B were obtained, showing coincidences between the x-rays and the three gamma rays.

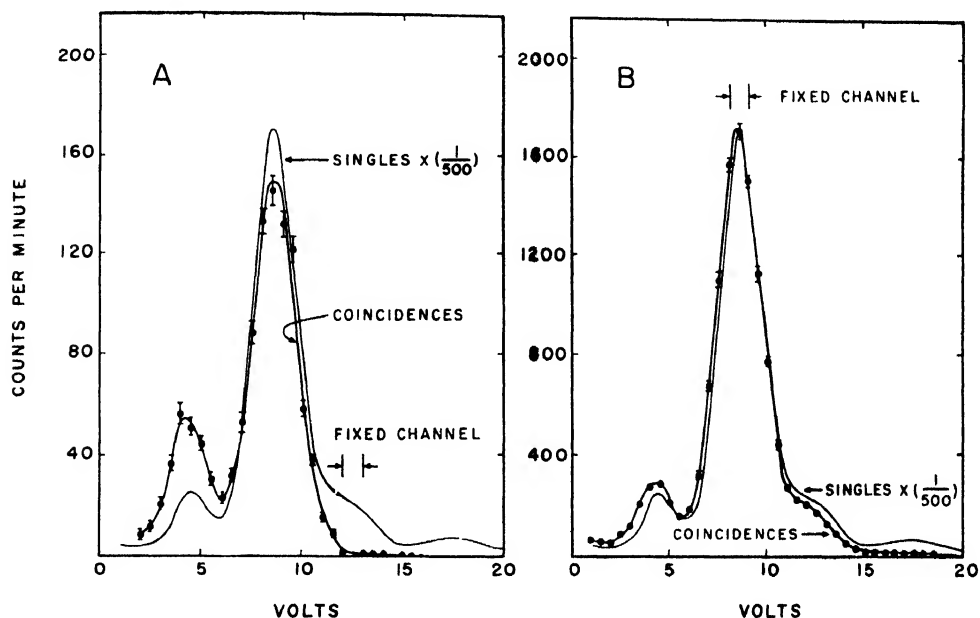


Fig. 5. (A) Gamma-gamma coincidences with 99 kev gamma ray.
(B) Gamma-gamma coincidences with 65 kev x-rays.

The total conversion coefficients of the various gamma rays have been previously measured, and when they are combined with the relative intensities of the presently measured unconverted quantum radiations, the transition probabilities of Table I are obtained. From a consideration of these transition intensities, it can be concluded that the 31 kev gamma ray is the first emitted of the cascade.

TABLE I

Energy, kev	Unconverted quantum intensities	a_T	Reference	Relative transi- tion probability
31	1	7.3	De-Shalit	8.3
99	12	9 3.15	De-Shalit Steffen	120 49.8
130	2	1.28	Steffen	4.8

Depending upon which of the two values of the conversion coefficient of the 99 kev gamma ray is employed, the percent of capture transitions terminating at the

130 kev level is calculated to be 11 or 23. Previously reported values are 10 and 35 percent.

The decay scheme of Au^{195} is shown in figure 6. The ground state spin $1/2$ of Pt^{195} has been measured by Jaeckel and Kopfermann (1936) in agreement with

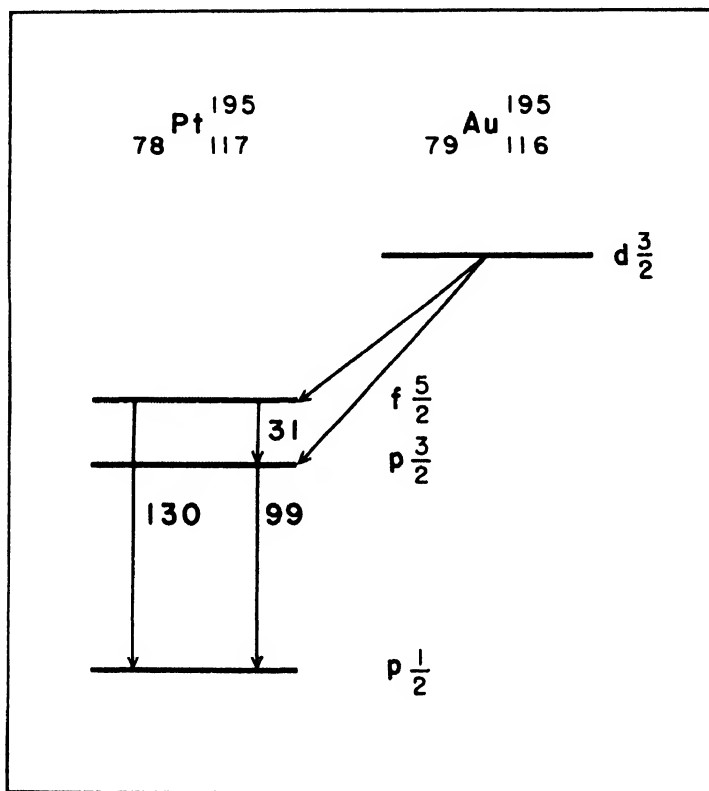


Fig. 6. Decay scheme for Au^{195} .

the orbital $p_{\frac{1}{2}}$ as indicated by the shell model. The data of Cork *et al* (1954) on the conversion in K- and L- shells for 31 and 99 kev gamma rays favour an assignment of M1 for both the gamma rays. The shell model indications of orbitals $p_{3/2}$ and $f_{5/2}$ to 99 and 130 kev levels agree with these assignments. With these assignments the 130 kev gamma-ray becomes E2 in nature. The measured conversion coefficients for this gamma ray (referred to in Table I) are not totally inconsistent with this classification. A spin of $d_{3/2}$ could be assigned to the ground state of Au^{195} on the shell model considerations.

The foregoing results are to be compared with those obtained by Cork *et al* (1954) and Potnis *et al* (1956) who have investigated energy levels in Pt^{195} by

way of the decay of Pt^{195m} . In the work of Cork *et al*, the cross-over transition was not reported, whereas it was observed by the second group of authors. Their work is confirmed by the present investigation.

ACKNOWLEDGMENTS

The author wishes to acknowledge the keen interest of Dr. W. F. G. Swann, Director of the Bartol Research Foundation, and Dr. C. E. Mandeville for helpful suggestions, and to thank Dr. W. B. Keighton for chemical purification, to Mrs. Patterson and Mrs. Brandt for making drawings, and to Mrs. Rodgers for typing the manuscript. The author's visit to the United States was made possible by a scholarship granted by Bartol Research Foundation.

REFERENCES

- Bernstein, E. M. and Lewis, H. W. 1955, *Phys. Rev.* **100**, 1345.
Cork *et al*, 1954, *Phys. Rev.* **94**, 1218.
De-Shalit, Huber and Schneider, 1952, *Helv. Phys. Acta*, **25**, 279.
Gillon *et al*, 1954, *Phys. Rev.* **93**, 124.
Jaeckel, B., and Kopfermann, 1936, *Zeits. f. Physik*, **99**, 492.
Potnis, Mandeville, and Burlow, 1956, *Phys. Rev.* **101**, 753.
Steffen, Huber, and Humbel, 1949, *Helv. Phys. Acta*, **22**, 167.
Steffen, R. M., and Roberts, D. M., 1951, *Phys. Rev.*, **82**, 332.
Steffen, R. M., 1953, *Phys. Rev.* **89**, 665.
Stelson P. M. and McGowan, F. K., 1955, *Phys. Rev.* **99**, 112.

ON THE RAMAN SPECTRA OF 1,1-DICHLOROETHANE AND 1,1,1-TRICHLOROETHANE IN THE VAPOUR STATE*

MONOMOCHAN MAZUMDER

OPTICS DEPARTMENT, INDIAN ASSOCIATION FOR THE CULTIVATION OF SCIENCE
JADAVPUR, CALCUTTA-32.

(Received for publication June 12, 1956)

Plate IX

ABSTRACT. The Raman spectra of 1,1-dichloroethane and 1,1,1-trichloroethane in the vapour state at 100°C and 125°C respectively have been studied and compared with those of the substances in the liquid state at about 30°C and at temperatures nearly equal to those of the vapours mentioned above. It is observed that there is no appreciable change in the spectra with the change of temperature of the liquids, but as soon as the liquids are transformed into the vapour phase, the frequency-shifts of some prominent lines increase and a few prominent Raman lines become much broader. These changes have been explained on the assumption that one half of the molecule in each case rotates freely about the C-C bond in the vapour state and probably the frequencies of the corresponding vibrations in the molecules in which the two halves are mutually orientated in such a way that the C-H bond in the two halves are in the same plane (eclipsed), may be slightly different from those due to the molecules in which one of the C-H bonds is rotated from the orientation mentioned above through 60° about the C-C bond (staggered). It is also pointed out that in the liquid phase intermolecular field prevents such free rotation about the C-C bond.

INTRODUCTION

The Raman spectra of 1, 1-dichloroethane and 1, 1, 1-trichloroethane both in the liquid and solid states have been investigated by Bishui (1948) and Biswas (1953) respectively. In the case of 1, 1-dichloroethane Bishui (1948) observed that there are too many Raman lines in the spectrum to be produced by the fundamental modes of the single molecule. It was pointed out that as there is hardly any probability of the existence of two rotational isomers, namely *trans* and *gauche*, in such a liquid, the extra lines appear because of the formation of some associated groups of molecules due to the influence of intermolecular field between neighbouring molecules of the liquid. While discussing the Raman spectra of 1,1,1- and 1,1,2-trichloroethane in the liquid and solid states Biswas (1953) pointed out that the influence of intermolecular field in the liquid and solid states on C—Cl stretching oscillations could be determined only by studying

* Communicated by Prof. S. C. Sirkar.

the Raman spectra of those substances in the vapour state. It was observed previously (Mazumder, 1953) that in the case of 1,2-dichloroethane, the ratio of the intensities of the lines 654 cm^{-1} and 755 cm^{-1} changes abruptly with the change from liquid to vapour state and also with the change from liquid to solid state. No such changes take place with the change from liquid to solid state in the case of 1,1-dichloroethane and 1,1,1-trichloroethane. It was not known however, whether any change in the relative intensities of any of the lines takes place with vaporization of the liquids. The Raman spectra of the substance in the vapour state have, therefore, been investigated and the results have been discussed in the present paper.

EXPERIMENTAL

The experimental arrangement was similar to that used by the author in his previous investigation (Mazumder, 1955). The liquids 1, 1-dichloroethane and 1, 1, 1-trichloroethane were distilled several times in vacuum before being introduced in the thick-walled Wood's tube of special design (Mazumder, 1954). The temperature of the tube containing requisite quantity of liquid was raised to about 100°C in the case of 1, 1-dichloroethane (B.P. 57.3°C) and 125°C in the case of 1,1,1-trichloroethane (B.P. 74°C). The pressure developed inside the Wood's tube at those temperatures of the vapours of the corresponding liquids was about 3.5 atmospheres in each case.

The Adam Hilger two-prism spectrograph which was used by the author in previous experiments was used in the present experiment also. Ilford Zenith plates were used to photograph the spectra. In both the cases the Raman spectra of the liquids at room temperature and at temperatures nearly equal to those of the vapours were also photographed for comparison. Three spectrograms were obtained for the vapour state in each case in order to avoid spurious results. Microphotometric records of all the spectrograms were taken with a Kipp and Zonen type self-recording microphotometer.

RESULTS AND DISCUSSION

The Raman spectra of 1, 1-dichloroethane in the vapour state at 100°C and in the liquid state at 100°C and 30°C are reproduced in figures 1(a), 1(b) and 1(c) of Plate IX. The spectra for 1,1,1-trichloroethane in the vapour state at 125°C and in the liquid state at 150°C and 30°C respectively are reproduced in figures 2(a), 2(b) and 2(c) in the same plate. The frequency-shifts are given in Tables I and II. Microphotometric records of the Raman lines of both the substances having frequency-shifts in the range 200 cm^{-1} to 800 cm^{-1} are reproduced in figures 3 and 4.

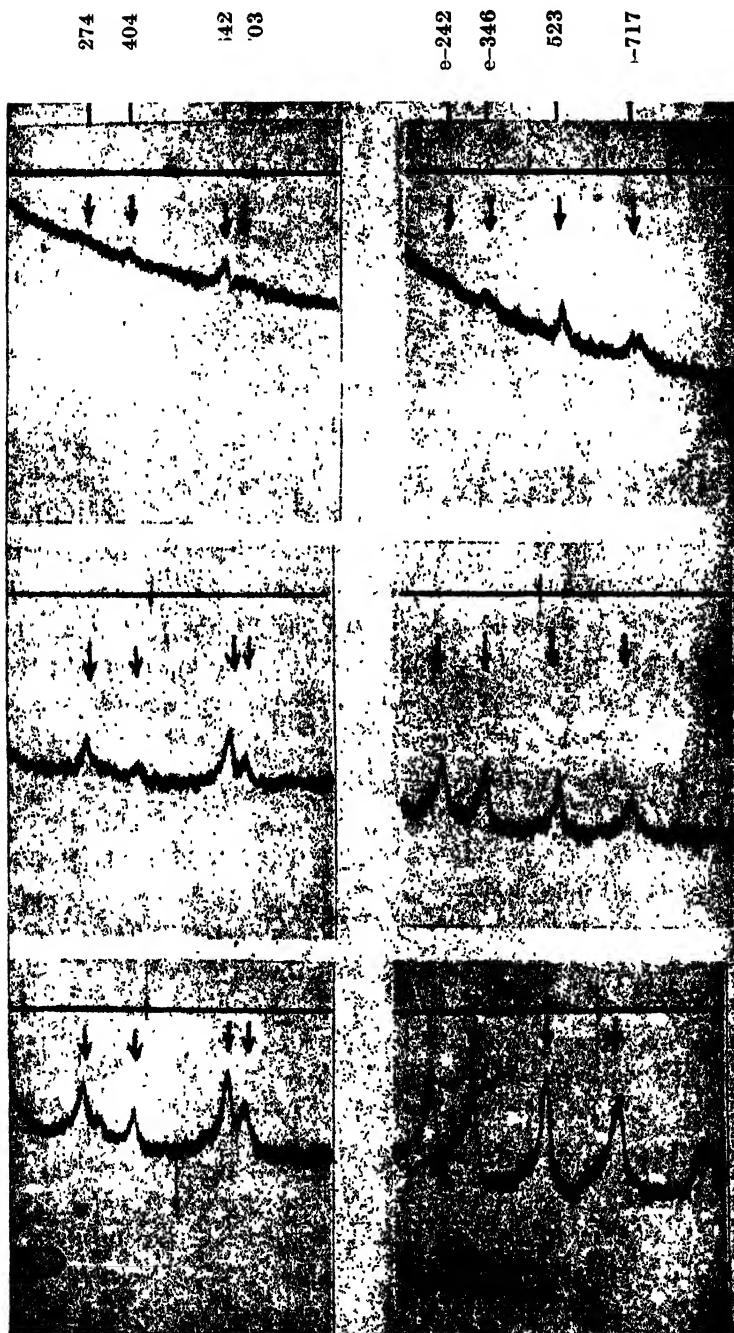
It can be seen from Table I that when 1, 1-dichloroethane in the liquid state is heated from 30°C to 100°C , its Raman spectrum does not change appreciably.

274
404
142
03

Vapour
at 100°C

Liquid
at 100°C

Liquid
at 30°C



Vapour
at 125°C

Liquid
at 150°C

Liquid
at 30°C

Microphotometric records of Raman spectra.

Fig. 3. 1,1-dichloroethane

Fig. 4. 1,1,1-trichloroethane

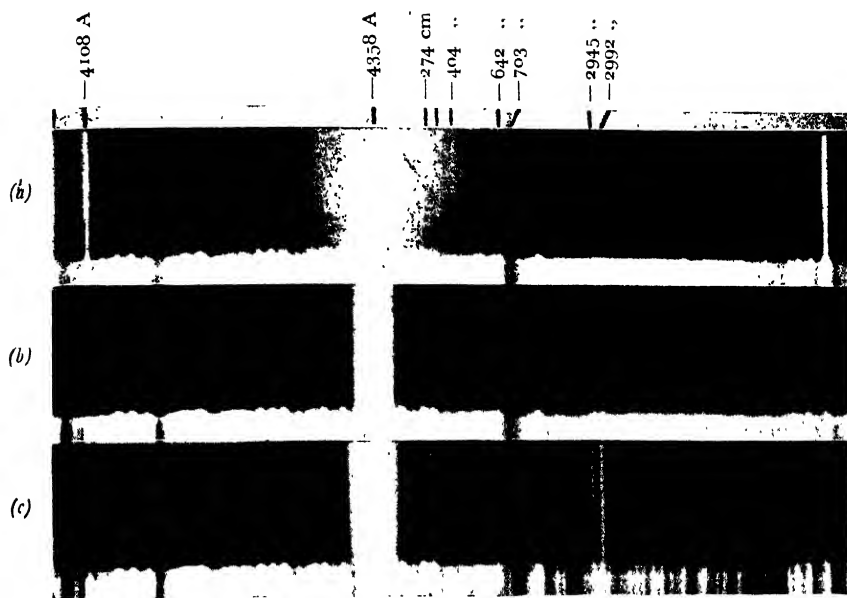


Fig. 1.

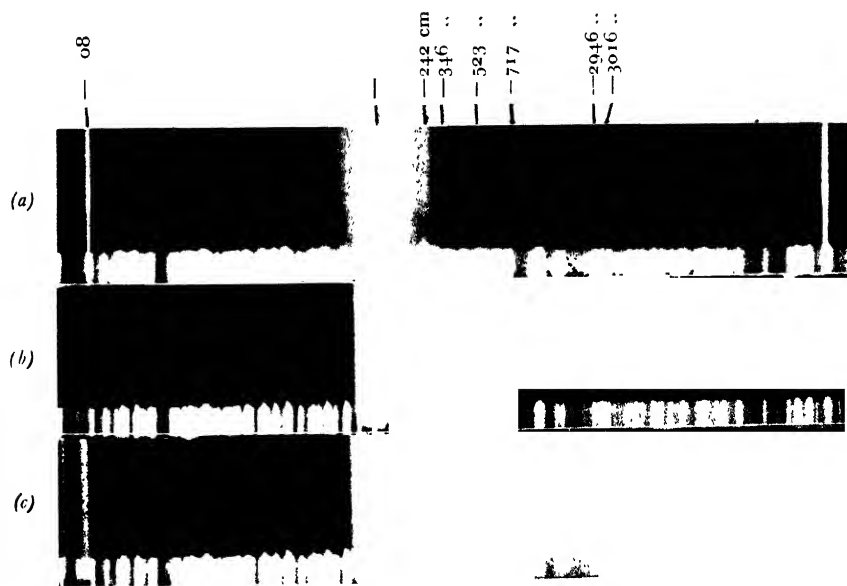


Fig. 2.

Raman spectra.

Fig. 1. 1, 1-dichloroethane

(a) Vapour at 100°C

(b) Liquid at 100°C

(c) " " 30°C

Fig. 2. 1, 1, 1-trichloroethane

(a) Vapour at 125°C

(b) Liquid at 150°C

(c) " " 30°C

The Raman spectrum, however, undergoes considerable changes with change from the liquid state at 100°C to the vapour phase at 100°C. The lines 320 cm^{-1} and 690 cm^{-1} shift respectively to 325 cm^{-1} and 703 cm^{-1} and the first line becomes much stronger. The lines 274, 325 and 703 cm^{-1} due to the vapour are much broader than the corresponding lines due to the liquid phase. Also the lines 2935 and 2987 cm^{-1} due to C—H stretching vibrations shift respectively to 2945 and 2992 cm^{-1} and the latter line becomes broader in the spectrum due to the vapour.

Similar changes are also found in the spectrum due to 1, 1, 1-trichloroethane with the change from liquid to vapour phase. The lines 242, 346, 712 and

TABLE I
1, 1-Dichloroethane.
 $\Delta\nu$ in cm^{-1}

Liquid state		Vapour state
at 30°C	at 100°C	at 100°C
274 (5) \pm e, k	274 (4) \pm e, k	274 (2b)
320 (1) e, k	320 ($\frac{1}{2}$) e, k	325 (1b)
404 (4) \pm e, k	404 (3) \pm e, k	404 (3)
640 (8) e, k	640 (6) e, k	642 (5)
690 (4) e, k	690 (2) e, k	703 (2b)
975 (2) e, k	975 (1) e, k	975 (1)
1054 ($\frac{1}{2}$) o, k	1054 (1) e, k	1071 (1)
1086 (2) e, k	1086 ($\frac{1}{2}$) e, k	
1270 (1) e, k		
1350 (0) e, k		
1440 (3) e, k	1440 ($\frac{1}{2}$) o, k	
2935 (7) e, k	2935 (5) e, k	2945 (5)
2987 (7b) e, k	2987 (5b) e, k	2992 (2b)
3060 (1) e	3061 (1)	

3007 cm^{-1} become broader, while the lines 523 and 2937 cm^{-1} remain as sharp in the case of the vapour as in the spectrum due to the liquid. The lines 712, 2937 and 3007 cm^{-1} shift respectively to 717, 2946 and 3016 cm^{-1} .

The lines which become broader in the vapour state of the two compounds are either due to antisymmetric oscillations or due to bending vibrations. The broadening of these lines in the spectra observed with vaporization of these

TABLE II

1, 1, 1-Trichloroethane

 $\Delta\nu$ in cm^{-1}

Liquid state		Vapour state
at 30°C	at 150°C	at 125°C
242 (7) \pm e, k, i	242 (4)	242 (1b)
346 (8) \pm e, k	346 (5)	346 (2b)
523 (10) \pm e, k	523 (6)	523 (4)
712 (5b) e, k	712 (3b)	717 (1b)
1070 (1) e, k	1070 (0)	
1084 (2) e, k	1984 (0)	
1186 (0) k		
1360 (1) e	1360 (0)	
1425 (1) e, k	1425 (0)	
1448 (2) e, k	1448 (0)	
2937 (6) e, k, i	2937 (3)	2946 (4)
3007 (3b) e, k	3007 (1b)	3016 (1b)

two substances clearly indicates that it is produced by the rotation of one half of the molecules about the C-C bond. Probably, the frequencies of the corresponding vibrations in the molecules in which the two halves are mutually orientated in such a way that the C-H bonds in the two halves are in the same plane (eclipsed), may be slightly different from those of the molecules in which one of the C-H bonds is rotated from the orientation mentioned above through 60° about the C-C bond (staggered). This difference seems to be larger in the case of 1, 1-dichloroethane than in the case of 1, 1, 1-trichloroethane probably because of the symmetric distribution of the Cl atoms about the C-C bond in the latter case. When one half of the molecule rotates freely about the C-C bond, the frequency changes continuously between the two limits and a broad band is produced. It is also expected theoretically that the symmetrical oscillations involving C-C stretching and C-Cl stretching will not be affected very much by such rotation of the two halves. If there would be a mixture of two forms of the molecules in the vapour state with the different mutual orientations of the two halves of the molecules as mentioned above, each of the lines due to the liquids mentioned above would be split up into two lines in the vapour state. But actually, a broad band instead of two sharp lines is observed in each case in the vapour state in place of such a single line.

The results mentioned above thus furnish evidence for the existence of free rotation of one half of the molecule about the C-C bond in the vapour state of the two compounds studied in the present investigation. In the case of disubstituted ethanes in which the substituents are present in both the halves of the molecules no such free rotation has been observed. But the difference in the frequencies of the C-Cl symmetric oscillations for two configurations of the molecules was found to be much greater (Mizushima *et al*, 1938) than that in the case of the molecules studied in the present investigations. This difference is evidently due to the influence of intermolecular field in the liquid state on the substituents as pointed out earlier (Mazumder, 1953). In the liquid state the two compounds studied in the present investigation give sharp lines. This shows that there is no such freedom of rotation of one half of the molecules probably due to the fact that the intermolecular field acting on one half of the molecule containing the substituent produces a single stable configuration of the molecule.

Table I shows that the two lines 1054 cm^{-1} and 1086 cm^{-1} coalesce to form a line at 1072 cm^{-1} when 1, 1-dichloroethane is vaporized. One of these two lines may be due to the associated groups of molecules which may be present in the liquid state. This probably confirms the suggestion made by Bishui (1948) that in the liquid state some of the molecules may be associated with each other. The shift of the line 690 cm^{-1} with the change from liquid to solid (Bishui, 1948) and from liquid to vapour state may be due to strengthening of the virtual bond in the solid state and its dissociation in the vapour state. In the case of 1,1, 1-trichloroethane also the line 712 cm^{-1} shifts slightly with the changes of state in the same way as the line 690 cm^{-1} in the case of 1, 1-dichloroethane and this shift may be due to the same reason in both the cases.

ACKNOWLEDGMENT

The author is indebted to Professor S. C. Sirkar, D.Sc., F.N.I., for his kind interest and constant guidance throughout the progress of the work.

REFERENCES

- Bishui, B. M., 1948, *Ind. J. Phys.*, **22**, 319.
Biswas, D. C., 1953, *Ind. J. Phys.*, **27**, 379.
Mazumder, M., 1953, *Ind. J. Phys.*, **27**, 406.
„ 1954, *Ind. J. Phys.*, **28**, 297.
„ 1955, *Ind. J. Phys.*, **29**, 361.
Mizushima, S., and Morino, Y., 1938, *Proc. Ind. Acad. Sc.*, **A.8**, 315.

CIRCULAR ARC ANTENNAS

S. BALARAM RAO

COLLEGE OF ENGINEERING, GUINDY, MADRAS.

(Received for publication December 1, 1955; after revision March 14, 1956)

ABSTRACT. This paper deals with the general problem of a radiating element bent in the form of an arc of a circle assuming a sinusoidal current-distribution along the length of the arc. The far field in the plane of an isolated circular arc current-filament is derived. This leads to the derivation of the radiation fields of two types of symmetrical composite arc antennas in the horizontal plane. The vertical radiation patterns of the composite types of arc antennas are also derived. In the experimental section of the paper, the horizontal patterns of the composite types of antennas are verified for cases where the radius of the arc is small compared to the wave length.

SECTION I

INTRODUCTION

In this paper an attempt is made to determine the radiation fields of circular arc antennas. The present investigation appears to be the first general one into the problem of circular arc antennas.

The previous work on circular antennas has been restricted to closed circular loops and open circular loops. While there have been quite a few references to circular loop antennas in literature (Sherman, 1944 ; Moullin, 1946 ; Foster, 1944 ; Glinsky, 1947), the most general ones appear to be those of Sherman and of Glinsky. Sherman has investigated closed and open circular loops whose circumferences are an integral number of wavelengths, assuming a sinusoidal distribution of current. He has deduced the far field in the plane of the loops and along the axes of the loops. Glinsky takes into account the attenuation of the current along the loop in deriving the radiation field of the loop, the circumference being of the order of half a wavelength.

By a circular arc antenna is meant a radiating element bent in the form of an arc of a circle. The radiation field due to such an arc in the plane containing the arc is derived. Neither the length of the arc nor the angle subtended by it at the centre is restricted.

These results lead to the derivation of the horizontal radiation patterns of two symmetrical composite circular arc antennas.

The radiation pattern of the composite antennas in a vertical plane containing the line of symmetry of the antennas, is also derived.

The theoretical radiation patterns in the horizontal plane of the composite types of antennas are verified experimentally for a few particular cases where the radius of the arc is small compared to the wavelength. The horizontal radiation pattern of a horizontal half-wave dipole has also been obtained to check the degree of agreement between the observed and theoretical patterns under the experimental conditions. The experimental observations are in fair agreement with the theoretical patterns.

In the last section of the paper, a short account of the method of evaluation of the integrals concerned is given. The M. K. S. system of units is used.

SECTION II

THE BASIC CIRCULAR ARC ANTENNA

In figure 1, AB is an arc of a circle, centre O , radius a and subtending an angle β at O . OA is along OX . The arc AB is the antenna and is fed at A by some method, so that assuming a sinusoidal distribution of current along the arc, at B , there is a current node. The positive direction of current at an intermediate point, Q , is for convenience, assumed to be anti clockwise. Our problem is to evaluate the radiation field at P , a distant point in the plane containing the arc AB . Since P is a very distant point, QP and OP can be considered parallel.

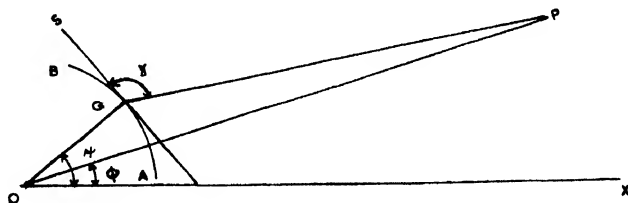


Fig. 1. The basic circular arc antenna.

The current I at Q on AB in terms of the maximum value I_m of the current at a current antinode is given by

$$\begin{aligned} I &= I_m \sin \left(\frac{2\pi a \beta}{\lambda} - \frac{2\pi a \psi}{\lambda} \right) \\ &= I_m \sin (A\beta - A\psi) \end{aligned} \quad \dots (1)$$

where $\psi = \text{angle } AOQ$, $A = \frac{2\pi a}{\lambda}$.

$\lambda = \text{wavelength of the radiation in free space and}$
 $\beta = \text{angle } AOB$

The magnetic field at P due to a small element of length $ad\psi$ of the antenna at Q is given by

$$dH = j \frac{Iad\psi}{2\lambda z} \sin \gamma e^{j\omega(t-z/c)} \quad \dots (2)$$

where γ = angle SQP , SQ being the tangent at Q to the arc
 $z = PQ$
 c = velocity of electromagnetic radiation in free space
 ω = angular frequency corresponding to the wavelength λ
 ϕ = angle XOP
 t = time
 $j = \sqrt{-1}$

From the geometry of figure 1, noting that $OP \gg AB$

$$\gamma = 90^\circ + (\psi - \phi) \quad \dots (3)$$

$$z = z_0 - a \cos(\psi - \phi) \quad \dots (4)$$

where $z_0 = OP$.

In equation (2) the z in the denominator can be substituted directly by z , while the more refined substitution of equation (4) should be carried out in the phase term in accordance with the practice in radiation theory.

Carrying out the substitution of equations (3) and (4) in (2) we have

$$dH = j \frac{I_m a}{2\lambda z_0} \sin(A\beta - A\psi) \cos(\psi - \phi) e^{j\omega \left[t - \frac{z_0}{c} + \frac{a}{c} \cos(\psi - \phi) \right]} d\psi \quad \dots (5)$$

To obtain the field at P due to the entire antenna we have to integrate the expression between the limits O and β of ψ . Calling the total field H_1 we have

$$H_1 = \int_0^\beta dH$$

$$= \int_0^\beta j \frac{I_m a}{2\lambda z_0} \sin(A\beta - A\psi) \cos(\psi - \phi) e^{j\omega \left[t - \frac{z_0}{c} + \frac{a}{c} \cos(\psi - \phi) \right]} d\psi \quad \dots (6)$$

The evaluation of the integral is rather involved and the method of evaluation is given in the final section.

The value of the field H_1 is obtained as

$$H_1 = j \frac{a I_m}{2\lambda z_0} \left\{ \sum_{n=0}^{n=\infty} j^n \left[\frac{J_n(A)}{A^n} - \frac{J_{n+2}(A)}{(n+1)^2} \right] \right.$$

$$\times [A \cos(n+1)(\beta - \phi) - A \cos A\beta \cos(n+1)\phi - (n+1) \sin A\beta \sin(n+1)\phi]$$

$$\left. + j \frac{J_1(A)}{A} (1 - \cos A\beta) \right\} e^{j\omega(t - z_0/c)} \quad \dots (7)$$

where $j = \sqrt{-1}$

n = any positive integer including zero,

$J_1(A)$, $J_n(A)$ etc are Bessel's function of argument A and order 1, n , etc.

In figure 2, we have the circular arc radiator which can be considered as the complement of the antenna of figure 1. It carries a current that is the "return" for that of figure 1. $A' B'$ is the antenna fed from A' . The nomenclature of the different points in figure 2 is the same as in figure 1 except for the primes. The current at an intermediate point Q' on the antenna is given by equation, (1), the positive direction being anti-clockwise along the arc. The distant point at which the field is considered is P as before.

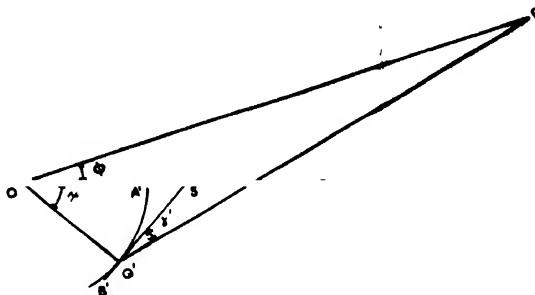


Fig. 2. The complementary basic circular arc antenna.

From the geometry of the figure we have

$$\begin{aligned}\gamma' &= 90^\circ - (\psi + \phi) \\ z' &= z_0 - a \cos (\psi + \phi)\end{aligned}$$

The field at P due to the entire antenna $A' B'$ is given by

$$H_z = \int_0^\beta j \frac{a I_m}{2 \lambda z_0} \cos (\psi + \phi) \sin (A \beta - A \psi) e^{j \omega \left[t - \frac{z_0}{c} + \frac{a}{c} \cos (\phi + \psi) \right]} d \psi$$

On evaluating the integral we have,

$$\begin{aligned}H_z &= j \frac{a I_m}{2 \lambda z_0} \left\{ \sum_{n=0}^{\infty} j^n \frac{[J_n(A) - J_{n+2}(A)]}{A^2 - (n+1)^2} [A \cos (n+1)(\phi + \beta) \right. \\ &\quad \left. - A \cos A \beta \cos (n+1)\phi + (n+1) \sin A \beta \sin (n+1)\phi] \right. \\ &\quad \left. + j \frac{J_1(A)}{A} (1 - \cos A \beta) \right\} e^{j \omega (t - z_0/c)} \quad \dots \quad (8)\end{aligned}$$

In the equations (7) and (8), some terms become indeterminate when $A = (m+1)$. These can be evaluated using the usual methods of evaluating indeterminate forms.

SECTION III

HORIZONTAL RADIATION PATTERN OF THE COMPOSITE CIRCULAR ARC ANTENNA—TYPE I

This type of antenna is illustrated in figure 3. The radiation pattern in the plane containing the antenna (referred to as the horizontal plane) can now be deduced from the equations (7) and (8).

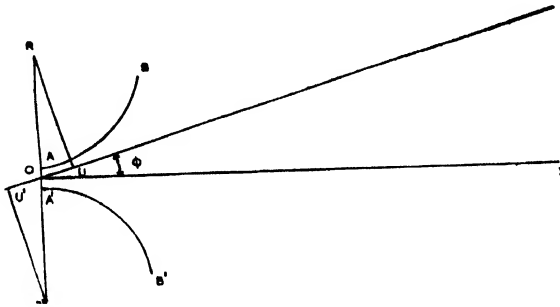


Fig. 3. The composite circular arc antenna—Type I. (For the horizontal pattern)

AB and $A'B'$ are the antenna elements. The transmission line feeds the antenna at A and A' . (This feed arrangement means that if at any point in AB , the instantaneous direction of current is counter-clockwise, then in $A'B'$ at the corresponding point the direction is also counter-clockwise. (See section II.). R and R' are the centres of the arcs. O is the centre of $R'R$, and is the origin.

The radiation pattern of AB is known with respect to its centre R , taking RO as the initial line. The required change in the azimuth of P , to make equation (7) apply to this case, is obtained by substituting $90^\circ + \phi$ for ϕ in equation (7). P is the point at which the field is being considered. The necessary change in the phase term is effected by expressing RP in terms of OP and other related parameters. From the geometry of the figure, noting that P is a distant point, we have

$$RP = z_0 - a \sin \phi \quad \dots \quad (9)$$

$$\text{since } RP = PU = OP - OU = z_0 - a \sin \phi.$$

The z_0 of equation (7) has to be replaced by $z_0 - a \sin \phi$ (in the phase term only) and ϕ of equation (7) replaced by $90^\circ + \phi$. The z_0 of equation (7) in the amplitude term need not be changed in conformity with the practice in antenna theory since the effect on the amplitude is relatively insignificant. Carrying out these

substitutions and the necessary simplifications we have, for the field at P due to AB ,

$$\begin{aligned}
 H_1 = j \frac{aI_m}{2\lambda z_0} e^{j\omega(t - \frac{z_0}{c} + \frac{a}{c} \sin \phi)} \left\{ j \frac{J_1(A)}{A} (1 - \cos A\beta) \right. \\
 + \sum_{q=1,3,5 \dots} j^{2q+1} \frac{[J_q(A) - J_{q+2}(A)]}{A^2 - (q+1)^2} [A \sin (q+1)(\beta - \phi) \\
 - A \cos A\beta \cos (q+1)\phi - (q+1) \sin A\beta \sin (q+1)\phi] \\
 + \sum_{p=0,2,4 \dots} j^{2p} \frac{[J_p(A) - J_{p+2}(A)]}{A^2 - (p+1)^2} [A \sin (p+1)(\beta - \phi) + A \cos A\beta \sin (p+1)\phi \\
 \left. - (p+1) \sin A\beta \cos (p+1)\phi] \right\} \dots \quad (10)
 \end{aligned}$$

where

q = any positive odd integer

p = any positive even integer

$J_p(A)$, $J_q(A)$ etc. are Bessel's functions.

In a similar fashion the field due to $A'B'$ in the juxta-position given in figure 2, can be obtained from equation (8) by substituting $-(90^\circ - \phi)$ for ϕ and $z_0 + a \sin \phi$ for z_0 in that equation. Carrying out these substitutions and the necessary simplifications, we have for the field at P due to $A'B'$,

$$\begin{aligned}
 H_2 = j \frac{aI_m}{2\lambda z_0} e^{j\omega(t - \frac{z_0}{c} - \frac{a}{c} \sin \phi)} \left\{ j \frac{J_1(A)}{A} (1 - \cos A\beta) \right. \\
 + \sum_{q=1,3 \dots} j^{2q+1} \frac{[J_q(A) - J_{q+2}(A)]}{A^2 - (q+1)^2} [A \cos (q+1)(\phi + \beta) - A \cos A\beta \cos (q+1)\phi \\
 - (q+1) \sin A\beta \sin (q+1)\phi] \\
 + \sum_{p=0,2 \dots} j^{2p} \frac{[J_p(A) - J_{p+2}(A)]}{A^2 - (p+1)^2} [A \sin (p+1)(\phi + \beta) - A \cos A\beta \sin (p+1)\phi \\
 \left. - (p+1) \sin A\beta \cos (p+1)\phi] \right\} \dots \quad (11)
 \end{aligned}$$

The total field at P is given by the addition of H_1 and H_2 and we have after some simplification

$$H = H_1 + H_2$$

$$\begin{aligned}
 = j \frac{aI_m}{\lambda z_0} \left\{ j \frac{J_1(A)}{A} (1 - \cos A\beta) \cos (A \sin \phi) - \sum_{q=1,3,5} \frac{[J_q(A) - J_{q+2}(A)]}{A^2 - (q+1)^2} \right. \\
 \times [jA \cos (A \sin \phi) \cos (q+1)\phi \{ \cos (q+1)\beta - \cos A\beta \} \\
 + \sin (A \sin \phi) \sin (q+1)\phi \{ (q+1) \sin A\beta - A \sin (q+1)\beta \}] \\
 + \sum_{p=0,2,1 \dots} \frac{[J_p(A) - J_{p+2}(A)]}{A^2 - (p+1)^2} [jA \sin (A \sin \phi) \sin (p+1)\phi \{ \cos A\beta - \cos (p+1)\beta \} \\
 \left. + \cos (p+1)\phi \cos (A \sin \phi) \{ A \sin (p+1)\beta - (p+1) \sin A\beta \}] \right\} e^{j\omega(t - z_0/c)} \dots \quad (12)
 \end{aligned}$$

The symmetry of the pattern as defined by equation (12) about the axis OX is apparent on substitution $-\phi$ for ϕ when the value of H remains unaltered both with regard to the amplitude and phase. On substituting $180^\circ - \phi$ for ϕ , the quadrature terms remain unaltered while the in-phase terms reverse in sign. This does not alter the amplitude of the field which is the square root of the sum of the squares of the quadrature terms and the in-phase terms.

SECTION IV

HORIZONTAL RADIATION PATTERN OF COMPOSITE ARC ANTENNA—TYPE II

This type of the arc antenna is illustrated in figure 4 and is made up of the two basic types. The transmission line feeds at A and A' . The positive direction of current at any two corresponding points of the antenna have already been mentioned in the section on the basic circular arc antennas. (See section II).

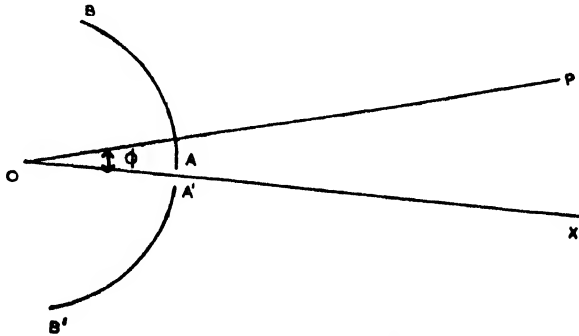


Fig. 4. The composite circular arc antenna—Type II. (For the horizontal pattern)

The field at the distant point P due to AB and $A'B'$ is obtained by adding the fields due to AB and $A'B'$ separately as given by equations (7) and (8).

Performing the addition

$$H = j \frac{aI_m}{\lambda z_0} e^{jw(t - z_0/c)} \left\{ j \frac{J_1^{(A)}}{A} (1 - \cos A\beta) + \sum_{n=0}^{n=\infty} j^n \frac{[J_n^{(A)} - J_{n+2}^{(A)}]}{A^2 - (n+1)^2} A \cos (n+1)\phi [\cos (n+1)\beta - \cos A\beta] \right\} \quad \dots \quad (13)$$

SECTION V

VERTICAL RADIATION PATTERN OF THE COMPOSITE CIRCULAR ARC ANTENNA—TYPE I

Figure 5 illustrates the composite circular arc antenna Type I. The field pattern in the plane XOZ is required, XOZ being referred to as the vertical plane.

Q and Q' are two corresponding points on the two arcs, AB and $A'B'$ of the antenna. The positive directions of current at Q and Q' are from Q to B and from Q' to A' respectively (See section II). The tangents at Q and Q' are inclined to the X axis at angles of ψ on either side of OX .

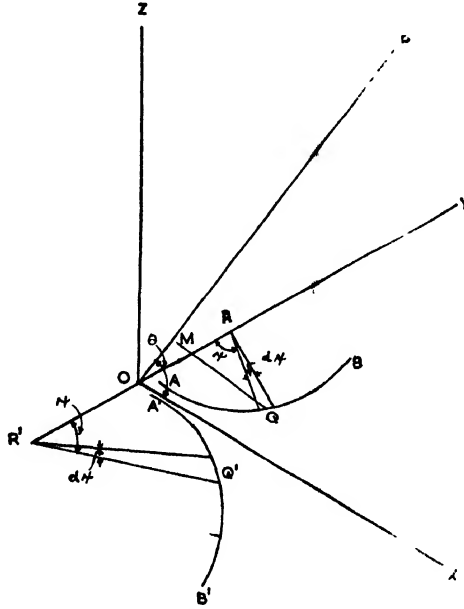


Fig. 5. The composite circular arc antenna—Type I. (For the vortical pattern).

Take small elements of the antenna, $ad\psi$, about Q and Q' and split them into components along OX and OY respectively. Let us write down the elementary fields in the plane XOZ , due to the two components each at Q and Q' of the elements, $ad\psi$, of the antenna.

$$dH_1 = j \frac{I_a}{2\lambda z} \sin \psi e^{j\omega(t-z/c)} d\psi \quad (14)$$

$$dH_2 = j \frac{I_a}{2\lambda z} \cos \psi e^{j\omega(t-z/c)} d\psi \quad (15)$$

$$dH_3 = j \frac{I_a}{2\lambda z} \sin \psi e^{j\omega(t-z/c)} d\psi \quad (16)$$

$$dH_4 = -j \frac{I_a}{2\lambda z} \cos \psi e^{j\omega(t-z/c)} d\psi \quad (17)$$

where dH_1 and dH_3 are respectively the fields due to the components along OY due to the elements of the antenna at Q and Q' .

dH_2 and dH_4 are respectively the fields due to the components along OX due to the elements of the antenna at Q and Q' .

$z = QP = Q'P$, P being the point where the field is being considered.

$\theta = \text{angle } XOP$, the elevation of P .

The other symbols have already been explained.

The value of dH_4 is negative because of the direction of current at Q' relative to that at Q .

The total field at P due to the small elements of the antenna at Q and Q' is given by

$$\begin{aligned} dH &= dH_1 + dH_2 + dH_3 + dH_4 \\ &= j \frac{I_a}{\lambda z} \sin \psi e^{j\omega(t-z/c)} d\psi \end{aligned} \quad \dots (18)$$

$$\text{Now } \omega = QP = OP - OM = z_0 - a \sin \psi \cos \theta \quad \dots (19)$$

where $z_0 = OP$ and QM is perpendicular to OP .

and,

$$I = I_m \sin (A\beta - A\psi) \quad \dots (1)$$

Making these substitutions in (18) we have

$$dH = j \frac{I_m a}{\lambda z_0} \sin (A\beta - A\psi) \sin \psi e^{j\omega(t-z_0/c)} \frac{a}{c} \sin \psi \cos \theta d\psi \quad \dots (20)$$

The total field at P is given by

$$\begin{aligned} H &= \int_0^\beta dH \\ &= \int_0^\beta j \frac{I_m a}{\lambda z_0} \sin (A\beta - A\psi) \sin \psi e^{j\omega(t - \frac{z_0}{c} + \frac{a}{c} \sin \psi \cos \theta)} d\psi \end{aligned}$$

This integration though involved can be performed and we have finally

$$\begin{aligned} H &= j \frac{a I_m}{\lambda z_0} e^{j\omega(t - \frac{z_0}{c})} \left\{ j_1(k)(1 - \cos A\beta) \right. \\ &\quad - \sum_{q=1,3,\dots} j A \frac{[J_q(k) - J_{q+2}(k)]}{A^2 - (q+1)^2} [\cos (q+1)\beta - \cos A\beta] \\ &\quad \left. + \sum_{p=0,2,\dots} \frac{J_p(k) - J_{p+2}(k)}{[A^2 - (p+1)^2]} [A \sin (p+1)\beta - (p+1) \sin A\beta] \right\} \quad \dots (21) \end{aligned}$$

where $k = A \cos \theta$

The angle of elevation θ is involved in the pattern only as the argument of the Bessel function i.e. $A \cos \theta$. Putting $-\theta$ for θ does not alter $A \cos \theta$ and hence the field pattern as defined by equation (21) is symmetrical about OX .

On substituting $180^\circ - \theta$ for θ , $A \cos \theta$ becomes negative. We have as a property of Bessels functions,

$$J_n(k) = J_n(-k), \text{ if } n \text{ is even}$$

$$J_m(k) = -J_n(-k), \text{ if } n \text{ is odd}$$

This means that all the quadrature terms reverse in sign. But this does not alter the amplitude of the field which is the square root of the sum of the squares of the quadrature terms and the in-phase terms respectively.

SECTION VI

VERTICAL RADIATION PATTERN OF THE COMPOSITE CIRCULAR ARC ANTENNA—TYPE II

Figure 6 illustrates the circular arc antenna—type II. The far field at any point P in the plane XOZ is required.

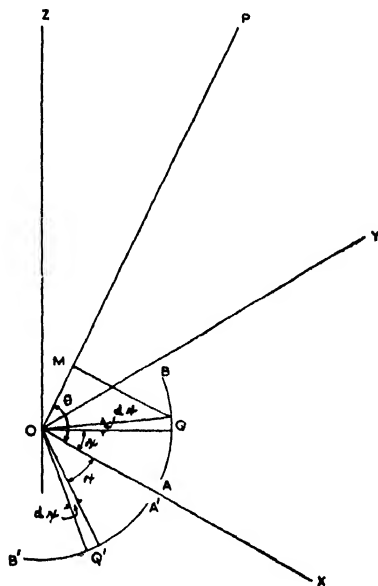


Fig. 6. The composite circular arc antenna—Type II. (For the vertical pattern).!

Following arguments identical with that given in the previous section, the differential field at P due to differential elements $ad\psi$ of the antenna at Q and Q' is given by

$$dH = j \frac{I_m a}{\lambda Z_0} \sin(A\beta - A\psi) \cos \psi e^{j\omega(t - \frac{z_0}{c} + \frac{a}{c} \sin \psi \cos \theta)} d\psi$$

The total field at P due to the entire antenna is given by

$$H = \int_0^\beta dH = \int_0^\beta j \frac{I_m a}{\lambda z_0} \sin(A\beta - A\psi) \cos \psi e^{j\omega(t - \frac{z_0}{c} + \frac{a}{c} \sin \psi \cos \theta)} d\psi$$

On performing the integration we have,

$$H = j \frac{a I_m}{\lambda z_0} e^{j\omega(t - \frac{z_0}{c})} \left\{ j \frac{J_1(k)}{A} (1 - \cos A\beta) + \sum_{n=0}^{n=\infty} j^n \cdot A \cdot \frac{[J_n(k) - J_{n+2}(k)]}{A^2 - (n+1)^2} \left[\cos(n+1)\beta - \cos A\beta \right] \right\} \quad \dots (24)$$

where $k = A \cos \theta$

In a manner identical to that used in the previous section it can be seen that the pattern as defined by (24) is symmetrical as far as the amplitude is concerned about the axes OX and OZ . Equation (24) for the value of $\theta = 0$, will agree with the value of equation (13) for the value $\phi = 0$, as both equations for these two particular values define the field at any point along the axis OX .

SECTION VII

EXPERIMENTAL VERIFICATION

The horizontal relative radiation intensity patterns of the composite types of circular arc antennas have been obtained experimentally in three cases where the values of A were small. The relative intensities at different azimuths are with respect to the intensity at the azimuth equal to 0° . The type and particulars of the antenna under test are given in the figures concerned. Since the patterns are symmetrical, only the values of the relative intensities for one quadrant are given.

The observed relative intensity pattern of a linear half wave dipole has been obtained under the same conditions under which the other patterns were obtained. This was to check, under the conditions of the experiment, the extent of agreement between the observed values of the relative intensities and the theoretical values for an antenna whose radiation pattern can be considered to be well established. This also helped to decide that the observed relative field intensities were reliable and that they had not been vitiated by extraneous factors like haphazard reflections, pick up from the ammeter leads, etc.

The antenna under test was used as the receiving antenna and the relative intensity pattern was obtained by rotating the receiving aerial. The output from the aerial was rectified using a crystal diode and the detector current indicated on a micro-ammeter placed some distance away.

The frequency used was 246 Mc/s. The transmitter was of the U.S. Navy type CWS-52244 with a rated output of 25 watts. The distance between the transmitting aerial and the receiving aerial was about 50 yards. The transmitting aerial was arranged to radiate horizontally polarised waves with a fairly sharp beam to minimise the effects of haphazard reflections.

The figures 7, 8 and 9 give the theoretical and observed relative intensities for the composite circular antennas. The details pertaining to the antenna of each figure are given along with the figure concerned. The theoretical pattern is shown by a continuous line while the observed values are marked by crosses.

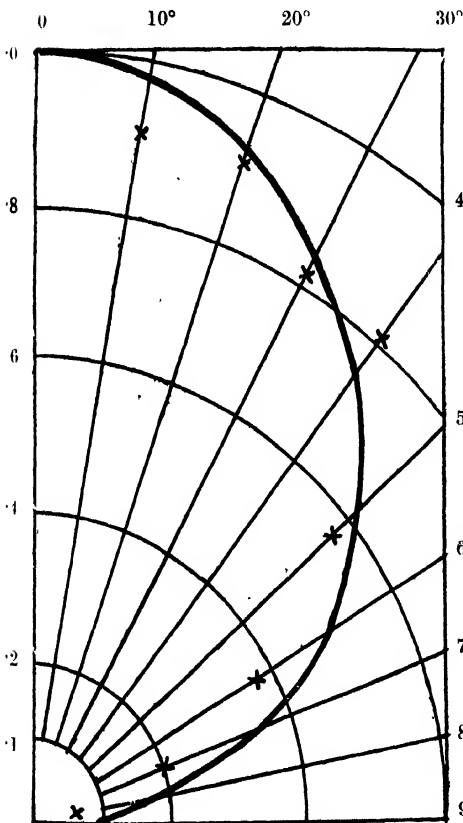


Fig. 7. Horizontal relative radiation pattern of the composite circular arc antenna—Type I. Theoretical and observed values ($A = 0.5$, $\beta = \pi$).

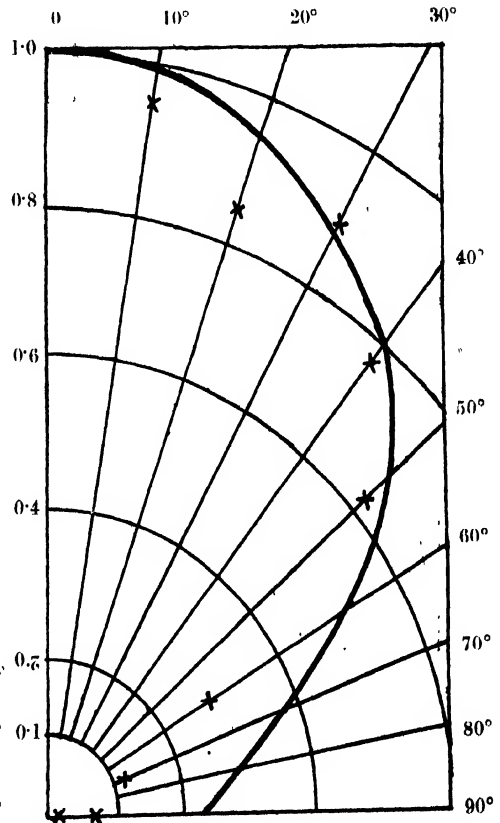


Fig. 8. Horizontal relative radiation pattern of the composite circular arc antenna—Type I: Theoretical and observed values ($A = 1$, $\beta = \pi/2$).

× Observed values
— Theoretical pattern

Figures 10 gives the relative intensity pattern of a half wave dipole and the observed values of the relative intensities. The agreement with the theoretical values can be seen from the figures.

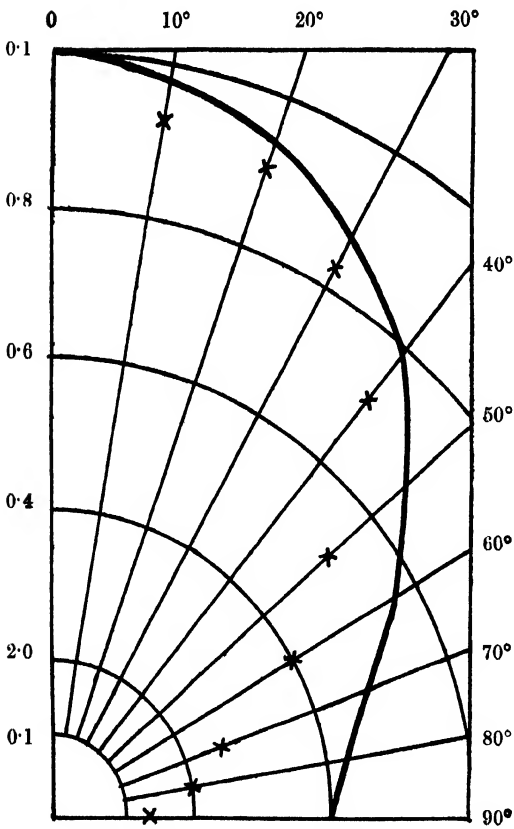


Fig. 9. Horizontal relative radiation pattern of the composite circular arc antenna —Type II: Theoretical and observed values.($A = 1, \beta = \pi/2$).

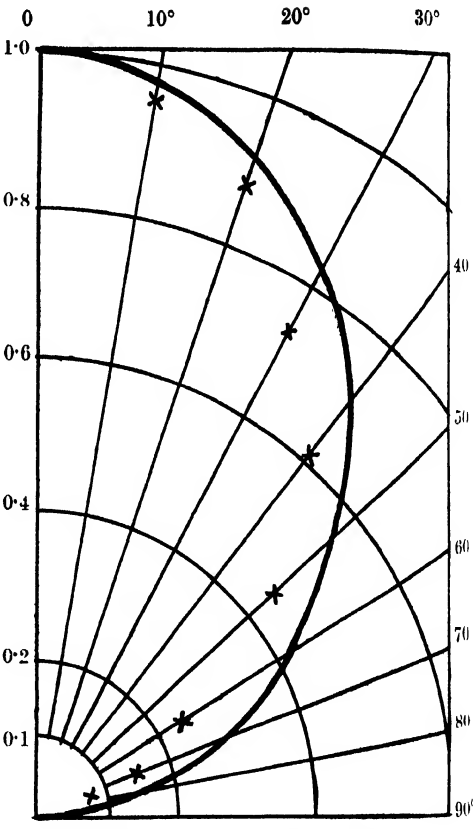


Fig. 10. Horizontal relative radiation pattern of horizontal half wave linear dipole: Theoretical and observed values.

× Observed values
— Theoretical values

The actual micro-ammeter readings are given in the tables that follow,

TABLE I

Composite circular arc antenna—Type I

 $A = 0.5, \beta = \pi$ (See figure 7)

Azimuth	Micro-am- meter read- ing in μa	Observed relative intensity	Theoretical relative intensity
0	48.0	1.00	1.00
10	44.0	0.92	0.98
20	44.0	0.92	0.93
30	39.5	0.82	0.84
40	39.0	0.81	0.74
50	28.0	0.58	0.62
60	18.0	0.38	0.50
70	9.5	0.20	0.35
80	4.0	0.08	0.18
90	0	0.00	0.08

TABLE II

Composite circular arc antenna—Type I

 $A = 1, \beta = \frac{\pi}{2}$ (See figure 8)

Azimuth	Micro am- meter read- ing in μa	Observed relative intensity	Theoretical relative intensity
0	42.5	1.00	1.00
10	41.0	0.96	0.99
20	36.0	0.85	0.94
30	38.0	0.89	0.88
40	33.0	0.78	0.80
50	22.5	0.53	0.68
60	11.5	0.28	0.52
70	4.5	0.11	0.38
80	0.5	0.01	0.29
90	3.5	0.08	0.24

TABLE III

Composite circular arc antenna—Type II

$$A = 1, \beta^i = \frac{\pi}{2} \text{ (See figure 9)}$$

Azimuth in degrees	Micro-am- meter read- ing in μa	Observed relative intensity	Theoretical relative intensity
0	49.5	1.00	1.00
10	46.0	0.93	0.98
20	45.0	0.91	0.94
30	41.0	0.83	0.87
40	35.5	0.72	0.78
50	26.0	0.53	0.66
60	20.0	0.40	0.58
70	13.5	0.27	0.48
80	10.0	0.20	0.42
90	6.5	0.13	0.40

TABLE IV

(See figure 10)

Horizontal half-wave dipole. (Dipole perpendicular to 0° azimuth)

Azimuth in degrees	Micro-am- meter read- ing in μa	Observed relative intensity	Theoretical relative intensity
0	24.5	1.00	1.00
10	23.5	0.96	0.98
20	21.5	0.88	0.91
30	18.0	0.73	0.82
40	15.0	0.61	0.70
50	11.0	0.45	0.55
60	6.0	0.24	0.42
70	4.0	0.16	0.29
80	2.0	0.08	0.16
90	0	0.00	0.00

SECTION VIII

METHOD OF EVALUATION OF THE INTEGRALS

The integrals to be evaluated in the previous sections of the paper are of the following form.

$$\int_0^\pi \sin(A\beta - A\psi) \cos(\psi + \phi) e^{jA \cos(\psi + \phi)} d\psi \quad (25)$$

In the expression (25) all the constant factors have been omitted.

The main difficulty in the integration of (25) is the presence of the factor $e^{jA \cos(\psi + \phi)}$ which cannot be directly integrated. This difficulty is got over by expanding $e^{jA \cos(\psi + \phi)}$ using the well known Fourier Bessel expansions, namely,

$$e^{jA \cos(\psi + \phi)} = J_0(A) + 2 \sum_{n=1}^{\infty} j^n J_n^{(A)} \cos n(\psi + \phi)$$

Once this substitution is made, the terms of the resulting series are integrable term by term after judicious grouping of the terms. A few salient steps in the process are given below.

$$\begin{aligned} f(\psi) &= \sin(A\beta - A\psi) \cos(\psi + \phi) e^{jA \cos(\psi + \phi)} \\ &= \frac{1}{2} [\sin(A\beta - A\psi + \psi + \phi) + \sin(A\beta - A\psi - \psi - \phi)] \left[J_0(A) \right. \\ &\quad \left. + 2 \sum_{n=1}^{\infty} j^n J_n^{(A)} \cos n(\psi + \phi) \right] \\ &= \frac{1}{2} J_0(A) [\sin(A\beta - A\psi + \psi + \phi) + \sin(A\beta - A\psi - \psi - \phi)] \\ &\quad + \frac{1}{2} \sum_{n=1}^{\infty} j^n J_n^{(A)} \{ \sin[A\beta - A\psi + (n+1)(\psi + \phi)] + \sin[A\beta - A\psi - (n-1)(\psi + \phi)] \\ &\quad + \sin[A\beta - A\psi - (n+1)(\psi + \phi)] + \sin[A\beta - A\psi + (n-1)(\psi + \phi)] \} \end{aligned}$$

$f(\psi)$ can now be regrouped as follows noting that the $(n+2)^{\text{th}}$ term has some of the terms in common with the n^{th} term and taking care to include terms which may be left out of the regrouping.

$$\begin{aligned} f(\psi) &= \frac{1}{2} \sum_{n=0}^{\infty} j^n [J_n^{(A)} - J_{n+2}(A)] \{ \sin[A\beta - A\psi + (n+1)(\psi + \phi)] \\ &\quad + \sin[A\beta - A\psi - (n+1)(\psi + \phi)] \} + j J_1^{(A)} \sin(A\beta - A\psi) \quad \dots \quad (26) \end{aligned}$$

Expression (26) can now be integrated term by term and the limits inserted to obtain the results given in the previous sections.

This method of evaluating the integral has been used by Moullin (1949). It should be noted that with this method there is no restriction on the values of β and A .

It should be noted that when A is an integer, one term each of the equations (7), (8), (12), (21) and (24) become indeterminate. These terms can be evaluated using the usual methods of evaluating indeterminate forms.

ACKNOWLEDGMENTS

The author is indebted to the University of Madras for permission to publish this paper, the material of which formed part of the thesis submitted to the University in 1954 for the Master's degree. The author thanks Dr. K. Sukumaran, Ex-Head of the Department of Electrical and Telecommunication Engineering, College of Engineering, Madras, under whose guidance this work was carried out. The author is grateful to Prof. K. S. Hegde, the present Head of the Department of Telecommunication Engineering, College of Engineering, Madras, for his suggestions and criticisms during the course of the investigation.

REFERENCES

- Foster. D., 1944, *Proc. Inst. Radio Engrs.*, **32**, 603-607.
Glinasky. G., 1947, *J. Appl. Phys.* **18**, 638-644.
Moullin. E. B., 1946, *Proc. Inst. Elec. Engrs.*, **93** pt. III, 345-351.
" (1949), "Radio Aerials" Oxford Clarendon Press, 223.
Sherman. J. B., 1944, *Proc. Inst. Radio Engrs.*, **32**, 534-537.

ON THE FLUORESCENCE OF PARA-BROMOTOLUENE, ORTHO-BROMO AND ORTHO-CHLOROTOLUENE IN THE SOLID STATE AT LOW TEMPERATURE.*

D. C. BISWAS

OPTICS DEPARTMENT, INDIAN ASSOCIATION FOR THE CULTIVATION OF SCIENCE,
JADAVPUR, CALCUTTA-32

(Received for publication, April 20, 1956)

Plate X

ABSTRACT. The fluorescence spectra of *p*-bromotoluene in the solid state at -40°C and -180°C and those of *o*-bromotoluene and *o*-chlorotoluene at -180°C and the spectra of these molecules dispersed in frozen solutions in different solvents have been investigated using mainly the group of Hg lines at 3650 \AA as the exciting radiation. The fluorescence spectra of these substances undergo changes when they are dispersed in different frozen solvents, the nature of the change being dependent on the nature of the solvent used. Finally, it is pointed out that the nature of the fluorescence bands given by these substituted toluenes is almost the same, but the position of the band system depends on the mode of the substitution and that this fact precludes the possibility of attributing this fluorescence to the presence of some common impurity in all these compounds.

INTRODUCTION

Fluorescence spectra of *p*-chlorotoluene in the solid state at different low temperatures and dispersed in frozen solutions in different organic solvents have been studied recently (Sirkar and Biswas, 1956; Biswas, 1956). It has been observed that the intensity of this fluorescence increases rapidly with lowering of temperature of the solidified mass and the band system is appreciably altered when the substance is dissolved in *n*-heptane, methyl cyclohexane, methyl alcohol etc., but the influence of the environment is found to be much less when the solvents are either carbon tetrachloride or tetrachloroethylene. Further, the intensity of fluorescence of *p*-chlorotoluene is reduced abruptly when the substance is dissolved in carbon disulphide and the strength of the solution is lowered from 15% to 5% by volume.

Such fluorescence is also exhibited by many other disubstituted benzenes (Sanyal, 1953; Biswas, 1954). The object of the present investigation was to find out how such fluorescence depends on the environments and temperature in the case of *p*-bromotoluene, *o*-bromotoluene and *o*-chlorotoluene. The fluorescence of these compounds in the solid state and in frozen solutions in benzene, *n*-heptane,

*Communicated by Prof. S. C. Sirkar.

ethyl alcohol and carbon tetrachloride have been studied in the present investigation.

EXPERIMENTAL

The liquids studied in the present investigation were supplied by Eastman Kodak Co., N. Y. and were of chemically pure quality. The solvents and the liquids were repeatedly distilled in vacuum.

The experimental arrangement is exactly the same as that described earlier (Biswas, 1956). The same ultraviolet light filter was placed in the path of the incident beam to transmit mainly the 3650\AA group of Hg lines. The samples were sealed in pyrex glass containers and were solidified by dipping the tube in liquid oxygen contained in a pyrex glass Dewar vessel. The spectra were recorded on Ilford Zenith plates with the help of two different Fuess glass spectrographs having dispersions of about 11\AA and 12.5\AA per mm. respectively in the 4047\AA region. As the bands are broad, the width of the slit of the spectrograph was increased to about 0.7 mm. to reduce the time of exposure except in the case of *o*-chlorotoluene in the pure state.

Besides the fluorescence spectra of the pure substances the fluorescence due to the frozen solutions of these substances in benzene, *n*-heptane, carbon tetrachloride and ethyl alcohol at -180°C was also investigated. The concentrations of these solutions varied from 3% to 7% and these mixtures, when frozen and cooled down to -180°C , appeared as translucent masses.

RESULTS AND DISCUSSION

The positions, approximate widths, relative intensities and the intervals between the fluorescence bands produced by *p*-bromotoluene at -40°C and -180°C , of *o*-bromotoluene and *o*-chlorotoluene at -180°C and those due to the frozen solutions of these compounds in benzene, *n*-heptane, methyl alcohol and carbon tetrachloride are given in Tables I, II and III. The intensities of the bands are indicated as very strong (v.s.), strong (s) etc. in the tables.

Some of the spectrograms are reproduced in Plate I.

p-Bromotoluene :

It is seen from the spectrograms reproduced in figure 1 that two very broad, ill-defined and weak fluorescence bands appear when *p*-bromotoluene is solidified and cooled down to -40°C . When the temperature is lowered down to -180°C , the bands become sharper and the number of bands increases from two to eight and these bands are quite well defined and are much more intense than those due to the substance at -40°C . When a 5% solution of *p*-bromotoluene in benzene is frozen and cooled down to -180°C , practically the same band system is observed but the relative intensities as well as the widths of the bands are found

Fig. 1.

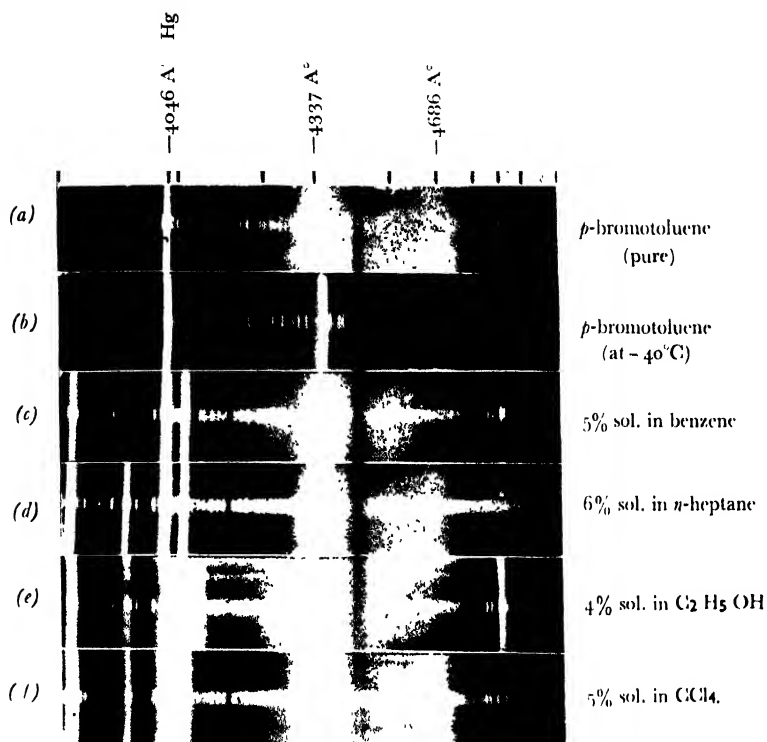


Fig. 2.



Fig. 3.

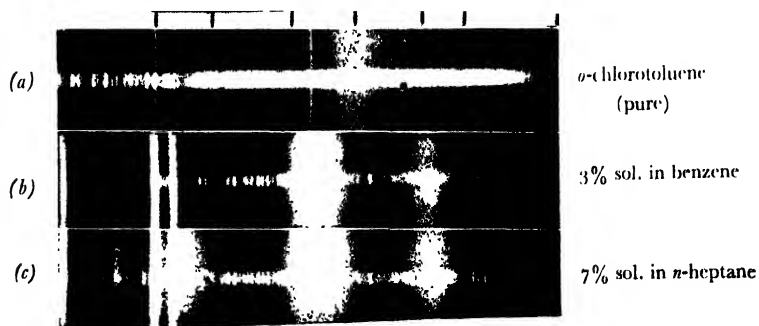
Fluorescence spectra at -180°C

TABLE I

Fluorescence spectra of *p*-Bromotoluene

Substance	Position of the band in A.U.	Width in A.U.	Position of the band in cm^{-1}	Successive diff. in cm^{-1}
Pure substance	4337 (m)	156	23051	
at -40°C	4686 (m)	187	21334	1717
	4060 (m)	121	24624	
	4233 (m)	55	23617	1007
	4337 (s)	136	23051	566
	4547 (m)	66	21986	1065
Pure substance at -180°C	4686 (s)	124	21334	652
	4810 (v.w)	—	20784	550
	4912 (w)	21	20353	431
	5054 (v.w)		19781	572
	4060 (w)		24624	
	4233 (m)		23617	1007
5% sol. in benzene at -180°C	4337 (m)	195	23051	566
	4547 (m)		21986	1065
	4691 (m)	200	21311	675
	4830 (?)		20698	613
	4060 (w)		24624	
	4238 (w)		23589	0135
6% sol. in <i>n</i> -heptane at -180°C	4318 (m)	28	23152	437
	4410 (m)	107	22669	483
	4556 (w)	57	21943	726
	4680 (s)	110	21361	582
	4840 (w)	45	20655	706
	4060 (w)	45	24624	
	4345 (m)	157	23008	1616
4% sol. in ethyl alcohol at -180°C	4694 (m)	150	21298	1710
	4848 (m)	21	20621	677
	weak continuum from 4236 \AA° to 4768 \AA°			
	4060 (w)		24624	
	4233 (w)	64	23617	1007
	4337 (s)	140	23051	566
	4547 (w)	68	21986	1065
5% sol. in CCl_4 at -180°C	4686 (s)	126	21334	652
	4810 (v.w)		20784	550

TABLE II
Fluorescence spectra of *o*-Bromotoluene

Substance	Position of the band in A.U.	Width in A.U.	Position of the band in cm^{-1}	Successive diff. in cm^{-1}
Pure substance at -180°C	3977 (m)	66	25137	
	4143 (v.w)	—	24130	1007
	4257 (v.s)	118	23484	646
	4455 (w)	52	22440	1044
	4582 (v.s)	141	21818	622
	4800 (v.w)	25	20827	991
	4938 (w)	45	20245	582
5% sol. in benzene at -180°C	3966 (s)	88	25207	
	4140 (?)	—	24148	1059
	4252 (v.s.)	138	23512	636
	4443 (w)	75	22501	1011
	4579 (v.s.)	166	21833	668
	4800 (w)	26	20827	1006
	4938 (m)	50	20245	582
4% sol. in CCl_4 at -180°C	3977 (m)	70	25137	
	4143 (?)	—	24130	1007
	4257 (v.s)	117	23484	646
	4455 (w)	52	22440	1044
	4582 (v.s.)	150	21818	622
	4810 (w)	28	20784	1034
	4960 (m)	65	20156	628
3% sol. in <i>n</i> -heptane at -180°C	3962 (m)	32	25233	
	4140 (?)	—	24148	1085
	4244 (s)	79	23556	592
	4442 (w)	39	22506	1050
	4562 (s)	104	21914	592
	4741 (v.w)	—	21087	827
	4842 (v.w)	—	20647	440
	4969 (w)	20	20119	528

TABLE III
Fluorescence spectra of o-Chlorotoluene

Substance	Position of the band in A.U.	Width in A.U.	Position of the band in cm^{-1}	Successive in diff. in cm^{-1}
Pure substance at -180°C	4143 (m)	101	24130	988
	4320 (w)	—	23142	712
	4457 (s)	127	22430	1046
	4675 (w)	—	21384	596
	4809 (m)	121	20788	1636
	5220 (v.w)	—	19152	
weak continuous fluorescence throughout the visible region				
3% sol. in benzene at -180°C	4100 (m)	125	24383	732
	4227 (w)	54	23651	858
	4386 (s)	194	22793	831
	4552 (v.w)	—	21962	691
	4700 (s)	193	21271	1337
	5015 (?)	—	19934	
7% sol. in n-heptane at -180°C	4100 (m)	130	24383	1215
	4315 (w)	32	23168	560
	4422 (s)	136	22608	1410
	4716 (s)	212	21198	1264
	5015 (?)	—	19934	
4% sol. in CCl_4 at -180°C	4143 (m)	88	24130	988
	4320 (w)	31	23142	712
	4457 (s)	147	22430	1046
	4675 (w)	25	21384	596
	4809 (m)	80	20788	

to be altered slightly. Thus when the solution is frozen, the band at 4233\AA becomes stronger than that at 4060\AA . Similarly the intensity of the band at 4547\AA becomes comparable to that of the band at 4686\AA , although the latter band is stronger in the case of the pure substance. Further, the widths of the individual

bands are larger in the case of the frozen solution than in the case of the pure substance.

When a 6% solution of *p*-bromotoluene in *n*-heptane is frozen and cooled to -180°C the strong band at 4337\AA appears to split up into two components at 4318 and 4410\AA respectively and only one weak band is observed at 4840\AA in place of the three such bands of the pure substance. Except the changes mentioned above, the other bands of the system undergo little changes either in their positions or in their relative intensities.

When a 4% solution of *p*-bromotoluene in ethyl alcohol is frozen and cooled to -180°C only the strong bands are observed against a weak continuous background radiation extending from 4236\AA to about 4770\AA . In case of a 5% solution of the substance in carbon tetrachloride at -180°C , the bands at 4060 , 4233 and 4547\AA diminish in intensity and the weak bands at 4912 and 5054\AA are not observed.

On comparing the band system of *p*-bromotoluene with that of *p*-chlorotoluene published earlier by the author (1956) it is found that these two compounds produce exactly similar fluorescence spectra in the visible region, the effect of replacement of the Cl-atom by a Br-atom being only to shift the band system as a whole towards longer wavelengths. Similar environments also produce some similar changes in the fluorescence spectra of these two substances in the case of the solutions in benzene and *n*-heptane. The influences of the field due to molecules of CCl_4 on the fluorescence spectra of *p*-chloro and *p*-bromotoluene in the frozen state are, however, different from each other and this difference can be attributed to the difference in the chemical affinity of chlorine and bromine atoms. When the molecules are dispersed in frozen CCl_4 , the fluorescence spectra of *p*-chlorotoluene suffer very little change while in the case of *p*-bromotoluene the bands at 4060 , 4233 and 4547\AA become weaker in this solution. This observed diminution in the intensities of these bands with dissolution of the substance in carbon tetrachloride corroborates the view put forward earlier (Biswas, 1956) that these bands in *p*-bromotoluene which correspond to the bands at 4038 , 4219 and 4529\AA of *p*-chlorotoluene are produced mainly by the interaction between the bromine atom of the *p*-bromotoluene molecules and the hydrogen atoms provided by the surrounding molecules.

o-Bromotoluene :

The fluorescence bands produced by *o*-bromotoluene in the solid state at -180°C are similar to those due to *p*-bromotoluene or *p*-chlorotoluene, but the system of bands due to *o*-bromotoluene as a whole is shifted towards shorter wavelengths by about 80 A.U. from its position in the case of *p*-bromotoluene. When a 5% solution of the ortho compound in benzene is frozen and cooled down

to -180°C , the bands are observed to shift slightly towards shorter wavelengths from the positions in the spectrum due to the pure substance. Similar shifts towards shorter wavelengths are also observed when a 3% solution of the substance in *n*-heptane is frozen at a temperature of -180°C . In the case of a 4% solution in CCl_4 cooled down to -180°C , no change in the positions of the bands with respect to those in the pure liquid is observed. So, it is evident that in this particular case the bands undergo changes only when the molecules are surrounded by molecules containing hydrogen atoms and molecules containing chlorine atoms but no hydrogen atoms exert very little influence on the energy levels of the *o*-bromotoluene molecule.

o-Chlorotoluene :

The main features of the fluorescence spectrum excited in solidified *o*-chlorotoluene at -180°C are quite similar to those of the other substituted toluenes described earlier. In the case of this particular compound, however, there is in addition to the regular band system, a weak continuous fluorescence extending throughout the visible region. In the case of dilute solutions of this substance in benzene or in *n*-heptane, the prominent fluorescence bands are found to be shifted towards shorter wavelengths and this shift is as large as 100\AA in the case of the strong band at 4809\AA . However, when a 4% solution of this compound in CCl_4 is frozen and cooled down to -180°C no change in the positions or in the intensities of the bands takes place. The widths of the bands are also considerably increased when the molecules are dispersed in benzene or *n*-heptane in the frozen state at -180°C . It is thus evident that the hydrogen atoms of the neighbouring molecules are responsible for bringing about changes in the band system of the molecules of *o*-bromotoluene and *o*-chlorotoluene, mentioned above.

It is easily seen from the results given in the Tables for the frozen solutions of these different compounds that the influence of the solvent molecules on the fluorescence spectrum depends largely on the relative positions of the substituent halogen atom in the molecule. In the intermolecular field of benzene or of *n*-heptane molecules in the solid state the fluorescence spectra of both ortho-bromotoluene and ortho-chlorotoluene undergo similar changes while the changes observed in the case of the para-compounds under similar conditions are different from those observed for the ortho-compounds.

Finally on comparing together the fluorescence spectra of all the four substituted toluenes, it is observed that the nature of the band system in all these compounds is almost the same, but the position of the spectrum depends on the mode of substitution. This may indicate the genuineness of the fluorescence spectrum and may justify the correctness of their assignments to the respective molecules.

ACKNOWLEDGMENT

The author is indebted to Professor S. C. Sirkar, D. Sc., F.N.I. for his kind interest and guidance during the progress of this work.

REFERENCES

Biswas, D. C., 1954, *Ind. J. Phys.*, **28**, 423

" 1956, *Ind. J. Phys.*, **30**, 143

Sanyal, S. B., 1953, *Ind. J. Phys.*, **27**, 447.

Sirkar, S. C. and Biswas, D. C., 1956, *J. Chem. Phys.*, **24**, 470.

L_{2,3} AND K EMISSION SPECTRA OF MAGNESIUM, ALUMINIUM AND LITHIUM IN HIGHER ORDERS.

A. K. SEN

KHAIRA LABORATORY OF PHYSICS, 92, UPPER CIRCULAR ROAD, CALCUTTA

(Received for publication May 11, 1956)

ABSTRACT. L_{2,3} and K emission spectra of magnesium, aluminium and lithium have been studied in higher orders by a newly built soft x-ray ruled grating vacuum spectrograph of one metre radius. The band width, band structures and the edge breadths have been determined accurately from the calibration curve. The agreement between the band widths of K valence band and L₃ band has been discussed in the case of magnesium and aluminium.

†

INTRODUCTION

The design and the construction of one metre ruled grating grazing incidence vacuum spectrograph has been reported (Das Gupta *et al.*, 1955) earlier. In the present paper the author gives the details of the setting and the calibration of the spectrograph, the results in connection with the study of L_{2,3} and K emission spectra of aluminium, magnesium and lithium in higher orders with elements in very pure state. The edge breadth, the band width and the band structures have been studied in the observed high order emission spectra with better resolution. The results have been discussed along with the K emission spectra of magnesium and aluminium obtained by Das Gupta (1946) in this laboratory.

EXPERIMENTAL TECHNIQUE

The design of the spectrograph is essentially the same as that used by Skinner (1937). The x-ray tube is exactly similar as that used by Das Gupta (1955). The concave grating that has been used has 1152 lines per mm, total number of lines 34114, ruled area 10 × 30 mm of one metre radius ruled on glass by Professor Manne Siegbahn and presented to the Calcutta University for our work.

The width of the slit of the spectrograph used for most of the experiments is about .02 to .03 mm. A second slit is introduced in between the grating and the slit of the spectrograph and by adjusting the width and position of the second slit the width of the grating utilised is limited to about 15 mm which is close to the theoretically optimum value for best focussing. The grating is set at an angle of 5°.5 grazing and the Rowland circle is of 50 cms radius and is accurately set in position by a number of trial experiments.

The entire arrangement of the slit system, the grating holder and the cassette are mounted within a hollow cylinder consisting of two halves. The shorter half

holds the entire arrangement and the longer part rolls along the rails of a heavy metal bench. The union of the two halves is effected by a rubber gasket. The hollow cylinder, that is the spectrograph chamber, is evacuated by a Leybold rotary pump (D 10) giving an ultimate vacuum of 10^{-5} mm of mercury. The rotary pump is connected through a sylphon by means of a gasket to the bottom of the fixed half of the spectrograph chamber. A liquid air trap is used over the pump in order to keep the spectrograph chamber free from any oil vapour and in better ultimate vacuum. The slit of the spectrograph is kept covered except during the exposure time by means of a shutter fixed to a metal cone to be operated in vacuum from outside.



Fig. 1. Ruled grating vacuum spectrograph for soft x-ray spectroscopy.

- A : The target in vertical position with graduated circular disc at the top.
- B : The tungsten coil evaporator in horizontal position facing the target.
- C : The oxide coated cathode facing the target.
- D : The liquid air trap running close to the target.
- E : Sylphon gasket joint with the vacuum system.
- F : X-ray tube fixed to the slit system of the spectrograph.
- G : Concave grating within the grating-holder.
- H : Cassette : the circle of focus.
- I : The contra board.

The x-ray tube is made of glass built by a local glass blower, using standard quickfit cone joints. The tube is directly joined to the slit of the spectrograph

using a very thin layer of Edward's high vacuum piecein. The x-ray tube is connected to the pumping system by means of gasket joint through a sylphon tube for facilities of alignment and to check the vibration of the system. The pumping system consists of a three stage oil diffusion pump (OT100) backed by Leybold rotary (D5). The speed of the diffusion pump is 100-120 litres per second at a pressure of 10^{-4} mm of mercury. A liquid air trap is fitted over the diffusion pump. The diffusion pump rests on ball bearings to allow smooth movements along the grooves on a metal base plate to prevent any strain on the glass x-ray tube during the process of vacuum.

The target i.e. the source of soft x-ray is a square sectioned copper tube of about one millimetre wall thickness with water cooling arrangements. The hollow metal cone of the target is separately cooled by water circulation. The target at its upper end carries a graduated circular disc facing a fixed pointer so that by rotating the target to the optimum position any one of the four faces may become the source of x-rays. The filament is a directly heated one and consists of a spiral of nickel wire coated with oxides of barium and strontium. Surrounding the filament there is an insulated cylindrical nickel shield to focus the electron beam on the right position of the target face. The sample under investigation is taken in a very pure state and evaporated in a very high vacuum in front of the target face so as to get the deposit of a thin film on the target. The evaporation unit consists of a conical tungsten spiral with a rectangular nickel shield and is placed on the side of the target opposite the filament. A liquid air trap is introduced in the x-ray tube by the side of the target to produce high local vacuum.

The high tension unit consists of two mercury valve rectifiers connected for full-wave rectification and is smoothed by two 0.1 m.f condensers. The maximum voltage and current obtainable from the unit is 10kV and 200mA. The voltage employed in our work ranges from 3 to 5kV and the control is effected by using a variac. The current utilised for exposure ranges from 10-100 mA and passes through relay contacts which controls the maximum value of the tube current. If the current exceeds the maximum value the high tension unit is automatically switched off. The control of the maximum value is effected by means of a rheostat and the relay circuit is operated from 220 volt D.C. main. The positive side of the high tension set is earth connected and the negative end is connected to one end of the filament coil. Thus the filament of the x-ray tube is at a negative high tension and the target is at the earth potential. The filament current is controlled by varying the filament voltage by means of a variac.

The photographic plates used are special Q 1 plates supplied by Messrs. Ilford Ltd. These are thin glass plates about 1/3 mm thick coated on one side with Q1 emulsion. The plates are bent round the cassette with a supporting thin metal back plate and fixed in position by a number of catches attached to the cassette.

The target face is thoroughly cleaned by means of a scraper before introducing into the x-ray tube. Silicone grease is introduced in all the cone joints to avoid carbon contamination in the tube. The photographic plate is put in proper position within the spectrograph. The vacuum is attained in about half an hour and the glass x-ray tube is heated to about 100°C for degassing. The target is bombarded with electron beam at 3–4 kV and 30 to 40 mA to raise the temperature of the target to about 300° to 400°C and maintained for about half an hour for degassing. The target temperature is recorded by using a thermocouple introduced within the target. Evaporation of the specimen metal is effected within one and half hours time from the starting of the vacuum pumps. Exposure is usually maintained at 3 kV and 50–80 mA and care is taken to avoid the appearance of any bright speck on the target face. After every one hour a new target face with a fresh deposit on it is brought before the filament to avoid any contamination of the specimen. With an exposure of about 6 hours at 3 kV 60 mA four orders of aluminium $L_{2,3}$ spectra have been recorded.

EXPERIMENTAL RESULTS

A dispersion curve has been drawn with grating set at $5^{\circ}.5$ grazing incidence. The prominent structure of carbon at 44.78 Å has been selected in seven orders of carbon K band to draw the dispersion curve. The band width, edge breadth

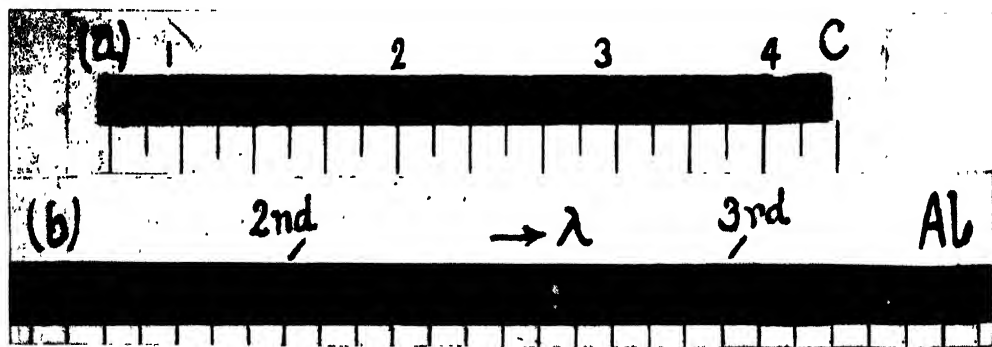


Fig. 2. (a) Four orders of carbon K spectra. (b) Second and third orders of aluminium $L_{2,3}$ spectra.

and the band structures have been determined from the dispersion curve. In Table I the results of L_3 spectra of magnesium in first order, of aluminium in second and third order and K spectra of lithium in second order are given along with Skinner's data.

TABLE I

Observed edge breadths ($\text{e v} \times 100$) at 300°K along with Skinner's values

Edge breadth	Li (2nd order)	Mg	Al (1st order)	Al (2nd order)	Al (3rd order)
Observed	25	20	22	22	21
Skinner's data	30 (1st order)	20			

K and L Band Widths:					
	Li (2nd order)	Mg	Al (1st order)	Al (2nd order)	Al (3rd order)
K— Band width	3.7 eV	8.0 eV	12.5 eV
L Band width	..	7.1 eV	13.0 eV	13.1 eV	13.2 eV

The author takes special interest in studying the edge breadth which has been found to be profoundly affected even due to the presence of the slight trace

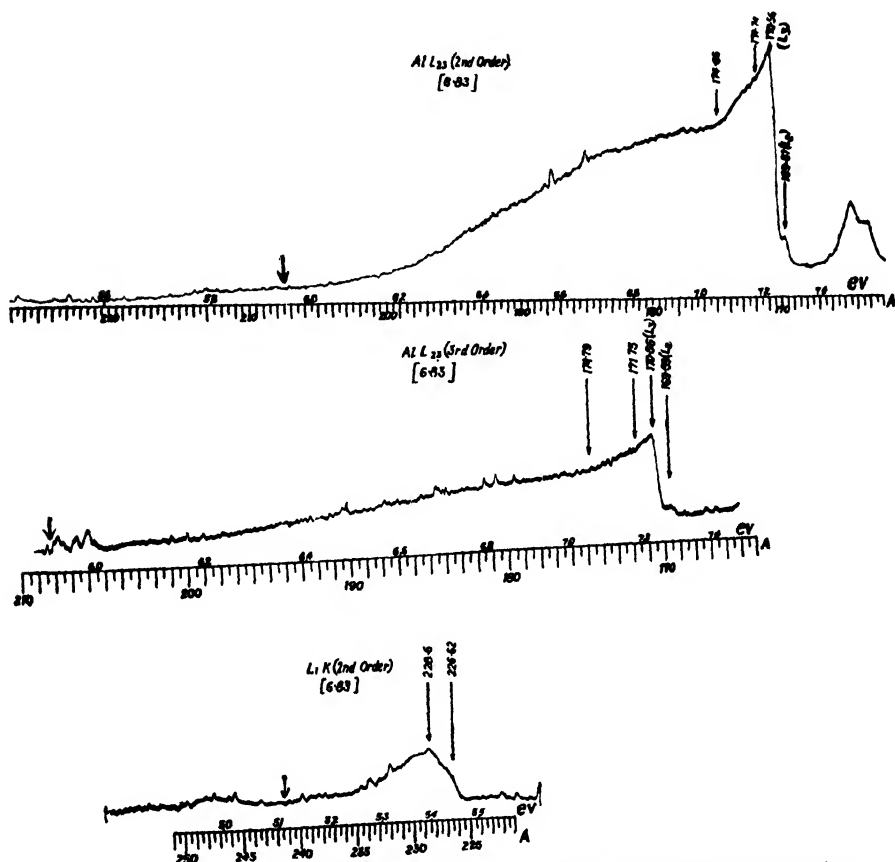


Fig. 3. Original photometer records of K and L_{2,3} spectra of lithium and aluminium.

of impurity in the metal. With this in view for better resolution $L_{2,3}$ spectra in third and fourth orders have been studied. The main difficulty in getting higher order spectra is the necessity of giving a prolonged exposure and it is really difficult to maintain the purity of the surface of the evaporated metal film on the target face during the long period of exposure. The results obtained with aluminium is hopeful since the calculated edge breadth agrees accurately with theoretically estimated value and the observed value of Skinner.

The kinks in L_3 spectra of aluminium appear at 174.86 and 171.74 Å and the most intense peak appears slightly shifted towards the longer wavelength side of the L_3 edge at 170.56 Å.

The edge breadth of lithium K is 0.25 e.v. and the band has got structures. In figure 4 the K valence band spectra of sodium, magnesium and aluminium as obtained by Das Gupta (1946) is shown along with the $L_{2,3}$ spectra of these metals.

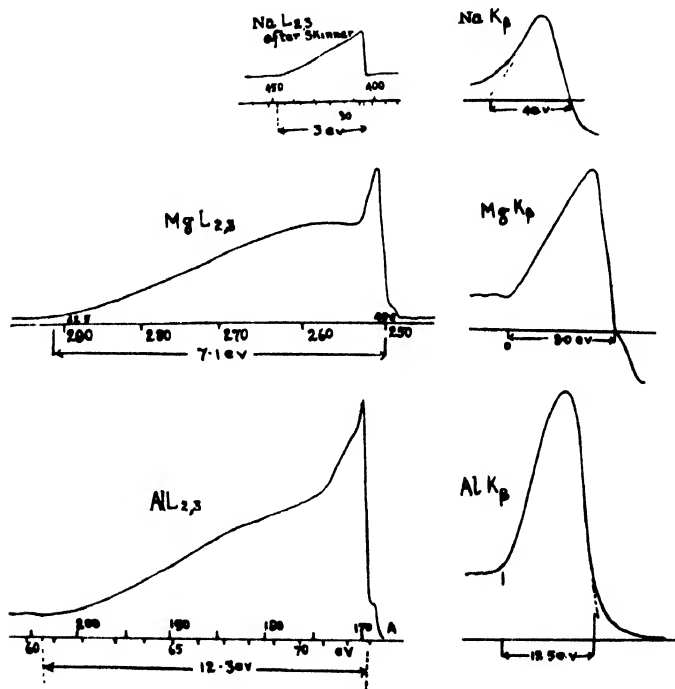


Fig. 4. K and $L_{2,3}$ spectra of sodium, magnesium and aluminium.

Although there is hardly any similarity between the K and $L_{2,3}$ spectra so far as their band structure is concerned there is fairly good agreement in total band width. In L_3 spectrum we get a mixture of $N_s(E)$ and $N_d(E)$ while in K spectrum we get a reflection of $N_p(E)$. The agreement in band width between K and L_3 spectra of these metals indicate that s , p and d wave functions pervade throughout the filled band of these metals. Accepting a complete overlapping

of *s*, *p* and *d* it is again difficult to explain the band structures as observed in these metals. In *L₃* spectrum of sodium there is a very slight trace of kink near the emission edge and a kink in similar position is very prominent in magnesium. In aluminium there are two prominent kinks in *L₃* spectrum but the *K* spectrum does not show any structure. From the study of *K* and *L_{2,3}* spectra of these metals it may be concluded that the *p* wave function pervades throughout the filled band otherwise it is difficult to explain the agreement in band widths of *K* and *L_{2,3}* valence emission spectra.

We can tentatively draw the distribution curve for *3s*, *3p* and *3d* electrons such that the superposition of these curves explain the observed kinks in sodium, (Jones *et al.* 1934) magnesium and aluminium. With the idea introduced by Jones, Mott and Skinner, that is the determination of the transition probability *f(E)* is largely an atomic problem one can make an attempt to explain the observed kinks in these metals by introducing an idea of double transition. Let us try to explain the kinks in *L₃* spectrum of aluminium. The number of kinks being two it should require at least partial overlapping of *3s*, *3p* and *3d* distributions. In trivalent aluminium the top of the Fermi surface should be drawn conveniently at such a position as to include a part of *3d* curve which means that the conduction electrons of aluminium have at least some per cent *3d* character. To explain an emission with initial *2p* vacancy and final *3p* vacancy we suggest the following mechanism : initially there is a vacancy in *2p* level, this is filled by a transition of *3s* electron and the *3s* hole is immediately filled up by a *3p* electron near the top of the Fermi surface and the net result is a *3p* hole in filled band. If such a transition process should exist the two kinks as observed in *L₃* spectrum of aluminium is easily explained.

In the case of magnesium, electrons in the conduction band are characterised by *3s* and *3p* wave functions, *3s* being more prominent near the bottom of the band while *3p* wave function characterises electrons near the top of the Fermi surface. To explain the intense peak near the short wavelength edge of the *L* emission band we have put forward a mechanism of double transition to avoid the difficulty arising out of the selection rule.

In the case of sodium, there is slight *p* character for the electrons near the top of the Fermi surface and this gives rise to an indication of kink near the short wavelength edge of *L₃* spectrum of sodium. Introducing the idea of overlapping of *3s*, *3p* and *3d* levels in different proportions in these metals one can draw tentative diagrams indicating the degree of overlapping from actual *L₃* spectra of these metals by graphical method. The prominent peak in *L₃* spectrum of magnesium metal near the short wavelength edge can be explained in the following way: the initial state is a vacancy in *L₃* level (*2p*), filled up by a transition of *3s* electron of the conduction band and the *3s* hole is immediately filled up by an electron having *3p* character near the top of the conduction band and in the process of emission the final state is characterised by a vacancy in *3p* level.

ACKNOWLEDGMENTS

The work has been carried out in the Khaira Laboratory of Physics, University College of Science, Calcutta. The author is thankful to Dr. K. Das Gupta, the Investigator in Charge of the Scheme 'Soft X-ray Spectroscopy of Metals, Alloys, Semi-conductors and Fluorescent Solids' under Council of Scientific and Industrial Research, Government of India, New Delhi, for introducing him to the technique and for his valuable guidance throughout the work. The author is grateful to Professor S. N. Bose, Khaira Professor of Physics for his kind encouragement and interest in the work.

REFERENCES

- Das Gupta, Sen and Bhattacharya, 1955, *Journal of Scientific and Industrial Research*, **14B**, 129.
Das Gupta, K., 1946, *Ind. J. Phys.*, **20**, 227.
Das Gupta, K., 1955, *Phil. Mag.* **46**, 77.
Jones, Mott and Skinner, 1934, *Phys. Rev.*, **45**, 370.
Skinner and Johnston, 1937, *Proc. Roy. Soc.*, **A 161**, 420.

SURFACE TENSION-TEMPERATURE RELATION FROM FREE-VOLUME CONCEPT

SHASHANKA SHEKHAR MITRA

RANDALL LABORATORY OF PHYSICS, UNIVERSITY OF MICHIGAN, ANN ARBOR (Mich.), U.S.A.

(*Received for publication February 22, 1956.*)

ABSTRACT. By applying the concept of free volume in liquids, the temperature variation of surface tension has been explained. Similarity in the behaviour of surface tension with that of viscosity and vapour pressure has been traced out and thereby a logarithmic type of equation has been suggested, a justification of which has been furnished from the free-space concept. The equation is

$$\log S = a + \frac{b}{T} - c \log T$$

being of the same type as those of Kirchoff's vapour pressure and Eyring's viscosity equations, though derived from somewhat different standpoints.

INTRODUCTION

In a number of communications (Mitra, 1953, 1954*a*, 1954*b*, Mitra and Srivastava, 1954*a*, Mitra and Chakravarty, 1954, Mitra and Sanyal, 1955, Mitra 1955*c*, Sanyal and Mitra, 1956) the author has investigated the systematics in the physico-chemical properties of liquids. From these investigations it appears that surface tension of liquids is quite similar in mechanism to that of viscosity and vapour pressure, specially as regards its temperature variation. It is a well known fact that the temperature-dependence of viscosity of simple liquids can be expressed by Andrade's (1934) logarithmic equation of the type

$$\log \eta = A + \frac{B}{T} \quad \dots (1)$$

Similarly, the temperature-dependence of vapour pressure is represented by the integrated Clausius Clapeyron's equation:

$$\log p = A + \frac{B}{T} \quad \dots (2)$$

From the consideration of the above two equations it appears at once that surface tension should also behave in a similar fashion; actually by eliminating η between equation (1) and Newton Friend (1942, 1943) and Mukherjee's (1953) viscosity-surface tension relation

$$\log \eta + a \log S = b \quad \dots (3)$$

the author (Mitra and Srivastava, 1954*b*) has obtained a relation of the type:

$$\log S = A + \frac{B}{T} \quad \dots (4)$$

for the temperature-dependence of the latter quantity. But it has also been shown that this equation is of a very approximate nature and cannot express the variation well even for very simple liquids. The cause may not only be traced out in the approximate nature of Andrade's equation but also in that of the viscosity-surface tension relation (3). Improvements in these directions have been made (Mitra and Chakravarty, 1955) and also two modifications of equation (4) have been suggested on empirical grounds. They are

$$\log S = \log S_0 + \frac{K}{T^n} \left(1 - \frac{T_0}{T} \right)$$

and

$$\log S = \log S_0 + \frac{L}{(\log T)^m} \left(1 - \frac{T_0}{T} \right)$$

and have been found to express the experimental data very well. The present communication aims to explain on theoretical grounds an already suggested surface tension-temperature relation by the author, which is of an almost similar type as the above equations. This equation is

$$\log S = a + \frac{b}{T} - c \log T$$

and is of a corrected form of equation (4) with a Kirchhoff or Eyring type $\log T$ factor.

SURFACE TENSION AND FREE-VOLUME

The proportionality of fluidity with free volume affords a good means of correlating the former quantity with temperature since the free volume is known as a function of the thermal state. The above method has been used by the author (Mitra, 1955*a, b*) to find a relation between η and T . So in this section we shall try to establish a relation between free-volume and surface-tension from a very simplified physical structure of a liquid.

The attractive force exerted by the molecules in the bulk of a liquid on those on the surface is the cause of surface tension. This force is a function of the distance between the surface layer and the neighbouring layer. More specifically, this function is of an inverse power type. So

$$F \propto \frac{1}{r^n} \quad \dots (5)$$

Now, in the hole theory of liquids, a liquid is supposed to be constituted of a random distribution of molecules in a vast sea of free space. This may be divided into a large number of smaller units, known as holes. The holes are assumed to be moving within the volume of the liquid. Almost all the physico-chemical properties of liquids can be explained with the aid of this picture. The flow of a liquid may be imagined to be the jump of molecules from one hole to the other by the action of some shearing stress, and hence, may be regarded as dependant on the number of such holes in a given quantity of liquid. The surface tension is explained as the attractive force exerted by the molecules inside the bulk on those at the surface separated by the holes.

From this geometrical picture (Mitra, loc. cit.) it can be easily shown that the free volume, v_f , in a liquid is related to liquid volume v , as

$$v_f = c^3(v^{1/3} - d)^3 \quad \dots (6)$$

c being the packing factor and other symbols having their usual meanings.

Relation (6) at once signifies that if we assume a cubical structure of the liquid, which is nearly the case for normal liquids, r of equation (5) is of the order of $v_f^{1/3}$. Hence,

$$F \propto \frac{1}{v_f^{n/3}}$$

But this force F is actually proportional to surface tension and so

$$S \propto \frac{1}{v_f^{n/3}}$$

or

$$v_f \propto S^k$$

k being some constant.

FREE-VOLUME AND FREE-ENERGY

The free volume and partition function of a liquid molecule are shown to be related by Eyring and Hirschfelder(1937) as

$$f = \frac{(2\pi mkT)^{3/2} V_f}{h^3} f_v f_r e^{\frac{\Delta E_{vap}}{RT}} \quad \dots (8)$$

where f is the partition function of a molecule, f_v and f_r being the vibrational and rotational contributions to it; and ΔE_{vap} is the energy of vaporization per mol. = $L - RT_0$, L being the normal latent heat of vaporization and T_0 being the boiling point. V_f represents the free volume for a gm. mole of the substance. But the free energy of such a system containing N indistinguishable particles is given by

$$F = -RT \ln(f/N)$$

Hence we can obtain the partition function as a function of the free energy or work function F :

$$f = Ne^{-F/RT} \quad \dots (9)$$

Combining equations (8) and (9) one gets

$$V_f = \frac{h^3 N}{(2\pi mkT)^{3/2} f_v f_r} e^{-(F + \Delta E_{vap})/RT} \quad \dots (10)$$

expressing the free volume as a function of free-energy.

SURFACE TENSION AND TEMPERATURE

The free energy is a function of temperature and pressure. But under the experimental condition of measuring surface tension, pressure is generally constant and hence F may be supposed to be changing with temperature only. F , as a first approximation (Mukherjee, 1951) is generally expressed as a linear function of temperature of the form

$$F = \alpha + \beta T$$

So we may now get free volume as a function of temperature only

$$V_f = \frac{h^3 N}{(2\pi mkT)^{3/2} f_v f_r} e^{-(\alpha' + \beta T)/RT} \quad \dots (11)$$

Here α' includes the energy of vaporization..

Since we know surface tension as a function of free-volume, it is now possible to express surface tension as a function of temperature. From equations (7) and (11) one gets

$$S^k = \frac{A}{T^{3/2} f_v f_r} e^{-(\alpha' + \beta T)/RT} \quad \dots (12)$$

Generally in the liquid state the variations in partition functions of rotation and interatomic and intermolecular vibrations with temperature are negligible, so f_v and f_r may be considered to be constants; hence

$$S^k = \frac{A'}{T^{3/2}} e^{-(\alpha' + \beta T)/RT}$$

or taking logarithms one gets

$$\log S = a + \frac{b}{T} - c \log T \quad \dots (13)$$

where a , b and c are constants obtaining the desired relation.

ACKNOWLEDGMENTS

The author is highly grateful to Prof. G. B. B. M. Sutherland, F.R.S. and Prof. G. E. Uhlenbeck for their interest in the investigation.

REFERENCES

- Andrade, 1934, *Phil. Mag.*, **17**, 497, 698.
- Eyring and Hirschfelder, 1937, *J. Phys. Chem.*, **41**, 249.
- Mitra, S. S., 1953, *Current Science*, **22**, 329.
- Mitra, S. S., 1954a, *J. Chem. Phys.*, **22**, 349; *Erratum, Ibid.* **22**, 1471.
- Mitra, S. S., 1954b, *J. Ind. Chem. Soc.*, **31**, 444.
- Mitra, S. S., 1955a, *Current Science*, **24**, 44.
- Mitra, S. S., 1955b, *J. Ind. Chem. Soc.*, **32**, 297.
- Mitra, S. S., 1955c, *Sci. and Cult.*, October.
- Mitra, S. S. and Chakravarty, D. N., 1954, *J. Chem. Phys.* **22**, 1775.
- Mitra, S. S. and Chakravarty, D. N., 1955, *Z. Phys. Chem.* **205**, 1.
- Mitra, S. S. and Sanyal, N. K., 1955, *J. Chem. Phys.*, **23**, 1737, 1955.
- Mitra, S. S. and Srivastava, S. N., 1954a, *J. Chem. Phys.*, **22**, 1134.
- Mitra, S. S. and Srivastava, S. N., 1954b, *J. Ind. Chem. Soc.*, **31**, 813.
- Mukherjee, A. K., 1951, *J. Ind. Chem. Soc.*, **28**, 519.
- Mukherjee, A. K., 1953, *J. Ind. Chem. Soc.*, **30**, 670.
- Newton Friend, 1942, *Nature* **150**, 432; 1943, *Phil. Mag.*, **34**, 643.
- Sanyal, N. K. and Mitra, S. S., 1956, *J. Chem. Phys.*, **24**, 473.

THE INVERSE KINETIC ENERGY MATRIX ELEMENTS FOR THE OUT-OF-PLANE VIBRATIONS IN FURAN THIOPHENE, CYCLOPENTADIENE AND THEIR SUBSTITUTED COMPOUNDS

V. SANTHAMMA

DEPARTMENT OF PHYSICS, ANDHRA UNIVERSITY, WALTAIR

(Received for publication October 10, 1955)

ABSTRACT. The inverse kinetic energy matrix elements for the torsional vibrations, out-of-plane bending vibrations and the interaction between the above two are derived for furan, pyrrole, thiophene, and cyclopentadiene using the vector expressions given by Malhiot and Ferigle (1955). The applicability of these expressions to the substituted compounds of the above parent molecules and the limitations imposed are discussed.

INTRODUCTION

In the process of computing the vibrational frequencies of polyatomic molecules using the well-known Wilson's $F-G$ matrix method the calculation of the inverse kinetic energy matrix elements is the most important step. The inverse kinetic energy matrix element is defined for a pair of internal coordinates k and k' by Wilson (1939, 1941) as

$$g_{KK'} = \sum_{t=1}^N \mu_t \vec{s}_{kt} \cdot \vec{s}_{k't} \quad \dots (1)$$

where \vec{s}_{kt} is a vector representing the contribution of the t^{th} atom. The summation is done over all the atoms. This matrix is transformed into another matrix (G) by means of a transformation matrix U and its transpose U' , the details and the application of which are given already elsewhere. (Santhamma, 1954).

Decius (1948) gave general formulae for the inverse kinetic energy matrix elements in terms of three types of internal coordinates* only. He considered 33 possible acyclic configurations in which case, the distinct types of configurations were specified following a definite notation (Decius, 1948) for the acyclic configuration of atoms defining super-positions of coordinates k and k' .

Malhiot and Ferigle (M and F, 1954), while discussing the consistency of Wilson's treatment with the Eckart conditions in the molecular vibrations, arrived at two important relations with regard to these \vec{s}_{kt} vectors, namely

$$\sum_t \vec{s}_{kt} = 0 \quad \dots (2)$$

* Bond stretching, inter-bond bending and torsion coordinates.

$$\Sigma \vec{r}_i^0 \times \vec{s}_{kt} = 0 \quad \dots (3)$$

where \vec{r}_i^0 is the equilibrium position vector of the t^{th} atom with respect to the centre of mass of the molecule. These two relations together with the gradient properties of \vec{s}_{kt} vectors led to expressions of the vectors for all the four types of internal coordinates (Decius, 1949) of vibrations of polyatomic molecules. The vector expressions for the end atoms defining the torsion coordinate are the same as derived by Decius (1948) and all the four for the out-of-plane bending coordinate are same as given by Lohman (1951).

The purpose of the present paper is

(a) to derive vector expressions for another important class of molecules furan, pyrrole, thiophene and cyclopentadiene when torsion and out-of-plane bending coordinates are considered using the notation and expressions of Malhiot and Ferigle (1955), (b) to compute inverse kinetic energy matrix elements $g_{kk'}$ with the help of the expressions given in (a) and equation (1) and (c) to discuss the applicability of the expressions given in (a) and (b) for the substituted furans, pyrroles, thiophenes and cyclopentadienes and the limitations imposed.

(a) Vector Expressions

1. General case of five membered ring compound

At first a general case of a pentacyclic compound is taken where the angles and bond lengths in the equilibrium position are all different from one another, atoms of the ring are numbered from 1 to 5 consecutively around the ring in the cyclic manner shown in figure 1, a, b, c, d, e in this figure indicate atoms.

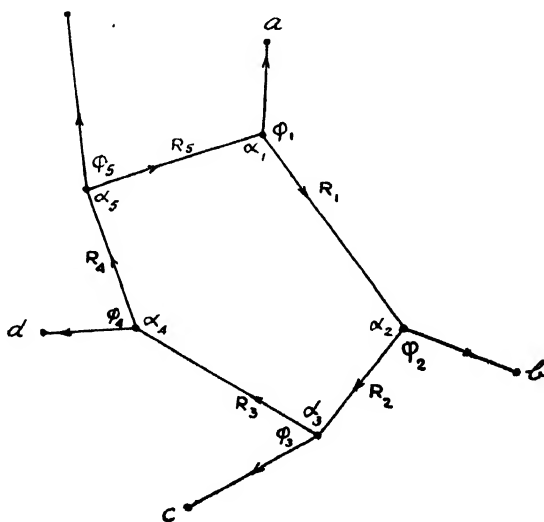


Fig. 1

The equilibrium angles, distances and the direction of the unit vectors along the bonds are indicated in the figure 1. The five torsion coordinates are designated by

$$\tau_{12}^{53}, \tau_{23}^{14}, \tau_{34}^{25}, \tau_{45}^{31} \text{ and } \tau_{51}^{42}.$$

following the notation of M and F, but these are here simply written as $\tau_1, \tau_2, \tau_3, \tau_4$ and τ_5 . The complete set of vector expressions in this case are presented in Table I.

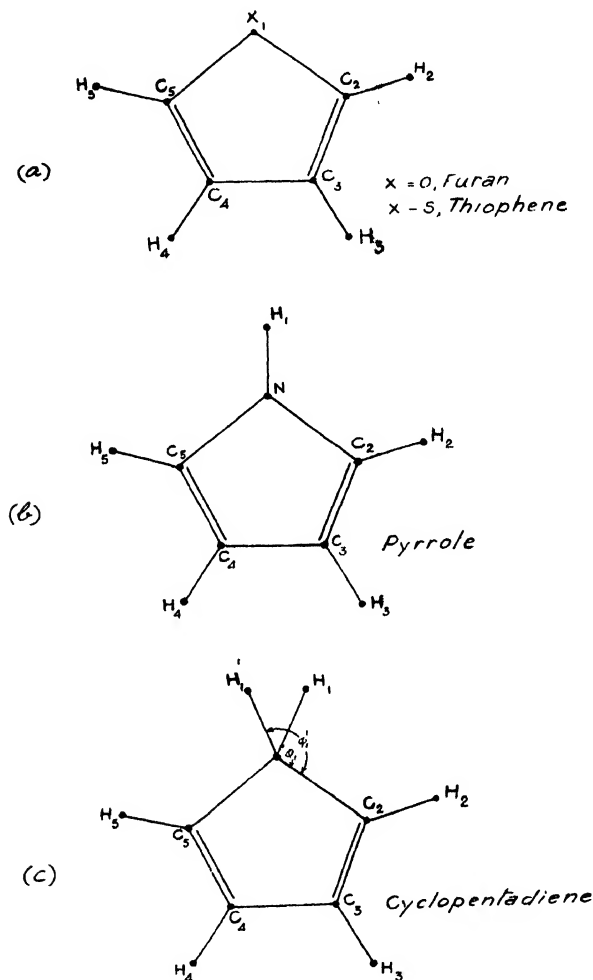


Fig. 2

2. Particular case (Furan, Pyrrole, Thiophene, and Cyclopentadiene).

In Table II expressions are given which refer to the particular case of furan, thiophene, pyrrole and cyclopentadiene (ref. Fig. 2). In these R_1, R_2, R_3 stand for the equilibrium distances of C—X (where X stands for O, S, NH or CH_2) C=C and C—C respectively.

TABLE I

Atoms of the ring	Coordi- nates	τ^{53}_{12}, τ_1	τ^{14}_{23}, τ_2	τ^{25}_{34}, τ_3	τ^{31}_{45}, τ_4	τ^{42}_{51}, τ_5
1		$-\vec{V} \left[\frac{1}{R_5} \operatorname{cosec} a_1 - \frac{1}{R_1} (\cot a_1 + \cot a_2) \right]$	$\frac{\vec{V}}{R_1} \operatorname{cosec} a_2$		$-\frac{\vec{V}}{R_5} \operatorname{cosec} a_5$	$-\vec{V} \left[\frac{1}{R_1} \operatorname{cosec} a_1 - \frac{1}{R_5} (\cot a_1 + \cot a_5) \right]$
2		$-\vec{V} \left[\frac{1}{R_2} \operatorname{cosec} a_2 - \frac{1}{R_1} (\cot a_1 + \cot a_2) \right]$	$-\vec{V} \left[\frac{1}{R_1} \operatorname{cosec} a_2 - \frac{1}{R_2} (\cot a_2 + \cot a_3) \right]$	$\frac{\vec{V}}{R_2} \operatorname{cosec} a_3$		$-\frac{\vec{V}}{R_1} \operatorname{cosec} a_1$
3		$-\frac{\vec{V}}{R_1} \operatorname{cosec} a_2$	$\frac{\vec{V}}{R_1} \left[\frac{1}{R_3} \operatorname{cosec} a_3 - \frac{1}{R_2} (\cot a_2 + \cot a_3) \right]$	$-\vec{V} \left[\frac{1}{R_2} \operatorname{cosec} a_3 - \frac{1}{R_3} (\cot a_3 + \cot a_4) \right]$	$\frac{\vec{V}}{R_3} \operatorname{cosec} a_3$	
4			$-\frac{\vec{V}}{R_3} \operatorname{cosec} a_3$	$\frac{\vec{V}}{R_4} \operatorname{cosec} a_4 - \frac{1}{R_3} (\cot a_3 + \cot a_4) \right]$	$-\vec{V} \left[\frac{1}{R_3} \operatorname{cosec} a_3 - \frac{1}{R_4} (\cot a_4 + \cot a_5) \right]$	$\frac{\vec{V}}{R_4} \operatorname{cosec} a_5$
5		$\frac{\vec{V}}{R_5} \operatorname{cosec} a_1$	$-\frac{\vec{V}}{R_4} \operatorname{cosec} a_4$	$\frac{1}{R_3} (\cot a_3 + \cot a_4) \right]$	$-\vec{V} \left[\frac{1}{R_5} \operatorname{cosec} a_5 - \frac{1}{R_4} (\cot a_4 + \cot a_5) \right]$	$-\vec{V} \left[\frac{1}{R_4} \operatorname{cosec} a_5 - \frac{1}{R_5} (\cot a_5 + \cot a_1) \right]$

TABLE II

Atmos of the ring	Co-ordi nates	τ_1	τ_2	τ_3	τ_4	τ_5
$C_1, O,$		$-\frac{\vec{V}}{R_1} \left[\text{cosec } \delta_1 + \right.$	$\frac{\vec{V}}{R_1} \text{ cosec } \delta_2$		$-\frac{\vec{V}}{R_1} \text{ cosec } \delta_2$	$\frac{\vec{V}}{R_1} \left[\text{cosec } \delta_1 + \right.$
S, N		$\left. \cot \delta_1 + \cot \delta_2 \right]$				$\cot \delta_1 + \cot \delta_2 \left. \right]$
C_2		$-\frac{\vec{V}}{R_2} \left[\frac{1}{R_2} \text{ cosec } \delta_2 + \right.$	$-\frac{\vec{V}}{R_2} \left[\frac{1}{R_1} \text{ cosec } \delta_2 + \right.$	$\frac{\vec{V}}{R_2} \text{ cosec } \delta_3$		$\frac{\vec{V}}{R_1} \text{ cosec } \delta_1$
		$\left. \frac{1}{R_1} (\cot \delta_2 + \cot \delta_1) \right]$	$\frac{1}{R_2} (\cot \delta_2 + \cot \delta_3) \left. \right]$			
C_3		$-\frac{\vec{V}}{R_2} \text{ cosec } \delta_2$	$-\frac{\vec{V}}{R_3} \left[\frac{1}{R_3} \text{ cosec } \delta_1 + \right.$	$-\frac{\vec{V}}{R_2} \left[\frac{1}{R_2} \text{ cosec } \delta_3 + \right.$	$\frac{\vec{V}}{R_3} \text{ cosec } \delta_3$	
			$\left. \frac{1}{R_2} (\cot \delta_2 + \cot \delta_3) \right]$	$\frac{2}{R_3} \cot \delta_3 \left. \right]$		
C_4			$-\frac{\vec{V}}{R_3} \text{ cosec } \delta_3$	$\frac{\vec{V}}{R_2} \left[\frac{1}{R_2} \text{ cosec } \delta_3 + \right.$	$-\frac{\vec{V}}{R_3} \left[\frac{1}{R_3} \text{ cosec } \delta_3 + \right.$	$\frac{\vec{V}}{R_2} \text{ cosec } \delta_2$
				$\left. \frac{2}{R_3} \cot \delta_3 \right]$	$\frac{1}{R_2} (\cot \delta_2 + \cot \delta_3) \left. \right]$	
C_5		$-\frac{\vec{V}}{R_1} \text{ cosec } \delta_1$		$-\frac{\vec{V}}{R_2} \text{ cosec } \delta_3$	$-\frac{\vec{V}}{R_1} \left[\frac{1}{R_1} \text{ cosec } \delta_2 + \right.$	$-\frac{\vec{V}}{R_2} \text{ cosec } \delta_2 +$
					$\left. \frac{1}{R_1} (\cot \delta_2 + \cot \delta_1) \right]$	$\frac{1}{R_1} (\cot \delta_2 + \cot \delta_1) \left. \right]$

TABLE III

Atoms of Co-ordi- the ring nates	$\gamma_{a_{512}}, \gamma_1$	$\gamma_{b_{123}}, \gamma_2$	$\gamma_{c_{234}}, \gamma_3$	$\gamma_{d_{345}}, \gamma_4$	$\gamma_{e_{451}}, \gamma_5$
a	$\rightarrow -\frac{V}{r_1} \sin \varphi_1 \operatorname{cosec} \alpha_1$				
b		$\rightarrow -\frac{V}{r_2} \sin \varphi_2 \operatorname{cosec} \alpha_2$			
c			$\rightarrow -\frac{V}{r_3} \sin \varphi_3 \operatorname{cosec} \alpha_3$		
d				$\rightarrow -\frac{V}{r_4} \sin \varphi_4 \operatorname{cosec} \alpha_4$	
e					$\rightarrow -\frac{V}{r_5} \sin \varphi_5 \operatorname{cosec} \alpha_5$
1	$\rightarrow \frac{V \sin \varphi_1 \operatorname{cosec}^3 \alpha_1}{\left[\frac{1}{r_1} \sin^2 \alpha_1 + \frac{1}{R_5} \sin \phi_1 \right]}$ $\sin \alpha_1 + \frac{1}{R_1} (\cos \alpha_1 \cos \beta_1 - \cos \varphi_1)$	$\rightarrow -\frac{V}{R_1} \sin^2 \varphi_2 \operatorname{cosec}^2 \alpha_2$			$\rightarrow -\frac{V}{R_5} \sin \varphi_5 \operatorname{cosec}^2 \alpha_5$ ($\cos \alpha_5 \cos \beta_5 \cos \phi_5$)
2	$\rightarrow -\frac{V}{R_1} \sin \varphi_1 \operatorname{cosec}^3 \alpha_1$ ($\cos \alpha_1 \cos \beta_1 - \cos \phi_1$)	$\rightarrow \frac{V \sin \varphi_2 \operatorname{cosec}^2 \alpha_2}{\left[\frac{1}{r_2} \sin^2 \alpha_2 + \frac{1}{R_1} \sin \varphi_2 \right]}$ $\sin \alpha_2 + \frac{1}{R_2} (\cos \alpha_2 \cos \beta_2 - \cos \varphi_2)$	$\rightarrow -\frac{V}{R_2} \sin^2 \varphi_3 \operatorname{cosec}^2 \alpha_3$		

TABLE III (contd.)

Atoms of Co-ordi- the ring nates	γ_{511}^a, γ_1	γ_{103}^b, γ_0	γ_{031}^c, γ_3	γ_{345}^d, γ_4	γ_{451}^e, γ_5
3		$-\frac{\vec{V}}{R_2} \sin \varphi_2 \operatorname{cosec}^3 \alpha_2$ $(\cos \alpha_2 \cos \beta_2 - \cos \varphi_2)$	$\vec{V} \sin \varphi_3 \operatorname{cosec}^3 \alpha_3$ $\left[\frac{1}{r_3} \sin 2\alpha_3 \right.$ $\left. + \frac{1}{R_2} \sin \varphi_3 \sin \alpha_3 + \frac{1}{R_3} \right.$ $\left. (\cos \alpha_3 \cos \beta_3 - \cos \varphi_3) \right]$	$-\frac{\vec{V}}{R_3} \sin 2\varphi_4 \operatorname{cosec}^2 \alpha_4$	
4			$-\frac{\vec{V}}{R_3} \sin \varphi_3 \operatorname{cosec}^3 \alpha_3$ $(\cos \alpha_3 \cos \beta_3 - \cos \varphi_3)$	$\vec{V} \sin \varphi_4 \operatorname{cosec}^3 \alpha_4$ $\left[\frac{1}{r_4} \sin^2 \alpha_4 \right.$ $\left. + \frac{1}{R_3} \sin \varphi_4 \sin \alpha_4 \right.$ $\left. + \frac{1}{R_4} (\cos \alpha_4 \cos \beta_4 - \cos \varphi_4) \right]$	$-\frac{\vec{V}}{R_4} \sin 2\varphi_4 \operatorname{cosec}^2 \alpha_4$
5	$-\frac{\vec{V}}{R_5} \sin^2 \varphi_1 \operatorname{cosec}^2 \alpha_1$			$-\frac{\vec{V}}{R_4} \sin \varphi_4 \operatorname{cosec}^3 \alpha_4$ $(\cos \alpha_4 \cos \beta_4 - \cos \varphi_4)$	$\vec{V} \sin \varphi_5 \operatorname{cosec}^3 \alpha_5$ $\left[\frac{1}{r_5} \sin^2 \alpha_5 \right.$ $\left. + \frac{1}{R_4} \sin \varphi_5 \sin \alpha_5 \right.$ $\left. + \frac{1}{R_5} (\cos \alpha_5 \cos \beta_5 - \cos \varphi_5) \right]$

$$\beta_i = 360 - (\varphi_i + \alpha_i)$$

TABLE IV

Atoms of the molecule	co- ordi- nates	H_1, γ_{512}	H_2, γ_{123}	H_3, γ_{234}	H_4, γ_{345}	H_5, γ_{451}	H'_1, γ'_{512}
H_1	$\vec{V} \sin \varphi_1 \operatorname{cosec} \alpha_1$						
H_2	$-\vec{V} \sin \varphi_2 \operatorname{cosec} \alpha_2$						
H_3	$\vec{V} \sin \varphi_3 \operatorname{cosec} \alpha_3$						
H_4	$-\vec{V} \sin \varphi_3 \operatorname{cosec} \alpha_3$						
H_5	$-\vec{V} \sin \varphi_2 \operatorname{cosec} \alpha_2$						
H_1	$\vec{V} \sin \varphi_1 \operatorname{cosec}^3 \alpha_1$						
$C_1, S,$ O, N	$\left[\frac{1}{r_1} \sin^2 \alpha_1 + \frac{2}{R_1} \sin \alpha_1 \sin \varphi_1 \right]$	$\vec{V} \sin \varphi_1 \operatorname{cosec}^3 \alpha_1$	$-\frac{\vec{V}}{R_1} \sin^2 \varphi_2 \operatorname{cosec}^2 \alpha_2$				$-\frac{\vec{V}}{r'_1} \sin \varphi'_1 \operatorname{cosec} \alpha_1$
							$\vec{V} \sin \varphi'_1 \operatorname{cosec}^3 \alpha_1$
							$\left[\frac{1}{r'_1} \sin^2 \alpha_1 \right]$
							$\frac{2}{R_1} \sin \varphi'_1 \sin \alpha_1$
C_2	$\vec{V} \sin \varphi_2 \operatorname{cosec}^3 \alpha_2$	$\vec{V} \sin \varphi_2 \operatorname{cosec}^3 \alpha_2$	$-\frac{\vec{V}}{R_2} \sin^2 \varphi_3 \operatorname{cosec}^2 \alpha_3$				$\vec{V} \sin^2 \varphi'_3 \operatorname{cosec}^2 \alpha_1$
		$\left[\frac{1}{r_2} \sin^2 \alpha_2 \right]$					$-\frac{\vec{V}}{R_1} \sin^2 \varphi'_3 \operatorname{cosec}^2 \alpha_1$
		$+\left(\frac{1}{R_1} + \frac{1}{R_2} \right)$					
		$\sin \alpha_2 \sin \varphi_2$					

TABLE IV (contd.)

Atoms of the molecule.	co- ordi- nates.	H_1 γ_{512}, γ_1	H_2 γ_{123}, γ_2	H_3 γ_{234}, γ_3	H_4 γ_{345}, γ_4	H_5 γ_{451}, γ_5	H_1 γ_{512}, γ'_1
C_3			$-\frac{\vec{V}}{R_3} \sin^2 \varphi_2 \operatorname{cosec}^2 \alpha_2$	$\frac{\vec{V}}{R_3} \sin \varphi_3 \operatorname{cosec}^3 \alpha_3$	$-\frac{\vec{V}}{R_3} \sin^2 \varphi_3 \operatorname{cosec}^2 \alpha_3$		
			$\left[\frac{1}{r_3} \sin^2 \alpha_3 + \left(\frac{1}{R_2} + \frac{1}{R_4} \right) \right]$				
			$\sin \varphi_3 \sin \alpha_3$				
C_4			$-\frac{\vec{V}}{R_3} \sin^2 \varphi_3 \operatorname{cosec}^2 \alpha_3$	$\frac{\vec{V}}{R_3} \sin \varphi_3 \operatorname{cosec}^3 \alpha_3$	$-\frac{\vec{V}}{R_2} \sin^2 \varphi_2 \operatorname{cosec}^2 \alpha_2$		
				$\left[\frac{1}{r_4} \sin^2 \alpha_4 - \left(\frac{1}{R_3} + \frac{1}{R_2} \right) \right]$			
				$\sin \varphi_3 \sin \alpha_3$			
C_5		$-\frac{\vec{V}}{R_1} \sin^2 \varphi_1 \operatorname{cosec}^2 \alpha_1$		$-\frac{\vec{V}}{R_2} \sin^2 \varphi_3 \operatorname{cosec}^2 \alpha_3$	$\frac{\vec{V}}{R_2} \sin \varphi_2 \operatorname{cosec}^3 \alpha_2$	$-\frac{\vec{V}}{R_6} \sin^2 \varphi'_1 \operatorname{cosec}^2 \alpha_1$	
				$\left[\frac{1}{r_5} \sin^2 \alpha_2 + \left(\frac{1}{R_2} + \frac{1}{R_1} \right) \right]$			
				$\sin \varphi_2 \sin \alpha_2$			

TABLE A

Coordinates k	k'	μ_X	μ_C
τ_1	τ_1	$\frac{1}{R_1^2} (\text{cosec } \delta_1 + \cot \delta_1 + \cot \delta_2)^2$	$\left[\left\{ \frac{1}{R_2} \text{cosec } \delta_2 + \frac{1}{R_1} (\cot \delta_2 + \cot \delta_1) \right\}^2 + \frac{1}{R_2^2} \text{cosec }^2 \delta_2 + \frac{1}{R_1^2} \text{cosec }^2 \delta_1 \right]$
τ_5	τ_5		
τ_5	τ_5	$\frac{1}{R_1^2} \text{cosec}^2 \delta_2$	$\left[\left\{ \frac{1}{R_1} \text{cosec } \delta_2 + R_2 (\cot \delta_2 + \cot \delta_3) \right\}^2 - \frac{1}{R_3^2} \text{cosec }^2 \delta_3 - \right.$
τ_4	τ_4		$\left. \left\{ \frac{1}{R_3} \text{cosec } \delta_3 + \frac{1}{R_2} (\cot \delta_2 + \cot \delta_3) \right\}^2 \right]$
τ_3	τ_3		$2 \left[\frac{1}{R_2^2} \text{cosec }^2 \delta_3 + \left(\frac{1}{R_2} \text{cosec } \delta_3 - \frac{2}{R_1} \cot \delta_3 \right)^2 \right]$
τ_1	τ_5	$-\frac{1}{R_1^2} \text{cosec } \delta_2 (\text{cosec } \delta_1 + \cot \delta_1 + \cot \delta_2)$	$-\left[\left\{ \frac{1}{R_2} \text{cosec } \delta_2 + \frac{1}{R_1} (\cot \delta_2 + \cot \delta_1) \right\} \left\{ \frac{1}{R_1} \text{cosec } \delta_2 + \frac{1}{R_2} (\cot \delta_2 + \cot \delta_3) \right\} \right.$
τ_4	τ_5		$\left. + \frac{1}{R_1} \text{cosec } \delta_2 \left\{ \frac{1}{R_3} \text{cosec } \delta_3 + \frac{1}{R_2} (\cot \delta_2 + \cot \delta_3) \right\} \right]$
τ_2	τ_3		$\left[\frac{1}{R_2} \text{cosec } \delta_3 \left\{ \frac{1}{R_2} \text{cosec } \delta_2 + \frac{1}{R_1} (\cot \delta_2 + \cot \delta_1) \right\} + \frac{1}{R_2} \text{cosec } \delta_2 \right.$
			$\left. \left\{ \frac{1}{R_2} \text{cosec } \delta_3 + \frac{2}{R_3} \cot \delta_3 \right\} - \frac{1}{R_1 R_2} \text{cosec } \delta_1 \text{cosec } \delta_3 \right]$
τ_1	τ_4	$\frac{1}{R_1^2} \text{cosec } \delta_2 (\text{cosec } \delta_1 + \cot \delta_1 + \cot \delta_2)$	$\left[-\frac{1}{R_2 R_3} \text{cosec } \delta_2 \text{cosec } \delta_3 + \frac{1}{R_1} \text{cosec } \delta_1 \left\{ \frac{1}{R_1} \text{cosec } \delta_2 + \frac{1}{R_2} (\cot \delta_2 + \cot \delta_3) \right\} \right]$

TABLE A (contd)

Coordinates $k \quad k'$	μ_X	μ_C
$\tau_1 \quad \tau_5$	$-\frac{1}{R_1^2} (\text{cosec } \delta_1 + \cot \delta_1 + \cot \delta_2)^2$	$\left[-\frac{2}{R_1} \text{cosec } \delta_1 \left\{ \frac{1}{R_2} \text{cosec } \delta_2 + \frac{1}{R_1} (\cot \delta_1 + \cot \delta_2) \right\} \right]$
$\tau_2 \quad \tau_3$		$-\left[\frac{1}{R_2} \text{cosec } \delta_3 \left\{ \frac{1}{R_1} \text{cosec } \delta_2 + \frac{1}{R_2} (\cot \delta_2 + \cot \delta_3) \right\} \right] +$
$\tau_3 \quad \tau_4$		$\left\{ \frac{1}{R_3} \text{cosec } \delta_3 + \frac{1}{R_2} (\cot \delta_2 + \cot \delta_3) \right\} \left\{ \frac{1}{R_2} \text{cosec } \delta_3 + \frac{2}{R_3} \cot \delta_3 \right\} +$
		$\frac{1}{R_3} \text{cosec } \delta_3 \left(\frac{1}{R_2} \text{cosec } \delta_3 + \frac{2}{R_3} \cot \delta_3 \right) \right]$
$\tau_3 \quad \tau_4$	$-\frac{1}{R_1^2} \text{cosec }^2 \delta_2$	$\left[\frac{2}{R_3} \text{cosec } \delta_3 \left\{ \frac{1}{R_3} \text{cosec } \delta_3 + \frac{1}{R_2} (\cot \delta_2 + \cot \delta_3) \right\} \right]$
$\tau_3 \quad \tau_5$	$\frac{1}{R_1^2} \text{cosec } \delta_2 (\text{cosec } \delta_1 + \cot \delta_1 + \cot \delta_2)$	$\left[\frac{1}{R_1} \text{cosec } \delta_1 \left\{ \frac{1}{R_3} \text{cosec } \delta_2 + \frac{1}{R_2} (\cot \delta_2 + \cot \delta_3) \right\} - \frac{1}{R_2 R_3} \text{cosec } \delta_2 \text{ cosec } \delta_3 \right]$
$\tau_3 \quad \tau_5$		$\left[-\frac{1}{R_1 R_2} \text{cosec } \delta_1 \text{ cosec } \delta_2 + \frac{1}{R_2} \text{cosec } \delta_2 \left(\frac{1}{R_2} \text{cosec } \delta_3 + \frac{2}{R_3} \cot \delta_3 \right) + \right.$
	$g_{kk'} = g_{k'k}$	$\left. \frac{1}{R_2} \text{cosec } \delta_3 \left\{ \frac{1}{R_2} \text{cosec } \delta_2 + \frac{1}{R_1} (\cot \delta_2 + \cot \delta_1) \right\} \right]$

TABLE B (contd.)

Coordinates k	k'	μ_H	μ_X	μ_C
γ_2	$\left. \begin{matrix} \gamma_4 \\ \gamma_3 \end{matrix} \right\}$			$\left\{ \frac{1}{r_{3,4}} \sin^2 \alpha_3 \cdots \left(\frac{1}{R_2} + \frac{1}{R_3} \right) \sin \varphi_3 \sin \alpha_3 \right\}$
γ_3				$\frac{1}{R_2 R_3} \sin^2 \varphi_2 \sin^2 \varphi_3 \operatorname{cosec}^2 \alpha_2 \operatorname{cosec}^2 \alpha_3$
γ_2	γ_5		$\frac{1}{R_1^2} \sin^4 \varphi_2 \operatorname{cosec}^4 \alpha_2$	
γ_3	γ_4			$\left[-\frac{1}{R_3} \sin^3 \varphi_3 \operatorname{cosec}^5 \alpha_3 \left\{ \frac{1}{r} \sin^2 \alpha_3 + \frac{1}{r_4} \sin^2 \alpha_3 \right. \right.$
			$\left. \left. 2 \left(\frac{1}{R_2} + \frac{1}{R_3} \right) \sin \varphi_2 \sin \alpha_3 \right. \right]$	
γ_2	$\left. \begin{matrix} \gamma_1' \\ \gamma_1 \end{matrix} \right\}$			$\left[-\left(\frac{1}{R_1} \sin^2 \varphi_1' \sin \varphi_2 \operatorname{cosec}^2 \alpha_1 \operatorname{cosec}^2 \alpha_2 \right) \right.$
γ_3			$\left(\frac{1}{r_1} \sin^2 \alpha_1 + \frac{2}{R_1} \sin \varphi_1' \sin \alpha_1 \right)$	$\left. \left(\frac{1}{r_{2,5}} \sin^2 \alpha_2 + \left(\frac{1}{R_1} - \frac{1}{R_2} \right) \sin \alpha_2 \sin \varphi_2 \right) \right]$
γ_1	γ_1'			$\left[\left(\sin \varphi_1 \sin \varphi_1' \operatorname{cosec}^2 \alpha_1 \right) \right.$
			$\left(\frac{1}{r_1} \sin^2 \alpha_1 + \frac{2}{R_1} \sin \alpha_1 \sin \varphi_1 \right)$	$\left. \left[\frac{2}{R_1^2} \sin^2 \varphi_1 \sin^2 \varphi_1' \sin^4 \alpha_1 \right] \right]$
			$\left(\frac{1}{r_1'} \sin^2 \alpha_1 + \frac{2}{R_1} \sin \varphi_1' \sin \alpha_1 \right)$	
γ_3	γ_1'			$\frac{1}{R_1 R_2} \sin^2 \varphi_1 \sin^2 \varphi_1' \operatorname{cosec}^2 \alpha_3 \operatorname{cosec}^2 \alpha_1$
γ_4	γ_1'			

The first suffix with regards to r is to be associated always with the first pair of coordinates in the brackets under the first column . The same notation follows for the second suffix also.

TABLE C

Coordinates k		μ_X	μ_C
τ_1	γ_1	$-\left\{\frac{1}{R_1} \sin \varphi_1 \operatorname{cosec}^3 a_1 (\operatorname{cosec} \delta_1 + \cot \delta_1 + \cot \delta_2) \right. \\ \left. \left(\frac{1}{r_1} \sin 2a_1 + \frac{2}{R_1} \sin a_1 \sin \varphi_1\right)\right\}$	$-\left[\frac{1}{R_1} \sin 2\varphi_1 \operatorname{cosec}^2 a_1 \left\{\frac{1}{R_2} \operatorname{cosec} \delta_2 + \frac{1}{R_1} (\cot \delta_2 + \cot \delta_1)\right\} \right. \\ \left. + \frac{1}{R_1^2} \sin 2\varphi_1 \operatorname{cosec}^2 a_1 \operatorname{cosec} \delta_1\right]$
τ_2	γ_2	$-\frac{1}{R_1^2} \sin 2\varphi_2 \operatorname{cosec}^2 a_2 \operatorname{cosec} \delta_2$	$-\left[\sin \varphi_2 \operatorname{cosec}^3 a_2 \left\{\frac{1}{R_1} \operatorname{cosec} \delta_2 + \frac{1}{R_2} (\cot \delta_2 + \cot \delta_3)\right\} \right. \\ \left.\left\{\frac{1}{r_2} \sin 2a_2 + \left(\frac{1}{R_1} + \frac{1}{R_2}\right) \sin a_2 \sin \varphi_2\right\} + \frac{1}{R_2} \sin 2\varphi_2 \operatorname{cosec}^2 a_2 \right. \\ \left.\left\{\frac{1}{R_3} \operatorname{cosec} \delta_3 + \frac{1}{R_2} (\cot \delta_2 + \cot \delta_3)\right\}\right]$
τ_3	γ_3		$-\left[\frac{1}{R_2^2} \sin 2\varphi_3 \operatorname{cosec}^2 a_3 \operatorname{cosec} \delta_3 + \left(\frac{1}{R_2} \operatorname{cosec} \delta_3 + \frac{2}{R_3} \cot \delta_3\right) \right. \\ \left.\left\{\sin \varphi_3 \operatorname{cosec}^3 a_3\right\}\left\{\frac{1}{r_3} \sin 2a_3 + \left(\frac{1}{R_2} + \frac{1}{R_3}\right) \sin \varphi_3 \sin a_3\right\} + \right. \\ \left.\frac{1}{R_3} \sin 2\varphi_3 \operatorname{cosec}^2 a_3 \left(\frac{1}{R_2} \operatorname{cosec} \delta_3 + \frac{2}{R_3} \cot \delta_3\right)\right]$
τ_4	γ_4		$-\left[\frac{1}{R_2^2} \sin 2\varphi_3 \operatorname{cosec}^2 a_3 \operatorname{cosec} \delta_3 + \left\{\frac{1}{R_3} \operatorname{cosec} \delta_3 + \frac{1}{R_2} (\cot \delta_2 + \cot \delta_3)\right\} \right. \\ \left.\sin \varphi_3 \operatorname{cosec}^3 a_3 \left\{\frac{1}{r_3} \sin 2a_3 + \left(\frac{1}{R_3} + \frac{1}{R_2}\right) \sin \varphi_3 \sin a_3\right\} + \right. \\ \left.\frac{1}{R_2} \sin 2\varphi_3 \operatorname{cosec}^2 a_3 \left\{\frac{1}{R_1} \operatorname{cosec} \delta_2 + \frac{1}{R_2} (\cot \delta_2 + \cot \delta_3)\right\}\right]$

TABLE C (contd)

Coordinate k	k'	μ_X	μ_C
τ_5	γ_5	$-\frac{1}{R_1^2} \sin^2 \varphi_2 \operatorname{cosec}^2 \alpha_2 (\operatorname{cosec} \delta_1 + \cot \delta_1 + \cot \delta_2)$	$-\left[\frac{1}{R_2^2} \sin^2 \varphi_2 \operatorname{cosec}^2 \alpha_2 \operatorname{cosec} \delta_2 + \left\{ \frac{1}{R_2} \operatorname{cosec} \delta_2 + \frac{1}{R_1} (\cot \delta_2 + \cot \delta_1) \right\} \right.$ $\left. \sin \varphi_2 \operatorname{cosec}^3 \alpha_2 \left\{ \frac{1}{r_5} \sin^2 \alpha_2 + \left(\frac{1}{R_2} + \frac{1}{R_1} \right) \sin \varphi_2 \sin \alpha_2 \right\} \right]$
τ_1	γ_2	$\frac{1}{R_1^2} \sin^2 \varphi_2 \operatorname{cosec}^2 \alpha_2 (\operatorname{cosec} \delta_1 + \cot \delta_1 + \cot \delta_2)$	$\left[\left\{ \frac{1}{R_2} \operatorname{cosec} \delta_2 + \frac{1}{R_1} (\cot \delta_1 + \cot \delta_2) \right\} \left\{ \sin \varphi_2 \operatorname{cosec}^3 \alpha_2 \right\} \right.$ $\left. \left\{ \frac{1}{r_2} \sin^2 \alpha_2 + \left(\frac{1}{R_1} + \frac{1}{R_2} \right) \sin \alpha_2 \sin \varphi_2 \right\} + \frac{1}{R_2^2} \sin^2 \varphi_2 \operatorname{cosec}^2 \alpha_2 \operatorname{cosec} \delta_2 \right]$
τ_1	γ_3		$-\left[\frac{1}{R_2} \sin^2 \varphi_3 \operatorname{cosec}^2 \alpha_3 \left\{ \frac{1}{R_2} \operatorname{cosec} \delta_2 + \frac{1}{R_1} (\cot \delta_2 + \cot \delta_1) \right\} \right.$ $\left. + \frac{1}{R_2} \sin \varphi_3 \operatorname{cosec}^3 \alpha_3 \operatorname{cosec}^2 \delta_2 \left\{ \frac{1}{r_3} \sin^2 \alpha_3 + \left(\frac{1}{R_2} + \frac{1}{R_1} \right) \sin \varphi_3 \sin \alpha_3 \right\} \right]$
τ_1	γ_4		$\left[\frac{1}{R_2 R_3} \operatorname{cosec} \delta_2 \operatorname{cosec}^2 \alpha_3 \sin^2 \varphi_3 + \frac{1}{R_1 R_2} \operatorname{cosec} \delta_1 \operatorname{cosec}^2 \alpha_3 \sin^2 \varphi_3 \right]$
τ_1	γ_5	$\frac{1}{R_1^2} \sin^2 \varphi_2 \operatorname{cosec}^2 \alpha_2 (\operatorname{cosec} \delta_1 + \cot \delta_1 + \cot \delta_2)$	$\left[\frac{1}{R_1} \sin \varphi_2 \operatorname{cosec}^3 \alpha_2 \operatorname{cosec} \delta_1 \left\{ \frac{1}{r_5} \sin^2 \alpha_2 + \left(\frac{1}{R_2} + \frac{1}{R_1} \right) \sin \varphi_2 \sin \alpha_2 \right\} \right]$
τ_2	γ_1	$\frac{1}{R_1} \sin \varphi_1 \operatorname{cosec}^3 \alpha_1 \operatorname{cosec} \delta_2 \left(\frac{1}{r_1} \sin^2 \alpha_1 + \frac{2}{R_1} \sin \alpha_1 \sin \varphi_1 \right)$	$\left[\frac{1}{R_1} \sin^2 \varphi_1 \operatorname{cosec}^2 \alpha_1 \left\{ \frac{1}{R_1} \operatorname{cosec} \delta_2 + \frac{1}{R_2} (\cot \delta_2 + \cot \delta_1) \right\} \right]$
τ_2	γ_3		$\left[\frac{1}{R_2} \sin^2 \varphi_3 \operatorname{cosec}^2 \alpha_3 \left\{ \frac{1}{R_1} \operatorname{cosec} \delta_2 + \frac{1}{R_2} (\cot \delta_2 + \cot \delta_1) \right\} \right.$ $\left. + \sin \varphi_3 \operatorname{cosec}^3 \alpha_3 \left\{ \frac{1}{R_3} \operatorname{cosec} \delta_3 + \frac{1}{R_2} (\cot \delta_2 + \cot \delta_1) \right\} \right]$

TABLE C (contd.)

Coordinates k k'		μ_X	μ_C
γ_2	γ_4		$\left\{ \frac{1}{r_3} \sin^2 a_1 - \left(\frac{1}{R_2} + \frac{1}{R_3} \right) \sin \varphi_3 \sin a_3 \right\} - \frac{1}{R_3^2} \sin^2 \varphi_3 \operatorname{cosec}^2 a_3 \operatorname{cosec} \delta_3$ $- \left[\frac{1}{R_3} \sin^2 \varphi_3 \operatorname{cosec}^2 a_3 \left\{ \frac{1}{R_3} \operatorname{cosec} \delta_3 + \frac{1}{R_2} (\cot \delta_2 + \cot \delta_3) \right\} \right.$ $\left. + \frac{1}{R_3} \sin \varphi_3 \operatorname{cosec}^3 a_3 \operatorname{cosec} \delta_3 \left\{ \frac{1}{r_4} \sin^2 a_3 + \left(\frac{1}{R_3} + \frac{1}{R_2} \right) \sin \varphi_3 \sin a_3 \right\} \right]$
γ_2	γ_5	$-\frac{1}{R_2^2} \sin^2 \varphi_2 \operatorname{cosec}^2 a_2 \operatorname{cosec} \delta_2$	$\frac{1}{R_2 R_3} \sin^2 \varphi_2 \operatorname{cosec}^2 a_2 \operatorname{cosec} \delta_3$
γ_3	γ_2		$\left[\frac{1}{R_2} \sin \varphi_2 \operatorname{cosec}^3 a_2 \operatorname{cosec} \delta_3 \left\{ \frac{1}{r_2} \sin^2 a_2 + \left(\frac{1}{R_1} + \frac{1}{R_2} \right) \sin a_2 \sin \varphi_2 \right\} \right]$ $+ \frac{1}{R_2} \sin^2 \varphi_2 \operatorname{cosec}^2 a_2 \left(\frac{1}{R_2} \operatorname{cosec} \delta_3 + \frac{2}{R_3} \cot \delta_3 \right)]$
γ_3	γ_4		$\left[\frac{1}{R_3} \sin^2 \varphi_3 \operatorname{cosec}^2 a_3 \left(\frac{1}{R_2} \operatorname{cosec} \delta_3 + \frac{2}{R_3} \cot \delta_3 \right) \right]$ $+ \sin \varphi_3 \operatorname{cosec}^3 a_3 \left(\frac{1}{R_2} \operatorname{cosec} \delta_3 + \frac{2}{R_3} \cot \delta_3 \right) \left\{ \frac{1}{r_4} \sin^2 a_3 + \left(\frac{1}{R_2} + \frac{1}{R_3} \right) \sin \varphi_3 \sin a_3 \right\} + \frac{1}{R_2^2} \sin^2 \varphi_3 \operatorname{cosec}^2 a_3 \operatorname{cosec} \delta_3$
γ_3	γ_5		$- \left[\frac{1}{R_2} \sin^2 \varphi_2 \operatorname{cosec}^2 a_2 \left(\frac{1}{R_2} \operatorname{cosec} \delta_3 + \frac{2}{R_3} \cot \delta_3 \right) + \frac{1}{R_2} \sin \varphi_2 \operatorname{cosec}^3 a_2 \operatorname{cosec} \delta_3 \left\{ \frac{1}{r_2} \sin^2 a_2 + \left(\frac{1}{R_1} + \frac{1}{R_2} \right) \sin a_2 \sin \varphi_2 \right\} \right]$

TABLE C (contd.)

Coordinates k, k'		μ_X	μ_C
τ_4	γ_1	$-\frac{1}{R_1} \sin \varphi_1 \operatorname{cosec}^2 \alpha_1 \operatorname{cosec} \delta_2 \left(\frac{1}{r_1} \sin^2 \alpha_1 + \frac{2}{R_1} \sin \alpha_1 \sin \varphi_1 \right) - \left[\frac{1}{R_1} \sin^2 \varphi_1 \operatorname{cosec}^2 \alpha_1 \left\{ \frac{1}{R_1} \operatorname{cosec} \delta_2 + \frac{1}{R_2} (\cot \delta_2 - \cot \delta_3) \right\} \right] - \frac{1}{R_2 R_3} \sin^2 \varphi_2 \operatorname{cosec}^2 \alpha_2 \operatorname{cosec} \delta_3$	
τ_4	γ_2	$\frac{1}{R_1^2} \sin^2 \varphi_1 \operatorname{cosec}^2 \alpha_2 \operatorname{cosec} \delta_2$	
τ_4	γ_3		$\left[\frac{1}{R_3} \sin \varphi_3 \operatorname{cosec}^2 \alpha_3 \operatorname{cosec} \delta_3 \left\{ \frac{1}{r_3} \sin^2 \alpha_3 + \left(\frac{1}{R_2} + \frac{1}{R_3} \right) \sin \varphi_3 \sin \alpha_3 \right\} - \frac{1}{R_2} \sin^2 \varphi_3 \operatorname{cosec}^2 \alpha_3 \left\{ \frac{1}{R_2} \operatorname{cosec} \delta_3 + \frac{1}{R_2} (\cot \delta_2 - \cot \delta_3) \right\} \right]$
τ_4	γ_5	$\frac{1}{R_1^2} \sin^2 \varphi_2 \operatorname{cosec}^2 \alpha_2 \operatorname{cosec} \delta_2$	$\left[\frac{1}{R_2} \sin^2 \varphi_2 \operatorname{cosec}^2 \alpha_2 \left\{ \frac{1}{R_1} \operatorname{cosec} \delta_3 + \frac{1}{R_2} (\cot \delta_2 + \cot \delta_3) \right\} + \sin \varphi_2 \operatorname{cosec}^2 \alpha_2 \left\{ \frac{1}{R_1} \operatorname{cosec} \delta_1 + \frac{1}{R_2} (\cot \delta_2 - \cot \delta_3) \right\} \right. \\ \left. \left\{ \frac{1}{r_3} \sin^2 \alpha_2 + \left(\frac{1}{R_2} - \frac{1}{R_1} \right) \sin \varphi_2 \sin \alpha_2 \right\} \right]$
τ_5	γ_1	$\frac{1}{R_1} \sin \varphi_1 \operatorname{cosec}^2 \alpha_1 (\operatorname{cosec} \delta_1 + \cot \delta_1 - \cot \delta_2)$	$\left[\frac{1}{R_1} \sin^2 \varphi_1 \operatorname{cosec}^2 \alpha_1 \operatorname{cosec} \delta_1 - \frac{1}{R_1} \sin^2 \varphi_1 \operatorname{cosec}^2 \alpha_1 \right. \\ \left. \left\{ \frac{1}{R_2} \operatorname{cosec} \delta_2 (\cot \delta_1 - \cot \delta_2) \right\} \right]$
τ_5	γ_2	$-\frac{1}{R_1^2} \sin^2 \varphi_2 \operatorname{cosec}^2 \alpha_2 (\operatorname{cosec} \delta_1 - \cot \delta_1 - \cot \delta_2)$	$-\left[\frac{1}{R_1} \sin \varphi_2 \operatorname{cosec}^2 \alpha_2 \operatorname{cosec} \delta_1 \left\{ \frac{1}{r_2} \sin^2 \alpha_2 + \left(\frac{1}{R_1} + \frac{1}{R_2} \right) \sin \varphi_2 \sin \alpha_2 \right\} \right]$

TABLE C (contd.)

Coordinates k k'	μ_X	μ_C
$\tau_3 \quad \gamma_3$		$\left[\frac{1}{R_2 R_1} \sin^2 \varphi_3 \operatorname{cosec}^2 \alpha_3 \operatorname{cosec} \delta_1 - \frac{1}{R_2 R_3} \sin^2 \varphi_3 \operatorname{cosec}^2 \alpha_3 \operatorname{cosec} \delta_2 \right]$
$\tau_5 \quad \gamma_4$		$\left[\frac{1}{R_2} \sin \varphi_3 \operatorname{cosec}^2 \alpha_3 \operatorname{cosec} \delta_2 \left\{ \frac{1}{r_4} \sin^2 \alpha_3 - \left(\frac{1}{R_2} - \frac{1}{R_3} \right) \sin \varphi_3 \sin \alpha_3 \right\} + \right.$ $\left. - \frac{1}{R_2} \sin^2 \varphi_3 \operatorname{cosec}^2 \alpha_3 \left[\frac{1}{R_2} \operatorname{cosec} \delta_2 + \frac{1}{R_1} (\cot \delta_1 + \cot \delta_2) \right] \right]$
$\tau_1 \quad \gamma'_1$	$-\frac{1}{R_1} (\operatorname{cosec} \delta_1 + \cot \delta_1 + \cot \delta_2) \sin \varphi'_1 \operatorname{cosec}^2 \alpha_1$	$-\left[\frac{1}{R_1} \sin^2 \varphi'_1 \operatorname{cosec}^2 \alpha_1 \left\{ \frac{1}{R_2} \operatorname{cosec} \delta_2 + \frac{1}{R_1} (\cot \delta_1 - \cot \delta_2) \right\} + \right.$
$\tau_2 \quad \gamma'_1$	$\left(\frac{1}{r'_1} \sin^2 \alpha_1 + \frac{2}{R_1} \sin \varphi'_1 \sin \alpha_1 \right)$	$\frac{1}{R_1^2} \sin^2 \varphi'_1 \operatorname{cosec}^2 \alpha_1 \operatorname{cosec} \delta_1$
$\tau_2 \quad \gamma'_1$	$\frac{1}{R_1} \sin \varphi'_1 \operatorname{cosec}^2 \alpha_1 \operatorname{cosec} \delta_2 \left(\frac{1}{r'_1} \sin^2 \alpha_1 + \frac{2}{R_1} \sin \varphi'_1 \sin \alpha_1 \right)$	$\left[\frac{1}{R_1} \sin^2 \varphi'_1 \operatorname{cosec}^2 \alpha_1 \left\{ \frac{1}{R_1} \operatorname{cosec} \delta_2 - \frac{1}{R_2} (\cot \delta_2 + \cot \delta_3) \right\} \right]$
$\tau_4 \quad \gamma'_1$	$-\frac{1}{R_1} \sin \varphi'_1 \operatorname{cosec}^2 \alpha_1 \operatorname{cosec} \delta_2 \left(\frac{1}{r'_1} \sin^2 \alpha_1 + \frac{2}{R_1} \sin \varphi'_1 \sin \alpha_1 \right)$	$-\left[\frac{1}{R_1} \sin^2 \varphi'_1 \operatorname{cosec}^2 \alpha_1 \left\{ \frac{1}{R_1} \operatorname{cosec} \delta_2 + \frac{1}{R_2} (\cot \delta_2 + \cot \delta_3) \right\} \right]$
$\tau_5 \quad \gamma'_1$	$\frac{1}{R_1} \sin \varphi'_1 \operatorname{cosec}^2 \alpha_1 (\operatorname{cosec} \delta_1 + \cot \delta_1 + \cot \delta_2)$	$\left[\frac{1}{R_1^2} \sin^2 \varphi'_1 \operatorname{cosec}^2 \alpha_1 \operatorname{cosec} \delta_1 - \frac{1}{R_1} \sin^2 \varphi'_1 \operatorname{cosec}^2 \alpha_1 \right.$
	$\left(\frac{1}{r'_1} \sin^2 \alpha_1 + \frac{2}{R_1} \sin \varphi'_1 \sin \alpha_1 \right)$	$\left. \left\{ \frac{1}{R_2} \operatorname{cosec} \delta_2 + \frac{1}{R_1} (\cot \delta_2 + \cot \delta_1) \right\} \right]$
$g_{\tau_3 \gamma'_1} = g_{\tau_3 \gamma_1} = 0$		$g_{kk'} = g_{k'k}$

The significance of various symbols can be found in the text. The applicability of these with regard to the substituted Furans, thiophenes, and pyrroles is mentioned in the text i.e., subjected to the statements 5.....9 stated therein.

As all the ring angles are found to be obtuse for the above molecules, the supplementary values of the α 's are introduced and denoted by δ with the proper change in sign as regards the trigonometrical expressions.

The expressions are the same for any substituted compound of the above molecules, if,

- (i) the equilibrium angles and distances are assumed to remain unaltered,
- (ii) planar structure of the molecule is retained, and
- (iii) substitution is made on the H atoms. They will hold even if the substitution is made on the H atoms of the (CH_2) group in cyclopentadiene and the H atom of N—H bond in case of pyrrole (figure 2c).

But when substitution is made on the ring atom the general expressions in Table I should be used, as the equilibrium distances and angles are expected to vary.

In Table III are given the s vector expressions for the atoms when out-of-plane bending coordinates are considered using the expressions given by Malhiot and Ferigle (1955).

The particular expressions applicable to furan, pyrrole, thiophene and cyclopentadiene are shown separately in Table IV. While reading the Table IV the following points are to be noted ;

1. The expressions under 1st and 6th columns do not arise in case of furan, thiophene and their substitutions as there are no bonds on atom (1) defining γ in the above cases.
2. Column 1 should be used along with the other columns in case of pyrrole and its substitutions. However, column 6 should be omitted in this case also.
3. All the 6 columns should be used for cyclopentadiene and its substitutions where the 1st and the last columns represent the out of plane bending of the two C—H bonds of (CH_2) group.
4. In all the above cases except in cyclopentadiene

$$\phi_1 = W - \frac{\alpha_i}{2} \text{ where } i = 1, 2 \text{ and } 3.$$

But in case of cyclopentadiene $\phi_1' = \phi_1 +$ the angle formed between the two C—H bonds of CH_2 group. And the remaining ϕ 's satisfy

$$\phi_i = W - \frac{\alpha_i}{2}$$

where i now stands for 2 and 3 only (Fig. 2abc).

5. In all the above cases it is seen from the experimental data that $r_1' = r_1$ (equilibrium C—H bond length of CH_2 group in cyclopentadiene) and $r_2 = r_3$

$= r_4 = r_5$ equilibrium C—H bond length in all the molecules. The Table IV is applicable for all the substituted compounds if it is assumed that.

6. The angles of the ring of the substituted compound remain unaltered from those of its parent molecule.

7. The bond distances of the ring in the equilibrium position also remain unaltered for the substituted compounds and

8. The orientation of the bonds remain unaltered for the substituted compounds. Assumptions 6, 7, 8 are considered to be fairly justifiable if the substitutions are made not on the ring but on the H atoms of the parent molecules.

9. The other factors being satisfied, Table IV is applicable even if different substitutions are made on the H atoms. It is for this purpose only r_i 's are retained in the Table IV without taking into consideration the statements of 5. (Otherwise Table III should be referred to, which is applicable even if the ring atom is substituted for). In all these tables \vec{V} stands for the unit vector upwards perpendicular to the equilibrium plane of the molecule.

(b) *Inverse kinetic energy matrix elements*

Using Tables II and IV and the equation 1, the elements of the inverse kinetic energy matrix of torsional vibrations, out-of-plane bending vibrations and the interaction between the above two are derived, and are separately given in Tables A, B & C. While reading these tables, the first column represents the pair of the coordinates contributing to the matrix μ_C , μ_H and μ_X , are the reciprocal masses of carbon atom, hydrogen atom and O, N, S or C according as the atom is oxygen, nitrogen, sulphur or carbon. The coefficients of the reciprocal masses are given under the corresponding columns. The absence of expression under any column and against any row means that, the particular μ vanishes in the corresponding element g . In order to read a particular $g_{kk'}$, the expressions against that pair of coordinates are to be first multiplied by the corresponding μ 's and then finally added up, for example $g_{\gamma_1\gamma_1}$ in Table B $g_{\gamma_1\gamma_1}$ is

$$\mu_H \frac{1}{r_1^2} \sin^2 \phi_1 \operatorname{cosec}^2 \alpha_1 + \mu_X \left[\sin^2 \phi_1 \operatorname{cosec}^2 \alpha_1 \left(\frac{1}{r_1} \sin^2 \alpha_1 + \frac{2}{R_1} \sin \alpha_1 \sin \phi_1 \right)^2 \right] + 2\mu_C \frac{\sin^4 \phi_1 \operatorname{cosec}^2 \alpha_1}{R_1^2}$$

In all these tables it is to be noted that $g_{kk'} = g_{k'k}$. The elements can be directly used to arrive at the (G) matrix elements for the out-of-plane modes of vibrations for furan, pyrrole, thiophene, cyclopentadiene and their substitutions, leading ultimately to values of the out-of-plane valence force constants for these molecules.

ACKNOWLEDGMENTS

The author is highly indebted to Prof. K. R. Rao for his invaluable guidance and keen interest during the progress of this work. She is equally indebted to the Government of India for awarding a Senior Research Scholarship.

REFERENCES

- Decius, J. C. 1948, *J. Chem. Phys.*, **16**, 1025.
Decius, J. C., 1949, *J. Chem. Phys.*, **17**, 1315.
Lohman, J. B., 1951, Office of Naval Research, Tech. Report, 17.
Miller, F. A., and Crawford Jr., B. L., 1946, *J. Chem. Phys.*, **14**, 282.
Robert, J. Malhiot and Slavador, M. Ferigle, 1955, *J. Chem. Phys.*, **23**, 30.
Robert, J. Malhiot and Salvador M. Ferigle, 1954, *J. Chem. Phys.*, **22**, 717.
Santhamma, V., 1954, *Proc. Natl. Inst. Sci. India*, **20**, 245.
Wilson Bright (Jr), 1939, *J. Chem. Phys.*, **7**, 1045.
Wilson Bright (Jr), 1941, *J. Chem. Phys.*, **9**, 76.

MAGNETIC MOMENTS OF THE NUCLEONS

S. K. KUNDU

DEPARTMENT OF THEORETICAL PHYSICS, INDIAN ASSOCIATION FOR THE CULTIVATION OF
SCIENCE, CALCUTTA-32

(Received for publication April 28, 1956)

ABSTRACT. It has been shown here how the magnetic moment of the neutron varies with cut-off limit of the momentum of the meson which the neutron emits and reabsorbs. Moreover, the influence of the magnetic field on the proton is included in the energy denominator of the perturbation matrix elements.

Both the proton and neutron have values for the magnetic moments different from what one would expect from Dirac's theory. This difference is explained by the hypothesis that the proton (or the neutron) dissociates into a neutron (or a proton) and a positive (or negative) meson. As the meson has spin and charge, it will have a magnetic moment which has a larger value than that of the proton on account of the smallness of the meson mass. What we observe as the magnetic moment of the proton is really the time average of the protonic and mesonic magnetic moments. The self energy of a proton, subjected to a weak homogeneous magnetic field, would arise from the virtual emission and reabsorption of mesons by the protons, if we calculate the energy for the above process, the term appearing as co-efficient to H , the magnetic field strength, is identified as the additional magnetic moment. The evaluation of such an addition to the magnetic moment involves an integration over the different momentum values of the virtual meson; theoretically a meson may be emitted with any value of the momentum, however the integral becomes infinite if we put ∞ as the upper limit for the meson momentum. Various attempts have been made to eliminate this difficulty. One of them is to put a maximum limit for the meson momentum which is the well known cut-off procedure.

In the present paper, we have tried to show in which way the magnetic moments of the proton and the neutron vary with the cut-off limit of the meson momentum. Further, it may be worthwhile to see how the inclusion of the magnetic energy of the proton in the denominator of the perturbation matrix elements influences the cut-off limits.

From the perturbation theory, the self energy of a neutron, which arises from the interaction with the corresponding meson field in the presence of a weak homogeneous magnetic field H , is given by (Fröhlich and others, 1938)

$$W_N = \frac{-H'_{01}H'_{10}}{E_0 - E_1} \quad \dots \quad (1)$$

H'_{01} denotes the matrix element for the emission of the negative meson by the neutron and H'_{10} denotes its reabsorption by the same nucleon. The spin of the virtual meson is in the direction of the magnetic field. E_0 and E_1 are the energies of the system in the initial and intermediate states respectively. Accordingly (putting $\chi = \frac{M_Y c}{\hbar}$ and $p = k\hbar$, where M_Y and p are the mass and momentum of the virtual meson emitted)

$$E_0 - E_1 = - \left(\frac{e\hbar}{2M_{p,c}} H + \frac{-e\hbar}{2M_{Y,c}} H + \hbar c \sqrt{k^2 + \chi^2} \right) \quad \dots \quad (2)$$

where the first two terms in the right hand side of (2) correspond to the energy of the proton and the virtual meson in the magnetic field H and the last term denotes the free energy of the emitted meson.

Taking the Lagrangian density of the charged vector meson to be of the form

$$\begin{aligned} L = & -\chi^2 (\psi^*_{\mu} \psi_{\mu} + \frac{1}{2} G^*_{\mu\nu} G_{\mu\nu}) \\ & -\chi^2 (g \tau_{NP} v_{\mu} \psi^*_{\mu} + g^* \tau_{PN} v^*_{\mu} \psi_{\mu}) \\ & -\chi^2 (f \tau_{NP} \frac{1}{2} U_{\mu\nu} (G^*_{\mu\nu} + f^* \tau_{PN} \frac{1}{2} U^*_{\mu\nu} G_{\mu\nu} \bar{v})) \quad \dots \quad (3) \end{aligned}$$

where

$$\begin{aligned} G_{\mu\nu} &= \frac{1}{\chi} \left(\frac{\partial}{\partial x_{\mu}} \psi_{\nu} - \frac{\partial}{\partial x_{\nu}} \psi_{\mu} \right) \\ v_{\mu} &= \Phi_N^{\dagger} \gamma_{\mu} \Phi_P, \quad u_{\mu\nu} = \Phi_N^{\dagger} \gamma_{\mu} \gamma_{\nu} \phi_P \end{aligned}$$

g and f denote the strength of the interaction.

Assuming the nucleon to be at rest the matrix element for the emission and absorption of the negatively charged transverse meson will be (vide March, 1951)

$$H'_{n^{-}jk, n^{-}jk+1} = \sum_{j=1,2} \sum_k \chi f \sqrt{\frac{\hbar c}{2V}} (n^{-}_{jk} + 1)^{1/2} (k^2 + \chi^2)^{-1/4} \left[\vec{\sigma} \cdot \text{curl} \left(\vec{r}_{jk} e^{i \vec{k} \cdot \vec{X}} \right) \right] \tau_{NP}^{(0)} \quad \dots \quad (4)$$

and

$$H'_{n^{-}jk+1, n^{-}jk} = - \sum_{j=1,2} \sum_k \chi f^* \sqrt{\frac{\hbar c}{2V}} \sqrt{n^{-}_{jk}} (k^2 + \chi^2)^{-1/4} \left[\vec{\sigma} \cdot \text{curl} \left(\vec{r}_{jk} e^{i \vec{k} \cdot \vec{X}} \right) \right] \tau_{PN}^{(0)} \quad \dots \quad (5)$$

where $\vec{\epsilon}_{jk}$ is a unit vector in the direction of polarisation corresponding to all possible values of k , for the transverse meson $j = 1, 2$ and for the longitudinal meson $j = 3$, with $\vec{\epsilon}_{3k}$ in the direction of k . V is the volume in which the field is confined and in which all the functions are assumed to be periodic. σ denotes the spin matrix of the nucleon.

The index (0) indicates that the expressions in brackets have to be taken at the point occupied by the nucleon.

Now remembering that the meson is subjected to a weak homogeneous magnetic field H , we find on using (4) and (5)

$$H'_{01} = -i\chi f \sqrt{\hbar c/2v} \sum_{j=1,2} \sum_k \left[\frac{\hbar c}{\hbar c \sqrt{k^2 + \chi^2} + 2M_Y c} - \frac{e\hbar}{2M_Y c} H \right] \left[\vec{\sigma}(\vec{\epsilon}_{jk} \times \vec{k}) \right] e^{-i(\vec{k} \cdot \vec{X}(0))} \tau_{NP} \quad \dots (6)$$

and

$$H'_{10} = i\chi f^* \sqrt{\hbar c/2v} \sum_{j=1,2} \sum_k \left[\frac{\hbar c}{\hbar c \sqrt{k^2 + \chi^2} + 2M_Y c} - \frac{e\hbar}{2M_Y c} H \right] \left[\vec{\sigma}(\vec{\epsilon}_{jk} \times \vec{k}) \right] e^{+i(\vec{k} \cdot \vec{X}(0))} \tau_{PN} \quad \dots (7)$$

Since we are concerned with a meson having spin in the direction of the magnetic field H , using (6) and (7), the self energy takes the form.

$$W_N = \frac{1}{3} f f^* \chi^2 (\hbar c/2V) \sum_{j=1,2} \sum_k \left[\frac{\hbar c}{\hbar c \sqrt{k^2 + \chi^2} + 2M_Y c} - \frac{e\hbar}{2M_Y c} H \right] \frac{\left[\vec{\sigma}(\vec{\epsilon}_{jk} \times \vec{k}) \right] \left[\vec{\sigma}(\vec{\epsilon}_{jk} \times \vec{k}) \right]}{-\hbar c \left[\sqrt{k^2 + \chi^2} - \frac{eH}{2M_Y c^2} \left(1 - \frac{M_Y}{M_P} \right) \right]} \tau_{NP} \tau_{PN}$$

Summing over the two polarisations $j = 1, 2$, replacing \sum_k by the integral $\int d\Omega \int dk \frac{v}{(2\pi)^3} k^2$ and multiplying both the numerator and denominator by $\left[(k^2 + \chi^2) + \frac{eH}{M_Y c^2} \sqrt{k^2 + \chi^2} \left(1 - \frac{1}{2} \frac{M_Y}{M_P} \right) + \frac{e^2 H^2}{4M_Y c^4} \left(1 - \frac{M_Y}{M_P} \right) \right]$, W_N simplifies to
(neglecting terms containing H^2)

$$W_N = -\frac{1}{6} \frac{ff^*\chi^2}{\pi^2} \int_0^\infty \frac{k^4 dk}{k^2 + \chi^2} - \frac{1}{6} \frac{ff^*\chi^2}{\pi^2} \frac{eH}{M_Y c^2} \left(1 - \frac{1}{2} \frac{M_Y}{M_P}\right) \int_0^\infty \frac{k^4 dk}{(k^2 + \chi^2)^{3/2}} \quad \dots (8)$$

As mentioned previously the co-efficient of H in the expression for W_N corresponds to μ'_N , the additional magnetic moment of the neutron due to virtual meson. Using (8) we write

$$\mu_N = -\frac{4}{3\pi} \left(\frac{ff^*\chi^4}{4\pi\hbar c} \right) \mu_0 \frac{M_P}{M_Y} \left(1 - \frac{1}{2} \frac{M_Y}{M_P}\right) \frac{1}{\chi^2} \int_0^\infty \frac{k^4 dk}{(k^2 + \chi^2)^{3/2}} \quad \dots (9)$$

where

$$\mu_0 = \frac{e\hbar}{2M_P c}$$

The above integral becomes infinite if the upper limit of k is equal to ∞ , so we put the upper limit to be $x\chi$ where x is any number the value of which will be adjusted to make the theoretical value agree with the experimental one. Hence

$$\mu_N = -0.573 \mu_0 \left[\frac{1}{2} x \sqrt{1+x^2} - \frac{3}{2} \log(x + \sqrt{1+x^2}) + x/\sqrt{1+x^2} \right] \quad (10)$$

where $M_P/M_Y = 6.6$ and $(ff^*\chi^4/4\pi\hbar c) = 0.22$ (the constants of the vector potential are determined from the deuteron binding energies by the method of Fröhlich, Haug and Sneddon, 1947).

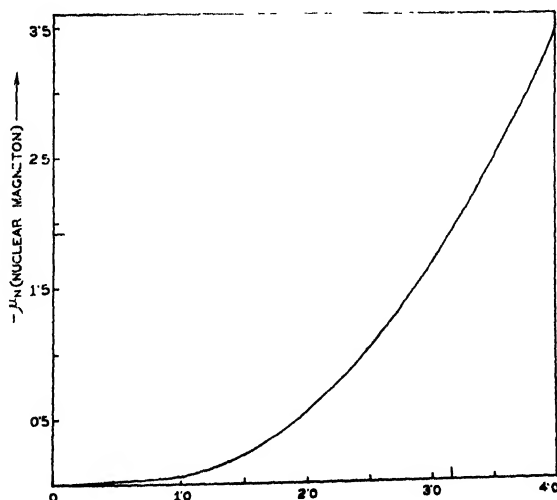


Fig. 1

In figure 1, we have plotted how μ_N varies with x , it is found that for $x = 3.16$ which is very close to the value of π , the theoretical value agrees with the experimental value. In our calculation

$$\mu_P = \mu_0 - \mu_N = 2.913 \mu_0$$

So it appears that if we take the upper limit of the meson momentum k to be $\pi\chi$, we get very good agreement with the experimental values of the magnetic moments of the neutron and proton. If, however, we neglect the energy of the proton due to the magnetic field, then to get fit with the experimental values, the value of x needs to be 3.06.

ACKNOWLEDGMENT

The author is indebted to Professor D. Basu for suggesting the problem and for his valuable guidance in the work.

REFERENCES

- Fröhlich, H., Heitler, W., Kemmer, N., 1938, *Proc. Roy. Soc. Lond.*, **A**, **166**, 154.
Fröhlich, H., Huang, K., Sneddon, I. N., 1947, *Proc. Roy. Soc. Lond. A.*, **191**, 61.
March, A., 1951, *Quantum Mechanics of Particles and Wave fields*.

CLOUD CHAMBER ANALYSIS OF COSMIC-RAY SHOWERS UNDER 10 TO 23 cm. OF LEAD.

P. K. SEN CHOUDHURY AND S. N. SENGUPTA

BAKER LABORATORY, PHYSICS DEPTT., PRESIDENCY COLLEGE, CALCUTTA

(Received for publication April 2, 1956; after revision June 5, 1956)

Plate XI

ABSTRACT. A counter-controlled cloud chamber study of different types of showers in Pb, under 10 to 23 cm. has been made to investigate the controversial existence of higher maximum in Rossi curve and its probable origin. The chamber and the counters in triple coincidence were specially arranged to detect the formation of a charged pair or particle by the decay or dissociation of an unstable neutral particle in air under the Pb absorber. The triple coincidence frequency rises by about 28% over the background under about 16 cm. of Pb. Analysis of the shower photographs, however, shows that this rise is largely due to a single charged particle mostly mesons coming from the top absorber which by subsequent knock-on process or otherwise produces the triple coincidence. These singles may account for about 12% of the total rise. About 10% of the total rise may be attributed to mixed meson and meson showers.

Analysis of shower photographs by neutral component shows that out of about thousand photographs we have obtained only one penetrating pair with its apex in air under 16 cm. of Pb and this may be due to a V-type of decay. But we have obtained many other photographs mainly under 15 to 20 cm. of Pb which show isolated pairs of very low energy (inferred from range and angular divergence) formed by a neutral component. These type of showers may account for the remaining 6 to 8% of the total rise at the second maximum. The origin of such pairs particularly in some photographs, by photon or indirectly by neutron is not very clear. There is a third possibility that these pairs are produced by the decay of a neutral particle of very low mass. This possibility may further be checked by a multiple plate chamber as we propose to do.

INTRODUCTION

The aim of this investigation has been to clarify the long persisting controversy over the existence of higher maximum in Rossi curve and to identify the radiation and the mechanism that might contribute to the formation of such a maximum. The senior author (1951) previously reported the existence of a second maximum like many other workers e.g. Clay (1949), Bothe (1950), Kameda and Miura (1950) and others, although some other workers denied its existence. A reference to all the earlier works may be found in the literature referred to above. The old controversy is still persisting and when the present investigation was completed we came across the abstracts of some papers of Bothe and his coworkers (1955) where they report that the previously reported sharp second maximum by them might be due to some defect in the electronics of the complicated circuits

used by them. Negative results have also been reported by Pfozter (1955). Harding (1955) reported a definite rise in the shower frequency by about 3% in the region of second maximum under certain experimental conditions. But McCusker and others (1955) detected a rise by about 2% using counters only but failed to detect any appreciable maximum by the cloud chamber investigation. Choudhury *et al* (1955) have reported a sharp second maximum.

In the previous analysis the senior author came to the conclusion that some of these controversies might be due to differences in geometrical arrangements. In some of the arrangements it seems to the author that there was a greater possibility of the second maximum being masked by oblique showers in the extended absorber or by the side showers coming not through the absorber. Whereas the failure of some recent workers, as for instance, McCusker and others (1955) to find an appreciable second maximum might be due to their experimental arrangements being biased for detecting penetrating secondary radiations only, as the lower tray of counters was covered with 10 to 2.5 cm. of lead absorber. The senior author (1951) from various considerations came to the conclusion that this maximum might be due to the formation of a new unstable neutral particle which subsequently decays or dissociates into a pair of very low energy content. Bothe (1953) and Pfozter (1953) also previously came to the conclusion that it is necessary to postulate the existence of a new type of unstable particle to explain this maximum and Bothe (1954) afterwards suggested that this new particle might be simply a neutral V-particle formed in the absorber.

In view of all these the present cloud chamber investigation was undertaken to test the various suggestions mentioned above or to identify if any other agency and mechanism are the origin of this second maximum.

EXPERIMENTAL ARRANGEMENTS

An automatic controlled Wilson chamber of Blackett's (1934) model was set up with the modification that the metallic piston in the back chamber was replaced by a rubber diaphragm which was found to give a much better type of sharp tracks. The front chamber is of diameter 1' and depth $3\frac{1}{2}$ ". A 2.5 cm. thick lead plate is placed at its centre to identify the penetrating and the soft component. Following the accepted custom, a particle which passes through this plate without multiplication is considered to be a penetrating one, like meson etc. The chamber was filled with argon. Alcohol with water in the ratio of 75 : 25 was used as the condensant. In order to avoid any complexity due to electronics, oblique showers etc., we used the simplest arrangement of three counters in coincidence and therefore the coincidence frequency is much smaller in comparison with others. In order to detect if there be the formation of any neutral unstable particle in the absorber which after leaving the absorber decays or dissociates in air; the two counters, separated by a distance of about 2 cm., were placed below

the lead absorber at a distance of about 70 cm. from it and the cloud chamber was placed immediately above the two counters. The third counter was placed just a little above the cloud chamber. The counters were of dimensions about 20 cm. length and 3 cm. diameter. The lead absorbers used in this experiment

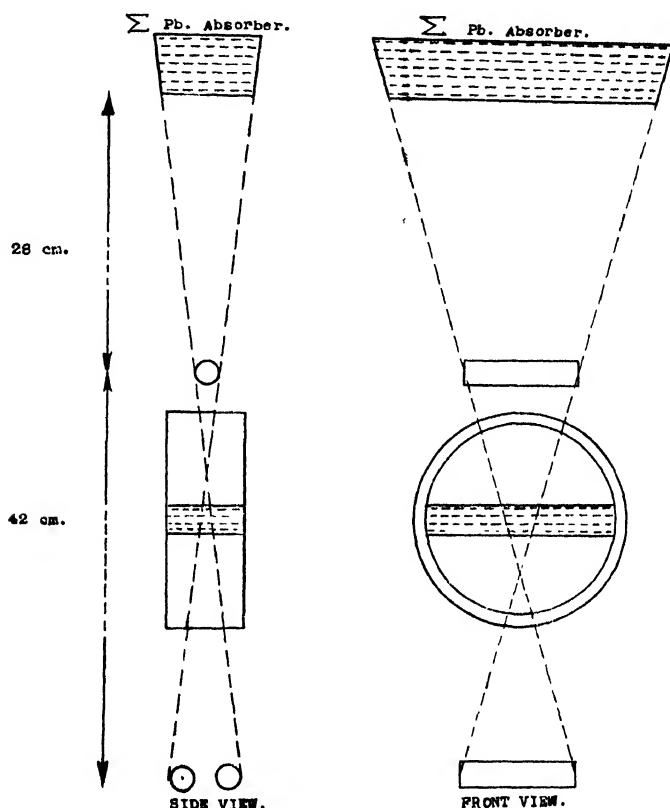


Fig. 1. Experimental arrangements.

are sheets of chemically pure lead and of dimension $1' \times 1' \times 1/8''$. Stereoscopic photographs were taken with a camera of two lenses. The actual experimental arrangements are shown in the figure 1. The present experiment was set up in the ground floor of a three-storied building, e.g. Baker Laboratory, Presidency College, Calcutta, whereas the previous investigation by the senior author was done in open air.

EXPERIMENTAL RESULTS

The main experimental results and the analysis of the shower photographs are shown in Table I. By single shower, two-particles shower and more than two particles shower as are given under different columns in Table I, we mean the

corresponding number of ionising particles entering the chamber from the top absorber. A single can produce a triple coincidence either by cascade multiplication in the inner lead plate if it is an electron or by knock-on electrons from the inner lead plate or from the lower chamber wall if it is a meson. A single ionising particle can also produce triple coincidence if it be associated with a neutral component e.g. a photon or an unstable particle which afterwards produces more charged particles. A photon can produce charged particles either by Compton process or by a pair formation and an unstable neutral particle can produce a charged pair by decay or dissociation. Many photographs are obtained by us where a single charged particle is associated with another pair of very low energy content mostly produced just at the bottom of the inner lead plate and sometimes in air. Typical photograph is shown in the photograph No. 2 (Plate XI) obtained under 16 cm. of lead. We have also obtained many cases of such isolated pair formation without association of any charged particle. These are given under a separate column in Table I. A typical photograph is shown in photograph No. 3 under 16 cm. of lead which shows simultaneous production of two such pairs.

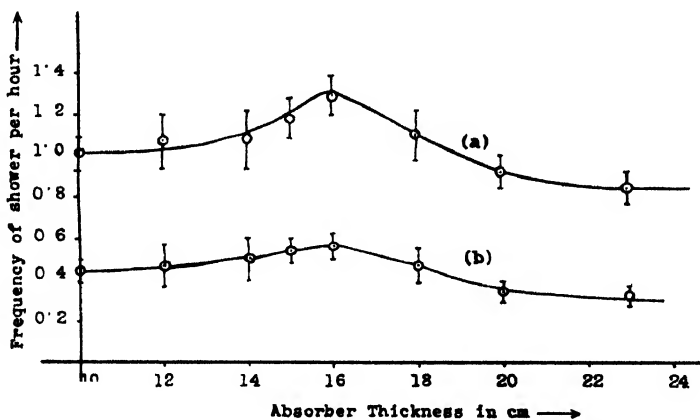


Fig. 2. (a) Total shower frequency curve.
(b) Single frequency curve.

We have plotted the total shower frequency against the corresponding absorber thickness in figure 2 (Curve *a*). We have also plotted the frequency of singles in figure 2 (Curve *b*). The results given in Table I as well as both the transition curves show a maximum under about 16 cm. of lead absorber. The rise in the total shower frequency under 16 cm. lead is about 28% higher than that under 10 cm. of lead. Such difference is much beyond the standard error. For statistical significance of the results we particularly concentrated our observations under 10, 15, 16, 20 and 23 cm. of lead. Again to check any periodic or abrupt variation of total cosmic ray intensity we measured

coincidence rates under each thickness in two different periods showing the same results with minor variations. The frequency of two particle-shower does not show any significant increase in the region of second maximum but the frequency of more than two-particle shower shows an increase in the region under 16 to 20 cm. of lead though the standard deviation is fairly large. We have also obtained some blank photographs which under 16 cm. of lead is about 15% of the total number of photographs and the percentage of blanks under other thicknesses of absorber also do not significantly vary from this. In view of the geometrical arrangement of the counters and the limited depth of focus of the camera etc. such a percentage of blanks may be quite reasonable.

For further analysis the showers of at least two particles containing one meson, two or more mesons are shown separately in Table II. As most of the penetrating particles are mesons, we have classified them as meson associated showers. Their respective frequencies are also given. The frequency of meson shower containing at least two mesons are separately given under the last column in Table II. The total frequency of meson associated shower as well as that of meson shower are separately plotted, in figure 3. against the corresponding absorber

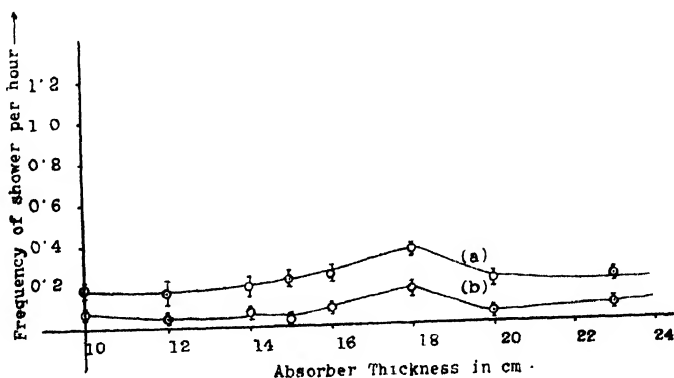


Fig. 3. (a) Meson associated shower frequency curve.
(b) Frequency of two or more meson associated showers.

thicknesses of lead. Though the shower frequency is very small in comparison with the total shower frequency still the meson associated shower shows a distinct rise in the region under 16 to 18 cm. of lead. The meson shower frequency shows an abrupt rise under 18 cm. of lead. Such abrupt rise may be accidental or the penetrating particles may be either very short-lived or their energy is very small so that these are easily lost by decay, scattering or absorption. Some typical photographs of meson shower are also shown in the photograph No.4 and No. 5. (Plate XI) The photograph No. 4 obtained under 16 cm. of lead shows the tracks of 4 mesons whereas the photograph No. 5 under 20 cm. of lead

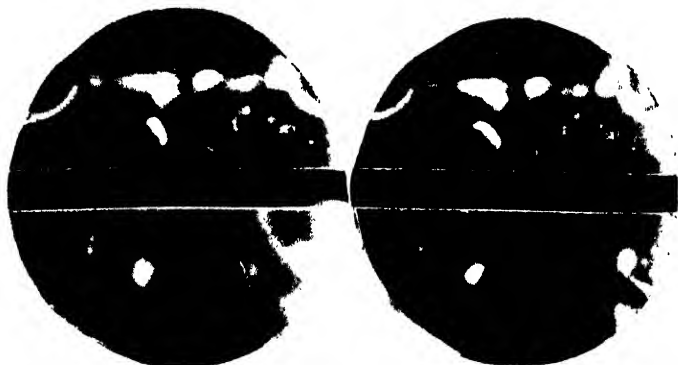
shows the tracks of about 6 mesons. These two may be pure penetrating showers.

A few bursts and nuclear interactions have also been photographed all in the neighbourhood of second maximum under 15 to 20 cm. of lead. Typical photographs are shown in the photographs No. 6, 7 and 8. Photograph No. 6 obtained under 18 cm. of lead shows at least one meson associated with a nucleonic pair (to the extreme left) produced by a neutral particle in the inner lead plate. Photograph No. 7 obtained under 15 cm. of lead shows a shower which may be a star produced by a neutral radiation. Photograph No. 8 obtained under 20 cm. of lead shows a burst of probably hundreds of particles. In this connection a reference may be made to the workers of Mohr and Stafford (1944) who obtained a hump using an ionisation chamber under about 20 cm. of lead. Also Schöpper, Höcker and Kuhn (1951) using photographic emulsion have obtained a second maximum starting from 15 upto 24 cm. of lead.

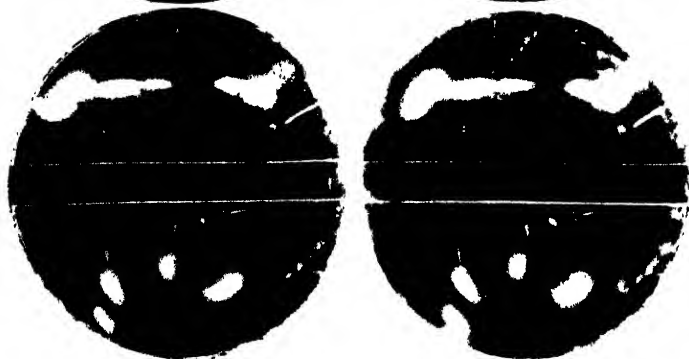
DISCUSSION ON THE PROBABLE ORIGIN OF SECOND MAXIMUM

The above analysis of the shower photographs shows that the meson associated shower and meson shower may only account for an increase in the shower frequency by less than 10% of the total rise which is about 28% in the region of second maximum. But the frequency of singles, which is about 50% of the total frequency, shows a definite maximum coincident with that of the total frequency. It appears therefore that the showers with single observable charged particles from the top absorber largely contribute to the origin of the second maximum and may account for about 12% of the total rise. An analysis of the singles together with the triple coincidences produced by neutral component under different thicknesses of lead absorber are given in the Table III which shows that majorities of these are either simple meson or meson which has produced knock-on showers in the inner lead plate. A few of these have produced cascade but another appreciable fraction shows singles associated with another pair of very low energy content. The simple mesons which have not produced any knock-on shower in the inner lead plate may also be associated with a non-ionising component which can generate a charged particle or a charged pair as in the previous case to produce triple coincidence. The possibility of a knock-on shower from the thin glasswall of the chamber is very small. Clay (1949) and his co-workers suggested that the second maximum may be due to knock-on showers by a meson. The maximum occurs when the rate of accumulation of the soft component by knock-on process is just equal to the rate of absorption of this component. But Pfozter (1953) showed that such a mechanism can produce a maximum under much lower thickness of the absorber e.g. about 4 cm. of lead. Harding (1955) very recently suggested that the second maximum may be due to mesons of sharp range about 18 cm. of lead which stopping in the ground immediately below the lower

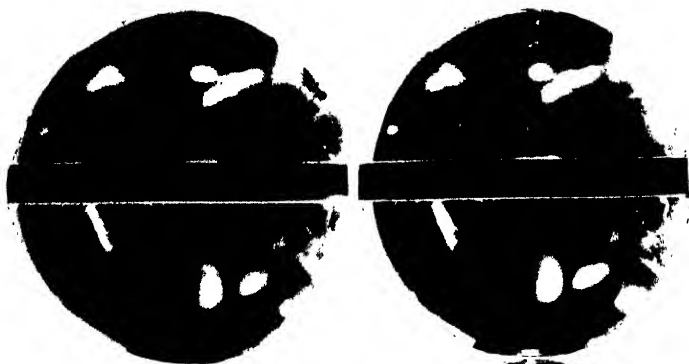
1.



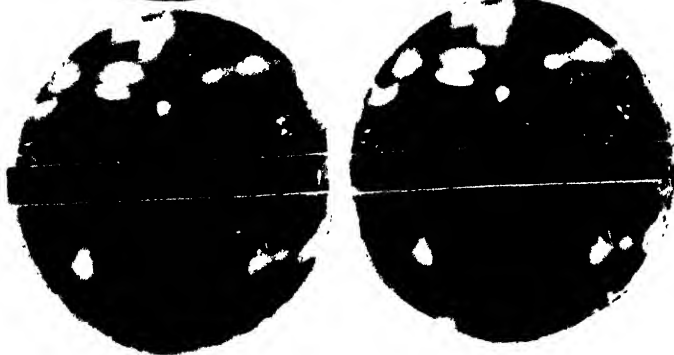
2.



3.

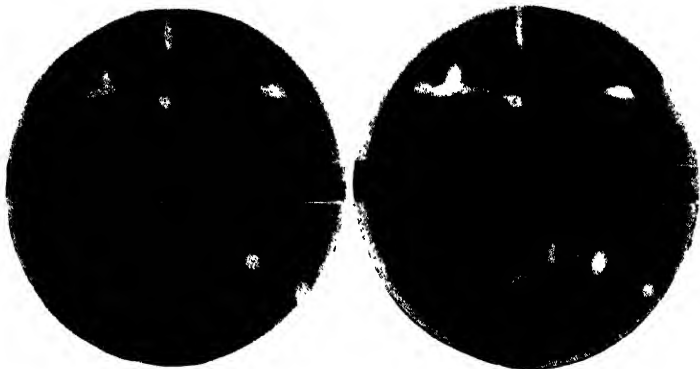


4.

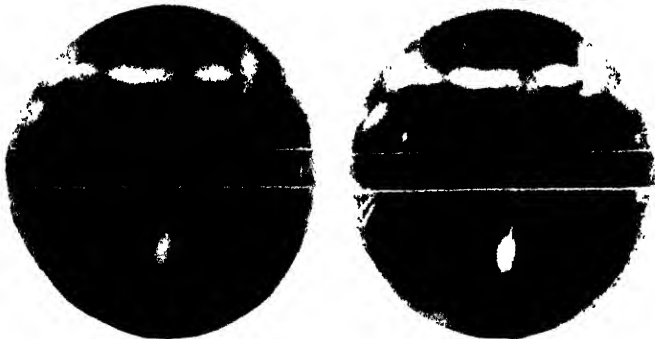


Typical shower photographs.

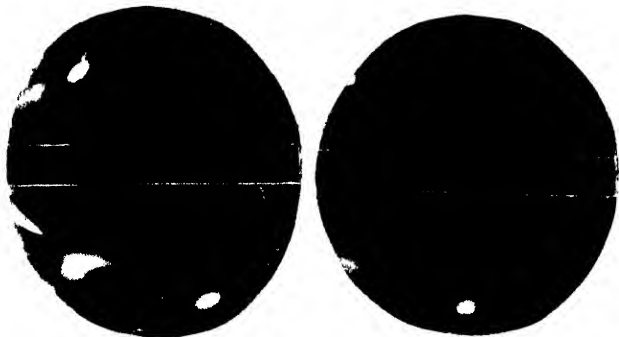
5.



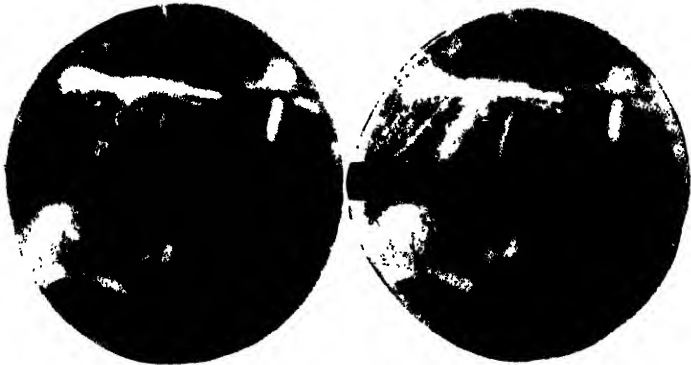
6.



7.



8.



Typical shower photographs.

counter tray emit decay electrons in the upward direction. Our chamber was about $1\frac{1}{2}'$ above the ground but we have not detected any such decay electron either entering the chamber from below or generating any shower in the inner lead plate. In the energy spectrum of meson at sea level also it is not known that there is a sharp peak in the region of second maximum.

Kameda and Miura (1950) obtained a very sharp second maximum which they inferred to be produced by the nucleonic component from the absorption mean free path of the primary rays. Hayakawa and Nishimura (1950) from a theoretical analysis of the results of the previous authors concluded that the second maximum consists of the overlapping of two kinds of secondary ionising particles. One type of secondaries have a definite range of about 16 cm. of lead whereas the other type has much longer range. They also further conclude that the sharp secondary maximum obtained by Kameda and Miura are due to the solid angle subtended by their counter train being very small and consequently the ratio J_N/J_E i.e. the vertical intensity ratio of the nucleonic component to the soft component, is much larger than that of the wide angle primaries. For wide angle primaries, the tail of the cascade shower and the back-ground knock-on electrons would mask the second maximum. In our arrangements also since the lower counters were placed at a distance of about 70 cm. below the absorber the solid angle is very small but our results, though show a maximum due to penetrating components, can account for less than 10% of the total rise under second maximum. In this connection a reference may also be made to the work of George (1947) and others who reported a maximum of penetrating showers under about 15 cm. of lead. The secondaries are of range of about 50 cm. of lead. Walker (1950) also pointed out that the penetrating showers have two kinds of secondaries of ranges of about 15 cm. of lead and 1 cm. of lead.

Bothe and Schemeiser (1938) originally suggested that the second maximum might be due to narrow meson pairs. But in our investigation out of more than one thousand photographs we have obtained only one such narrow pair under 23 cm. of lead. Similarly we have obtained only one photograph, No. 1, under 16 cm. of lead which shows a pair of penetrating particle with its apex in air or just on the top counter above the cloud chamber. Such a pair may be produced by V-type of decay of a hyparon e.g. $V^0 \rightarrow P + \pi + Q$. $Q = 37\text{Mev}$; but its frequency is so small that such V-particles cannot give rise to the second maximum. Again considering the probable contribution to second maximum due to neutral component, as shown in Table III, we have obtained many photographs which show isolated pairs of very low energy content (indicated by the angle of emission and the range in the chamber) either associated with another single soft ionising particle or without any such ionising particle. We have also some soft ionising particles absorbed in the inner lead plate. For triple coincidence such particles must be associated with other soft neutral component. These cases are represented under the last five columns of Table III to-

gether with the frequency of such showers under different thicknesses and though the statistical error is large the results show a definite increase of this type of shower under 15 to 20 cm. of lead in comparison to that under 10 and 23 cm. of Pb. The abundance of these showers is such that it may contribute 7 to 8% rise to the total shower frequency at the second maximum. Again whenever we observe such a pair (mostly absorbed in the chamber gas) there must be simultaneous formation of other such pairs to produce triple coincidences and as such their probability of detection is much smaller than the total triple coincidences that may be produced by a single such pair associated with a charged particle.

Now to explain the formation of such soft component particularly the soft pairs by neutral component under 15 to 20 cm. of Pb, there are three possibilities i.g. (1) pair formation by a photon below critical energy present in the tail of the cascades as shown by Greisen and others (1948), (2) pair formation by photon originating from neutron capture or inelastic scattering of neutron in Pb and (3) pair formation by the decay or dissociation of a new unstable neutral particle of very low mass. But the photons below the critical energy are rapidly absorbed in Pb and as such these cannot explain the increase or even the steady value of such shower frequency in the region from 15 to 20 cm. of Pb. Similarly the increase of such shower frequency may not be due to neutron component as the neutron transition curve in Pb investigated by Tongiorgi (1949) does not show any increase in the region under investigation. So there remains the third alternative in support of which the typical photographs No. 3 obtained under 16 cm. of Pb may be significant. The photograph shows simultaneous formation of two such pairs just at the bottom of the inner Pb plate without any appreciable Compton electron or cascade shower in the chamber. From the angle of the emission it appears that the energy of the photons (if photons are supposed to be the origin of these pairs) is near to 1 Mev. only. As such, the probability of pair formation by such photon is much smaller in comparison with that of Compton scattering. Moreover, the formation of two such simultaneous pairs is highly improbable. If these pairs are produced by the decay of a new unstable particle its rest mass must also be very small. In this connection reference may be made to the previous works of the senior author (1951, 1954) on anomolous gamma-ray absorption where also the possible existence of such a particle was suspected.

In the light of the above analysis of the results we are undertaking a further investigation with a multiple-plate cloud chamber to check the probable formation of such a new unstable particle.

ACKNOWLEDGMENTS

In conclusion we express our thanks to the Government of West Bengal for a research grant by which this investigation has been possible. We also express our grateful thanks to the Principal, Presidency College, Calcutta, and to Prof. Dr. K. C. Kar and Prof. Dr. R. L. Sengupta for their helpful co-operation.

REFERENCES

- Blackett, P. M. S., 1934, *Proc. Roy. Soc.* **146A**, 281.
- Bothe, W. and Schmeiser K., 1938, *Ann. d. Physic.* **32**, 161.
- Bothe, W. and Thurn H., 1950, *Phys. Rev.* **79**, 544.
- Bothe, W., 1953, *Z. Naturforschg.* **8a**, 393.
- Bothe, W. and Kraemer, H., 1954, *Phys. Rev.* **95**, 1402.
- Bothe, W., 1955, *Z. Naturforschg.* **10a**, 794.
- Chaudhury, R. M. 1955, *Nature*, **176**(4488), 876.
- Clay, J., 1949, *Rev. Mod. Phys.*, **21**, 82.
- George, E. P. and Jason A. C., 1947, *Nature*, **160**, 327.
- Greisen, (1949), *Phys. Rev.*, **75**, 1063, 1071.
- Harding, J. B. 1955, *Proc. Phys. Soc. A*, **68**, 352.
- Hayakawa, S. and Nishimura, J., 1950, *Prog. Theor. Phys.* **6**, 948.
- Kameda T. and Miura I. 1950, *Prog. Theor. Phys.*, **5**, 323.
- McCormack, P. D., McCusker C. B. A. and Wilson B. G., 1955, *Proc. Phys. Soc., A*, **68**, 1088.
- McCusker, C. B. A. and Wilson B. G., 1955, *Prog. Phys. Soc., A*, **68**, 1086.
- Mohr and Stafford, 1944, *Proc. Roy. Soc.* **A183**, 54.
- Pfotzer, G., 1953, *Z. Naturforschg.* **8a**, 335.
- Pfotzer, G., 1953, *Z. Naturforschg.* **8a**, 353.
- Pfotzer, G., 1955, *Z. Naturforschg.* **10a**, 718.
- Schöpper, E., Höcker, K. H. and Kuhn G., 1951, *Phys. Rev.* **82**, 444.
- Sen Chaudhury, P. K., 1951, *Ind. J. Phys.* **25**, 539.
- Sen Chaudhury, P. K., 1951, *Phys. Rev.* **81**, 274.
- Sen Choudhury, P. K., 1954, *Z. Naturforschg.* **9a**, 175.
- Tongiorgi, 1949, *Phys. Rev.*, **4**, 517.
- Walker, W. D., 1950, *Phys. Rev.* **77**, 686.

ON THE DETERMINATION OF ELECTRON DENSITY DISTRIBUTION IN THE IONOSPHERIC REGIONS FROM $h'-f$ RECORDS.

A. K. SAHA

INSTITUTE OF RADIO PHYSICS AND ELECTRONICS, UNIVERSITY COLLEGE OF TECHNOLOGY
92, UPPER CIRCULAR ROAD, CALCUTTA

(Received for publication May 21, 1956)

ABSTRACT. Comparative studies have been made of the various available methods for the determination of the height distribution of electrons in the ionospheric layers. It is concluded that, for routine ionospheric work, Ratcliffe's method is the quickest though, under restricted conditions, some of the other methods yield more accurate results. Methods which take into account the effect of earth's magnetic field have also been studied. It was, however, found that the errors due to the neglect of the magnetic field are of the same order as the limits of observational errors in height measurement. The complications involved in including the magnetic field are, therefore, not warranted. This is particularly because, the inclusion of the magnetic field affects only the thickness of the layer and not its height of maximum ionization, and the MUF is mainly controlled by the latter.

INTRODUCTION

The determination of height distribution of electron density in the ionospheric regions is one of the basic problems of ionospheric physics. Because of the simple relation that exists between the electron density and the reflected frequency, the problem is equivalent to that of determining the true height of reflection for the various exploring frequencies. A simple method of obtaining the true height would be to fit the $h'-f$ pattern (apparent height *vs.* frequency) to a known mathematical function. Unfortunately such fits are not always possible. Various other methods have, therefore, been suggested for obtaining the true height distribution of ionization from the observed $h'-f$ pattern. The methods may be divided into two broad classes (Piggot, 1954) : (1) model methods and (2) integral equation methods.

Model methods are based on the fitting of the observed $h'-f$ patterns with patterns calculated from simplified models. Since the variation of electron density near the maximum of a layer is often parabolic, the parabolic model methods developed by Appleton and Beynon (1940, 1947) and by Booker and Seaton (1940) are used widely to deduce the position of maximum density in the ionized layers. The procedures have been described in detail by Mitra (1952). In these methods, only a few points on the $h'-f$ curve near the high frequency end are utilised. In the model method suggested by Ratcliffe (1951) a simple mathematical

form (parabolic, linear, etc.) is assumed for the electron distribution, and the resulting $h'-f$ curve is calculated. By comparing the observed $h'-f$ curve with the calculated, it is possible to decide whether the actual distribution approximates to that assumed.

The integral equation methods are based on the solution of the integral

$$h'(f) - \int_0^{h_r} \mu' dz \quad \dots \quad (1)$$

where h_r = height of reflection of frequency f above the ground
 μ' = 'group refractive index'.

= $\frac{\text{velocity of light in free space}}{\text{vertical component of group velocity of the wave}}$

When the effects of electron collisions and the earth's magnetic field are neglected the form of the function μ' is such that the integral can be reduced to Abel's integral equation (Appleton, 1930) for which an analytical solution is known (Abel, 1881). The result has been applied by Rydbeck (1940) and others, using planimetric integration or other graphical procedures, to evaluate the rather larger number of integrals involved. An improved procedure for the numerical evaluation has been developed by Kelso (1952) based on the use of the Gauss-Christoffel quadrature formula.

Both the model method and the integral equation method are only approximately valid for the ordinary ray reflections when the earth's magnetic field is taken into account. Several methods have, therefore, been developed (Shinn and Whale, 1952; Shinn, 1953; Kelso, 1954; Budden, 1954) which include the effect of the magnetic field. All these methods, in their present forms, are too laborious and are not suitable for routine use. Shinn and Whale (1952) have shown that for a parabolic layer, estimates of the height of maximum ionization made with and without consideration of the effect of the earth's magnetic field are nearly identical. The layer thickness is found to be smaller when the magnetic field is taken into account. However, the effect of the magnetic field on the layer thickness calculations is very small when the angle of dip of the earth's magnetic field is not large, i.e. at low magnetic latitudes.

In the present paper the $h'-f$ records obtained at Calcutta and Haringhata stations have been treated by some of the above methods mainly with the object of testing the relative merits of these methods in terms of accuracy and suitability of application.

2. OUTLINES OF THE METHODS ADOPTED

(a) *Ratcliffe's method : Parabolic layer method neglecting earth's magnetic field.*

Ratcliffe has treated the case of a single layer and also that of a composite layer formed by the overlapping of two layers assuming parabolic distribution

of ionization for both. For a single parabolic layer Appleton (1937) has shown that the apparent height of reflection of a pulse of frequency $f(< f_c)$ is given by

$$h' = h_m + y_m \phi \left(\frac{f}{f_c} \right) \quad \dots (2)$$

where f_c = critical penetration frequency

h_m = height of maximum electron density

y_m = semi-thickness of the layer

and

$$\phi \left(\frac{f}{f_c} \right) = \frac{1}{2} \left(\frac{f}{f_c} \right) \log_e \left| \frac{f_c + f}{f_c - f} \right| - 1 \quad \dots (3)$$

If a pulse of frequency $f(> f_c)$ penetrates the layer and is reflected from another layer situated at the level h_m , then the apparent height of reflection is increased on account of group retardation in the half parabola below h_m . This retardation is given by

$$\Delta h' = y_m \phi \left(\frac{f}{f_c} \right) \quad \dots (4)$$

Note: Computations of the values of $\Delta h'$ in Eqn. (4) are necessary for the estimation of the retardation produced in an upper layer (F2) trace by a lower layer (F1.). The retardation produced by only the half parabola below the h_m for the lower layer is considered above, following Booker and Seaton (1940), because the F1 region may be assumed to consist of half of a parabola, the bottom of the F2 layer seldom rising sufficiently above h_m F1. However, in computing the retardation produced in the F1 layer the E region should be considered as a complete parabola.

For our computations the function $y_m \phi \left(\frac{f}{f_c} \right)$ was plotted (after Ratcliffe) for different values of y_m (50, 100, 150, 200 km) and choosing the frequency and height scales to correspond to those of the automatic $h'-f$ records obtained at Haringhata, Calcutta (figure 1). The $h'-f$ records are projected (in an enlarged) on the computed curves and the values of y_m and h_m are read off by direct comparison. The curves in figure 1 are drawn for $f_c = 3\text{Mc/s}$. The frequency scale being logarithmic, the curves for other values of f_c will be identical and measurements may be made by simply sliding the scale along the frequency axis. Curves on the right hand side of figure 1 (drawn for $y_m = 50$ and $y_m = 100$ kms. only) are used for calculating the retardation produced in an upper layer (F2) trace by a lower layer (F1). Procedures for these measurements have been described in detail by Ratcliffe (1951).

For the case of two parabolic layers, partially overlapping the retardation produced by the shaded portion of figure 2 for reflection produced by the upper layer is according to Ratcliffe,

$$\Delta h' = y_m \left(\frac{f}{f_r} \right) \log_e \left\{ \sqrt{1 - (f_B/f_c)^2} + \frac{1+f/f_c}{\sqrt{(f/f_c)^2 - (f_B/f_c)^2}} \right\} \quad \dots (5)$$

where f_B is the frequency which just penetrates the shaded layer. A set of curves have been drawn (corresponding to the scale of automatic $h'-f$ records

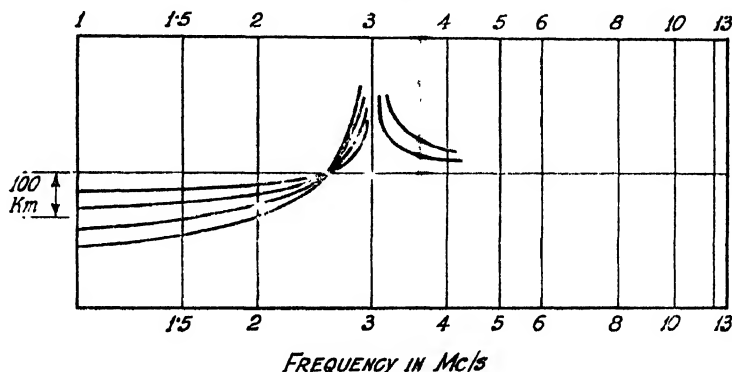


Fig. 1. Theoretical $h' - f$ curves for parabolic distribution. The curves have been constructed for semi-thicknesses (y_m) of 50, 100, 150 and 200 km after Ratcliffe's method. The frequency and height scales used correspond to those of the automatic $h' - f$ records. The curves on the right hand side are drawn for $y_m = 50$ and 100 kms only.

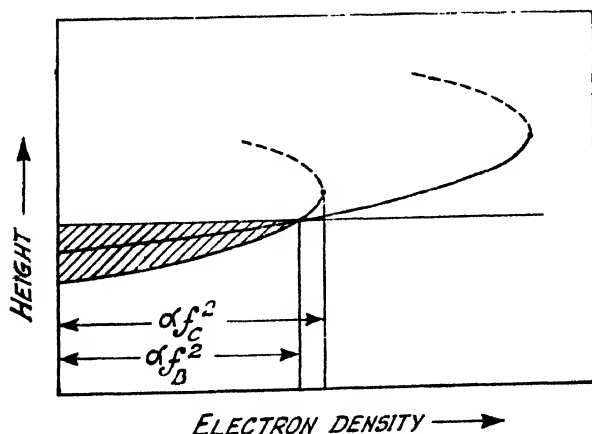


Fig. 2. Illustrating a case of vertical distribution where a composite ionospheric layer is produced by two overlapping parabolas.

of Calcutta) for different values of f_B/f_c and for $y_m = 50$ and $y_m = 100$ kms. These curves (for $f_c = 3$ Mc/s) are given in figure 3.

(b) *Kelso's method (1): Integral equation method neglecting earth's magnetic field.*

It has been shown by Pekeris (1940) that the integral Eq.(1) may be transformed to give the true height of reflection h_v for a given frequency in terms of

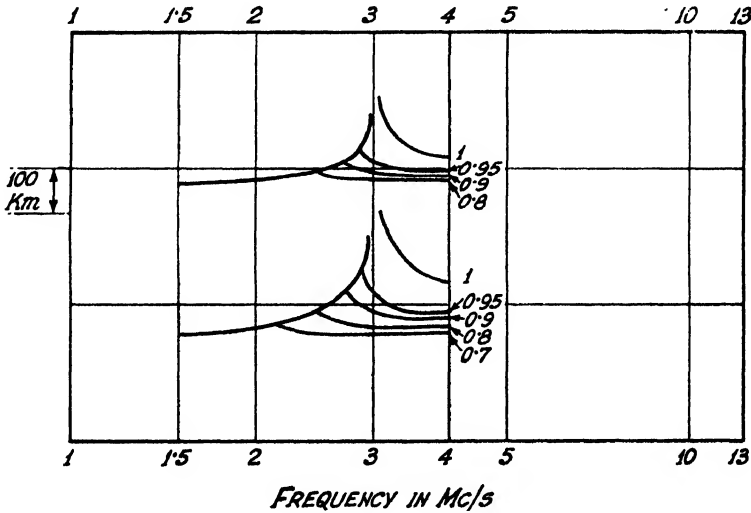


Fig. 3. Theoretical $h'-f$ curves for electron distributions as shown in Fig. 2. Curves are drawn on the same scale as in Fig. 1.

the apparent height h' and the operating frequency f . This expression is

$$h_v = \frac{2}{\pi} \int_0^{f_v} \frac{h'(f)df}{\sqrt{f_v^2 - f^2}} \quad \dots (6)$$

Eqn. (6) can be evaluated by putting $f = f_v \cos \theta$ and solving the equation

$$h_v = \frac{1}{2} \int_0^{\pi} h'(\cos \theta) d\theta \quad \dots (7)$$

Kelso (1952) has shown that if we determine from the experimental $h'-f$ curve the apparent heights h'_k corresponding to a set of frequencies given by

$$f_k = f_v \cos \theta_k$$

where
$$\theta_k = \frac{2k-1}{2n} \pi ; k = 1, 2, \dots, n, \quad \dots (8)$$

then the true height for frequency f_v is

$$h_v = \frac{1}{n} \sum_{k=1}^n h'_k$$

The ratios $\frac{f_k}{f_v} = \cos \theta_k$ are completely determined by the value of n . The values of $\cos \theta_k$ for $n = 5$ and $n = 10$ are given in Table I. The values for $n = 5$ are used wherever the experimental $h'-f$ curve is smooth and those for $n = 10$ near cusps or discontinuities. The values of f_k for a given value of f_v may be obtained readily from figure 4.

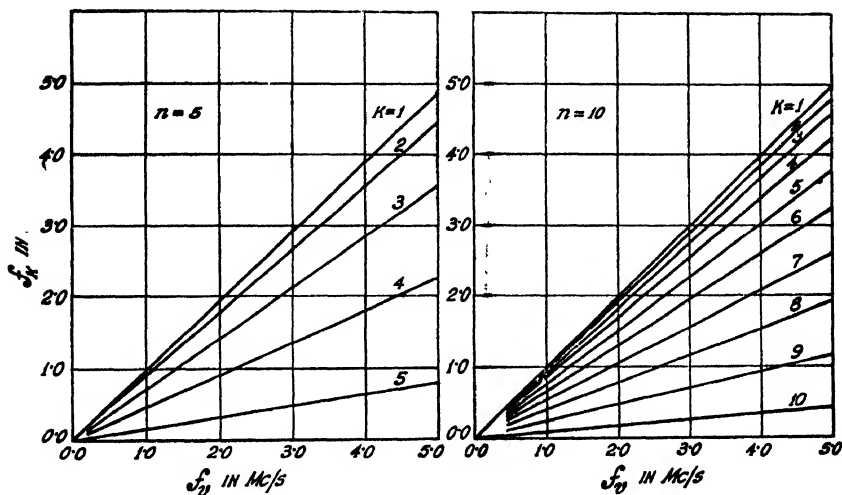


Fig. 4. Plots of $f_k = f_v \cos \frac{2k-1}{2n} \pi$ against f_v , for different values of k and for $n=5$ and $n = 10$ (after Kelso). The values of f_k required for the computation of true height of reflection at f_v by Kelso's method are readily obtained from this diagram.

TABLE I
Values of f_k/f_v for $n = 5$ and $n = 10$

$n = 5$	$n = 10$	
0.9877	0.9969	0.6945
0.8910	0.9724	0.5225
0.7071	0.9239	0.3827
0.4540	0.8526	0.2334
0.1564	0.7604	0.0785

(c) *Whale and Shinn's method: Parabolic layer method including earth's magnetic field.*

The integral equation (1) may be written as

$$h'(f) = \int_{z_r} \mu' dz + h_0 \quad \dots \quad (10)$$

where z_r = the height of the point of reflection of frequency f above the lower boundary of the layer.

In the absence of magnetic field, the form of the function μ' is such that in the case of a parabolic layer, Eqn. (10) may be transformed to

$$h' = h_0 + y_m X \left(\frac{f}{f_c} \right) \quad \dots (11)$$

where

$$X = \frac{1}{2} \left(\frac{f}{f_c} \right) \cdot \log_e \left| \frac{f_c + f}{f_c - f} \right|$$

which is simply Eqn. (2), expressed in a different form.

In the presence of the earth's magnetic field, however, the form of the function μ' becomes complicated and depends on the strength and direction of the field. Eqn. (11) then becomes

$$h'(f) = h_0 + y_m(X + Y) \quad \dots (12)$$

where Y is a function of f, f_c, f_H and ϕ ,

f_H = gyro-magnetic frequency,

ϕ = angle of dip of the earth's magnetic field.

It may be shown that Y is dependent on the ratios f/f_c and f_H/f_c and not on the actual values of f, f_c and f_H . So that

$$Y = Y \left(\frac{f}{f_c}, \frac{f_H}{f_c}, \phi \right) = \frac{1}{y_m} \int_{\infty}^{z_r} \mu' dz - X$$

Y is equal to zero when f/f_c is zero, when f_H/f_c is zero or when ϕ is zero.

Shinn and Whale (1952) and Shinn (1953) have made detailed computations of Y for different values of $f/f_c, f_H/f_c$ and ϕ by numerical integration using the EDSAC electronic computer. They have expressed their results as functions of X, k and s , where

$$k = \frac{6.4 f_H}{6.4 f_H + f_c}$$

or

$$\frac{f_c}{f_H} = 6.4 \left(\frac{1}{k} - 1 \right)$$

and

$$s = \sec \frac{\phi}{2}$$

For Haringhata (Calcutta) $\phi = 32^\circ$, so that $s = \sec \frac{\phi}{2} = 1.04$. The value of H in the F-region over Calcutta has been given by Baral and Mitra (1950) as

0.36 oersted (from examination of a large number of records of critical frequencies for the region for ordinary and extraordinary rays). This gives $f_H = 1.01$ Mc/s.

We have extrapolated the value of X tabulated by Shinn (1953) for different values of X , k and for $s = 1.04$, and assuming $f_H = 1.01$ Mc/s, have constructed Table II giving the values of $X + Y$ for different values of X (i.e. f/f_c) and f_c .

It is obvious from Eqn. (12) that if h' (from the $h' - f$ records) be plotted against $X + Y$, then such plots will be straight lines. The slope of the straight line will give the semi-thickness of the parabolic layer and the intercept on the h' -axis will be the lower boundary of the layer. (This is similar to Appleton and Beynon's method, where the magnetic field is neglected and h' is plotted against X , instead of $X + Y$.)

TABLE II
Values of $10^3(h' - h_0)/Y_m = 10^3(X + Y)$
for sec $\phi = 1.04$ and $f_H = 1.01$ Mc/s

k		0.35	0.4	0.45	0.5	0.55	0.6	0.65	0.7	0.75	
X	f/f_c	f_c	11.99	9.70	7.91	6.48	5.29	4.32	3.49	2.79	2.16
0.6	0.697	618	620	623	625	628	630	632	634	636	
0.9	0.806	924	928	932	935	938	941	945	949	953	
1.2	0.878	1239	1244	1250	1256	1261	1265	1271	1276	1282	
1.5	0.925	1554	1560	1567	1574	1581	1587	1594	1602	1610	
1.8	0.955	1878	1885	1894	1903	1911	1918	1926	1934	1942	
2.1	0.974	2201	2212	2223	2235	2246	2255	2263	2272	2280	
2.4	0.985	2538	2550	2561	2572	2577	2582	2590	2602	2615	

(d) *Kelso's method (2): Integral equation method including earth's magnetic field.*

In this method (Kelso, 1954) the earth's magnetic field is taken into account and the true height is obtained by solving, in a convergent series of integrals, the integral equation (1). The integration have to be carried out through the use of three formulae obtained from the Gauss-Christoffel quadrature formula. We describe here the main steps of the procedure to be employed for the computation of true height by this method:

(i) Following the method described in Sec. 2(b), the true height for the no-magnetic field case is determined for various frequencies f_r . These give the zero order true height values $h_0(f_r)$.

(ii) Using graphical differentiation the derivative

$$h_0'(f_r^2) = \frac{1}{2f_v} \frac{dh_0}{df_r}$$

is obtained for several values of f and the results plotted as a function of f^2 .

(iii) For a number of f^2 values integrations are carried out by the application of the Gauss-Christoffel quadrature formula to obtain

$$\begin{aligned}\phi(f^2) = & 0.1338 h_0'(x_1 f^2)[G(x_1)-1] \\ & + 0.2992 h_0'(x_2 f^2)[G(x_2)-1] \\ & + 0.4382 h_0'(x_3 f^2)[G(x_3)-1] \\ & + 0.5382 h_0'(x_4 f^2)[G(x_4)-1] \\ & + 0.5905 h_0'(x_5 f^2)[G(x_5)-1]\end{aligned}$$

where $x_1 = 0.0517$ $x_3 = 0.5390$ $x_5 = 0.9779$
 $x_2 = 0.2523$ $x_4 = 0.8125$

$$G(x) = \mu't = \mu'\sqrt{1-x}, \text{ where } x = \frac{f_0^2}{f^2} \quad t = 1 - \frac{f_0^2}{f^2}$$

and $f_0^2 = \frac{Ne^2}{\pi m}$ proportional to electron density N
 e = charge of electron in e.s.u.
 m = mass of electron in gms.

The values of $G(x)$ are obtained from figure 5, where $G(x) = \mu't$ (for the ordinary ray) has been plotted against x for the magnetic latitude of Calcutta, i.e.

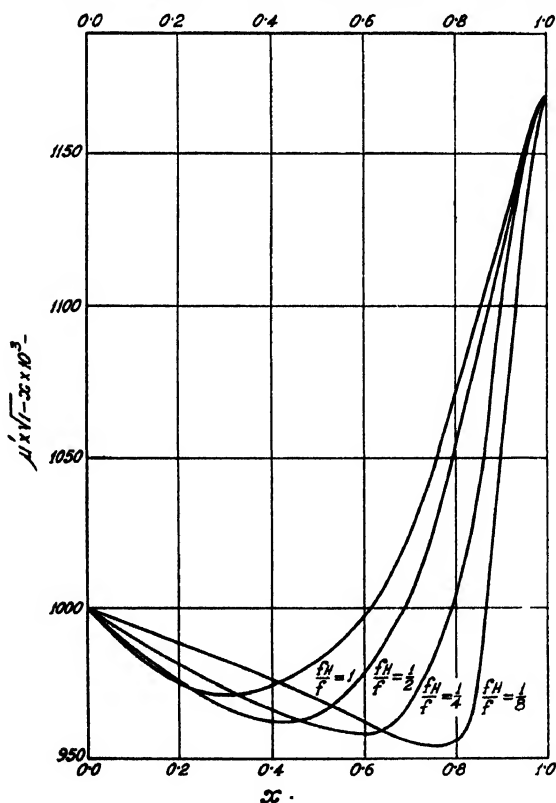


Fig. 5. Values of the function $G(x) = \mu'\sqrt{1-x}$ for the ordinary ray and for the magnetic latitude of Calcutta ($\varphi = 32^\circ$).

for $\phi = 32^\circ$ and for $\frac{f_H}{f} = \frac{1}{8}, \frac{1}{4}, \frac{1}{2}, 1$. The curves have been constructed by extrapolating to $\phi = 32^\circ$ the table of $\mu't$ computed by Shinn (1954) for different values of ϕ and $\frac{f_H}{f}$

$\phi(f^2)$ values are obtained for a sufficient number of f^2 values so that a reasonably well defined curve of $\phi(f^2)$ vs. f may be plotted.

(iv) Taking the same values of f_r as used in (i) the $\phi(f^2)$ vs. f curve is integrated with the help of the Gauss-Christoffel formula to obtain

$$\begin{aligned} h_1(f_r) = & -f_r^2 [0.003685 \phi(0.1667 f_r) \\ & + 0.02922 \phi(0.5035 f_r) \\ & + 0.08969 \phi(0.6598 f_r) \\ & + 0.1642 \phi(0.8696 f_r) \\ & + 0.2132 \phi(0.9851 f_r)] \end{aligned}$$

(v) The process may be repeated using $h_1(f_r)$ in the same manner as $h_0(f_r)$ to obtain $h_2(f_r)$ and so on.

(vi) The true height of reflection at frequency f_r is then given by the sum of all the $h_i(f_r)$; $i = 0, 1, 2, \dots$

The process is a convergent one and may be terminated according to the desired accuracy.

3. APPLICATION TO CALCUTTA RECORDS

The methods described above have been used to find the distribution of electron density at E and F regions over Calcutta and Haringhata from $h'-f$ records obtained with (i) a manual recorder of high height resolution (± 0.5 km) and having a frequency range of 1.5 to 4.1 Mc/s, and (ii) an automatic ionosphere recorder (± 5 km accuracy in height measurement) having a frequency sweep of 1.0 to 13.0 Mc/s.

(a) *Electron distribution in Region E.*

E-region electron density distribution has been deduced from $h'-f$ records obtained with the manual recorder. Variation of true height of reflection with frequency has been obtained by the application of the parabolic layer method (Appleton and Beynon) and the integral equation method of Kelso (1). The analysis of a sample record is illustrated in figure 6(a). It may be noted that, in the parabolic layer method the true heights of reflection for low frequencies can be obtained by extrapolating the h_r-f curve. For computation of the same by the Kelso method, however, the apparent height data near the low frequency end are needed. In the analysis of the record shown in figure 6(a) it was assumed that the apparent height had the constant value of 100 km below 1.5 Mc/s. It

may be seen in figure 6(a) that the values of h_m and the thickness of the layer obtained by the two methods differ slightly. This may indicate slight departure of the E layer from the perfect parabolic shape.

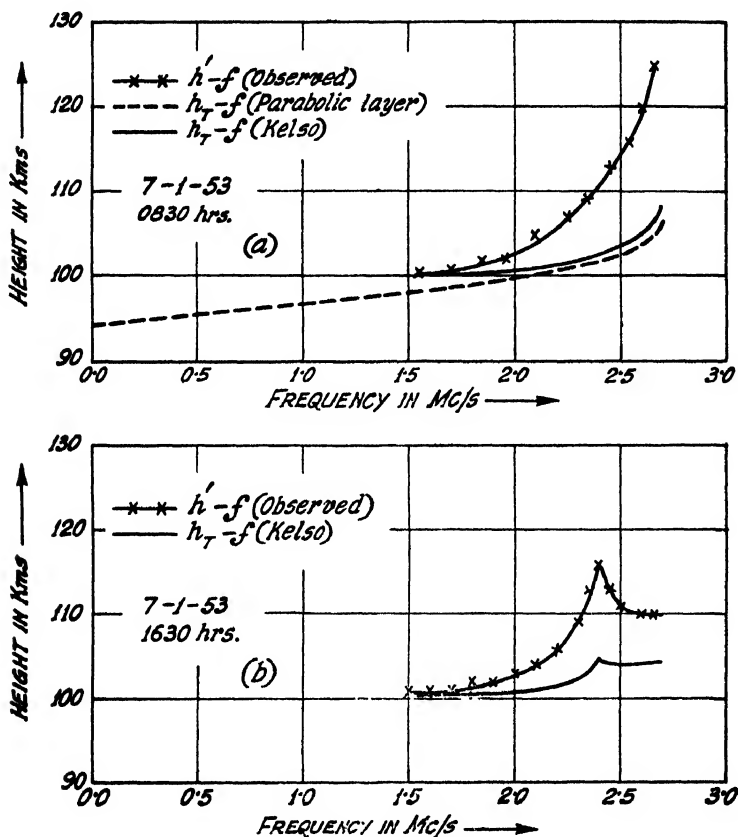


Fig. 6. Experimental apparent height and computed true height curves for (a) normal E-layer and (b) E-region in the presence of sporadic E ionization.

Figure 6(b) gives the variation of true height of reflection from the E-region in the presence of sporadic E, deduced by the Kelso method (1). The parabolic layer method is not applicable to sporadic E reflections. The cusp in the $h_r - f$ curve near foE has no physical significance, but comes out even when the computations are carried out with $n = 10$ [see Sec. 2(b)]. The sampling procedure of Kelso is not adequate near cusps in the $h' - f$ curve.

From a study of a number of E-region electron distributions, deduced by the Kelso method, it has been noticed that, generally, in presence of sporadic E, the distribution of normal E-layer ionization deviates appreciably from the parabolic law.

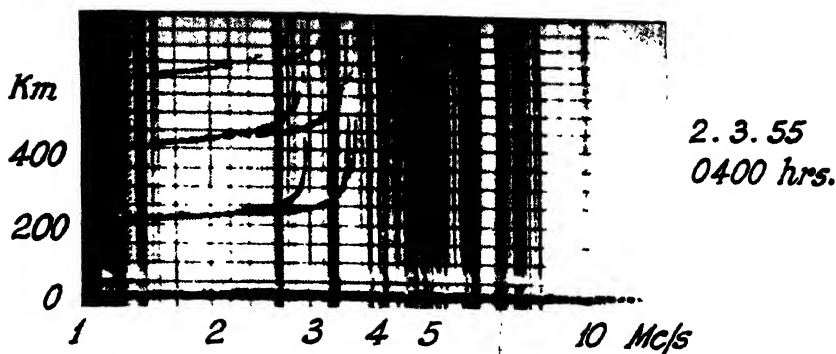
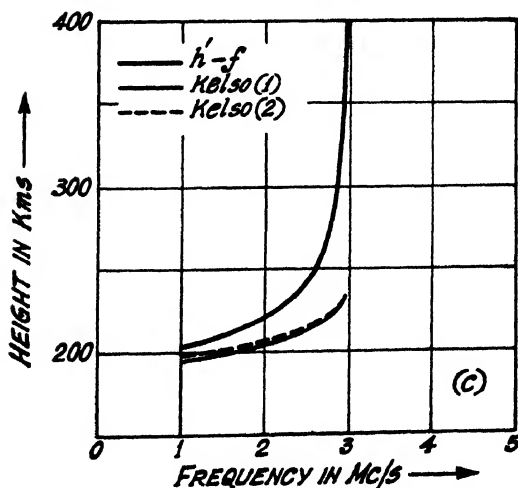
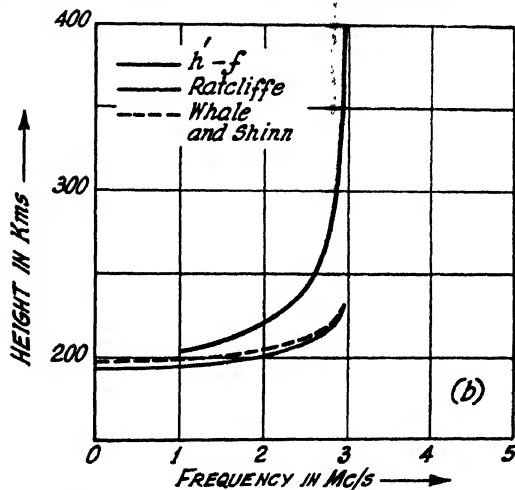


Fig. 7(a). A night-time $h'-f$ record containing the F-trace only.



F (b) & 7(c). $h'-f$ curves and computed true height curves corresponding to the record shown in Fig. 7(a).

(b) *Electron distribution in the Region F.*

F-region electron density distribution has been deduced from $h'-f$ records obtained with the automatic recorder. The variation of true height with frequency deduced from a night-time $h'-f$ record [figure 7(a)] containing the F-trace only by the parabolic layer methods and by the integral equation methods are shown in figures 7(b) and 7(c) respectively. The true height variation corresponding to a day time $h'-f$ record [figure 8a], containing the E, F_1 and F_2 layer traces are shown in figure 8(b) and (8(c)).

It will be seen that the true heights obtained by the methods of Ratcliffe and of Kelso neglecting magnetic field are in close agreement only for the night time record and not for the day time F_1 and F_2 records, the heights obtained by Kelso method being systematically lower. The reason for this is that in the Kelso method the h_r-f curves are obtained as integrated effect of the experimental results over the entire range of observed frequencies, whereas in the Ratcliffe method a chosen range of frequencies is considered in the true height deductions for a particular layer. It should be noted that the Kelso method gives the distribution of electron density with height instead of indicating the best parabolic fit given by the Ratcliffe method. However, the true height values near cusps in the $h'-f$ records (near foE fo F_1) obtained by Kelso method are not dependable because of the approximations involved in the sampling procedure. Although the solutions given by Ratcliffe method are of an approximate nature, the ease with which these can be obtained makes the method specially suitable for routine measurements.

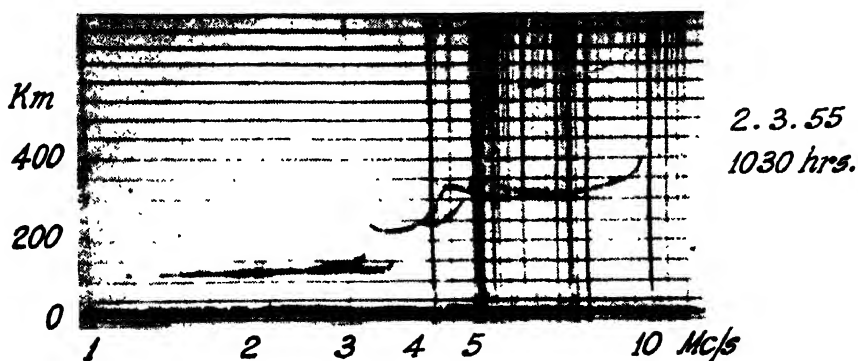


Fig. 8(a). A day-time $h'-f$ curve containing E, F_1 and F_2 layer traces.

In figures 7(b) and 8(b) the true height data for the F_2 layer obtained by Whale and Shinn method (including the effect of the earth's magnetic field) have also been presented. In figure 7(c) the true height data obtained by Kelso method (2) is also given. It will be seen that the value of h_m obtained after inclusion of

the effect of magnetic field is practically the same as that obtained when the field is not considered. The thickness, however, is less by about 10% when the effect of the field is taken into account. Thus the result of neglecting the earth's magnetic field in true height calculations from $h'-f$ records obtained at our latitude ($\phi = 32^\circ$) is to overestimate the layer thickness by about 10% without introducing appreciable error in the h_m value. It is to be noted that in actual radio

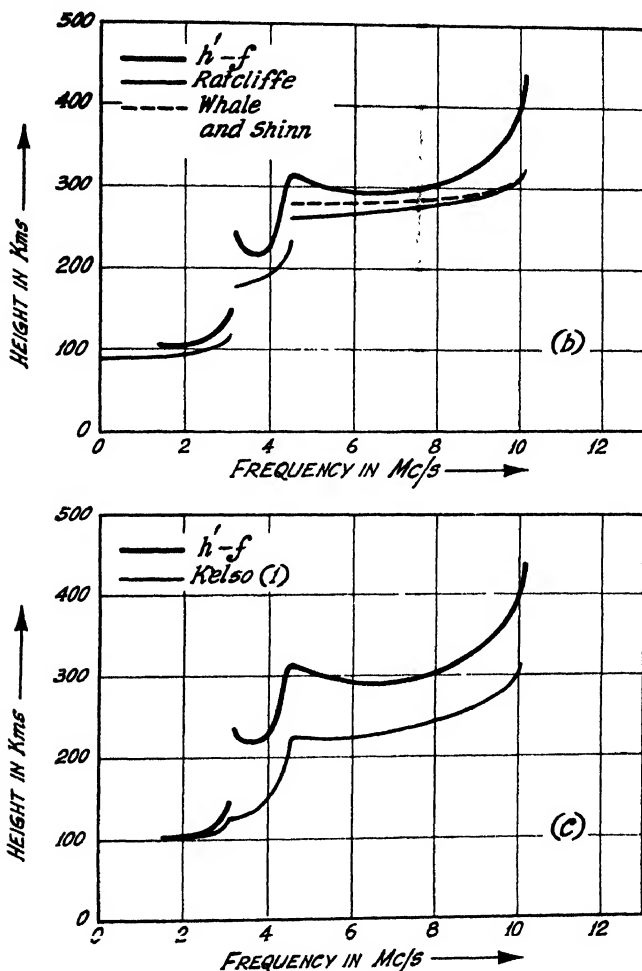


Fig. 8(b) & (c). Apparent height and true height curves corresponding to the $h'-f$ record shown in Fig. 8(a).

communication the variation in MUF is mainly controlled by the variation in h_m only. As the inclusion of the magnetic field has negligible effect on h_m and the correction is laborious the determination of true height neglecting the effect of the earth's magnetic field is justified for all practical purposes.

Figure 9(a) shows the diurnal variation of true height of reflection at 3, 4, 5, 7 and 10 Mc/s obtained by applying Ratcliffe's method to the automatic $h'-f$ curves for a typical quiet day. Figure 9(b) shows similar curves for a disturbed day.

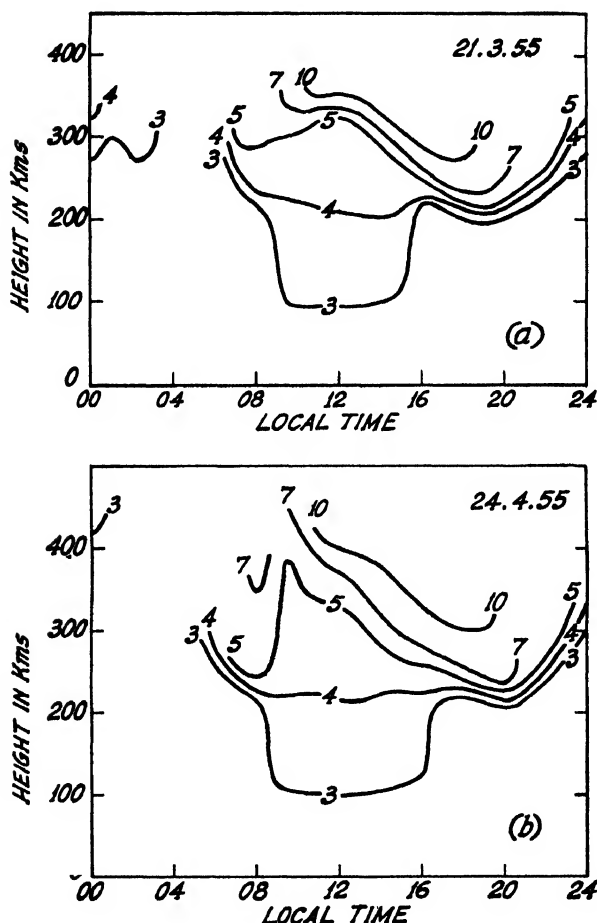


Fig. 9. Diurnal variation of true height of reflection at 3, 4, 5, 7 and 10 Mc/s obtained by Ratcliffe's method from $h'-f$ records for (a) a quiet day and for (b) a disturbed day.

Preliminary results of applying the Kelso method to hourly $h'-f$ records for 24 hours for a number of quiet days during the period March-September, 1955 have shown that on about 60% of the daylight hours the F_2 region has a true parabolic distribution of ionization. During night-time the F-region is found to be parabolic in almost all the cases.

CONCLUDING REMARKS

It may be concluded from the above study that the determination of height distribution of electrons by Ratcliffe's method is the most convenient for routine work. The other methods, although more accurate under special conditions (e.g. Kelso method as applied to E-region or to night-time F-region records), are more laborious. For the latitudes round Calcutta the distributions as computed by neglecting the earth's magnetic field are sufficient for all practical purposes. The errors resulting from the neglect of the magnetic field do not exceed those involved in the actual height measurement with the apparatus used. Further, the inclusion of the magnetic field affects only the thickness of the layer and not its height of maximum ionization. And it is known that in practical radio communication the height of maximum ionization has a much greater control than the thickness of an ionospheric layer.

ACKNOWLEDGMENTS

The work forms part of the programme of the Radio Research Committee of the Council of Scientific & Industrial Research, Government of India.

The author is indebted to Professor S. K. Mitra for constant help and guidance and to Dr. J. N. Bhar for encouragement and advice. Thanks are also due to Dr. S. S. Baral for some valuable discussions.

REFERENCES

- Abel, N. H. 1881, *Œuvres*, t.1, p.11. Christiania
Appleton, E. V., 1930, *Proc. Phys. Soc.*, **42**, 321.
Appleton, E. V. and Beynon, W. J. G., 1940, *Proc. Phys. Soc.*, **52**, 518.
Appleton, E. V. and Beynon, W. J. G., 1947, *Proc. Phys. Soc.*, **59**, 58.
Baral, S. S. and Mitra A. P., 1950, *J. Atmos. Terr. Phys.*, **1**, 95.
Booker, H. G. and Seaton, S. L., 1940, *Phys. Rev.*, **57**, 87.
Budden, K. G., 1954, *Physics of the Ionosphere*, Report of the Physical Society Conference p. 332.
Kelso, J. M., 1952, *J. Geophys. Res.*, **57**, 357.
Kelso, J. M., 1954, *J. Atmos. Terr. Phys.*, **5**, 11.
Mitra, S. K., 1952, *The Upper Atmosphere*, Asiatic Society, Calcutta.
Pekeris, C. L., 1940, *Terr. Mag. Atmos. Elec.*, **42**, 205.
Piggot, W. R., 1954, *J. Atmos. Terr. Phys.*, **5**, 201.
Ratcliffe, J. A., 1951, *J. Geophys. Res.*, **56**, 463.
Rydbeck, O. E. H., 1940, *Phil. Mag.*, **30**, 282.
Shinn, D. H., 1953, *J. Atmos. Terr. Phys.*, **4**, 240.
Shinn, D. H., 1954, *Physics of the Ionosphere*, Report of the Physical Society Conference p. 402.
Shinn, D. H. and Whale, H. A., 1952, *J. Atmos. Terr. Phys.*, **2**, 85.

ULTRAVIOLET ABSORPTION SPECTRA OF PYRIDINE IN THE LIQUID AND SOLID STATES*

S. B. BANERJEE

OPTICS DEPARTMENT, INDIAN ASSOCIATION FOR THE CULTIVATION OF SCIENCE,
JADAVPUR, CALCUTTA-32.

(Received for publication June 28, 1956)

ABSTRACT. The ultraviolet absorption spectra of pyridine in the liquid and solid states have been investigated and the results have been compared with those for the vapour and solutions reported by previous workers.

In the case of the liquid as well as the solid only one system of bands in the region 2400—2650Å has been observed corresponding to the bands due to $\pi \rightarrow \pi^*$ transition found in the case of the vapour. The 0,0 band is found to shift towards the longer wavelengths with the liquefaction of the vapour and also with the solidification of the liquid. The bands due to $n \rightarrow \pi^*$ transition lying in the region 2700Å—2900Å observed in the case of the vapour by previous workers are absent in the spectra due to the liquid and the solid. These results have been interpreted in the present paper by assuming that in the liquid and solid states pyridine molecules form associated groups through weak virtual bonds formed through the nitrogen atoms and the hydrogen atoms of neighbouring molecules, preventing thereby the $n \rightarrow \pi^*$ transition. It is pointed out that these results corroborate the assignment of the system in the long wavelength region to $n \rightarrow \pi^*$ transition in the case of the vapour.

INTRODUCTION

The detailed classification of the absorption spectrum of pyridine in the vapour state was reported first by Sponer and Stücklen (1946) who observed only one system of bands with the ν_0 -band at 34769 cm^{-1} and a large number of narrow headless bands. From theoretical considerations and from a study of the spectra of pyridine in solutions it was suggested by Kasha (1950) that there are probabilities of two types of transitions in pyridine, one of these involving the excitation of one of the nitrogen nonbonding electrons to π -molecular orbital being designated as $n \rightarrow \pi^*$ transition and the other a singlet-singlet $\pi \rightarrow \pi^*$ transition. The former transition was expected to be weaker than the latter. The band system due to the vapour was re-examined by Rush and Sponer (1952) and it was concluded that there is a second system in the spectrum at 38350 cm^{-1} . The first system of bands (called Transition I) of Sponer and Stücklen was recognised to be that due to the $n \rightarrow \pi^*$ transition and the second system (called Transition II) to the $\pi \rightarrow \pi^*$ transition. It can also be seen from the spectrograms of the

*Communicated by Prof S. C. Sirkar.

absorption spectra of pyridine vapour for different vapour pressures reported by Herington (1950) that with very low vapour pressure the bands on the shorter wavelength side (Transition II) are observed while with considerably high vapour pressure the weak bands on the longer wavelength side make their appearance. This also shows that the bands due to the $n \rightarrow \pi^*$ transitions are very weak.

Stephenson (1954) studied the ultraviolet absorption spectrum of pyridine dissolved in ethyl alcohol. His absorption curve does not show the bands corresponding to Transition I ($n \rightarrow \pi^*$ transition) while the bands corresponding to Transition II are quite intense, with the ν_0 -band at about 38000 cm^{-1} . He suggested that these results might be interpreted by assuming that in alcohol the nitrogen nonbonding electron becomes involved in the formation of hydrogen bond, thus causing Transition I to move well into the region of Transition II so as to be obscured by the latter transition. The absorption spectra of pyridine in alcohol ether solution at -183°C reported by Zanker (1954) shows only the bands of Transition II with the position of the ν_0 -band remaining almost undisplaced with respect to that reported by Stephenson (1954) for the solution in alcohol in the liquid state.

Recently, Kastha (1956) studied the Raman spectrum of pure pyridine in the solid state at -180°C and also that of frozen solution of pyridine in ethyl alcohol at -180°C . He observed that pure pyridine in the solid state at -180°C shows low frequency Raman lines which are absent in the case of the frozen solution of the substance in ethyl alcohol at -180°C and are replaced by a continuous wing extending up to 95 cm^{-1} . From this and other results he concluded that in the solid state at -180°C the pyridine molecules probably form associated groups and this association breaks up and the pyridine molecules probably form complex molecules with the ethyl alcohol molecules through hydrogen bonding in the solution.

It seems that none of the previous workers studied the ultraviolet absorption spectra of pure pyridine in the liquid and solid states. The object of the present investigation was to study the ultraviolet absorption spectra of the pure substance in the liquid and solid states at low temperatures and to compare the results with those obtained for the vapour and for solutions at different temperatures. These results have been discussed in the present paper and attempts have been made to correlate the results with those observed in the investigations on the Raman spectra of the substance in different states.

EXPERIMENTAL

Chemically pure pyridine was first fractionated and the fraction boiling at about $115^\circ\text{--}116^\circ\text{C}$ was redistilled under reduced pressure before use. The spectra were photographed on Ilford HP3 films with a Hilger E 1 spectrograph. Very thin films of thickness less than .01 mm were used in the case of the liquid

and solid states. Iron arc spectrum was taken on each film as a comparison. Microphotometric records of the spectrograms were taken with a Kipp and Zonen type Moll microphotometer. The absorption spectra were calibrated with the help of microphotometric records of iron arc lines using the method described earlier (Banerjee, 1956).

RESULTS AND DISCUSSIONS

The microphotometric records of the absorption spectra of pyridine in the liquid and solid states are reproduced in figure 1. The wave numbers of the cen-

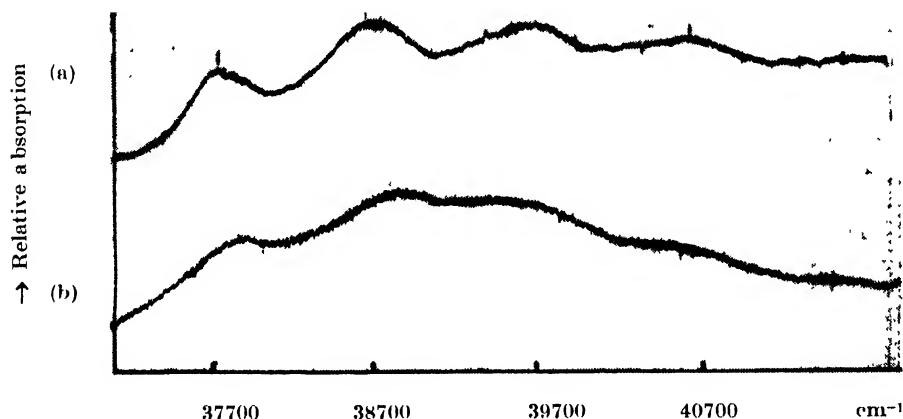


Fig. 1. Microphotometric records of the ultraviolet absorption spectra of pyridine.
(a) Solid at -180°C . (b) Liquid at 32°C .

tres of absorption bands are given in Table I. The bands of Transition I could not be detected even using films of considerably greater thickness.

TABLE I

Absorption bands of Pyridine

Liquid at 32°C		Solid at -180°C	
Wave no. (cm^{-1}) and intensity	assignment	Wave no. (cm^{-1}) and intensity	assignment
37881 (ms)	ν_0	37724 (ms)	ν_0
38793 (s)	$\nu_0 + 912$	38703 (s)	$\nu_0 + 979$
39702 (s)	$\nu_0 + 2 \times 912$	39686 (s)	$\nu_0 + 2 \times 979$
40613 (ms)	$\nu_0 + 3 \times 912$	40654 (ms)	$\nu_0 + 3 \times 979$

In the case of the liquid and solid only one system of bands on the shorter wavelength side consisting of four broad bands is observed. The system of bands

on the longer wavelength side corresponding to $n \rightarrow \pi^*$ transition observed in the case of the vapour (Sponer and Stücklen, 1946) could not be detected for the liquid or the solid state. The ν_0 -band observed in the spectrum due to the liquid is at 37881 cm^{-1} and the other bands indicate a progression of vibrational frequency 912 cm^{-1} . Probably this system corresponds to the system of bands due to $\pi \rightarrow \pi^*$ transition observed in the case of the vapour (Rush and Sponer, 1952) with the ν_0 -band at about 38350 cm^{-1} . The ν_0 -band of this system thus shifts by about 469 cm^{-1} towards the longer wavelengths with the change from vapour to the liquid state. The ν_0 -band due to the solid is at 37724 cm^{-1} and the other bands represent a progression of the frequency 979 cm^{-1} . Thus with the solidification of the liquid and cooling to -180°C the ν_0 -band further shifts towards longer wavelengths by 157 cm^{-1} . It is seen that the major shift in the position of the ν_0 -band occurs when the change from vapour to liquid state takes place. This indicates that the pyridine molecules probably form associated groups when the vapour is liquefied and that this association becomes a little stronger with solidification of the liquid and cooling to -180°C .

Stephenson (1954) studied the ultraviolet absorption spectrum of pyridine in solution in ethyl alcohol and observed the bands recognised to be due to $\pi \rightarrow \pi^*$ transition with the ν_0 -band at about 38000 cm^{-1} . He concluded that the nitrogen nonbonding electron gets involved in hydrogen bond formation in alcohol, thus accounting for the absence of the bands corresponding to the $n \rightarrow \pi^*$ transition (called Transition I). The absence of the bands due to $n \rightarrow \pi^*$ transition in the pure liquid may be explained by assuming that a large number of pyridine molecules form associated groups among themselves due to formation of weak virtual bonds through the nitrogen nonbonding electrons and the hydrogen atoms of the neighbouring molecules and the number of such electrons available in the liquid for $n \rightarrow \pi^*$ transition (Transition I) being very small it would be difficult to get the bands due to this transition which are themselves expected to be weak compared to those due to $\pi \rightarrow \pi^*$ transition. Also, the associated groups of molecules in the liquid may require higher energy for excitation as was suggested for complex molecules in alcohol solution by Stephenson (1954). In the case of the solid at -180°C where the association becomes stronger the probability of obtaining the bands of Transition I would be still smaller.

The probability of such association among neighbouring pyridine molecules is also corroborated by the results obtained by Kastha (1956) in an investigation on the Raman spectra of pyridine in the liquid state and in the solid state at -180°C as well as in solutions in ethyl alcohol at different temperatures. He observed that with solidification of the pure substance some of the frequencies representing the C—H vibration are affected while in the case of the solution the line 995 cm^{-1} due to symmetric vibration of the ring is strongly affected and also the line 1575 cm^{-1} due to a degenerate mode of the ring is split up into two components. From these results he concluded that whereas in the case of

the solution in alcohol regular bond between the nitrogen atom and the O-H group is formed, only weak linkages between neighbouring molecules are established when the pure liquid is solidified and cooled to -180°C .

The results discussed above thus furnish conclusive evidence for the formation of associated groups of molecules in the liquid and solid states of pyridine.

ACKNOWLEDGMENT

The author is indebted to Professor S. C. Sirkar, D. Sc., F.N.I. for his kind interest and constant guidance throughout the progress of the work.

REFERENCES

- Banerjee, S. B., 1956, *Ind. J. Phys.*, **30**, 106.
Herington, E. F. G., 1950, *Discussions of the Faraday Society*, **9**, 26.
Kasha, M., 1950, *Discussion of the Faraday Society*, **9**, 14.
Kastha, G. S. 1956, Unpublished results.
Rush, J. H., and Sponer, H., 1952, *J. Chem. Phys.*, **20**, 1847.
Sponer, H. and Stücklen, H., 1946, *J. Chem. Phys.*, **14**, 101.
Stephenson, H. P., 1954, *J. Chem. Phys.*, **22**, 1077.
Zanker, V., 1954, *Z. Phys. Chem.*, Band **2**, 52.

DEFORMATION OF A FIXED-FREE BAR UNDER A COMPRESSIVE IMPACT OF SHORT DURATION.

S. K. GHOSH

DEPARTMENT OF PHYSICS, CHANDERNAGORE COLLEGE, W. BENGAL

(Received for publication September 20, 1953)

ABSTRACT. The present paper gives a quantitative explanation, from the theory already developed by the author in a series of papers, of the fact regarding the deformation of a fixed-free bar under a compressive impact of short duration. The experimental data supplied by E. T. Habib are used in testing the theory. The agreement between author's theory and experiment is found to be satisfactory.]

In a series of paper already published (Ghosh and Ghosh, 1951, 1952; Ghosh, 1953) the elastic and plastic behaviour of a bar under a compressive impact by an elastic or inelastic load have been studied. In the present paper attempt has been made by the help of the theory developed, to explain quantitatively the experimental results obtained by Habib (1948) who in course of his study on high-speed compression tests on small copper cylinders measured the deformation undergone by a specimen fixed at one end and struck at the free end by a compressive force of short duration. The deformations i.e. the displacements (ω_l) at the impact end for different values of time of collision with respective values of striking velocities of impact are calculated from equations (20) (Ghosh, 1953)

Thus during $0 < t < \theta_1$,

$$\omega_l = f_1(t) - \frac{1}{2}\eta_1 f_1'(t),$$

After time $t = \theta_1 = \frac{2l}{c}$ the second term no longer vanishes, so,

during $\theta_1 < t < 2\theta_1$,

$$\omega_l = f_1(t) - \frac{1}{2}\eta_1 f_1'(t) + 2f_2(t_1) - 2f_1(t_1) - \frac{1}{2}\eta_1\{3f_2'(t_1) - 2f_1'(t_1) - 2\theta_1 f_2''(t_1) + 2\theta_1 f_1''(t_1)\},$$

and during

$$2\theta_1 < t < 3\theta_1,$$

$$\omega_l = (\omega_e)_{\theta_1 < t < 2\theta_1} + 4f_3(t_2) - 6f_2(t_2) + 2f_1(t_2)$$

$$- \frac{1}{2}\eta_1\{8f_3'(t_2) - 9f_2'(t_2) + 2f_1'(t_2) - 8\theta_1 f_3''(t_2) + 12\theta_1 f_2''(t_2) - 4\theta_1 f_1''(t_2)\}$$

and so on, where $\eta_1 = \eta/E_1$ and the values of the functions $f_1(t)$, $f_2(t)$, $f_3(t)$, and their derivatives are easily obtained from equations (12d.) of Part I. (Ghosh and Ghosh, 1952, 1953)

Before actually calculating the theoretical values of the displacement, it is obviously necessary to find out, from a knowledge of the time of deformation, the interval during which the impacting pressure terminates.

The compression tests performed by Habib (1947, 1948) utilised as the test specimen an annealed copper cylinder of length $\frac{1}{2}$ " and diameter 0.33". The impacting load consisted of several pistons made of tool steel and hardened Rockwell C45 having the following dimensions:

1" hollow piston, weight = 8g (0.176 lb), $\frac{1}{2}$ " diameter.	
1" piston " = 25g (0.55 lb), $\frac{1}{2}$ " "	
3" piston, " = 75g (0.165 lb), $\frac{1}{2}$ " "	

Taking an average value of $\eta = 10^3$ Poise and Young's modulus $E_1 = 1.7 \times 10^4$ lbs/in² for copper, the deformations at the impacted end are calculated at different values of time and striking velocities from the above equations. It is needless to mention that the author has conveniently used the hard load in evaluating the above equations for the deformations just to comply with the experimental condition where sufficiently hard tool steel pistons are employed. In this way, by the help of equations (19d) (Ghosh, 1953) and their derivatives, the displacements are calculated as shown in the Table I given below.

TABLE I

Mass of the load in lb.	Time of deformation in micro sec.	Striking velocity v_0 in/sec.	Deformation in inch.	
			Theory	Expt.
1" Hollow Piston .0176	40	1000	0.023	0.02
1" Piston — .055	80	1000	0.051	0.04
	64	800	0.037	0.03
3" Piston— .165	120	1000	0.086	0.08
	127	900	0.063	0.06

The experimental values of the deformations at different striking velocities using different pistons as the impacting load are quoted from a study of the figures 4, 5, 6, 7 in Habib's paper. The table shows satisfactory agreement between author's theory and experimental tests in the same line.

ACKNOWLEDGMENT

The author wishes to thank Dr. M. Ghosh D.Sc., Professor of Physics, City College, Calcutta, for his kind help during the preparation of this paper.

REFERENCES

- Ghosh, M. and Ghosh, S. K. 1951, Part I, *Ind. J. Phys.*, **25**, 153.
 " " 1952, Part II, **26**, 463.
 Ghosh, S. K. 1953, Part III, *Ind. J. Theo. Phys.* **1**, 25,
 Habib, E. T., 1948, *J. of Appl. Mech. Trans. ASME.*, **70**, 248.
 " 1947, *J. of Appl. Phys.*, **18**, 645.

Letters to the Editor

The Board of Editors will not hold itself responsible for opinions expressed in the letters, published in this section. The notes containing reports of new work communicated for this section should not contain many figures and should not exceed 500 words in length. The contributions must reach the Assistant Editor not later than the 15th of the second month preceding that of the issue in which the Letter is to appear. No proof will be sent to the authors.

THE ULTRAVIOLET ABSORPTION SPECTRA OF *o*-, *m*-, *p*-FLUOROBROMOBENZENES.

S. L. N. G. KRISHNAMACHARI

PHYSICS DEPARTMENT, ANDHRA UNIVERSITY, WALTAIR

(Received for publication July 4, 1956)

In continuation of the work on the *o*, *m*, *p*-fluorochlorobenzenes (author, 1955, 56, 56), the ultraviolet absorption spectra of *o*-, *m*-, *p*-fluorobromobenzenes in the vapour state were investigated. There is no previous work on the ortho and meta compounds where as the para compound was studied in hexane solution by Conrod-Billroth (1936) and in the vapour state by Dima and Tintea (1940). The latter authors identified only three frequencies in the upper and none in the lower state.

The path lengths and temperatures employed in the present work are the same as in the earlier investigations. The general appearance of the spectra are quite similar to the corresponding fluorochlorobenzenes. The regions of absorption, the number of bands measured, the position of the 0,0 band, the prominent *v*, *v* separations and the nature of the electronic transitions giving rise to the discrete spectra are given in Table I. The excited and ground state frequencies, their correlation with the Raman data and the probable assignments are given in Table II. Details of the analyses will be published shortly.

TABLE I

Characteristic features of the ultraviolet absorption of *o*, *m*, *p*-FC₆H₄Br.

Region of absorption		{ Number of bands	0,0 band	Prominent <i>v</i> , <i>v</i> separations	Nature of the electronic transition
1) Discrete	2) Continuous				
Ortho 2830-2450A	below 2150A	135	36985 cm ⁻¹	83,131 cm ⁻¹	A' - A'
Meta 2810-2430A	"	150	36963 cm ⁻¹	81 cm ⁻¹	A' - A'
Para 2900-2475A	„	190	36221 cm ⁻¹	30 cm ⁻¹	A ₁ - B ₁

TABLE II

Ground and excited state frequencies of *o*-,*m*-,*p*-FC₆H₅B₄.

	Raman data			U. V. absorption data		Probable assignment
	$\Delta\nu$	Int	ρ	Ground state	excited state	
Ortho	(author 1956)			(author)		
	298	St Sh	.36	294	249 (w)	{ one of the ϵ^+g components of
	654	St Vsh	.16	656	599 (St)	benzene
	821	St Sh	.18	823	791 (Vst)	C-Br stretching
	1026	St Vsh	.15	1028	942 (Vst)	} Totally symmetric carbon vibrations
	1234	St Sh	.15	1244	1245 (ms)	
						C-F stretching
Meta	(author, 1956)					
	666	St Vsh	.11	668	607 (m)	C—Br stretching
	859	m d	.25	863	831 (ms)	
	1002	Vst Sh	.05	1004	962 (Vst)	Carbon ring breathing
	1056	St Sh	.02	1062	1001 (w)	
	1215	St Vd	.01	1229	1211 (mw)	C—F stretching
Para	(Nielsen et al. 1956)					
	290	Vst Sh	.30	276	251 (m)	One of the ϵ^+g components of C ₆ H ₆
	596	m Sh	.15	597	513 (mw)	C—Br stretching
	810	Vst Sh	.10	812	788 (Vst)	} Totally symmetric C—C vibrations
	1066	Vst Sh	.40	1066	1016 (st)	
	1228	St —	.50	1235	1230 (ms)	C—F stretching

The author is grateful to Dr. G. C. Finger for the gift of the samples, and to the Government of India for the award of a senior research scholarship. The author is deeply indebted to Prof. K. R. Rao for his valuable guidance.

REFERENCES

- Krishnamachari, S. L. N. G., 1955, *Ind. Jour. Phys.*, **29**, 603.
 " 1956,, " " " **30**, 151.
 .. 1956, " " " (in. press)
 .. 1956, *Curr. Science*, **25**, 185.
 .. 1956, " " (in press)
 Conrad-Billroth, H and Forster, G. 1936, *Zeit. Fur. Phys. Chem.* **33**, 311.
 Dima, G. A. and Tintea, H. 1940, *Bull. Sect. Sci. Acad. Rou.* **23**, 34-5.
 Nielsen, J. R. et al., 1956, *Jour. Chem. Phys.*, **24**, 420.

BOOK REVIEW

PARAMAGNETIC NUCLEAR RESONANCE—By Pierre Grivet. (In French).
Pp 298. Centre National de la Recherche Scientifique. Paris. 1955.
Price 1800 francs.

This book has been actually written by seven specialists under the general supervision of Prof. Grivet who has himself written the introduction dealing with general features of nuclear magnetism. The second chapter dealing with the establishment and integration of Bloch equation according to the macroscopic theory has been written by R. Gabillard. In this chapter the integration of the Bloch equation for slow sweep and rapid sweep and also the simplified theory in the case of rapid sweep have been discussed in detail. The quantum theory of nuclear resonance and relaxation in spin-medium has been given in detail by Y. Ayant in the next chapter. He has also included in this chapter discussion on the study of nuclear resonance in water, other liquids and paramagnetic solutions. The experimental methods have been described and explained in Chapter IV by R. Gabillard. He has discussed separately the methods of measuring long and short relaxation times, including in each case theoretical calculations. He has also included an elaborate discussion on the experimental methods of detecting nuclear spin-echoes developed by Hahn and has given detailed accounts of the method of measuring the times of relaxation, T_1 and T_2 , from spin-echo patterns developed independently by himself and Bradford & Clay in 1951. Beautiful photographs of such patterns have been reproduced to explain this method. In the next chapter M. Soutif and R. Gabillard have given some more details of practical experimental arrangements including details of circuit components. Chapter VI written by G. J. Bene, P. M. Denis and R. C. Extermann deals with the production of stationary magnetic field required for the study of nuclear magnetic resonance. In the next chapter on gyromagnetic ratio, Y. Ayant has discussed the corrections to be applied to this ratio due to the phenomena of "shifts" and G. J. Bene has given a long table containing the numerical values of nuclear magnetic moments. In Chapter VIII, Y. Ayant has given the theory of quadrupolar resonance and relaxation and M. Buyle-Bodin has discussed the theory of the experimental arrangement suitable for detecting such a resonance. In Chapter IX on gyromagnetic ratio and nuclear magnetic moment G. J. Benne, P. M. Denis and R. C. Extermann have discussed the regularities observed in the distribution of nuclear magnetic moments and their relation to "magic numbers".

In each chapter references to original papers have been included and numerous diagrams have been used to facilitate elucidation. From the summary

of the contents given above it will be quite evident that attempts have been made to present in the volume up-to date and exhaustive treatments of the theoretical aspects of the phenomena connected with nuclear magnetic resonance. The book will be immensely helpful to both specialists working in this line and physicists who want to be acquainted with this line of research. Considering the get up and quality of the diagrams, the price seems to be quite reasonable.

S. C. S.

ERRATA

THE INVERSE KINETIC ENERGY MATRIX ELEMENTS, ETC.,

By V. SANTHAMMA

DEPARTMENT OF PHYSICS, ANDHRA UNIVERSITY, WALTAIR.

Indian Journal of Physics, Vol. XXX, September, 1956.

1. Page 434—Table heading ; read $\gamma_{512}^a \gamma_1$ for $\gamma_{512}^a \gamma_1$ and $\gamma_{234}^c \gamma_3$ for $\gamma_{234}^c \gamma_3$
2. „ 435— „ „ ; read $\gamma_{512}^a \gamma_1$ for $\gamma_{511}^a \gamma_1, \gamma_{123} \gamma_2$ for $\gamma_{103}^b \gamma_0$ and
 $\gamma_{234}^c \gamma_3$ for $\gamma_{034}^c \gamma_3$
3. „ 436—Tatal IV, sixth line ; read H_1' for H_1
4. „ 437 Table heading ; read $\gamma_{345} \gamma_4$ for $\gamma_{345} \sigma_4$
5. „ 441 Table B (*contd*), third line read

$$\left[-\frac{1}{R_3} \sin^3 \phi_3 \operatorname{cosec}^5 \alpha_3 \left\{ \frac{1}{r_3} \sin^2 \alpha_3 + \dots \right. \right.$$

$$\left. \text{for } \left[-\frac{1}{R_3} \sin^3 \phi_3 \operatorname{cosec}^5 \alpha_3 \left\{ \frac{1}{r} \sin^2 \alpha_3 + \dots \right. \right. \right.$$

6. „ 446— Table C (*contd*), third line, read $\tau_5 \gamma'_1$ for $\tau_1 \gamma'_1$.

RESOLUTION OF SPECTRAL LINES OF UNEQUAL INTENSITY

K. C. CHATURVEDI AND M. S. SODHA

156-D, KAMALA NAGAR, DELHI-8

(Received for publication August 10, 1956)

ABSTRACT. In this paper the authors have discussed the dependence of resolving power on intensity ratio of the two lines to be resolved, detecting instrument and the stage of resolution desired when (i) instrumental line width is negligible and (ii) when natural line width is negligible.

INTRODUCTION

In general the spectral lines, sought to be resolved are not of equal intensity. This fact has not been given sufficient importance and there are no results, regarding the variation of resolving powers of instruments with the intensity ratio of the two spectral lines to be resolved, except those of Sparrow (1916) and Sodha (1952) for non-absorbing prism. The latter's results are not correct since he took the central minimum as the point of intersection of the component two intensity patterns.

Sparrow (1916) has suggested that two spectral lines, to be resolved, should have no dip in the resultant intensity pattern at the limit of resolution. In other words, resolution to non-resolution occurs, when the central minimum of the resultant intensity pattern of the two lines, just vanishes. It is obvious that the visibility

$$V = \frac{I_{max} - I_{min}}{I_{max} + I_{min}}$$

becomes zero at the limit of resolution, when Sparrow's criterion is applied. Hence Sparrow's criterion merely sets an upper limit for the resolving power.

Tolansky (1947) modified the Rayleigh criterion, when the spectral lines are of unequal intensity and stated that the two lines can be resolved when they are separated such that at the point of overlap the intensity of the stronger has fallen to two-fifths of the maximum intensity of the weaker line. In this modification Tolansky has obviously overlooked the following facts.

- (i) The weaker maximum of the resultant intensity pattern is different from the maximum intensity of the weaker line. The tail of the stronger line also contributes to it.
- (ii) For lines of unequal intensity, the central minimum does not occur at the point of intersection of the two component intensity patterns.

Keeping the above facts in view, Sodha (1952) modified the Rayleigh criterion for resolution of lines of unequal intensity and stated that at the limit of resolution the central minimum of the resultant intensity pattern should be $8/\pi^2$ times the weaker maximum.

Ditchburn (1930) has pointed out that the value of $(I_{min}/I_{max}) = C$, of the resultant intensity pattern at limiting resolution is characteristic of the detecting instrument and the stage of resolution desired. It may be added that in discussing resolution of lines of unequal intensity I_{max} should refer to the weaker maximum of the resultant intensity pattern.

In this communication, the authors have investigated the variation of resolving power with the intensity ratio $b (> 1)$ of the two spectral lines to be resolved for various values of C ($0.4 \leq C \leq 0.98$) in the following two cases :

(i) When instrumental width is negligible and the intensity distribution of the line is governed by Doppler effect.

(ii) When Doppler width is negligible and the intensity distribution is governed by the instrument (Fabry Perot etalon).

NEGLECTIBLE INSTRUMENTAL WIDTH

The intensity distribution of a spectral line of wave number ν_0 due to Doppler effect is given by

$$I' = I_0 e^{-\beta(\nu - \nu_0)^2}$$

where $\beta = \mu c^2_0/2RT\nu_0^2$, μ being the mass of radiant atoms.

The intensity distribution of another spectral line of wave number $\nu_0 + \Delta\nu$ and an intensity b times the first is given by

$$I'' = bI_0 e^{-\beta(\nu - \nu_0 - \Delta\nu)^2}$$

if $\Delta\nu$ is small (β same for both lines)

Putting $\sqrt{\beta}(\nu - \nu_0) = x$ and $\sqrt{\beta}\Delta\nu = a$, the resultant intensity pattern is given by

$$\frac{I}{I_0} = e^{-x^2} + be^{-(x-a)^2} \quad \dots (1)$$

Neglecting shrinkage effect, the weaker maximum of the resultant intensity pattern ($x_{max} = 0$) is given by—

$$\frac{I_{max}}{I_0} = 1 + be^{-a^2} \quad \dots (2)$$

The value of $x(=x_{min})$ for which the minimum of the resultant intensity pattern occurs, is given by

$$\frac{1}{I_0} \frac{dI}{dx} = -xe^{-x^2} + b(a-x)e^{-(a-x)^2} = 0$$

or

$$\phi(x) = b\phi(a-x) \quad \dots (3)$$

where

$$\phi(x) = xe^{-x^2}$$

For $b = 1$, Eqn. (3) gives

$$x_{min} = a/2 \quad (3a)$$

The minimum of the resultant intensity pattern is given by

$$\frac{I_{min}}{I_0} = e^{-x_{min}^2} + be^{-(a-x_{min})^2} \quad \dots (4)$$

For optimum resolution

$$C = \frac{I_{min}}{I_{ma}} \quad \dots (5)$$

The resolving power is given by

$$\frac{\lambda}{d\lambda} = \frac{\nu_0}{\Delta\nu} = \frac{\sqrt{\beta}}{a} \cdot \nu_0 = \alpha \cdot C_0 \sqrt{\frac{\mu}{2RT}} \quad \dots (6)$$

where

$$\alpha =$$

The details of calculation are given in Table I which gives the variation of α with C for $b = 1, 2, 3, 4$ and 5 . The table is illustrated by figure 1.

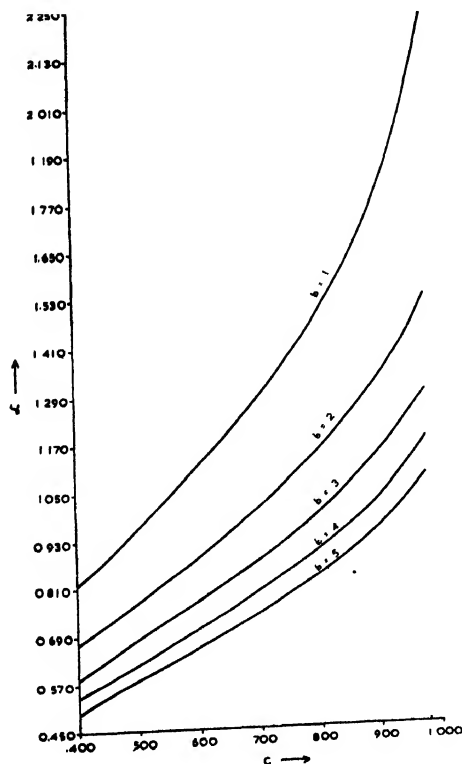


Fig. 1. Variation of α with C when instrumental width is negligible.

TABLE I

Variation of α with C for $b = 1, 2, 3, 4$ and 5 when instrumental width is negligible.

b	x_{min}	$\phi(x_{min})$	$\phi(a=x_{min})$ $\frac{1}{b} \phi(x_{min})$	$a-x_{min}$	$\frac{a}{a-x_{min}}$ $=x_{min} +$	$\frac{I_{min}}{I_0}$	$\frac{I_{max}}{I_0}$	$C = \frac{I_{min}}{I_{max}}$	α
1	0.806	—	—	0.806	1.612	1.0427	1.0743	0.971	0.620
1	0.837	—	—	0.837	1.674	0.9932	1.0608	0.937	0.597
1	0.894	—	—	0.894	1.788	0.8986	1.0400	0.863	0.559
1	1.000	—	—	1.000	2.000	0.7358	1.0183	0.722	0.500
1	1.049	—	—	1.049	2.098	0.6658	1.0123	0.658	0.477
1	1.095	—	—	1.095	2.190	0.6024	1.0083	0.597	0.457
1	1.183	—	—	1.183	2.366	0.4932	1.00370	0.491	0.423
1	1.225	—	—	1.225	2.450	0.4462	1.00248	0.445	0.408
2	0.632	0.4239	0.2119	1.365	1.997	0.9817	1.0368	0.947	0.501
2	0.775	0.4252	0.2126	1.363	2.138	0.8602	1.0206	0.843	0.468
2	0.894	0.4018	0.2009	1.391	2.285	0.7395	1.0108	0.732	0.439
2	1.000	0.3679	0.1839	1.433	2.433	0.6250	1.0054	0.622	0.411
2	1.140	0.3106	0.1553	1.457	2.597	0.5125	1.0024	0.511	0.385
2	1.225	0.2733	0.1366	1.561	2.786	0.3974	1.0009	0.397	0.359
3	0.548	0.4057	0.1352	1.565	2.113	0.9996	1.0347	0.966	0.473
3	0.707	0.4289	0.1430	1.542	2.249	0.8841	1.0190	0.868	0.445
3	0.837	0.4155	0.1385	1.555	2.392	0.7633	1.0099	0.756	0.418
3	1.049	0.3492	0.1164	1.623	2.672	0.5491	1.0023	0.548	0.374
3	1.140	0.3106	0.1035	1.667	2.807	0.4586	1.0011	0.458	0.356
3	1.183	0.2917	0.0972	1.690	2.873	0.4184	1.0008	0.418	0.348
4	0.447	0.3661	0.0915	1.712	2.159	1.0323	1.0377	0.995	0.465
4	0.548	0.4057	0.1014	1.674	2.222	0.9840	1.0286	0.957	0.450
4	0.632	0.4239	0.1060	1.658	2.290	0.9257	1.0212	0.906	0.437
4	0.775	0.4252	0.1063	1.657	2.432	0.8046	1.0109	0.796	0.411
4	0.894	0.4018	0.1005	1.678	2.572	0.6877	1.0005	0.687	0.389
4	1.000	0.3679	0.0920	1.710	2.710	0.5836	1.0000	0.584	0.369
4	1.095	0.3298	0.0825	1.748	2.843	0.4888	1.0012	0.488	0.352
4	1.140	0.3106	0.0777	1.768	2.908	0.4471	1.0008	0.447	0.344
4	1.183	0.2917	0.0729	1.789	2.972	0.4098	1.0005	0.409	0.336
5	0.447	0.3661	0.0732	1.788	2.235	1.0227	1.0337	0.989	0.447
5	0.632	0.4239	0.0848	1.738	2.370	0.9144	1.0181	0.898	0.422
5	0.775	0.4252	0.0850	1.737	2.512	0.7929	1.0091	0.786	0.398
5	0.894	0.4018	0.0804	1.756	2.650	0.6792	1.0054	0.676	0.377
5	1.000	0.3679	0.0736	1.786	2.786	0.5727	1.0021	0.571	0.359
5	1.095	0.3298	0.0660	1.823	2.918	0.4820	1.0010	0.482	0.343
5	1.183	0.2917	0.0583	1.861	3.044	0.4038	1.0005	0.403	0.329

*Obtained by trial and error.

The variation of α with b for various values of C is given in Table II, which has been tabulated from figure 1.

TABLE II

Variation of α with b for various values of C when instrumental width is negligible.

$C \downarrow b \rightarrow$	1	2	3	4	5
0.4	0.393	0.359	0.345	0.335	0.328
0.5	0.425	0.383	0.364	0.354	0.346
0.6	0.458	0.406	0.384	0.372	0.363
0.7	0.492	0.430	0.405	0.391	0.381
0.8	0.529	0.456	0.428	0.412	0.401
Rayleigh's criterion					
0.9	0.576	0.484	0.454	0.435	0.423
0.98	0.624	0.515	0.478	0.457	0.444
Abbe's criterion					

Table II has been illustrated by figure 2.

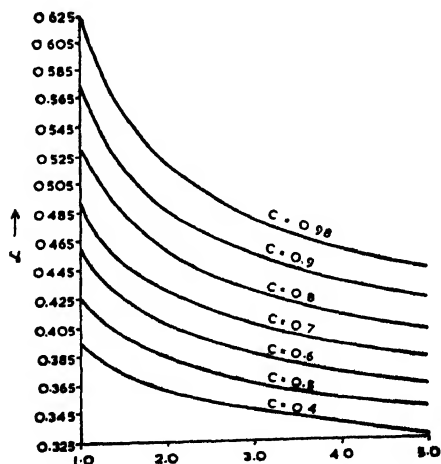


Fig. 2. Variation of α with b , when instrumental width is negligible.

FABRY PEROT ETALON

The intensity pattern of a spectral line in the order (n_0+n) , where n is a fraction and n_0 an integer is given for Fabry Perot etalon by

$$I' = \frac{I_0}{1+F \sin^2 \pi(n_0+n)} = \frac{I_0}{1+x^2}$$

where F is the coefficient of fineness and $x = \pi n F^{\frac{1}{2}}$.

The intensity distribution of another spectral line, separated by an order Δn , of an intensity b times the first is given by

$$I'' = \frac{bI_0}{1+F \sin^2 \pi(n_0+n-\Delta n)} = \frac{bI_0}{1+(x-a)^2}$$

where

$$a = \pi \Delta n F^{\frac{1}{2}}$$

The resultant intensity pattern is given by

$$\frac{I}{I_0} = \frac{1}{1+x^2} + \frac{b}{1+(x-a)^2} \quad \dots (7)$$

The values of x for which the maxima or minimum of the resultant intensity pattern occur are given by

$$-\frac{1}{2I_0} \frac{\alpha I}{\alpha x} = \frac{x}{(1+x^2)^2} - \frac{b(a-x)}{\{1+(a-x)^2\}^2} = 0$$

or

$$F(x) = bF(a-x) \quad \dots (8)$$

$$\text{where } F(x) = \frac{x}{(1+x^2)^2}$$

The weaker maximum will occur near $x = 0$ and can be obtained by solving Eqn. (8) by the method of successive approximations given by Sodha (1955).

The minimum and weaker maximum of the resultant intensity pattern are given by

$$\frac{I_{min}}{I_0} = \frac{1}{1+x_{min}^2} + \frac{b}{1+(a-x_{min})^2} \quad \dots (9)$$

and

$$\frac{I_{max}}{I_0} = \frac{1}{1+x_{max}^2} + \frac{b}{1+(a-x_{max})^2} \quad \dots (10)$$

For optimum resolution

$$C = \frac{I_{min}}{I_{max}}$$

The resolving power is given by

$$\frac{\lambda}{d\lambda} = \frac{n_0}{\Delta n} = \frac{\pi}{\alpha} \cdot n_0 F^{\frac{1}{2}} = \alpha n_0 F^{\frac{1}{2}} \quad \dots (11)$$

where

$$\alpha = \pi/a$$

The details of calculation are given in Table III, which gives the variation of α with C for $b = 1, 2, 3, 4$ and 5 . The table is illustrated by figure 3.

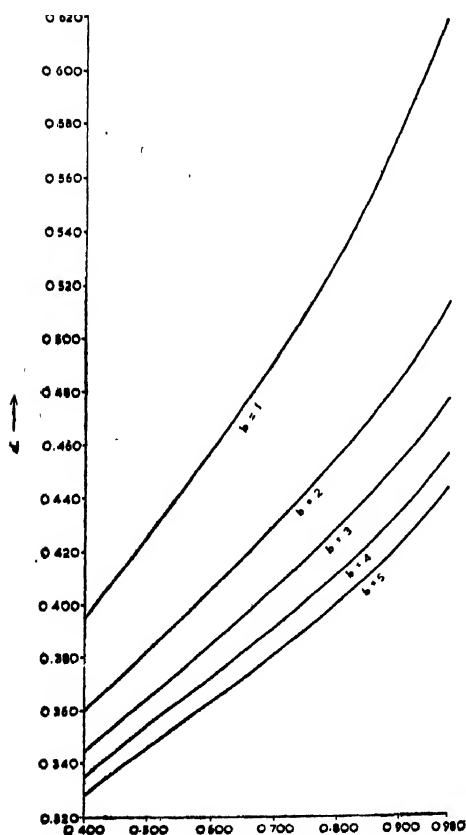


Fig. 3. Variation of α with C for F. P. etalon.

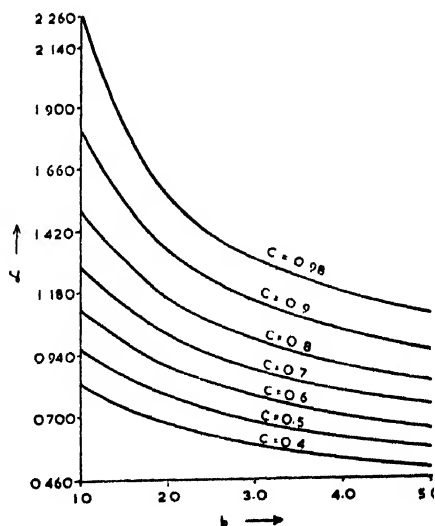


Fig. 4. Variation of α with b for F. P. etalon.

TABLE III

Variation of α with C for $b = 1, 2, 3, 4$ and 5 for F.P. etalon.

b	x_{min}	$F(x_{min})$	$\frac{F(a-x_{min})}{F(x_{min})}$	$a-x_{min}$	$\frac{a}{a-x_{min}} + x_{max}$	I_{min} I_0	I_{max} I_0	$C = \frac{I_{min}}{I_{max}}$	α	
1	0.70	—	—	0.70	1.4	0.229	1.3423	1.3719	0.978	2.247
1	0.80	—	—	0.80	1.6	0.155	1.2195	1.3004	0.934	1.964
1	0.90	—	—	0.90	1.8	0.117	1.1050	1.2474	0.886	1.746
1	1.00	—	—	1.00	2.0	0.090	1.0000	1.2071	0.828	1.571
1	1.15	—	—	1.15	2.3	0.062	0.8611	1.1626	0.741	1.366
1	1.25	—	—	1.25	2.5	0.050	0.7805	1.1403	0.684	1.257
1	1.40	—	—	1.40	2.8	0.037	0.6757	1.1144	0.606	1.122
1	1.60	—	—	1.60	3.2	0.0255	0.5618	1.0897	0.516	0.982
1	1.85	—	—	1.85	3.7	0.0174	0.4522	1.0684	0.423	0.849
1	1.90	—	—	1.90	3.8	0.016	0.4338	1.0650	0.407	0.827
2	0.65	0.321	0.1605	1.395	2.045	0.210	1.382	1.416	0.976	1.536
2	0.80	0.297	0.1485	1.460	2.260	0.145	1.247	1.344	0.928	1.390
2	1.00	0.250	0.1250	1.610	2.610	0.096	1.0564	1.271	0.831	1.204
2	1.20	0.201	0.1005	1.800	3.000	0.065	0.8816	1.2038	0.732	1.047
2	1.40	0.159	0.0795	2.010	3.410	0.044	0.7346	1.1602	0.633	0.921
2	1.60	0.126	0.0630	2.220	3.820	0.032	0.6183	1.1293	0.548	0.823
2	1.80	0.100	0.0500	2.440	4.240	0.024	0.5234	1.1059	0.473	0.741
2	2.00	0.080	0.0400	2.680	4.680	0.020	0.4445	1.0876	0.409	0.671
3	0.70	0.315	0.1050	1.750	2.460	0.200	1.4033	1.4527	0.966	1.277
3	0.80	0.297	0.0990	1.810	2.610	0.155	1.3114	1.4035	0.934	1.204
3	1.00	0.250	0.0833	1.960	2.960	0.100	1.1196	1.3169	0.850	1.061
3	1.20	0.201	0.0670	2.170	3.370	0.070	0.9354	1.2474	0.750	0.932
3	1.40	0.159	0.0530	2.390	3.790	0.050	0.7848	1.1977	0.655	0.829
3	1.60	0.126	0.0420	2.630	4.230	0.0365	0.6598	1.1601	0.569	0.743
3	1.80	0.100	0.0333	2.900	4.700	0.027	0.5546	1.1307	0.490	0.669
3	2.00	0.080	0.0266	3.140	5.140	0.0205	0.4753	1.1099	0.428	0.611
4	0.67	0.319	0.0797	2.000	2.670	0.220	1.4902	1.5253	0.977	1.177
4	0.70	0.315	0.0787	2.015	2.715	0.215	1.4616	1.5078	0.969	1.157
4	0.90	0.275	0.0687	2.140	3.040	0.140	1.2694	1.4059	0.903	1.033
4	1.20	0.201	0.0503	2.450	3.650	0.075	0.9813	1.2846	0.764	0.861
4	1.50	0.142	0.0355	2.810	4.310	0.046	0.7573	1.2066	0.628	0.729
4	1.80	0.100	0.0250	3.200	5.000	0.030	0.5917	1.1610	0.510	0.628
4	2.00	0.080	0.0200	3.500	5.500	0.023	0.5019	1.1285	0.445	0.571
4	2.20	0.064	0.0160	3.800	6.000	0.017	0.4303	1.1084	0.388	0.524
5	0.77	0.303	0.0607	2.260	3.030	0.185	1.4465	1.5167	0.954	1.037
5	0.90	0.275	0.0550	2.350	3.250	0.142	1.3191	1.4495	0.910	0.967
5	1.20	0.201	0.0402	2.670	3.870	0.081	1.0249	1.3191	0.777	0.812
5	1.50	0.142	0.0284	3.070	4.570	0.049	0.7873	1.2307	0.640	0.688
5	1.80	0.100	0.0200	3.500	5.300	0.032	0.6132	1.1729	0.523	0.593
5	2.10	0.072	0.0144	3.940	6.040	0.0215	0.4874	1.1338	0.430	0.520
5	2.30	0.058	0.0116	4.260	6.560	0.0170	0.4201	1.1138	0.377	0.479

*obtained by trial and error.

The variation of α with b for various values of C is given in Table IV, which has been tabulated from figure 3.

TABLE IV

Variation of α with b for various values of C , for F.P. etalon

$b \rightarrow$	1	2	3	4	5
0.4	0.822	0.666	0.565	0.534	0.492
0.5	0.954	0.768	0.678	0.618	0.576
0.6	1.110	0.882	0.774	0.702	0.654
0.7	1.284	1.005	0.876	0.798	0.738
0.8 Rayleigh's criterion	1.500	1.152	0.990	0.906	0.834
0.9	1.800	1.338	1.146	1.026	0.954
0.98 Abbe's criterion	2.250	1.548	1.308	1.194	1.092

Table IV is illustrated by figure 4.

ACKNOWLEDGMENTS

The authors are grateful to Dr. D. S. Kothari, Scientific Adviser to the Ministry of Defence, for permission to publish this paper.

REFERENCES

- Sparrow, 1916, *Astrophys. J.*, **44**, 76.
 Ditchburn, 1930, *Proc. Roy. Irish. Acad.*, **39**, 58.
 Tolansky, 1947, *High Resolution Spectroscopy* (Methuen & Co., London), 87.
 Sodha, 1952, *Sc. & Cult.*, **18**, 248.
 Sodha, 1955, *Ind. J. Phys.*, **29**, 461.

THEORY OF SPHERICAL SYMMETRY METHOD FOR MEASUREMENT OF THERMAL NEUTRON ABSORPTION

A. M. GHOSE AND N. K. GANGULY

BOSE INSTITUTE, CALCUTTA

(Received for publication May 30, 1956)

ABSTRACT. A new method has been developed for measuring thermal neutron absorption cross-section. The method is a variant of the beam attenuation technique. It is an absolute method requiring no standard neutron absorber for calibration. In this method the spherical symmetry of the experimental arrangement has been exploited to balance out the effect of scattering. Detailed examination has been made of the circumstances under which this balancing takes place. Effects of non-radial neutrons, scattering and absorption in the moderator, variation of detector efficiency for scattered neutrons, multiple scattering and absorption processes, thermalisation of scattered epithermal neutrons and non-attainment of thermal equilibrium in the moderator have been studied. Possible extension of this method to other energies of neutrons as well as to other types of radiations, have been discussed.

1. INTRODUCTION

Technological as well as theoretical importance of the interactions of thermal neutrons with matter has resulted in the accumulation of voluminous data on thermal neutron cross-sections. Nevertheless a study of the methods involved immediately reveals the fact that whereas the precise measurement of σ_t , the total interaction cross-section for thermal neutrons, is of comparatively little experimental difficulty, determination of absorption or scattering cross-sections separately, is rendered difficult by numerous sources of error. The principal methods which have been employed hitherto for the measurement of σ_a , the thermal neutron absorption cross-section, are the following ;

(a) The beam attenuation technique. This method is applicable only to very good absorbers in which the effect of scattering is negligible (Havens and Rainwater, 1946; Wu *et al* 1947 etc.)

- (b) **Activation method.** This method is applicable to absorbers in which neutron absorption leads to the formation of beta-active nuclei. This method is a relative one requiring a standard absorber to calibrate the neutron beam used for activation. (Houtermans, 1941; Maurer and Ramm, 1942; Seren *et al*, 1947 etc.)
- (c) **Methods based on local reduction of neutron density in a solution or mixture, due to the presence of the absorber in it.** This is also a relative method, requiring a standard absorber for calibration (Lapointe and Rasetti, 1940; Coltman and Goldhaber, 1946).
- (d) **Reactor methods, based on the diminution of power level in a nuclear reactor due to the presence of the absorber.** In both, 'the danger coefficient' and the 'oscillation method', the two principal methods which fall under this category, the depression of neutron flux is required to be calibrated by a standard absorber, which is usually boron. (Anderson *et al*, 1947; Weinburg and Schweinler, 1948; Harris *et al*, 1950; Pomerance and Hoover, 1948; Pomerance, 1951; Raievski and Yvon, 1950 etc.)
- (e) **Methods based on the free decay of neutron flux in a moderator solution containing the absorber.** This is an absolute method applicable only to absorbers obeying $1/v$ law of neutron absorption. So far this method has been applied to boron containing compounds only (Scott *et al*, 1954; Dardel and Sjostrand, 1954).

It will be observed that most of the above methods are relative ones and their accuracy thus depends entirely on the accuracy with which the thermal neutron absorption cross-section of standard boron absorber is known. The experimental value of this important nucleonic constant has changed from time to time with the improvement of the measuring technique and in Table I we have collected some of the values used for thermal neutron capture cross-section of boron to show this trend. We must note in this connection that the word 'thermal' in connection with neutrons refers to the Maxwellian distribution of neutron velocities corresponding to a temperature of 300°K. If the neutron velocity distribution is different, then corrections for this deviation must be included in discussing the cross-section value. We have corrected pre-war values quoted in Table I in this manner. Details of this correction will be discussed in a subsequent section.

Although the latest determination of the capture cross-section of boron has removed greatly the difficulty in fixing the capture value of standard absorber, it is obviously desirable to develop an absolute method for determining the thermal neutron absorption cross-section applicable to absorbers of not too large

cross-section. The present method was developed with the idea of meeting this requirement.

TABLE I

Thermal neutron capture cross-section of natural boron

Author.	Thermal neutron cross-section in barns (at the standard neutron velocity of 2.2×10^5 cm/sec., wherever possible)
Pre-war value quoted by Lapointe and Rasetti (1940)	Varies from 500-700 barns when uncorrected; average value of 600 barns were used by the authors; corresponding corrected value is 664 barns
Ross and Story (1949)	710 ± 21
Neutron cross-section Advisory Group AECU (1952)	751.3 (3990 barns for B^{10} isotope which is 18.8% abundant)
Argonne Lab. Standard Hammermesh <i>et al</i> (1953)	755 ± 5
Brookhaven Lab. Standard Carter <i>et al</i> (1953)	749 ± 4
Harwell standard. Egelstaff (1953)	782 ± 5
Scott <i>et al</i> (1954)	744 ± 20
Dardel and Sjostrand (1954)	764 ± 3

II METHOD

The method we have employed is a variant of the beam attenuation technique*. The fundamental relation between the transmission factor ψ and the parameters involved in the passage of a neutron beam through an absorber can always be expressed in the form

$$\psi = I/I_0 = \exp.[-K N \rho S/M], \quad \dots (1)$$

where I_0 and I are the neutron intensities recorded in the detector before and after the introduction of the absorber respectively, N is Avogadro's number, while ρ , M and S are the density, molecular weight and thickness of the absorber along

* (Reported to AEC India 1948; Bose Inst. Annual Report, 1949).

neutron path respectively. The interpretation of the constant K depends essentially on the geometry of the arrangement used. For a 'good' geometry transmission experiment in which all the scattered neutrons are excluded from the detector, the value of K is obviously equal to σ_t , the total cross-section, provided the thickness of the absorber is such as to render the effect of multiple scattering negligible. As the geometry of the experiment is made 'poorer' more of the scattered neutrons strike the detector and the value of K gets smaller than σ_t . In the extreme case when the absorber is a spherical shell of small thickness surrounding the source and there is no limiting diaphragm between the source and the detector, as many neutrons are scattered into the detector (for instance neutron marked ' α ' in figure 1) as are scattered out of the direct beam (neutron marked

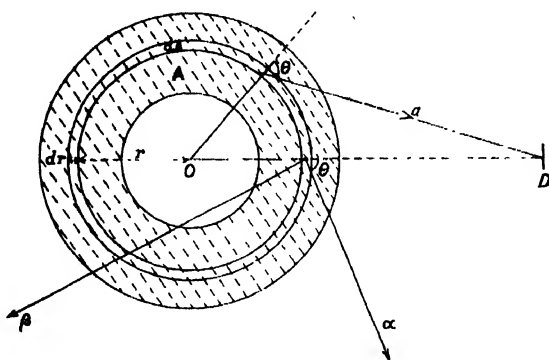


Fig. 1

α in figure 1); in this case the value of K is equal to σ_a , the absorption cross-section, provided certain simple conditions, which we are going to consider presently, are satisfied.

To analyse the situation in detail, let us consider the experimental arrangement schematically represented in figure 1. O is a source of thermal neutrons situated at the centre of a spherical absorber shell A , while D is a detector of thermal neutrons. Let the neutron intensities at distances r and $r + dr$ from the source be n and $n + dn$ respectively.

Obviously
$$-dn = dn_a + dn_s \quad \dots (1a)$$

where dn_a is the number of neutrons absorbed in the infinitesimal shell dA as shown in figure, while dn_s represents the drop in neutron intensity through scattering in dA . The expression for dn_a is $Nn\sigma_a\rho dS/M$, where dS is the average pathlength of neutrons through dA . Now, the neutron intensity n at r is composed of both primary as well as scattered neutrons; the path followed by the latter is not radial, in general, even if the primary beam happens to be radial. Hence

dS in the expression for dn_a is not, in general, equal to dr . However, if the source emits radial neutrons and if the absorber thickness is so small that the number of scattered neutrons is small enough to allow us to neglect the obliquity of their path in considering their contribution to n , we can write $dS = dr$ in the above expression for dn_a . Hence with these assumptions

$$dn_a = Nn \sigma_a \rho dr/M. \quad \dots (1b)$$

While considering the expression for dn_s we note that the neutrons which are scattered in the forward direction (i.e. angle of scattering is not greater than $\pi/2$), e.g. the neutron marked α in figure 1, are available for absorption by nuclei outside the elementary shell and hence they do not cause any drop in the neutron intensity for transmission through dA . Neutrons which are scattered by more than $\pi/2$, e.g. the neutron marked β in the figure, will cross dA at points such as C and will be available for absorption, provided we can neglect the drop in neutron intensity through absorption between the points of scattering and the points of re-entrance. As before, we have neglected the effect of obliquity of the path of scattered neutrons with respect to their unscattered path. Under these assumptions, we can therefore set dn_s to zero and hence (1a) becomes

$$\frac{dn}{n} = -\frac{N\sigma_a\rho}{M} dr,$$

leading to

$$n = n_0 \exp.[-\sigma_a N\rho S/M] \quad \dots (1c)$$

If the efficiency of the detector is independent of the direction of incidence of the neutron actuating it, so that scattered neutrons are detected with the same efficiency as the unscattered ones, the measured transmission will be equal to n/n_0 and hence we will get finally

$$= \frac{I}{I_0} = \frac{n}{n_0} = \exp.[-\sigma_a N\rho S/M] \quad \dots (2)$$

which is the same as Eqn. (1) with K replaced by σ_a .

Collecting the assumptions made in deriving the above formula, we note that the following conditions must hold good, if the effect of scattering is to be balanced out by spherical geometry of the apparatus.

(1) The neutron flux is radial so that S in equation (2) is the radial thickness of the absorber.

(2) The thickness of the absorber is so small that the effect of the obliquity of the path of scattered neutrons compared to that of the unscattered ones is

negligible; we note that this condition is less stringent than that of neglecting multiple processes altogether.

(3) There is no absorber or scatterer between the source and the absorber whose cross-section is under investigation.

(4) Efficiency of the detector is independent of the angle of incidence of the neutron striking it.

(5) We have also tacitly assumed in the above that the absorber does not generate fresh thermal neutrons through slowing down by scattering of epithermal neutrons.

Deviations from the above assumptions occur in practice and in the subsequent sections we will examine them in detail.

III. NON-RADIAL FLUX OF NEUTRONS

To produce a spherically symmetrical thermal neutron beam in the laboratory using natural sources, the obvious and straight forward way is to surround a Ra-Be source with a spherical moderator of sufficient thickness to thermalise the fast neutrons issuing out of the source. It is well-known, however, that the neutrons emerging from the moderator surface are not radial and therefore the assumption (1) stated in the previous section is violated. In calculating the modified transmission factor, we will have to take into account the variation of the neutron path length S with its inclination with the radius, together with the angular distribution of the neutrons emerging from the moderator. A reference to figure 2 at once shows that the expression for S is given by

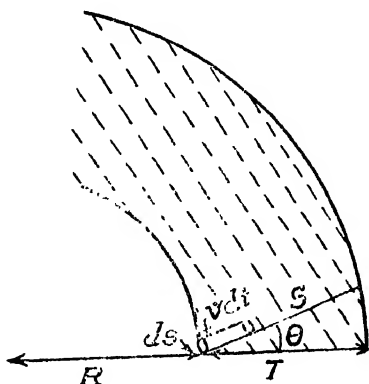


Fig. 2

$$S = S(\mu) = [R^2\mu^2 + T(T + 2R)]^{1/2} - \mu R, \quad \dots (3)$$

where $\mu = \cos \theta$, R is the inner radius of the absorber which is assumed to be placed directly on the moderator and T is the radial thickness of the absorber.

The problem of determining the angular distribution of neutrons at the moderator surface is more complicated. If the dimensions of the moderator surface is large compared to the mean free path for scattering of thermal neutrons in it, we can apply the results which have been derived for semi-infinite plane moderators. Using certain simple assumptions Fermi deduced a simple angular distribution law for the neutron intensity (Fermi, 1936; Bethe, 1937). If we normalise to unit neutron density, the density distribution function is given by

$$\phi(\mu) = (1 + \sqrt{3}\mu)/(1 + \sqrt{3}/2), \quad \dots (4)$$

where $\phi(\mu)d\mu$ is the neutron density between directions defined by μ and $\mu + d\mu$. The problem of neutron distribution from the surface of a semi-infinite moderator, which neither absorbs nor multiplies the neutrons, is completely analogous to the Milne problem in the astrophysics. The problem has been solved by Weiner and Hopf (Weiner and Hopf, 1931; Hopf, 1934). A modified derivation which is suitable for numerical calculations has been given by Plackzek and Seidel (Plackzek and Seidel, 1947; Plackzek, 1947). The new distribution function is given by

$$\phi(\mu) = \frac{1}{2(1+\mu)^{1/2}} \exp. \left[\frac{1}{\pi} \int_0^{\pi/2} x \frac{\tan^{-1}(\mu \tan x)}{1 - x \cot x} dx \right] \quad (5)$$

Tables of numerical values of $\phi(\mu)$ have also been given by Plackzek, which shows that Fermi's function is accurate within a fraction of one per cent. More exact but complicated solutions of the problem at hand has been derived, but the error caused by using (5) in our calculations being of the order of a tenth of a per cent, we have refrained from using them. Experimentally the distribution function has been verified by Hoffman and Livingston and more recently by Jonker and Blok (Hoffman and Livingston, 1938; Jonker and Blok, 1949).

To find out the numerical distribution function from the density distribution function, let us consider an elementary area dS of the moderator surface (figure 2). For simplicity let us assume that all neutrons travel with the same velocity v . Neutrons which are emitted at an angle θ in an interval of time dt will be contained in a cylinder with a base dS and slant height $v dt$. Hence the number of neutrons within the angles defined by μ and $\mu + d\mu$ is $\phi(\mu) \cdot \mu \cdot v dt \cdot d\mu ds$, showing that the numerical distribution function is proportional to $\mu\phi(\mu)$.

Hence the expression (2) for transmission is modified to

$$\psi = \int_0^1 \mu\phi(\mu) \exp. \left[-S(\mu)N\rho\sigma_a/M \right] d\mu / \int_0^1 \mu\phi(\mu) d\mu \quad \dots (6)$$

The above expression cannot be directly integrated and solved for σ and one has to take recourse to geometrical or algebraic methods. Using the geometrical constants of the apparatus used, one can tabulate corresponding values of ψ and $f = N\rho\sigma_a/M$. From this set of values either a graph of ψ vs f may be drawn

to get f and hence σ_a from any measured value of ψ , or the usual interpolation formula may be applied for the same purpose. Alternatively, the universal transmission curves derived in the following paragraphs may be used.

Let us express all distances in terms of λ , the absorption mean free path of thermal neutrons in the absorber, where

$$\lambda = \frac{1}{f} = \frac{M}{N\rho\sigma_a} \quad (7)$$

The equation (3) now becomes

$$s(\mu) = \frac{S(\mu)}{\lambda} = [\mu^2 a^2 + t(t+2a)]^{\frac{1}{2}} - a\mu$$

where

$$a = R/\lambda \quad \text{and} \quad t = T/\lambda. \quad \text{Therefore,}$$

$$s(\mu) = t[\mu^2 r^2 + (1+2r)]^{\frac{1}{2}} - r\mu \quad (8)$$

where $r = a/t$ is the ratio of inner radius of the absorber shell to the thickness of the absorber used and $\alpha(r, \mu)$ is the function

$$\alpha(r, \mu) = [\mu^2 r^2 + (1+2r)]^{\frac{1}{2}} - r\mu \quad \dots \quad (9)$$

The function $\alpha(r, \mu)$ is given for various values of r and μ in Table II and figure. 3.

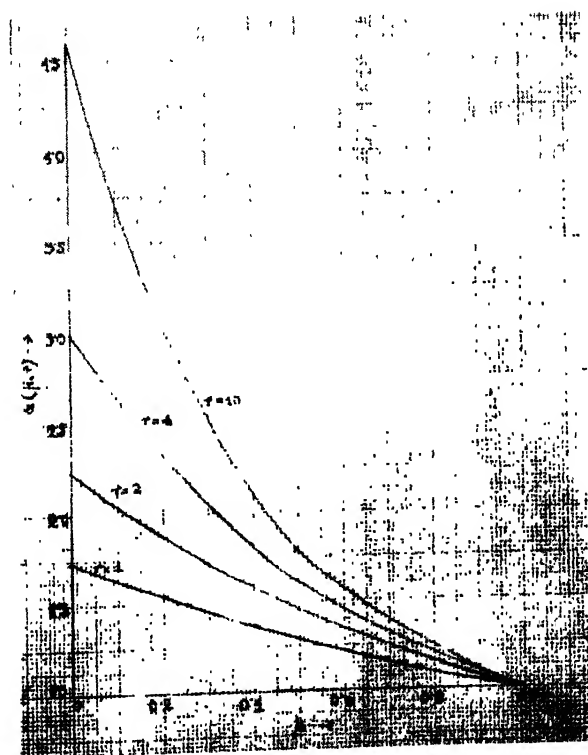


Fig. 3 $\alpha(r, \mu)$ as function of r and μ

TABLE II

Function $\alpha(r, \mu)$ for various values of r and μ

$\mu \backslash r$	1	2	3	4	5	6	7	8	9	10
0	1.7320	2.2361	2.6457	3.0000	3.3166	3.6056	3.8730	4.1231	4.3589	4.5826
0.1	1.6349	2.0450	2.3627	2.6265	2.8541	3.0551	3.2357	3.4000	3.5508	3.6904
0.2	1.5436	1.8716	2.1129	2.3048	2.4641	2.6000	2.7182	2.8227	2.9159	3.0000
0.3	1.4578	1.7152	1.8946	2.0311	2.1401	2.2299	2.3057	2.3707	2.4273	2.4772
0.4	1.3776	1.5749	1.7052	1.8000	1.8730	1.9313	1.9791	2.0192	2.0533	2.0828
0.5	1.3028	1.4495	1.5414	1.6056	1.6533	1.6904	1.7202	1.7446	1.7650	1.7823
0.6	1.2330	1.3377	1.4000	1.4419	1.4721	1.4951	1.5131	1.5277	1.5397	1.5498
0.7	1.1682	1.2382	1.2779	1.3036	1.3219	1.3353	1.3458	1.3541	1.3583	1.3666
0.8	1.1079	1.1495	1.1721	1.1863	1.1962	1.2033	1.2088	1.2131	1.2166	1.2195
0.9	1.0519	1.0705	1.0802	1.0861	1.0902	1.0981	1.0953	1.0970	1.0984	1.0995
1.0	1.0000	1.0000	1.0000	1.0000	1.0000	1.0000	1.0000	1.0000	1.0000	1.0000

The expression (6) for transmission is now modified to

$$\begin{aligned}
 \psi &= \int_0^1 \mu \phi(\mu) \exp. [-s(\mu)] d\mu \bigg/ \int_0^1 \mu \phi(\mu) d\mu \\
 &= \int_0^1 \mu \phi(\mu) \exp. [-t \cdot \alpha(r, \mu)] d\mu \bigg/ \int_0^1 \mu \phi(\mu) d\mu \quad \dots \quad (10)
 \end{aligned}$$

This is a function of t and r . This functional relation is shown in Table III and figure. 4, the latter being the universal transmission curves applicable to different geometrical dimensions of the apparatus used. These curves may be utilised as follows: From the dimensions of the apparatus we first determine the ratio $r = R/T$. Figure 4 is then used to determine the set of corresponding values of ψ and t , with the help of which the transmission curve (ψ vs. t) pertaining to the apparatus is drawn. Alternatively Table III may be used for the same purpose employing usual algebraic methods. In either case, the value of t corresponding to any experimentally obtained value of ψ is determined. From the value

of t thus obtained and the value of T is cms. measured directly, the value of σ_a is calculated by using the relation

$$\sigma_a = \frac{M}{N\rho\lambda} = \frac{Mt}{N\rho T} \quad \dots (11)$$

In Tables II and III and figures 3 and 4 we have covered the range $r = 1$ to 10 and $t = 0$ to 1.0; we can extend them to include values other than those considered here, in the manner indicated in the above paragraphs.

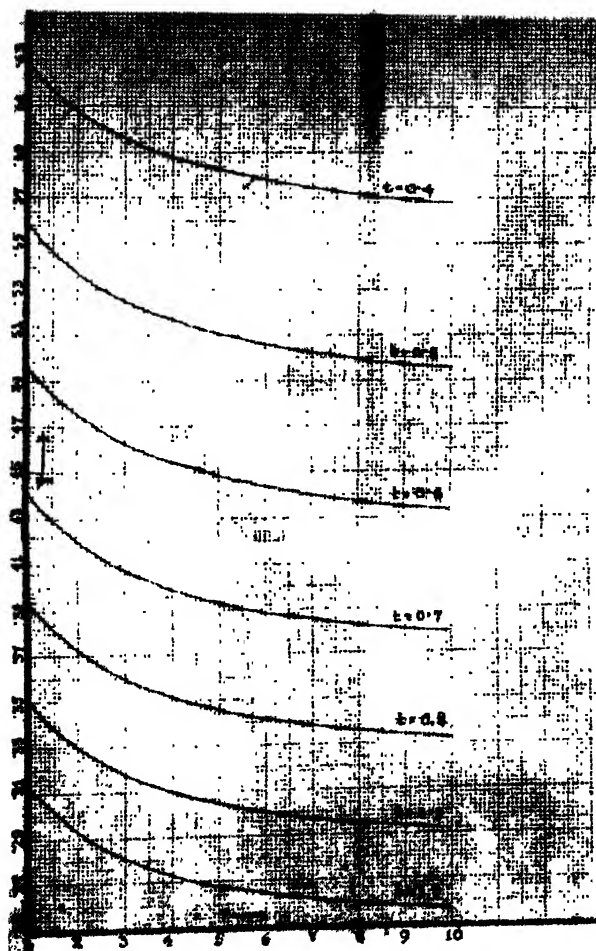


Fig. 4(a). $\psi(r, t)$ as function of r and t

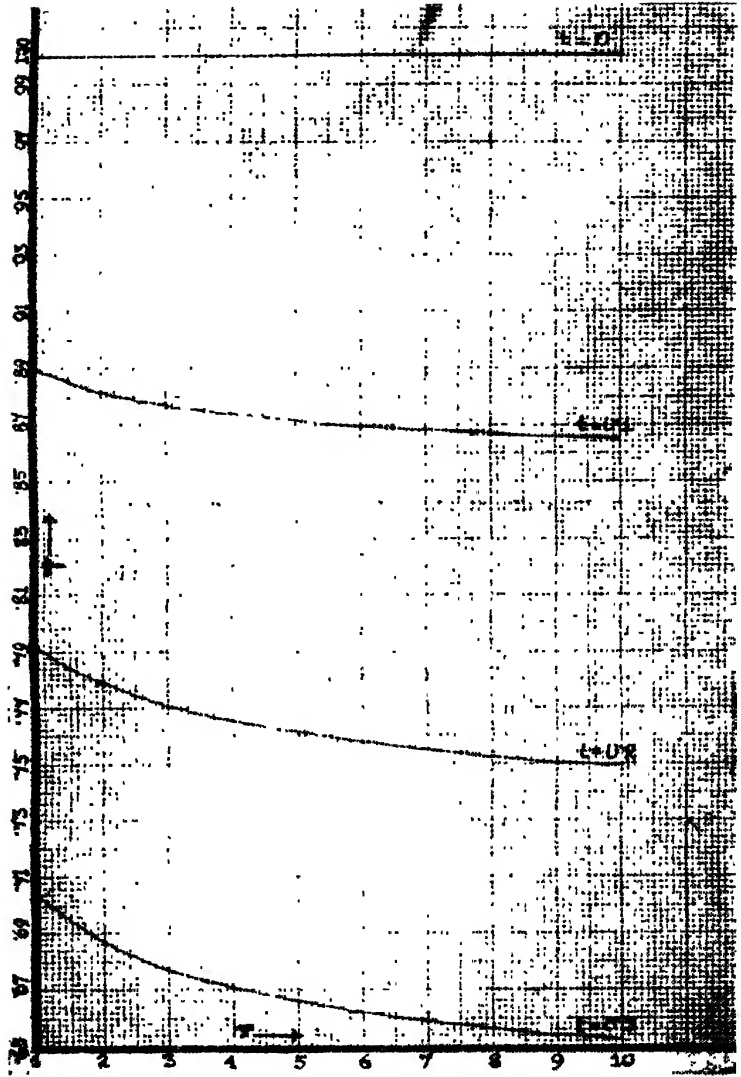


Fig. 4(b)

TABLE III
Transmission function $\psi(r, t)$ for various values of r and t

$t \backslash r$	1.	2	3	4	5	6	7	8	9	10
0.0	1.0000	1.0000	1.0000	1.0000	1.0000	1.0000	1.0000	1.0000	1.0000	1.0000
0.1	0.8891	0.8814	0.8777	0.8746	0.8721	0.8702	0.8687	0.8674	0.8663	0.8653
0.2	0.7914	0.7787	0.7710	0.7657	0.7616	0.7585	0.7560	0.7539	0.7522	0.7506
0.3	0.7040	0.6877	0.6778	0.6710	0.6660	0.6622	0.6590	0.6564	0.6544	0.6525
0.4	0.6266	0.6076	0.5963	0.5887	0.5831	0.5788	0.5753	0.5725	0.5703	0.5682
0.5	0.5578	0.5371	0.5250	0.5169	0.5111	0.5066	0.5030	0.5001	0.4978	0.4958
0.6	0.4966	0.4750	0.4625	0.4543	0.4484	0.4439	0.4404	0.4371	0.4353	0.4332
0.7	0.4422	0.4202	0.4078	0.3996	0.3938	0.3894	0.3860	0.3833	0.3811	0.3792
0.8	0.3939	0.3720	0.3597	0.3518	0.3462	0.3420	0.3387	0.3361	0.3341	0.3322
0.9	0.3509	0.3294	0.3175	0.3099	0.3046	0.3006	0.2976	0.2951	0.2932	0.2915
1.0	0.3127	0.2918	0.2804	0.2732	0.2682	0.2645	0.2617	0.2594	0.2577	0.2561

The error in the above table is within 0.2%, which is enough for the purpose at hand. For the sake of comparison we have given in Table IV, the values of ψ for radial distribution of neutrons. They are obviously equal to $\psi(0, t)$ in our previous notation.

TABLE IV
Transmission ψ , in absence of angular distribution of neutrons

	0.0	0.1	0.2	0.3	0.4	0.5	0.6	0.7	0.8	0.9	1.0
ψ	1.0000	0.9048	0.8187	0.7408	0.6703	0.6065	0.5488	0.4966	0.4493	0.4066	0.3679

IV. MULTIPLE PROCESSES

When the absorber thickness reaches a value not small compared to the scattering mean free path λ_s of the neutrons, the error caused by the absorption of scattered neutrons cannot be neglected. Major contribution to this error comes from singly scattered neutrons; the effect of multiple scattered neutrons will be felt only when the absorber thickness becomes larger than λ_s . In this discussion we will confine our attention to first order corrections alone, as this is sufficient to cover most of the cases which will occur in practice. Referring to sec. II condition (2) for the validity of the transmission equation, we find that

multiple processes affect our result through the alternation in the path-length of scattered neutrons from the path they would have followed in absence of scattering. Since on an average the length of the scattered path is greater than the corresponding undeviated path, more of the neutrons will be absorbed, as a result of which the apparent value of the absorption cross-section σ'_a will be greater than its true value. A rough estimate of the error caused may be obtained in the following manner. To find the order of increase in the neutron path due to scattering we note that if we pair off the neutrons scattered in the opposite directions, the total change in the path length remains of the same order as we shift the point of scattering from the inner to the outer surface of the absorber. At thickness $T/2$ of the absorber, the neutron pair scattered at angles 0° and 180° suffer a total increment of path length by T . Hence as a rough estimate we can suppose that the path-length increase through scattering is $T/2$ per neutron. Let ψ' and ψ be transmission in presence and in absence of scattering respectively. Hence the number of primary neutrons absorbed is $(1-\psi)$.

Number of primary neutrons scattered is then obviously $\frac{\sigma_s}{\sigma_a}(1-\psi)$ where σ_s is the scattering cross-section of the absorber. Of these scattered neutrons nearly $\frac{1}{2}(1-\psi)$ fraction will be absorbed due to increase in path length alone. Hence neglecting second and higher order scattering

$$1-\psi' = 1-\psi + \frac{1}{2} \frac{\sigma_s}{\sigma_a} (1-\psi)^2$$

showing that the fractional error p in estimating absorption is of the order of

$$p = \frac{1}{2} \frac{\sigma_s}{\sigma_a} (1-\psi) \simeq \frac{1}{2} \frac{\sigma_s}{\sigma_a} (1-\psi')$$

If the value of $\frac{\sigma_s}{\sigma_a}$ is approximately known, then the above relation may be used to estimate the order of error involved.

A semi-empirical approach to the problem may be made as follows. The increase in absorption due to scattering is a function of absorber thickness T . This increased absorption may be imagined as due to a virtual source at the centre, the strength of the virtual source being a monotonically increasing function of T ; we can write this source-strength as $n_0 f(T)$, as it is proportional to the real source-strength n_0 for obvious reasons. Hence the measured transmission is related to the corrected transmission by an equation of the form

$$n_0(1-\gamma') = n_0[1+f(T)](1-\psi')$$

or,

$$\psi' = \psi + f(T)\psi - f(T) \quad \dots \quad (13)$$

Since $\psi \leq 1$, ψ' is always greater than ψ , $f(T)$ being essentially positive. Now the expression for ψ when all neutrons are radial is

$$\psi = \exp. [-T\sigma_a N\rho/M] \quad \dots (14a)$$

When the neutrons follow an angular distribution law, we assume that when T is varied keeping the moderator radius constant we can express the above equation in the form

$$\psi = \exp. [-\beta(T)\sigma_a N\rho/M] \quad \dots (14b)$$

Similarly expressing ψ' in the form

$$\psi' = \exp. [-\beta(T)\sigma'_a N\rho/M] \quad \dots (14c)$$

where σ'_a is the apparent absorption cross-section measured without heed to the scattering. Comparing (14a), (14b) and (14c) and remembering that by Plackzek and Seidel distribution law most of the neutrons are emitted from the moderator surface making small angles with the radius, it is evident that for not too large value of T , we can expand $\beta(T)$ in the form

$$\beta(T) = T(A_0 + B_0T + C_0T^2 + \dots). \quad (15a)$$

When the absorber thickness T is very small, elementary considerations show that the strength-function $f(T)$ is also very small showing that $f(T) \rightarrow 0$ as $T \rightarrow 0$. For moderate values of T we can therefore write

$$f(T) = T(A_1 + B_1T + C_1T^2 + \dots) \quad \dots (15b)$$

Now, on substituting (14b) and (14c) in (13) and taking \ln of both sides we have

$$\begin{aligned} \sigma'_a &= \sigma_a + \frac{M}{N\rho} \cdot \frac{1}{\beta(T)} \ln \left[1 + f(T) \left(1 - \frac{1}{\psi} \right) \right] \\ &= \sigma_a + \frac{M}{N\rho} \cdot \frac{1}{\beta(T)} \left[f(T) \left(1 - \frac{1}{\psi} \right) + \text{higher terms} \right] \end{aligned}$$

using (15a), (15b) and expansion of $\frac{1}{\psi} = \exp. \left[T \cdot \sigma_a \frac{N\rho}{M} \right]$, we have

$$\begin{aligned} \sigma'_a &= \sigma_a + \frac{M}{N\rho} \frac{(A_1 + B_1T + C_1T^2 + \dots)}{(A_0 + B_0T + C_0T^2 + \dots)} \left[T \cdot \frac{\sigma_a N\rho}{M} + \text{higher terms} \right] \\ &= \sigma_a (1 + AT + BT^2 + \dots) \quad \dots (16) \end{aligned}$$

When a series of measurements of σ'_a is available for several values of T ,

we can fit them into the above relation to find the true value of the absorption cross-section σ .

V. ABSORPTION AND SCATTERING IN MODERATOR

If the moderator used in slowing down the neutrons has an appreciable absorption cross-section, a fraction of the scattered neutrons which encounter the moderator in their scattered path will be absorbed. This effect should be extremely small in all normal moderators, for which σ_a is only a small fraction of σ_t . On the other hand, most of the neutrons incident on the moderator will suffer multiple scattering within it. We can, in fact, assume that these neutrons, irrespective of their previous history, will emerge out from the surface of the moderator obeying the angular distribution law discussed in Sec. II.

A crude estimate of the correction factor, similar to Eqn. (12) above, may be derived easily if T is small compared to R , so that most of the neutrons scattered by more than $\pm\pi/2$ will strike the moderator. We neglect the increase in path between the point of scattering in the absorber and the point of incidence on the moderator; we assume however that the average change in path length for neutrons scattered through angles less than $\pm\pi/2$ is of the order of $T/2$. With these assumptions we can easily show that the presence of the moderator modifies the Eqn. (12) to

$$p \simeq \frac{1}{2} \left\{ \frac{\sigma_s}{\sigma_a} \frac{1}{2} (1 - \psi') + \frac{\sigma_s}{\sigma_a} (1 - \psi') \right\} = \frac{3}{4} \frac{\sigma_s}{\sigma_a} (1 - \psi') \quad \dots (17)$$

Like Eqn. (12), the above equation is one useful only for indicating order of the error involved and no other significance should be attached to it.

The nett effect of the presence of the moderator will be an increase in the neutron absorption, the increase being proportional to the number of primary neutrons scattered by the absorber. As discussed in the previous section, we can associate this absorption to imaginary sources at the centre and hence the form of the empirical correction formula as given by Eqn. (16) retains its validity and may be applied to derive the true value of σ_a .

VI. DETECTOR EFFICIENCY FOR SCATTERED NEUTRONS

Efficiency of a detector depends, in general, on the length of the path of the radiation through the active volume of the detector. Since the scattered neutrons follow a path different from the unscattered ones, efficiency and hence the number of neutrons recorded will vary with the magnitude of scattering by the absorber. The calculation of the relative efficiency of a detector depends, in general, on the type of the detector, the mode of its use as well as on its shape and size. In this discussion we will discuss a foil type neutron detector, the beta-

activity induced on the exposed surface being taken as a measure of the neutron flux. We will also suppose that it is a circular disc of diameter d , with its axis passing through the centre of the absorber and moderator spheres. When a flux of neutrons is incident on the foil at an angle θ to the normal, the number of active nuclei produced between depths x and $x+dx$ is proportional to $dx \sec \theta \exp. (-\mu x \sec \theta)$, where μ is the absorption coefficient per cm. of the material of the detector for thermal neutrons. When the foil is presented for counting the activity produced, the recorded intensity will be approximately given by

$$\int \exp. (-\mu x \sec \theta) \sec \theta \exp. (-\mu' x) dx,$$

where μ' is the "absorption coefficient" for the beta rays emitted by the foil. In all practical cases $\mu' \gg \mu$. Hence the recorded activity and hence the efficiency of the detector is proportional to $\sec \theta$. The maximum value of θ (θ_m say) when the centre of the spheres is at a distance D is obtained by solving the equation (figure 5)

$$d = 2[D \tan \theta_m - (R+T) \cos \theta_m] \quad (18)$$

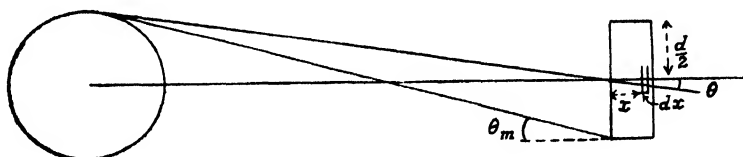


FIG. 5

We note that of the σ_s/σ_a ($1-\psi$) scattered neutrons, about half will be rescattered by the moderator in a manner similar to the primary neutrons. Hence they do not cause any change in the efficiency of the detector. The remaining half will be scattered through a mean angle of the order of $\frac{1}{2}\theta_m$. Hence the measured transmission will be

$$\psi' = \psi + \frac{1}{2} \frac{\sigma_s}{\sigma_a} \left(\sec \frac{\theta_m}{2} \right) - 1 \quad (1-\psi)$$

showing that the fractional error in estimating the absorption is of the order of

$$p' = -\frac{1}{2} \frac{\sigma_s}{\sigma_a} \frac{1-\psi}{\psi} \left(\sec \frac{\theta_m}{2} - 1 \right) \quad \dots \quad (19)$$

due to alteration in efficiency of the detector.

VII. SCATTERING OF EPITHERMAL NEUTRONS

A fast neutron source surrounded by a moderator of finite dimensions always emits epithermal neutrons in addition to the flux of thermal neutrons. In presence of the absorber, some of these neutrons will be thermalised by scattering, especially when these scattered neutrons encounter the moderator in their path. These neutrons can not be distinguished from the primary thermal neutrons and thus the detector will register an apparent increase in the value of ψ which will lower the measured absorption cross-section. The number of thermalised epithermal neutrons is a monotonic function of the absorber thickness T and tends to zero as T is made vanishingly small. Hence we can apply the semi-empirical equation (16) to correct for this effect as well.

VIII. ERROR DUE TO NON-ATTAINMENT OF THERMAL EQUILIBRIUM

In the moderating material surrounding the source, neutrons lose their energy through elastic and inelastic collisions till their energy is comparable to the energy of thermal agitation of the atoms of the slowing-down medium. We have assumed hitherto that the velocity of the neutrons eventually attains a Maxwellian distribution characteristic of the temperature T_0 of the moderator. This is, however, strictly true only in a moderator of infinite dimensions which scatter the neutrons but do not absorb them. The actual velocity distribution from a finite, moderator, will therefore, show deviation from the Maxwellian distribution. Experiments have shown that we can approximate the distribution closely by a Maxwellian distribution corresponding to a temperature T' , different from T_0 , over which is superimposed a pronounced tail of relatively fast neutrons extending far into the epithermal region. The contribution of epithermal neutrons can be experimentally determined by the usual cadmium difference technique. On the other hand, the estimation of the temperature T' characterising the velocity distribution cannot be determined in a simple manner. When strong sources are available one can employ the velocity selector techniques to determine the actual distribution. When the moderator is in room-temperature experiments of Manley *et al* (1946) and of Rainwater and Havens (1946) may be interpreted as showing that when a paraffin moderator of linear dimensions about 10 ± 5 cms. is used T' is given by $390^\circ \pm 10^\circ \text{K}$, if D—D neutrons are used. For Ra-Be source, the dimensions of the moderator are to be increased to take into account the higher initial energy of neutrons. Hence for spheres of paraffin of diameters lying between 15 and 25 cms., we expect the above value of T' to remain valid.

It is usual to define thermal neutrons as neutrons with Maxwellian velocity distribution corresponding to a temperature of 300°K . For low absorbers, therefore, the cross-section $(\sigma_a)T'$, measured for neutrons at temperature T' has to

corrected by the following relation to get σ_a , the true thermal neutron absorption cross-section.

$$\sigma_a = (\sigma_a)T' \left(\frac{T''}{T'} \right)^{\frac{1}{2}} \quad \dots \quad (20)$$

Inserting the value of T' stated above for paraffin spheres we have

$$\sigma_a = (1.1402 \pm 0.0145) (\sigma_a)T' \quad \dots \quad (20a)$$

We have used this correction factor in Table I.

For absorbers not obeying $1/v$ law partial compensation for non-attainment of thermal equilibrium may be obtained by lowering the moderator temperature. When strong sources are available a better plan is to use large amount of graphite moderator, which has a low absorption cross-section, as is done in atomic reactors for getting thermal neutron flux.

IX. SMALL DEVIATIONS FROM SPHERICAL SYMMETRY

If the absorber and the moderator spheres are not concentric, then the absorber thickness on one side will be greater than the opposite side. If, however, the centres are separated by a distance small compared to the absorber thickness, and detector is made to record the neutron intensity at different directions with respect to the spheres keeping its mean distance from the centres constant, then the increase in the number of scattered neutrons from one side will almost compensate the decrease in their number from the other side. The compensation in the value of the mean recorded intensity will not be exact but it will obviously be of second order of smallness. The degree of attainment of spherical symmetry can be obtained by noting the relation between the intensity I and the distance D between the detector and the mean centre of the source and the absorber. If the geometry of the arrangement is exactly spherical, for a point detector ID^2 should be constant. For a detector of finite size I/Ω should be constant, where Ω is the solid angle subtended by the detector at the centre of the spheres.

Small local variations of the density of the absorber, and other small deviations from the spherical symmetry are likewise smoothed out and their effects rendered insignificant, if measurements are taken in different directions as indicated above.

CONCLUSION

The above considerations show that the spherical symmetry method is realisable practically and it rests on firm theoretical foundations. Experimental details of the arrangement developed in our laboratory will be communicated in a separate paper.

The method can obviously be extended to other neutron energies provided a spherically symmetric source of such neutrons as well as a detector which responds uniformly to neutrons of different energies are available. The method can also be extended to study the absorption processes of other radiations, isolated from their scattering effects provided suitable sources and detectors are available. An important extension of the process is possible in the field of gamma rays, where account must be taken for the degeneracy and hence the variation of the detector efficiency through Compton effect. Experiment along this line is under way in the laboratory.

The authors wish to claim equal share in the publication of this work.

ACKNOWLEDGMENT

Thanks are due to Dr. D. M. Bose, Ph.D., F.N.I., Director, Bose Institute for his kind interest throughout the progress of this work.

REFERENCES

- Anderson, Fermi, Watterberg, Weil and Zinn., 1947, *Phys. Rev.*, **72**, 16.
 Bethe, 1937, *Rev. Mod. Phys.*, **9**, 132.
 Carter, Palevsky, Meyers and Hughes, 1953, *Phys. Rev.*, **92** 716.
 Coltman and Goldhaber, 1946, *Phys. Rev.*, **69**, 411.
 Dardel and Sjostrand, 1954, *Phys. Rev.*, **96**, 1566.
 Egelstaff AERE Harwell Report, 1953, N/M 62.
 Fermi, 1936, *Ricerca Scient.*, **7**, 13.
 Hammermesh, Ringo and Wexler, 1953, *Phys. Rev.*, **90**, 603.
 Harris, Muelhaue, Rasmussen, Schroeder and Thomas, 1950, *Phys. Rev.*, **80**, 342.
 Havens and Rainwater, 1946, *Phys. Rev.*, **70**, 136, 154.
 Hoffman and Livingston, 1938, *Phys. Rev.* **53**, 1021.
 Hopf, 1934, *Camb. Tract.* No. 31.
 Houtermans, 1941, *Z. Phys.*, **118**, 424.
 Jonker and Block, 1949, *Physica*, **15**, 1032.
 Lapointe and Rasetti, 1940, *Phys. Rev.*, **58**, 544.
 Manley, Hawroth and Leubke., 1946, *Phys. Rev.*, **69**, 405.
 Maurer and Ramm, 1942, *Z. Phys.*, **119**, 609.
 Neutron cross section Advisory Group, 1952, AECU 2040.
 Plackzek, 1947, *Phys. Rev.*, **72**, 556.
 Plackzek and Seidel, 1947, *Phys. Rev.*, **72**, 550.
 Pomerance, 1951, *Phys. Rev.*, **83**, 641.
 Pomerance and Hoover, 1948, *Phys. Rev.*, **73**, 1265.
 Raievski and Yvon, 1950, *Compt. Rend.*, **231**, 345.
 Rainwater and Havens, 1946, *Phys. Rev.* **70**, 136.
 Ross and Story, 1949, *Rep. Prog. Phys.*, **12**, 291.
 Scott, Thomson and Wright, 1954, *Phys. Rev.*, **95**, 582.
 Seren, Friedlander and Turkel, 1947, *Phys. Rev.*, **72**, 888.
 Weinberg and Schweinler, 1948, *Phys. Rev.*, **74**, 851.
 Weiner and Hopf, 1931, *Berl. Ber. Math. Phys. Klasse* 696.
 Wu, Rainwater and Havens, 1947, *Phys. Rev.*, **71**, 174.

RAMAN SPECTRA OF PYRIDINE AND ITS SOLUTIONS IN ETHYL ALCOHOL AT DIFFERENT TEMPERATURES*

G. S. KASTHA

OPTICS DEPARTMENT, INDIAN ASSOCIATION FOR THE CULTIVATION OF SCIENCE,
JADAVPUR, CALCUTTA-32

(Received for publication July 6, 1956)

Plate XII

ABSTRACT. The results obtained in the investigations on the Raman spectra of pure pyridine in the liquid and solid states and those for solutions in ethyl alcohol of strengths 38% and 56% in the liquid and frozen states have been discussed. In the Raman spectrum due to solid pyridine four low frequency lines in the neighbourhood of the Rayleigh line appear at 58, 82, 97 and 137 cm^{-1} . In the case of the solutions only a strong band at 95 cm^{-1} is observed. From considerations of the similarities between the low frequency spectra due to solid pyridine and solid benzene at -180°C , it has been concluded that these lines originate from the vibration in small groups of associated pyridine molecules, and in the case of the frozen solutions the band at 95 cm^{-1} is assigned to vibration in the complex molecules formed by the combination of pyridine molecules with alcohol molecules.

The changes observed in the spectra due to the single molecules with dissolution and solidification also support this view.

INTRODUCTION

The Raman spectra of frozen solutions of toluene in ethyl alcohol of strengths 81% and 35% and of 35% solution of benzene in ethyl alcohol and other aliphatic solvents were studied recently (Kastha, 1956) to find out the influence of environment on the nature of new Raman lines in the low frequency region exhibited by these two compounds in the solid state. In the case of the frozen 81% solution of toluene, a strong band at 95 cm^{-1} superposed on a continuous wing extending from the Rayleigh line to about 95 cm^{-1} was observed in place of the discrete lines yielded by the pure substance at -180°C . In case of the frozen 35% solution of toluene the band disappears but the continuous wing up to 95 cm^{-1} from the Rayleigh line persists. From these results it was concluded that these lines in the case of pure toluene in the solid state are due to groups of toluene molecules formed by virtual linkages among neighbouring molecules in the solid state. In the case of 81% solution the groups contain molecules of both the solute and the solvent and the band at 95 cm^{-1} is due to such groups. When the strength of the solution is diminished to 35%, these groups break up but new groups in which alcohol molecules surround the toluene molecules are formed and these produce the continuous wing.

In the Raman spectra of 35% frozen solution of benzene in ethyl alcohol at -180°C , the low frequency lines appear with undiminished intensity at the

*Communicated by Prof. S. C. Sirkar

same positions as in the case of pure benzene in the solid state. From this result and results obtained with other solutions of benzene frozen at -180°C , it was concluded that these lines are due to oscillation in small groups of benzene molecules which persist in solutions also.

It is known that benzene and pyridine have the same structure excepting that one of the C-H groups is replaced by a single nitrogen atom. When the Raman spectra due to both these compounds in the liquid states are compared, they are found to be different. In fact, the symmetry of benzene molecule is D_{6h} and that of pyridine is C_{2v} . However, the ring frequency 992 cm^{-1} appears in both the cases. Pyridine is slightly basic and is known to form complex molecules with many compounds containing an OH group in contrast to the complete indifference of neutral benzene towards the hydroxyl group.

Ichishima (1949) studied the Raman spectra of pure pyridine in the solid state at low temperature in order to account for the origin of the low frequency lines, observed in this case. But as the results were not accessible to us, it was thought worthwhile to reinvestigate the spectrum due to pure pyridine in the solid state and to compare with each other the low frequency lines due to both solid pyridine and benzene. The Raman spectrum of pyridine at -180°C has, therefore, been reinvestigated and it has been compared with the Raman spectra of the frozen solutions of pyridine in an aliphatic alcohol. These results have been discussed in the present paper.

EXPERIMENTAL

The arrangements for photographing the Raman spectrum of pure pyridine and that of solutions of pyridine in the solid state at -180°C were the same as those described in the previous paper (Kastha, 1956).

Chemically pure, water-free pyridine was repeatedly distilled under reduced pressure and was used in the present investigation as the solute, ethyl alcohol being used as a solvent. The solvent was of chemically pure quality and was repeatedly distilled under reduced pressure before use. Pure pyridine was sealed under vacuum in a cylindrical pyrex glass container. The Raman spectra due to the substance was photographed keeping the container always immersed in liquid oxygen during the exposure. In the case of the solution of pyridine in ethyl alcohol such solutions of strengths 38% and 56% were sealed in long containers of pyrex glass and were frozen by immersing the containers in liquid oxygen. The frozen masses appeared to be transparent and homogeneous. The Raman spectra due to these transparent masses were recorded in the same way as those of frozen solutions of toluene in ethyl-alcohol (Kastha, 1956).

A Fuess glass spectrograph having a dispersion of about 11 Å/mm in the region $\lambda 4047\text{ Å}$ and Ilford Zenith plates were used to photograph all the Raman spectra.

RESULTS AND DISCUSSION

The spectrograms due to pure pyridine in the solid state at -180°C and of solutions of pyridine in ethyl alcohol in the liquid and frozen states are reproduced in figures 1-5, Plate XII. The spectrogram due to pure alcohol in the solid state at -180°C is given in figure 6, Plate XII. Spectrograms showing the low frequency lines in solid pyridine and the band due to frozen solutions are shown enlarged in figures 7a, 7b and 7c, Plate XII. The Raman frequencies of pure pyridine in the liquid state and in the solid state at -180°C together with those for the solutions in the liquid and frozen states are given in Table I; those due to solid benzene at -180°C have also been included for comparison.

TABLE I
Solutions of pyridine in ethyl alcohol*

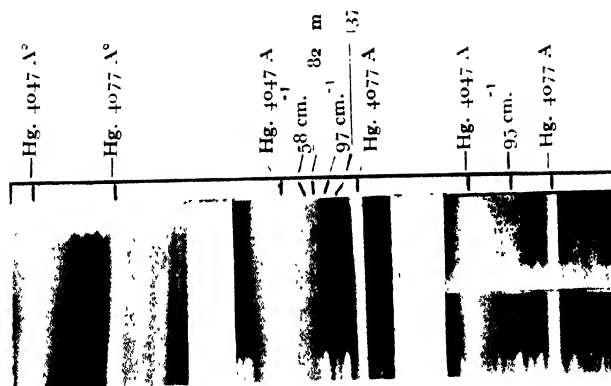
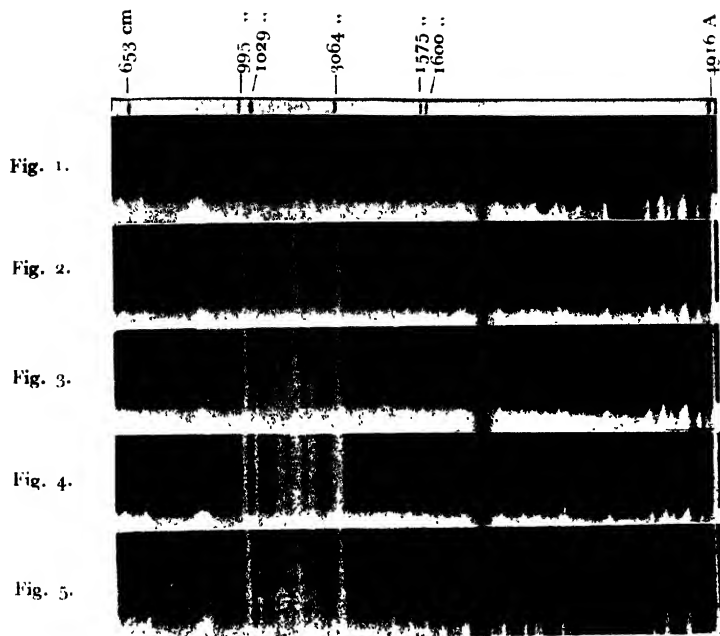
Liquid pyridine at 28°C $\Delta\nu$ in cm^{-1}	Solid pyridine at -180°C $\Delta\nu$ in cm^{-1}	38%		56%		Solid benzene at 180°C $\Delta\nu$ in cm^{-1} (Sirkar and Ray 1950).
		$\Delta\nu$ in cm^{-1}		$\Delta\nu$ in cm^{-1}		
		at 28°C	at -180°C	at 28°C	at -180°C	
Continuous wing extend- ing up to 100 cm^{-1}	58 (3)	Continuous wing extend- ing up to 90 cm^{-1}		Continuous wing extend- ing up to 100 cm^{-1}		47 (1)
	82 (3)					53 (2)
	97 (3)		95 (4b)		95 (4b)	78 (5)
	137 (1)					95 (1b)
603 (1)	603 (1)	603 (1)		603 (1)		134 (3)
656 (3)	656 (3)	656 (3)	656 (3)	656 (3)	656 (3)	603 (1)
995 (10)	995 (8)	994 (2)		994 (4)	995 (0)	989 (10)
		1000 (10)	1005 (10)	1000 (10)	1002 (10)	
1029 (10)	1034 (6)	1029 (6)	1034 (4)	1029 (6)	1034 (5)	1174 (4)
1219 (3)	1208 (1)	1219 (3)	1219 (3)	1219 (3)	1219 (3)	
	1224 (3)					
1482 (3)	1482 (2)	1482 (2)	1482 (2)	1482 (2)	1482 (2)	
1575 (3b)	1576 (3)	1575 (2)	1575 (2)	1575 (3)	1575 (2)	1581 (3)
	1600 (0)	1595 (2)	1595 (2)	1595 (2)	1595 (2)	1602 (2)
2919 (2)	2919 (2)					
2955 (1)						3042 (2)
	3031 (2b)					3046 (2)
3064 (10)	3064 (10)	3064 (10)	3064 (10)	3064 (10)	3064 (10)	3063 (5)
3150 (1)	3148 (1)					

*The Raman frequencies due to the solvent have been excluded.

In the Raman spectrum due to pure pyridine at 28°C a strong wing extending up to about 100 cm^{-1} accompanies the Rayleigh line. However, when the liquid is solidified and cooled to -180°C , the wing is replaced by four discrete lines at 58, 82, 97 and 137 cm^{-1} . The intensities of the first three lines are the same as that of the line 656 cm^{-1} while the line 137 cm^{-1} is weaker than this line. It can be seen from Table I that in the spectrum due to solid benzene at -180°C the low frequency lines appear at 47, 53, 78, 95 and 135 cm^{-1} . The similarity in the low frequency spectra due to these two compounds in the solid state at -180°C is not surprising, for they have almost the same molecular structures. It has been shown by Sirkar and Ray (1950) from a study of the temperature dependence of the intensities of the low frequency lines and recently by the present author (Kastha, 1956) from the study of the Raman spectra of frozen solutions of benzene, that these lines do not originate from the angular oscillations of benzene molecules pivoted in the lattice of benzene crystals but they may be due too scillations in very small associated groups of benzene molecules which persist even in a 18% solution. As the low frequency lines due to solid pyridine are almost at the same positions as in the case of benzene these lines also may have the same origin.

It can be seen from Table I that the lines 1029, 1219 and and 1575 cm^{-1} undergo changes and a new line at 3031 cm^{-1} appears with solidification of the liquid. The splitting up of the line 1219 cm^{-1} into two lines and the appearance of the new line at 3031 cm^{-1} may be due to the fact that the virtual bonds are formed between some of the neighbouring molecules through the hydrogen atoms and consequently the new lines slightly displaced from the original lines are formed. It may be pointed out in this connection that when regular bond is formed between the free electron of the nitrogen atom and the hydrogen atom of the OH group in alcohol, the 995 cm^{-1} line is accompanied by a new line (Hatem *et al*, 1949). So, when only a weaker virtual bond is formed no such change is expected, but the lines due to vibrations in which these atoms are involved are affected appreciably. The changes observed in the case of frozen solutions and discussed later also corroborate this view.

It can be seen in the spectrograms due to 38% and 56% solutions of pyridine in ethyl alcohol in the liquid state that the continuous wing extends upto 90 cm^{-1} to 100 cm^{-1} respectively, from the centre of the Rayleigh line. In the spectra due to the frozen solutions of the above mentioned strengths (figures 7b and 7c) this wing and discrete low frequency lines found in the spectra due to solid pyridine are absent and they are replaced by a moderately intense broad band at 95 cm^{-1} . On examining the spectrum due to solid ethyl alcohol at -180°C (figure 6) neither any band nor any continuous wing is observed in the neighbourhood of the Rayleigh line. Hence the band at 95 cm^{-1} observed in the spectra due to the solutions at -180°C cannot be due to vibration in the ethyl alcohol lattice. The appearance of such a band in the spectra due to frozen solutions of toluene in ethyl alcohol was observed previously (Kastha, 1956) and the



Raman spectra of pyridine

Fig. 1. Pure Solid at -180°C .Fig. 2. 38% Solution in ethyl alcohol at 28°C Fig. 3. " " " " -180°C Fig. 4. 56% " " " " 28°C Fig. 5. " " " " -180°C Fig. 6. Solid alcohol at -180°C .

Fig. 7 (a) Solid pyridine (Showing low frequency lines)

Fig. 7 (b) Frozen 38% soln. (Showing the band at 95 cm.⁻¹)

Fig. 7 (c) " 56% " (" " " " ")

band was assigned to vibration in toluene-alcohol complex. Therefore, it can similarly be concluded that the band at 95 cm^{-1} may originate from vibration in groups of complex molecules formed between pyridine and ethyl alcohol molecules. The disappearance of the other discrete lines is evidently due to the dissolution of the groups containing pyridine molecules alone in the solutions of pyridine in ethyl alcohol.

On examining the spectrograms due to 38% and 56% solutions of pyridine in ethyl alcohol at 28°C it is found that the line at 995 cm^{-1} due to pure pyridine becomes much weaker than the line at 1029 cm^{-1} and a strong new line at about 1000 cm^{-1} appears in both the cases. This was first observed by Hatem *et al* (1949). From a study of the Raman spectra of solutions of pyridine in ethyl alcohol in the liquid state at gradually diminishing strengths, they observed that the line at 992 cm^{-1} becomes fainter in comparison with the line 1028 cm^{-1} as the concentration of pyridine in the solution is decreased and finally vanishes when the ratio of pyridine to ethyl alcohol becomes 1 : 5. On the other hand, the line at 1002 cm^{-1} attains a maximum of intensity when the concentration of pyridine in ethyl alcohol is in the ratio 1 : 1. From these results they concluded that complex molecules between pyridine and ethyl alcohol molecules are formed probably through the nonbonding electrons of the nitrogen atom.

From a comparison of spectrograms due to frozen solution of strength 38% and 56% (figures 3 and 5) with those due to the solution at room temperature it is seen that the line at 995 cm^{-1} disappears and the new line at 1000 cm^{-1} observed in case of the solutions at 28°C shifts to 1005 cm^{-1} and 1002 cm^{-1} respectively when the solutions are frozen and cooled to -180°C . So, in the solution at 28°C some of the pyridine molecules are not associated with alcohol molecules, but in the solid state all of them are linked to the alcohol molecules. Thus solidification accelerates the formation of the bonds between the pyridine and alcohol molecules probably due to the fact that the molecules come closer together in the solid state. The line 1029 cm^{-1} due to the solution at 28°C also shifts to 1034 cm^{-1} when the solution is frozen and cooled to -180°C . This shows that the ring of any molecule is attached to that of a neighbouring molecule at other points in the ring so as to change this particular ring frequency. The line 1575 cm^{-1} due to the pure liquid splits up into two components at 1575 and 1595 cm^{-1} in case of the solutions but the intensities of the two lines become equal when the solutions are frozen. This may be due to the fact that this line corresponds to the mode e_{2g} in benzene molecule and that the two components of the degenerate mode which give rise to the line 1575 cm^{-1} in the benzene molecule separate out from each other when the complex is formed by pyridine molecule with alcohol molecules. In the case of the concentrated solution the line 1575 cm^{-1} due to the free pyridine molecules is superposed on the two lines due to the complex molecule and therefore, the line 1575 cm^{-1} is more intense in this case than the line 1595 cm^{-1} .

In case of the crystals of pure pyridine no such complex is formed, but only weak virtual bonds are formed between neighbouring molecules. So, such splitting of the 1575 cm^{-1} line does not take place in the case of pure pyridine but the faint line at 1600 cm^{-1} observed in this case may be due to a combination frequency $(603+995)\text{ cm}^{-1}$.

These conclusions are also supported by the results obtained by Banerjee (1956) who studied the ultraviolet absorption spectra of pure pyridine in the liquid and solid states. He found that the first of the two systems of bands corresponding to $n\rightarrow\pi^*$ and $\pi\rightarrow\pi^*$ transitions which have been observed in the absorption spectra due to pyridine vapour by previous workers is absent in the absorption spectra obtained in case of pyridine both in the liquid and solid states. The results have been explained by him on the assumption that in the liquid and solid states the pyridine molecules form virtual bonds through the nitrogen nonbonding electrons and hydrogen atoms of the neighbouring molecules.

Thus the results obtained from a study of the Raman spectra of pyridine in the liquid and solid states and also in the liquid and frozen solutions of ethyl alcohol furnish strong evidences to show that pyridine molecules form associated groups in the solid state which give rise to four lines in the low frequency region and complexes with alcohol molecules are formed in the frozen solutions which produce a single band at 95 cm^{-1} .

ACKNOWLEDGMENT

The author is indebted to Professor S. C. Sirkar, D.Sc., F.N.I. for his keen interest and helpful guidance throughout the progress of the work.

REFERENCES

- Banerjee, S. B., 1956, *Ind. J. Phys.*, **30**, .
Hatem, S., Valladas, Dubois, S. and Volkminger, H., 1949, *Compt. rend.*, **228**, 182-4.
Ichishima, I., 1949, Repts. Radiation chem. Research Inst., Tokyo University, No. 4, 9-10.
Kastha, G. S., 1956, *Ind. J. Phys.*, **30**, 313.
Sirkar, S. C. and Ray, A. K., 1950, *Ind. J. Phys.*, **24**, 189.

SOMMERFELD'S FINE STRUCTURE FORMULA FROM A SECOND ORDER EQUATION WITHOUT THOMAS CORRECTION

C. C. BANERJJI

DEPARTMENT OF THEORETICAL PHYSICS

INDIAN ASSOCIATION FOR THE CULTIVATION OF SCIENCE, JADAVPUR, CALCUTTA-32

(Received for publication May 7, 1956)

ABSTRACT. Dirac has shown that the spin of the electron is a consequence of the Hamiltonian; that is why the second order equation of a free electron does not show its spin characteristics. However, when the electromagnetic interactions are introduced in the Dirac equation and we go over to the second order equation, we find that the latter shows the existence of spin by giving the correct magnitude of the magnetic moment of the electron. The second order equation derived from Dirac equation having only the Coulomb field contains certain spin terms. The evaluation of these terms, it is shown here, leads to Sommerfeld's fine structure and they take the place of Thomas spin-orbit interaction as introduced by Pauli.

The Bohr model of an electron moving in a Coulomb field in circular orbits explains the spectrum of hydrogen in general terms but fails to interpret the fine structure of the lines. Sommerfeld's extension of Bohr model to include elliptic orbits does not add any new energy levels; for a given total quantum number n , the energy levels of the possible elliptic orbits coincide with that of the circular orbit for the same n . However, if the electron moves according to the laws of special theory of relativity rather than that of Newtonian mechanics, the energy levels depend on the ellipticity of the orbit which enabled Sommerfeld to explain correctly the fine structure of hydrogen lines.

The Schrödinger's theory of the hydrogen atom gives the same results as were obtained by Sommerfeld from Newtonian mechanics. Taking the Klein-Gordon equation which is the relativistic analogue of the Schrödinger equation Sommerfeld obtained a fine structure formula which differs slightly from his earlier relation deduced from the old quantum theory, this quantum mechanical formula which takes into account the relativity effect does not agree with the experimental findings.

During this time the idea of spinning electron was postulated by Goudsmit and Uhlenbeck. Following the suggestion of Thomas (1926), Pauli (1927) introduced a spin-orbit interaction term in Schrödinger's equation and obtained a correction to the energy levels due to spin only; this also disagrees with the experimental observations. However, if we add the corrections due to relativity (Sommerfeld) and spin (Pauli) we obtain an expression which agrees with the

correct fine-structure formula in the first approximation. However, Dirac's linear equations which incorporate spin and relativity effects in an inseparable way and lead to the exact formula for the fine-structure.

The second order equation of Schrödinger's form obtained from two first order Dirac equations shows certain additional terms in the expression for the interaction besides those which appear due to relativistic effects in Klein-Gordon equation. These extra terms are due to spin and thus the effects of spin and relativity are separately shown in the interaction. The author calculates the energy correction for hydrogen levels for spin from these terms and obtained an expression for fine structure which to a first approximation agrees with Sommerfeld's formula.

DERIVATION OF SOMMERFELD'S FORMULA

Dirac's wave equation (1928) which is linear in time differential and invariant under Lorentz transformation, describes an electron by four wave functions (ψ_1, ψ_2, ψ_3 and ψ_4). Darwin (1928) has obtained a solution of Dirac equation for scalar potential $V(r)$ which is a function of r only and zero vector potential. The radial parts of the solution for ψ , denoted by F and G , satisfy simultaneous differential equations of the form

$$\alpha F_l + \frac{dG_l}{dr} - \frac{l}{r} G_l = 0 \quad \dots (1a)$$

$$-\beta G_l + \frac{dF_l}{dr} + \frac{l+2}{r} F_l = 0 \quad \dots (1b)$$

where
$$\alpha = \frac{W - V + mc^2}{\hbar^2 c^2} \text{ and } \beta = \frac{W - V - mc^2}{\hbar^2 c^2}$$

As the energy of the electron involved is very much less than the rest energy, F_l which represents the radial part of the solution for ψ_1 and ψ_2 contributes very little to the solution. Eliminating F_l from (1a) and (1b), we have,

$$\frac{d^2 G_l}{dr^2} + \left(\frac{2}{r} - \frac{\alpha}{\beta} \right) \frac{dG_l}{dr} + \left\{ \alpha\beta - \frac{l(l+1)}{r^2} + \frac{l}{r} \frac{\alpha'}{\alpha} \right\} G_l = 0 \quad \dots (2)$$

Substituting $G_l = \frac{\sqrt{\alpha}}{r} g_l$ in the equation (2), we get

$$\frac{d^2 g_l}{dr^2} + \left[k^2 - \frac{l(l+1)}{r^2} - U(r) \right] g_l = 0 \quad \dots (3)$$

where

$$k^2 = \frac{W^2 - m^2 c^4}{\hbar^2 c^2} \quad \dots (3a)$$

$$\text{and} \quad U(r) = -\frac{2WV}{\hbar^2 c^2} + \frac{V^2}{\hbar^2 c^2} + \frac{l+1}{r} \frac{\alpha'}{\alpha} - \frac{3}{4} \left(\frac{\alpha'}{\alpha} \right)^2 + \frac{1}{2} \frac{\alpha''}{\alpha} \quad \dots \quad (3b)$$

A similar equation for g_{-l-1} may be obtained by replacing l by $-(l+1)$.

The equation (3) reduces to the Klein-Gordon form if $\frac{\alpha'}{\alpha}$, $\left(\frac{\alpha'}{\alpha}\right)^2$ and $\frac{\alpha''}{\alpha}$ are neglected and further if E or $V \ll mc^2$ the Klein-Gordon equation reduces to the Schrödinger form. Since the Klein-Gordon equation takes special theory of relativity into account and since the first two terms of (3b) are present in Klein-Gordon equation, the last three terms represent the contribution due to spin only. We now calculate the contributions of these three terms to the energy levels of the hydrogen atom and examine to what extent this contribution along with energy eigen values given by Klein-Gordon equation represent experimental data.

Let us denote $U_s(r)$ to represent the above mentioned three terms.

$$\text{Therefore,} \quad U_s(r) = -\frac{l+1}{r} \frac{\alpha'}{\alpha} - \frac{3}{4} \left(\frac{\alpha'}{\alpha} \right)^2 + \frac{1}{2} \frac{\alpha''}{\alpha} \quad \dots \quad (4)$$

$$\begin{aligned} &= \frac{l+1}{r} \left(-\frac{ze^2}{r^2} \right) - \frac{3}{4} \left(-\frac{ze^2}{r^2} \right)^2 + \frac{1}{2} \frac{2ze^2}{r^3} \\ &= -\frac{ze^2}{W-V+mc^2} \frac{l+1}{r^3} - \frac{3}{4} \frac{z^2 e^4}{(W-V+mc^2)^2 r^4} + \frac{ze^2}{(W-V+mc^2)r^3}. \end{aligned}$$

Neglecting the second term and in the approximation $W-V+mc^2 \approx 2mc^2$ we have,

$$U_s = -\frac{lze^2}{2mc^2} \cdot \frac{1}{r^3}$$

$$\text{Energy due to spin} \quad E_s = -\frac{\hbar^2}{2m} \left(-\frac{ze^2}{2mc^2} \cdot \frac{l}{r^3} \right) \quad \dots \quad (5)$$

Average value of this energy

$$\begin{aligned} E_s &= (-) \frac{ze^2 \hbar^2 \cdot l}{2 \cdot 2m^2 c^2} \left(\frac{1}{r^3} \right) \\ &= (-) \frac{ze^2 \hbar^2 l}{2 \cdot 2m^2 c^2} \cdot \frac{z^3}{a^3 n^3 l(l+\frac{1}{2})(l+1)} \\ &= (-) \frac{Rhca^2}{2n^3(l+\frac{1}{2})(l+1)} = (-) \frac{Rhca^2}{n^4} \left[\frac{n}{l+1} - \frac{n}{l+\frac{1}{2}} \right] \quad \dots \quad (6) \end{aligned}$$

where $a = \text{Bohr radius} = \frac{\hbar^2}{mc^2}$ and $\alpha = e^2/\hbar c$

We know that the correction term for relativity obtained from Klein-Gordon equation, which of course means our equation (3) with first two terms in the expression for $U(r)$, is given by

$$E_{rel} = (-) \frac{Rhc\alpha^2}{n^4} \left[\frac{n}{l+\frac{1}{2}} - \frac{3}{4} \right] \quad \dots (7)$$

The energy for the Balmer term may also be obtained from our equation (3) by introducing non-relativistic approximation and it is given by

$$E_n = - \frac{Rhc}{n^2} \quad \dots (8)$$

Hence sum of the energies represented by (6), (7) and (8) gives us the energy value of the various levels, thus

$$\begin{aligned} E_{nl} &= E_n + E_{rel} + E_s \\ &= - \frac{Rhc}{n^2} - \frac{Rhc\alpha^2}{n^4} \left[\frac{n}{l+\frac{1}{2}} - \frac{3}{4} \right] - \frac{Rhc\alpha^2}{n^4} \left[\frac{n}{l+1} - \frac{n}{l+\frac{1}{2}} \right] \\ &= - \frac{Rhc}{n^2} - \frac{Rhc\alpha^2}{n^4} \left[\frac{n}{l+1} - \frac{3}{4} \right] \quad \dots (9) \end{aligned}$$

As already mentioned a similar formula may be obtained by substituting $-(l+1)$ for l in the expression for $U(r)$ or E_{nl} .

Sommerfeld's formula when expanded and terms involving higher powers than α^2 are neglected gives exactly the equation (9) and it explains the energy levels of spectral lines in the visible region.

DISCUSSION

The last three terms of equation (3b) which appear in the potential energy term are regarded as taking into account the spin effect; they depend on the first and the second differential of the potential energy rather than on the potential energy, whereas the relativistic terms depend on the kinetic and potential energy. It appears that equation (3) reduces to the Klein-Gordon form. The energy correction terms due to spin and relativity (c.f. equations (6) and (7)) have the same coefficient which indicates a close relationship between spin and relativity. The influence of spin (for states of $l > 0$) is to split up the Bohr energy level into two levels—one higher and the other lower than it; the effect of relativity is to bring down both such levels from the Bohr level. In Dirac's equation, the spin comes as a consequence of the linearization of the Hamiltonian, the present paper shows that even if we make a second order equation from the first order

equations, the spin terms retain their form, though in a different way and give correct energy levels. These spin terms occurring naturally in the second order equation take the place of the externally introduced spin-orbit interaction due to Thomas. The Thomas term contains only the first differential of the potential energy, where as ours includes both the first and second differentials. Pauli's treatment of the spin-orbit interaction has an ambiguity for $l = 0$, our method is free from it.

ACKNOWLEDGMENT

The author wishes to express his sincere thanks to Prof. D. Basu, Ph.D., for his helpful discussion throughout the progress of the work.

REFERENCES

- Dirac, P. A. M., 1928, *Proc. Roy. Soc.* A117, 810; A118, 351.
and A118, 654.
Pauli, W., 1927, *Zeit. f. Physik.* 43, 601.
Sommerfeld, A., 1916, *Ann. d. Phys.*, 51, 1.
Thomas, L. H., 1926, *Nature*, 107, 514.

RAMAN SPECTRA OF THREE MONOSUBSTITUTED BENZENE COMPOUNDS IN THE SOLID STATE AT LOW TEMPERATURES*

D. C. BISWAS

OPTICS DEPARTMENT, INDIAN ASSOCIATION FOR THE CULTIVATION OF SCIENCE,
JADAVPUR, CALCUTTA-32

(Received for publication June 4, 1956)

Plate XIII

ABSTRACT. The Raman spectra of $C_6H_5.COCH_3$, $C_6H_5.OC_2H_5$, and $C_6H_5.CHO$ in the liquid and in the solid state at different low temperatures have been investigated and the results have been compared with the available data on the ultraviolet absorption spectra of the substances obtained under similar conditions. Acetophenone produces four new lines at 34, 50, 83 and 94 cm^{-1} respectively in the solid state at -90°C , while phenetole gives rise to a single new line at 96 cm^{-1} when the substance is solidified and cooled to -90°C . With lowering of temperature to -180°C , the low-frequency lines of acetophenone become sharper and the two lines at 83 and 94 cm^{-1} shift to 80 and 96 cm^{-1} respectively, while phenetole, under a similar change of temperature, gives rise to a second line at 83 cm^{-1} . Amongst the intramolecular lines, some of the lines due to C-H oscillations in both acetophenone and phenetole undergo some changes with change from liquid to solid phase.

Contrary to the case of the above two substances benzaldehyde does not produce any distinct line in the low frequency region when this compound is solidified, but instead it gives rise to a feeble continuous wing extending upto about 100 cm^{-1} from the Rayleigh line.

Attempts have been made to interpret these results.

INTRODUCTION

The Raman spectra of a few monosubstituted benzene compounds in the solid state at low temperatures were studied by Ray (1950; 1951; 1952) and Biswas (1955). It was observed that the number, intensities and positions of the low-frequency lines are different for the different compounds, and they depend on the nature of the substituent group. Further, it was pointed out (Biswas, 1955) that in the case of methyl and ethyl benzoate the changes in the ultraviolet absorption spectra with change of state of these compounds furnish useful information regarding the appearance of low frequency lines in the Raman spectra of these substances in the solid state at low temperatures.

The compounds mentioned above have simple substituents excepting ethyl benzoate. The Raman spectra due to the solid phase of monosubstituted benzenes which have comparatively long and complicated substituent groups attached to the ring were not investigated by any previous worker. As the study

*Communicated by Prof. S. C. Sirkar

of the Raman spectra of a few such monosubstituted benzenes in the solid state and a comparison of the results with the available data on their ultraviolet absorption spectra obtained under similar conditions might throw more light on the origin of these low-frequency lines, the Raman spectra of acetophenone, phenetole and benzaldehyde representing three different types of substituted benzenes have been studied in liquid and solid states and the results for two of these compounds have been compared with those for the ultraviolet absorption spectra studied under similar conditions by previous authors.

EXPERIMENTAL

The liquids acetophenone and benzaldehyde used in the present investigation were procured from E. Merck and phenetole was supplied by Fisher Scientific & Co. U.S.A. They were distilled in vacuum as usual before being introduced in pyrex glass containers in which these substances were sealed and exposed to the incident radiation from a mercury arc. The technique and the experimental procedure for recording the Raman spectra of these substances in the solid state at different low temperatures were the same as described earlier (Biswas, 1954). The spectra were photographed on Ilford Zenith plates using a Fuess glass spectrograph of dispersion of about 11\AA per mm. in the 4046\AA region. On each spectrogram, iron arc spectrum was photographed for comparison.

RESULTS AND DISCUSSIONS

The Raman shifts observed for the three substances in the liquid and solid phase at different temperatures are given in Tables I–III. Some available data on the Raman spectra of these substances in the liquid phase as reported by earlier workers are also included in these tables. The low-frequency spectrum of acetophenone in the solid state at -90°C and -180°C respectively enlarged about four times are reproduced in figure 1, Plate XIII.

Acetophenone.

When this substance is solidified and cooled down to -90°C , four new lines at 34, 50, 83 and 94 cm^{-1} respectively appear in the low-frequency region. All these lines are quite intense and the two lines at 83 and 94 cm^{-1} are broad. When the temperature on the solidified mass is lowered to -180°C , the broad lines become sharper and the components of the pair at 83 and 94 cm^{-1} shift to 80 and 96 cm^{-1} respectively. In order to understand the origin of these lines in acetophenone, it would be interesting to compare the changes mentioned above with those observed in the ultraviolet absorption spectra of the substance by Deb (1951) with solidification of the liquid. He observed that when the substance is solidified and cooled down to -180°C , the absorption bands become much sharper and in place of the first broad band at 35744 cm^{-1} due to the liquid three sharper bands at 34170, 35249 and 36315 cm^{-1} respectively are recorded in the spectro-

gram due to the solid phase. Evidently, these three bands coalesce into one in the case of the liquid due to increase in the width of the individual bands. Moreover, the results given by the above author show that the ν_0 -band as a whole shifts towards longer wavelength side by about 500 cm^{-1} with change from liquid to solid phase. Deb concluded that these changes on the absorption band with solidification are brought about as a result of intermolecular association amongst the molecules of the substance in its solid phase at low temperature.

Such association restricts the freedom of angular oscillation of the molecules about their axes and makes the bands sharper. The appearance of strong low-frequency lines in the Raman spectra due to solidified acetophenone both at -90°C and -180°C can be attributed to this phenomenon of intermolecular association in this substance. This case of acetophenone is very much similar to that of methyl benzoate described earlier (Biswas, 1955).

Amongst the Raman lines due to the single molecules of the substance the broad line at 162 cm^{-1} appears to shift to 166 cm^{-1} and the line at 1681 cm^{-1} to 1675 cm^{-1} . Moreover, the line at 3063 cm^{-1} due to C-H stretching oscillation appears to become stronger and the line 2920 cm^{-1} weaker when the substance is solidified and cooled to low temperatures. The two other lines at 2965 and 3007 cm^{-1} respectively due to C-H vibration seem to merge into one another to produce a line at 2998 cm^{-1} in the solid state. These changes may indicate that the association takes place mainly through these hydrogen bonds.

Phenetole:

When phenetole is solidified and cooled down to -90°C a new Raman line appears at 96 cm^{-1} . When the temperature is further lowered to -180°C , this line shifts to 99 cm^{-1} and another comparatively weak line appears at 83 cm^{-1} . These results on the low-frequency spectrum of phenetole can be correlated with those on the ultraviolet absorption spectra of the substance obtained by Deb (1953) in the solid state at -180°C . He observed that the absorption bands of phenetole become sharper in the solid state at -180°C , but their positions are not appreciably altered with change from liquid to solid state. The diminution in the width of the bands is due to the restriction on the angular oscillations of the molecules which is brought about probably as a result of the formation of virtual linkages amongst the neighbouring molecules in the crystal lattice of the substance. The appearance of low-frequency Raman lines in solidified phenetole may be attributed to the oscillations of the molecules connected through these virtual bonds. In this particular case at -90°C , the molecules may not be linked to each other at more than one point, but at -180°C new linkages may occur giving rise to the line 83 cm^{-1} . As the substituent group is rather large, the phenyl group is not surrounded by other phenyl groups in the lattice and therefore the virtual linkages formed at particular points of the molecule do not affect the excited electronic state of the molecule appreciably.



Fig. 1

Low frequency Raman spectrum of acetophenone

(a) Solid at -180°C; (b) Solid at about -90°C

TABLE I
Acetophene
 $\Delta \nu$ in cm^{-1}

Liquid		Solid (Present author)	
Murray <i>et al</i> (1942)	Present author	At about -90°C	At -180°C
	Continuous wing extending upto about 119cm^{-1}	34 (3)	34 (3)
		50 (3)	50 (4)
		83 (4b)	80 (3)
		94 (4b)	96 (5)
165 (5b)	162 (6b)	166 (4b)	166 (4b)
371 (3)	371 (2)	371 (1b)	371 (1b)
404 (0)	—	—	—
461 (0)	467 (0)	—	—
588 (3)	589 (1)	—	—
617 (5)	617 (4)	617 (2)	617 (2)
732 (6)	728 (5)	731 (3)	731 (3)
767 (2)	755 (1)	—	—
852 (1)	—	—	—
896 (0)	—	—	—
958 (3)	955 (2)	955 (0)	955 (0)
1002 (10)	999 (10)	999 (7)	999 (7)
1027 (6)	1023 (4)	1023 (3)	1023 (3)
1076 (6)	1077 (5)	1081 (3)	1081 (3)
1161 (4)	1154 (3)	1154 (1)	1154 (1)
1180 (3)	1181 (1)	—	—
1267 (7)	1262 (5)	1262 (4)	1262 (4)
1301 (0)	—	—	—
1427 (1)	—	—	—
1447 (1)	1443 (0)	—	—
1493 (3)	1491 (2)	1491 (0)	1491 (0)
1597 (10)	1595 (12)	1595 (8)	1595 (8)
1684 (10)	1681 (10)	1675 (7)	1675 (7)
2921 (6)	2920 (5)	2920 (1)	2920 (1)
2967 (2)	2965 (1)	2998 (2)	2998 (2)
3006 (2)	3007 (1)	—	—
3065 (10)	3063 (6b)	3063 (7)	3063 (7)
3187 (1)	—	—	—

TABLE II**Phenetole** $\Delta \nu$ in cm^{-1}

Liquid	Solid (Present author)	
	At about -90°C	At -180°C
Continuous wing extending upto about 114 cm^{-1}		83 (2)
	96 (3)	99 (3)
177 (2)	177 (0)	177 (0)
241 (3b)	241 (0b)	245 (0b)
348 (5)	348 (2)	348 (3)
429 (3)	429 (1)	429 (2)
585 (1)	—	
614 (3)	614 (0)	614 (1)
762 (2)	—	762 (0)
799 (5)	799 (2)	799 (3)
923 (2)	923 (0)	923 (0)
998 (10)	998 (6)	998 (8)
1028 (5)	1028 (2)	1028 (3)
1117 (2)	1117 (1)	1117 (1)
1158 (3)	1158 (1)	1158 (2)
1245 (4)	1245 (2)	1245 (3)
1451 (1)	1451 (0)	1451 (0)
1490 (0)	—	—
1589 (4b)	1587 (2)	1587 (3)
1599 (6)	1599 (2)	1599 (3)
2884 (2)	2884 (1)	2884 (1)
2937 (6)	2932 (2)	2932 (3)
—	—	2977 (1)
2986 (3)	2986 (1b)	2986 (1)
	3063 (6)	3063 (8)
3065 (8b)	3074 (7)	3074 (9)

TABLE III

Benzaldehyde

 $\Delta \nu$ in cm^{-1}

Liquid		Solid (Present author)	
Magat (1936)	Present author	At about -105°C	At -180°C
	Feeble wing extending upto about 95cm^{-1}	Feeble wing extending up to about 100cm^{-1}	Feeble wing extending upto about 100
137 (10b)	134 (4b)	134 (0b)	134 (0b)
234 (5b)	238 (3b)	238 (1b)	238 (1b)
439 (8)	435 (5)	435 (2)	435 (2)
613 (8)	605 (5)	605 (2)	605 (2)
646 (4)	652 (2)	652 (0)	652 (0)
745 (1)	747 (0)	---	---
827 (6)	826 (5)	826 (3)	826 (3)
---	850 (0)	---	---
1000 (15)	1000 (9)	1005 (6)	1005 (6)
1022 (4)	1020 (1)	1020 (0)	1020 (0)
1164 (12)	1167 (7)	1167 (4)	1167 (4)
1201 (12)	1200 (8)	1207 (0)	1207 (5)
1390 (3)	1389 (2)	1389 (0)	1389 (1)
1456 (3)	1459 (1)	1459 (0)	1459 (0)
1492 (3)	1490 (1)	1490 (0)	1490 (0)
1595 (15)	1594 (12)	1594 (8)	1594 (6)
---	1655 (2b)	1665 (1)	1665 (1)
1696 ± 13 (15b)	1701 (12b)	1701 (8b)	1701 (8b)
3060 (4)	3062 (7b)	3062 (5b)	3062 (5b)
Continuum	---	---	---
4358-4816 Å			

With solidification of phenetole no other intramolecular oscillations except those due to the C-H oscillations undergo any appreciable change. In the case of the Raman lines due to C-H stretching oscillation however, the broad line due to the liquid at 3065 cm^{-1} is replaced in the solid state by two intense lines at 3063 and 3074 cm^{-1} respectively. Moreover, a comparatively weak line appears at 2977 cm^{-1} when the solid is cooled to -180°C . These changes in the Raman lines due to C-H oscillations indicate that these hydrogen atoms are mainly responsible for the intermolecular interaction in the solid state of this substance.

Benzaldehyde:

In the solid state at low temperatures, benzaldehyde does not exhibit any distinct Raman line in the low-frequency region, but a weak and continuous wing extending upto about 100 cm^{-1} on the longer wavelength side of the Rayleigh line appears to be superposed on the feeble wing which is present in the spectrum of the incident light. The wing accompanying the Rayleigh line due to the liquid is weak in comparison with such wing observed in other ordinary substituted benzene compounds. Thus it appears that when the wing due to the liquid is feeble, the new Raman lines of the low-frequency region are also very weak. The neighbouring molecules of benzaldehyde probably get associated in the liquid state through the OH virtual bonds and these associated groups being large, the wing due to the liquid phase is weaker. This happens because (1) the phenyl groups of adjacent molecules cannot come close together and (2) the associated groups being large the rotational freedom is restricted. It is presumed that the contribution to the intensity of the wing comes partly from oscillations in closely packed groups of the adjacent benzene rings in the liquid and also from the rotation of the single molecules.

Amongst the lines due to intramolecular oscillations the strong line at 1000 cm^{-1} due to the liquid phase shifts to 1005 cm^{-1} when the substance is solidified and cooled to low temperatures. It is observed from the data given by Magat (1936) that some previous authors have reported the existence of a continuous background in the visible region in the Raman spectrum of benzaldehyde in the liquid state. It is, however, observed in the present investigation that when the incident light is filtered through a dilute aqueous solution of NaNO_2 , the continuous background in the visible region is completely absent. The presence of the continuum which was reported earlier may, therefore, be due to fluorescence excited in liquid benzaldehyde by the ultraviolet light of the incident beam.

ACKNOWLEDGMENT

The author is indebted to Prof. S. C. Sirkar, D.Sc., F. N.I. for his kind interest and guidance during the progress of this work.

REFERENCES

- Biswas, D. C., 1954, *Ind. J. Phys.*, **28**, 85.
Biswas, D. C., 1955, *Ind. J. Phys.*, **29**, 503.
Deb, A. R., 1951, *Ind. J. Phys.*, **25**, 433.
Deb, A. R., 1953, *Ind. J. Phys.*, **27**, 457.
Magat, M., 1936, *Annual Tables of constants and Numerical Data.*, p. 26-81.
Murray, M. J. Cleveland, F., and Saunders, R. H., 1942, *J. Am. Chem. Soc.*, **64**, 1181.
Ray, A. K. 1950, *Ind. J. Phys.*, **24**, 111.
Ray, A. K., 1951, *Ind. J. Phys.*, **25**, 131.
Ray, A. K., 1952, *Ind. J. Phys.*, **26**, 226.

THE CRYSTAL STRUCTURE OF ANTHRACENE AT DIFFERENT TEMPERATURES*

G. S. R. KRISHNA MURTI

OPTICS DEPARTMENT, INDIAN ASSOCIATION FOR THE CULTIVATION OF SCIENCE,
JADAVPUR, CALCUTTA-32

(Received for publication, June 16, 1956)

Plate XIV

ABSTRACT. The crystal structure of anthracene at -180°C , 32°C , 55°C and 80°C has been investigated by studying the Debye-Scherrer patterns. It is found that at a temperature of about -180°C the dimensions of the unit cell are given by $a = 8.547$ A.U., $b = 6.000$ A.U., $c = 11.090$ A.U. and $\beta = 125^{\circ}10'$. These values a , b and c being slightly lower than those at the room temperature. The mean values of α_a , α_b and α_c , the coefficients of expansion along the three crystallographic axes a , b and c respectively are found to be 77.5×10^{-6} , 27.52×10^{-6} and 31.05×10^{-6} respectively. The dimensions of the unit cell of the crystal at 80°C are $a = 8.696$ A.U., $b = 6.150$ A.U., $c = 11.310$ A.U. and $\beta = 124^{\circ}28'$. It appears that the coefficient of expansion is low upto about 55°C but a tenfold increase in the values takes place in the range from 55°C to 80°C . The values for α_a , α_b and α_c in the range from 32°C to 80°C are 32.55×10^{-5} , 39.36×10^{-5} and 27.45×10^{-5} respectively.

INTRODUCTION

The crystal structure of anthracene was first determined by Bragg (1923) by the X-ray reflection method who observed that the crystal belongs to a space group C_{2h}^5 with the unit cell dimensions, $a = 8.58$ A.U., $b = 6.02$ A.U., $c = 11.18$ A.U. and $\beta = 125^{\circ}$. The space group was confirmed by Banerjee (1930) who studied the Debye-Scherrer patterns and the rotation photographs due to the crystal. The structure was determined more accurately by Robertson (1933) employing the double Fourier series method and by Mathieson, Robertson and Sinclair (1950) by the triple Fourier series method. These authors reported the same space group for the crystal, but slightly different unit cell dimensions. The values given by them are $a = 8.561$ A.U., $b = 6.036$ A.U., $c = 11.163$ A.U. and $\beta = 124^{\circ}42'$.

The mean values of coefficients of expansion α_{11} , α_{22} and α_{33} over the range 20° to -195°C were reported by Kozhin and KitaiGorodskii (1953) to be 111.7×10^{-6} , 13.4×10^{-6} and 20.3×10^{-6} respectively. They reported the unit cell dimensions at 20°C as $a = 8.544$ A.U., $b = 6.023$ A.U., $c = 11.145$ A.U. and $\beta = 124^{\circ}42'$ and at -195°C as $a = 8.441$ A.U., $b = 6.006$ A.U., $c = 11.08$ A.U. and

* Communicated by Prof. S. C. Sirkar.

$\beta = 125^\circ 35'$. So there is no change in the lattice of crystal in the temperature range from 20°C to -195°C .

It is known now that the lattice of *p*-dichlorobenzene changes when the crystal is heated to about 45°C . It was thought worthwhile to find out whether the structure of anthracene remains unaltered or changes above room temperature. The Debye-Scherrer pattern of the crystal was therefore studied at 55°C and 80°C and also at -180°C in order to compare with each other the structures at these temperatures.

EXPERIMENTAL

Anthracene used was of chemically pure quality supplied by J. T. Baker Chemical Co., U.S.A. The substance was powdered well in a mortar and packed inside a glass tube of diameter 0.7 mm and the Debye-Scherrer pattern was photographed at different temperatures. The methods for keeping the powder at the temperature of liquid oxygen and also at temperatures higher than 32°C were the same as those described by Krishna Murti and Sen (1956).

A Seifert X-ray tube running at 26 ma, 32 kV was used to photograph the patterns. An exposure of about $2\frac{1}{2}$ hrs was sufficient to get the pattern recorded with moderate density. The rings obtained were sharp since the diameter of the sample was about $\frac{1}{2}$ mm. The X-ray tube was provided with a copper target and a nickel filter was used to cut off the $K\beta$ wavelengths. Two cylindrical cameras were used and the radii of the cameras were measured accurately by taking the Debye-Scherrer pattern of rocksalt. For the high temperature camera, the distance from the film to the specimen is 2.84 cms and for the low temperature and room temperature camera, it is 5.25 cms. Several photographs under the same conditions were taken for each specimen to test the genuineness of the results. Spacings were calculated from the diameters of the Debye-Scherrer rings which were measured correct to about 0.1 mm.

RESULTS AND DISCUSSION

The spacings deduced from the Debye-Scherrer patterns due to the crystal at different temperatures mentioned above are given in Table I in which the spacings calculated from the data of Mathieson, Robertson and Sinclair (1950) are also included in the first column for comparison. The intensities of the ring are recorded as very strong (vs), strong (s), medium (m), weak (w) and very weak (vw). Some of the representative photographs of the Debye-Scherrer patterns obtained under different conditions are reproduced in Plate XIV.

It can be seen from Table I that the spacings observed for the crystal at room temperature (32°C) agree fairly well with the spacings calculated from the data given by Mathieson, Robertson and Sinclair (1950). The assignment of indices to the planes was made by taking the structure factors of different planes

TABLE I
Spacings of crystals of anthracene

From the data of Mathieson, Robertson & Sinclair (1950)		Present Investigation				Cooled to 180°C and brought back to 32°C
Planes	Spacings	at 32°C	at 55°C	at 80°C	at 180°C	
001	9.128	9.120 w			*9.083 vw	9.120 w
101	8.318					
100	7.041					
010	6.036					
102	5.526					
011	5.034					
111	4.885	4.888 w	4.888 vw	*4.977 vw	*4.867 vw	4.888 w
110	4.581	4.577 vs	4.577 vs	*4.666 vs	*4.557 vs	4.577 w
002	4.564					
101	4.478					
201	4.179	4.184 s	4.184 s	*4.244 s	*4.144 s	4.184 s
202	4.159					
112	4.076					
103	3.651					
012	3.641					
111	3.596					
200	3.520	3.525 s	3.525 s	3.584 s	3.490 s	3.525 s
203	3.483					
211	3.436	3.440 s	3.440 s	3.494 s	3.419 s	3.440 s
104	3.349					
102	3.107					
003	3.043					
210	3.040	3.042 s	3.042 s	*3.094 s	*3.018 s	3.042 s
020	3.018					
113	2.868					
021	2.866	2.866 w	2.866 vw	*2.925 vw	*2.848 vw	2.866 w
121	2.836					
201	2.794					
120	2.774	2.777 w	2.777 vw	*2.825 vw	*2.759 vw	2.777 w
204	2.763					
112	2.761					
013	2.717					
301	2.672					
211	2.535					
022	2.517					
121	2.503					
221	2.446					
311	2.443	2.444 m	2.444 m	2.482 m	2.428 w	2.444 m
114	2.433					
103	2.348					
300	2.347					
220	2.291					
004	2.282	2.280 w	2.280 vw	*2.333 vw	2.268 w	2.280 w
202	2.239					
205	2.217					
113	2.189					
310	2.187					
122	2.165					
014	2.134					
212	2.092					
105	2.078					

TABLE I (Contd.)

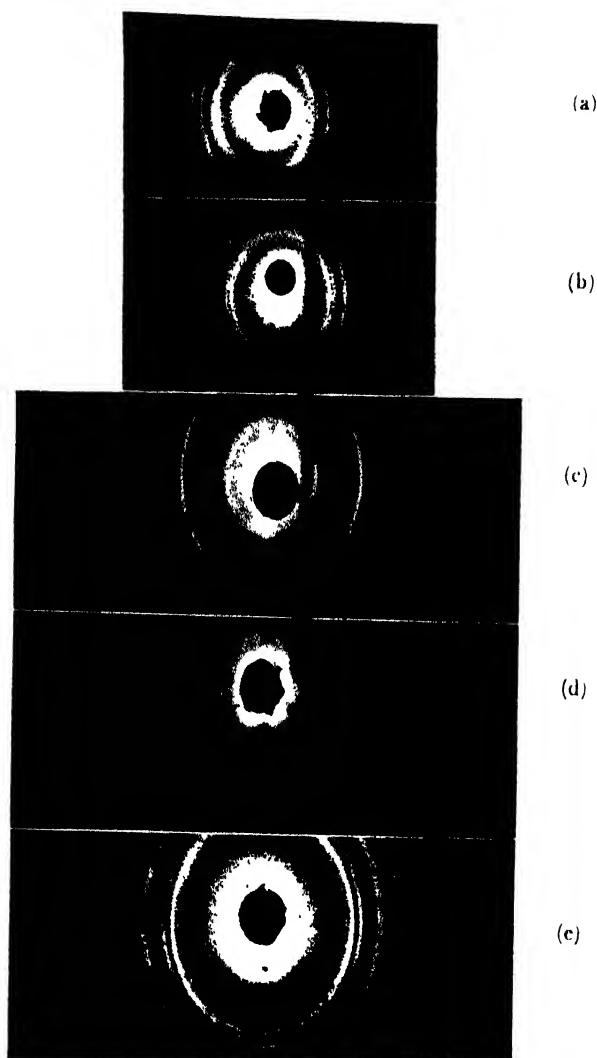
Planes	From the data of Mathieson, Robertson & Sinclair (1950) Spacings	Present Investigation				Cooled to -180°C and -brought back to 32°C
		at 32°C	at 55°C	at 80°C	at -180°C	
221	2.050	2.052 mw	2.052 mw	2.080 vw	2.035 w	
224	2.038			(broad)		
301	2.015					
030	2.012					
321	2.001	2.004 vw			1.987 vw	2.004 vw
031	1.964	1.968 vw				1.968 vw
131	1.956					
130	1.934	1.930 vw			1.922 vw	1.930 vw
311	1.912					
104	1.879					
411	1.853	1.855 m	1.855 m	1.884 m	1.840 m	1.855 m
320	1.852					
203	1.841					
131	1.835					

* These spacings are used to calculate dimensions of the unit cell.

TABLE II

Planes	Spacings in A.U. at -180°C		Spacings in A.U. at 80°C	
	Calculated from unit cell dimensions	observed	Calculated from unit cell dimensions	observed
200	3.493	3.493	3.584	3.584
211	3.420	3.419	3.494	3.494
311	2.428	2.428	2.482	2.482
004	2.267	2.268		
221	2.035	2.035	2.090	
321	1.988	1.987	2.070	2.080 (broad)
130	1.922	1.921		
411	1.841	1.840	1.885	1.884

into consideration. It can be seen from Table I that the spacings at 32°C agree with those given by Mathieson, Robertson and Sinclair (1950) and therefore the dimensions of unit cell are given as $a = 8.561$ A.U., $b = 6.036$ A.U., $c = 11.163$ A.U. and $\beta = 124^\circ 42'$ as reported by those authors.



Debye-Scherrer patterns of anthracene

- (a) Specimen at 80°C (Radius of Camera : 2.84 cms)
- (b) Specimen at 55°C (Radius of Camera : 2.84 cms)
- (c) Specimen at 32°C (Radius of Camera : 5.25 cms)
- (d) Specimen at - 180°C (Radius of Camera : 5.25 cms)
- (e) Specimen once cooled to - 180°C and brought back to 32°C (Radius of Camera : 5.25 cms).

It is further evident from the Table I that all the spacings for the crystal maintained at -180°C are consistently shorter than the corresponding spacings for the crystal at 32°C and when the crystal is brought back to 32°C , after it is once cooled to -180°C , the spacings agree with those at room temperature. Since new Debye-Scherrer rings do not appear in the pattern obtained for the crystal at -180°C , it can be concluded that the unit cell only contracts at -180°C and no appreciable distortion takes place. The dimensions of the unit cell calculated from the spacings of the planes (001), (111), (110), (120), (210) and (021) for the crystal at -180°C are given below.

$$\begin{aligned} a &= 8.547 \text{ A.U.} & b &= 6.000 \text{ A.U.} \\ c &= 11.090 \text{ A.U. and} & \beta &= 125^{\circ}10'. \end{aligned}$$

Taking the dimensions of the unit cell for the crystal at room temperature as those reported by Mathieson *et al* (1950) the mean coefficients of expansions, α_a , α_b and α_c in the directions along the three crystallographic axes in the range 32°C to -180°C can be calculated. The calculated values are

$$= 77.5 \times 10^{-6}, \quad \alpha_b = 27.52 \times 10^{-6} \quad \alpha_c = 31.05 \times 10^{-6}.$$

The dimensions of the unit cell for the crystal at -195°C reported by Kozhin and KitaiGordskii (1953) agree fairly well with those obtained in the present investigation excepting the value of a . But since they reported values for the dimensions of the unit cell at 20°C lower than those reported by Mathieson *et al* (1950) the mean values of coefficients of expansion do not agree with those obtained from the data reported by them.

It can be seen from Table I that the spacings for the crystal at 80°C are comparatively higher than those obtained for the crystal at 32°C . But as no new rings appear in the Debye-Scherrer pattern nor does the pattern change even slightly when the crystal is heated to 80°C , it can be concluded that only thermal expansion of the unit cell takes place with the rise of temperature to 80°C . The dimensions of the unit cell in the crystal at 80°C calculated from spacings of (11 $\bar{1}$), (110), (120), (004), (021) and (20 $\bar{1}$) are found to be

$$\begin{aligned} a &= 8.696 \text{ A.U.} & b &= 6.150 \text{ A.U.} \\ c &= 11.310 \text{ A.U. and} & \beta &= 124^{\circ}28'. \end{aligned}$$

The mean values of coefficients of expansion α_a , α_b and α_c in the range from 32°C to 80°C are obtained as

$$\alpha_a = 32.85 \times 10^{-6}, \quad \alpha_b = 39.36 \times 10^{-6} \quad \text{and} \quad \alpha_c = 27.45 \times 10^{-6}.$$

It can be seen that the mean values of coefficients of expansion in the high temperature range are about ten times higher than those in the low temperature region.

It can be seen from Table I that the values of spacings in the crystal at 55°C are almost the same as those for the crystal at 32°C. This might be due to the reason that in this temperature range the coefficient of expansion is small so that appreciable change in the spacings does not take place. The spacings, however, increase abruptly when the temperature is raised above 55°C and the coefficient of expansion increases enormously. The values of the spacings of other planes calculated from the dimensions of the unit cell for the crystal at low and high temperatures are given in Table II together with those observed. It can be seen that these two sets of values agree fairly well with each other.

The low frequency Raman lines of anthracene at different temperatures have not been investigated thoroughly and it would be interesting to find out whether these lines undergo abrupt changes with the change in the temperature of the crystal from 32°C to 80°C, because in the case of *p*-dichlorobenzene such a change has been observed by previous authors.

ACKNOWLEDGMENT

The author wishes to express his indebtedness to Professor S. C. Sirkar, D.Sc., F.N.I. for his kind help and invaluable guidance throughout the progress of this work.

REFERENCES

- Banerjee, K., 1930, *Ind. J. Phys.*, **4**, 557.
Bragg, Sir William, 1923, *Proc. Phys. Soc. Lond.*, **35**, 167.
Krishna Murti, G. S. R., and Sen, S. N., 1956, *Ind. J. Phys.*, **30**, 242.
Kozhin, V. M., and KitaiGorodskii, A. I., 1953, *Zhur. fiz. Khim.*, **27**, No. 11, 1276.
Mathieson, A. M., Robertson, J. M., and Sinclair, V. C., 1950, *Acta. cryst.*, **3**, 245.
Robertson, J. M., 1933, *Z. Krist.*, **84**, 321.
.. 1933, *Proc. Roy. Soc. Lond.*, **A140**, 79.

ON DEPENDENCE OF RESOLVING POWER ON BACKGROUND INTENSITY, STAGE OF RESOLUTION AND DETECTING INSTRUMENT

K. C. CHATURVEDI AND M. S. SODHA

156-D, KAMLANAGAR, DELHI-6

(Received for publication, May 2, 1956)

ABSTRACT. In this paper the authors have discussed the variation of resolving power of prism, grating, reflecting echelon and Fabry-Perot etalon with background intensity, stage of resolution desired and the detecting instrument, when natural line width is negligible. The case when instrumental width is negligible has also been discussed.

INTRODUCTION

Ditchburn (1930) has pointed out that the resolving power of an instrument depends on the stage of resolution desired and the detecting instrument. A given combination of detecting instrument and the stage of resolution desired is characterized by c , the ratio of minimum to maximum of the resultant intensity pattern of two lines for optimum resolution. For example, when the spectrogram is examined by a microphotometer we have.

- i) Detection of inhomogeneity in radiation when $c = 0.98$.
- ii) Partial resolution (approximate measurement of wavelength separation) when $c = 0.8$.
- and iii) Complete resolution (measurement of wavelength separation and relative intensities) when $c = 0.4$.

The variation of resolving power of various instruments with c has been studied by Sharma and Sodha (1954) and Mitra (1954), when the background intensity is zero. Sodha (1954) has discussed the variation of resolving power, with background intensity on Rayleigh's criterion ($c = 0.8$).

In this paper the authors have investigated the dependence of resolving power on k and c i.e. detecting instrument, stage of resolution desired and the background intensity present. Two important cases have been distinguished,

- i) when instrumental width is negligible and the intensity distribution of a line is governed by Doppler effect
- ii) when Doppler width is negligible and the intensity distribution of a line is governed by the instrument.

NEGLIGIBLE INSTRUMENTAL WIDTH

The intensity distribution of a spectral line of wave number ν_0 due to Doppler effect is given by

$$I' = I_0 \exp \{-\beta(\nu - \nu_0)^2\}$$

where $\beta = \mu c_0^2 / 2RT\nu_0^2$, μ being the mass of radiant atoms.

The intensity distribution of another spectral line of wave number $(\nu_0 + \Delta\nu)$ and same intensity is

$$I'' = I_0 \exp \{-\beta(\nu - \nu_0 - \Delta\nu)^2\}$$

if $\Delta\nu$ is small (β same for both lines).

Putting $\sqrt{\beta}(\nu - \nu_0) = x$ and $\sqrt{\beta} \cdot \Delta\nu = a$, the resultant intensity pattern in the presence of a background intensity kI_0 is given by

$$I = kI_0 + I_0 e^{-x^2} + I_0 e^{-(x-a)^2}$$

Neglecting the shrinkage effect, the intensity maximum ($x = 0$ or a) and intensity minimum ($x = a/2$) are given by

$$\frac{I_{max}}{I_0} = 1 + k + e^{-a^2}$$

and

$$\frac{I_{min}}{I_0} = k + 2e^{-a^2/4}$$

Putting

$$\frac{I_{min}}{I_{max}} = c$$

we have

$$k = \{c(1 + e^{-a^2}) - 2e^{-a^2/4}\} / (1 - c) \quad \dots (1)$$

The resolving power is given by

$$\frac{\lambda}{d\lambda} = \frac{\nu_0}{\Delta\nu} = \frac{\sqrt{\beta}}{a} \cdot \nu_0 = \alpha \cdot c_0 \sqrt{\frac{\mu}{2RT}} \quad \dots (2)$$

where

$$\alpha = \frac{1}{a} \quad \dots (3)$$

Table I, computed from equations (1) and (3), illustrates the variation of α with k and c . The results have been illustrated by figures 1 and 2.

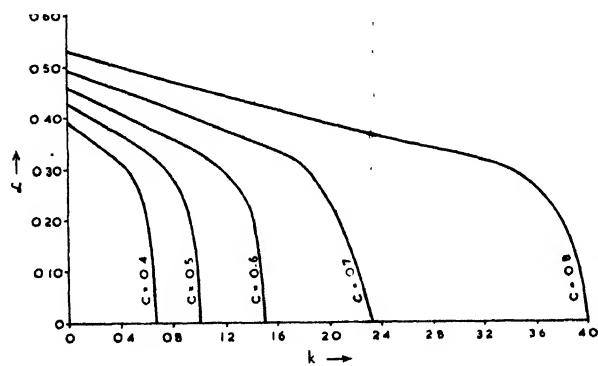


Fig. 1. Variation of α with k and c (0.4–0.8) when instrumental width is negligible.

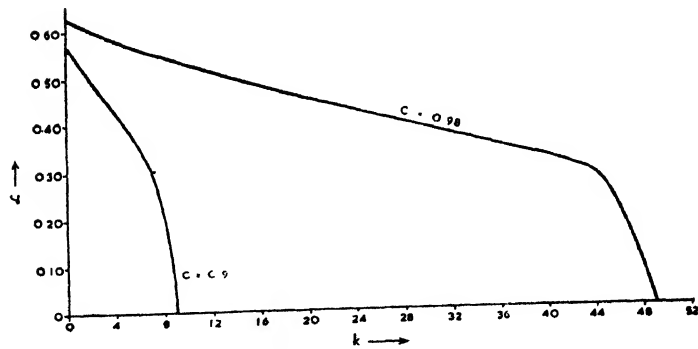


Fig. 2. Variation of α with k and c (0.9–0.98) when instrumental width is negligible.

TABLE I

Variation of α with k and c when the instrumental width is negligible

k	$c = 0.4$	$c = 0.5$	$c = 0.6$	$c = 0.7$	$c = 0.8$	$c = 0.9$	$c = 0.98$
0.00	—	—	—	—	0.53	—	—
0.04	—	—	—	—	—	—	—
0.08	0.38	—	0.45	—	—	—	—
0.11	—	0.41	—	—	—	—	—
0.14	—	—	—	0.48	—	—	—
0.22	0.35	—	—	—	—	—	—
0.39	—	—	0.41	—	0.50	0.56	—
0.44	—	—	—	0.45	—	—	—
0.46	—	0.35	—	—	—	—	—
0.50	0.29	—	—	—	—	—	—
0.666	0.00	—	—	—	—	—	—
0.80	—	0.29	—	—	—	—	—
0.82	—	—	0.35	—	—	—	—
0.85	—	—	—	0.41	—	—	—
1.00	—	0.00	—	—	—	—	—
1.02	—	—	—	—	0.46	—	—
1.09	—	—	0.32	—	—	—	—
1.25	—	—	0.29	—	—	—	—
1.43	—	—	—	0.35	—	—	—
1.50	—	—	0.00	—	0.42	—	—
1.79	—	—	—	0.32	—	0.50	—
1.99	—	—	—	—	0.39	—	—
2.33	—	—	—	0.00	—	—	0.60
2.50	—	—	—	—	0.36	—	—
3.00	—	—	—	—	0.33	0.46	—
3.50	—	—	—	—	0.29	—	—
3.97	—	—	—	—	0.20	—	—
4.00	—	—	—	—	0.00	—	—
4.56	—	—	—	—	—	0.41	—
6.07	—	—	—	—	—	—	0.56
6.30	—	—	—	—	—	0.35	—
9.00	—	—	—	—	—	0.00	—
13.11	—	—	—	—	—	—	0.50
19.28	—	—	—	—	—	—	0.46
24.52	—	—	—	—	—	—	0.42
26.81	—	—	—	—	—	—	0.41
36.37	—	—	—	—	—	—	0.35
44.02	—	—	—	—	—	—	0.29
49.00	—	—	—	—	—	—	0.00

FABRY-PEROT ETALON

The intensity pattern of a spectral line in the order $(n_0 + n)$ where n is a fraction and n_0 an integer is given for Fabry Perot etalon by

$$I' = \frac{I_0}{1 + F \sin^2 \pi(n_0 + n)} = \frac{I_0}{1 + x^2}$$

where F is the coefficient of fineness and $x = \pi n F$.

The intensity pattern of another spectral line of equal intensity maximum and separated by a small order Δn is given by

$$I'' = \frac{I_0}{1 + F \sin^2 \pi(n_0 + n - \Delta n)} = \frac{I_0}{1 + (x - a)^2}$$

where

$$a = \pi \cdot \Delta n \cdot F$$

The resultant intensity pattern, in the presence of a background intensity, which is equal to k times the intensity maximum, is given by

$$\frac{I}{I_0} = k + \frac{1}{1 + x^2} + \frac{1}{1 + (x - a)^2}$$

Neglecting shrinkage effect, the maximum ($x = 0$ or a) and minimum ($x = a/2$) of the resultant pattern are given by

$$\frac{I_{max}}{I_0} = k + 1 + \frac{1}{1 + a^2}$$

and

$$\frac{I_{min}}{I_0} = k + \frac{2}{1 + a^2/4}$$

For limiting resolution, putting

$$\frac{I_{min}}{I_{max}} = c$$

we have

$$a^4(c + ck - k) - a^2(5k - 5ck + 8 - 6c) - 4(k + 2 - ck - 2c) = 0$$

or

$$a^2 = \frac{(5k - 5ck + 8 - 6c) + \sqrt{(5k - 5ck + 8 - 6c)^2 + 16(c + ck - k)(k + 2 - ck - 2c)}}{2(c + ck - k)} \dots (4)$$

since a is real,

The resolving power of the Fabry Perot etalon is given by

$$\frac{\lambda}{d\lambda} = \frac{n_0}{\Delta n} = \frac{\pi}{\alpha} \cdot n_0 F^{\frac{1}{2}} = \alpha \cdot n_0 F^{\frac{1}{2}} \quad \dots (5)$$

where

$$\alpha = \pi/a \quad \dots (6)$$

and the value of a is given by equation (4).

Table II illustrates the variation of α with k and c . The results have been illustrated in figures 3 and 4.

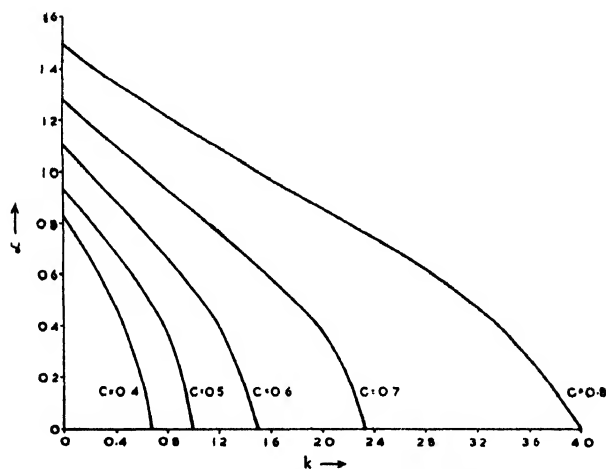


Fig. 3. Variation of α with k and c (0.4–0.8) for F. P. etalon.

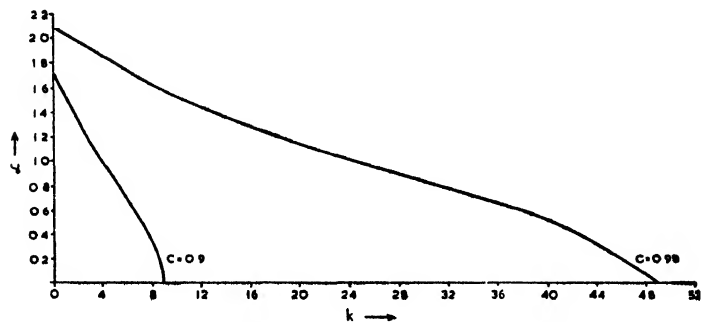


Fig. 4. Variation of α with k and c (0.9–0.98) for F. P. etalon.

TABLE II
Variation of α with k and c for F.P. etalon.

k	$c = 0.4$	$c = 0.5$	$c = 0.6$	$c = 0.7$	$c = 0.8$	$c = 0.9$	$c = 0.98$
0.0	0.82	0.96	1.11	1.28	1.49	1.76	2.10
0.1	0.74	—	—	—	—	—	—
0.2	0.66	0.83	1.00	—	—	—	—
0.4	0.48	0.69	—	1.10	1.34	—	—
0.6	—	0.55	0.78	—	—	—	—
0.666	0	—	—	—	—	—	—
0.8	—	0.38	—	0.93	—	—	—
1.0	—	0	0.55	—	1.15	—	—
1.2	—	—	0.41	0.76	—	—	—
1.5	—	—	0	—	—	—	—
1.6	—	—	—	0.58	—	—	—
2.0	—	—	—	0.38	0.85	1.34	—
2.333	—	—	—	0	—	—	—
3.0	—	—	—	—	0.56	—	—
4.0	—	—	—	—	0	1.01	—
6.0	—	—	—	—	—	0.72	—
8.0	—	—	—	—	—	0.38	—
9.0	—	—	—	—	—	0	—
10.0	—	—	—	—	—	—	1.52
20.0	—	—	—	—	—	—	1.15
30.0	—	—	—	—	—	—	0.84
40.0	—	—	—	—	—	—	0.54
49.0	—	—	—	—	—	—	0

GRATING, REFLECTING ECHELON AND PRISM

The intensity of a spectral line diffracted by a grating or a reflecting echelon is given by

$$\frac{I'}{I_0} = \frac{1}{N^2} \cdot \frac{\sin^2 N\beta}{\sin^2 \beta}$$

where I_0 is the intensity maximum, N is the number of lines of the grating or the number of steps in the reflecting echelon and 2β the phase difference between two adjacent beams.

Putting $x = N\beta$, we have

$$\frac{I'}{I_0} = \frac{\sin^2 x}{x^2}$$

when β is small.

The above expression also represents the intensity distribution in a prism if

$$x = \frac{\pi l}{\lambda} \sin \theta$$

The intensity distribution of another line of the same intensity and an angular separation corresponding to $\Delta x = a$ is given by

$$\frac{I''}{I_0} = \frac{\sin^2(x-a)}{(x-a)^2}$$

The resultant intensity distribution of the two lines, when the background intensity is kI_0 , is given by

$$\frac{I}{I_0} = k + \frac{\sin^2 x}{x^2} + \frac{\sin^2(x-a)}{(x-a)^2}$$

Neglecting shrinkage effect the intensity maximum ($x = 0$ or a) and minimum ($x = a/2$) of the resultant pattern are given by

$$\frac{I_{max}}{I_0} = 1 + k + \frac{\sin^2 a}{a^2}$$

and

$$\frac{I_{min}}{I_0} = k + \frac{2 \sin^2(a/2)}{(a/2)^2}$$

For limiting resolution, putting

$$\frac{I_{min}}{I_{max}} = c$$

we have

$$k = \frac{c}{1-c} \left(1 + \frac{\sin^2 a}{a^2} \right) - \frac{8 \sin^2(a/2)}{a^2(1-c)} \quad (7)$$

The resolving power of the *grating* or the *reflecting echelon* is given by

$$\frac{\lambda}{d\lambda} = \frac{\pi \cdot n}{\Delta\beta} = \frac{\pi}{a} \cdot Nn = \alpha \cdot Nn \quad (8)$$

and the resolving power of the *prism* is given by

$$\frac{\lambda}{d\lambda} = \alpha \cdot t \left(\frac{d\mu}{d\lambda} \right) \quad (9)$$

where

$$\alpha = \pi/a \quad (10)$$

the value of a being given by equation (7).

Table III illustrates the variation of α with k and c . The results have been illustrated in figures 5 and 6.

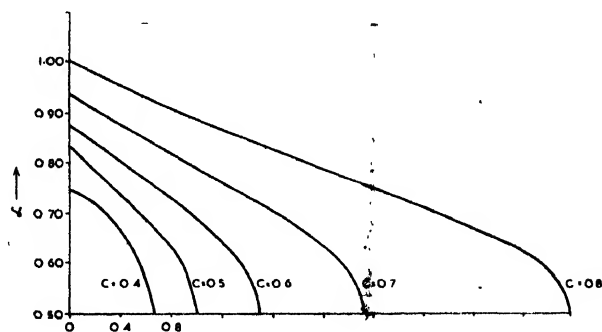


Fig. 5. Variation of α with k and c (0.4—0.8) for grating, reflecting echelon and prism.

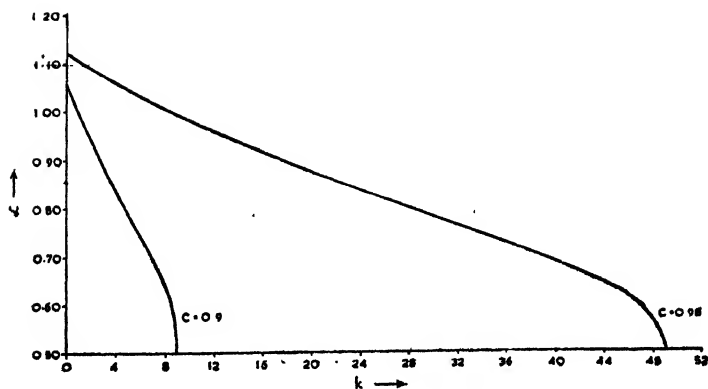


Fig. 6. Variation of α with k and c (0.9—0.98) for grating, reflecting echelon and prism

TABLE III

Variation of α with k and c for grating, reflecting echelon and prism.

k	$c = 0.4$	$c = 0.5$	$c = 0.6$	$c = 0.7$	$c = 0.8$	$c = 0.9$	$c = 0.98$
0.00	—	—	—	—	1.00	—	1.115
0.01	—	0.83	—	—	—	—	—
0.09	—	—	—	—	—	1.05	—
0.17	—	—	—	0.91	—	—	—
0.26	0.71	—	0.83	—	—	1.04	—
0.51	0.63	0.71	—	—	—	—	—
0.63	0.55	—	—	—	—	—	—
0.67	0.50	—	—	—	—	—	—
0.69	—	—	—	0.83	—	—	—
0.76	—	—	—	—	0.91	—	1.11
0.82	—	0.63	—	—	—	—	—
0.89	—	—	0.71	—	—	1.00	—
0.96	—	0.55	—	—	—	—	—
1.00	—	0.50	—	—	—	—	—
1.28	—	—	0.63	—	—	—	—
1.46	—	—	0.55	—	—	—	—
1.50	—	—	0.50	—	—	—	—
1.55	—	—	—	0.71	0.83	—	—
2.05	—	—	—	0.63	—	—	—
2.28	—	—	—	0.55	—	—	—
2.33	—	—	—	0.50	—	—	—
2.83	—	—	—	—	0.71	—	—
3.60	—	—	—	—	0.63	—	—
3.92	—	—	—	—	0.55	—	—
4.00	—	—	—	—	0.50	—	—
4.13	—	—	—	—	—	0.83	—
4.49	—	—	—	—	—	—	1.05
6.72	—	—	—	—	—	0.71	—
6.86	—	—	—	—	—	—	1.02
8.23	—	—	—	—	—	0.63	—
8.47	—	—	—	—	—	—	1.00
8.86	—	—	—	—	—	0.55	—
9.00	—	—	—	—	—	0.50	—
16.69	—	—	—	—	—	—	0.91
24.76	—	—	—	—	—	—	0.83
37.79	—	—	—	—	—	—	0.71
45.28	—	—	—	—	—	—	0.63
48.34	—	—	—	—	—	—	0.55
49.00	—	—	—	—	—	—	0.50

ACKNOWLEDGMENTS

The authors are grateful to Dr. D. S. Kothari, Scientific Adviser to the Ministry of Defence, for permission to publish this paper.

REFERENCES

- Ditchburn, 1930, *Proc. Roy. Irish. Acad.*, **39**, 58.
 Sodha and Sharma, 1954, *Ind. J. Phys.*, **28**, 437.
 Mitra, 1954, *Ind. J. Phys.*, **28**, 543.
 Sodha, 1954, *Ind. J. Phys.*, **28**, 141.

ULTRAVIOLET ABSORPTION SPECTRA OF *o*-METHOXY-PHENOL AND 2, 4, 6-TRICHLOROPHENOL IN DIFFERENT STATES*

S. K. SEN

OPTICS DEPARTMENT, INDIAN ASSOCIATION FOR THE CULTIVATION OF SCIENCE,
JADAVPUR, CALCUTTA-32

(Received for publication, July 18, 1956)

ABSTRACT. Absorption spectra of *o*-methoxyphenol and 2,4,6-trichlorophenol in different states have been studied and the results have been compared with those of chlorophenols reported by previous authors. Raman spectra of the liquids have also been investigated.

Major change is observed to occur in the spectrum of *o*-methoxyphenol on liquefaction of the vapour with a shift of the 0,0 band by 550 cm^{-1} towards longer wavelengths. In the spectrum due to the solid state at low temperatures, the 0,0 band is observed to be displaced towards shorter wavelengths by 100 cm^{-1} from its position in the spectrum due to the liquid and the bands become sharper.

The 0,0 band of 2,4,6-trichlorophenol is also found to shift by 495 cm^{-1} towards longer wavelengths on liquefaction of the vapour. With solidification and cooling down to -180°C , the 0,0 band shifts by 390 cm^{-1} towards shorter wavelengths and the bands are found to be sharper.

By comparing the results with those for chlorophenols it is concluded that the perturbing field resulting in the changes in the electronic spectra depends on the presence or absence of permanent electric moment. So, it has been suggested that in the case of substituted benzenes, Davydov splitting alone cannot account for the observed changes.

INTRODUCTION

Swamy (1953) reported some changes in the absorption spectra of chlorophenols in the solid state at low temperature, the changes depending on the nature and relative positions of the substituents. The 0,0 band of *o*-chlorophenol was found to shift by 272 cm^{-1} towards shorter wavelengths with solidification of the liquid and cooling down to -180°C , while there was a smaller shift in the case of *p*-chlorophenol. Shifts of the 0,0 bands were also observed in the case of *o*-, *m*- and *p*-cresols (Swamy, 1952) with the change from the liquid to solid state at low temperatures. In the case of *p*-cresol, the companions of the 0,0 band could be represented by transitions to higher harmonics of the mode of frequency of the carbon ring. In order to find out the nature of the influence of intermolecular field on the absorption spectra of other substituted phenol compounds at low temperatures the ultraviolet absorption spectra of *o*-methoxy phenol

* Communicated by Prof. S. C. Sirkar.

($\text{OHC}_6\text{H}_4\text{CH}_3\text{O}$) and 2, 4, 6-trichlorophenol ($\text{OHC}_6\text{H}_2\text{Cl}_3$) in different states have been studied in the present investigation and the results have been compared with those due to other substituted phenols. As no data were available regarding the absorption spectra of these two compounds in the vapour state, these spectra have, therefore, been investigated in order to find out the changes which take place in the spectrum with liquefaction of the vapours. A tentative analysis of each of these two spectra has also been included.

EXPERIMENTAL

Chemically pure samples of *o*-methoxyphenol (E. Merck) and 2, 4, 6-trichlorophenol (Scherring-Kahlbaun, Berlin) were distilled several times under reduced pressure before being used in the present investigation.

The experimental set up was the same as that used in an earlier investigation by the author (Sen, 1955). Spectrograms were taken on HP3 films with a Hilger EI quartz spectrograph having a dispersion of 3 A.U. per mm in the region 2600\AA . The absorption spectrum of *o*-methoxyphenol in the vapour state at room temperature was photographed with a sealed absorption tube of length 30 cm. and of diameter 14 mm, quartz windows being cemented to the ends of the tube with Araldite. The spectrum of 2,4,6-trichlorophenol in the vapour state required a similar tube of length 50 cm. which was also evacuated and then sealed. The tube in this case was kept at 85°C by means of an electric heater, the liquid container attached to the tube being kept at a temperature at least 10°C below that of the tube by means of another heater. The time of exposure required in the case of the spectra due to the vapour state was one hour. Very thin films of thickness of the order of a few microns were required for the spectra due to the liquid states, the time of exposure varying from 10 to 15 minutes. The spectra due to the solid state were photographed with one hour's exposure in each case. Iron arc spectrum was photographed on each spectrogram as comparison. Microphotometric records were obtained with a self-recording microphotometer supplied by Kipp and Zonen. The frequencies of the bands were measured using the microphotometric records of the iron lines and superposing records of two known iron lines as reference lines on the record due to the absorption spectrum by making linear scratches on the latter spectrum in place of these two lines.

RESULTS

The microphotometric records of the spectrograms due to the substances in the liquid, solid and vapour states are given in figures 1 and 2. The frequencies of the bands due to the vapours with probable assignments are given in Tables I and III. Such data for the liquid and solid states are given in Tables II and IV. As usual, the relative intensities are indicated by the letters (s), (m) and (w) respectively.

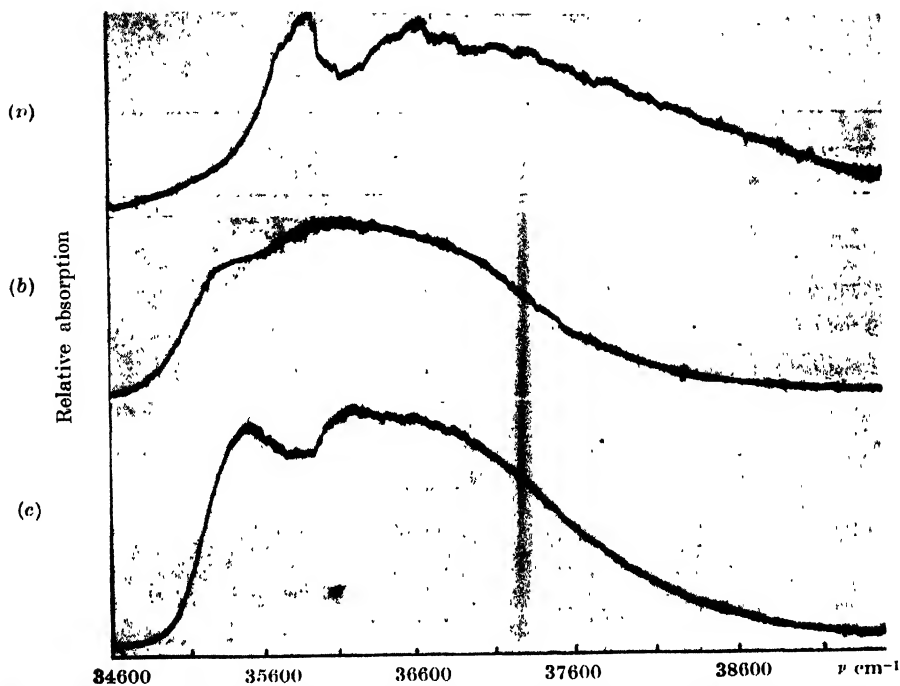


Fig. 1. Microphotometric records of the ultraviolet absorption spectra of *o*-methoxyphenol: (a) Vapour at 32°C. (b) Liquid at 32°C. (c) Solid at -180°C.

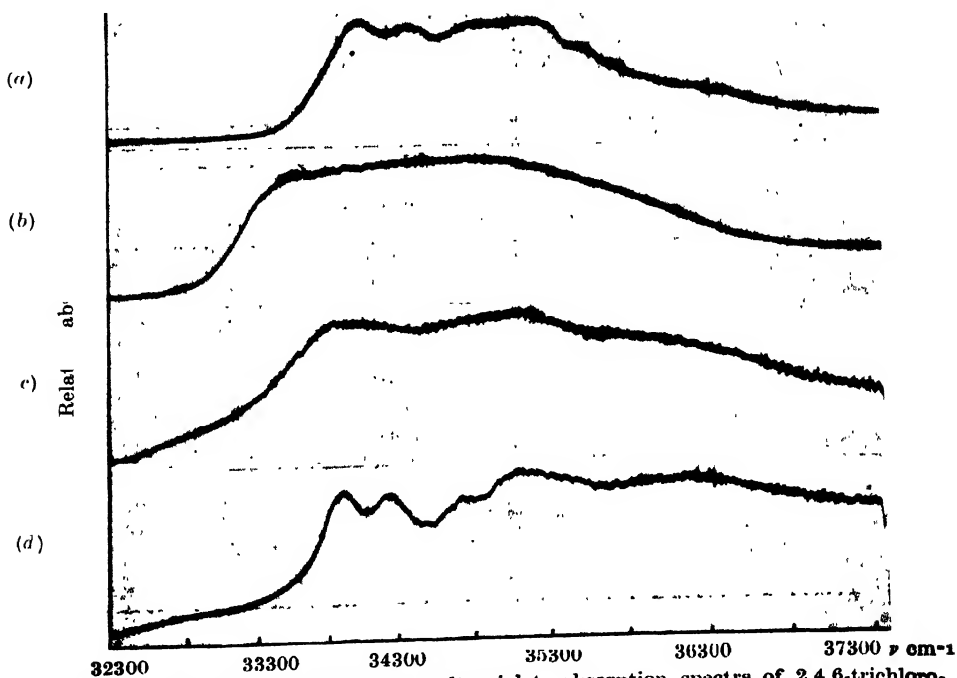


Fig. 2. Microphotometric records of the ultraviolet absorption spectra of 2,4,6-trichlorophenol: (a) Vapour at 85°C. (b) Liquid at 70°C, (c) Solid at 32°C and (d) Solid at -180°C

TABLE I

Absorption bands of *o*-methoxyphenol in the vapour state at 32°C

ν in cm^{-1}	Difference from 0,0 band	Assignment	ν in cm^{-1}	Difference from 0,0 band	Assignment
			36424 (s)	487	0+487
35691 (m)	-246	0-246	36659 (s)	722	0+722
35752 (r)	-185	0-185	36866 (s)	929	0+929
35798 (r)	-139	0-139	37191 (m)	1254	0+323+929
35854 (s)	-83	0-83	37386 (m)	1449	0+722 \times 2
35897 (s)	-40	0-40	37492 (m)	1555	0+163+422+487 \times 2
35937 (s)	—	0,0	37618 (m)	1681	0+237+722 \times 2
36035 (m)	98	0+98	37700 (m)	1763	0+323+722 \times 2
36100 (m)	163	0+163	37886 (m)	1949	0+98+929 \times 2 0+487+722 \times 2
36174 (m)	237	0+237	37959 (w)	2022	0+163+929 \times 2
36260 (m)	323	0+323	38105 (w)	2168	0+722 \times 3
36359 (m)	422	0+422	38346 (w)	2409	0+237+722 \times 3

TABLE II

Absorption bands of *o*-methoxyphenol in the liquid and solid states.

Liquid at 32°C			Solid at -180°C		
ν in cm^{-1}	Difference from 0,0 band	Assignment	ν in cm^{-1}	Difference from 0,0 band	Assignment
35387 (s,vb)	—	0,0	35488 (s,b)	—	0,0
36123 (s,vb)	736	0+736	36009 (s,b)	521	0+521
36862 (w,vb)	1475	0+736 \times 2	36197 (s,b)	709	0+709
			36413 (m,b)	925	0+925
			36717 (w,b)	1229	0+521+709
			36935 (w,b)	1447	0+521+925

TABLE III

Absorption bands of 2,4,6-trichlorophenol in the vapour state at 85°C

ν in cm^{-1}	Difference from 0,0 band	Assignment
34026 (s)	—	0,0
34366 (s)	340	0 + 340
34712 (m)	680	0 + 340 \times 2
34829 (s)	803	0 + 803
35172 (s)	1146	0 + 1146 0 + 340 + 803
35513 (m)	1487	0 + 340 \times 2 + 803 0 + 340 + 1146
35854 (w)	1828	0 + 340 \times 2 + 1146 0 + 340 \times 3 + 803
36317 (w)	2291	0 + 1146 \times 2 0 + 340 \times 2 + 803 \times 2

TABLE IV

Absorption bands of 2,4,6-trichlorophenol in the liquid and solid states

Liquid at 70°C			Solid at 32°C			Solid at -180°C		
ν in cm^{-1}	Diff. from 0,0 band	Assign- ment	ν in cm^{-1}	Diff. from 0,0 band	Assign- ment	ν in cm^{-1}	Diff. from 0,0 band	Assignment
A very broad band extend- ing from 33450 cm^{-1} to 35535 cm^{-1}	—	Long wave- length edge at 33531 cm^{-1} taken as the 0,0 band	33843 (s,b)	—	0,0	33921 (s)	—	0,0
			34845 (w,b)	1002	0 + 1002	34228 (s)	307	0 + 307
			35152 (s,b)	1309	0 + 1309	34683 (m)	762	0 + 762
			35844 (w,b)	2001	0 + 1002 \times 2	35087 (s)	1166	0 + 1166
			36151 (w,b)	2308	0 + 1002 + 1309	35295 (m)	1374	0 + 307 \times 2 + 762
						35854 (w)	1933	0 + 762 + 1166
						36250 (w)	2329	0 + 1166 \times 2

TABLE V

Raman spectrum of *o*-methoxyphenol in the liquid state at room temp.

Reitz and Ypsilanti (1935) $\Delta\nu$ in cm^{-1}	Present author $\Delta\nu$ in cm^{-1}
184 (7b)	183 (4)
237 (3)	238 (1)
308 (5)	305 (2)
349 (4)	348 (2)
458 (3)	455 (0)
492 (3)	495 (4)
536 (6)	537 (4)
583 (5)	581 (3)
726 (2)	
759 (14)	758 (10)
832 (5)	831 (3)
1028 (3)	
1041 (6)	1039 (8)
1159 (8)	1156 (6)
1204 (2)	
1260 (9)	1261 (7)
1302 (4)	1299 (2)
1354 (3b)	1357 (2)
1456 (5b)	1453 (3)
1499 (3)	1497 (1)
1600 (9b)	1598 (7b)
2842 (4)	2840 (2)
2932 (2b)	
3023 (2)	
3071 (9b)	3073 (5b)
3544 (0)	

DISCUSSION

o-Methoxyphenol ($\text{OH C}_6\text{H}_4\text{OCH}_3$)

The absorption spectrum of *o*-methoxyphenol in the vapour state has been analysed assuming the 0,0 band to be at 35937 cm^{-1} . The bands on the longer wavelength side of the 0,0 band give some ground state vibration frequencies which should agree with Raman frequencies which were reported earlier by Reitz and Ypsilanti (1935). The Raman spectrum was also reinvestigated to test the purity of the liquid and the frequencies are given in Table V along with those reported by previous authors. There are two Raman lines at 183 and 238 cm^{-1} and a wing extending upto 145 cm^{-1} in this spectrum. So the ground state vibration frequencies $139, 185, 246 \text{ cm}^{-1}$ may be identified with the Raman frequencies the first one being hidden in the wing accompanying the Rayleigh line in the Raman spectrum. The bands at 40 and 83 cm^{-1} may be due to $\nu \rightarrow \nu$ transitions. The bands show excited state vibration frequencies 98, 163, 237, 323, 422, 487, 722 and 929 cm^{-1} . The corresponding ground state frequencies may be 139, 187, 301, 346, 495, 537, 752 and 1039 cm^{-1} respectively, as given by the Raman spectrum.

The spectrum due to the liquid state shows three very broad bands with the 0,0 band at 35387 cm^{-1} , the frequency difference between successive bands being 736 cm^{-1} . The 0,0 band thus shifts by 550 cm^{-1} towards longer wavelengths with liquefaction of the vapour. Such a shift indicates the influence of strong intermolecular field acting on the molecules which lowers the excited electronic state. In the case of *o*-chlorophenol (Swamy, 1953) practically no shift of the 0,0 band was observed with the change from vapour to liquid phase. It is well known that in the *o*-chlorophenol molecule the chlorine atom is attached to the OH group through a virtual linkage (Pauling, 1939; Ghosh, 1955). It is thus evident that when the chlorine atom is not free to form virtual linkage with the neighbouring molecule no perturbing intermolecular field acts on the electronic state of the molecule in the liquid phase. It is proved by this fact that the shift of the 0,0 band with liquefaction is not due to ordinary Van der Waal forces but it is due to formation of virtual linkages.

With the solidification of the liquid and lowering of temperature to -180°C , the spectrum changes giving sharper bands with the 0,0 band at 35488 cm^{-1} , which is displaced by about 100 cm^{-1} towards shorter wavelengths from its position in the liquid state. The successive bands show progression of excited state vibration frequencies 521 , 709 and 925 cm^{-1} . The shift of the 0,0 band of *o*-chlorophenol (Swamy, 1953) with the change from liquid to solid state at low temperature was slightly larger. Perhaps at short distances the chlorine atom in any molecule has tendency to be attached to the hydrogen atom of the neighbouring molecules although it is already linked to the OH group of the same molecule. Thus it gives scope for formation of associated groups of molecules at low temperatures, thereby causing a larger shift of the 0,0 band. In the present case, with the absence of chlorine atom, the bond between associated groups of molecules may not be rigid enough to diminish the amplitude of angular oscillation considerably at low temperatures giving only a little sharper bands and a smaller shift of the 0,0 band than in the case of *o*-chlorophenol.

2, 4, 6-Trichlorophenol ($\text{Cl}_3\text{C}_6\text{H}_2\text{OH}$)

The absorption spectrum due to 2, 4, 6-trichlorophenol in the vapour state has been studied and a tentative assignment of the bands has been made assuming the 0,0 band to be at 34026 cm^{-1} . As the data for the Raman spectrum were not available, the Raman spectrum of the liquid was also investigated. A feeble Raman spectrum was observed and the Raman frequencies observed are 198 , 387 , 864 , 1154 and 1617 cm^{-1} . The absorption spectrum gives progression of excited state frequencies 340 , 803 , 1146 cm^{-1} which may correspond to the ground state frequencies 387 , 864 , 1154 cm^{-1} as given by the Raman spectrum.

The spectrum due to the liquid state gives a very broad band with its long wavelength edge at 33531 cm^{-1} and extending upto 35535 cm^{-1} . If the 0,0 band

The spectrum due to the substance in the solid state at room temperature gives five broad bands with the 0,0 band at 33843 cm^{-1} displaced by 312 cm^{-1} towards shorter wavelengths from its position in liquid state. The bands get slightly sharpened but they are still very broad and progression of excited state frequencies $1002, 1309\text{ cm}^{-1}$ has been observed. These are probably mean values of different frequencies.

When the solidified mass is cooled to -180°C , seven sharp bands are observed, the 0,0 band being at 33921 cm^{-1} . This band thus shifts by 78 cm^{-1} towards shorter wavelengths when the solid mass is cooled down from room temperature to -180°C . Assignment of the bands shows a progression of excited state frequencies 307, 762 and 1166 cm^{-1} . The sharpening of the bands with lowering of temperature may be due to cessation of angular oscillations owing to the formation of new virtual linkages among the molecules. In the case of *p*-chlorophenol (Swamy, 1953) the 0,0 band was observed to be in the same position both in the vapour and the solid state at low temperature, whereas in the present case in which the molecule has a larger dipole moment the 0,0 band due to the solid state is found to be displaced by 105 cm^{-1} towards longer wavelengths from its position in the vapour state. It may be pointed out that in the theory put forward by Davydov (1948) the perturbing field acting on the electronic state of the molecule in the lattice is determined by the Coulomb forces between the various charges in the atoms of neighbouring molecules, but the results discussed above show that the perturbing field depends on the presence or absence of permanent electric moment in the molecule and also on the nature of substituent atoms in the molecule. It appears, therefore, that in substituted benzenes the Davydov splitting alone cannot account for the observed changes in the electronic spectra.

ACKNOWLEDGMENT

The author is indebted to Professor S. C. Sirkar, D.Sc., F.N.I. for his kind interest and constant guidance throughout the progress of the work.

REFERENCES

- Davydov, A., 1948, *Zhur. eksp. teor. Fiz.*, **18**, 210.
Ghosh, D. K., 1955, *Ind. J. Phys.*, **29**, 450.
Pauling, L., 1939, The nature of the chemical bond, Cornell University Press.
Reitz, A. W. and Ypsilanti Gr. Prinz, 1935, *Monatsh*, **66**, 285-98.
Swamy, H. N., 1952, *Ind. J. Phys.*, **26**, 119.
" 1953, *Ind. J. Phys.*, **27**, 119.
Sen, S. K., 1955, *Ind. J. Phys.*, **29**, 561.

ON THE RADIAL PULSATION OF MAGNETIC STARS

S. P. TALWAR AND J. N. TANDON

DEPARTMENT OF PHYSICS, UNIVERSITY OF DELHI, DELHI

(Received for publication, June 22, 1956)

ABSTRACT. The general equation governing the radial pulsations of magnetic stars has been derived and the integral formula for the frequency of pulsations deduced. The magnetic field is assumed to be continuous across the surface of the star.

The problem of the pulsations of a magnetic star has been the subject of investigation during recent years¹. Schwarzschild (1949); Gjellestad (1952); Ferraro and Memory (1952); Cowling (1952). More recently Chandrasekhar and Limber (1954) deduced an integral formula for the frequency of pulsations of a star in which a permanent magnetic field is assumed to be prevalent. They assumed the field to vanish at the surface of the star which is not always a valid assumption. Keeping this in view we consider in this note the radial pulsations of a star, having body currents so that the magnetic field is continuous across the surface.

Since the mass of a layer at a distance r_0 from the centre of the unperturbed star is conserved during pulsations, we can write the equation of continuity as,

$$\left(\frac{r}{r_0} \right)^2 \frac{\rho}{\rho_0} \frac{\partial r}{\partial r_0} = 1 \quad \dots (1)$$

The equation of motion, choosing the time t and the distance r_0 as the independent variables, can be written in the following form

$$\rho \frac{\partial^2 r}{\partial t^2} = - \frac{\partial p}{\partial r} - \frac{Gm}{r^2} \rho + (\mathbf{j} \times \mathbf{H})_{\text{radial}} \quad \dots (2)$$

where ρ denotes the density, p the pressure, G the gravitational constant. H and j are the magnetic field and the current density, satisfying the equations,

$$\text{Curl } \mathbf{H} = 4\pi \mathbf{j} \quad \dots (3)$$

and

$$\text{div } \mathbf{H} = 0$$

Distinguishing the values of various parameters for the equilibrium configuration by the subscript zero and writing,

$$r = r_0 + \delta r, p = p_0 + \delta p, \rho = \rho_0 + \delta \rho, \mathbf{H} = \mathbf{H}_0 + \delta \mathbf{H}, \mathbf{j} = \mathbf{j}_0 + \delta \mathbf{j}$$

we find that the equations governing the radial oscillations of a small amplitude are

$$\frac{2\delta r}{r_0} + \frac{\partial \delta r}{\partial r_0} = -\frac{\delta \rho}{\rho_0} \quad \dots \quad (5)$$

$$\begin{aligned} \text{and} \quad \rho_0 \frac{\partial^2 \delta r}{\partial p^2} + \left[-\frac{Gm}{r_0^2} \rho_0 + (\mathbf{j}_0 \times \mathbf{H}_0)_{\text{radial}} + \frac{\partial \delta p}{\partial r_0} \right] \left(1 + \frac{2\delta r}{r_0} + \frac{\partial \delta r}{\partial r_0} \right) \\ + \rho_0 \frac{Gm}{r_0^2} \left(1 - \frac{2\delta r}{r_0} + \frac{\delta \rho}{\rho_0} \right) - [(\mathbf{j}_0 + \delta \mathbf{j}) \times (\mathbf{H}_0 + \delta \mathbf{H})]_{\text{radial}} = 0 \quad \dots \quad (6) \end{aligned}$$

where in equation (6) we have used

$$\frac{\partial p_0}{\partial r_0} = -\frac{Gm}{r_0^2} \rho_0 + (\mathbf{j}_0 \times \mathbf{H}_0)_{\text{radial}} \quad \dots \quad (7)$$

which must hold in equilibrium.

For adiabatic pulsations

$$\delta p = \Gamma \frac{\delta \rho}{\rho_0} p_0 \quad \dots \quad (8)$$

Thus using equations (5) and (7) we obtain

$$\frac{\partial \delta p}{\partial r_0} = \Gamma \left[\frac{\delta \rho}{\rho_0} \left\{ -\frac{Gm}{r_0^2} \rho_0 + (\mathbf{j}_0 \times \mathbf{H}_0)_{\text{radial}} \right\} - p_0 \frac{\partial}{\partial r_0} \left(\frac{2\delta r}{r_0} + \frac{\partial \delta r}{\partial r_0} \right) \right] \quad \dots \quad (9)$$

Putting

$$\frac{\delta r}{r_0} = \xi = \xi_0 e^{i\omega t} \quad \dots \quad (10)$$

and using equation (9), the Eddington's equation for radial pulsation, modified in the presence of the permanent magnetic field, takes the form

$$\begin{aligned} \frac{\partial^2 \xi}{\partial r_0^2} + \frac{\partial \xi}{\partial r_0} \left[\frac{4}{r_0} - \frac{Gm}{r_0^2} \frac{\rho_0}{p_0} + \frac{(\Gamma - 1)(\mathbf{j}_0 \times \mathbf{H}_0)_{\text{radial}}}{\Gamma p_0} \right. \\ \left. + \xi \frac{\sigma^2 \rho_0}{\Gamma p_0} + \frac{(4 - 3\Gamma)}{\Gamma} \frac{Gm}{r_0^2} \frac{\rho_0}{p_0 r_0} + \frac{(\mathbf{j}_0 \times \mathbf{H}_0)_{\text{radial}} (3\Gamma + 1)}{\Gamma p_0 r_0} \right] \\ + \frac{[(\mathbf{j}_0 \times \delta \mathbf{H}) + (\delta \mathbf{j} \times \mathbf{H}_0)]_{\text{radial}}}{\Gamma p_0 r_0} = 0 \quad \dots \quad (11) \end{aligned}$$

This equation is true for all types of current distribution, within the sphere, governed by equations (3) and (4).

Now the change in the magnetic field, $\delta \mathbf{H}$, following the motion is given by

$$\delta \mathbf{H} = \text{curl}(\delta \mathbf{r} \times \mathbf{H}_0) + (\delta \mathbf{r} \cdot \text{grad}) \mathbf{H}_0 \quad \dots \quad (12)$$

To simplify matters, we assume

$$\xi_0 = \text{constant} \quad \dots \quad (13)$$

which is a usual assumption made in the theory of adiabatic pulsations of a star (Ledoux, 1945; Chandrasekhar and Limber 1954). Thus equation (12) gives

$$\delta \mathbf{H} = -2 \xi \mathbf{H}_0 \quad (14)$$

which on substitution in equation (3) gives

$$\delta \mathbf{j} = -3 \xi \mathbf{j}_0 \quad (15)$$

Using equations (14) and (15) in equation (11) we get

$$\sigma^2 r_0 = (3\Gamma - 4) \left[\frac{Gm}{r_0^2} - \frac{(\mathbf{j}_0 \times \mathbf{H}_0)_{\text{radial}}}{\rho_0} \right]$$

Multiplying by r_0 and integrating over the entire mass we get

$$\sigma^2 = (3\Gamma - 4) \frac{\Omega + \int \int \int \mathbf{r} \cdot (\mathbf{j} \times \mathbf{H}) d\tau}{I} \quad (16)$$

where $d\tau = r^2 \sin \theta dr d\theta d\phi$, is the volume element, I and Ω denote the moment of inertia and the gravitational energy of the system respectively.

Because the nature of the field outside a star is a matter which is not easily decided, we consider here, for the sake of illustration, the model of current system adopted by Ferraro (1954). The equations (3) and (4) give

$$H_r = -\frac{1}{r^2 \sin \theta} \frac{\partial U}{\partial \theta}, \quad H_\theta = -\frac{1}{r \sin \theta} \frac{\partial U}{\partial r}$$

where U is the Stokes potential given by (cf. Equation (26) Ferraro (1954))

$$U = k \left[\frac{r^4}{10} - \frac{1}{6} R^2 r^2 \sin^2 \theta \right] \quad (k \text{ is a constant})$$

we find

$$\int \int \int \mathbf{r} \cdot (\mathbf{j} \times \mathbf{H}) d\tau = \frac{2}{315} k^2 R^7 - M \quad (17)$$

where M is the magnetic energy of the configuration and therefore the frequency of the radial pulsations is given by

$$\sigma^2 = (3\Gamma - 4) \frac{\Omega + M}{I} \quad \dots \quad (18)$$

This expression is, as expected, identical with that obtained by Chandrasekhar and Limber for the particular case of the magnetic field vanishing at the surface of the star.

This equation (18) clearly shows that the effect of the magnetic field is to decrease the frequency of pulsations. Further, the critical magnetic energy for the dynamical stability of a magnetic sphere is evidently equal to the gravitational energy, since above this limit the frequency of pulsations becomes imaginary. In the model adopted here, the critical polar field H_p is given by,

$$H_p^2 = \frac{42}{25} \frac{GM^2}{R^4} \quad \dots \quad (19)$$

REFERENCES

- Chandrasekhar, S. and Limber, D. N., 1954, *Ap. J.*, **119**, 10.
 Cowling, T. G., 1952, *M.N.*, **112**, 527.
 Ferraro, V. C. A. and Memery, D. J., 1952, *M.N.*, **112**, 361.
 Ferraro, V. C. A., 1954, *Ap. J.*, **119**, 407.
 Gjellestad, G., 1952, *Ann. d'ap.*, **15**, 276.
 Ledoux, P., 1945, *Ap. J.*, **102**, 143.
 Schwarzschild, M.; 1949, **12**, 148.

FLUORESCENCE SPECTRA OF METHYL BENZOATE, *m*-CHLOROTOLUENE AND *m*-BROMOTOLUENE*

D. C. BISWAS

OPTICS DEPARTMENT, INDIAN ASSOCIATION FOR THE CULTIVATION OF SCIENCE,
JADAVPUR, CALCUTTA-32

(Received for publication, July 17, 1956)

Plate XV

ABSTRACT. Fluorescence spectra given by methyl benzoate in the visible region in the solid state at -180°C and in dilute solutions in ethylene chlorhydrin and *n*-heptane have been investigated using ultraviolet light as exciting radiation. An analysis of the bands due to the crystals of the pure substance shows that ν_0 -band is at 25451 cm^{-1} and the other bands are due to transitions in which the various vibrational frequencies of the molecule are coupled with the electronic state of this molecule. The spectra due to the solutions are different from those due to the pure substance and the solvent molecules are observed to exert a great influence on the spectrum.

The fluorescence spectra due to meta chloro- and meta bromotoluene have also been investigated and the results have been compared with the spectra due to other similar molecules.

INTRODUCTION

The fluorescence spectra of a few halogen substituted toluenes in the solid state and in different frozen solutions at -180°C have been studied recently (Sirkar and Biswas, 1956; Biswas, 1956a; 1956b). It has been observed that the nature of the spectrum depends on the relative positions of the substituents in the benzene ring. The study of the fluorescence spectra due to frozen solutions of these compounds shows that the same solvent produces some similar changes in the fluorescence spectra of different ortho substituted or different para substituted toluenes.

Besides the disubstituted benzenes mentioned above, methyl benzoate also produces fluorescence in the visible region in its solid state at low temperature (Biswas, 1955). This compound differs from the above substituted toluenes in having only one long substituent group attached to the benzene ring. It would, therefore, be interesting to investigate how the fluorescence spectrum of this compound is altered by environments and to find out whether the main characteristics of the fluorescence spectrum produced in these compounds are determined by the benzene ring or by the substituent groups. The fluorescence spectra of this compound in different frozen solutions have therefore been investigated.

* Communicated by Prof. S. C. Sirkar.

In earlier investigations only ortho- and para-chlorotoluenes and bromotoluenes were investigated under different conditions. These investigations have been extended to metachloro- and meta bromotoluene and the results have been included in the present paper.

EXPERIMENTAL

The liquid methyl benzoate was supplied by Fisher Scientific Co., N.Y., U.S.A. and meta chloro- and meta bromotoluene were secured from Dr. Theodor Schuchardt and City Chemical Corporation, N.Y. respectively. The liquids were of chemically pure quality and were distilled carefully under reduced pressure before use.

Besides the spectra due to the pure substances in the solid state those due to the frozen solutions of methyl benzoate in ethylene chlorhydrin and *n*-heptane have been studied. The solvents were purified by distillation in the same way as stated above. The purity of these solvents was assured by the fact that they did not produce any fluorescence in the visible region when they were frozen and cooled to -180°C .

The experimental arrangement and procedure adopted in the present investigation were the same as that given earlier (Biswas, 1956a). The spectra were photographed on Ilford Special Rapid plates with the help of two different Fues glass spectrographs of dispersion about 11\AA and 12.5\AA respectively per mm. in the 4046\AA region. The slit width varied from .25 to .75mm.

The fluorescence spectra due to 10% solutions of methyl benzoate in ethylene chlorhydrin and *n*-heptane in the frozen state were studied. The solution in ethylene chlorhydrin formed transparent mass when it was frozen by suddenly dipping it in liquid oxygen while the other solution formed nearly an opaque mass under a similar treatment. The 10% solution in *n*-heptane in the liquid state was also found to exhibit feeble fluorescence.

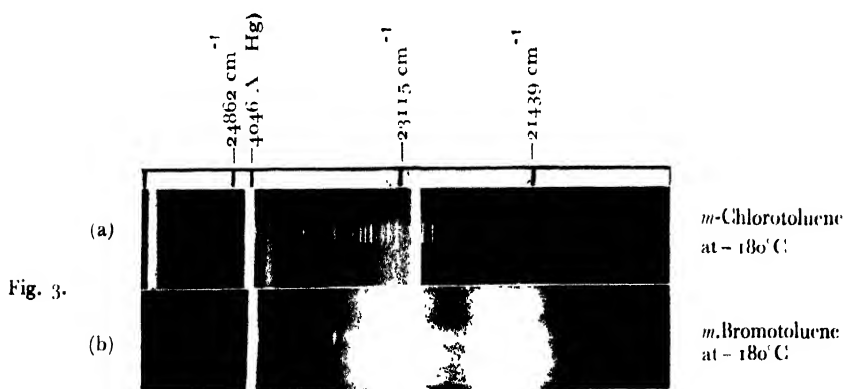
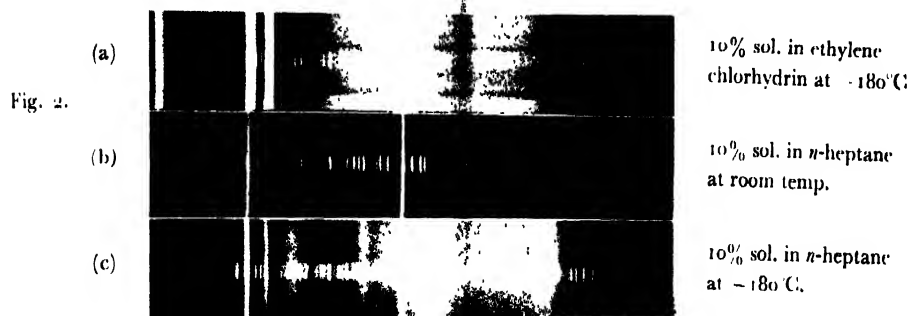
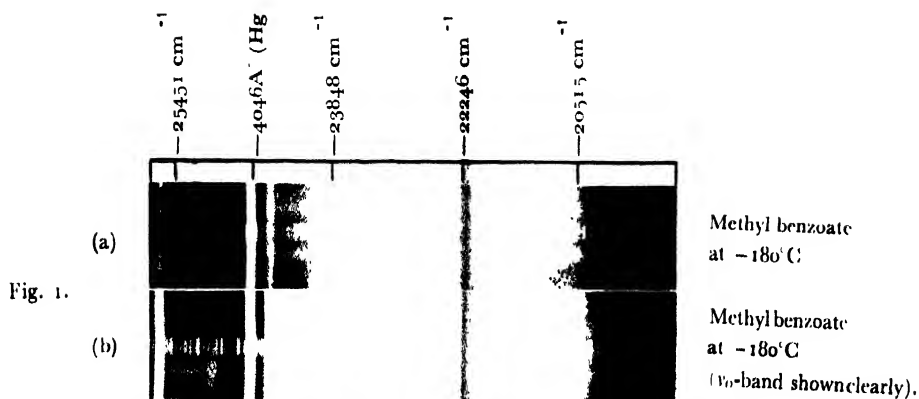
RESULTS AND DISCUSSION

The positions and the relative intensities of the fluorescence bands produced by methyl benzoate under different conditions are given in Table I. Tentative assignments for the fluorescence bands due to the pure substance are also given in Table I. Table II contains the data on the fluorescence spectra of *m*-chloro- and *m*-bromotoluene in the solid state at -180°C . The relative intensities of the bands are indicated as strong (s), medium (m) etc. in the tables.

The spectrograms are reproduced in figures 1, 2 and 3, Plate XV

Bands due to methyl benzoate under different conditions :

Methyl benzoate in the solid state at -180°C produces fifteen fluorescence bands in the visible region and a continuous spectrum extending from 24455 cm^{-1}



Fluorescence Spectra.

to 24066 cm^{-1} . The assignment of these bands due to the pure substance in the solid state given in column 2, Table I shows that the bands can be assigned to transitions in which the vibrational frequencies 174, 219, 360, 1003, 1173, 1600 and 1722 cm^{-1} are involved. These frequencies also correspond to some

TABLE I
Fluorescence bands of methyl benzoate

Pure substance at -180°C		10% sol. in ethylene chlorhydrin at -180°C ν in cm^{-1}	10% sol. in <i>n</i> -heptane at room temp. ν in cm^{-1}	10% sol. in <i>n</i> -heptane at -180°C ν in cm^{-1}
ν in cm^{-1}	Assignment			
25451 (w)	ν_0			
25277 (w)	$\nu_0 - 174$			
25232 (w)	$\nu_0 - 219$	25232 (w)		25207 (v.w)
		24807 (w)		24819 (m)
Continuous fluorescence from 24455 to 24066 cm^{-1}		24276 (v.w)		24189 (m)
				23980 (v.w)
23848 (s)	$\nu_0 - 1603$			23803 (w)
23735 (m)	$\nu_0 - 1716$		23713 (v.w)	
23528 (m)	$\nu_0 - (1720 + 203)$	23601 (s)		23573 (w)
23271 (m)	$\nu_0 - (1600 + 360 + 215)$			23407 (m)
		23168 (s)	23195 (w)	23185 (w)
22726 (m)	$\nu_0 - (1723 + 1002)$	22644 (s)		
			22445 (w)	22542 (s)
22246 (s)	$\nu_0 - 2 \times 1602$			22196 (w)
22128 (m)	$\nu_0 - (1600 + 1723)$			
21924 (m)	$\nu_0 - (1600 + 1722 + 210)$			21996 (w)
21771 (m)	$\nu_0 - (1600 + 1722 + 360)$	21852 (s)		
		21244 (s)	21705 (w)	21761 (m)
21078 (m)	$\nu_0 - (2 \times 1600 + 1173)$		21078 (w)	21398 (w)
20515 (m)	$\nu_0 - (2 \times 1600 + 1736)$	20634 (w)		20862 (s)
			20075 (v.w)	
19930 (v.w)	$\nu_0 - (2 \times 1600 + 1736 + 220 + 365)$	19828 (v.w)		19930 (v.w)?

of the Raman frequencies of the molecule (Biswas, 1955). Hence the bands are due to the molecule of the substance. Of the frequencies mentioned above, the 1600 and 1722 cm^{-1} are those of vibrations of the ring and of the C = O group

respectively. It is observed that the intense bands are due to coupling of these two vibrations with the electronic state.

TABLE II
Fluorescence spectra

Meta chlorotoluene at -180°C ν in cm^{-1}	Meta bromotoluene at -180°C ν in cm^{-1}
24862 (m)	24875 (w)
23578 (m)	23551 (s)
23115 (s)	23110 (s)
21904 (m)	21890 (s)
21439 (s)	21371 (s)
20336 (w)	20258 (m)

The frequencies 360, 1003 and 1173 cm^{-1} are not observed as independent transitions probably because the ν_0 —360 cm^{-1} band is superposed on a mercury line and the other two bands coalesce with other neighbouring bands producing a continuous fluorescence in the region 24455 cm^{-1} to 24066 cm^{-1} . Comparison of the fluorescence spectrum of methyl benzoate with those produced by some halogen substituted toluenes (Biswas, 1956a, 1956b) shows that the spectrum due to the former differs almost entirely from that due to any halogenated toluene. This fact also suggests that the fluorescence is due to the molecule itself.

The fluorescence bands due to solutions of methyl benzoate in ethylene chlorhydrin and in *n*-heptane given in Table I show that the spectrum is quite different from that due to the pure substance. Such a phenomenon is also observed in the case of other organic compounds. For instance, in the case of naphthalene the spectrum due to the pure substance is different from that due to the solution in alcohol (Pringsheim, 1949).

As pointed out previously (Biswas, 1956a) the fluorescence in pure crystal may be due to slight distortion of the molecule produced by association of the molecules with each other and in the case of solutions groups of molecules may be formed by association of molecules of the solvent with those of the solute. As observed previously in the case of chloro- and bromotoluenes, solvents containing chlorine atom or only hydrogen atoms in their molecules produce different changes in the fluorescence spectrum of methyl benzoate. The present results thus confirm the conclusion drawn earlier in the case of chloro- and bromotoluenes that virtual bonds formed through halogen atoms of the solvent produce

changes in the fluorescence spectrum which are different from those produced by the virtual bonds formed through the hydrogen atoms of the solvent.

Bands due to meta chloro- and meta bromotoluene:

The fluorescence spectrum of *m*-chlorotoluene has close resemblance with that produced by any other halogen substituted toluene studied earlier (Biswas, 1956a, 1956b). In the case of the spectrum due to *m*-bromotoluene, however, the relative intensities of the bands differ from those observed in the case of the other halogenated toluenes. In the former case all the bands between 23600 cm^{-1} and 21300 cm^{-1} are almost equally intense while in the latter cases the bands occur alternately with strong and medium intensities. Moreover, in *m*-bromotoluene the bands are, in general, broader and the components of the strong pairs at 23551 and 23110 cm^{-1} and at 21890 and 21371 cm^{-1} respectively are hardly resolved from each other. Further, on comparing the durations of exposure and the widths of the slit employed in these different cases it is observed that the fluorescence in both these meta compounds is much weaker than that of the para- or of the ortho substituted toluenes studied earlier. From the results of these investigations it becomes evident that all chloro- and bromotoluenes exhibit fluorescence bands in the visible region in their solid state at low temperatures.

ACKNOWLEDGMENT

The author is indebted to Professor S. C. Sirkar, D.Sc., F.N.I. for his kind help and guidance during the progress of this work.

REFERENCES

- Biswas, D. C., 1955, *Ind. J. Phys.*, **29**, 503.
 „ 1956a, *Ind. J. Phys.*, **30**, 143.
 „ 1956b, *Ind. J. Phys.*, **30**, 407.
 Pringsheim, P., 1949, *Fluorescence and Phosphorescence*, p. 408.
 Sirkar, S. C. and Biswas, D. C., 1956, *J. Chem. Phys.*, **24**, 470.

ON THERMOLUMINESCENCE SPECTRA

B. C. DUTTA* AND A. K. GHOSH

KHAIRA LABORATORY OF PHYSICS, UNIVERSITY COLLEGE OF SCIENCE AND TECHNOLOGY,
UNIVERSITY OF CALCUTTA

(Received for publication, June 28, 1956)

ABSTRACT. The construction of a rapid-scanning spectrophotometer capable of recording spectrum in one second is reported in this paper. The thermoluminescence spectra of KCl and its analysis, along with a brief description of the demountable cathode ray tube and the temperature recording system used in the experiment, are also given.

INTRODUCTION

In studying thermoluminescence it has been found that peaks in the thermoluminescence glow curves differ in the spectral nature of the emission. Up till now all attempts to record spectrographically the spectrum of the thermoluminescence peaks have failed. The failure is due to the transient nature of the glow and its low intensity. In order to make a detailed study of the spectral nature of various thermoluminescence peaks a rapid-scanning of the weak transient emission is necessary. A spectrophotometer suitable for this purpose has been designed and constructed under the guidance of Prof. S. N. Bose. The part of the paper dealing with its design and construction was reported earlier by Prof. Bose at the International Crystallography Conference, held in Paris in July, 1954.

EXPERIMENTAL TECHNIQUE & EQUIPMENT

The apparatus assembly consists of various parts:

- (1) For excitation - demountable cathode ray tube fitted with sample holder.
- (2) For recording thermoluminescence spectra—a rapid-scanning spectrophotometer with a recording system.
- (3) For recording temperature—a thermocouple and a galvanometer.

The construction of the demountable cathode ray tube of pyrex glass will be clear from figure 1. The finely powdered sample is rubbed on the flat surface of the silver bulb of the sample holder without using any adhesive. The upper part of the sample holder is double-walled and made of brass. Close to the surface where the sample is rubbed, a cromel-alumel thermocouple is mounted to give the temperature of the phosphors. Obviously silver is used to minimise any

* Now at Birkbeck College, London.

temperature difference that may creep in between the phosphor and the thermocouple. Silver specimen-holder, by virtue of its low thermal capacity, is very convenient to heat at a high rate. In the hollow of the silver bulb an electric heater

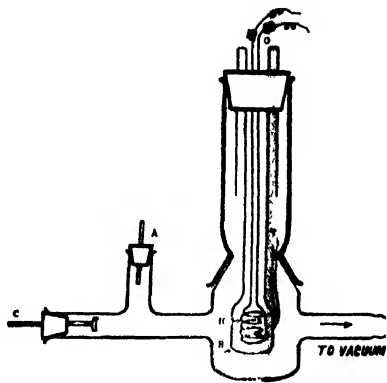


Fig. 1. Diagrammatic representation of the demountable cathode-ray tube.

- A—Anode,
- B—Silver bulb of the sample holder,
- C—Cathode,
- H—Heater,
- T—Thermocouple,
- O—Opening for pouring liquid oxygen.

is fitted, which is run at 20–30 volts and 20–30 amps. current from a transformer. The double-walled portion of the sample holder passes through a rubber cork (as shown in the figure) which can be fitted in a glass cone. Thus the sample holder can be rotated to expose different faces of it to cathode ray, so that fresh surface can be used when necessary. Liquid oxygen is poured in the bulb of the sample holder through the opening at the top which projects outside the discharge tube. A quartz window is provided in the discharge tube. When a vacuum sufficient for cathode discharge is obtained, the bulb of the sample-holder is filled with liquid oxygen to maintain the sample at the low temperature required.

The cathode ray tube is run by a rectified high voltage power unit operating at 10 KV with electronic current of approximately 400 mA. The advantage of using this rectified H.V. power unit is that it protects the sample from the hazards of ionic bombardments. During the thermoluminescence experiments, the sample is initially bombarded continuously for at least ten minutes, so that all the trapping centres might be saturated.

It is seen that, if the initial bombardment is poor, only the shallow traps are filled, while the deeper traps remain inoperative. Thus the yield of the thermoluminescence glow depends somewhat on the initial bombardment, and hence

irradiation is continued for an appreciable amount of time so that the traps may be filled to saturation.

The spectrophotometer consists of two slits, a 60° quartz prism, two concave mirrors, and a plane mirror of stainless steel. The plane mirror is placed on a turning table which is connected to a cam rotated by a synchronous motor so that the mirror oscillates through 3° (approximately) in 9/10ths of a sec., and flies back again to the initial position instantaneously.

The light emitted by the phosphors is collected by a condensing lens system (one convex and one cylindrical) and is concentrated on the entrance slit of the spectrophotometer and it passes on to the collimating concave mirror. The rays of light rendered parallel by reflection from the collecting concave mirror are dispersed by the quartz prism. The dispersed rays are then received by the plane mirror which reflects the ray to a second concave mirror. The rays after reflection from the concave mirror are focussed on the exit slit. The oscillation of the plane mirror causes the spectrum to sweep in front of the exit slit in 9/10ths of a second and to fly back to the initial position instantaneously. A photomultiplier tube of 19 dynodes and of very high gain transforms the weak spectrum on the exit slit into electrical signals which, after suitable amplification, are displayed on a cathode ray oscillograph. The cam drive also supplies the trigger for the horizontal sweep of the oscillograph which makes every spectrum to start at the left and to end at the right of the screen. Thus in every second a curve of the spectral distribution of the emission is obtained on the oscillograph screen. It is photographed with a specially constructed camera with a 3.5 Tesser lens and autosequence release synchronised with the oscillograph sweep. The spectrum calibration of the record is done by taking reference lines of various known sources e.g., He or Hg discharge lamps. Thus the instrument performs the dual role of a spectrograph and a microphotometer and can be very conveniently adopted to carry on studies of (1) fluorescence and phosphorescence, (2) thermoluminescence spectra, (3) temperature-dependence of luminescence (both fluorescence and phosphorescence), (4) correlation of colour centres and other known trapping centres with luminescence, (5) development of emission centres in the phosphor during X-ray or cathode ray irradiation and (6) near infra-red absorption and emission spectra etc. Minor variations of the experimental technique may extend the usefulness of the present apparatus to many other fields.

The various part of the spectrophotometer as shown in figure 2, are rigidly mounted on a horizontal, square ($20'' \times 20''$) heavy cast iron base, supported on a tripod stand with three levelling screws.

The accuracy of the spectroscopic results depends on the proper alignment of the light source, condensing lens system and the entrance slit of the scanning spectrophotometer in relation to one another and of all of them with respect to the first concave mirror. For this purpose, the condensing lens system and the source are mounted on a heavy optical bench 60 cms. long.

The diagram illustrates the optical system of the Van de Graaff generator. It shows a central vertical axis with a 'CORONA DISCHARGE' at the top. Below this, a 'CORONA DISCHARGE' is shown with a 'CORONA DISCHARGE' label. The central part of the diagram shows a 'SLIT (CONTINUOUS)' and a 'SLIT (PULSED)'. The bottom part shows a 'PHOTO TUBE' connected to a 'TO ELECTROMAGNETIC SYSTEM OF THE CAMERA'. The diagram also includes labels for 'OSCILLOGRAM', 'Y AMPLIFIER', 'PULSE AMPLIFIER', 'TO -VE HIGH VOLTAGE', '100V', '10KΩ', '100V', and 'EARTH'.

Concave mirrors. The concave mirrors are of stainless steel having a focal length of 25 cms and aperture $f/4.2$. The collimating concave mirror is placed at a distance of 25 cms from the entrance slit. The mirrors are mounted on a stand with arrangement for raising or lowering them at will (rack and pinion) and also for rotating them about the vertical axis. Additional adjustment facilities are provided for a tight spring and a movable screw which tilts the mirrors

around a horizontal axis. Finally the entire system is fixed to a plate, screwed to the base of the instrument by vertical screws and vertical springs, which make the base of the mirror capable of slight movements around a vertical axis. With these highly flexible arrangements, all possible motions of the mirrors guarantee accurate alignments and correct optical paths, yet obeying the fundamental requirements of rigidity.

Prism and prism table : A 60° quartz prism 4 cms high, is made by cementing together two 30° cornu prisms, one right-handed and the other left-handed. The overall refracting base of the prism is 7 cms and the prism is placed on a two-fold circular prism table with three levelling screws. This is mounted on a vertical support provided with a fixing screw to enable the prism table to be fixed at any suitable height and position around the vertical axis. A micrometer screw, with a large drum-head having 100 divisions, makes the prism table amenable to further small adjustments around the vertical axis and is intended to receive and fix any desired spectral range. This movement may be noted from a straight scale held close to the drum head; the desired wavelength region may be extrapolated from the reading of the scale accurately which in turn has been compared and calibrated with different spectral lines.

Plane mirror : The stainless steel plane mirror is clamped on a vertical stand held upright by a cylindrical tube fixed to the base of the instrument. The mirror-stand is rotatable with a jerk-free motion inside the cylindrical tube by means of two sets of ball bearings fitted at different heights. Slightly above the cylindrical tube which holds it, the mirror-stand has a grooved joint where two circular plates are fitted, the bottom one being rivetted to the lower portion of the stand. The upper plate, containing a fiducial mark, may be rotated slightly relative to the lower one containing a graduated scale. This slight motion which is very helpful in the final stages of alignment, is actuated by means of a slide-screw having movements similar (though differing in mechanical details) to those described in connection with the motion of the prism table.

Cam : The plane mirror stand is connected to a shaft (10 cms). The end of the shaft terminates in a small roller having a frictionless drive on ball-bearings. The roller rests on a cam rotating the plane mirror by 3° . To eliminate objectionable mechanical vibrations, the roller and the camedges are lined with rubber.

Camera : The automatic operation of the camera makes it suitable to record the one-second sequence photographs of the spectra displayed on the oscillograph screen. The camera is coupled with a system, electromagnetically operated, which automatically actuates the advance of the film, cocks the shutter to take exposure – all in perfect synchronisation with the oscillograph sweep. The cam drive of the plane mirror operates a micro-switch which in its turn operates the electromagnet system. A magazine of 50 ft. film can be fed into the camera which makes it possible to photograph thermoluminescence spectra of repeated experiments on the same film.

The photomultiplier is enclosed in an aluminium casing with a small window in front of the photo cathode surface. The space between the photomultiplier tube and the casing wall is filled with a dehydrating silicate jelly in order to prevent any surface leakage.

This high gain, low noise photomultiplier of 19 dynodes is run by a highly stabilized power unit giving variable voltages from 200-2800 volts. The outputs of the stabilized units are connected to the bleeder circuit ($-ve$ H.T. terminals to the photocathode) by means of long, shielded cables. There is a meter on the front panel of the stabilized power supply to give directly the voltage applied to the photomultiplier. As the intensity of the thermoluminescence spectrum is very weak, the photomultiplier out-put current is very very small (only of the order of 5—10 microamps). This low output current is properly amplified by a high-gain amplifying system. The output of the amplifying system is then applied to the vertical plates of the oscillograph. The amplifying system has three fixed gains which are actuated by a band-switch. All the circuit elements are properly shielded.

For recording temperature during thermoluminescence a micro-moll galvanometer, with a time period of 0.3 sec., which is critically damped with suitable resistance, is used. The movements of the galvanometer are recorded on a strip of 35 mm. film of length 40 cms. The galvanometer exciter lamp is operated by a micro-switch coupled with the external sweep of the oscillograph in such a way that when the oscillograph spot comes to the middle position of the oscillograph screen, the microswitch is set on momentarily and a spot of light from the galvanometer excitor lamp focussed by a cylindrical lens (40 cms long), falls on the film strip. At the beginning of each experiment, a spot in the film strip is obtained at liquid air temperature, which serves as the reference spot and the temperature of any subsequent spot can be obtained by measuring the distance of the spot, under consideration, from the reference spot. A few known temperature (starting from liquid oxygen temperature to 300°C) spots are obtained on the film and the distance of each of these spots is measured from the reference spot corresponding to liquid oxygen temperature. Then a graph, drawn with the temperature in $^{\circ}\text{K}$ against the distance of the spot, serves as the calibration curve. The galvanometer is placed on a highly insulated platform which rests on sand to make it free from vibrations. The galvanometer, with the exciter lamp and the film holder, is placed in a wooden chamber under the working table.

The thermoluminescence glow shows variation due to the different rates of heating of the sample, and, in the initial part of the experiment, the rate of temperature rise depends on the amount of liquid oxygen present in the specimen-holder just at the moment when heating is started. So the sample-holder is filled with liquid oxygen up to a fixed height before heating is started.

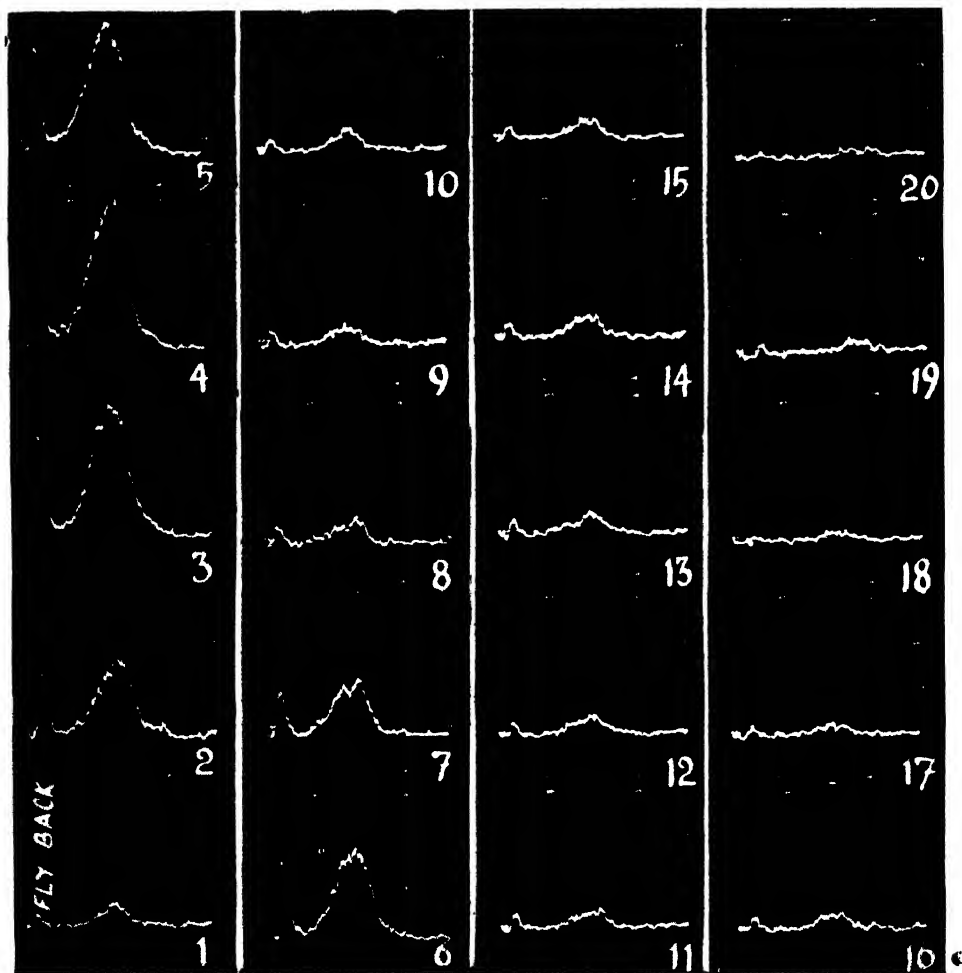


Fig. 3 (a) Thermoluminescence spectra of KCl excited at 90°K.

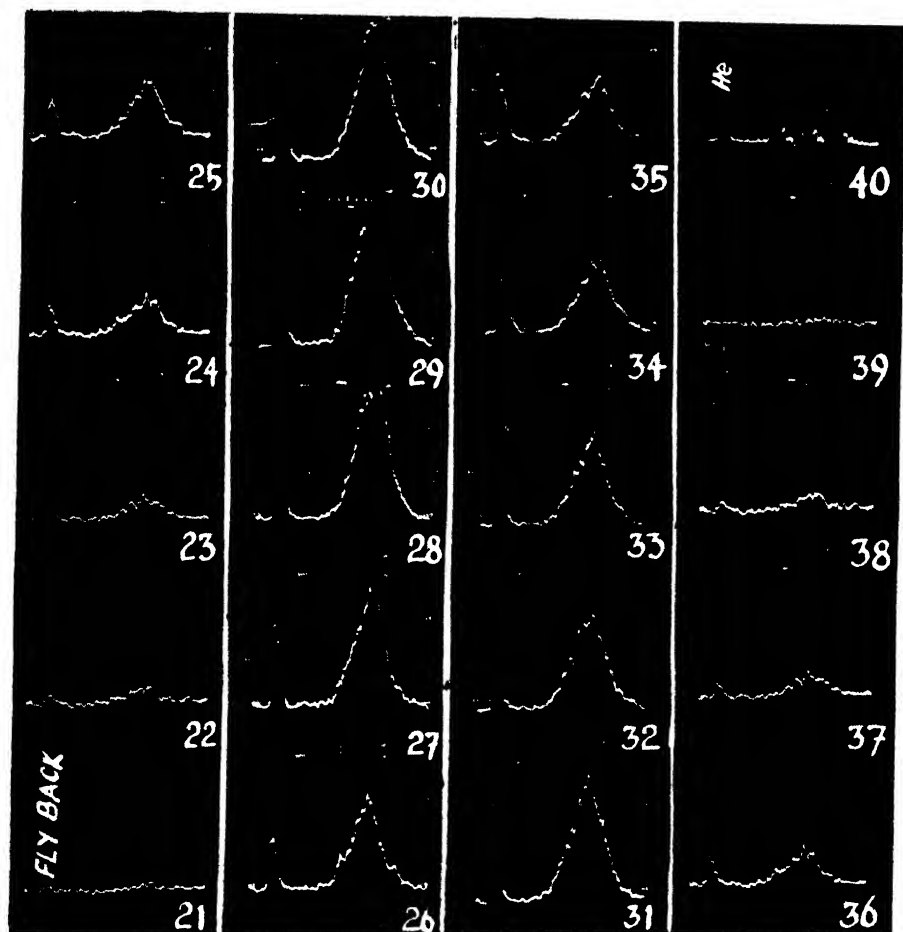


Fig. 3 (b) Thermoluminescence spectra of KCl excited at 90°K.

The experiment is performed in a dark room. After exciting the sample in the dark by cathode rays at liquid oxygen temperature for about 10 minutes or more, the excitation source is cut off. The high voltage power supply for the photomultiplier tube and the heater current of the specimen-holder are switched on. The oscillograph spot-movements are watched, and as soon as the vertical shifts of the oscillograph spot start, the electro-magnet system of the camera and the exciter lamp of the galvanometer are switched on. This is done to save unnecessary wastage of the film. The heating and the recording are continued till the entire stored energy is given out and the sample does not give any more thermoluminescence glow.

EXPERIMENTAL RESULTS

Pure potassium chloride on bombardment with cathode rays at room temperature becomes deep blue and the sample fluoresces weakly. The thermoluminescence glow is too weak for spectroscopic analysis—showing that the energy stored in potassium chloride excited at about 300°K is mostly released by nonradiative mechanism. But this colour at the temperature of liquid oxygen looks pinkish.

The thermoluminescence of potassium chloride excited at 90°K consists of two strong glow peaks at 120°K and 549°K (approximately) and a weaker peak at about 200°K. The peak at 549°K is the strongest. The glow peaks have emissions at different spectral regions. The first thermoluminescence spectrum at 106°K with peak at 434 $m\mu$ is recorded in frame No. 1. There is a gradual increase in the height of the peak up to the frame No. 4, wherein it attains maximum intensity having peak at 440 $m\mu$, half-width extension of 383 $m\mu$ —483 $m\mu$, at a temperature of 120°K. The shape of the bands in frames No. 3-9 appears to be changing. This may be due to temperature shifts towards longer wavelengths which is a common phenomenon. In these spectra, weak appearance of longer wavelength band is perceptible which becomes stronger in the high temperature glow peak. It should be mentioned that exact peak positions of the diffused bands are difficult to measure and the measurements become more uncertain where the emission intensity is poor; the measurements are more reliable near the glow peak temperatures. The emission during the second glow peak (at 200°K) is very poor in intensity and the corresponding spectral nature is very diffuse; this may be seen from frame Nos: 12-21. The peak positions and extensions cannot be measured properly; it can, however, be said that the spectral nature of emission during the second glow peak is not the same as those during the first or the third glow peak; emission here consists of short wavelength (blue) part only.

The third glow peak appears at frame No. 22 corresponding to the temperature 479°K, and it attains maximum intensity in frame No. 29; the spectral nature of emission at different stages of this glow peak has been recorded in frames numbering 22-36 i.e., at temperature between 479°K and 619°K. As may be seen

from the figure (frame No. 22-36) and table, there are distinct changes in the peak position of the thermoluminescence emission band during the third glow peak: shifts in the peak positions are not always in the same direction with increase in temperature. At the low temperature end (frame No. 22; temp. 479°K) the emission band shows a peak at 510 m μ ; near about the glow temperature (frame No. 28—29; temperature 439°K—549°K) the thermoluminescence is comparatively rich in longer wavelength emission and shows a peak at 525 m μ ; at still higher temperature band maximum shifts towards short wavelength, e.g. at 619°K band maximum is at 513 m μ .

TABLE I

Potassium chloride excited at 90°K.

Frame No.	Peak m μ	Half-width m μ	Temperature °K
1	434	—	106
2	432	385—481	110
	590		
3	432	372—483	115
4 (Max)	440	383—483	120
	590		
5	430	380—483	125
6	430	380—483	131
7	409	—	137
	448		
8	409	—	145
	448		
9	430	—	153
10	440	—	161
11	440	—	169
12	440	—	177
13	440	—	185
14—21	(Max, at 200°K corresponding to Frame No. 15)		
22	510	—	479
23	513	—	489
24	513	455—582	499
25	513	453—582	509
26	513	453—582	519
27	513	453—582	529
28	525 (out of scale)		539
29 (Max)	525 (out of scale)		549
30	525	462—580	559
31	520	462—580	569
32	518	456—602	579
33	515	451—602	589
34	515	451—602	599
35	513	451—602	609
36	513	—	619

Dutton and Maurer (1953) have measured the electrical conductivity of X-rayed potassium chloride during heating of the sample from the low temperatures and have found two conductivity peaks (temp. 128°K and 205°K) associated with changes in colour centres. They have also noticed thermoluminescence accompanying the conductivity peaks.

They have ascribed the peak at 128°K to the destruction of V_1 -band. Sharma (1952) has found that the V_2 -band disappears with the peak at 205°K; which Dutton and Maurer have ascribed to F' -centre. But in our measurements it is found that the peak at about 200°K is the weakest of the three. Dutton and Maurer have worked with single crystal while Sharma has used powdered sample. Sharma detected the bleaching of the bands by measuring the total diffuse reflectance of light monochromatised by filters. Further, the thermoluminescence curves for potassium chloride recorded by Sharma as also by Bose (1955) are distinctly different from that observed in the present investigation. The second glow peak at 200°K is very poor in intensity compared to the first and third glow peaks, whereas the second glow peak is very strong compared to others in the measurements of Sharma and Bose. This difference in thermoluminescence characteristics may be due to thermal history of the sample and is not well understood at present. The results of the present measurements have better agreement with those of Dutton and Maurer: as such bleaching temperatures reported by these authors are only taken into consideration to interpret the thermoluminescence glow of potassium chloride.

DISCUSSION

Thermoluminescence emission during the first glow peak (120°K) seems to be changing in spectral character with increasing temperature and the short wavelength part (band maximum at 440 m μ) is much more intense compared to longer wavelength band with maximum at 590 m μ (the 590 m μ is only just perceptible in the spectrum). In the next glow peak (at 200°K) the emission is poor and the long wavelength part is no longer perceptible. During the third glow peak (at about 549°K), one of these bands seems to be present in the emission and a strong long wavelength band with maximum at 525 m μ is observed instead. Thus most of the energy is released during this high temperature glow peak. The study of diffuse reflectance measurements show that the highest glow temperature (549°K) of potassium chloride is coincident with the bleaching temperature for F -centres. In this case also we find that bleaching of F -centres is somehow related with thermoluminescence emission, although it is known that optical excitation in F -band does not produce any luminescence. The other two glows peaks occur at the bleaching temperatures of V_1 and F' -centres. The difference in the spectra leads us to the conclusion that the responsible emission mechanisms must be different in each case.

Excitation of potassium chloride at 300°K reduces the luminescence efficiency considerably, so that, on bleaching, intensity of emission is too poor to be recorded. The effect is due to the non-radiative energy levels provided by the higher aggregates of F -centres which are more likely to be produced in this temperature

range. This is a general behaviour with almost all the alkali halides (i.e., intense colouration always reduces the luminescence intensity). In the case of potassium chloride, the effect is very pronounced for excitation at room temperature (300°K).

ACKNOWLEDGMENTS

We are grateful to Prof. S. N. Bose for his valuable guidance and constant interest in the work. Thanks are due to Mr. H. N. Bose for his helpful discussions, and to the Ministry of Education, Government of India, for granting scholarships to both the authors.

REFERENCES

- Dutton, D. and Maurer, R. J., 1953, *Phys. Rev.*, **90**, 126.
Dutton, Heller and Maurer, 1951, *Phys. Rev.*, **84**, 363.
Sharma, J. 1952, D. Phil. dissertation, Calcutta University.
Bose, H. N., 1955, *Proc. Phys. Soc.*, **B68**, p. 249-252.

Letter to the Editor

The Board of Editors will not hold itself responsible for opinions expressed in the letters, published in this section. The notes containing reports of new work communicated for this section should not contain many figures and should not exceed 500 words in length. The contributions must reach the Assistant Editor not later than the 15th of the second month preceding that of the issue in which the Letter is to appear. No proof will be sent to the authors.

DIPOLE MOMENTS OF TRI-SUBSTITUTED BENZENES. PART I

D. V. G. L. NARASIMHA RAO

PHYSICS DEPARTMENT, ANDHRA UNIVERSITY, WALTAIR

(Received for publication, August 27, 1956)

Following the author's previous work on tri-substituted benzenes (Rao, 1955-56) the dipole moments of a few other similar molecules (the substituent groups being Cl and NO₂) are determined in solution in benzene at 30°C. The calculations are extended to include 1, 2, 3 substitution also. The results are presented in the following table.

TABLE

Compound	observed	calculated
2, 4-Dichlorotoluene	1.95 D	1.95
2, 6-Dichlorotoluene]	1.11	0.75
3, 4-Dichlorotoluene	2.95	2.82
4-Chloro 2-Nitrotoluene	3.63	3.68
6-Chloro 2-Nitrotoluene]	2.95	2.83
4-Chloro 3-Nitrotoluene	4.82	4.88
6-Chloro 3-Nitrotoluene	3.11	2.92
2-Chloro 4-Nitrotoluene	4.05	3.88

It will be seen from the table that the agreement between the calculated and the observed values is satisfactory.

Full details will be communicated shortly.

ACKNOWLEDGMENTS

The author is deeply indebted to Prof. K. R. Rao for his kind and invaluable guidance throughout the progress of the work. He is also grateful to the Government of India for the award of a Senior Research Scholarship.

REFERENCES

- Rao Narasimha, D. V. G. L., 1955 *Ind. J. Phys.*, **29**, 49.
„ 1956, *Ibid* ' **30**, 91.

GROWING OF ORGANIC PHOSPHORS FOR SCINTILLATION COUNTERS

RANGALAL BHATTACHARYYA, UMA BASU ROY

AND

SANTIMAY CHATTERJEE

INSTITUTE OF NUCLEAR PHYSICS, CALCUTTA

(Received for publication August 9, 1956)

ABSTRACT. A simple furnace has been designed and constructed for organic phosphor-crystals. The furnace is described and its mode of operation explained. Conditions for good crystal growth are discussed.

INTRODUCTION

Organic compounds, like anthracene, stilbene, diphenyl, etc. are now commonly used for detection of nuclear radiations when they are used in conjunction with photomultipliers. There are three main features which a phosphor must possess in order to be useful as a radiation detector, viz. (a) the material should be crystallisable in big form so that the mass absorption coefficient for γ -rays is high, (b) the fluorescent band produced by the phosphor when excited by the incident radiation should correspond to the spectral response of the photomultiplier tube, (c) the scintillation decay time should be very small. A simple arrangement for growing fairly large-size organic crystals which conform to the above three features to a quite satisfactory extent and can be conveniently used for detecting alpha, beta and gamma rays is presented in what follows. A review on the mechanism of crystal growth has been published in the Proceedings of Faraday Society (1949), No. 5.

Growing of organic crystals for scintillation counters is greatly affected by the state of purity of the sample used. It has been found that the same material of different manufacturers exhibits different spectral characteristics. Purity of the sample is also important for growing big single crystals. So when samples of of requisite purity are not readily available they have to be purified by the absorption chromatographic methods. It is also important to remove the suspended impurities. Because of the great importance of these crystals, crystal growing has undergone extensive research, theoretical and experimental in all industrial countries. The review of such works can be found in literature. But in most cases technical details are lacking. In the present work we have presented the details as far as necessary.

*Part of this work was reported at the Indian Science Congress in January 1956.

In general organic crystals can be grown from solutions or from melts; for our purpose the latter is most suitable and can be accomplished in two ways (a) the stationary crucible method (Stockberger, 1936, Huber, 1949) and (b) the dropping crucible method (Leninger, 1952). A furnace was erected earlier following the method (a). The temperature control had to be done manually which is extremely tedious.

Later another furnace has been developed using the method of dropping crucible. The same principle has been employed by Leninger for growing stilbene. The furnace developed here is much more simple and can be employed for growing any organic sample having a melting point less than 250°C. The dropping of the crucible was initially automatically controlled by a water-clock which was later replaced by a motor and gear arrangement.

DESCRIPTION OF THE FURNACE

The furnace is described in figure 1. (1) is the melting furnace and consists of a copper tube of diameter 2" and length 13.5" on which nicrome wire has been evenly wound keeping proper insulation and the whole of it again is wound by asbestos paper. (2) is the annealing furnace made of pyrex tubing of diameter 3" and length 19.5" with nicrome wire wound around it. (3) is the crystallising furnace described separately, (4) are soft glass envelopes of diameter 4.8" (4a) is pyrex tube within which the container with the grown crystal rests at the end. (5) is the wheel which supports the crucible through a wire, and the spindle of the wheel is connected to a motor and gear arrangement (6) which controls the rate of fall of the crucible. The whole arrangement rests on a base plate (7) and cast iron structure (8). The current in the two furnaces are separately controlled by two variacs (9). The indicator lamps (10) show whether a furnace is running and the meter (11) records the current. It has been found that during the process of crystallisation the slightest mechanical shock given to the crystal container disturbs the crystal growth and as such the whole arrangement has to be made shock-proof. This is achieved by placing the furnace on sand kept in a wooden box of proper size, the box itself, in its turn, being placed on shock-absorbing rubber-studs (not shown in the diagram).

The crystallising furnace is shown in figure 2. In the crystallising furnace the space between the melting furnace and the annealing furnace is enclosed with heat-insulating material like asbestos. There are two thick brass plates (a) and (b) at top and bottom clamped to syndenio plates (c) and (d) and with a thin walled copper cylinder (e). The whole enclosure is packed with asbestos keeping space for (i) the crystal container to drop vertically at the centre, (ii) a dimetrical hole (f) by which the crystal growth can be seen and (iii) three small horizontal holes for inserting thermocouples to measure temperature. In the viewing hole the mica sheets provide heat insulation.

The sample from which the crystal has to be grown is distilled in an arrangement shown in figure 3, under reduced pressure. The crystal container of pyrex-



Fig. 1

tubing also shown in figure 3 is taken out and sealed. The conical shape of the bottom has been found important and necessary as it facilitates the growth of the seed crystal.

The temperature characteristic of the crystallising furnace is first studied for various values of the currents flowing through the melting furnace and the annealing furnace. It has been found that the temperatures become steady in about four hours and any steady temperature gradient can be maintained inside the crystallising furnace and that is not much affected by the daily variation of the room temperature. The rate at which the container is lowered is also measured

and this rate is controlled by the rate of water drops falling at (6) of figure 1. It is not difficult to obtain a rate of falling of the container equal to $1/8''$ per hour.

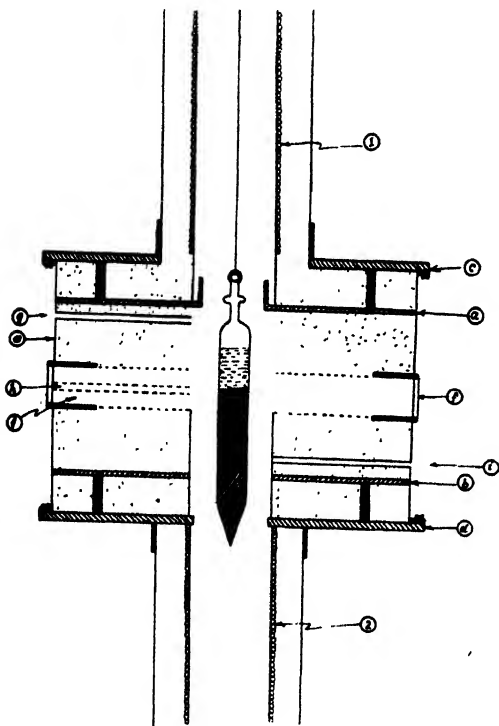


Fig. 2

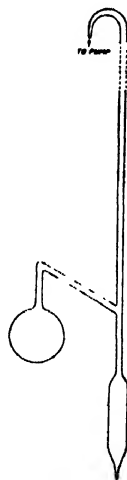


Fig. 3

Growing of the crystal: The sample sealed in the container is hung by means of a fine wire from the wheel above (5) in figure 1, through a fine hole at the centre of the sydenio plate at the top of the melting furnace. The furnaces are mounted vertically so that the container can reach the bottom without touching the sides anywhere. Initial position of the container in the melting furnace is adjusted by putting requisite amount of water on the water-float bath. The furnaces are then started. The melting furnace should be set at about 10°C above the melting point of the sample so that the sample is brought into the liquid state. At a temperature about 3°C above the crystallising temperature the molten mass comes to a viscous state and it has been found that good crystals can not be grown if we start from this state. In the case of diphenyl it is kept at 85°C (melting point 71°C). The temperature at the top of the crystallising furnace has to be kept at about 75°C , 69°C at the middle and about 60° at the bottom. The corresponding temperatures for stilbene are 130°C , 120°C and 103°C respectively. In our case copper-constantan thermocouples have been used to measure these temperatures. Occasionally, during the growth of the crystal these temperatures have to be checked. The thermo-e.m.f. measurements have been made with a Tinsley potentiometer within an accuracy of $\pm 0.5^{\circ}\text{C}$.

With the help of this apparatus single crystals of stilbene and diphenyl have been grown. Fairly large crystals of diameter upto 1" and length 3" have been grown. After cutting and proper polishing they have been used in conjunction

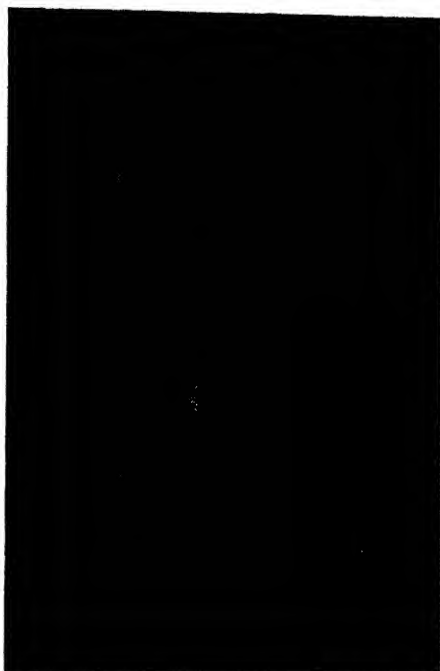


Fig. 4. Photograph of an unpolished stilbene phosphor. The scale is in inches.

with photomultipliers where they have given satisfactory service. A photograph of the crystal is shown in figure 4.

ACKNOWLEDGMENT

The authors are indebted to Late Prof. M. N. Saha, F.R.S. for his constant encouragement and to Prof. A. K. Saha for very helpful suggestions during the progress of the work.

REFERENCES

- Hubér, Von, V. *et al.*, 1949, *Helv. Phys. Acta.*, **22**, 418.
- Leninger, R. F., 1952, *R. S. I.*, **23**, 127.
- Stockberger, D. C., 1936, *R. S. I.*, **7**, 133.

ULTRAVIOLET ABSORPTION SPECTRA OF SOLUTIONS OF BROMOTOLUENES IN ISOBUTYL ALCOHOL AT DIFFERENT TEMPERATURES*

S. B. ROY

OPTICS DEPARTMENT, INDIAN ASSOCIATION FOR THE CULTIVATION OF SCIENCE,
CALCUTTA-32

(Received for publication, July 30, 1956)

ABSTRACT. Ultraviolet absorption spectra of 0.2% and 40% solutions of ortho-, meta- and para-bromotoluene in isobutyl alcohol in the liquid state and in the solid state at -180°C have been investigated and the results have been compared with those obtained in the case of pure substances in different states, as reported by previous workers. The splitting of the absorption bands in the case of ortho- and meta-bromotoluene in the solid state observed by previous workers is found to be absent in the case of 0.2% frozen solution, but the spectrum due to 40% frozen solution in each case shows broad band system which seems to be composed of two systems of bands, one due to 0.2% frozen solution and another due to the pure substance in the solid state. The absorption spectrum of 0.2% solution of para-bromotoluene resembles that due to the vapour and that due to 40% solution resembles that due to the pure liquid. The absorption spectra of frozen solutions of the para compound do not show any splitting as in the case of pure crystals. It has been concluded that splitting of the absorption band is not due to lattice field but may be due to the presence of strongly assymetric groups of molecules in the crystals.

INTRODUCTION

The ultraviolet absorption spectra of the solutions of ortho-, meta- and para-chlorotoluene in isobutyl alcohol in the liquid state and in the solid state at -180°C were investigated recently (Roy, 1956) in order to find out the influence of environments on the nature of absorption spectrum of the molecule in the solid state at -180°C . In the case of the pure ortho- and meta compounds in the solid state at -180°C , Swamy (1952) observed splitting of the band systems, while in the case of the solution in the solid state no such splitting was observed (Roy, 1956). It was concluded that when the molecules are surrounded by similar molecules in the solid state the influence of the intermolecular field is largest, because owing to presence of permanent electric moment the molecules become strongly associated with each other through virtual linkages and such association causes splitting of the energy level. But in the case of the frozen solutions of ortho- and meta-chlorotoluene the molecules are highly dispersed as single molecules and so the influence of the intermolecular field due to molecules of the solvent is not large enough to cause a splitting of the energy level.

* Communicated by Prof. S. C. Sirkar.

Swamy (1953) studied the ultraviolet absorption spectra of ortho- and para-bromotoluene in the solid state at -180°C . In the case of ortho-bromotoluene each absorption band was found to be split up into three components, while in the case of para-bromotoluene no much splitting was observed. Recently, Sen (1956) studied ultraviolet absorption spectra of meta-bromotoluene both in the liquid and solid states at -180°C and observed splitting of the energy level as in the case of the ortho compound in the solid state.

In order to study how the environments affect the intermolecular field when these substances are dissolved in suitable solvents in various proportions and frozen and cooled to -180°C , an investigation of the ultraviolet absorption spectra of frozen solutions of ortho-, meta- and para bromotoluene in isobutyl alcohol of different concentrations was undertaken and the results which are discussed in the present paper support the conclusions drawn earlier (Roy, 1956) that the splitting of the energy level is due to formation of associated groups of the molecules in the solid state.

EXPERIMENTAL

The experimental arrangement in the present investigation was the same as that described in the previous paper (Roy, 1956). The bromotoluenes were of chemically pure quality. The purity of isobutyl alcohol used as solvent was tested by studying its absorption spectrum. All the liquids were distilled under reduced pressure before use. Solutions of two different concentrations were studied. In each case solutions of strength 0.2% and 40% were used. When the dilute solution was frozen it was transparent and homogeneous. In this case the absorption cell, described in the previous investigation (Roy 1956) was used. The 40% solution was translucent in the frozen state. In this case the absorption cell used was the same as that used by Swamy (1952), but the thickness was controlled by using aluminium foil of thickness of the order of .01 mm. A hydrogen discharge tube running at 3 KV served as the source of continuous spectrum. Spectrograms were taken on Ilford HP3 film. Microphotometric records of these spectrograms were taken with a Kipp and Zonen type self-recording microphotometer. Iron arc spectrum was recorded on each spectrogram as comparison. The frequencies of the absorption bands were measured with the help of these microphotometric records of the absorption spectra in which records of the two known iron lines were taken as reference lines, and the records of the iron arc spectrum.

RESULTS

The microphotometric records of the spectra are reproduced in figures 1, 2 and 3 and the wave numbers of the bands and their probable assignments are given in Tables I, II, III, IV, V and VI.

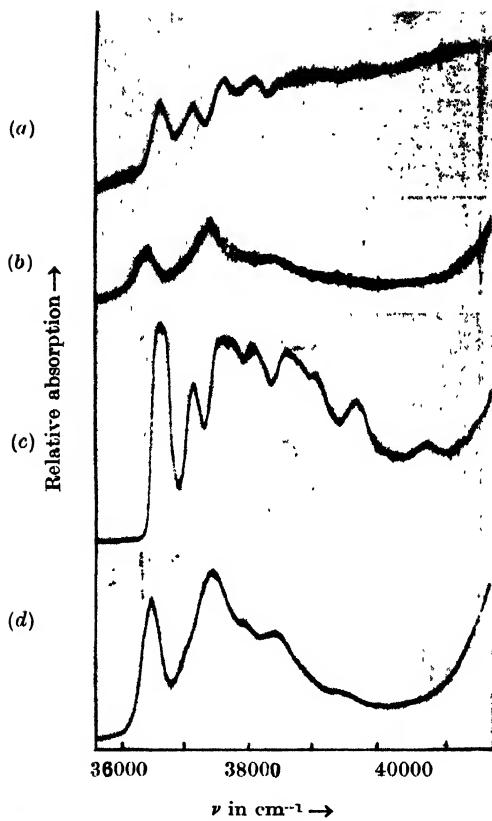


Fig. 1. Michrophotometric records of the ultraviolet absorption spectra of solutions of *o*-bromotoluene in isobutyl alcohol.

- (a) 40 % Frozen solution at -180°C
- (b) 40 % Solution at 30°C
- (c) 0.2 % Frozen solution at -180°C
- (d) 0.2 % Solution at 30°C

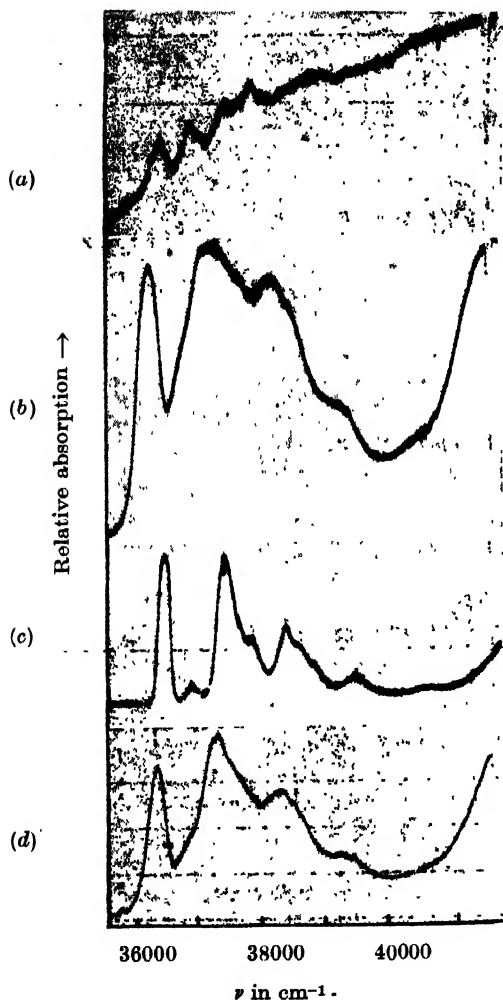


Fig. 2. Microphotometric records of the ultraviolet absorption spectra of solutions of *m*-bromotoluene in isobutyl alcohol.

- (a) 40% Frozen solution at -180°C .
- (b) 40% Solution at 30°C
- (c) 0.2% Frozen solution at -180°C .
- (d) 0.2% Solution at 30°C .

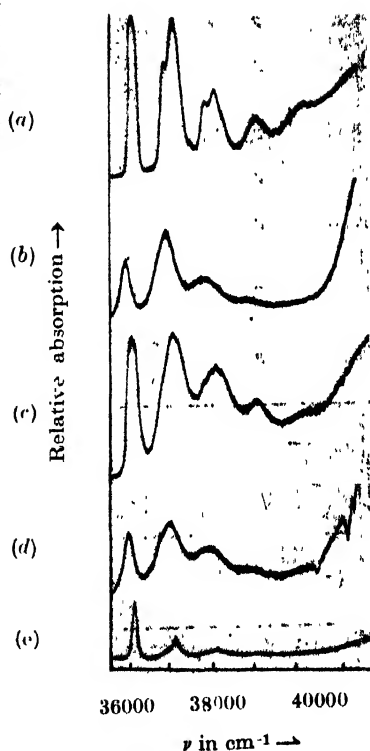


Fig. 3. Microphotometric records of ultraviolet absorption spectra of *p*-bromotoluene and its solution in isobutyl alcohol.

- (a) 40% Solution at -180°C
- (b) 40% Solution at 30°C
- (c) 0.2% Solution at -180°C
- (d) 0.2% Solution at 30°C
- (e) *p*-Bromotoluene at -180°C

TABLE I

Absorption spectra of *o*-bromotoluene

Vapour (Swamy, 1953)		Pure liquid (Swamy, 1953)		Soln. in isobutyl alcohol (Present author)			
ν in cm^{-1}	Assign- ment	ν in cm^{-1}	Assign- ment	0.2%		40%	
				ν in cm^{-1}	Assign- ment	ν in cm^{-1}	Assign- ment
		36450 (Vs,b)	ν_0				
36780	$\nu_0 - 74$			36512 (s)	ν_0	36472 (s)	ν_3
36854	ν_0			36998 (w)	$\nu_0 + 486$		
37280	$\nu_0 + 426$					37456 (s)	$\nu_3 + 984$
37330	$\nu_0 + 476$						
		37432 (S,b)	$\nu_0 + 982$				
37825	$\nu_0 + 971$			37512 (s)	$\nu_0 + 1000$		
37876	$\nu_0 + 1022$						
38796	$\nu_0 + 2 \times 971$			37997 (m)	$\nu_0 + 486$ $+ 1000$		
						38450 (m)	$\nu_3 +$ 2×984
38848	$\nu_0 + 971$ $+ 1022$	38420 (w)	$\nu_0 +$ 2×982	38489 (m)	$\nu_0 +$ 2×1000		
38900	$\nu_0 + 2 \times 1022$						
				39480 (w)	$\nu_0 + 3 \times 1000$		

TABLE II

Absorption spectra of *o*-bromotoluene

Pure solid at -180°C (Swamy, 1953)		Frozen solution in isobutyl alcohol (Present author)			
ν in cm^{-1}	Assignment	0.2%		40%	
		ν in cm^{-1}	Assignment	ν in cm^{-1}	Assignment
36730 (m)	C_0	36646 (V,s)	ν_0	36646 (s,b)	ν_0
36950 (w)	B_0				
37176 (s)	A_0	37117 (m)	$\nu_0 + 471$	37117 (s,b)	$\nu_0 + 471$
37690 (m)	C_1	37641 (s)	$\nu_0 + 995$	37641 (s,b)	$\nu_0 + 995$
37912 (w)	B_1				
38140 (s)	A_1	38111 (s)	$\nu_0 + 471 + 995$	38111 (s,b)	$\nu_0 + 471 + 995$
38655 (m)	C_2	38635 (s)	$\nu_0 + 2 \times 995$	38635 (m,b)	$\nu_0 + 2 \times 995$
38880 (w)	B_2				
39104 (w)	A_2				
\pm		39106 (m)	$\nu_0 + 471 + 2 \times 995$		
		39630 (m)	$\nu_0 + 3 \times 995$		
		40624 (w)	$\nu_0 + 4 \times 995$		

TABLE III
 Absorption spectra of *m*-bromotoluene

Vapour (Sen, 1956)		Pure liquid (Sen, 1956)		Soln. in isobutyl alcohol (Present author)			
				0.2%		40%	
ν in cm^{-1}	Assign-ment	ν in cm^{-1}	Assign-ment	ν in cm^{-1}	Assign-ment	ν in cm^{-1}	Assign-ment
		36197 (s,b)	ν_0				
36359 (s)	$\nu_0 - 167$			36360 (s)	ν_0	36286 (s)	ν_0
36526 (vs)	ν_0			36821 (w)	$\nu_0 + 455$		
36987 (m)	$\nu_0 + 461$					37246 (s)	$\nu_0 + 960$
		37223 (s,b)	$\nu_0 + 1026$	37330 (s)	$\nu_0 + 964$		
37492 (s)	$\nu_0 + 966$			37554 (m)	$\nu_0 + 1188$		
37730 (m)	$\nu_0 + 1204$	38247 (m,s,b)	$\nu_0 + 2 \times 1026$	37781 (m)	$\nu_0 + 455 + 964$	38201 (m)	$\nu_0 + 2 \times 960$
				38302 (m)	$\nu_0 + 2 \times 964$		
		39277 (w,b)	$\nu_0 + 3 \times 1026$	39250 (w)	$\nu_0 + 3 \times 964$	39160	$\nu_0 + 3 \times 960$

 TABLE IV
 Absorption spectra of *m*-bromotoluene

Pure Solid (Sen, 1956)		Frozen soln. in isobutyl alcohol (Present author)			
		0.2%		40%	
ν in cm^{-1}	Assignment	ν in cm^{-1}	Assignment	ν in cm^{-1}	Assignment
36123 (m)	C_0				
36570 (v,s)	A_0	36485 (V,s)	ν_0	36485 (s,b)	ν_0
37004 (s)	B_0	36917 (v,w)	$\nu_0 + 432$	36917 (s,b)	$\nu_0 + 432$
37108 (m)	C_1				
37554 (m)	A_1	37456 (s)	$\nu_0 + 971$	37456 (s,b)	$\nu_0 + 971$
		37667 (m)	$\nu_0 + 1182$	37667 (s,b)	$\nu_0 + 971 + 432$
		37882 (m)	$\nu_0 + 432 + 971$		
37992 (ms)	B_1				
38098 (w)	C_2				
38541 (w)	A_2	38420 (m)	$\nu_0 + 2 \times 971$	38420 (m,b)	$\nu_0 + 2 \times 971$
		38613 (m)	$\nu_0 + 971 + 1182$		
38982 (ms)	B_2	38851 (w)	$\nu_0 + 2 \times 971 + 432$		
		39404 (w)	$\nu_0 + 3 \times 971$		
		40361 (w)	$\nu_0 + 4 \times 971$		

TABLE V

Absorption spectra of *p*-bromotoluene

Vapour (Swamy, 1953)		Pure liquid (Swamy, 1953)		Solution in isobutyl alcohol (Present author)			
				0.2%		40%	
ν in cm^{-1}	Assignment	ν in cm^{-1}	Assignment	ν in cm^{-1}	Assignment	ν in cm^{-1}	Assignment
		35803 (vs,b)	ν_0	35986 (s)	ν_0	35947 (s)	ν_0
36173	ν_0			36754 (m)	$\nu_0 + 768$		
36928	$\nu_0 + 755$	36827 (s)	$\nu_0 + 1025$	36998 (s)	$\nu_0 + 1012$	36957 (s)	$\nu_0 + 1010$
37189	$\nu_0 + 1016$			37767 (m)	$\nu_0 + 768$		
		37849 (w)	$\nu_0 + 2 \times 1025$		$+1012$	37968 (m)	$\nu_0 + 2 \times 1010$
37954	$\nu_0 + 755$			38011 (m)	$\nu_0 + 2 \times 1012$		
	$+1016$						
38205	$\nu_0 + 2 \times 1016$			39020 (w)	$\nu_0 + 3 \times 1012$	38989 (w)	$\nu_0 + 3 \times 1010$

TABLE VI

Absorption spectra of *p*-bromotoluene

Pure solid Present author		Frozen solution in isobutyl alcohol (Present author)			
		0.2%		40%	
ν in cm^{-1}	Assignment	ν in cm^{-1}	Assignment	ν in cm^{-1}	Assignment
36129 (vs)	ν_0	36064 (s)	ν_0	36129 (v.s)	ν_0
36903 (m)	$\nu_0 + 774$	36852 (m)	$\nu_0 + 788$	36903 (m)	$\nu_0 + 774$
37150 (s)	$\nu_0 + 1021$	37081 (s)	$\nu_0 + 1016$	37150 (s)	$\nu_0 + 1021$
37925 (w)	$\nu_0 + 774 + 1021$	37871 (m)	$\nu_0 + 788 + 1016$	37925 (w)	$\nu_0 + 1021 + 774$
38154 (m)	$\nu_0 + 2 \times 1021$	38083 (m)	$\nu_0 + 2 \times 1016$	38156 (m)	$\nu_0 + 2 \times 1021$
		39096 (w)	$\nu_0 + 3 \times 1016$	39176 (w)	$\nu_0 + 3 \times 1021$
		40116 (w)	$\nu_0 + 4 \times 1016$	40200 (w)	$\nu_0 + 4 \times 1021$

DISCUSSION

o-Bromotoluene

It can be seen from Tables I and II that in the case of 0.2% solution of *o*-bromotoluene in isobutyl alcohol in the liquid state, the position of the 0,0 band is shifted towards shorter wavelengths from the position of the 0,0 band due to

pure liquid by 60 cm^{-1} and from its position in the vapour state by 342 cm^{-1} towards longer wavelengths. Thus the influence of the solvent molecules is a little smaller than that due to the molecules of the pure substance. When this solution is frozen the 0,0 band shifts by 130 cm^{-1} towards shorter wavelengths. On comparing the absorption spectrum of 0.2% frozen solution of *o*-bromotoluene with that due to the pure substance in the solid state as reported by Swamy (1953), it is found that the splitting of the band system into three systems observed in the case of the crystals of the pure substance does not take place in the case of 0.2% solution in the solid state. But the 0,0 band due to the frozen solution is shifted by about 208 cm^{-1} towards longer wavelengths with respect to the 0,0 band due to the vapour state. This shift of the 0,0 band shows that in the solid state the alcohol molecules surrounding the *o*-bromotoluene molecules exert a strong influence on the electronic energy level of the molecule, but the energy level is split up into three components only when the *o*-bromotoluene molecules are surrounded by the same molecules. The absorption spectrum due to a 40% solution of *o*-bromotoluene in the solid state shows that in this spectrum, the band system due to the pure substance in the solid state is superposed on that due to 0.2% solution in the frozen state. These results could be interpreted by assuming that the splitting of the bands is caused by the lattice field in the crystals of the pure substance and as the molecules are dispersed in the 0.2% frozen solution the lattice is absent and the splitting does not occur. If the above assumption were correct, it would be necessary to conclude that in 40% solution at -180°C some crystallites of the pure substance are present. Attempts were made to find out whether small crystals of *o*-bromotoluene separate out when the 40% solution is cooled. It was found, however, that the whole mixture freezes almost simultaneously and the frozen mass appears to be opaque. This shows that the molecules of *o*-bromotoluene are mixed up with those of the alcohol in the solid state. Probably most of them remain in small groups of associated molecules in the 40% frozen solution and as single molecules in 0.2% solution, so that the latter appears to be quite transparent while the former is opaque owing to the difference in the refractive indices of the groups of *o*-bromotoluene molecules. Hence it is to be concluded that the splitting of the energy level is due to the formation of such groups in 40% solution at -180°C and in the pure crystals of *o*-bromotoluene.

m-Bromotoluene.

It can be seen from Tables III and IV that in the case of 0.2% and 40% solution of *m*-bromotoluene in isobutyl alcohol in the liquid state the 0,0 band is displaced by about 160 cm^{-1} and 240 cm^{-1} respectively towards longer wavelengths with respect to its position in the spectrum due to the vapour phase. This shift in the case of the pure liquid is about 323 cm^{-1} . In the case of 0.2% solution the bands can be assigned to progressions of excited state frequencies 455, 964 and 1188 cm^{-1} as in the case of the vapour, but the spectrum due to 40%

solution in the liquid state resembles that due to the pure liquid with the difference that the excited state frequency 1026 cm^{-1} in the liquid state diminishes to 966 cm^{-1} in the case of 40% solution. When the solutions are frozen and cooled to -180°C , the 0,0 band due to 0.2% solution shifts further towards its position in the vapour state while that due to 40% solution seems to be a broad band composed of the 0,0 band due to the frozen 0.2% solution and that due to the pure crystal. In this case also the molecules are probably present in small groups as in the case of ortho compound.

p-Bromotoluene.

It can be seen from Tables V and VI that the absorption spectra of 0.2% solution of *p*-bromotoluene in isobutyl alcohol can be assigned to progressions of two excited state frequencies 768 cm^{-1} and 1012 cm^{-1} as in the case of the vapour. The absorption spectra due to 40% solution is almost similar to that due to pure liquid, the bands due to the progressions of excited state frequencies 755 cm^{-1} being absent. The displacement of the band system with the changes of state observed in this case is much smaller than that in the case of the ortho- or meta compound. Also the spectrum due to the pure crystals does not indicate any splitting of the bands observed in the case of the other two isomers. If the splitting would be due to the lattice field, it would take place in this case also. So the absence of any splitting in this case indicates that the splitting is not due to lattice field, but it is due to presence of strongly asymmetric groups of molecules in the crystal. Probably, owing to the small value of dipole moment in the *p*-bromotoluene molecule, the molecules do not form large groups of associated molecules. The small shift of the 0,0 band with liquefaction of the vapour, however, indicates that the intermolecular field has a small influence on the position of 0,0 band and this may be due to the formation of small symmetric groups. In the solid state the regular distribution of such groups around any molecule may diminish the resultant intermolecular field acting on the molecule.

Investigations with other liquids are in progress.

ACKNOWLEDGMENT

The author is indebted to Professor S. C. Sirkar, D.Sc., F.N.I. for his guidance throughout the progress of this work.

REFERENCES

- Roy, S. B., 1956, *Ind. J. Phys.*, **30**, 267.
- Sen, S. K., 1956 (unpublished results).
- Swamy, H. N., 1952, *Ind. J. Phys.*, **26**, 445.
- „ 1953, *Ind. J. Phys.*, **27**, 119.

EFFECT OF BACKGROUND INTENSITY ON RESOLVING POWER OF LUMMER GEHRCKE PLATE AND TRANSMISSION ECHELON

K. C. CHATURVEDI AND M. S. SODHA

156-D, KAMLA NAGAR, DELHI-6.

(Received for publication May 2, 1956)

ABSTRACT. This communication discusses the effect of background intensity on the resolving power of Lummer-Gehrcke plate and transmission echelon. A table and five figures illustrate the variation of resolving power with background intensity for various values of N_e and α .

INTRODUCTION

Sodha (1954) has discussed the effect of background intensity on resolving power of prism, grating, reflecting echelon and Fabry Perot etalon, when natural line width is negligible on Rayleigh's criterion for resolution of spectral lines. In this paper the effect of background intensity on resolving power of Lummer-Gehrcke plate and transmission echelon has been investigated.

INTENSITY CONSIDERATIONS

The intensity distribution of a spectral line diffracted by a Lummer-Gehrcke plate (Sodha, 1952) and transmission echelon (Sodha, 1953) is given by

$$\frac{I'}{I_0} = \frac{(1-a^N)^2 + 4a^N \sin^2 N\beta}{(1-a)^2 + 4a \sin^2 \beta} \quad \dots (1)$$

where N is the number of interfering beams,

2β is the phase difference between two adjacent beams,

$\alpha = e^{-kt/2}$, t being the height of a step and k the absorption coefficient of the material for transmission echelon,

and $a = Re^{-kt \sec \theta}$, R being the reflecting coefficient and t the thickness in case of L.G. plate.

The intensity distribution of another line of the same intensity and angular separation $\Delta\beta$ is given by

$$\frac{I''}{I_0} = \frac{(1-a^N)^2 + 4a^N \sin^2 N(\beta - \Delta\beta)}{(1-a)^2 + 4a \sin^2(\beta - \Delta\beta)} \quad \dots (2)$$

Hence the resultant intensity pattern of the two lines in presence of a background intensity, k times the intensity maximum of the two lines, is

$$\frac{I}{I_0} = \frac{k(1-a^N)^2}{(1-a)^2} + \frac{I'}{I_0} + \frac{I''}{I_0}$$

$$= \frac{k(1-a^N)^2}{(1-a)^2} + \frac{(1-a^N)^2 + 4a^N \sin^2 N\beta}{(1-a)^2 + 4a \sin^2 \beta} + \frac{(1-a^N)^2 + 4a^N \sin^2 N(\beta-\Delta\beta)}{(1-a)^2 + 4a \sin^2(\beta-\Delta\beta)} \quad \dots \quad (3)$$

The maxima ($\beta = m\pi$ or $m\pi + \Delta\beta$) and minimum ($\beta = m\pi + \Delta\beta/2$) of the resultant intensity pattern are given by

$$\frac{I_{max}}{I_0} = (k+1) \cdot \frac{(1-a^N)^2}{(1-a)^2} + \frac{(1-a^N)^2 + 4a^N \sin^2 N\Delta\beta}{(1-a)^2 + 4a \sin^2 \Delta\beta} \quad \dots \quad (4)$$

and

$$\frac{I_{min}}{I_0} = k \cdot \frac{(1-a^N)^2}{(1-a)^2} + 2 \frac{(1-a^N)^2 + 4a^N \sin^2 N(\Delta\beta/2)}{(1-a)^2 + 4a \sin^2 (\Delta\beta/2)} \quad \dots \quad (5)$$

RESOLVING POWER

Applying Rayleigh's criterion for resolution

$$\frac{I_{min}}{I_{max}} = 0.8$$

and putting

$$\Delta\beta = \frac{\pi}{N_e} \quad \dots \quad (6)$$

we obtain

$$k = \frac{(1-a)^2}{(1-a^N)^2} \left\{ \frac{4(1-a^N)^2}{(1-a)^2} + 4 \times \frac{(1-a^N)^2 + 4a^N \sin^2(N\pi/N_e)}{(1-a)^2 + 4a \sin^2(\pi/2N_e)} \right.$$

$$\left. - 10 \frac{(1-a^N)^2 + 4a^N \sin^2(N\pi/2N_e)}{(1-a)^2 + 4a \sin^2(\pi/2N_e)} \right\} \quad \dots \quad (7)$$

From Eqn. (6) the resolving power of Lummer-Gehrecke plate (Sodha, 1952) and transmission echelon (Sodha, 1953) in the m -th order can be easily shown to be given by

$$R = \frac{\lambda}{\Delta\lambda} = N_e \left\{ m - \frac{2t}{\cos r} \cdot \frac{d\mu}{d\lambda} \right\} \quad \dots \quad (8)$$

for L.G. plate,

TABLE I
Values of k for different (N, a) combinations.

[illegible]

and

$$R = \frac{\lambda}{d\lambda} = N_e \left\{ m - t \cdot \frac{d\mu}{d\lambda} \right\} \quad \dots (9)$$

for transmission echelon.

Table I gives the relationship between N_e and k for various values of N and a as calculated from Eqn. (7). The results have been illustrated in figures 1, 2, 3, 4 and 5.

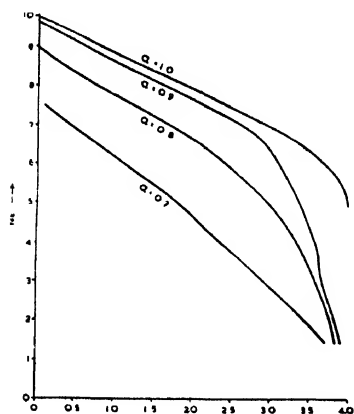


Fig. 1. Variation of N_e with k for $N = 10$.

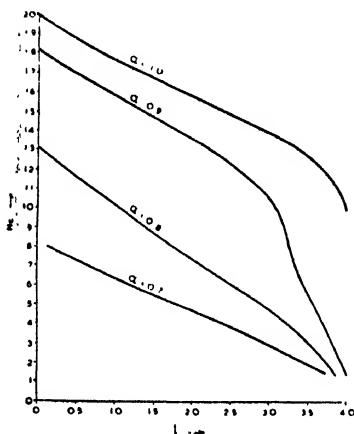


Fig. 2. Variation of N_e with k for $N = 20$.

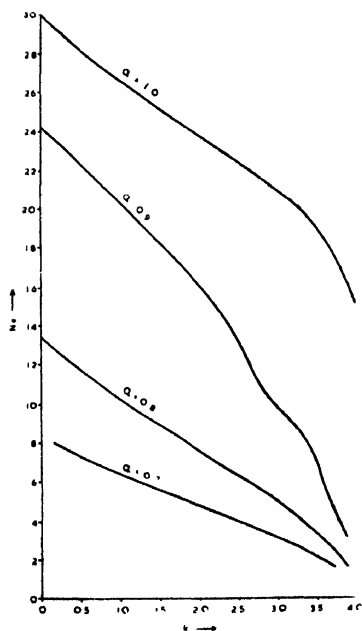


Fig. 3. Variation of N_e with k for $N = 30$.

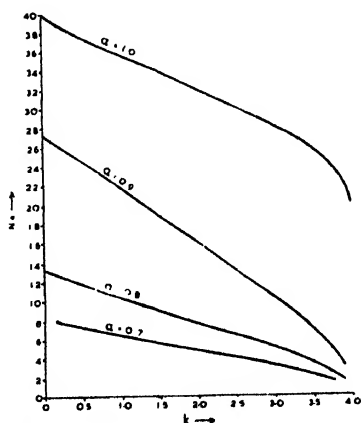


Fig. 4. Variation of N_e with k for $N = 40$.

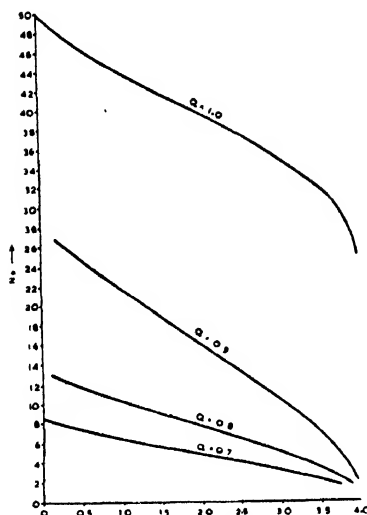


Fig. 5 Variation of N_e with k for $N = 50$.

ACKNOWLEDGMENT

The authors are grateful to Dr. D. S. Kothari, Scientific Adviser to the Ministry of Defence, for permission to publish this paper.

REFERENCES

- Sodha, 1952, *J.S.I.R.*, IIB, 395.
 Sodha, 1953, *Sc. & Cult.*, 18, 489.
 Sodha, 1954, *Ind. J. Phys.* 28, 141.

ERRATA

RESOLUTION OF SPECTRAL LINES OF UNEQUAL INTENSITY

K. C. CHATURVEDI & M. S. SODHA

Indian Journal of Physics, Vol. 30, No. 10.

Page 492, 2nd line from bottom : read $\frac{1}{2I_0} \frac{dI}{dx}$ instead of $\frac{1}{I_0} \frac{dI}{dx}$.

Page 494, Column 4, read $\varphi(a-x_{min})$ instead of $\varphi(a=x_{min})$
 $\frac{1}{b} \varphi(x_{min})$ $\frac{1}{b} \varphi(x_{min})$

Page 496, 12th line from bottom: read $-\frac{1}{2I_0} \frac{dI}{dx}$ instead of $-\frac{1}{2I_0} \frac{aI}{ax}$

Page 498, column 4: read $F(a-x_{min})$ instead of $F(a-xI_{min})$

" " 5 : There is an asterisk above $(a-x_{min})$

" " 8 heading : read $\frac{I_{min}}{I_0}$

" " 9 " : read $\frac{I_{max}}{I_0}$

" " 10 " : read $c = \frac{I_{min}}{I_{max}}$

In Fig. 2 and Fig. 3 the blocks have been interchanged.

ON THE INDUCTION DRAG OF A SPHERE MOVING IN A CONDUCTING FLUID IN THE PRESENCE OF A MAGNETIC FIELD

K. P. CHOPRA

PHYSICS DEPARTMENTS, DELHI UNIVERSITY, DELHI-8

(Received for publication May 20, 1956)

ABSTRACT. In this note the expressions for the induction drag experienced by (1) a uniformly magnetised sphere moving in an inviscid, incompressible, conducting fluid, and (2) an infinitely conducting sphere moving in an incompressible, inviscid and conducting fluid under the influence of an external uniform magnetic field are derived, subject to the condition that the currents do not seriously modify the magnetic field. It is found that the medium behaves as if it possesses viscosity of the order of $(\sigma/c^2)H_0^2a^2$. A comparison with viscous drag shows that the induction drag plays an important role when the condition,

$$H_0 a > c \sqrt{\eta/\sigma},$$

is satisfied. A possible application and limitations of the results are discussed in the last section.

INTRODUCTION

The electromagnetic induction gives rise to many interesting phenomena. If a conducting material, for example, moves through a magnetic field, electric currents are induced in the material. These currents interact with the permanent magnetic field to produce a force called 'induction drag'. Again a sphere moving in an inviscid, incompressible fluid would experience no resistance in the absence of external forces. On the other hand, if the hydrodynamic motion takes place in an electrically conducting fluid in the presence of a magnetic field, it will experience a resistance on account of the above mentioned interaction. The following two cases are of immediate interest:

- 1) The motion of a uniformly magnetised sphere (of intensity H_0) in an inviscid, incompressible fluid of electrical conductivity σ .
- 2) The motion of a sphere of infinite electrical conductivity (and zero magnetic permeability) in an inviscid, incompressible, fluid of electrical conductivity σ , under the influence of an external permanent uniform magnetic field H_0 .

For all points external to the sphere, in either case, it behaves as if a dipole of moment $\mu(=H_0 a^3/2)$ were placed at the centre of the sphere with its axis (1) parallel to the field in the first case, and (2) antiparallel to the field in the second case; 'a' being the radius of the sphere. If H is the dipolar field at any point P ,

(external to the sphere) then the hydrodynamical motion of the sphere interacts with the field \mathbf{H} to produce the induced electric field \mathbf{E} given by

$$\mathbf{E} = \frac{1}{c} (\mathbf{v} \times \mathbf{H}). \quad \dots (1)$$

The induced electric field \mathbf{E} generates currents of density

$$\mathbf{j} = \frac{\sigma}{c} (\mathbf{v} \times \mathbf{H}). \quad \dots (2)$$

The currents thus generated raise the temperature of the fluid. The energy dissipated in this way is characterised by the function,

$$\phi = (\sigma/c^2)(\mathbf{v} \times \mathbf{H})^2. \quad \dots (3)$$

The total rate of dissipation of energy is obtained by multiplying the dissipation function ϕ with the volume element surrounding the point P , and integrating throughout the fluid. The principle of conservation of energy requires this energy to come from the system itself. If R is the resistance experienced by the sphere, then the rate of energy dissipation must equal Rv ; whence R is readily calculated. In the next two sections the expressions for translational drag and resisting moment of the sphere moving under the specified conditions are obtained. The last section deals with the discussion of the results obtained and their limitations.

TRANSLATIONAL DRAG

Consider a dipole of moment $\mu (=H_0 a^3/2)$ moving with uniform velocity v in a direction parallel to the dipole axis. It will be convenient to adopt the spherical polar coordinates with the origin at the centre of the sphere, such that the vector r makes an angle θ with the direction of motion. Then the components of the magnetic field H at any point $H(r, \theta, \phi)$, and the components of velocity are:

$$\left. \begin{aligned} H_r &= \frac{H_0 a^3}{r^3} \cos \theta, & H_\theta &= \frac{H_0 a^3}{2r^3} \sin \theta, & H_\phi &= 0, \\ v_r &= v \cos \theta, & v_\theta &= -v \sin \theta, & v_\phi &= 0. \end{aligned} \right\} (r < a) \quad \dots (4)$$

The induced electric field \mathbf{E} is given by

$$E_r = E_\theta = 0, \quad E_\phi = \frac{3H_0 a^3 v}{2cr^3} \sin \theta \cos \theta. \quad \dots (5)$$

The current density \mathbf{j} has the components

$$j_r = j_\theta = 0, \quad j_\phi = \frac{3\sigma H_0 a^3 v}{2cr^3} \sin \theta \cos \theta. \quad \dots (6)$$

so that the energy dissipation function Φ becomes

$$\Phi = \frac{9\sigma H_0^2 a^6 v^2}{4c^2 r^6} \sin^2 \theta \cos^2 \theta. \quad \dots (7)$$

The rate of energy dissipation is then given by

$$\begin{aligned} Rv &= \int_0^\pi \int_a^\infty \frac{9\sigma H_0^2 a^6 v^2}{4c^2 r^6} \sin^2 \theta \cos^2 \theta \cdot 2\pi r^2 \sin \theta \, d\theta \, dr, \\ &= (2\pi/5)(\sigma/c^2)H_0^2 a^3 v^2. \end{aligned} \quad \dots (8)$$

(Since the term involving r in the integrand is $1/r^4$, the upper limit of r , to a good degree of approximation, is taken as infinity). From (8) the expression for the resistance R , viz.,

$$R = (2\pi/5)(\sigma/c^2)H_0^2 a^3 v, \quad \dots (9)$$

is readily obtained. The expression (9) can also be obtained by calculating the retarding force on the dipole due to the currents given by (6).

ROTATIONAL INDUCTION DRAG

Consider a dipole of moment $\mu (= H_0 a^3/2)$ rotating in an incompressible conducting fluid with a uniform angular velocity ω . Then the components of the magnetic field H at any point $P(r, \theta, \phi)$ and of the velocity v are :

$$\begin{aligned} H_r &= \frac{H_0 a^3}{r^3} \cos \theta, & H_\theta &= \frac{H_0 a^3}{2r^3} \sin \theta, & H_\phi &= 0_{(r>a)}, \\ v_r &= 0, & v_\theta &= 0, & v_\phi &= r\omega. \end{aligned} \quad \dots (10)$$

The induced electric field E produced by the interaction of hydrodynamical motion and the magnetic field has the components

$$E_r = -\frac{H_0 a^3 \omega}{2cr^2} \sin \theta, \quad E_\theta = \frac{H_0 a^3 \omega}{cr^2} \cos \theta, \quad E_\phi = 0, \quad \dots (11)$$

so that

$$E = \frac{H_0 a^3 \omega}{2cr^2} [1 + \cos^2 \theta]^{1/2} \quad \dots (12)$$

This induced electric field E generates currents of density

$$j = \sigma E = \frac{\sigma H_0 a^3 \omega}{2cr^2} \left[1 + \cos^2 \theta \right]^{\frac{1}{2}} \quad \dots (13)$$

and the energy dissipation function Φ is given by

$$\Phi = \frac{\sigma H_0 a^6 \omega^2}{4c^2 r^4} \left[1 + \cos^2 \theta \right] \quad \dots (14)$$

The rate of energy dissipation is then given by

$$D\omega = \frac{4\pi}{3} (\sigma/c^2) H_0^2 a^5 \omega^2, \quad \dots (15)$$

whence the rotational resisting moment D is

$$D = \frac{4\pi}{3} (\sigma/c^2) H_0^2 a^5 \omega. \quad \dots (16)$$

DISCUSSION

The resistance experienced by a sphere of radius a moving uniformly with velocity v in a fluid of coefficient of viscosity η is given by stokes law,

$$R_1 = 6\pi\eta av, \quad \dots (17)$$

while the opposing moment to a sphere rotating with angular velocity ω is given by

$$D_1 = 8\pi\eta a^3 \omega. \quad \dots (18)$$

Equations (9), (16), (17) and (18) combine to give the expressions for total drag and opposing moment of the sphere moving in an incompressible, viscous and electrically conducting fluid, viz:

$$R' = 6\pi av \left[\eta + \frac{1}{15} (\sigma/c^2) H_0^2 a^2 \right] \quad \dots (19)$$

$$\text{and} \quad D' = 8\pi a^3 \omega \left[\eta + \frac{1}{6} (\sigma/c^2) H_0^2 a^2 \right]. \quad \dots (20)$$

The expression $(\sigma/c^2) H_0^2 a^2$ has the dimensions of viscosity, and may be legitimately called 'electro-magnetic viscosity'. The numerical coefficients of this term in the parentheses of (19) and (20) suggest that, unlike ordinary viscosity, electro-magnetic viscosity is anisotropic in nature. Further, the inductive viscosity is important when the inequality,

$$H_0 a > c\sqrt{\eta/\sigma}, \quad \dots (21)$$

is satisfied.

Under the action of inductive viscosity, the kinetic energy of a body of mass m , radius a , and magnetic moment μ moving in a fluid of electrical conductivity σ would fall to $1/e$ -th of its value in a time

$$\tau \sim (\sigma/c^2)^{-1}(ma^3/\mu^2) \quad \dots (22)$$

We speak of τ as the decay time. For values of the various parameters in (22) comparable to those for the sun, viz.,

$$m \sim 10^{34} \text{ gm.}, \quad a \sim 10^{11} \text{ cm.}, \quad \mu \sim 10^{33} \text{ e.m.u.},$$

$$(\sigma/c^2) \sim 10^{-8} \text{ e.m.u.}, \quad (\text{inter-stellar gas ?}),$$

the decay time is $\tau \sim 10$ years.

This value of τ is too small compared with the age of the universe. The difficulty is, however, overcome if we assume that there is no relative motion between the body and a part of the fluid surrounding it to the extent of a radius, say a' . The evidence in support of such a view is not, however, lacking in astrophysics; the outer solar corona has a radius $a' \sim 10a$. According to our calculations, if τ is to be of the order of 10^9 years, a' should necessarily be of the order of $100a$.

This discrepancy is perhaps due, in the first place, to the assumption made in the above calculations, that the currents do not modify the field appreciably. However, if the currents seriously change the field, the picture is completely altered. The changes in H due to these currents cause an electric field to be produced in a direction opposite to $\frac{1}{c}(v \times H)$, thus reducing the currents considerably. When this happens, we must put

$$j = \sigma \left[E' + \frac{1}{c} (v \times H) \right], \quad \dots (23)$$

where

$$\text{curl } E' = - \frac{1}{c} \frac{dH}{dt} \quad \dots (24)$$

This effect is important when the currents flow in large volumes of the fluid say of dimensions $l > 1/4\pi\sigma v$, and is called 'electro-magnetic shielding'. If the shielding is perfect the motion of the sphere is unimpeded, while partial shielding merely increases the decay time. For $a' \sim 10a$, and $\tau \sim 10^9$ years, the shielding should be such that the net electric field is of the order of $10^{-2}(v \times H)/c$.

Apart from electromagnetic shielding, the mechanical effects on the sphere may be reduced by electrostatic shielding in which the electric force $\frac{1}{c}(v \times H)$ is balanced by an electric force E' of electrostatic origin. Here the current

$\frac{\sigma}{c}(v \times H)$ produces a piling up of positive charge in front of itself and of negative charge behind, so that the material becomes polarised. The sphere would proceed unimpeded, if the balance of E' with $\frac{1}{c}(v \times H)$ is very nearly exact. The balance cannot be nearly perfect unless the rate at which the polarisation charge is built up, is far greater than that at which it is dissipated by conduction through the surrounding material.

The electro-static shielding takes place, only if the currents \mathbf{j} satisfy the condition,

$$\text{div. } \mathbf{j} \neq 0. \quad \dots (25)$$

In the case of translational motion, the currents given by (6) do not satisfy this condition. However, in the case of a rotating sphere, the currents \mathbf{j} given by (13) satisfy (25), and it appears that the effect of electro-static shielding on the rotational motion of a magnetised sphere in a conducting fluid is worth investigation.

The detailed calculations of induction drag, taking into account of the shielding effects, appear to be extremely complicated, and will form the subject matter of a subsequent note.

ACKNOWLEDGMENT

The author wishes to thank Prof. D. S. Kothari for suggesting this investigation.

VARIATION OF THE BINDING ENERGIES OF NEUTRONS AND PROTONS IN HEAVY NUCLII

H. K. RAUT

DEPARTMENT OF PHYSICS, RAVENSHAW COLLEGE, UTKAL UNIVERSITY
CUTTACK.

(Received for Publication September 9, 1956)

ABSTRACT. The binding energy of the last neutron and of the last proton for different $N-Z$ values has been calculated from $_{80}\text{Hg}^{202}$ to $_{100}\text{centurium}^{255}$ from current mass data. The variation of binding energy has been studied and graphs have been plotted throughout this range. It has been observed from such studies that there are possibilities for the existence of magic numbers after 82 protons and 126 neutrons.

INTRODUCTION

According to the shell structure of the nucleus there are certain neutron and proton numbers which are called magic. Several nuclear properties show remarkable fluctuations around these numbers. The interest in shell structure began with a review by Mayer (1948) of the experimental information correlating abundance and stability with the higher magic numbers. Peaks in the binding energies for both neutrons and protons in light nuclei were observed at these numbers by Redlich (1952).

The masses of heavier nuclei and their isotopes were not known with sufficient accuracy to permit reliable calculation and to draw specific conclusions. Further, the number of isotopes known were small in number and masses of some of them were not determined. Since a number of data on masses from $_{80}\text{Hg}^{202}$ to $_{100}\text{centurium}^{255}$ have recently been reported by Segre (1953), Green (1955) and Duckworth, Benjamin and Pennington (1954), it was thought worthwhile to calculate and study the binding energies of neutrons and protons for heavy nuclei. The recent values of masses of neutron and neutral hydrogen atom as given by Li, Whaling, Fowler, and Lauritsen (1951) have also been taken into account for this purpose.

CALCULATION AND DESCRIPTION

The binding energy of the last neutron and of the last proton was calculated by the following relations:

$$B_n(A, N, Z) = M(A-1, N-1, Z) + m_n - M(A, N, Z)$$

$$B_p(A, N, Z) = M(A-1, N, Z-1) + m_H - M(A, N, Z)$$

where, B_n = Binding energy of last neutron
 B_p = Binding energy of last proton
 A = Mass number
 N = Number of neutrons
 Z = Atomic number or number of protons
 M = Isotopic mass
 m_n = Mass of the neutron = 1.008982 m.u.
 m_H = Mass of the neutral hydrogen
 Atom = 1.008142 m.u.

The binding energies, thus calculated are given in Table 1.

TABLE 1

Element	(Z)	(A)	(N)	(N-Z)	(M) m.u.	(B_n) m.m.u.	(B_p) m.m.u.
Hg	80	203	123	43	203.03550
		205	125	45	205.03980
Tl	81	203	122	41	203.03499
		204	123	42	204.03679	7.002	6.672
		205	124	43	205.03792	8.032	..
		206	125	44	206.04021	6.692	7.732
		207	126	45	207.04189	7.302	..
		208	127	46	208.04676	4.112	..
		209	128	47	209.05044	5.302	..
		210	129	48	210.05537	4.052	..
Pb	82	204	122	40	204.03612	..	7.012
		205	123	41	205.03831	6.792	6.802
		206	124	42	206.03859	8.702	7.472
		207	125	43	207.04034	7.232	8.012
		208	126	44	208.04140	7.922	8.632
		209	127	45	209.04623	4.152	8.672
		210	128	46	210.04958	5.632	9.002
		211	129	47	211.05450	4.062	9.012
		212	130	48	212.05791	5.572
		213	131	49	213.06268	4.212	..
		214	132	50	214.06633	5.332	..

TABLE I (contd.)

Element	(Z)	(A)	(N)	(N-Z)	(M) m.u.	(B _n) m.m.u.	(B _p) m.m.u.
Bi	83	207	124	41	207.04285	..	3.882
		208	125	42	208.04451	7.322	3.972
		209	126	43	209.04550	7.992	4.042
		210	127	44	210.04951	4.972	4.862
		211	128	45	211.05300	5.492	4.722
		212	129	46	212.05728	4.702	5.362
		213	130	47	213.06072	5.542	5.332
		214	131	48	214.06526	4.442	5.562
Po	84	215	132	49	215.06739	6.852	7.082
		208	124	40	208.04558	..	5.412
		209	125	41	209.04750	7.062	5.152
		210	126	42	210.04826	8.222	5.382
		211	127	43	211.05234	4.902	5.312
		212	128	44	212.05487	6.452	6.272
		213	129	45	213.05922	4.632	6.202
		214	130	46	214.06185	6.352	7.012
		215	131	47	215.06643	4.402	6.972
		216	132	48	216.06919	6.222	6.342
At	85	217	133	49	217.07354	4.632	..
		218	134	50	218.07676	5.762	..
		211	126	41	211.05317	..	3.232
		212	127	42	212.05675	5.402	3.732
		213	128	43	213.05925	6.482	3.762
		214	129	44	214.06299	5.242	4.372
		215	130	45	215.06562	6.352	4.372
		216	131	46	216.06967	4.932	4.902
		217	132	47	217.07225	6.402	5.082
		218	133	48	218.07638	4.852	5.302
Em	86	219	134	49	219.07865	6.712	6.252
		212	126	40	212.05621	..	5.102
		215	129	43	215.06562	..	5.512
		216	130	44	216.06750	7.102	6.262
		217	131	45	217.07155	4.932	6.262

TABLE I (*contd.*)

Element	(Z)	(A)	(N)	(N-Z)	(M) m.u.	(B _n) m.m.u.	(B _p) m.m.u.
Em	86	218	132	46	218.07351	7.022	6.882
		219	133	47	219.07776	4.732	6.762
		220	134	48	220.07993	6.812	6.862
		221	135	49	221.08385	5.062	..
		222	136	50	222.08663	6.202	..
Fr	87	217	130	43	217.07221	..	3.432
		218	131	44	218.07544	5.752	4.252
		219	132	45	219.07747	6.952	4.182
		220	133	46	220.08086	5.592	5.042
		221	134	47	221.08301	6.832	5.062
		222	135	48	222.08674	5.252	5.252
		223	135	49	223.08917	6.552	5.602
		224	137	50	224.09318	4.972	..
Ra	88	219	131	43	219.07824	..	5.342
		220	132	44	220.07950	7.722	6.112
		221	133	45	221.08276	5.722	6.242
		222	134	46	222.08450	7.242	6.652
		223	135	47	223.08788	5.602	7.002
		224	136	48	224.09001	6.852	7.302
		225	137	49	225.09344	5.552	7.882
		226	138	50	226.09574	6.682	..
		227	139	51	227.09982	4.902	..
		228	140	52	228.10212	6.682	..
		229	141	53	229.10448	6.622	..
		230	142	54	230.10555	7.912	..
Ac	89	221	132	43	221.08395	..	3.692
		222	133	44	222.08602	6.012	3.982
		223	134	45	223.08860	7.302	4.042
		224	135	46	224.09147	6.112	4.552
		225	136	47	225.09322	7.232	4.932
		226	137	48	226.09651	5.692	5.072
		227	138	49	227.09845	7.042	5.432
		228	139	50	228.10206	5.372	5.902

TABLE I (contd.)

Element	(Z)	(A)	(N)	(N - Z)	(M) m.u.	(B _n) m.m.u.	(B _p) m.m.u.
Ac	89	229	140	51	229.10366	7.382	6.602
		230	141	52	230.10722	5.422	5.402
Th	90	223	133	43	223.09036	..	4.702
		224	134	44	224.09116	8.182	5.582
		225	135	45	225.09381	6.332	5.802
		226	136	46	226.09525	7.542	6.112
		227	137	47	227.09836	5.872	6.292
		228	138	48	228.09981	7.532	6.782
		229	139	49	229.10279	6.002	7.412
		230	140	50	230.10472	7.052	7.082
		231	141	51	231.10817	5.532	7.192
		232	142	52	232.11034	6.812	..
		233	143	53	233.11382	5.502	..
		234	144	54	234.11650	6.302	..
		235	145	55	235.12037	5.112	..
Pa	91	225	134	43	225.09514	..	4.162
		226	135	44	226.09823	5.892	3.722
		227	136	45	227.09953	7.682	3.862
		228	137	46	228.10200	6.512	4.502
		229	138	47	229.10331	7.672	4.642
		230	139	48	230.10599	6.302	4.942
		231	140	49	231.10783	7.142	5.032
		232	141	50	232.11095	5.862	5.362
		233	142	51	233.11250	7.432	5.982
		234	143	52	234.11586	5.622	6.102
U	92	235	144	53	235.11854	6.302	6.102
		227	135	43	227.10166	..	4.712
		228	136	44	228.10232	8.322	5.352
		229	137	45	229.10469	6.612	5.452
		230	138	46	230.10553	8.142	5.922
		231	139	47	231.10818	6.332	5.952
		232	140	48	232.10947	7.692	6.502
		233	141	49	233.11193	6.522	7.162

TABLE I (contd.)

Element	(Z)	(A)	(N)	(N-Z)	(M) m.u.	(B _n) m.m.u.	(B _p) m.m.u.
		234	142	50	234.11379	7.122	6.852
		235	143	51	235.11704	5.732	6.962
		236	144	52	236.11912	6.902	7.562
		237	145	53	237.12231	5.792	..
		238	146	54	238.12493	6.362	..
		239	147	55	239.12869	5.222	..
		240	148	56	240.13101	6.662	..
Np	93	231	138	45	231.11026	..	3.412
		232	139	46	232.11236	6.882	3.962
		233	140	47	233.11322	8.122	4.392
		234	141	48	234.11568	6.522	4.392
		235	142	49	235.11723	7.432	4.702
		236	143	50	236.12017	6.042	5.012
		237	144	51	237.12158	7.572	5.682
		238	145	52	238.12514	5.422	5.312
		239	146	53	239.12730	6.822	5.772
		240	147	54	240.13002	6.262	6.812
Pu	94	241	148	55	241.13250	6.502	6.652
		232	138	44	232.11338	..	5.022
		233	139	45	233.11555	6.812	4.952
		234	140	46	234.11616	8.372	5.202
		235	141	47	235.11844	6.702	5.382
		236	142	48	236.11962	7.802	5.752
		237	143	49	237.12192	6.682	6.392
		238	144	50	238.12366	7.242	6.062
		239	145	51	239.12653	6.112	6.752
		240	146	52	240.12862	6.892	6.822
Am	95	241	147	53	241.13154	6.062	6.622
		242	148	54	242.13413	6.392	6.512
		243	149	55	243.13740	5.712	..
		237	142	47	237.12302	..	4.742
		238	143	48	238.12571	6.292	4.352
		239	144	49	239.12740	7.292	4.402

TABLE I (contd.)

Element	(Z)	(A)	(N)	(N-Z)	(M) m.u.	(B _n) m.m.u.	(B _p) m.m.u.
Am	95	240	145	50	240.13023	6.152	4.442
		241	146	51	241.13151	7.702	5.252
		242	147	52	242.13489	5.602	4.792
		243	148	53	243.13686	7.012	5.412
		244	149	54	244.14011	5.632	5.432
Cm	96	238	142	46	238.12713	..	4.032
		239	143	47	239.12941	6.702	4.442
		240	144	48	240.13044	7.952	5.102
		241	145	49	241.13223	7.192	6.142
		242	146	50	242.13420	7.012	5.452
		243	147	51	243.13694	6.242	6.092
		244	148	52	244.13880	7.122	6.202
		245	149	53	245.14138	6.402	6.872
Bk	97	243	146	49	243.13860	..	3.742
		244	147	50	244.14122	6.362	3.862
		245	148	51	245.14229	7.912	4.652
		246	149	52	246.14547	5.802	4.052
		249	152	55	249.15186
		250	153	56	250.15591	4.932	..
Cf	98	243	145	47	243.14131
		244	146	48	244.14211	8.182	4.632
		245	147	49	245.14368	7.412	5.682
		246	148	50	246.14543	7.232	5.002
		248	150	52	248.14920
		249	151	53	249.15180	6.382	..
		250	152	54	250.15395	6.832	..
		251	153	55	251.15725	5.682	..
		252	154	56	252.15988	6.352	..
		253	155	57	253.16321	5.652	..
	99	246	147	48	246.14657	..	5.252
		247	148	49	247.15011	5.442	3.462
		253	154	55	253.16296	..	5.062
Centurium	100	254	154	54	254.16570	..	5.402
		255	155	55	255.16886	6.022	..

From these values of binding energies for neutrons and protons, it is clearly seen that the binding energies for even numbers are always higher than that for odd ones. At magic numbers 82 and 126, for protons and neutrons respectively, the binding energy is maximum. These observations were also verified by drawing graphs between even or odd neutron and proton numbers and their binding energies for different $(N-Z)$ values. Also a smaller peak was obtained at 88 in the case of protons, for most of the $(N-Z)$ values. There was a gradual increase and decrease in the binding energies for neutrons and protons respectively for higher numbers.

The difference between the binding energy of a neutron, B_n in a nucleus with odd (or even) N and the average of that of its two neighbours with the same $(N-Z)$ and odd (or even) N is denoted by D_n .

$$D_n = B_n - [B_n(N+2) + B_n(N-2)]/2$$

The average of D_n for all available $(N-Z)$ values is denoted by $[D_n]_{AV}$ and plotted against N (figure 1.). Similarly $[D_p]_{AV}$ is defined and plotted against Z (figure 2.).

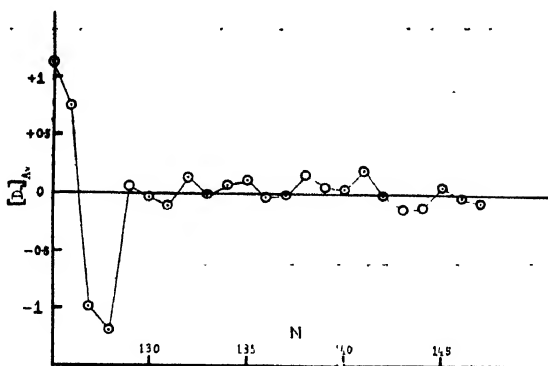


Fig. 1. Variation of $[D_n]_{AV}$ with N

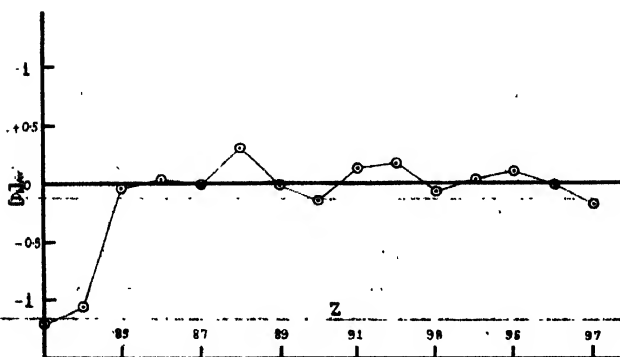


Fig. 2. Variation of $[D_p]_{AV}$ with Z .

For neutrons, the maximum $[D_n]_{AV}$ occurs at $N = 125$. It falls gradually to 126 after which the fall is very sharp. Smaller peaks were also obtained at neutron numbers 129, 132, 135, 138, 141, 145. Two adjacent smaller peaks were separated from each other by three neutron numbers, except in the case of $N = 145$.

For protons, the $[D_p]_{AV}$ curve also fluctuates. The minimum value of $[D_p]_{AV}$ occurs at $Z = 83$. Smaller peaks were observed at proton numbers 88, 92, 95. The adjacent smaller peaks are separated from each other by three proton numbers, nearly.

DISCUSSION

The binding energy of neutrons or protons reaches a high value at a magic number and rapidly falls after that. This actually happens in the case of 126 neutrons and 82 protons which are known to be magic numbers. It was pointed out by Redlich (1952) that the smaller peaks occurring at other neutron and proton numbers in ' $N-B_n$ ', ' $Z-B_p$ ', ' $N-[D_n]_{AV}$ ', or ' $Z-[D_p]_{AV}$ ' graphs might be due to these numbers being magic. At neutron numbers 11, 14, 20, 24 and 28 and at protons numbers 11, 14, 20, 28 smaller peaks were observed by him and among such numbers 14, 20 and 28 are now known to be magic numbers.

From these considerations, it is obvious that there might be magic numbers after 82 protons and 126 neutrons. Also the peak occurring at 88 protons is highest among all the smaller peaks. So this might be a magic number. But other factors are to be considered before arriving at any specific conclusion.

The periodicity in the variation of $[D_n]_{AV}$ and $[D_p]_{AV}$ is also significant and deserves considerations.

The increase in the binding energy of neutrons and protons for even N or Z values is due to their greater stability.

REFERENCES

- Duckworth, Henry E., Benjamin, G. and Pennington, Edwin, M., 1954, *Rev. Mod. Phys.*, **26**, 463.
 Green Alex, E. S., 1955, *Nuclear Physics*, P. 526.
 Li, C. W., Whaling, Ward, Fowler, W. A. and Lauritsen C. C., 1951, *Phys. Rev.*, **83**, 512.
 Mayer, M. G., 1948, *Phys. Rev.*, **74**, 235.
 Redlich, Martin, G., 1952, *Phys. rev.*, **88**, 38.
 Segre, E., 1953, *Experimental Nuclear Physic Vol.*, P. 756.

ON THE FLUORESCENCE IN DIAMOND EXCITED BY X-RAYS*

S. N. SEN AND B. M. BISHUI**

OPTICS DEPARTMENT, INDIAN ASSOCIATION FOR THE CULTIVATION OF SCIENCE, JADAVPUR,
CALCUTTA-32

PLATE XVI

ABSTRACT. The spectra of fluorescence excited by X-rays in seven specimens of diamond of Type I and one specimen of diamond of Type II have been photographed with an Adam Hilger glass spectrograph. The fluorescence efficiency at the 4156 Å band and ultra-violet absorption limits of the specimens were known. It has been observed that all the specimens of diamond of Type I show continuous fluorescence extending from 5200 Å to 3900 Å and only one specimen, namely D8, shows an absorption band at 4155 Å in the continuous fluorescence. The diamond of Type II also shows a very weak continuous fluorescence extending from 4045 Å to 5049 Å. It has been concluded from these results that the particular type of impurity which produces the fluorescence band at 4156 Å is not solely responsible for the continuous fluorescence produced by X-rays, but other impurities can produce the continuous fluorescence under X-ray excitation.

It has further been observed that the intensity of extra Laue spots in these diamonds reported earlier cannot be correlated with fluorescence under X-ray excitation. It has been pointed out that this fact corroborates the conclusion drawn earlier by Sirkar and Sen (1956) that the extra spots in Laue photographs of diamond are due to either mosaicity or irregularities of the spacings in the crystal and not due to chemical impurity.

INTRODUCTION

The fluorescence spectra of diamond excited by X-rays were compared previously by Ramchandran (1946) with the spectrum of fluorescence excited by ultra-violet light and it was observed that 4156 Å band appeared as an absorption band in the spectrum excited by X-rays although its companions on the longer wavelength side were present as emission bands. Fluorescence in some specimens of diamond excited by X-rays was later studied by Bishui (1951) in this laboratory who found that all the four specimens of diamond of Type I showed continuous fluorescence extending from 5660 Å to 3700 Å, and in the case of two specimens showing strong absorption band at 4156 Å, the fluorescence spectrum excited by X-rays showed an absorption band in this region accompanied by a few other similar bands on the short wave length side. He also observed that a diamond

* Communicated by Prof. S. C. Sirkar.

** Present address: Central Glass & Ceramic Research Institute, Calcutta-32.

of Type II did not show any fluorescence in the visible region when irradiated by X-rays. These results were explained on the hypothesis that fluorescence is due to the presence of chemical impurities in the lattice of diamond of Type I and that such impurities are absent in the diamond of Type II.

The fluorescence and absorption spectra in the visible region in the case of six specimens of diamond including one of Type II at temperatures ranging from -180°C to 275°C were studied by Bishui (1950) who observed that integrated intensity of the band at 4156 \AA increased at lower temperatures and diminishing gradually with the rise of temperature of the crystal, it vanishes abruptly at a temperature which is different for different crystals. It was further observed by him that the absorption band at 4156 \AA and its companions also disappear at 275°C , but the birefringence shown by the crystals is not altered very much at this temperature.

Later, Bishui (1952) studied the intensity of the fluorescence band 4156 \AA of eight new specimens of diamond at room temperature with respect to that of the Raman line 1332 cm^{-1} excited by the Hg line 4358 \AA and found that the transparency of the crystals for wavelengths shorter than 3000 \AA cannot be correlated with the intensity of the fluorescence band. These crystals did not exhibit any absorption band at 4156 \AA at room temperature, but at -180°C some of them showed a sharp absorption band at 4156 \AA . From these results it was concluded by Bishui (1950, 1952) that the fluorescence band behaves in the same way as impurity fluorescence and that the impurity is of chemical nature. He also found that the fluorescence band 4156 \AA is originated by some impurity which also produces two absorption bands at 2360 \AA and 2363.5 \AA , and diamonds which may not possess this impurity in appreciable quantities but possess some other impurities which produce absorption in the region 3000 \AA do not show the fluorescence band 4156 \AA with any appreciable intensity. It was pointed out that fluorescence is not due to lattice defect produced by strain in the tetrahedral lattice because there is no exact correlation between microscopic strain and fluorescence in diamonds of Type I..

It is not clear, however, whether the impurity which is responsible for the fluorescence band at 4156 \AA is also responsible for the continuous fluorescence spectrum in the region 3700 \AA to 5650 \AA which is observed when some specimens are excited by X-rays. It would be also worthwhile to investigate whether all diamonds which are transparent upto about 2300 \AA show continuous fluorescence when excited by X-rays. The object of the present investigation was to elucidate

these points more clearly. The spectra due to fluorescence excited by X-rays in eight specimens of diamond having ultraviolet absorption limits lying between 3000 \AA to 2240 \AA and of different thickness have, therefore, been studied in the present investigation.

Recently, it was observed by Sirkar and Sen (1956), who studied the positions and approximate relative intensities of extra spots accompanying the $\{111\}$ reflection in the Laue photographs of eleven specimens of diamond, that neither the intensities of extra reflection in the direction making an angle $2\theta_B$ with incident radiation nor those of extra reflection in other directions present in the Laue photographs of some of the crystals could be correlated either with the intensity of the band at 4156 \AA or with the impurity present in the crystal. Since the approximate relative intensities of the extra spots accompanying the $\{111\}$ reflection in Laue photograph could not be correlated with the intensity of the band at 4156 \AA it was thought worthwhile to study the X-ray fluorescence in some of these diamonds to find out whether the X-ray fluorescence could be correlated with intensities of extra reflection. The present paper deals with the results obtained in the case of diamonds D7, D8, D9, D10, D11, D12 and D14 of Type I and D13 of Type II used by Bishui (1952) in a previous investigation.

EXPERIMENTAL TECHNIQUE

A Seifert X-ray tube giving 26 milliamperes at 32 K.V. and provided with copper anticathode was used for the irradiation of crystals with X-rays. A lead disc about 0.5 cm thick and provided with a small hole was placed on the window to get a narrow beam of X-rays. The specimen of diamond was placed on a stand and it was completely covered by a light-tight cylindrical lead box blackened inside and provided with two rectangular windows 90° apart, through one of which the X-rays were incident on the crystal and through the other the light emitted by the crystal came out and was focussed with a lens on the slit of a spectrograph. A Fuess glass spectrograph was used to photograph the spectra. Special care was taken to see that no stray light could enter the slit of the spectrograph or the box containing the specimen of diamond. On observing visually through the spectrograph it was found that spectrum of light emitted by diamonds was a continuous one and it disappeared as soon as the X-ray tube was switched off. In the case of D12 and D13 it was found that the light emitted by the crystals was very feeble. The spectra were next photographed using in each case an exposure time of 6 hrs and keeping the current in the tube constant. The width of the slit of the spectrograph had to be increased to 0.5 mm in order to diminish the time of exposure. Ilford Zenith plates were used for photographing the spectra. Iron arc spectrum was recorded as comparison on each spectrogram.

RESULTS

The spectrograms obtained in the case of eight specimens of diamonds are reproduced in figures 1-8 in Plate XVI and the intensities of fluorescence excited by X-rays are entered in column (2) of Table I. The intensities of extra spots in the Laue photographs of these specimens of diamonds as given in column 3 are taken from the results of Sirkar and Sen (1956). The intensities of the fluorescence band λ 4156 and the ultraviolet absorption limits are taken from the results reported by Bishui (1952).

TABLE I

Diamond	Intensity of fluorescence excited by X-rays	Intensity of extra Laue reflection at $2\theta = 41^{\circ}36'$	$I_{\lambda 4156}/I_R$	Ultraviolet absorption limit in A.U.	Thickness of diamond in mm.
D 7	Strong	Medium	5.2	2560	1.353
D 8	Moderately strong absorption band at 4155 Å	Strong	1.5	3000	1.3
D 9	Moderately strong	Medium	9.26	2550	0.8
D 10	Very strong	Medium	8.4	2810	1.092
D 11	Strong	Weak	7.1	2270 absorption band at 2360	0.952
D 12	Weak	Strong	3.8	2720	0.647
D 13	Very weak	Weak	0	2240	0.838
D 14	Strong	Weak	6	2300 absorption band at 2360	0.812

DISCUSSION

It can be seen from the spectrograms reproduced in Plate XVI that all the specimens show continuous fluorescence extending from 3900 Å to 5200 Å in general except D13 which gives a feeble continuous spectrum extending from 4045 Å to 5049 Å. In the case of D 8, the spectrum shows a weak absorption band at 4155 Å and in the other cases the absorption band is totally absent. The absence of absorption band in the fluorescence spectra of these specimens of diamond can be explained by the fact observed by Bishui (1952) that the absorption spectra in the visible region for these specimens at room temperature did not show any absorption band at 4156 Å although the band appeared, except in the case of D13 and D14, when the crystals were cooled to -180°C .

The appearance of the absorption band in the fluorescence spectrum due to D 8 suggests that the crystal might exhibit a band in the absorption spectrum at room temperature and the band being weak might have been overlooked by Bishui (1952). In order to verify this, the absorption spectrum was studied again and a feeble band at 4155 \AA was detected. The microphotometric record reproduced in figure 9 shows that the absorption band at 4155 \AA is very feeble and the inten-

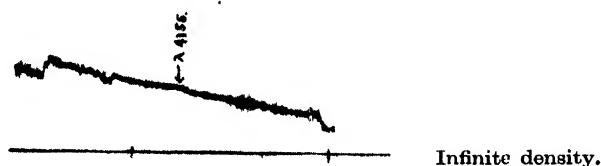
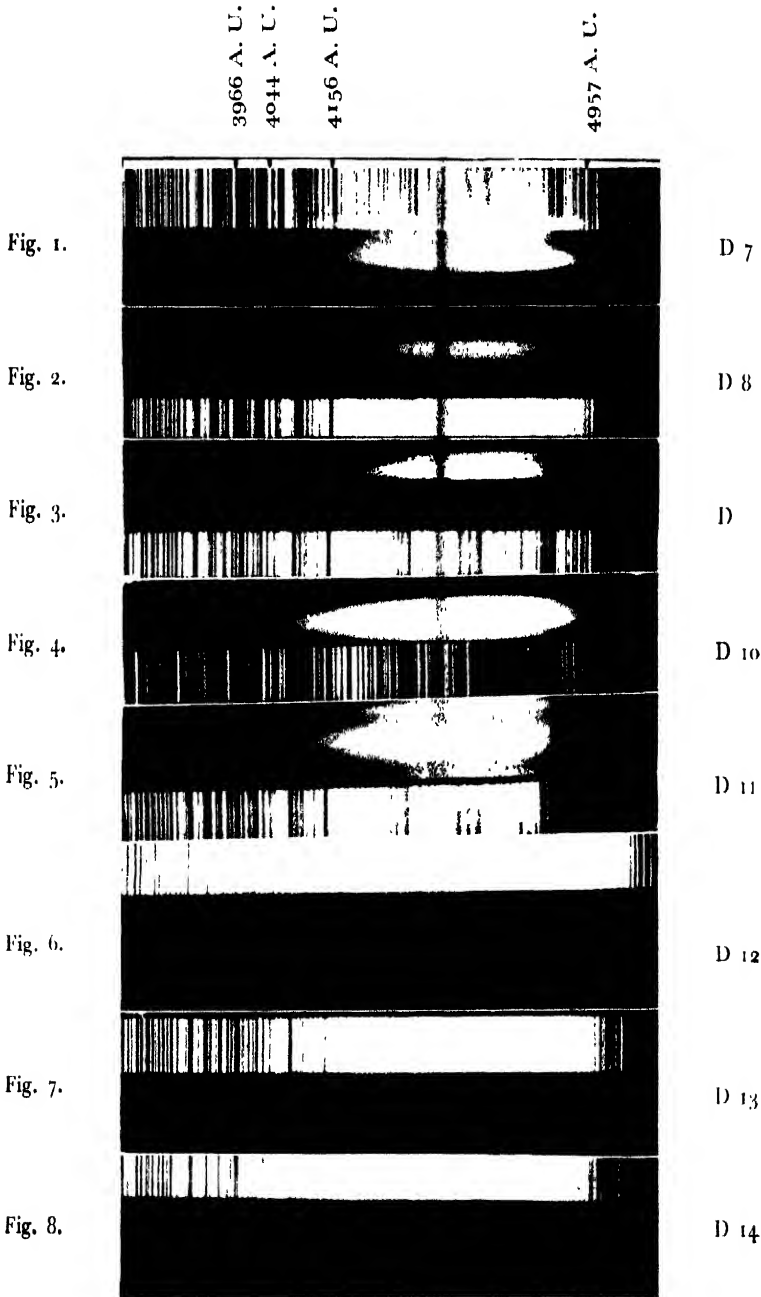


Fig. 9. Microphotometric record of absorption band $\lambda 4155$.

sity ratio I_F/I_R i.e., the ratio of intensities of the fluorescence band at 4156 \AA and the Raman line is affected only very slightly by this absorption, so that the value 1.5 for ratio reported by Bishui may be increased only to about 2.5 when this absorption is taken into consideration.

It is further observed that D 13 which is transparent upto about 2250 \AA and was classified by Bishui (1952) as a diamond belonging to Type II shows under X-ray excitation a very weak fluorescence which is continuous and extends from 4045 \AA to 5049 \AA . In the case of D 4 studied by Bishui no fluorescence was observed under X-ray excitation although it exhibited at -180°C a very feeble fluorescence band at 4156 \AA when excited by ultraviolet radiation. D 13 did not show any trace of this band. From these results he concluded that both these specimens of diamond belong to Type II and do not contain any chemical impurities. It appears, however, that there are some traces of a particular type of impurity in D 13 which gives rise to feeble continuous fluorescence under X-ray excitation but does not produce the fluorescence band at 4156 \AA when excited by ultraviolet rays.

Plate XVI shows that among the fluorescence spectra due to the eight specimens of diamond the spectrum due to D 10 is the most intense one and the ultraviolet absorption limit of this diamond is at 2810 \AA . The intensity of



Fluorescence of diamond excited by X-rays.

fluorescence due to some of the other specimens like D 8, D 13 or D 14 is much smaller than that of the fluorescence due to D 10. As the ultraviolet absorption limit of D 8 is at 3000 \AA which is longer than that of D 10 and the limits in the case of D 13 and D 14 are much shorter, being approximately at 2240 \AA and 2300 \AA respectively, the intensity of fluorescence due to X-ray excitation does not depend much on the ultraviolet absorption limit.

It can also be seen from columns 2 and 4 of Table I that there is no correlation between the intensity of the continuous fluorescence excited by X-rays and that of the fluorescence band 4156 \AA . Although both the 4156 \AA band and the continuous fluorescence excited by X-rays are weak in the case of D12 and D13, the intensity of the band 4156 \AA due to D 8 is very small but the fluorescence excited by X-rays in this specimen is very strong. Similarly, the intensity of the fluorescence band 4156 \AA due to D 9 is greater than that due to D 10, but the intensity of fluorescence excited by X-rays is larger in the latter case than in the former. These facts indicate that the impurities producing the band at 4156 \AA are of particular type while other impurities not producing this band can produce fluorescence under X-ray excitation.

Columns 2 and 3 of Table I again show that there is no correlation between intensity of X-ray fluorescence and that of extra spots in the Laue photographs. This is in conformity with the conclusion drawn earlier by Sirkar and Sen (1956) that some of the extra spots are due to mosaicity in the crystal and the other spots are due to irregularities in the spacing present in the crystal.

ACKNOWLEDGMENT

The authors are indebted to Prof. S. C. Sirkar, D.Sc., F.N.I. for this kind interest and constant guidance throughout the progress of the work.

REFERENCES

- Bishui, B. M., 1950, *Ind. J. Phys.*, **24**, 441.
,, 1951, *Ind. J. Phys.*, **25**, 575.
,, 1952, *Ind. J. Phys.*, **26**, 347.
Ramchandran, G. N., 1946, *Proc. Ind. Acad. Sciences*, **24A**, 176.
Sirkar, S. C. and Sen, S. N., 1956, *Ind. J. Phys.*, **30**, 29.

Letter to the Editor

The Board of Editors will not hold itself responsible for opinions expressed in the letters, published in this section. The notes containing reports of new work communicated for this section should not contain many figures and should not exceed 500 words in length. The contributions must reach the Assistant Editor not later than the 15th of the second month preceding that of the issue in which the Letter is to appear. No proof will be sent to the authors.

THEORY OF SPECIFIC HEAT OF LIQUID HYDROGEN.

S. C. MISRA

RAVENSHAW COLLEGE, CUTTACK

(Received for publication August 8, 1956)

As the three physical states are continuous, the liquid state may be taken as a transition from solid to the gaseous state. So, in the theory of specific heat of liquids we must consider the motion of oscillation of the particles as in the solid state and also the motion of translation of the particles as in the gaseous state. Hence total specific heat at any temperature will be determined by relative contribution of the two terms or $C_v \propto C_{ois} + C_{trans}$

By comparing the formulae of Debye (Debye's Theory of specific heat of solids) and Planck (Theory of black body radiation) it is found that

$$C_{ois} = 3R - C_v$$

where R is the usual gas constant

C_v is the Debye term and its characteristic temperature (θ_m) is to be determined by trial.

$$\text{and } C_{trans} = \frac{3}{2} R \left[1 - e^{-\lambda(T - T_m)} (1 - T_\lambda) \right]$$

where R is the usual gas constant

T is the temperature at which the specific heat is observed.

T_m is the melting point.

λ is an arbitrary constant independent of temperature.

In the case of liquid hydrogen it is found that the best results are obtained by assuming that $\theta_m = 24^\circ\text{K}$ and $\lambda = 0.04$.

The experimental values are taken from Eucken (1936). In the case of hydrogen the rotation starts at 50°K and it is not taken into account.

In the table below the last four readings are given separately, for one can notice a sudden change in the specific heat at 21.09°K . Such changes are observed in solids also (perhaps some change in the internal structure takes place here.) So, for these readings θ_m is taken to be 21°K .

Temp. (abs)	Sp. heat obs.	Sp. heat calc.	Temp. (abs)	Sp. heat obs.	Sp. heat calc.
15.33	2.54	2.56	20.5	2.98	2.96
15.86	2.56	2.60			
16.23	2.63	2.63			
16.87	2.70	2.68			
17.22	2.70	2.71			
17.88	2.78	2.76	21.00	2.93	2.92
18.92	2.84	2.84	21.40	2.94	2.95
19.5	2.89	2.89	22.10	3.00	3.00
20.0	2.92	2.92	23.10	2.99	3.06

Similarly, in the case of liquid heavy hydrogen we get the best values of the specific heat for $\theta_m = 54^\circ\text{K}$ and $\lambda = 0.02918$. On the whole in both the cases the agreement with our suggestion is quite satisfactory.

REFERENCES

Eucken, 1936, *Z. Electrochem*, **42**, 547.